INTERNATIONAL SYMPOSIUM on
ADVANCED ENGINEERING & APPLIED MANAGEMENT
– 40th ANNIVERSARY in HIGHER EDUCATION (1970-2010)
4 – 5 November, 2010, Hunedoara, ROMANIA

[1.]Caius PANOIU, [2.]Manuela PANOIU, [3.]Raluca ROB

PROGRAMMABLE GAIN AMPLIFIER USING PARALLEL PORT CONTROLLING

[1-3.] ELECTRICAL ENGINEERING AND INDUSTRIAL INFORMATICS DEPARTMENT, UNIVERSITY POLITECHNICA TIMISOARA, FACULTY OF ENGINEERING HUNEDOARA, HUNEDOARA, ROMANIA

ABSTRACT:
This paper presents a way to realize a programmable gain amplifier that can be software controlled using parallel port. The controlling scheme is made in LabVIEW, which permits visualisation of the both input and output of the amplifier and also gain control using parallel port.
KEYWORDS:
Programmable gain amplifier, parallel port, spectral characteristic

1. INTRODUCTION

Realizing a programmable gain amplifier is a difficult problem, especially if the purpose is obtaining a huge number of regulation steps and a good accuracy. In case of this amplifier, the controlling gain implies 255 equal steps, using a digital to analogue converter, whose reference current can be adjusted by controlling the digital inputs using parallel port.

2. METHODOLOGY

The application can acquire a signal using a real generator using the analogical inputs of the data acquisition board NI – 6221 [1]. This signal can be followed on a virtual oscilloscope display built in LabVIEW. As well, the input signal is added with a continuous signal in order to obtain a unipolar reference signal for digital analogical converter. Gain control can be made controlling digital inputs of the converter using parallel port. Block scheme of the application is represented in figure 1.

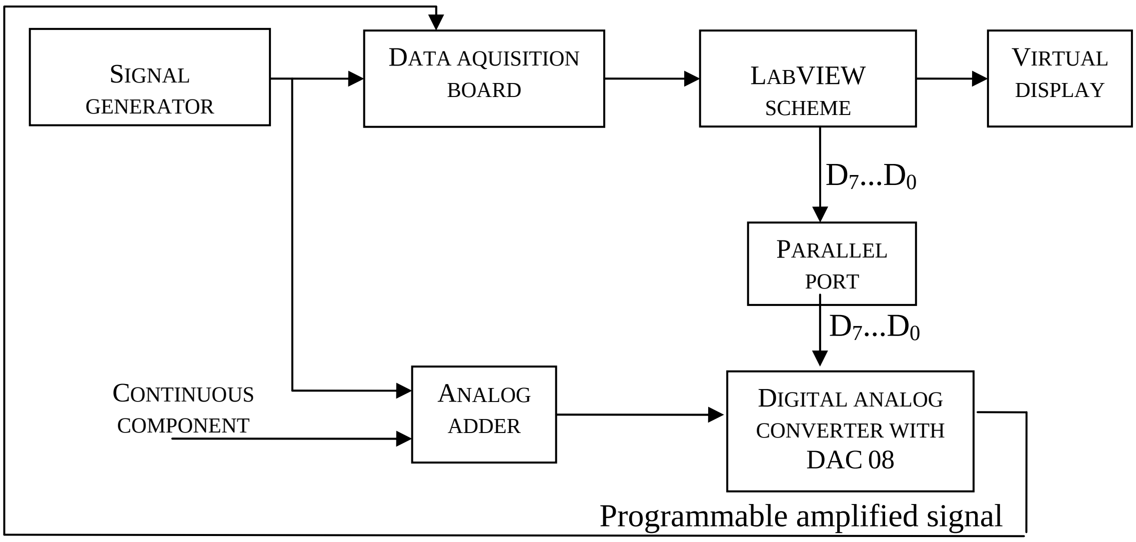

Fig.1. Block scheme of the application

In order to build a programmable gain amplifier of the input signal, the authors used an analogical adder realized with an operational amplifier μA741, like in figure 2. The output of the μA741 is connected at the reference input of a digital analogical converter with DAC 08.

LabVIEW scheme is completing with a $D_7...D_0$ byte generating system [4], byte that is sent on data lines of the parallel port using 378h address. This byte becomes digital input signal for DAC 08. In this way, according with the byte value, there can be obtained different values for the output current of the converter [5]. The analogical output represents the acquired signal from the signal generator and programmable amplified by the present application. This signal can be followed on the virtual oscilloscope display if it is connected to an analogical input of data acquisition board.

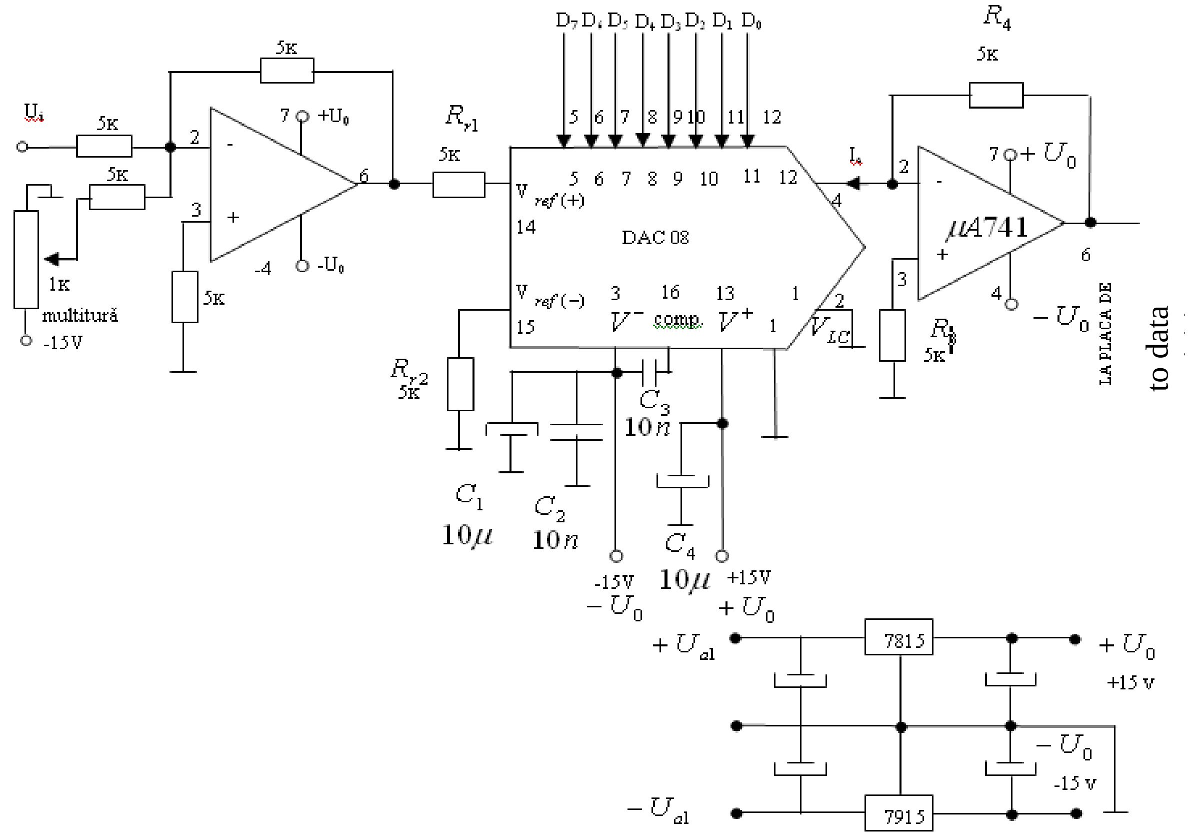

Fig.2. Electronic scheme of the application

Data acquisition board NI-6221

This application is realized using data acquisition board National Instruments NI – 6221, presented in figure 3.

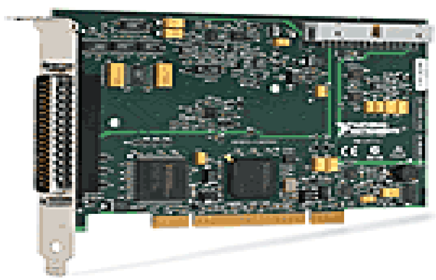

Fig.3. Data acquisition board PCI-6221.

Characteristics:

- 16 analogical inputs, 250 kS/s, resolution 16 bits
- 2 analogical outputs, 833 kS/s, resolution 16 bits
- 10 digital I/O compatible TTL
- 2 counter/timers on 32 bits
- Digital trigger
- Compatibility with Windows (2000/NT/XP), Linux and Mac OS X
- Integration with software components LabVIEW, CVI, Measurement Studio for Visual Studio NET.

Table 1. PCI-6221 Pins signification

AI 0	68	34	AI 8
AI GND	67	33	AI 1
AI 9	66	32	AI GND
AI 2	65	31	AI 10
AI GND	64	30	AI 3
AI 11	63	29	AI GND
AI SENSE	62	28	AI 4
AI 12	61	27	AI GND
AI 5	60	26	AI 13
AI GND	59	25	AI 6
AI 14	58	24	AI GND
AI 7	57	23	AI 15
AI GND	56	22	AO 0
AO GND	55	21	AO 1
AO GND	54	20	NC
D GND	53	19	P0.4
P0.0	52	18	D GND
P0.5	51	17	P0.1
D GND	50	16	P0.6
P0.2	49	15	D GND
P0.7	48	14	+5V
P0.3	47	13	D GND
PFI 11/P2.3	46	12	D GND
PFI 10/P2.2	45	11	PFI 0/P1.0
D GND	44	10	PFI 1/P1.1
PFI 2/P1.2	43	9	D GND
PFI 3/P1.3	42	8	+5V
PFI 4/P1.4	41	7	D GND
PFI 13/P2.5	40	6	PFI 5/P1.5
PFI 15/P2.7	39	5	PFI 6/P1.6
PFI 7/P1.7	38	4	D GND
PFI 8/P2.0	37	3	PFI 9/P2.1
D GND	36	2	PFI 12/P2.4
D GND	35	1	PFI 14/P2.6

3. DISCUSSION LabVIEW implementation

Control elements are rotary buttons, pushing buttons, circular dial and other input devices.

This paper is an oscilloscope application that is structured on two channels. Using NI-6221 data acquisition board, to each channel it can be provided a signal from a real generator. Different types of signal could be chosen depending on the generator capacity. Through LabVIEW program, there can be set the amplitude and the vertically position on each channel independently, like in figure 4. For these, there are used *Knob* control buttons [2].

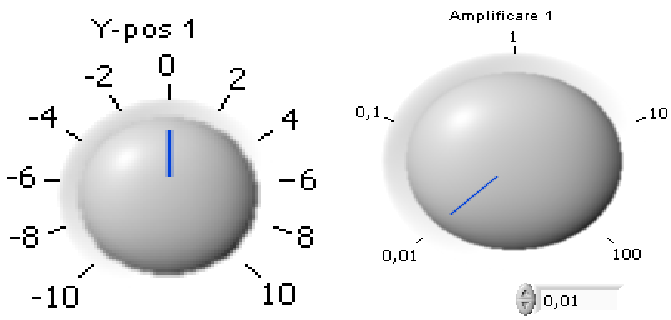

a) b)

Fig. 4. The electric scheme
a) Button for controlling the vertically position,
b) Button for controlling the amplification

The number of the acquired samples can be controlled using a control button placed on Front Panel.

In order to acquire signals on two different channels, there is using *DAQ Assistant* block that can determine the number of employed channels, sampling rate, amplitude, error, etc. For separating the desired channels, there is using *Trigger and Gate* block. With *Multiply* and *Add*, the user can control the amplitude and the vertically position.

For spectral analysis of the acquired signals in frequency domain, it is using *Spectral Measurements* block.

Time base scheme of the indicator display is presented in figure 6.

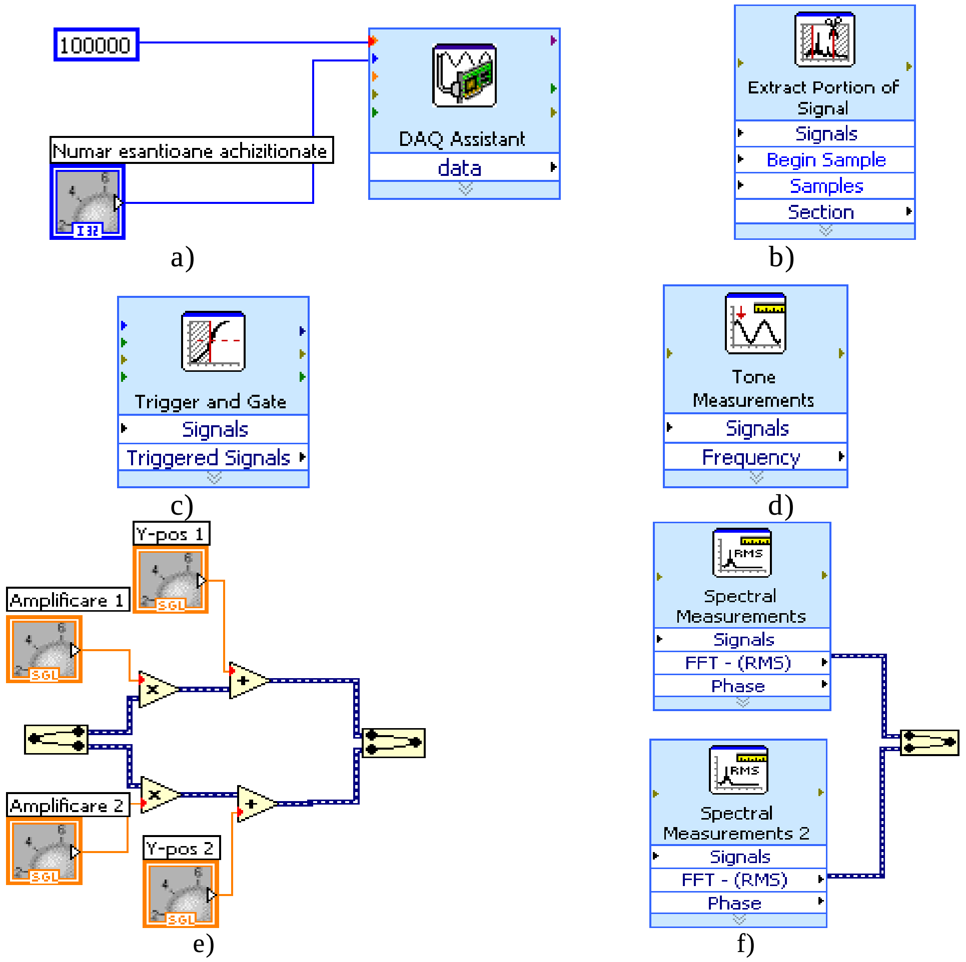

Fig. 5. a) DAQ Assistant, b) Extract Portion of Signal, c) Trigger and Gate, d) Tone Measurements, e) Mathematical blocks Multiply and Add, f) Spectral Measurements.

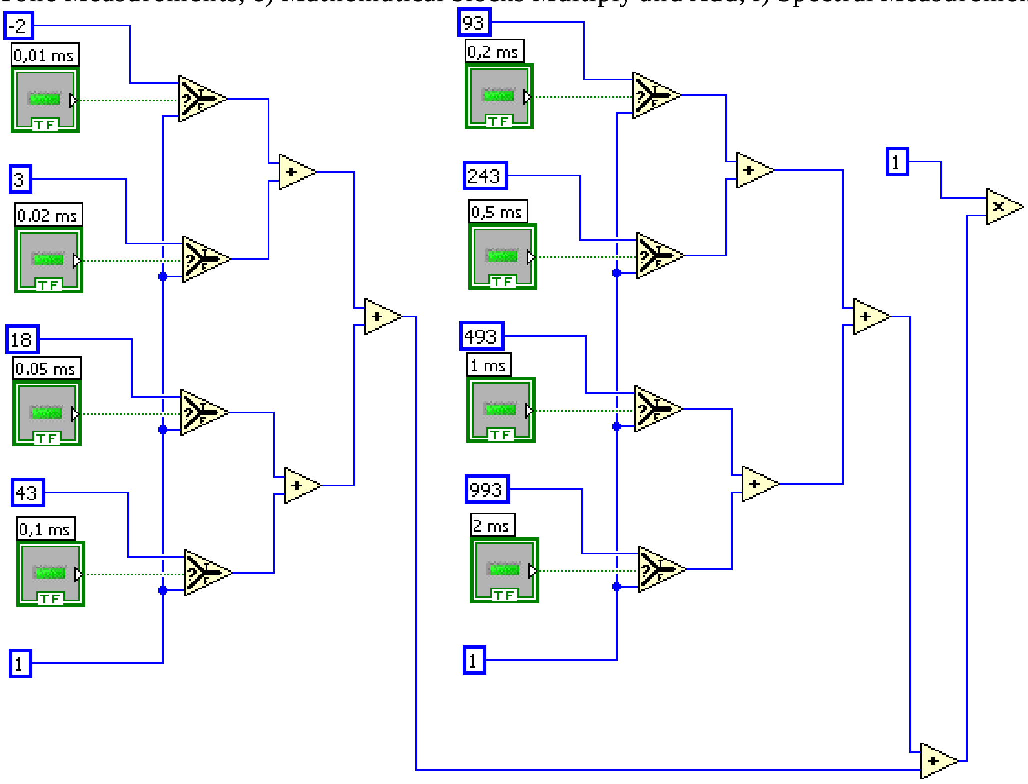

Fig. 6. Time base

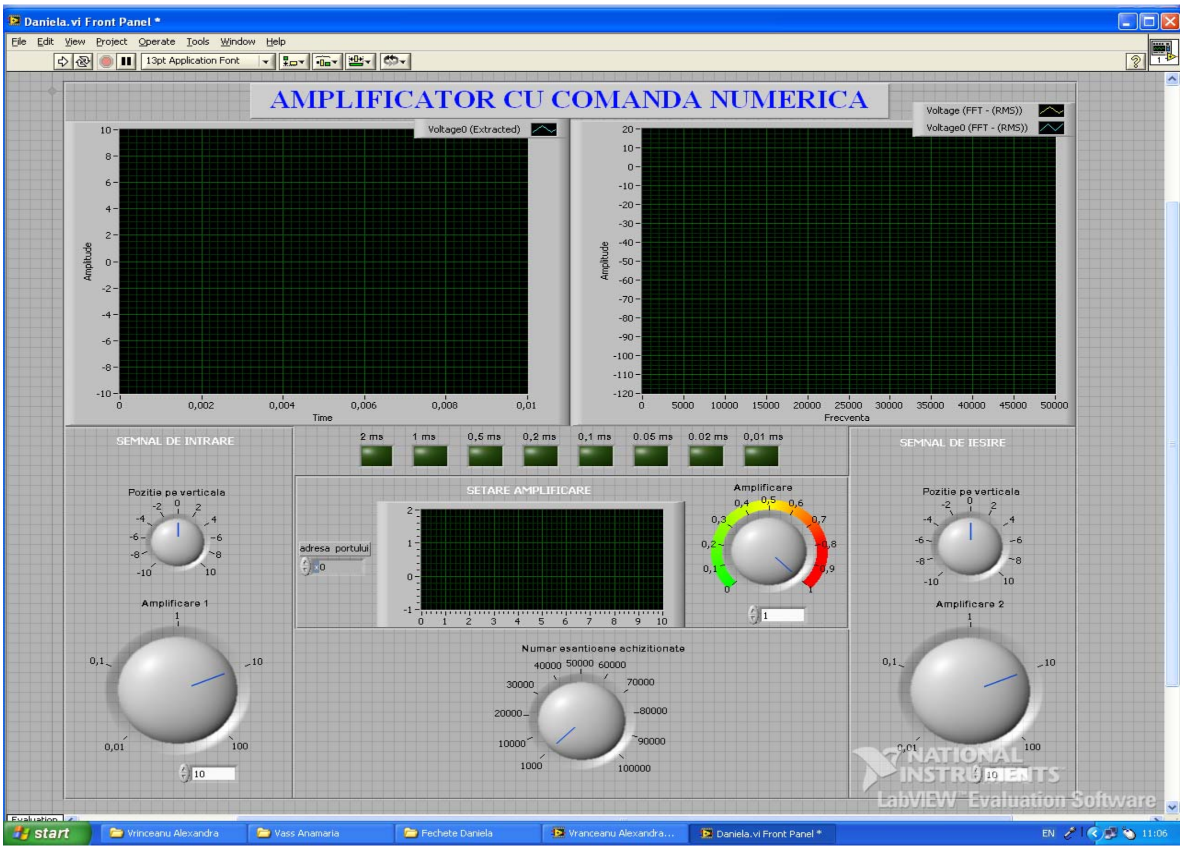

Fig. 7. Front panel of the application

The assumed signals according with the electrical scheme can be viewed on a display indicator placed on Front Panel [3] (two channels). On the first display can be viewed signals in time domain, on the second can be viewed signals in frequency domain, like in figure 7.

4. CONCLUSIONS

The programmable gain of the amplifier solves the accuracy problem, because realizing a high number of voltage steps, which represents a difficult problem. The application permits the input and output signals to be viewed on virtual displays in order the amplitude and vertically position to be adjusted.

REFERENCES

[1.] Liviu Toma, *Sisteme de achiziţii de date*, Editura de Vest, Timişoara, 1998.
[2.] Francis Cotet, Octavian Ciobanu, *Bazele programării în LabVIEW*, Editura Matrix Rom Bucureşti, 1998.
[3.] http://www.ctanm.pub.ro/academic/labview/Tutorial.htm
[4.] Mircea Popa, *Sisteme cu microprocesoare*, Editura Orizonturi Universitare, Timişoara, 2003.
[5.] Popa M, Marcu M, *Porturile paralel şi serie ale calculatorului PC*, Editura Orizonturi Universitare, Timişoara, 2001.

INTERNATIONAL SYMPOSIUM on ADVANCED ENGINEERING & APPLIED MANAGEMENT
– 40th ANNIVERSARY in HIGHER EDUCATION (1970-2010),

INTERNATIONAL SYMPOSIUM on
ADVANCED ENGINEERING & APPLIED MANAGEMENT
– 40th ANNIVERSARY in HIGHER EDUCATION (1970-2010)
4 – 5 November, 2010, Hunedoara, ROMANIA

[1]Ion COPACI, [2]Bogdan TĂNĂSOIU

ON THE DYNAMIC EXPERIMENTAL DETERMINATION OF THE CHARACTERISTICS OF SHOCK INSULATORS

[1] UNIVERSITY "AUREL VLAICU" ARAD, ROMANIA
[2] REMARUL „16 FEBRUARIE“ CLUJ-NAPOCA, ROMANIA

ABSTRACT:
The paper presents and compares two methods for establishing the dynamic characteristics of shock insulators and underlines the authenticity and scientific validity of the method of collision testing in specialized stands.
The paper also contains the experimental results obtained for a shock insulator with elastomer type elastic elements, together with a series of conclusions that regard the equipping of shock insulators with a high capacity for storing and dissipating potential deformation energy, as well as the importance of the 2β energy characteristic for the collision process.
KEYWORDS: shock insulators, potential deformation energy, buffers, transmitted forces

1. INTRODUCTION

The shock caused by collision [2] leads to the transmission of forces and accelerations that can determine unwanted consequences on the resistance structures, equipment, passengers and freight transported by railway vehicles.

In order to reduce the transmitted forces and accelerations and, consequently, the unwanted consequences of the shock, railway vehicles are equipped with shock insulators. The capacity of the shock insulators to store potential deformation energy, described by the 2β energy coefficient [1], directly influences the magnitude of the forces and accelerations transmitted to the vehicles, the level of the potential energy $(1 - 2\beta)E_p$ received by the vehicles, as well as the effects caused by the shock during the collision process. Therefore, during the design and execution of railway vehicles, there is a tendency to increase the storage capacity for potential deformation energy of shock insulators in order to reduce the levels of the forces and accelerations transmitted to the vehicles during the collision.

In regard to the use of railway vehicles there is a tendency to increase travel velocities, reduce the formation times of trains as well as increase the axle load. Consequently, the forces and accelerations transmitted to the vehicles as a result of collisions reach relatively high values that need to be considered during the conception, design and execution of railway vehicles.

2. DETERMINING THE DYNAMIC CHARACTERISTICS OF SHOCK INSULATORS EXPERIMENTALLY

Initially, the characteristic dynamic diagrams were obtained under the action of the shock caused by the free fall of a weight (ram), with a well determined mass, from different launching heights, on the buffer or central coupling dampener affixed to a rigid plane [2].

This adopted system differs significantly from the mechanical system encountered in the use of railway vehicles, specifically the one formed by the masses of the two cars separated by shock insulators, system which has a longitudinal freedom of motion.

The excitation function (system entry), specifically the momentum "mv" of the ram mass is applied through the buffer or central coupling dampener to a plane with a theoretically infinite mass. Thus, time variations of the force and contraction of the buffer or central coupling dampener are obtained, as response functions to the applied excitation, particular to the used mechanical system and different from those of the real system.

Consequently, through the use of this method, characteristic dynamic diagrams are obtained that can not lead to a correct qualitative appreciation of the shock insulator, resulting in erroneous dynamic characteristics.

Through the experimental determination process for the characteristic dynamic diagrams involving the falling ram we have established the diagram in figure 1 for a central coupling dampener type S-2V-90, used by the railway administrations of the former USSR countries. In figure 2 we have represented the characteristic dynamic diagram of the same type of dampener, determined by colliding two railway cars, each with a mass of ≈ 92t, at a collision velocity of 6,0km/h. The following observations can be made:

- the variation of the force as a function of contraction differs substantially. In the case of the diagram in figure 1 sudden increases of the force appear, followed by decreases. In the case of the diagram in figure 2, the evolution is approximately linear up to a contraction of ≈ 75mm;
- the stored potential deformation energy and the dissipation coefficient η for the same maximum contraction D_{max}=85mm have higher values for the collision, We=30,4KJ, η=0,88, tan in the situation of the falling ram, when We=21,8KJ, η=0,63.

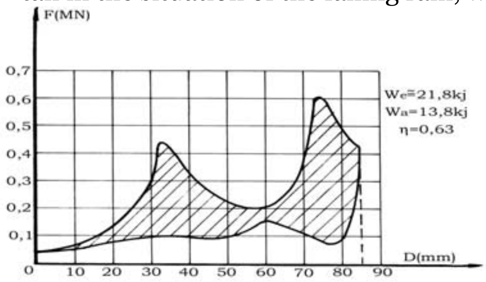

Fig.1

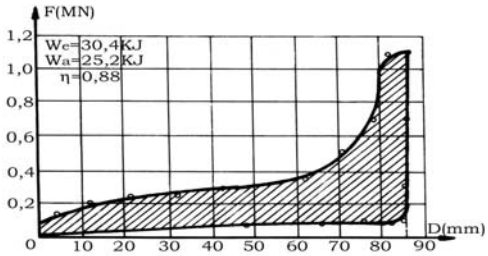

Fig. 2

Thus, significant differences are observed in regards to the obtained dynamic characteristics, which categorically imposes the option for determining the characteristic dynamic diagram for the shock insulators through the collision method.

3. FORCES TRANSMITTED TO THE VEHICLES DURING THE COLLISION

A series of authors have tried to theoretically establish mathematical expressions for the forces and accelerations transmitted to the vehicles during the collision process.

The general case of the collision of two railway cars is considered. The colliding car, with mass m_1 and velocity v_1, interacts with a collided car, with mass m_2 and velocity v_2, where $v_1 > v_2$. The cars are equipped with shock insulators (buffers or central coupling insulators).

During the collision process, part of the kinetic energy of the vehicles is transformed into potential deformation energy that is maximal at time t_{12} when the vehicles travel at the same velocity v_{12}. The expression for the potential deformation energy E_p is:

$$E_p = \frac{m_1 m_2}{m_1 + m_2}\frac{(v_1 - v_2)^2}{2} = \frac{m_1 m_2}{m_1 + m_2}\frac{v^2}{2} \tag{1}$$

where: m_1 – mass of the colliding car; m_2 – mass of the collided car; v– relative velocity between vehicles (collision velocity).

The energy factor that characterizes the efficiency of shock insulators is 2β, which represents the ratio between potential deformation energy stored by the shock insulators, W_e, and the total potential energy, which includes the potential energy stored by the elastic elements that represent the bearing structures, the elastic elements that form the suspension of the vehicle, the equipment and the existing load (freight, passengers):

$$2\beta = W_e / E_p \tag{2}$$

The theoretical expressions of the transmitted force established previously can be used only under the condition that the vehicles are equipped with shock insulators that show a linear variation between force and contraction, consequently we propose the following relations.

Railway vehicles can be equipped with shock insulators whose elastic elements show a nonlinear variation between force and contraction [2], [3].

In the case of a collision between two vehicles of the same type, with $m_1 = m_2 = m$, $K_{T1} = K_{T2} = K_T$, $p_1 = p_2 = p$, and $\beta_1 = \beta_2 = \beta$, the expression of the transmitted force becomes:

$$F_{max} = (v_1 - v_2)\sqrt{\frac{m}{4}2\beta\frac{K_T}{p}} \tag{3}$$

where:

- p = f(v) is the plenitude coefficient and represents the ratio between the stored potential deformation energy and the product between the maximum transmitted force and the maximum contraction of the shock insulator;
- K_T = f(v) is the convetional rigidity of the shock insulator (buffer) and represents the ratio between the maximum transmitted force and the maximum contraction of the shock insulator.

4. EXPERIMENTAL DETERMINATIONS

During the testing, the colliding car, launched from the inclined plane of the testing stand, collided at various velocities the standing, unbraked, collided car sitting on the level part of the stand. The used cars, colliding and collided, were 4 axle freight cars, loaded with uniform materials (sand, gravel, broken rock, etc.) up to a total mass of 80t/car. The colliding car was equipped with category A buffers and the collided car with category C buffers (studied with elastomer elastic element).

For each shock caused by the collision of the vehicles, during the collision process the following parameters were determined experimentally:

- collision velocity v;
- forces transmitted through the buffers $F_1(t)$, $F_2(t)$;
- contraction of the dampener of the collided car $D_1(t)$, $D_2(t)$.

Tables 1 and 2 show the experimental results obtained during the testing conducted.

The adnotations made in the tables represent:

- F_{total} – force transmitted during collision;
- $F_{med} = \frac{F_1 + F_2}{2}$ - average force transmitted through the buffer;
- $D_{med} = \frac{D_1 + D_2}{2}$ - average buffer contraction;
- W_{e1}, W_{e2} – potential deformation energy stored by the buffers of the collided vehicle (category C);
- W_{a1}, W_{a2} - potential deformation energy dissipated by the buffers of the collided vehicle (category C);
- η_1, η_2 – energy coefficients for the dissipation of potential deformation energy of the shock insulators: $\eta_1 = \frac{W_{a1}}{W_{e1}}$ and $\eta_2 = \frac{W_{a2}}{W_{e2}}$;
- $W_{emed} = \frac{W_{e1} + W_{e2}}{2}$ - average potential deformation energy stored by the category C buffers.

Table 1

V [km/h]	F_1 [MN]	F_2 [MN]	F_{total} [MN]	F_{med} [MN]	D_1 [mm]	D_2 [mm]	D_{med} [mm]
8,4	0,564	0,551	1,115	0,557	48,1		48,85
9,6	0,627	0,628	1,255	0,627	60	65,9	62,95
10,7	0,652	0,718	1,37	0,685	65,9	70,4	68,15
12,7	0,852	0,872	1,724	0,862	74,1	77,8	75,95
13,9	0,952	1,026	1,978	0,989	75,6	80,7	78,15
14,7	1,09	1,038	2,128	1,064	77	78,5	77,75
16	1,215	1,217	2,432	1,216	89	90,1	89,55

Table 2

V [km/h]	W_{e1} [KJ]	W_{a1} [KJ]	η_1	W_{e2} [KJ]	W_{a2} [KJ]	η_2	$W_{e\ med}$ [kJ]
8,4	15,1	13,4	0,887	15,3	14,3	0,934	15,2
9,6	23,4	20,5	0,876	25,5	22,5	0,882	24,45
10,7	28,6	24,7	0,863	31,6	28,1	0,889	30,1
12,7	38,8	34,6	0,892	41,8	37,8	0,904	40,3
13,9	46,5	41,6	0,995	48,7	45,4	0,932	47,6
14,7	48,5	43,6	0,9	51,8	48,8	0,94	50,15
16	70,5	65,5	0,93	74,5	69,7	0,93	72,5

Figures 3, 4, 5 and 6 show the diagrams of the force transmitted through the buffers as a function of the buffer contraction, together with the energy characteristics for the collisions at the marked velocities.

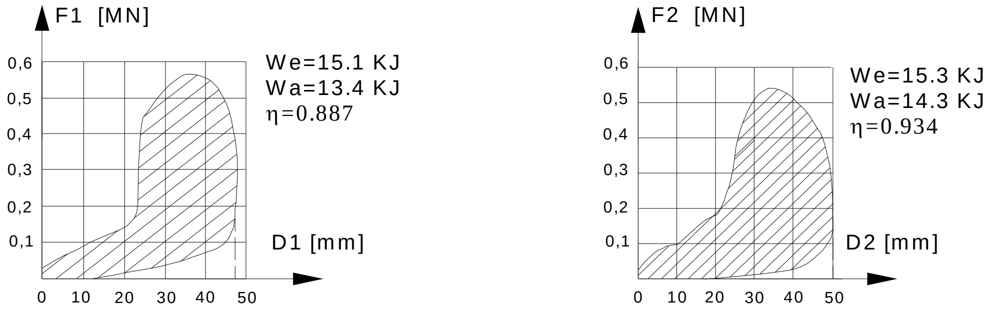

Fig. 3 V = 8,4Km/h

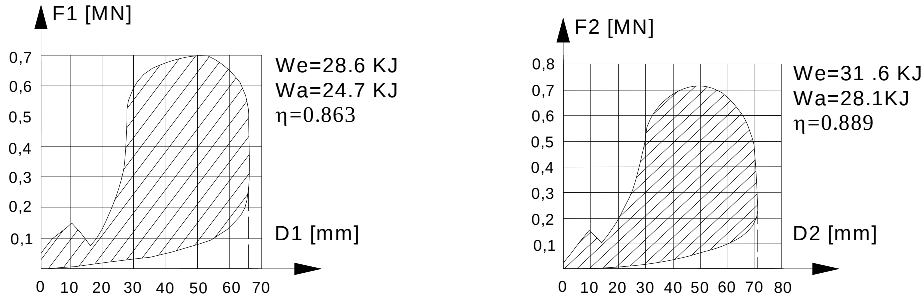

Fig. 4 V = 10,7Km/h

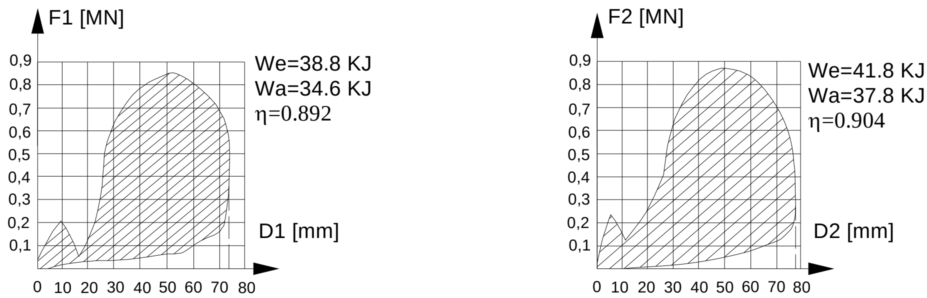

Fig. 5 V = 12,7Km/h

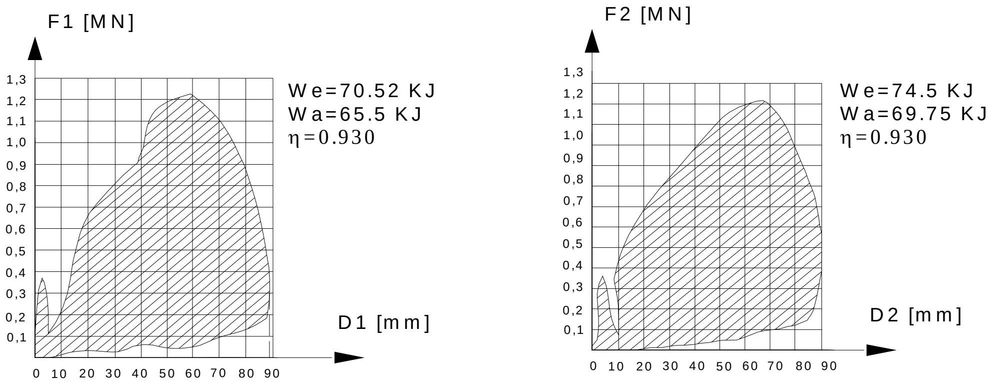

Fig. 6 V = 16Km/h

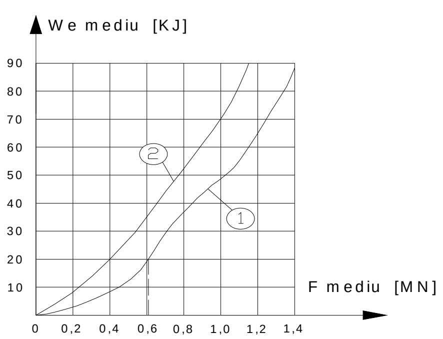

Fig. 7

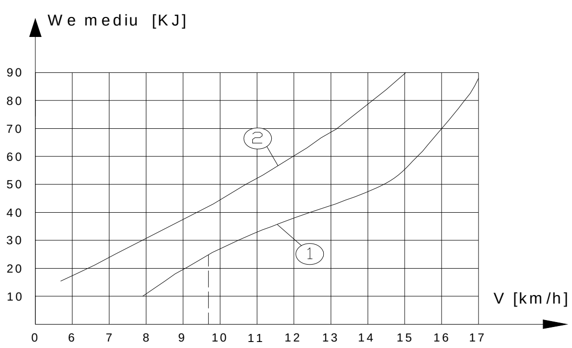

Fig. 8

Figures 7 and 8 show the variations of the average stored potential deformation energy of the category C buffers, as a function of the average force transmitted through the buffers and the collision velocity (curves 1). In the diagrams the same variations are shown for a category C buffer with a RINGFEDER type elastic element connected in parallel with a hydraulic dampener of own design (curves 2).

5. CONCLUSIONS

In order to establish the dynamic characteristics of the shock insulators (buffers, central coupling dampeners, long displacement dampeners), the method of the collision is imposed, which offers the real characteristics. Following the analysis of the experimental results for a force of under 1,3MN and a collision velocity above the velocity of 15Km/h, the studied buffers store potential deformation energy above 70KJ and consequently they can be classified as being category C according to UIC 526 -1 in accordance to the type of testing conducted.

REFERENCES

[1.] Copaci I., Trif E. ş.a. „Aplicarea metodei tensometrice pentru calcularea forţei transmise şi a lucrului mecanic înmagazinat de amortizoarele de şoc în timpul tamponării". Revista Transporturilor şi Telecomunicaţiilor nr. 3 la al II-lea Simpozion Naţional de Tensometrie cu participare internaţională , Cluj Napoca – 1980, pg.33-39 .

[2.] Sebesan I., Copaci I., „Teoria sistemelor elastice la vehiculele feroviare", Editura Matrix Rom Bucuresti – 2008.

[3.] Tănăsoiu Aurelia, Copaci Ion, „Study on the Sock caused by Collision of Railway Vehicles", International Journal of Mechanics, ISSN 1998-4448, pag. 67-76, www.naun.org/journals/mechanics.

INTERNATIONAL SYMPOSIUM on ADVANCED ENGINEERING & APPLIED MANAGEMENT
– 40th ANNIVERSARY in HIGHER EDUCATION (1970-2010),

INTERNATIONAL SYMPOSIUM on
ADVANCED ENGINEERING & APPLIED MANAGEMENT
– 40th ANNIVERSARY in HIGHER EDUCATION (1970-2010)
4 – 5 November, 2010, Hunedoara, ROMANIA

[1]Gelu Ovidiu TIRIAN, [2]Camelia BRETOTEAN-PINCA,
[3]Cristian CHIONCEL, [4]Sergiu MEZINESCU

INDUSTRIAL IMPLEMENTATION OF THE PREDICTION, DETECTION, AND CRACK REMOVAL SYSTEM OF CONTINUOUS CASTING

[1,2,4] UNIVERSITY POLITEHNICA OF TIMISOARA, FACULTY OF ENGINEERING FROM HUNEDOARA, ROMANIA
[3] UNIVERSITY „EFTIMIE MURGU", RESITA, ROMANIA

ABSTRACT:
The paper presents the industrial FDS deployment of crack prediction and elimination, and also an adaptive system to eliminate slipping between the semi-finished and pulling rollers (FAS), when the FDS casting speed performs any corrections.
KEYWORDS:
Continuous casting, implementation, crack, slip

1. INTRODUCTION

Continuous casting facilities are currently managed by automated systems organized several hierarchical levels [3].

Control systems ensure the right working algorithms required by an appropriate system working – both technologically and generally speaking –, and also in case of classical systems based on PID numerical controller [7]. Usually, there are no measures for crack prediction, thus rejects results from the process (in terms of tenth of tones of steel). In such case, working staff changes the working methods of the installation, based on internal instructions.

The casting programmer is not appropriate and that has important economical implications. Worldwide, there is research [1], [2], [4], [5] who might lead to already-made crack detection (inside the crystallizing apparatus) and damaged goods. Currently used methods do not entirely eliminate the cracks.

In [6], [8], it is proposed a number of original solutions allowing the complete crack rejection from the cast material, outside the crystallizing apparatus. Therefore, we have designed a neural network [6] allowing us to detect any primary crack, by a thorough predictive analysis of the information received from a thermo-couple matrix [7]. Information is used by a system based on fuzzy logics [8], which enables corrections of the casting speed and of the cooling water flow. Since this method does not lead to a complete crack rejection (although specialized literature refers to correcting the casting speed alone, in addition to that we have proposed to change the cooling water flow as well), we have adopted a new predictive principle who diminishes any possible cracking. Thus, the fuzzy system [8] analyzes a number of characteristic measurements and, although the neural network [6] has not yet acknowledged any crack, but it considers they may occur they perform casting speed corrections and cooling water flow occurs. Certainly, the solution we have proposed also implies a more complex fuzzy controller, using two sets of distinct set of rules.

Because crack disposal system produces speed corrections they are applied as a step; it was necessary to analyze any potential slipping between the bars and poured pick rollers (this slip happens when the casting starts, but then is not important). To remove the slide, which may adversely affect the speed adjustment, we designed an adaptive fuzzy system [9]. This crack prediction and elimination fuzzy system software was implemented on a development board then, it was tested in the plant.

2. METHODOLOGY DISCUSSION

To validate industrial principles and methods of prediction and elimination of cracks, attempts have been implemented in a real continuous casting plant, in operation , fig. 1. Since it is an operating plant, implementation was accomplished without significant disruption of the production process, which would immediately lead to unacceptable economic loss to the firm.

Fig. 1. Real continuous casting plant

Major subassemblies of the installation and key operating parameters when the tests have been performed are presented in figure 2., in a print-screen of the process management system.

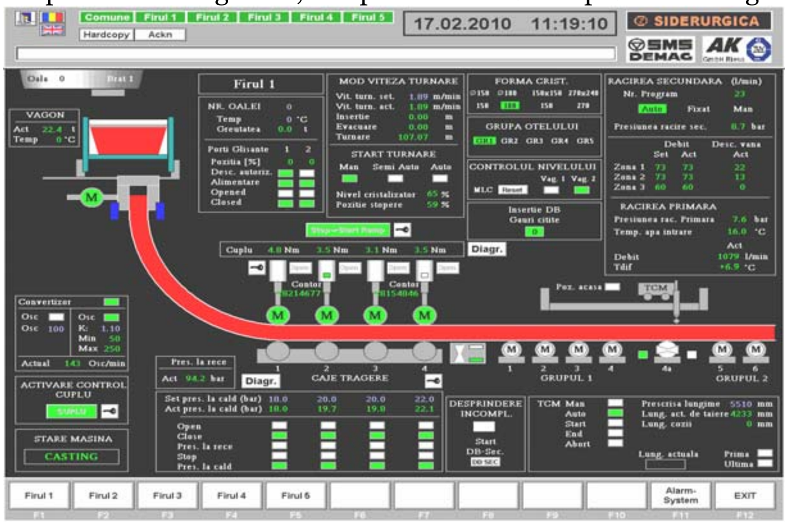

Fig.2. Continuous casting facility – print-screen of the industrial process management system

This was implemented under the FDS industrial cracks prediction and elimination adaptive system to eliminate slipping between semi finished-drawing rollers (FAS). Conditions in which attempts were made were very strict, with minimum disruption process and assistance of specialized hardware.

Implementing solutions within the industrial plant consisted mainly in the following:

Two plates full development were purchased, including related software.

A. On one plate we implemented ADF cracks prediction and elimination system, and on the other plate the adaptive system to eliminate slipping (FAS). Since the software implementation is performed in C-language, related programs were designed.

B. Specialists have introduced these systems in driving continuous casting process.

C. Technological parameters were performed during the casting: up to 1042 o'clock, cooling water flow was very high, the casting speed reached its average values, temperature distributor was high, the technological risk was high, and FDS considered a risk of cracks large enough; when we did a very small correction of cooling water flow rate and a large correction of the casting speed, which is 1.6 m/min. At 1043 o'clock, the distributor temperature was lower and become small. FDS noticed a decrease in the risk of a rupture, dictating a low speed correction, fig.3. Accordingly, the casting speed increased to 2 m/min. Following the rules, the first situation corresponds to rule 207, and the second to rule 205. From fig.3, recorded directly from the process, we conclude that FDS interpreted correctly the situations encountered and dictate related remedies.

D. To check the operation of the FAS, there were also a series of tests. Its implementation was carried out by specialists of the beneficiary, in accordance with their internal rules.

All the records presented were taken directly from the production control system. Implementation agreement with the FDS and the FAS has been very difficult, since this is private property multifunction with a continuous casting line in current production. This agreement was achieved and supported by business professionals of the company because research conducted by them was considered very interesting and useful, but they wanted a confirmation of their practice.

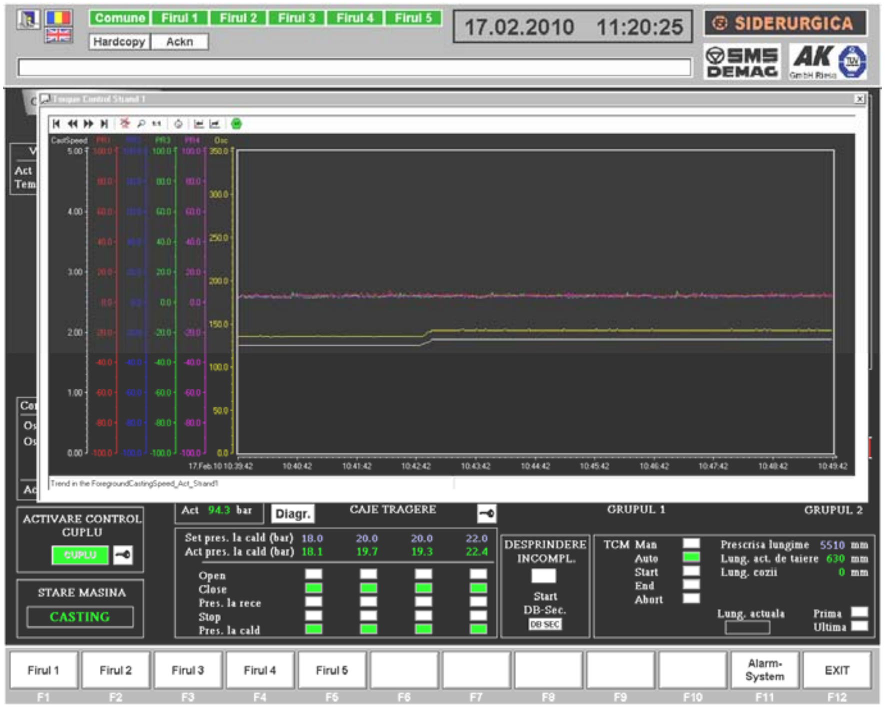

Fig.3. Evolution of casting speed to decrease the risk of a rupture

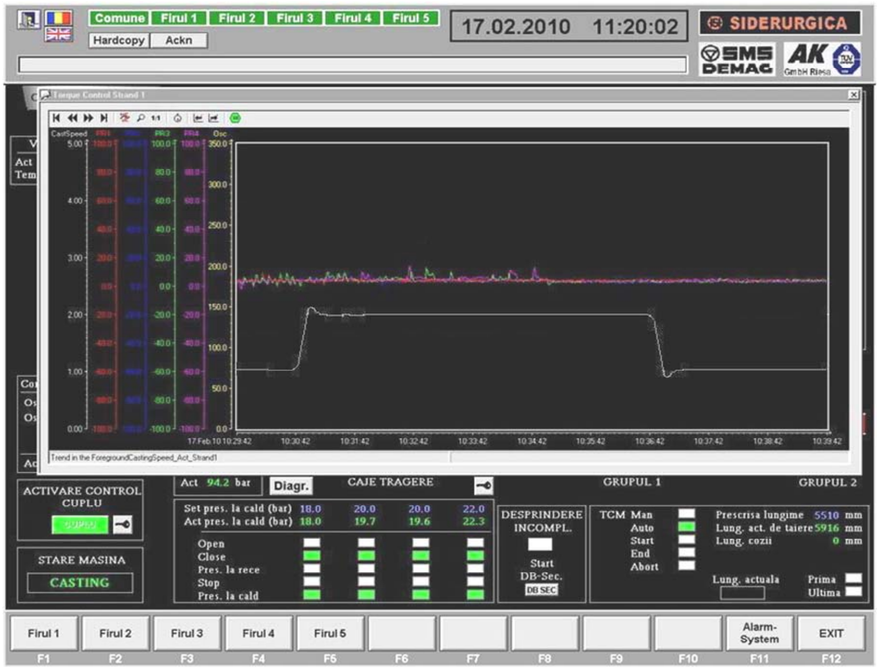

Fig.4. Variation of active wheel speed without FAS action

Initially, the FAS was no longer used. At 1030 o'clock, it required an increase in casting speed from 1-2 m/min. In fig.4 we see that there is an increase in active roll (with a small override for growth approximately 8 seconds). Because of this fast growth there is a slip between the roll and the cast material. Passive wheel speed changes as in fig.5, and lasts for 48 seconds, which is very much. At 1036 o'clock, the phenomena repeated in reverse order (we ordered a decreasing of the speed drawing). It was confirmed that in case slipping occurs more often the effective time of casting speed change.

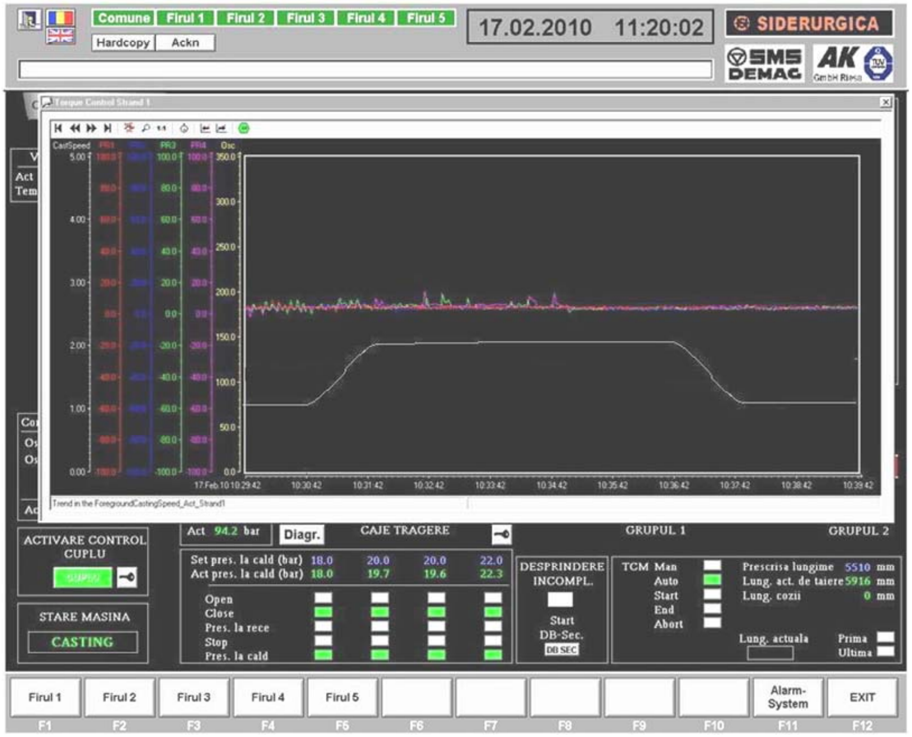

Fig.5. Variation of passive wheel speed without FAS action

Next, we put API into service. At 1041 o'clock we ordered to increase again the speed of 1-2 m/min, fig.6. Note that now the active drawing roller speed varies slowly (rise time approximately 18 seconds) and bar cast speed increase without sliding fig.7 in 18 seconds. In conclusion it appears that FAS acted under rule base.

Fig.6. Active wheel speed variation when FAS is in running

Fig.7. Variation passive roller speed when FAS is in running

3. CONCLUSIONS

We implemented an industrial FDS for crack prediction and elimination adaptive system to eliminate slipping semi-finished - roller drawing (FAS). Following implementation of the FDS and the FAS industry have achieved very good results, which led both to eliminate cracks and to eliminate slipping semi-finished - drawing roll.

REFERENCES

[1.] J. Adamy - *Device for Early Detection of run-out in continuous casting*, United States Patent, No.5, 904.202, Date of Patent May 18 (1999).

[2.] C. Avila, Y. Tsuji - *Crack width prediction of RC structures by Artificial Neural Networks, Adaptive and Natural Computing Algorithms*, Springer Vienna, pg.92-95, 12.dec. (2005).

[3.] S. Bouhouche, et. all - *Quality Monitoring Using Principal Component Analysis and Fuzzy Logic. Application in Continuous Casting Process*, American Journal of Applied Science (AJAS), 4 (9), ISSN: 1546-9239, 2007, pp.637-644.

[4.] T. Nakamura, K. Kazuho - *Breakout Prediction System in the continuous casting process*, the United States Patent, No.5, 548.520, Date of Patent Aug. 20 (1996). 5. F.P. Pleschiutschnugg - Method and apparatus for the early recognition of ruptures in the continuous casting of steel a year with Oscillating Mold, United States Patent, No. US 6,179,041 B1 Date of Patent Jan. 30 (2001).

[5.] G.O. Tirian - *Neural system for detecting cracks in the wire of the continuous casting*, 12th International Research/Expert Conference, Trends in the Development of Machinery and Associated Technology, pp 649-652 Istanbul, Turkey, August 2008.

[6.] G.O. Tirian, S. Anghel S., M. Pănoiu, C. Pinca-Bretotean - *Control of the Continuous Casting Process Using Neural Networks*, Proceedings of the 13th WSEAS International. Conference on Computers, Rhodes Island, Greece, July 23-25, ISSN :1790-5109, ISBN :978-960-474, 099-4, 2009, pp.199-204.

[7.] G.O. Tirian, O. Prostean, S. Anghel, Pinca B. C, D.Cristea - *Fuzzy Control System for Implementing the cracks During the continuous casting*, Annals of DAAAM & Proceedings of the 20th International Symposium DAAAM, Volume 20, No.1, ISSN 1726-9679, ISBN 978-3-901509-70-4, pp 1661-1662, 25-28th November 2009, Vienna, Austria.

[8.] G.O Tirian, G. Prostean, S. Rusu-Anghel, D. Cristea et. all - *Adaptive control system of continuous casting process based on the fuzzy logic mechanism* - IEEE International Joint Conferences on Computational Cybernetics, ICCC and Technical Informatics CONTI 2010, May 27-29, Timisoara, ISBN: 978-1-4244-7431-8, pp.379-382, 2010.

INTERNATIONAL SYMPOSIUM on
ADVANCED ENGINEERING & APPLIED MANAGEMENT
– 40th ANNIVERSARY in HIGHER EDUCATION (1970-2010)
4 – 5 November, 2010, Hunedoara, ROMANIA

[1.] Adrian DANILA

THE DYNAMIC MODEL OF THE CAPACITOR-RUN TWO-PHASE INDUCTION MOTOR - A VARIATIONAL APPROACH

[1.] TRANSYLVANIA UNIVERSITY OF BRASOV, ROMANIA

ABSTRACT:
The dynamic models of the three-phase electric machines are obtained within the classical approach with the direct- and quadrature-axis theory via two transformations of the dynamic set of equations, i.e. the Park and Clarke transformations. Several assumptions such as no magnetic saturation, no space-harmonics are used for simplification purposes. The variational method also called the Euler-Lagrange method is another approach for modeling the dynamic behaviour of the electric machines that relates to the physical energy of the drive. The Euler-Lagrange models are more suitable than the two-axis theory models when magnetic saturation or/and space harmonics are to be taken into account. In this paper, an analysis of the coarse start-up of a capacitor-run two-phase induction motor based on the variational approach is presented. The core of this approach is the Lagrangian of the system i.e. a real function describing the dynamic behaviour of the system, [1], [2]. The basics of this approach and its main characteristics are discussed into the first chapter. In the second chapter of the paper an expression for the Lagrangian for the capacitor-run two-phase induction motor is introduced. In the third chapter, the evolution with time of the values of the Lagrangian's components is detailed. The discussion is based on a set of experimental data and a dedicated software application. The results of the analysis show that the variation approach may provide not only basic information such as the values of the induced currents, but can also give additional information about the stability of the drive. The conclusions and further developments are presented in the last chapter of the paper.
KEYWORDS:
three-phase electric machines, variation approach

1. INTRODUCTION

The dynamic models of systems are representations such as functions, sets of differential equations and so that allow estimations on the outputs based on input measurements. There are two basic ways to determine the dynamic models of a given system (1) either using explanatory theories or (2) with input and output measurements and system identification algorithms.

In the basic approach, the dynamic models of the electric drives are obtained with the direct and quadrature-axis theory tailored to the specific class of the electric machine and power converter. The implementation of the direct and quadrature-axis theory provide models that allow estimating system's response in the time domain, [3]. The estimate's consistency is affected by the accuracy of the measurements and the consistency of the parameters' estimates. With the space vector definition, the time domain model of the machine may be transformed into the complex representation. The complex representation of the electric machine model provides the easiest way to transform the dynamic model from one reference coordinate system to another. In addition, in the complex representation the command of the three-phase inverters can be handled in the most appropriate manner.

With the notations generally accepted in the literature, index 1 for the stator and index 2 for the rotor, the dynamic set of equations in complex representation is as follows, [3].

$$\underline{u}_1 = R_1 \cdot \underline{i}_1 + \frac{d\underline{\Psi}_1}{dt} \text{ voltage equation – stator,} \tag{1}$$

$$0 = R_2 \cdot \underline{i}_2 + \frac{d\underline{\Psi}_2}{dt} + j \cdot \underline{\Psi}_2 \cdot \frac{d\gamma}{dt} \text{ voltage equation – rotor,} \tag{2}$$

$$\underline{\Psi}_1 = L_1 \cdot \underline{i}_1 + L_h \cdot \underline{i}_2 \quad \text{flux linkages equation – stator,} \tag{3}$$

$$\underline{\Psi}_2 = L_1 \cdot \underline{i}_1 + L_h \cdot \underline{i}_2 \quad \text{flux linkages equation – rotor,} \tag{4}$$

$$M_{el} = \frac{3}{2} \cdot p \cdot \mathrm{Im}\left(\underline{\Psi}_2 \cdot \underline{i}_2^*\right) = \frac{J}{p} \cdot \frac{d\gamma}{dt} + M_W \qquad \text{torque equation.} \tag{5}$$

Another approach issued from the quantum electro-dynamic theory relates to the Lagrangian function of the system represented as a function of two sets of generalized coordinates [1] as follows.

- the first is a set of complex numbers $q^c = \left(q_1, \ldots q_{2 \cdot n^c}\right)$ with $2 \cdot n^c = \overline{0,n}$ and (6)

- the second, a set of real numbers $q^r = \left(q_{2 \cdot n^c}, \ldots q_n\right)$ with $n^r = n - n^c$. (7)

The Lagrangian is a real-value and analytic function of complex variables, $\mathsf{L}\left(q^c, q^{c*}, q^r, \dot{q}^c, \dot{q}^{c*}, \dot{q}^r\right)$ related to the dynamic set of equations by the Euler-Lagrange equations on the following form.

$$\frac{d}{dt}\left(\frac{\partial \mathsf{L}}{\partial t}\right) = \frac{\partial \mathsf{L}}{\partial q_k} + S_k \,, \; k = \overline{0,n} \tag{8}$$

where the S_k -terms correspond to the non-conservative energy exchanges with the environment.

For the electrical drives, the dynamic set of equations, in variational form is as follows, [2].

$$\frac{d}{dt}\left(\frac{\partial \mathsf{L}}{\partial \dot{\gamma}}\right) - \frac{\partial \mathsf{L}}{\partial \gamma} = -M_W \qquad \text{torque equation,} \tag{9}$$

$$2 \cdot \frac{d}{dt}\left(\frac{\partial \mathsf{L}}{\partial \underline{i}_1^*}\right) - \frac{\partial \mathsf{L}}{\partial \underline{i}_1} = \underline{u}_1 - R_1 \cdot \underline{i}_1 \qquad \text{voltage equation - stator} \tag{10}$$

$$2 \cdot \frac{d}{dt}\left(\frac{\partial \mathsf{L}}{\partial \underline{i}_2^*}\right) - \frac{\partial \mathsf{L}}{\partial \underline{i}_2} = -R_2 \cdot \underline{i}_2 \qquad \text{voltage equation - rotor} \tag{11}$$

2. METHODOLOGY

The stator of the capacitor-run, two-phase induction machine has two distributed windings, the main and the auxiliary windings. The axes of these windings are located at 90 electrical degrees with respect to the air gap of the machine. The numbers of turns of these windings usually differ. The main winding is supplied directly from the grid whereas the auxiliary winding is supplied through a capacitor from the grid to produce the quadrature current component.

The rotor is symmetrical and similar to the rotor of the squirrel-cage three-phase induction machine. Due to these features, the stator produces an elliptic magnetic motion field into the air gap, [4].

The dynamic set of equations in complex representation with the stator asymmetry taken into account will be as follows.

$$\underline{u}_{S1} = R_{1m} \cdot \underline{i}_{S1} + \frac{d\underline{\Psi}_{S1}}{dt} - R_{1a} \cdot \underline{i}_{S1}^* \qquad \text{voltage equation – stator} \tag{12}$$

$$0 = R_2 \cdot \underline{i}_{R1} + \frac{d\underline{\Psi}_{R1}}{dt} + j \cdot \underline{\Psi}_{R1} \cdot \frac{d\gamma}{dt} \qquad \text{voltage equation - rotor} \tag{13}$$

$$\underline{\Psi}_{S1} = L_{hm} \cdot \left(1 + \sigma_1\right) \cdot \underline{i}_{S1} + L_{hm} \cdot \underline{i}_{R1} - L_{ha} \cdot \underline{i}_{S1}^* - L_{ha} \cdot \underline{i}_{R1}'^* \quad \text{flux linkage equation - stator} \tag{14}$$

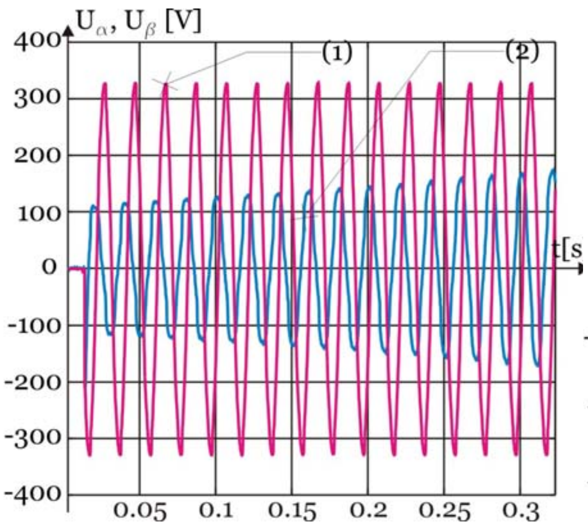

Figure 1: the input supply voltages at the motor terminals; (1) – the main winding supply voltage and (2) – the auxiliary winding supply voltage.

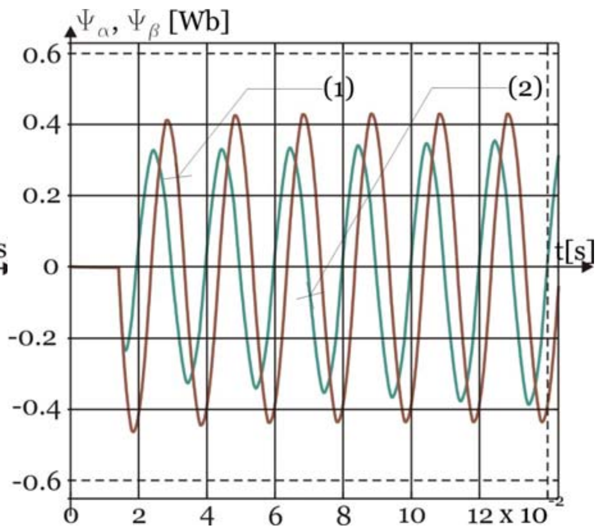

Figure 2: the components of the flux linkages within the air gap; (1) – the direct component and (2) – the quadrature component.

$$\underline{\Psi}'_{R1} = L_{hm}\cdot\left(1+\sigma_2\right)\cdot \underline{i}'_{R1} + L_{hm}\cdot \underline{i}_{S1} - L_{ha}\cdot \underline{i}^*_{S1} - L_{ha}\cdot \underline{i}^*_{R1}$$ flux linkage equation - rotor (15)

$$M_{el} = p\cdot \mathrm{Im}\left(L_{hm}\cdot \underline{i}_{S1}\cdot \underline{i}^*_{R1} - L_{ha}\cdot \underline{i}^*_{S1}\cdot \underline{i}^*_{R1} - L_{ha}\cdot\left(\underline{i}^*_{R1}\right)^2\right)$$ torque equation (16)

The magnetizing inductances over the two axes of magnetic asymmetry of the stator are given by the following expressions.

$$L_{hm} = \frac{L_{h\alpha}+L_{h\beta}}{2}\text{ , and } L_{ha} = \frac{L_{h\alpha}-L_{h\beta}}{2}\text{ respectively.} \tag{17}$$

We introduce the Lagrangian of the run-capacitor induction machine as follows.

$$\begin{aligned}&\mathrm{L}\left(\gamma,\dot{\gamma},\underline{i}_{R2},\underline{i}^*_{R2},\underline{i}_{S1},\underline{i}^*_{S1}\right) = \mathrm{L}_{mec} + \mathrm{L}_{mag}\\ &= \frac{J}{2}\cdot\dot{\gamma}^2 + \frac{L_{hm}}{2}\cdot\left|\underline{i}_{S1}+\underline{i}_{R2}\cdot e^{j\cdot\gamma}\right|^2 - \frac{1}{4}\cdot L_{ha}\cdot\left[\left(\underline{i}_{S1}+\underline{i}_{R2}\cdot e^{j\cdot\gamma}\right)^2 + \left(\underline{i}^*_{S1}+\underline{i}^*_{R2}\cdot e^{-j\cdot\gamma}\right)^2\right]+\\ &+\frac{L_{\sigma1}}{2}\cdot\left|\underline{i}_{S1}\right|^2 + \frac{L_{\sigma1}}{2}\cdot\left|\underline{i}_{R2}\right|^2\end{aligned} \tag{18}$$

With the magnetic fluxes given by the expressions:

$$\underline{\Psi}_{S1} = 2\cdot\frac{\partial L}{\partial \underline{i}^*_{S1}} \tag{19}$$

$$\underline{\Psi}_{R1} = 2\cdot\frac{\partial L}{\partial \underline{i}^*_{R1}}. \tag{20}$$

As seen from the notation (18), the magnetic Lagrangian has four components. An evaluation of the variation of these components at the coarse start-up of the capacitor-run induction machine is subsequently analysed.

3. DISSCUSIONS/RESULTS/ANALYSES

The motor under the investigation was of MSP311 type. The nominal parameters of the motor are given in Table 1.

Table 1: The Nominal Parameters of the MSP311 Motor

Denomination	Rated supply voltage	Rated frequency	Rated angular speed	Number of pair poles	Capacitance
Units	[V]	[Hz]	[rpm]	[-]	[μF]
Value	220	50	2820/420	1/6	14

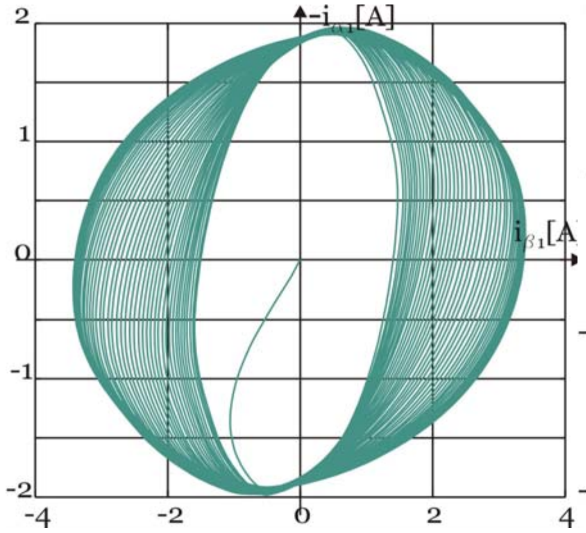

Figure 3: The space vector of the stator currents at coarse, no-load start-up.

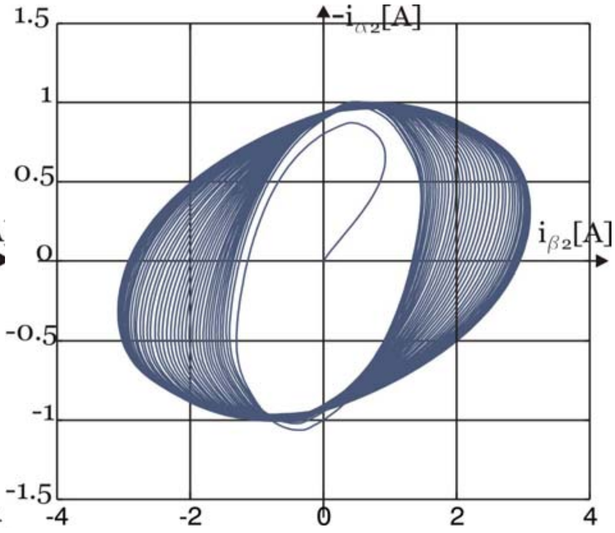

Figure 4: the estimated space vector of the rotor currents at coarse, no-load start-up.

The electrical and magnetic parameters of the motor had been earlier determined by direct measurements for the stator windings or had been computed through the FEM method for inductances, [5]. The results are presented in Table 2.

Table 2. The Electrical and Mechanical Parameters of the MSP311 Motor

Denomination	Stator resistance d/q axis	Stator self-in-ductance d/q axis	Mutual inductance d/q axis	Rotor resistance	Rotor self-in-ductance
Units	[Ω]	[H]	[H]	[Ω]	[H]
Value	20,8/57,5	0,358/0,665	0,275/0,504	17,0	0,523

The values were defined as follows.

- excitation values: $\underline{u}_{S1}$, M_W
- state values: $\underline{\Psi}_{S1}$, $\underline{\Psi}_{R1}$, ω

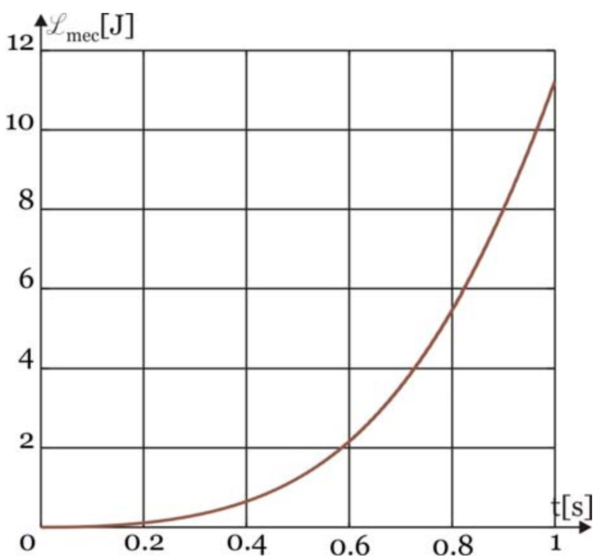

Figure 5: the mechanical component of the Lagrangian at coarse start-up.

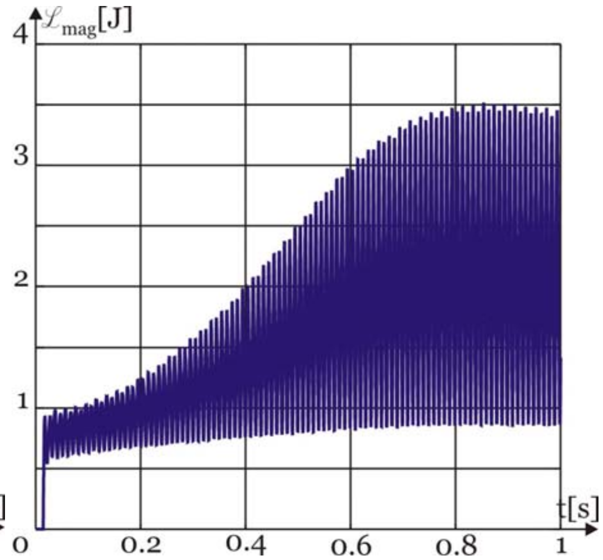

Figure 6: the magnetic Lagrangian at coarse start-up.

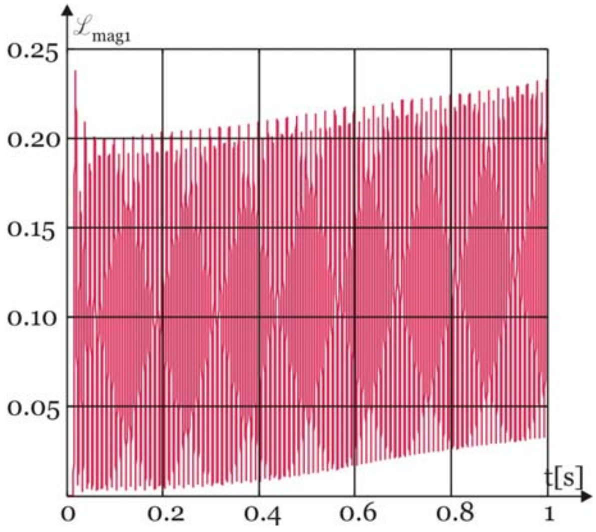

Figure 7: the symmetrical magnetizing component of the Lagrangian at coarse start-up.

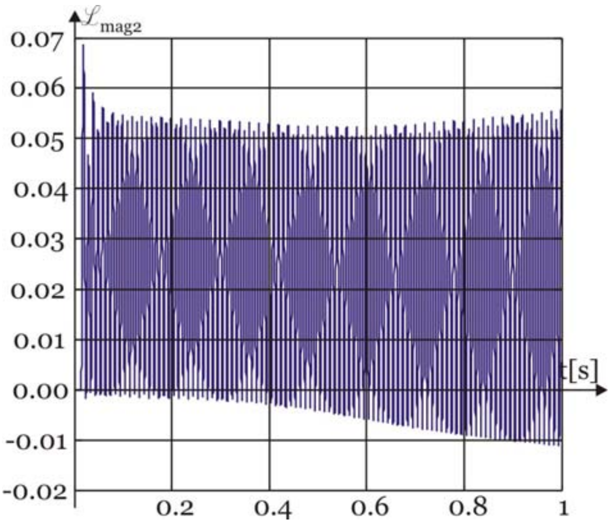

Figure 8: the asymmetrical magnetizing component of the Lagrangian at coarse start-up.

The supply voltage components were acquired on a dedicated test-band with a computer-aided measurement system. The state values and the Lagrangian were determinate through a dedicated Matlab application. The dynamic model used to estimate the rotor currents and fluxes was the flux model of the machine issued from the equations set (1) to (5).

The supply voltages dependencies with time and the components of the flux linkages within the air gap of the machine are presented in Figure 1 and Figure 2.

The space vectors of the stator and rotor currents are presented in Figures 3 and 4, respectively.

As shown in Figure 1, the auxiliary voltage increased to the steady state magnitude with a time constant of about 0.6 seconds. The magnetic motion field (mmf) into the air gap of the machine was highly elliptic during the start-up. In the steady-state operation the mmf became almost circular, Figures 3 and 4. However, in direct operation of the machine, the shape of the mmf is dependent on the load. Therefore, in direct operation, the efficiency of the machine cannot be optimized. To optimize the efficiency, an electronically controlled voltage supply must be added to the drive.

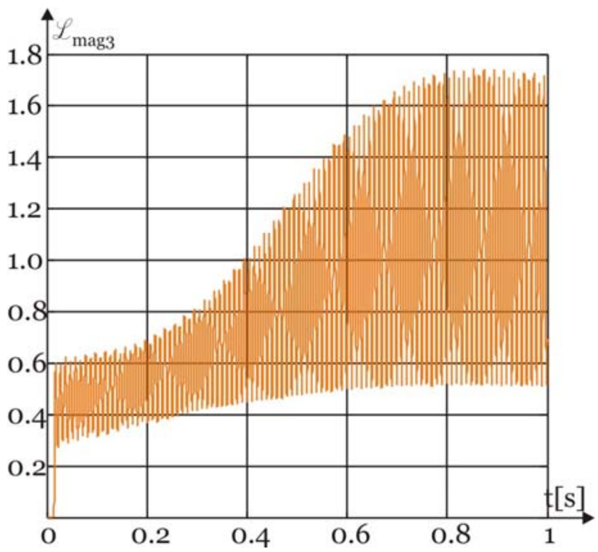

Figure 9: the symmetrical leakage magnetic component of the Lagrangian at coarse start-up

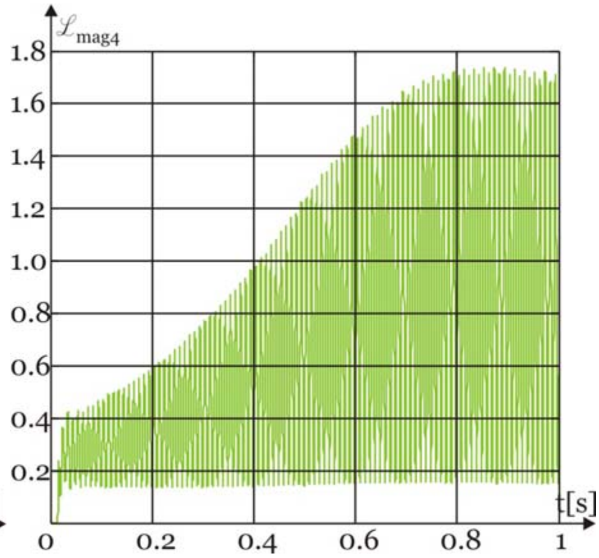

Figure 10: the asymmetrical leakage magnetic component of the Lagrangian at coarse start-up

In figures 5 and 6 the mechanical and the magnetic components of the Lagrangian are depicted. The mechanical Lagrangian represents the kinetic energy of the drive. The experiment was performed at no-load operation of the drive therefore the angular speed increased proportional with time. The magnetic Lagrangian takes into account the total amount of the magnetic energy into the machine. As seen from the plot, at the beginning of the process the magnetic circuitry of the machine was not magnetized. Therefore the start-up took some time until reaching the steady-state operation. This phenomenon is similar with the coarse start-up of the DC-shunt machine. The components of the magnetic Lagrangian are presented in Figures 7 to 10. As seen from the plots, the magnitude of the magnetizing components of the Lagrangian both symmetrical and asymmetrical parts are almost unchanged during the start-up process. However, the two magnitudes of the leakage components of the Lagrangian increase during the process. The maximum magnitude is achieved near the synchronous angular speed before the steady-state regime of the drive. In addition, the leakage components of the Lagrangian are much greater in comparison with the previous two components of the Lagrangian.

4. CONCLUSIONS/FURTHER PROPOSALS

In this paper, the variation of the Lagrangian of a capacitor-run two-phase induction motor during the coarse start-up of the drive has been investigated. The investigation proved an interesting similarity between the coarse start-up of the capacitor-run two-phase induction motor and the coarse start-up of the DC-shunt machine. As for the DC-shunt machine, the capacitor-run two-phase induction motor is not suitable for fast tracking servo-drives due to its large time constants.

The analysis also proved that the magnetic component of the Lagrangian has four components. The information regarding the dynamics of the start-up is mainly contained into the two leakage components of the Lagrangian. Because the Lagrangian and its components may not be measured through direct transducers, in the on-line applications, a digital signal processor should be used. Further developments consist in the use of the drive's Lagrangian to produce the command law for the drive system.

REFERENCES

[1.] D. Basic, F. Malrait, and P. Rouchon, Euler-Lagrange Models With Complex Currents of Three-Phase Electrical Machines and Observability Issues, IEEE Transactions on Automatic Control, Vol.55, No.1, 2010, pp. 212-217

[2.] I. Boldea and S. A. Nasar, The Induction Machine Handbook, CRC Press, 2002

[3.] G. Henneberger, Electrical Machines II. Dynamic Behavior, Converter Supply and Control, Aachen University, 2002

[4.] S. Bala, Dynamics of Single/Two Phase Induction Motors, University of Wisconsin-Madison, 2004

[5.] A. Danila, I.Margineanu, R. Campeanu, C. Suciu, I. Boian, The Optimization of the Single/Two Phase Induction Motor Start-Up with Electronically Switched Capacitor, 2008 IEEE International Conference on Automation, Quality and Testing, Robotics. Proceedings – Tome III pp 450-454

INTERNATIONAL SYMPOSIUM on
ADVANCED ENGINEERING & APPLIED MANAGEMENT
– 40th ANNIVERSARY in HIGHER EDUCATION (1970-2010)
4 – 5 November, 2010, Hunedoara, ROMANIA

[1] Anca IORDAN, [2] Manuela PĂNOIU, [3] Ionel MUSCALAGIU, [4] Raluca ROB

DESIGN OF AN EDUCATIONAL INFORMATICS SYSTEM FOR THE STUDY OF THE EUCLIDIAN VECTORS USING UML DIAGRAMS

[1-2] TECHNICAL UNIVERSITY OF TIMISOARA, ENGINEERING FACULTY OF HUNEDOARA, ROMANIA

ABSTRACT:
The informative society needs important changes in educational programs. The informational techniques needs a reconsideration of the learning process, of the programs, manuals structures, a reconsideration of the methods and organization forms of the didactic activities, taking into account the computer assisted instruction and self instruction. This paper presents the necessary stages in implementing an informatics system used for the study of euclidian vectors. The modeling of the system is achieved through specific UML diagrams representing the stages of analysis, design and implementation, the system thus being described in a clear and concise manner.
KEYWORDS:
Educational Software, Java, Vector, Distance Education, UML

1. INTRODUCTION

In the condition of informatics society whose principal source in the social–economic development is to produce and consumption the information, the complex and fast knowledge of the reality for rational, opportune, effective decisions is a desideratum which generate the necessity to form some superior level habituation in information manage for the whole population. The computers and their programs offer to the users powerful capabilities for the information manipulation: image and text visualize on the screen which can be manipulate later; memory storage of an important quantity of information, his accessing and selection of a part of them; possibility to realize a great volume of computation; possibility of equipment control and fast decisions; Computer Based Training [1].

This facilities offer to the microcomputers higher educational capabilities versus other technologies used in education and provide learning controlled based on many parameters: intellectual aptitude, level of knowledge, abilities, rhythm of work.

2. COMPUTER BASED TRAINING AS A DIDACTIC METHOD

The informatics society makes sensitive modification in education programs. In this scope, the school must prepare programmers, maintenance technicians, etc. In the same time it is necessary that the teacher make ready to use the computer in education process.

These informational techniques impose to reorganize the contents of the education process, of the programs, course books and manuals, to reconsider the methods and organization forms of didactic activities, which follow to be center on individualization of the teaching process [2].

The programmed teaching consist in information presentation in small units, logic structured, units that compose a program, the teaching program. The user will have possibility that after each sequence to have a knowledge about the measure of understanding the give information. The programmed teaching method organize the didactic action applying the cybernetic principles to the teaching-learning-evaluating activities level, considering like a complex and dynamic system, composed as an elements ensemble and inter-relations and develop his personal principles valid on the strategic level in any cybernetic organization form of teaching.

On the other hand, programmed teaching assumes some principles which the teaching program must respect [3]:

- The small steps principle consists in progressive penetration, from simple to complex, in a subject content which logic divided in simple units series lead to minimal knowledge, which later will form an ensemble. This principle regards the subject division in contents/information units that give to user the chance to succeed in his teaching activities;
- The principle of personal rhythm of study regard mannerism observance and capitalization of each user of the program which will be able to make the sequences of knowledge learning or control, in a personal rhythm appropriate to his psycho-intellectual development, without time limits. The user can progress in the program only if he accomplished the respective sequence requirement;
- The active participation principle, or active behavior, regard user effort trend into selection, understanding and applying the necessary information in elaboration of a correct answer. On each step the user is liable to an active participation to resolve the step job;
- The principle of inverse connection, regard positive or negative inputs of user competence, refer to the success or breakdown in task performed;
- The immediate and directly control of the task work precision with the possibility to progression to the next sequence, in case of success;
- The repetition principle, based to the fact that the programs are based on return to the users initial knowledge.

The combined programming interposes the linear and branch sequence according to teaching necessities.

After linear and branch programming the computer aided generative teaching has appear, where the exercises are gradually present, with different difficulty steps and answers on the students questions.

The expert system consists of self-teaching training programs, tutorial strategies, and the usage of natural language, mixed initiative and some complex representation of knowledge usage [4]. The computer based programmed teaching realize learning process with a inputs flow – the command, an executive controlled system, an output flux – control and a control system functions which correct measure establish.

In such a system have tree stages of teacher perceive: teaching, evaluating and the feedback loop closing, the computer being present in all of tree stages.

3. UML

Unified Modeling Language (UML) is a standardized general-purpose modeling language in the field of software engineering [5]. UML includes a set of graphical notation techniques to create abstract models of specific systems.

The Unified Modeling Language (UML) is an open method used to specify, visualize, construct and document the artifacts of an object-oriented software-intensive system under development. UML offers a standard way to write a system's blueprints, including conceptual components such as: actors, business processes, system's components and activities, as well as concrete things such as: programming language statements, database schemas and reusable software components.

UML combines the best practice from data modeling concepts such as entity relationship diagrams, business modeling (work flow), object modeling and component modeling. It can be used with all processes, throughout the software development life cycle, and across different implementation technologies. UML has succeeded the concepts of the Booch method, the Object-modeling technique (OMT) and Object-oriented software engineering (OOSE) by fusing them into a single, common and widely usable modeling language. It is very important to distinguish between the UML model and the set of diagrams of a system. A diagram is a partial graphical representation of a system's model. The model also contains a "semantic backplane" — documentation such as written use cases that drive the model elements and diagrams.

UML diagrams represent two different views of a system model [6]:

- Static view: Emphasizes the static structure of the system using objects, attributes, operations and relationships. The structural view includes class diagrams and composite structure diagrams.
- Dynamic view: Emphasizes the dynamic behavior of the system by showing collaborations among objects and changes to the internal states of objects. This view includes sequence diagrams, activity diagrams and state machine diagrams.

UML models can be exchanged among UML tools by using the XMI interchange format.

4. DEVELOPMENT STAGES OF THE EDUCATIONAL INFORMATICS SYSTEM

4.1. System's analysis

Using the UML modeling language, the analysis of an informatics system consists in drawing the use case and activity diagrams [7]. The software utility ArgoUML [8] was used to construct the diagrams.

The informatics system will be described in a clear and concise manner by representation of the use-cases. Each case describes the interaction between the user and the system. The use case diagram is represented in figure 1.

The presented diagram defines the system's domain, allowing visualization of the size and scope of the whole developing process. It contains:

- an actor - the user who represents the external entity with which the system interacts;
- six use cases describing the functionality of the system;
- relationships between the user and use cases (association relationships) and the relationships between use cases (generalization relationships).

For each use-case in the diagram presented earlier an activity diagram is constructed. Each diagram will specify the processes and algorithms that are behind the use cases studied. Activity diagrams [9] are represented by nodes (with partitions and branches) or conditional blocks (with decisions). The activity diagrams are used to visualize, specify, build and document dynamic issues related to the informatics system processes. They focus on flow control seeking the transition, in a certain order, from one activity to another.

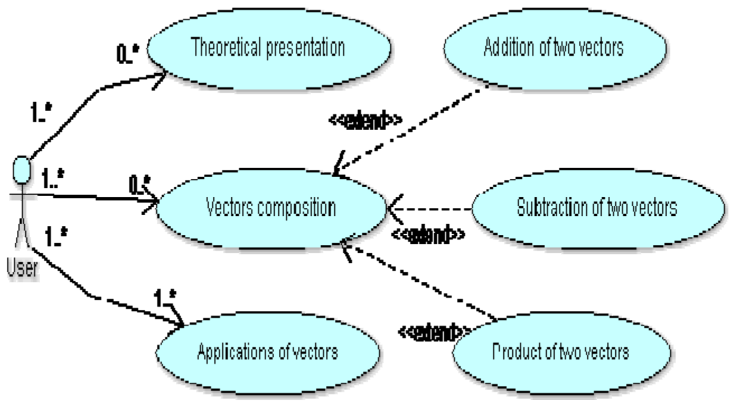

Figure 1 Use-cases Diagram

4.2. System's designing

Conceptual modeling [10] allows the identification of the most important concepts for the system. Since classes are concepts, the following two diagrams present the classes that will be used in the project.

Figure 2 presents the inheritance and achievement relationships used. It may be noted that all attributes and methods of the *Applet* class will apply to the derived class *Forta*, which implements two interfaces, *Runnable* and *ActionListener*.

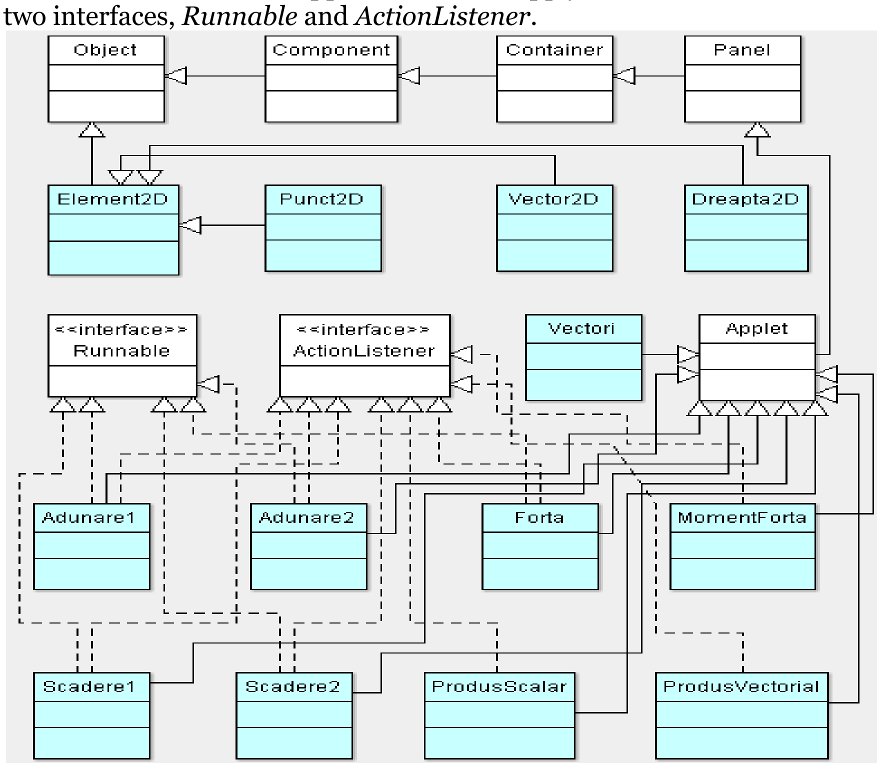

Figure 2 Class Diagram: the inheritance and achievement relationships

The composition relationships that exist between instances of the classes in the architecture are shown in figure 3. The difference of the composition relationship, with respect to aggregation, is that the instance of the whole could not exist without part objects. When looking at figure 3 one can see that a type *Vectori* instance consists of two *Punct2D* type items, one *Vector2D* object type, one *Dreapta2D* object type, five *JButton* object type and five *JTextField* object type. In such a relationship it is possible for an object to belong to several instances of a whole. For example object type *Vector2D* belongs to *Vectori, Adunare1, Adunare2, Scadere1, Scadere2, ProdusScalar, ProdusVectorial, MomentForta* and *Forta* type instances.

Both class diagrams shown contain specific classes to the application as well as existing classes and interfaces from Java.

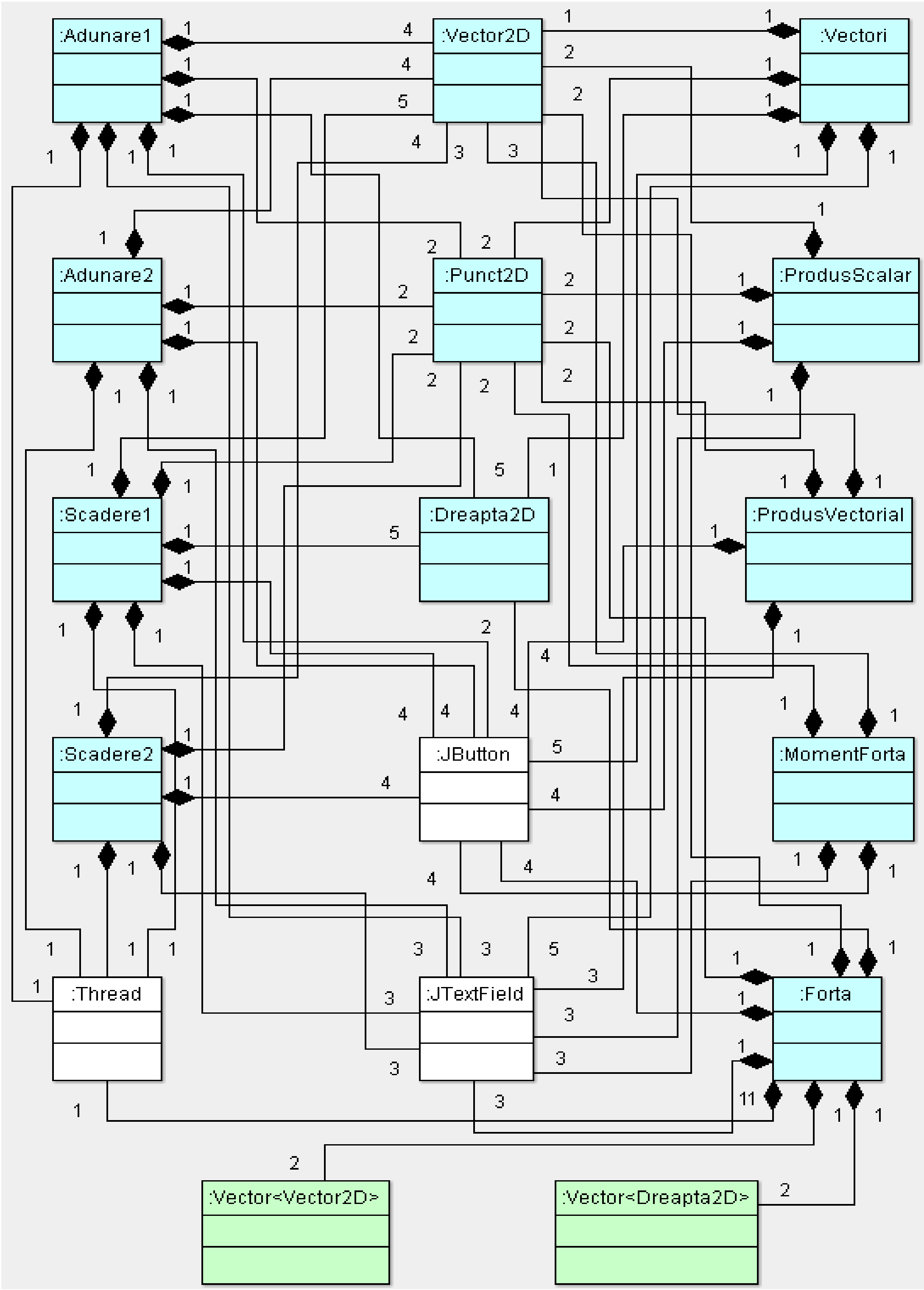

Figure 3 Class Diagram: The composition relationships

4.3. System's implementation

The component diagram [11] allows the visualization of the module in which the system is broken into and the dependencies between modules. The component diagram emphasis on physical software components (files, libraries, executables) and not on logic components, such as packages.

The diagram in figure 4 describes the collection of components that all together provide functionality for the educational informatics system.

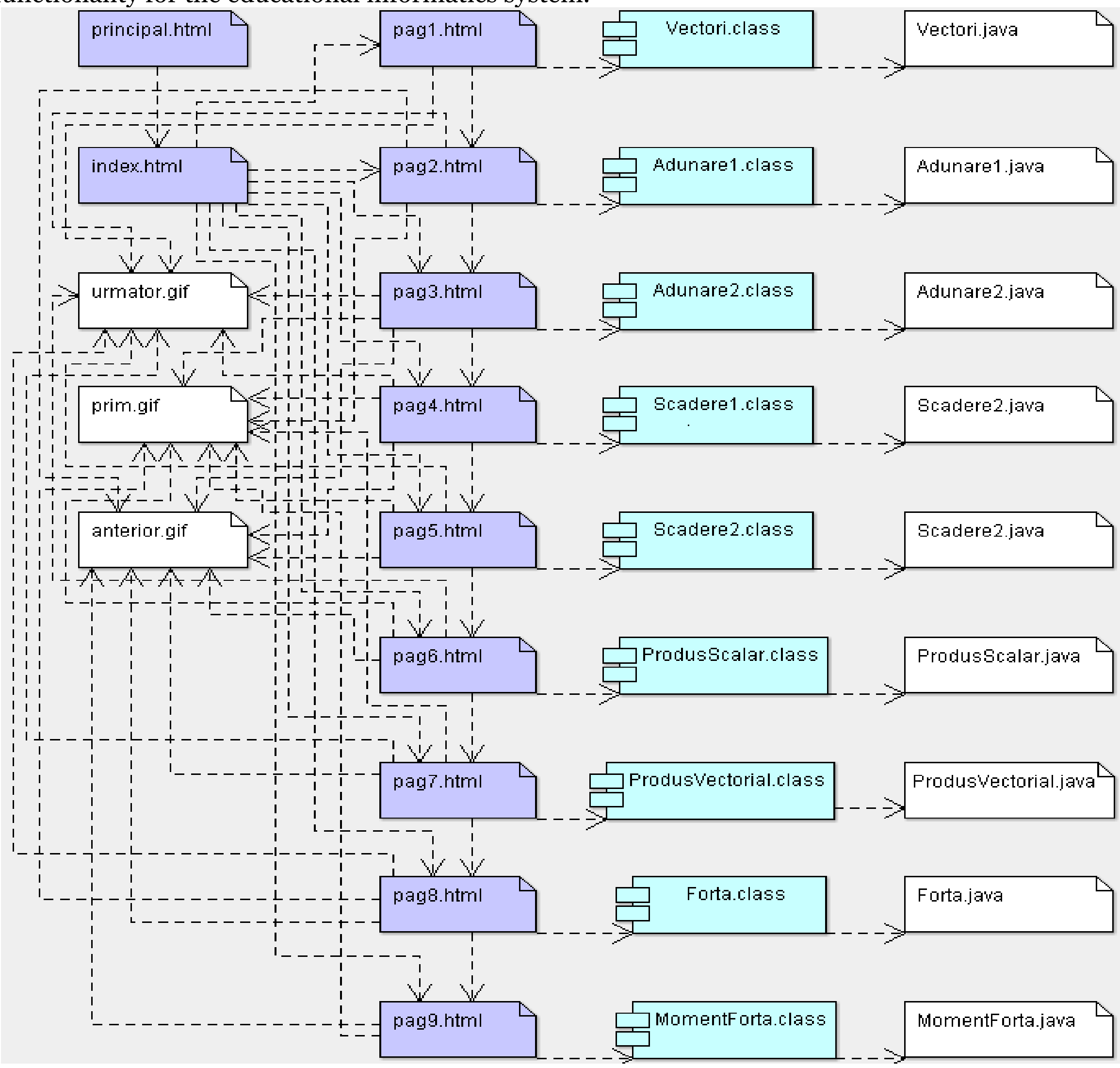

Figure 4 Component Diagram

5. USER INTERFACE

The educational informatics system is accomplished using the Java programming language [12]. The main page of the application contains buttons for selecting the following options: addition of two vectors using the parallelogram rule and the triangle rule (figure 5), subtraction of two vectors using the parallelogram rule and the triangle rule (figure 6), scalar product of two vectors, cross product of two vectors, total forces what reacts on a material point (figure 7) and force momentum in rapport with a point. The method of the class *Adunare2* which draw the addition of two vectors is presented forwards:

```
public void run() {  pas=3;
    for (int k=9;k>=0;k--) {double x,y,x1,y1;
    x=k/(double)10*v2.getOrigine().getX()+(1-k/(double)10)*v1.getExtremitate().getX();
    y=k/(double)10*v2.getOrigine().getY()+(1-k/(double)10)*v1.getExtremitate().getY();
    O=new Punct2D(x,y);
    x1=v1.getExtremitate().getX()+(v2.getExtremitate().getX()-v2.getOrigine().getX());
    y1=v1.getExtremitate().getY()+(v2.getExtremitate().getY()-v2.getOrigine().getY());
    x=k/(double)10*v2.getExtremitate().getX()+(1-k/(double)10)*x1;
```

```
y=k/(double)10*v2.getExtremitate().getY()+(1-k/(double)10)*y1;
E=new Punct2D(x,y); O.setId("O2'"); E.setId("E2'"); vaux=new Vector2D(O,E);
repaint(); pause(300); }  pas=4; double x1,y1;
x1=v1.getExtremitate().getX()+(v2.getExtremitate().getX()-v2.getOrigine().getX());
y1=v1.getExtremitate().getY()+(v2.getExtremitate().getY()-v2.getOrigine().getY());
E=new Punct2D(x1,y1); E.setId("E"); suma=new Vector2D(v1.getOrigine(),E);
String s1="O("+String.format("%.1f",suma.getOrigine().getX())+";";
s1+=String.format("%.1f",suma.getOrigine().getY())+")";
s1+="E("+String.format("%.1f",suma.getExtremitate().getX())+";";
s1+=String.format("%.1f",suma.getExtremitate().getY())+")  ";
s1+="p="+String.format("%.1f",suma.get_p());
s1+="q="+String.format("%.1f",suma.get_q());
t3.setText(s1);  repaint(); pause(300); }
```

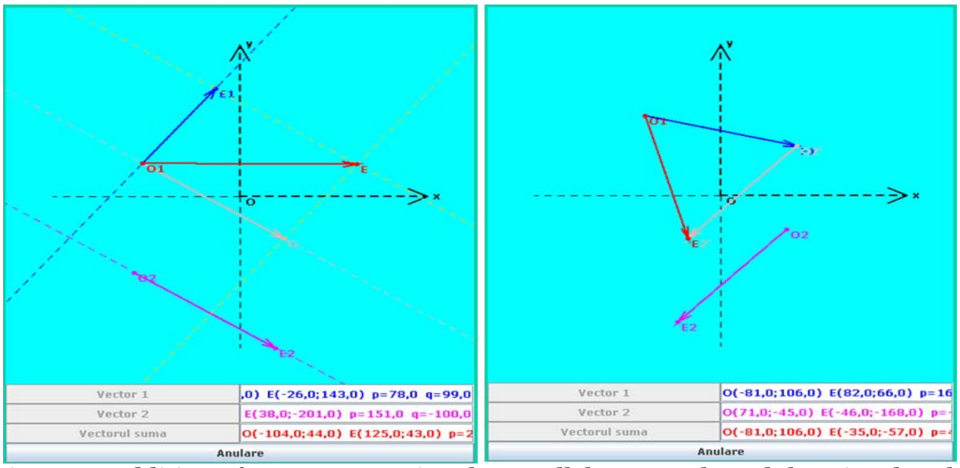

Figure 5. Addition of two vectors using the parallelogram rule and the triangle rule

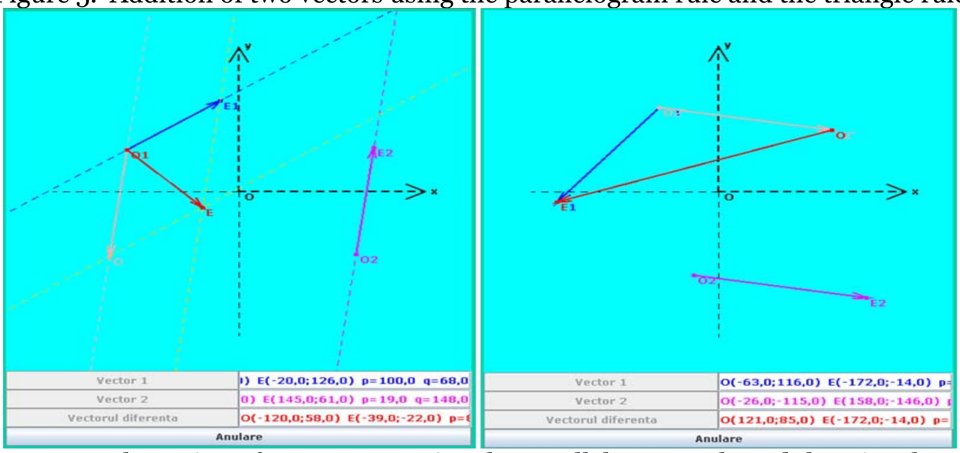

Figure 6. Subtraction of two vectors using the parallelogram rule and the triangle rule

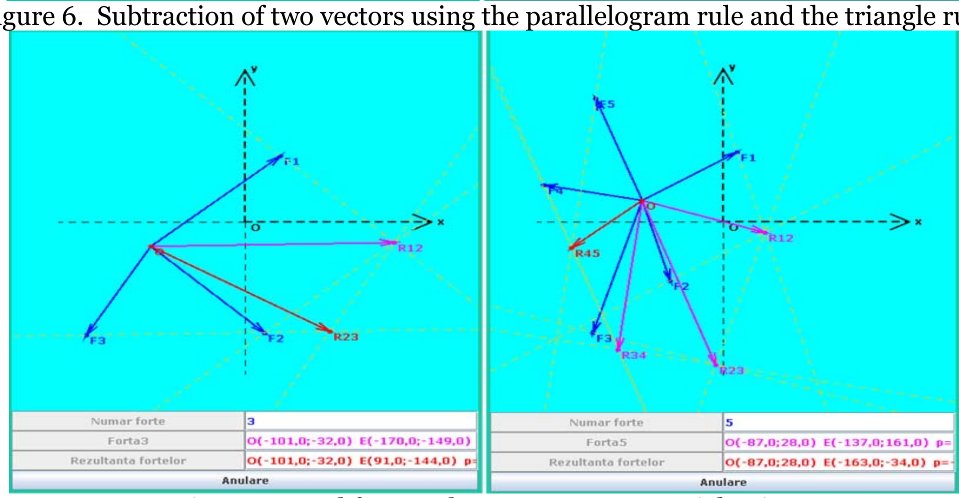

Figure 7. Total forces what reacts on a material point

6. CONCLUSIONS

Through the diagram representation all three phases: analysis, design and implementation, the educational informatics system has been described in a clear and concise manner. The use of the UML modeling language for the creation of the diagrams is characterized by rigorous syntactic, rich semantic and visual modeling support.

The diagrams were made using a new approach, multidisciplinary of the informatics application, encompassing both modern pedagogy methods and discipline-specific components. The link between teaching activities and scientific goals and objectives was established through the development of the new methods and the assimilation of new ways, capable of enhancing school performance, enabling students to acquire the knowledge and techniques required and apply them in optimum conditions.

REFERENCES

[1.] A. Adăscăliţei, *Instruire asistată de calculator. Didactica informatica*, Editura Polirom, 2007
[2.] D. Glusac, D. Radosav, D. Karuovic, D. Ivin, *Pedagogical and Didactic-Methodical Aspects of E-learning*, 6th WSEAS International Conference on E-ACTIVITIES, Tenerife, Spania, 2007, pp. 67-75
[3.] I. Negret-Dobridor, I. Panişoara, *Ştiinţa învăţării. De la teorie la practică*, Editura Polirom, 2005
[4.] I. Nicola, *Tratat de pedagogie şcolară*, Editura Aramis, 2003
[5.] G. Booch, J. Rumbaugh, I. Jacobson, *The Unified Modeling Language User Guide*, Addison Wesley, 1999
[6.] M. Fowler, K. Scott, *UML Distilled: A Brief Guide to the Standard Object Modeling Language*, Addison Wesley, Readings MA, USA, 2000
[7.] D. Bocu, *Iniţiere în modelarea orientată obiect a sistemelor soft utilizând UML*, Editura Albastră, Cluj-Napoca, 2002
[8.] http://argouml.tigris.org
[9.] J. Odell, *Advanced Object Oriented Analysis& Design using UML*, Cambrige University Press, 1998
[10.] J. Rumbaugh, I. Jacobson, G. Booch, *The Unified Modeling Language Reference Manual*, Addison Wesley, 1999
[11.] D. Bocu, *Modelare orientată obiect cu UML*, Editura Albastră, Cluj-Napoca, 2006
[12.] S. Tănasă, C. Olaru, S. Andrei, Java de la 0 la expert, *Polirom Press*, Iasi, 2007

INTERNATIONAL SYMPOSIUM on ADVANCED ENGINEERING & APPLIED MANAGEMENT
– 40th ANNIVERSARY in HIGHER EDUCATION (1970-2010),

INTERNATIONAL SYMPOSIUM on ADVANCED ENGINEERING & APPLIED MANAGEMENT
– 40th ANNIVERSARY in HIGHER EDUCATION (1970-2010),

INTERNATIONAL SYMPOSIUM on
ADVANCED ENGINEERING & APPLIED MANAGEMENT
– 40th ANNIVERSARY in HIGHER EDUCATION (1970-2010)
4 – 5 November, 2010, Hunedoara, ROMANIA

1. Susana ARAD, 2. Marius MARCU, 3. Dragos PASCULESCU, 4. Codrut PETRILEAN

ASPECTS OF THE ELECTRIC ARC FURNACE CONTROL

1-4. UNIVERSITY OF PETROSANI, ROMANIA

ABSTRACT:
Operating mode of electric arc furnace is influenced by a series of disturbances. These perturbations lead to growth of specific energy consumption and decrease in total electric oven We addressed the mathematical modeling of electric arc furnace (EAF) by analysis of related technological processes and the possibility of using simulation software model arc furnace as part of the grid. Mathematical modeling of electric arc furnace related processes (EAF) in order to optimize functional and technological performance of this complex aggregate has the direct positive consequences reducing specific consumption of electricity in steel development with about 15%, simultaneously obtaining a high quality steels electricity produced.

KEYWORDS:
electric arc furnace, energy consumption, modeling, optimize, control

1. INTRODUCTION

Electric arc furnaces (EAFs) are widely used in steelmaking and in smelting of nonferrous metals. Typical EAFs operate at power levels from 10MW to 100MW. The power level is directly related to production throughput, so it is important to control the EAF at the highest possible average power with a low variance to avoid breaker trips under current surge conditions. For efficient power control, good dynamic models of EAFs are required [2]. Melting metal in electric arc furnaces is based on the amount of heat developed in the arc and transmitted by radiation burden. Arc burning between solid electrodes and liquid (molten metal) in an ionized gaseous medium is the presence of an appropriate voltage [1].

Furnaces for steel development are generally three phase AC. Arcs are established between the electrodes and melt, representing oven with a consumer phase Y connection with isolated neutral. The three phase arc, unlike the single phase, has the advantage of load balancing supply network. In the system three- phases with the isolation of neutral, represented by arc furnace, the re-ignition of arc to one of three phase occurs more rapidly than for a single-phase arc, due to increasing pressure on this phase which contributes to increased stability of the arc combustion.

During operation of electric arc furnace, so that the power developed in the arc should have imposed, it is necessary that the distance between electrodes and solid or molten metal bath is kept constant. This distance and arc length is required so the voltage and current in the arc, the temperature and degree of ionization of the melting area.

The power indicators of the arc furnaces depend heavily on the current of arc. The variations are caused by current fluctuation in operating state. The dynamic characteristic V-I depends on the rapid variation of AC, which is not followed closely by voltage, especially at small currents due to thermal persistency of the arc-over which is reflected by different voltage in the same value of the current in arc [3].

2. ELECTRIC ARC FURNACE MODELLING

The notable contribution to EAF modeling was made by Morales et al [7]. An initial contribution was the study of the slag foaming where extensive slag data was collected and analyzed; the practical benefits of slag foaming by reduced electrical consumption and improved yield were reported from continued use a foaming on a plant [8].

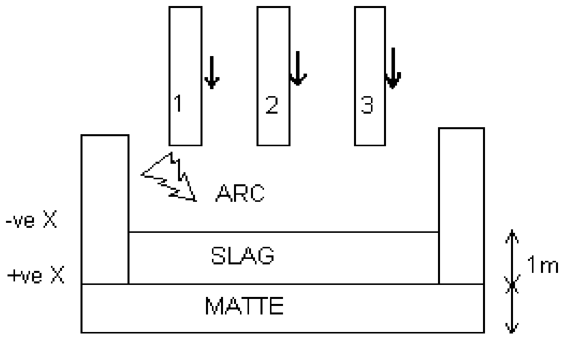

Fig. 1: Physical Model of EAF

Figure 1 shows the physical model of the electric arc furnace. In this particular EAF model, there are three electrodes that are moved vertically up and down with hydraulic actuators. Each of these electrodes has a diameter of roughly 1.5m, weighs approximately 40 tons and is 1 to 2 stories tall. In theory, the ore is melted with a huge power surge from the electrodes. The actual product is denser than the scrap and thus falls to the bottom of the furnace creating the matte. Above the matte lies the slag where the electrode tips are dipped. The tremendous heat created by these electrodes causes the ore to liquefy and separate. Thereupon more raw materials are placed in the furnace and the process repeats itself.

The arc furnace model employs non-linear differential equations1 as opposed to the traditional piecewise linear method resulting in more accurate and realistic simulation.

Arcing is a phenomenon that occurs when the electrodes are moved above the slag. As the electrode approaches the slag, current begins to jump from the electrode to the slag, creating electric arcs. Depending on the magnitude of the input voltages of the electrodes, the arcing distance can vary. Usually, arcing occurs in a region within centimeters of the slag (approximately 10- 15cm). Therefore, the EAF model must take into account the instances when x1, x2, x3 are negative (i.e. the electrodes are suspended above the slag). The factors that affect the arc furnace operation are the melting or refining materials, the electrode position, the electrode arm control scheme and supply system voltage and impedance. Thus, the description of an arc furnace load depends on the following items: arc voltage, arc current and arc length (which is determined by the position of electrode).

In general, the different methods for arc furnace modeling may be classified into the "time domain" and "frequency domain" methods [6]. The electric arc furnace is a highly variable non-linear load, which according to some studies, possesses what is described as a chaotic pattern.

Voltage flicker is a stochastic and time varying phenomenon that causes variation in voltage root mean square in the frequency range (0.5-25 Hz) [6]. To generate the dynamic behavior of the arc furnace using different models, the slop of the V-I curve should be changed as a sinusoidal function. Since the electrical arc is a nonlinear and time varying phenomenon, description of its behavior in the time domain is easier than in the frequency domain. Let "l" be the arc length, A and B are the coefficients from experimental formula, then

$$v_{at} = A + B \cdot l \tag{1}$$

where, v_{at} reflects the arc furnace operating condition.

Time domain methods are the basic methods for flicker study in electrical arc furnaces.

Time domain methods can be classified into V-I Characteristic (VIC), and Equivalent Circuit Methods (ECM) [6]. The arc resistance in the case of sinusoidal variation is defined as: the ECM methods can be obtained from arc operation; the periodic variation of arc voltage and the resistance that arc shows can be used to develop the arc furnace model [1]. Too much simplification in developing the model may affect the accuracy of the model.

The dynamic load models consider periodic change of the arc resistance about the value given for each model. The electric arc furnace model was studied as a part of the electrical network as depicted in Figure 2. In a simulated attempt to reduce voltage flicker, the size of the STATCOM (the converter solution for reliable and stable grids) in the network was varied, while the size of the capacitors and parameters of

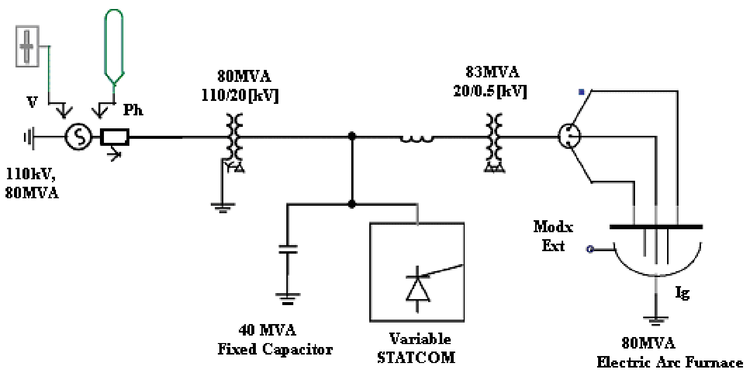

Fig. 2: Electric Arc Furnace System

the arc furnace remained fixed. The function of static compensator provides reactive power compensation to solve industrial system voltage fluctuation.

AC arc furnaces are a major source of grid disturbances. The frequent interruption of the arc leads to strong voltage fluctuations and unbalance between phases too. The converters operate as a 64 MVAr STATCOM on the grid supplying the furnace. It is possible to compensate the unbalanced load with the single phase control of the STATCOM and at the same time, supply the required reactive power to stabilize the grid voltage. In normal operation the mean value of current unbalance without operating converter was 8.6%. With the STATCOMs in operation the unbalance is reduced by a factor of nearly four.

Mathematical modeling of processes related to EAF electric arc furnace in order to optimize functional and technological performance of this complex aggregate was based on the following principles [10]: the analogy, the concepts and principles of hierarchically. According to these principles for developing mathematical models to go through stages:

- ❖ Identify target shape. This step has to satisfy the purpose and objectives of the system, while ensuring their compatibility;
- ❖ Defining criteria of efficiency, it is a correct step conditioned by defining objectives optimization solutions enable system and modeling;
- ❖ Develop options based on accesses of realistic solutions, effective and originals;
- ❖ Assessment of scenarios depending on efficiency criteria established;
- ❖ Fixing the final solution based on comparative analysis of various solutions of modeling.

These require detailed and accurate knowledge of the technological process optimization and implicitly to all installations and components of them and involve the need for develop a hierarchical models system in order to framework of decision and coordination of interactive subsystems shown like in Figure 3.

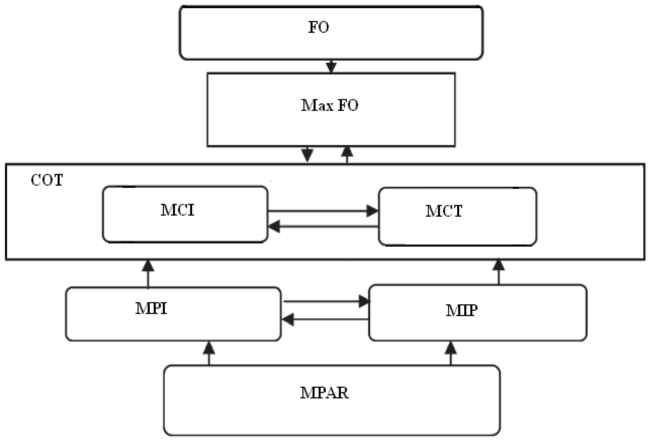

Fig. 3: Sequence algorithm modeling aggregate

Application of specific mathematical models to optimize the operation of arc furnaces, particularly the mathematical model to conduct the effectively melting MCT and the mathematical model of load preheating MPI (including the mathematical model for calculating the design of recovery burners related to preheating MPAR). The main component of furnace processes modeling EAF is the FO aim function of the system. Given the fact that the study related to technological processes EAF is responsible for obtaining high quality steel, the modeling system aim function FO is the quality/cost relation; the responsible model for maximizing the efficiency of the whole system and the aim function is *Max FO*.

Operative management of melting COT is done by mathematical models to calculate the load MCI and the mathematical model to conduct the effectively melting MCT. The modeling of the designed system for technological processes from EAF is composed of subsystems that describe the algorithm of the aggregate modeling. The mathematical model for calculating the design of recovery burners related to preheating MPAR has the positive consequence reducing specific consumption of electricity in steel elaboration with about 15%, simultaneously obtaining a high quality of steels and is directly correlated to MPI.

3. ELECTRIC ARC FURNANCE CONTROL

In order to maintain the arc length constant of the electric arc furnace, a control system for the electrode position according to the arc impedance is used. The automat system must rapidly change the position of the electrodes (1.5 ... 3 seconds) if a disturbance action sets up, therefore the time constants of the system components must be minimized. On three-phases electric furnaces, each electrode has its own control installation [9].

Whatever the electrodes' mode of action in automatic systems is, impedance Z_c is used as a parameter set furnace, Eq. (2), the ratio between the supply voltage $U = k_2 U_a$ (or a proportional size to the arc voltage measured with a voltage transformer or directly at the terminals of the arc) and the arc current $I = k_3 I_a$, (or a proportional size with the arc current measured with a current transformer) [9].

$$Z = k_1 \cdot Z_c = \frac{k_2 \cdot U_a}{k_3 \cdot I_a} \tag{2}$$

For a certain adjusted value of the impedance Z_0 results a deviation ΔU_0 like in Eq (3) and the result of the comparison, the Uo parameter, is transmitted to the controller which acts on the execution element (continual flow motor, three-phase induction motor or hydraulic operation shaft) and determines the transition of the electrodes in order to delete the difference and so, to re-establish the required value of the arc impedance.

$$\Delta U_0 = U_a - Z_0 \cdot I_a \tag{3}$$

The deletion of the automatic temperature control drawbacks, for example that at some stages of the technological process one can stock the furnace with energy of up to plus or minus 15% in relation to the optimal one, can be obtained by the use of on-line conduct systems and temperature control.

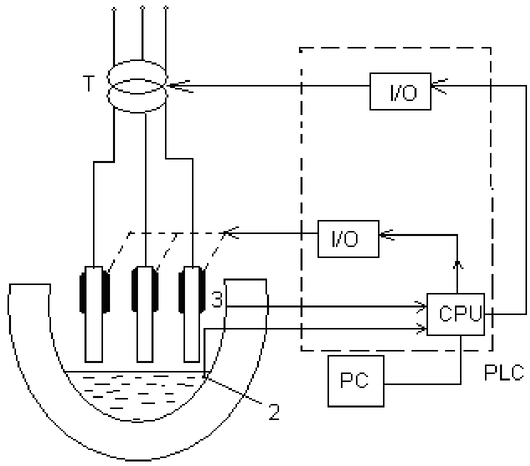

Fig. 4: Control system of power electric on arc furnace

The regulation and control scheme of the arc furnace through a logical programmable controller PLC is described in Figure 4.

PLC is robust and compact devices specially created to monitor and control some automation parameters. With their use various automation schemes can be implemented of medium complexity. Initially they were designed to implement binary control functions: combinational logical functions and automate programmable (control sequence). Hence there had been added more continuously adaptive control functions, communication features and functions for viewing and storing the collected data. With output interfaces, PLC controls various elements of digital performance (two-position). Outputs are usually voltaic isolated from the logical aspect to allow linkage of greater value voltages or currents and to protect the logical aspect of any accidental over-voltages. Depending on the building of PLC, there can be repeater contact, power transistor or thyristor type outputs.

LG Industrial Systems has introduced the range programmable controllers (PLC), GLOFA-GM series for medium and large applications which can use here.

Automatic system is to ensure as far as possible to optimum functioning furnace, quickly remove those disturbances.

Electrodes position adjustment is made regarding furnace current which receives information about heating regime using the programming logic controller PLC. The controller commands by the central processing unit power regulators which provide the amount of set energy for each stage of technological process.

The controller receives technological tasks (electrical parameters, metal temperature) from the programming device on Windows- Based Programmer and bases on them it establishes the necessary power and controls its insertion in the furnace through the power regulator. The controller may also perform other functions on the introduction of materials, oxygen and to optimize the process.

One of the main objectives of the three-electrode Electric Arc Furnace simulator study is to have the electrodes maintain constant power consumption. This is achieved by moving the electrodes to a given depth, obtaining the desired resistances (conductance), which leads to a constant power consumption. Identification system block diagram is shown in Figure 5.

The dynamic behavior is based on the arc length variations. The nonlinear and time varying characteristic of the arc length cause changes in arc resistance and so the slope of the V-I characteristic [6].

To attain this goal, the open-loop system described in the previous section must be closed in order to create an error signal. The control principle is accomplished by minimizing this error signal with specific controllers. For this system, although the power is to remain constant, since the power magnitudes are scalar multiples of the electrode currents, controlling the current will lead to power control as well. A feedback loop has now been added to the output of the open loop system.

The output currents are fed back into the negative port of an adder block, where they are combined with the initial step responses representing the desired current. The difference between the desired current and output current is then fed into a PID controller set appropriately to transform a current magnitude to a percent error. This percent error orders the hydraulic actuators to open the valves such that a new resistance sets the corresponding currents to converge to the desired currents.

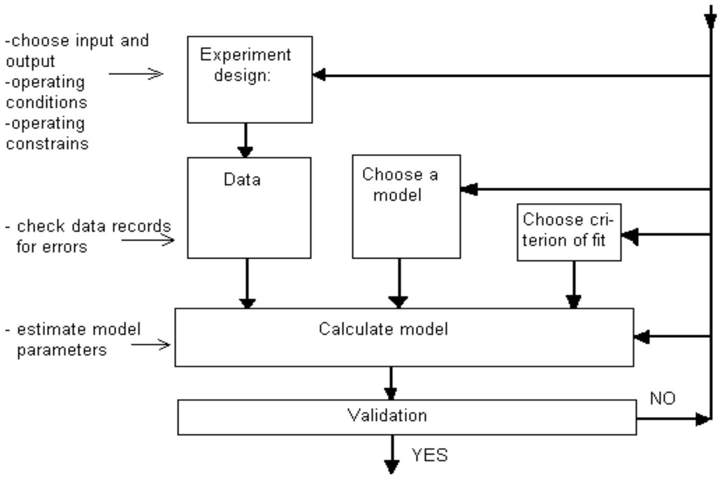

Fig. 5. The system identification loop

4. CONCLUSIONS

Application of specific mathematical models to optimize the operation of arc furnaces, particularly the mathematical model to conduct the effectively melting MCT and the mathematical model of load preheating MPI (including the mathematical model for calculating the design of recovery burners related to preheating MPAR).

The mathematical model for calculating the design of recovery burners related to preheating MPAR has the positive consequence reducing specific consumption of electricity in steel elaboration with about 15%, simultaneously obtaining a high quality of steels and is directly correlated to MPI.

The deletion of the automatic temperature control drawbacks, for example that at some stages of the technological process one can stock the furnace with energy of up to plus or minus 15% in relation to the optimal one, can be obtained by the use of on-line conduct systems and temperature control.

The regulation and control scheme of the arc furnace through a logical programmable controller PLC was proposed. Finally, a feedback loop was introduced to create a closed-loop system. The input step functions now represent the desired current to control the power.

REFERENCES

[1.] S. Arad, Electrotehnologii. Utilizarea energiei electrice in industrie. Focus Publishing, Petrosani 2009.
[2.] B. Boulet, V. Vaculik and G. Wong, "Control of High-Power Non-Ferrous Smelting Furnaces", IEEE Canadian Review, 1997.
[3.] D. Comşa, L. Pantelimon, Electrotemie, Didactical and Pedagogical Publishing House, Bucureşti, 1979.
[4.] D. Comşa, S. Darie, „Măsurarea mărimilor şi parametrilor cuptoarelor electrice cu arc", Energetica, 7(6), 1976, pp.289-294.
[5.] Cz. Flueraşu, C. Ionescu and C. Flueraşu, "Numerical Simulation of Over voltages Occurring at the Virtual Chopping of Currents in Electric Arc Furnaces", Proc. of Int. Conf in Electro Heating Equipment, Sibiu, 1991.
[6.] M. A. Golkar, M. Tavakoli Bina and S. Meschi, „A Novel Method of Electrical Arc Furnace Modeling for Flicker Study", Proc of Int. Conf. on Renewable Energies and Power Quality, ICREPQ'07, 2007
[7.] R.D. Morales, et al. „A mathematical simulator for the EAF steelmaking process using direct reduced iron". ISIJ International vol 41(5), 2001, pp 426-435,.
[8.] L.P. Rathaba,., „Model Fitting for Electric Furnace Refining", M. Eng. Thesis, University of Pretoria, 2004
[9.] A. Saimac, E. Roşu, et al. Utilizarea energiei electrice în metalurgie, Didactical and Pedagogical Publishing House, Bucureşti, 1980
[10.] A. Ioana,.A. Nicolae, et al Conducerea optimala a cuptoarelor cu arc electric, Fair Partners Publishing, Bucuresti, 2002.

INTERNATIONAL SYMPOSIUM on ADVANCED ENGINEERING & APPLIED MANAGEMENT
– 40th ANNIVERSARY in HIGHER EDUCATION (1970-2010),

INTERNATIONAL SYMPOSIUM on
ADVANCED ENGINEERING & APPLIED MANAGEMENT
– 40th ANNIVERSARY in HIGHER EDUCATION (1970-2010)
4 – 5 November, 2010, Hunedoara, ROMANIA

[1.]Raluca ROB, [2.]Caius PANOIU, [3.]Manuela PANOIU, [4.]Anca IORDAN

SIGNAL GENERATOR DESIGNED IN LabVIEW PROGRAM

[1-4.] ELECTRICAL ENGINEERING AND INDUSTRIAL INFORMATICS DEPARTMENT, UNIVERSITY POLITECHNICA TIMISOARA, FACULTY OF ENGINEERING HUNEDOARA, HUNEDOARA, ROMANIA

ABSTRACT:
In this paper the authors present a virtual signal generator that contains two independent channels. It was choosed the LabVIEW Tool for designing the generator, because it permits a practical graphical interface with the user. The generated signals can be visualizated using the indicated displays of the virtual instrument, as on a real osciloscope using a data acquisition board.

KEYWORDS:
Signal generator, Noise signal, Spectral analysis

1. INTRODUCTION

Signal generators are electric devices that are used as time variable voltage sources with a specified waveform and adjustable amplitude and frequency. These instruments are used in electrical laboratory at controlling, adjusting, measuring the electrical signals.

2. LABVIEW IMPLEMENTATION OF THE SIGNAL GENERATOR

INPUT DATA

The parameters of generated signals can be introduced in program using appropriate control elements: rotary buttons, pushing buttons, circular dial.

The signal generator is designed using two independent channels. Generated signals can be sinusoidal, rectangular, triangular, slope, continuous component. Input parameters: offset, frequency, amplitude and phase can be introduced using numeric control elements described in figure 1.

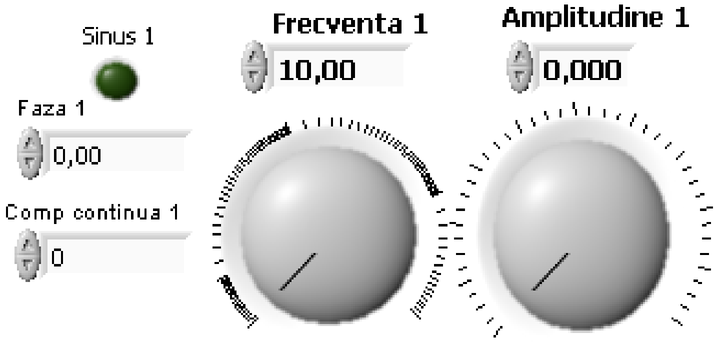

Fig.1. Numeric control elements

Signal selection can be made using two inputs multiplexers.

BLOCK DIAGRAM

The elements from block diagram that introduce the input data are presented in figure 2. In order to obtain different types of signals, the electric scheme contains *Simulate Signal* blocks that can be set to generate the desired signal.

The electric scheme can realize signal reversing operations, half wave and full wave rectification. Full wave rectification is done using *modulus* mathematical block [3]. Half wave rectification is made according with the following principle: signal is reversing, the result is subtracting from the full wave rectificated signal. The obtained signal is a half wave rectificated signal and amplified twice. The result is divided by 2, and the final signal represents the half wave rectificated signal (figure 3).

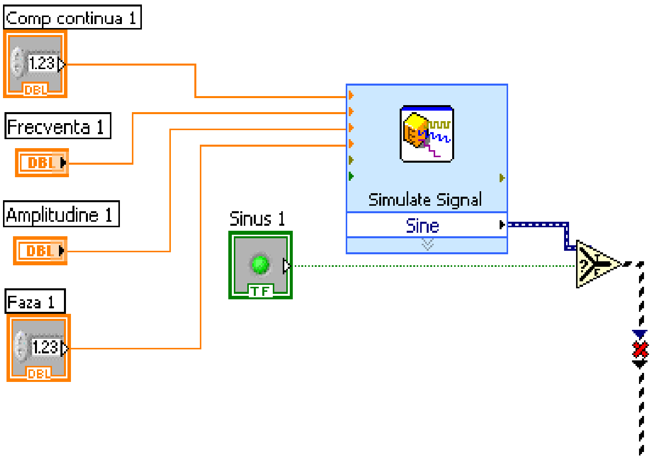

Fig.2 Simulate signal block

Each signal can be viewed with noise. The noise level can be adjusted. There were chosen the following noise types: Uniform, Gaussian, Periodic random, Bernoulli, MLS Sequence, Gamma, Poisson, and Binomial.

Noise signals are generated using *Simulate Signal* blocks set with *Numeric* and *Boolean* control elements [2].

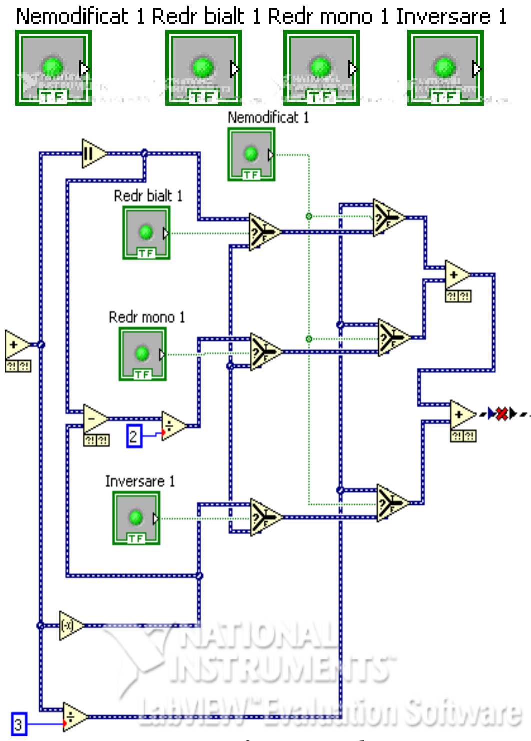

Fig.3. Rectification scheme

In order to obtain a continuous functioning, all elements of electric scheme are introduced in a *While* structure. Loop condition represents the *Stop* button placed on Front Panel.

Time base scheme of the indicator display is presented in figure 4.

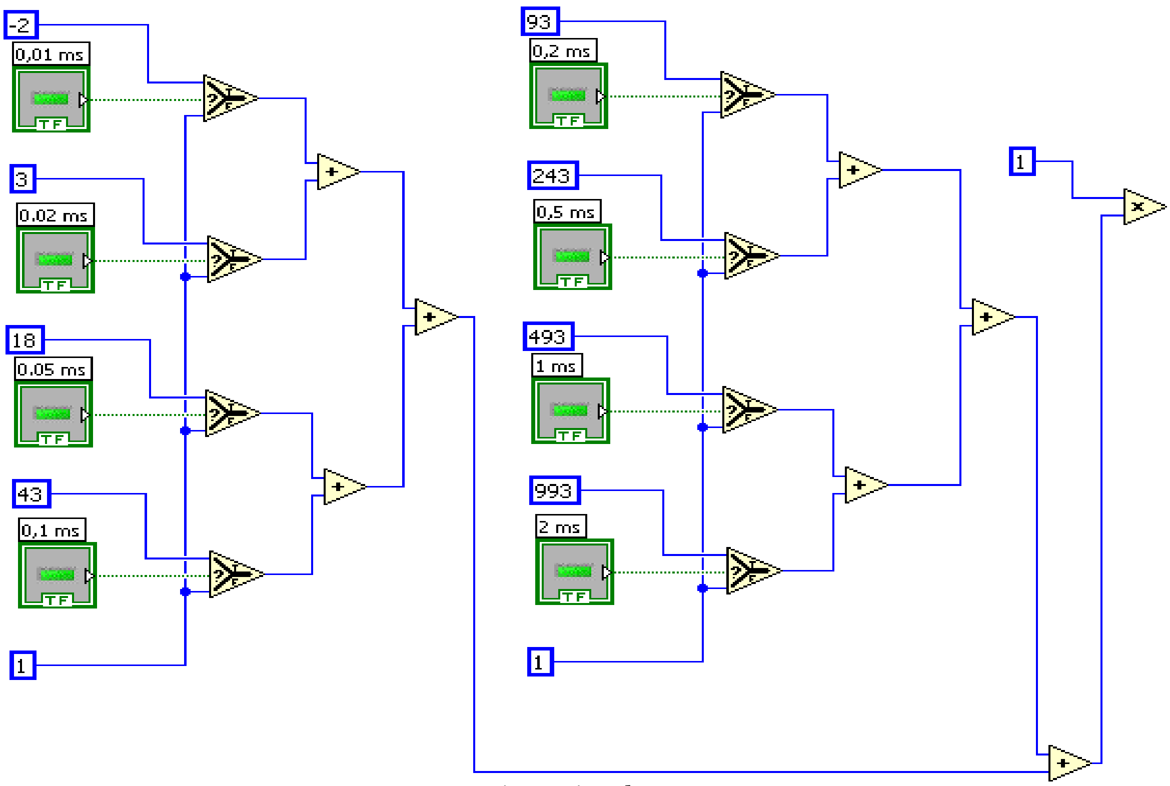

Fig.4. Time base.

The signals can be followed on a real oscilloscope display if it is connected to an analog input of data acquisition board, like NI-6221 (figure 5).

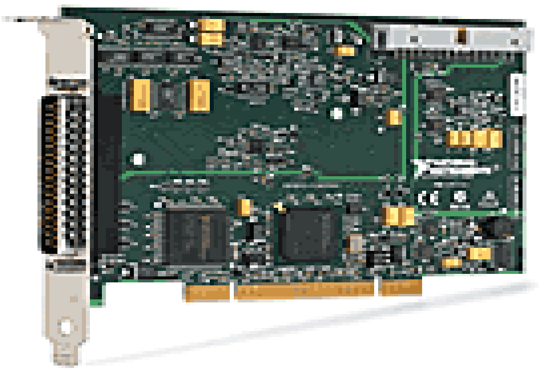

Fig.5. Data acquisition board PCI-6221.

Characteristics:

- 16 analog inputs, 250kS/s, resolution 16 bits
- 2 analog outputs, 833kS/s, resolution 16 bits
- 10 digital I/O compatible TTL
- 2 counter/timers on 32 bits
- digital trigger
- compatibility with Windows (2000/NT/XP), Linux
- integration with software components LabVIEW, CVI, Measurement Studio for Visual Studio NET

Figure 6 presents the front panel of the application.

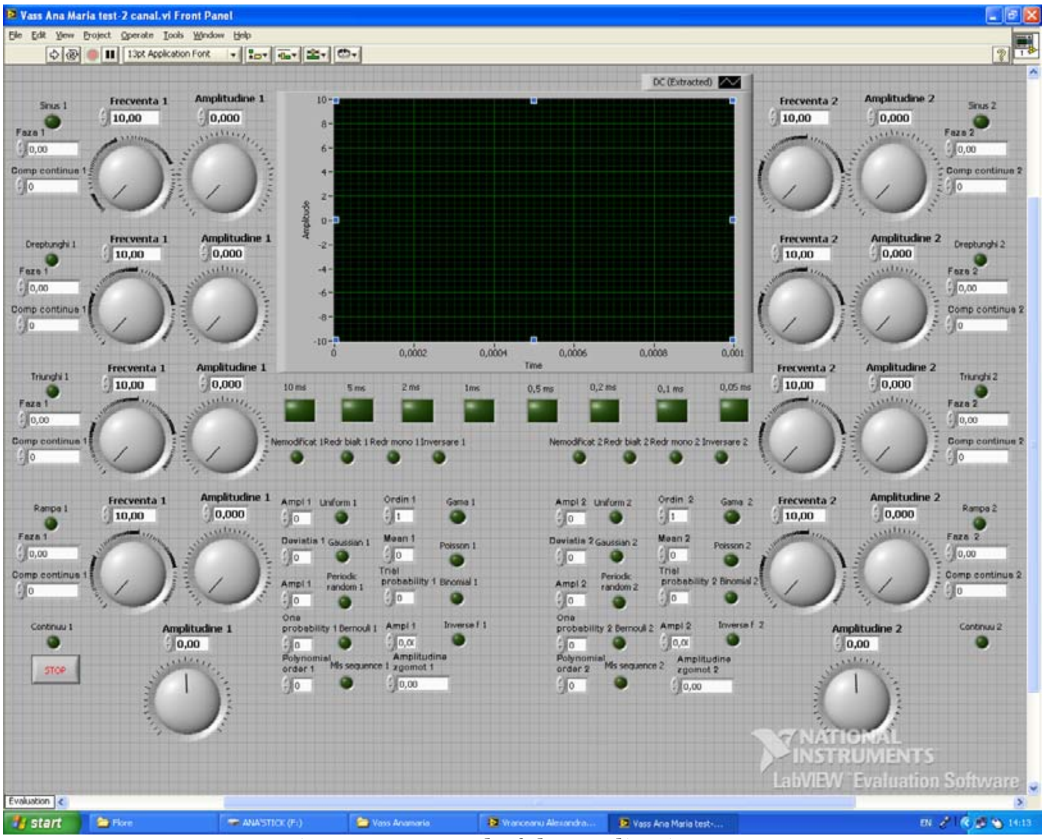

Fig.5. Front panel of the application

3. CONCLUSIONS

This application becomes very useful in electrical laboratorys, because it is a virtual instrument that simulates a real oscilloscope on two independent channels. In this way there can be simulated different types of signals that can be viewed on the virtual display. Using a data acquisition board [1], these virtual signals can be transformed in real voltage signals.

REFERENCES

[1.] Liviu Toma, *Sisteme de achiziţie de date*, Editura de Vest Timişoara, 1998
[2.] Francis Cottet, Octavian Ciobanu, Bazele programării în LabVIEW, Editura Matrix ROM Bucureşti, 1998
[3.] http://www.ctanm.pub.ro/academic/labview/Tutorial.htm

INTERNATIONAL SYMPOSIUM on ADVANCED ENGINEERING & APPLIED MANAGEMENT
– 40th ANNIVERSARY in HIGHER EDUCATION (1970-2010),

INTERNATIONAL SYMPOSIUM on
ADVANCED ENGINEERING & APPLIED MANAGEMENT
– 40th ANNIVERSARY in HIGHER EDUCATION (1970-2010)
4 – 5 November, 2010, Hunedoara, ROMANIA

[1] Corina Daniela CUNȚAN, [2]Ioan BACIU, [3]Manuela PĂNOIU, [4]Gabriel Nicolae POPA

DIGITAL CONTROL MODES OF THE SEMI-CONTROLLED THREE-PHASED RECTIFIERS

[1.-4] UNIVERSITY POLITEHNICA TIMIŞOARA, FACULTY OF ENGINEERING HUNEDOARA, ELECTRICAL ENGINEERING AND INDUSTRIAL INFORMATICS DEPARTMENT, ROMANIA

ABSTRACT:
In this work is presenting an interface circuit between a PC and a semi-controlled three-phsed rectifier. The circuit performs a numerical-analogue conversion using a CAN followed by a current-voltage conversion and a galvanic separation using opto-couplers that enter into a linearity circuit with the operational amplifiers. The output voltage is used to control the impulse forming circuits for the thyristor grids.
KEYWORDS: parallel port, numerical-analogue converter, opto-coupler, process control, power systems control, hybrid systems

1. INTRODUCTION

The numerical management of the industrial processes acquired today new valencies, both following the evolution of the management concept, and especially following the large scale evolution of the integrated circuits technology (LSI) and on very large scale (VLSI) of the a microprocessors, microcomputers and minicomputers. Thus, the modern concepts regarding the process management, materialized in large classes of adjusting and management algorithms, become operational and efficient following the development of the hardware instructions and the microprocessors on which are implemented with special performances.

The progress obtained in the field of interface systems with the industrial processes, of the data acquisition systems, of conversion and primary processing, as well as of the drive systems allowed the extension of the fields of utilization numerical computation technique in the management of the industrial processes.

Taking into account the processes' diversity, their complexity degree, the performance requirements imposed by the management systems, the knowledge level of them, there have been developped and implemented structures of management systems with different complexity degrees compatible both with relatively simple problems regarding the processes' numeric adjustment and with complex problems of the process management by global performance criteria.

2. WORK'S PRESENTATION

2.1. Semi-controlled three-phased rectifying bridge

The application diagram is presented in fig. 1.[1]

The three-phase bridge is formed by the diodes D_1, D_2, D_3 and thyiristors Th_1, Th_2, Th_3. Between phases R, S, T there is a phase difference of 120°. The current through R_L is closing successively by Th_3 and D_2 then by Th_2 and D_1 and, finally, by Th_1 and D_3. The circuits β AA 145 having the terminals 16 connected together and the same control voltage in the terminal 8, they open the thyristors at the same conduction angle (considered against each of the three grid voltages).

The ignition impulses will be identical as duration but dephased in time by 6,66 ms (corresponding to the 120°). Under load, it appears a voltage of which shape is strongly dependent by the value of the conduction angle φ.

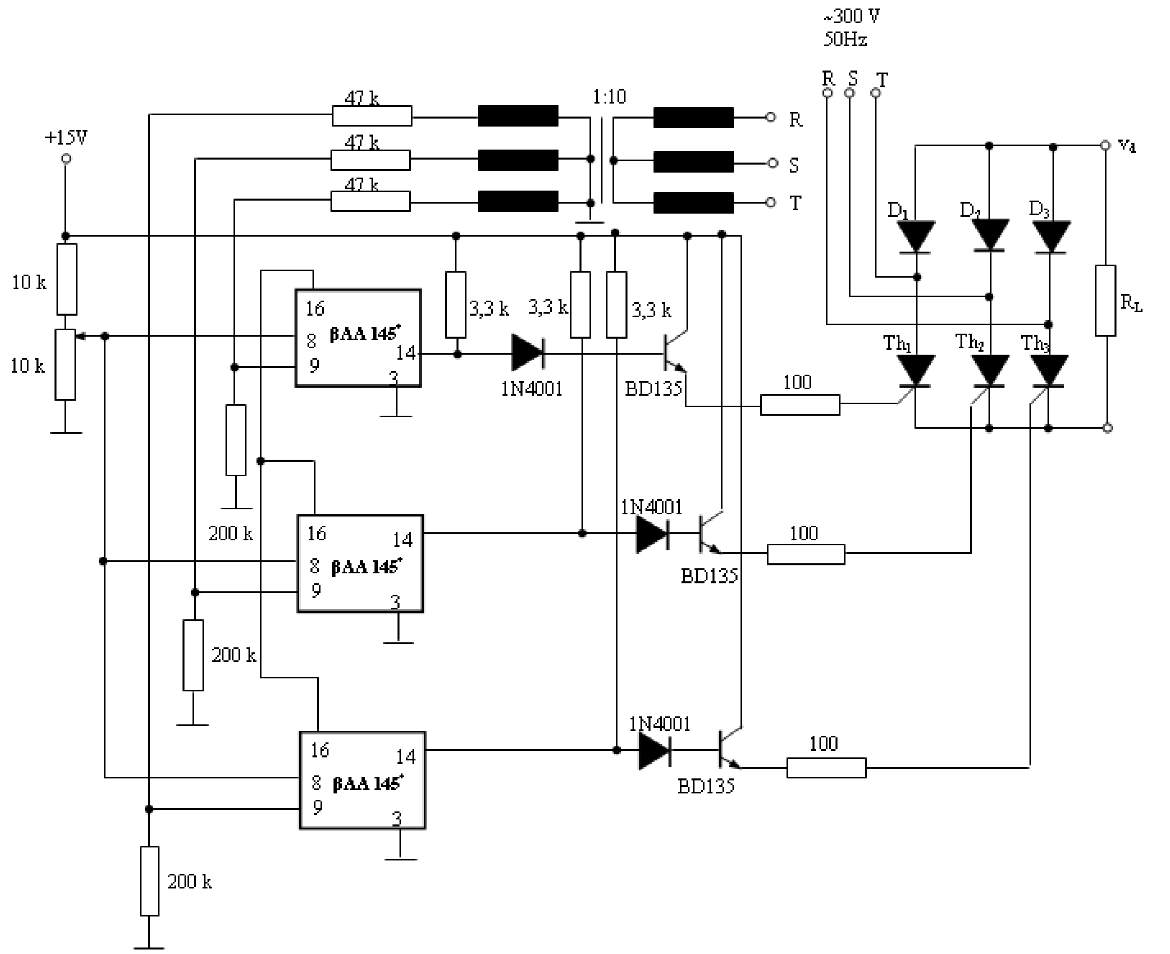

Fig. 1. The electric diagram of three-phase controll of a semi-controlled bridge

The average value of the rectified voltage in case of a rectifier with m phases becomes:

$$U_{do} = 2\frac{m}{2\pi}\int_{0}^{\pi/m}\sqrt{2}U_{2}\cos\omega t\, d(\omega t) = \sqrt{2}U_{2}\frac{\sin\pi/m}{\pi/m}, \tag{1}$$

where U_2 is the effective value of the voltage in the transformer's secondary; the index „o" featuring the situation of an ideal rectifier.

The above relation is valid for m = 2, 3,.....

For $m \to \infty, \lim\limits_{m\to\infty} U_{d0} = \sqrt{2}U_2$.

The effective value of the rectified voltage is calculated as follows:

$$U_{doef} = \sqrt{2\frac{m}{\pi}\int_{0}^{\pi/m}(\sqrt{2}U_{2}\cos\omega t)^{2}\, d(\omega t)} \tag{2}$$

obtaining the expression:

$$U_{doef} = \sqrt{\frac{mU_{2}^{2}}{\pi}\left|\omega t + \frac{\sin\omega t}{2}\right|_{0}^{\pi/m}} = U_{2}\sqrt{1+\frac{m}{2\pi}\sin\frac{2\pi}{m}}. \tag{3}$$

When $m \to \infty, \lim\limits_{m\to\infty} U_{d0ef} = \sqrt{2}U_2$.

An important issue arisen in case of the power application is to insure the protection of the controlled active element (thyristor, triac) against the possible accidents related to the malfunction of the reaction loop that has to ensure the on-load power stabilization. The integrated circuit β AA 145 that ensures the control can „interpret" this accident as a decrease of the power under load and as consequence to generate ignition impulses with increasing conduction angle, increasing unjustified the on-load power and putting in thermal destruction danger the controlled thyristor or triac.

The same effect can have also an accident in the cooling circuit of the radiator of a power thyristor, of which heat resistance has increased and which, therefore, can not disipate anymore the calculated maximum power.

For such accidents there are protection schemes, separated by the reaction loof of stabilizing the on-load power, that acts at the level of the thyristor's gate, blocking it when the temperature of the controlled active element's radiator decreases a certain value.

In case when the blocking is made directly on the thyristor's gate, then must be manipulaed big currents, which makes that the sensitivity of the protection circuit (in case it'a a circuit not too complex) to be small. Therefore, the thyristors' integrated control circuits are provided with a terminal with blocking priority of the ignition impulses. The circuit has a high sensitivity because it works at small currents (characteristic to an integrated circuit).

Terminal 6 of the circuit β AA 145 is the terminal with blocking priority. When terminal 6 is „put" to the supply voltage (e.g. short-circuited with terminal 7) the impulse generation on both outputs is inhibeted. In normal operation within the time interval passed from the null impulse generation until the appearance of the ignition impulse, the input impedance on terminal 6 is very high (there are only blocked junctions).

Any application diagram that uses terminal 6 for blocking the ignition impluses should respect this condition. If this condition is not taken into account, is possible to appear abbandoned ignition impulses.

The circuit β AA 145 is destined most exclusively to the on-phase control of the thyristors' (triacs') ignition. The increasing complexity of the thyristors' control circuits made that their monolitic achievement to be very attractive, as proven also by the great number of integrated circuits destined to the thyristors' and triacs' cocontrol.

In principle, the priming of a thyristor can be achieved with a circuit extremely simple. Utilization of a complex circuit or an integrated circuit is justified when is desired mot only the thyristor's priming but also the control of the disipated power in the anode circuit.

From the priming achievement's viewpoint, all the existent integrated circuits are identical: they supply current impulses (positive or negative) necessary to the control on the thyristor's grid. Howerever, the circuits are distinguished as regards the control mode of the power disipated in the thyristor's anode circuit's load. As result, hereby the expression „thyristors' control" refers to the control of the power from the load circuit. From this viewpoint, there are three control modes offered by the integrated circuits [1]:
(a) control through phase;
(b) control through zero with constant reference in time;
(c) control through zero with lineary variable reference in time.

2.2. The numerical-analogue conversion principle

There will be used balanced codes to present the the numerical information because they have the advantage of a natural expression and are compatible with the numerical calculation circuits. In case of such a code, a figure from a number has both the semnificance of its value itself, and the balance due to the position within the number. The numerical-analogue conversion assumes the transformation of the value and proportion of the number's figures into a corresponding analogue measure.

Is considered a binary integer of N bits, as [2]:

$$\overline{B_{N-1}B_{N-2}...B_{i-1}...B_1B_0} = \sum_{i=1}^{N-1} B_i 2^i \tag{4}$$

The figure B_{i-1} has the position i starting with the less significant bit (LSB) and has the balance 2^{i-1}, which means that the balance increases from right to left, the most significant bit (MSB) having the balance 2^{N-1}. The previous remarks are valid also for subunit binary numbers of N bits [2]:

$$\overline{B_1B_2...B_i...B_{N-1}B_N} = \sum_{i=1}^{N} \frac{B_i}{2^i}, \tag{5}$$

One can notice that the numerical-analogue conversion process is similar with the transformation procedure of a number from the binary numeration system, in the decimal numeration system, in this case to each binary figure "1" being associated a certain value of an electric measure (current or voltage) which is summed-up proportionally according to the rank that occupies within the numerical representation (for the figure "0" is associated the value zero of the same electric measure). Modification of the figures' balance with factors under form $1/2^i$ suggests a simple solution to achieve the balancing operation. This would be the utilization of some divisor rezistive grids, with more nodes, having between successive nodes the division ratio of 1/2. The resistances corresponding to the binary figures are introduced in the circuit when the associated binary figure is 1 or are disconnected in contrary case, by means of some electronic switches. The most usual types of grids are the ones with balanced resistances and with resistances R – 2R [3]. The electronic switches can be achieved with bipolar transistors or with transistors with field effect.

In the great converters family, the integrated circuit β DAC-08, 8-bit converter, occupies a position of industrial standard [4]. The circuit has a precision of 0,19% sufficient for the usual industrial applications. Being a speed circuit (set-up time of 100 ns order) can be used for data acquisition for the control of the industrial processes and numerical processing.

The circut has two current outputs noted I_0 and $\bar{I}_0$. These currents have the property that their sum is constant and equal with $\frac{255}{256} I_{REF}$, where I_{REF} is the current imposed from exterior. Thus, depending on the logical configuration, at the inputs $B_1,\ldots,B_8$ is obtained a current I_0 proportional with the numerical value of the binary word formed by the eight bits.

The maximum value at the current output I_0 is obtained when all the currents I_k are switched in this output.

$$I_0 = \sum_{k=1}^{8} I_k = I_{REF} \sum_{k=1}^{8} 1/2^k = \frac{255}{256} I_{REF} \tag{6}$$

The current I_{REF} is supplied from exterior by means of a current generator or from a voltage generator, V_{REF}, and a resistance, R_{REF}, that determines the current's value:

$$I_{REF} = \frac{V_{REF}}{R_{REF}} \tag{7}$$

The output current's conversion into voltage, maintaining a small value for the set-up time is very difficult. The end-scale current for β DAC 08 is set-up in 100 ns [1]. At output can be attached a load resistance in order to obtain an output voltage between 0 and -10 V.

Due to this time constant (RC), the conversion current/voltage is achieved usually with the diagram presented in fig. 2 [1]. The response time is limited now by the set-up time and by the value of the operational amplifier's slew-rate.

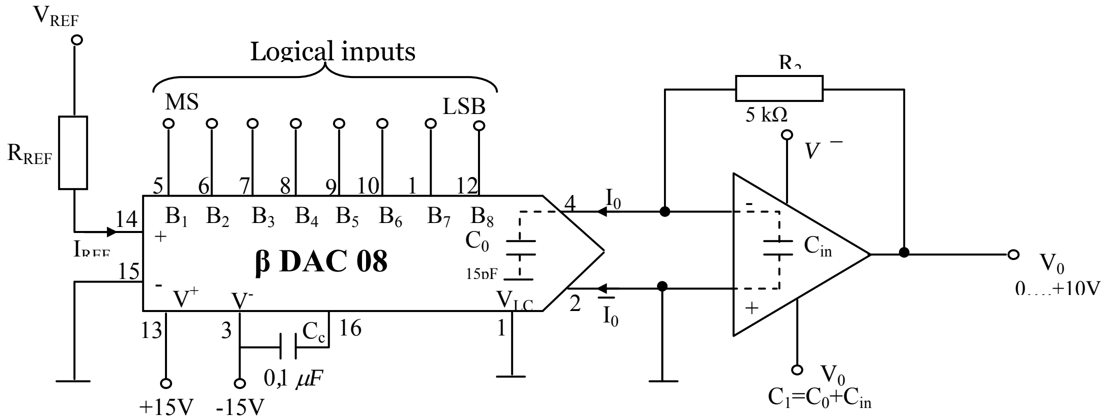

Fig.2. Electric diagram with current-voltage convertor at output

2.3. Galvanic insulation circuit

The process interfaces ensure the junction between the the computing system and the managed process, and as result should be taken safety measures in such way that the damaging of a component of the managed process (including transducers, execution elements) to not cause the damaging of the computing system [3]. Among the protection techniques used in such situations is also the galvanic insulation between the computer's and process' circuits.

The galvanic insulation consists in elimination of any direct electric connection between the computer's circuits and the ones corresponding the process. This is achieved ussualy electromagnetically (with transformers and relays), optically (with opto-couplers or optical insulators) and capacitive (with capacitive barriers).

Utilization of galvanic insulation in the acquisition and maangement systems ensure the protection of the system and the operator, reducing the noise and rejection of common mode voltages, especially of the ones caused by the mass loops.

The diagram of the galvanic separation circuit is the one from fig.3.

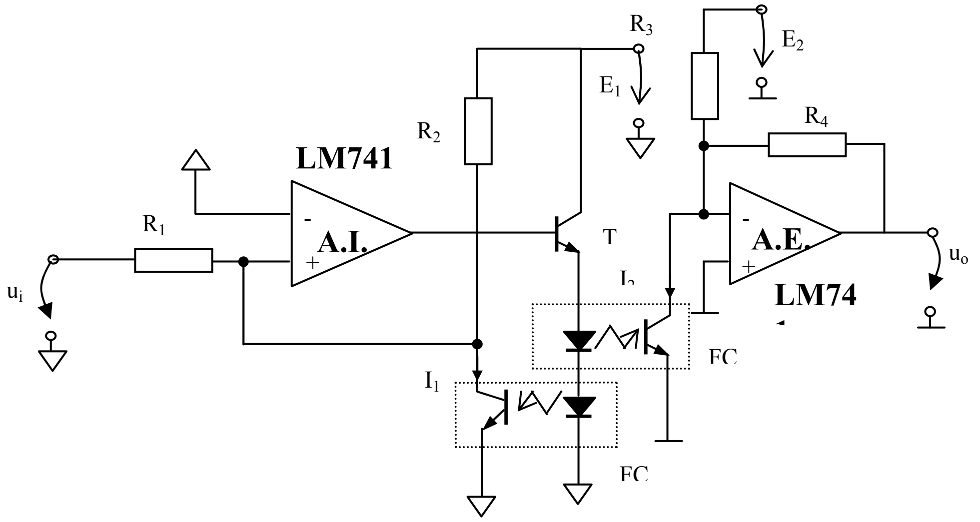

Fig. 3. The galvanic separation circuit

The transfer function of the insulation amplifier is made based on the hypothesis regarding the identity of the characteristics of the two photo-couplers [3].

$$I_1 = \frac{u_i}{R_1} + \frac{E_1}{R_2} \tag{8}$$

$$I_2 = \frac{u_O}{R_4} + \frac{E_2}{R_3} \tag{9}$$

where I_1 and I_2 represent the collector currents corresponding to the two photo-transistors. Because the diodes are connected in serial, it results that $I_1 = I_2$ resulting the transfer function of the insulation amplifier:

$$u_O = \frac{R_4}{R_1} u_i + R_4 \left(\frac{E_1}{R_2} - \frac{E_2}{R_3} \right) \tag{10}$$

It's determined that this transfer function is linear and independent by the photo-couplers' characteristics, with the condition regarding the identity of the two photo-couplers' characteristics.

2.4. Programming of the parallel port

The parallel port is used at the computer's communication with the peripheral equipments and for monitoring of different processes by PC [4].

The standardized connector of the parallel port is of D type, mother, with 25 pins [5].

The pin's number is the number inscribed on the connector in front of each pin. "**In**" represents the data transfer from peripheric to the port, and "**Out**" from the port to peripheric.

At the pins 1, 11, 14, 17 the signal is reversed by the hardware board and the pins from 18 to 25 represent the mass. Presentation of the parallel port's pins (fig. 4).

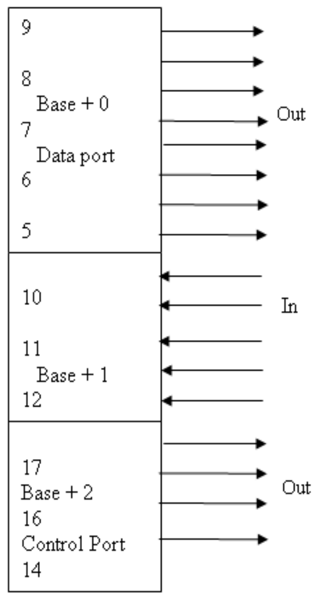

Fig. 4. Parallel Port

3. EXPERIMENTAL RESULTS

Following the experimental verifications, the output voltages from the numerical analogue converter block were noted U_{ies1} and respectively the galvanic separation circuit U_{ies2}, for the input measures between 0 – 255. The measured values are recorded in table 1.

Table 1 Output voltages CNA and for control of rectifying block

Input	U_{ies1}	U_{ies2}
0	1,1mV	300 mV
10	194 mV	590 mV
25	480 mV	1,15 V
50	969 mV	1,7 V
75	1,45 V	2,54 V
100	1,94 V	3,08 V
125	2,42 V	3,89 V
150	2,91 V	4,49 V
175	3,41 V	5,21 V
200	3,9 V	5,8 V
225	4,38 V	6,52 V
250	4,87 V	7,11 V
255	4,96 V	7,24 V

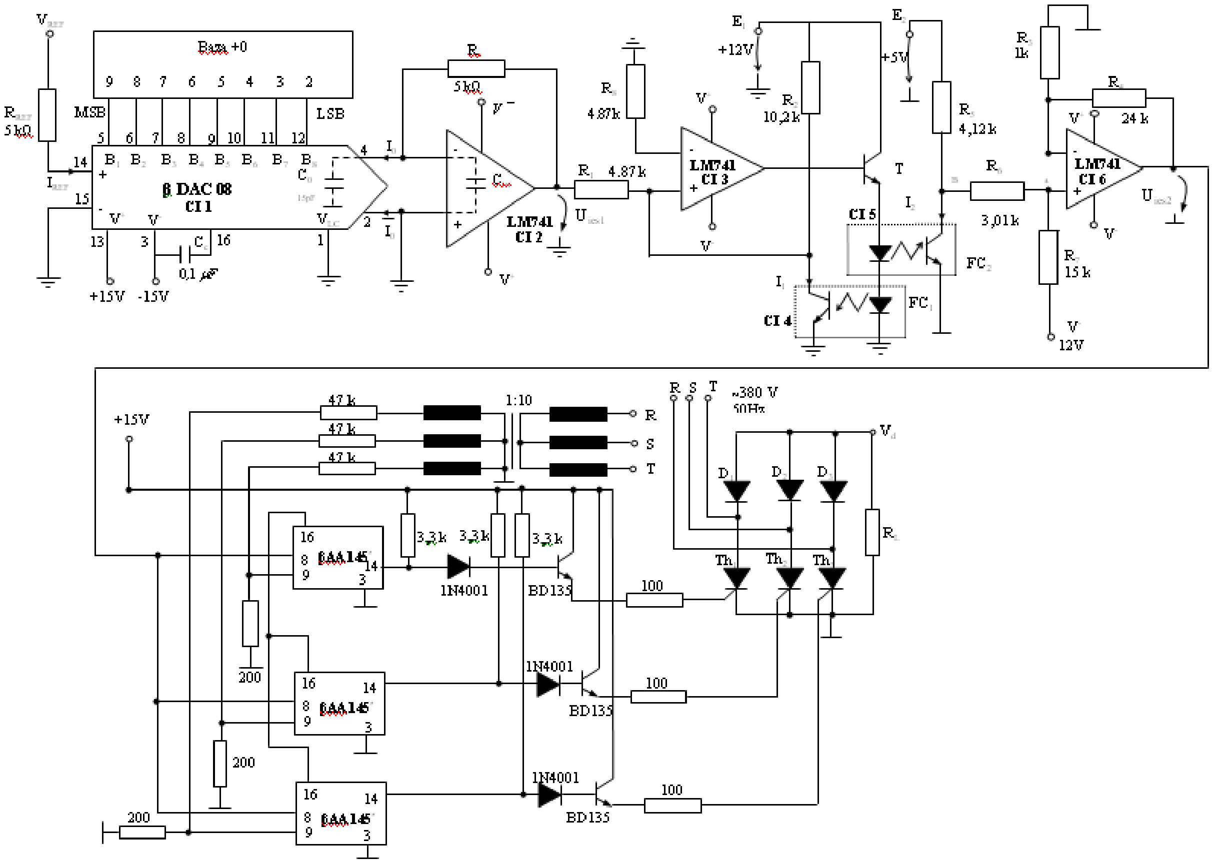

Fig. 5 Diagram of the three-phased rectifier's control interface

The control circuit represents in fact an interface between a computer and a three-phased power rectifier (fig. 5) that operates linearly on the entire variation scale of the numerical sequence on 8 bits (0-255). The program that allows to obtain at the parallel port the numerical sequence is achieved in C++ [6][7].

The thyristors of the rectifying bridge are independently controlled each by an integrated circuit β AA 145 specialized in thyristors controll, of which synchcronization is achieved trhough a three-phased transformer with the transformation factor 1:10, directly from the voltage of the supply system.

The control impulse is the one related to the positive alternance corresponding to each phase of the supply system.

Further, the obtained impulse is amplified in current by means of the medium power transistors of BD 135 type and which allow the direct connection to the thyristor grids of the rectifying bridge, without being necessary an additional galvanic separation circuit.

4. CONCLUSIONS

Analyzing the experimental data from table 1 one can notice a linear operation of each block in part, respectively of the conversion circuit, as well as of the galvanic separation circuit. The control circuit allows obtaining at output, directly proportional with a numerical value introduced from the keyboard, a maximum value that does not exceed 8 V, which represents also the maximum input voltage for the circuit βAA 145 which is the impulse former for the thyristors of the semicontrolled rectifying bridge.

Following the performed experiments was found that for the numerical values 0-10 as input in the control circuit is obtained a neglectable voltage at the rectifying bridge's output, which means that the thyristors are practically not controlled.

By introducing of a reaction loop can be obtained the adjustment of the output voltage automatically by bringing of a part form the output voltage tensiunea de ieşire to the computing system which determines the optimal control value.

REFERENCES

[1.] Bodea M., Vătăşescu A., Linear integrated circuits. Manual of utilization vol. IV, Technical Publishing House, Bucharest, 1985.
[2.] Toma L., Acquisition systems and numerical processing of signals, Western Publishing House, Timişoara, 1996;
[3.] Ignea A., Electric measurement of non-electric measures, Western Publishing House, Timişoara, 1996;
[4.] Popa M., Systems with microprocessors, "University Horizons" Publishing House, Timişoara, 2003;
[5.] Cristea D., Pănoiu C., Interfaces and peripherics, "Mirton" Publishing House, Timişoara, 2007;
[6.] Iordan A., Pănoiu M., Object-oriented programming. C++ Language. Laboratory guide, "Mirton" Publishing House, Timişoara, 2007;
[7.] Popovici D., Popovici I., C++ Object-oriented technology. Applications. "Teora" Publishing House, Bucharest, 2002.

INTERNATIONAL SYMPOSIUM on ADVANCED ENGINEERING & APPLIED MANAGEMENT
– 40th ANNIVERSARY in HIGHER EDUCATION (1970-2010).

INTERNATIONAL SYMPOSIUM on ADVANCED ENGINEERING & APPLIED MANAGEMENT
– 40th ANNIVERSARY in HIGHER EDUCATION (1970-2010),

INTERNATIONAL SYMPOSIUM on
ADVANCED ENGINEERING & APPLIED MANAGEMENT
– 40th ANNIVERSARY in HIGHER EDUCATION (1970-2010)
4 – 5 November, 2010, Hunedoara, ROMANIA

[1.]Adrian DANILA, [1.]Gabriela PAVEL, [1.]Radu MERA

A STUDY OF THE PARAMETER ESTIMATION OF THE SINGLE/TWO-PHASE INDUCTION MACHINES

[1-2.]TRANSYLVANIA UNIVERSITY OF BRASOV, ROMANIA

ABSTRACT:
A key point in simulation and control of the electrical drives is the accuracy of the available dynamic model. Especially for the squirrel-cage induction machines, the exact determination of the rotor's parameters i.e. resistances and inductances is not a straightforward task because these parameters cannot be determined through direct measurements during the drive's operation. Several techniques are used to obtain estimates for the machine's parameters as well as to obtain estimates for the process parameters such as flux-linkages components. Among these techniques, the observer-based methods are widely used in control engineering. The finite elements methods (FEM) are commonly used in design. In this work, the authors implemented both methods to determine the process parameters for a given single/two-phase induction machine. To validate the estimations, the results were compared with the measurements.

KEYWORDS:
electrical drives, simulation and control, finite elements methods, measurements

1. INTRODUCTION

The on-line estimation of the process parameters is essential in the adaptive control of the variable- parameters systems but also for the constant-parameters systems in the presence of stochastic disturbances, such are the electrical drives destinated to the control of speed and position.

In particular, the sensor-less estimation of the rotor's position is of major interest due to (1) the low cost implementation and (2) the increased maintenance issued from the elimination of the speed or position transducers. In addition, the on-line estimation of the process parameters allow the direct torque control and the implementation of advanced control algorithms such as the slider-mode control.

In this approach, the deterministic Luenberger's observer may be used to the angular speed reconstruction of the induction machine's rotor based on the measurements or estimated values of the torque and rotor's position. The Bocker's observer allows the reconstruction of the electromagnetic field's components based on the phase-voltages and currents, and the angular speed at the machine's shaft. In the same context, there are two applications of the extended Kalman filter that allow estimating the time constant of the rotor in presence of disturbances [1].

The typical applications of these algorithms are the control laws for the command of the three-phase inverters into the speed and position control of the induction machines electrical drives. Despite that from the theoretical point of view, the state observers are asymptotical stable, the convergence – and the estimate accuracy – depend on the accuracy of the parameters of the motor and finally on the electrical and mechanical parameters of the machine.

Because not all parameters of the machine may be determinate through direct measurements, numerical methods, based on the machine's geometry are often used, [2]. The commonly used approach is the use of the finite differences method, the finite elements method, integrals methods the frontier's elements methods. The field analysis allows determining the process parameters in the same manner as the observer-based methods and in addition the model's parameters or the physical parameters may also be determined.

Based on this idea, the paper presents an implementation of a state observer with the separation of the fast variables, the Pietrzak-David algorithm,[1], in comparison with the implementation of the FEM method to estimate the stator flux-linkages components within an single/two-phase induction machine.

2. METHODOLOGY

2.1. The Implementation of the FEM method to compute the inductances and the magnetic fluxes within the single/two-phase induction machine

The basis of the FEM method, [3] is the transformation of the solution of the electromagnetic potential, ψ into a linear combination of coordinate functions $\psi = \sum_{k=1}^{n} \alpha_k \cdot \varphi_k$. The unknown coefficients, $\alpha_k, k = \overline{1,n}$ result from a minimisation of the energetic functional associated to the field $F(\psi)$. There are various software applications that allow the FEM implementation to analyse the electromagnetic field both at low and high frequencies. In this paper, the Ansoft-Maxwell SV environment was used for the 2D analysis of the electrical machine, [4].

2.2. The Implementation of the Pietrzak-David State Estimator, [1]

The dynamic model of the induction machine is represented into a coordinate reference system related to the magnetic motion field as shown in the expressions below.

$$\frac{d}{dt}\begin{bmatrix}\Psi_{1d}\\ \Psi_{1q}\\ i_{1d}\\ i_{1q}\end{bmatrix} = \begin{bmatrix} 0 & \omega_e & -R_1 & 0 \\ -\omega_1 & 0 & 0 & -R_1 \\ \frac{R_2^{'}}{\sigma \cdot L_2^{'} \cdot L_1} & \frac{\omega}{\sigma \cdot L_1} & -\frac{1}{\sigma}\cdot\left(\frac{R_1}{L_1}+\frac{R_2^{'}}{L_2^{'}}\right) & \omega_1 - \omega_2 \\ -\frac{\omega}{\sigma \cdot L_1} & \frac{R_2^{'}}{\sigma \cdot L_2^{'} \cdot L_1} & -\omega_1 + \omega_2 & -\frac{1}{\sigma}\cdot\left(\frac{R_1}{L_1}+\frac{R_2^{'}}{L_2^{'}}\right) \end{bmatrix} \cdot \begin{bmatrix}\Psi_{1d}\\ \Psi_{1q}\\ i_{1d}\\ i_{1q}\end{bmatrix} + + \begin{bmatrix} 1 & 0 \\ 0 & 1 \\ \frac{1}{\sigma \cdot L_1} & 0 \\ 0 & \frac{1}{\sigma \cdot L_1} \end{bmatrix} \cdot \begin{bmatrix} v_{1d} \\ v_{1q} \end{bmatrix} \quad (1)$$

The time constants of the drive may be grouped into three categories as follows.

1	very slow time constants:	mechanical
2	slow time constants:	magnetic
3	fast time constants:	electrical

After eliminating the variations of the variables associated to the very slow and slow time constants, the dynamic model of the induction machine may be reduced to a second-order linear system as shown in the expressions below.

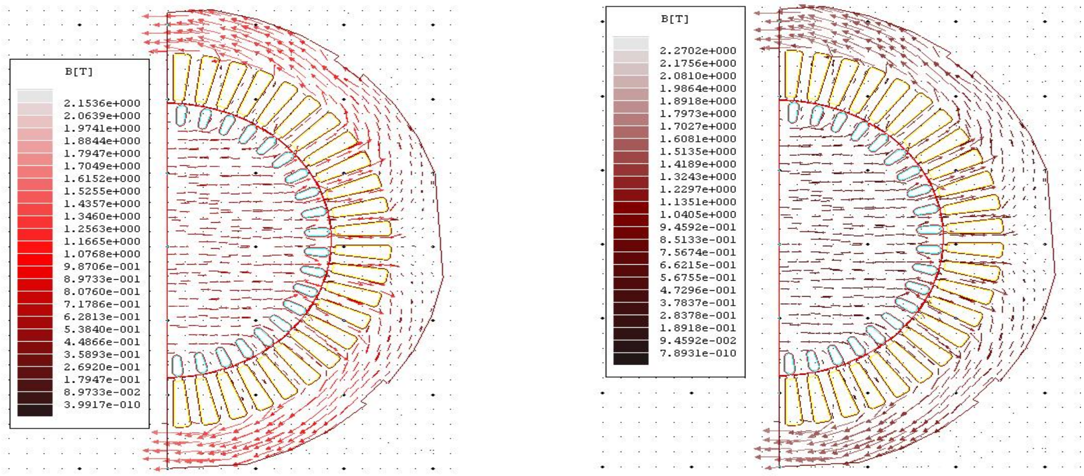

Figure 1: The spectra of the magnetic field determined with the FEM method; to the left - the (Od) axis component, to the right – the (Oq) axis component.

$$\left| \begin{aligned} &\frac{d\mathbf{Y_1}}{dt} = \mathbf{A} \cdot \mathbf{Y_1} + \mathbf{B} \cdot \mathbf{U_1} \\ &\mathbf{X_1} = \mathbf{C} \cdot \mathbf{Y_1} + \mathbf{D} \cdot \mathbf{U_1} \end{aligned} \right. \quad (2)$$

where the significance of the matrices is given in expressions (3) to (6).

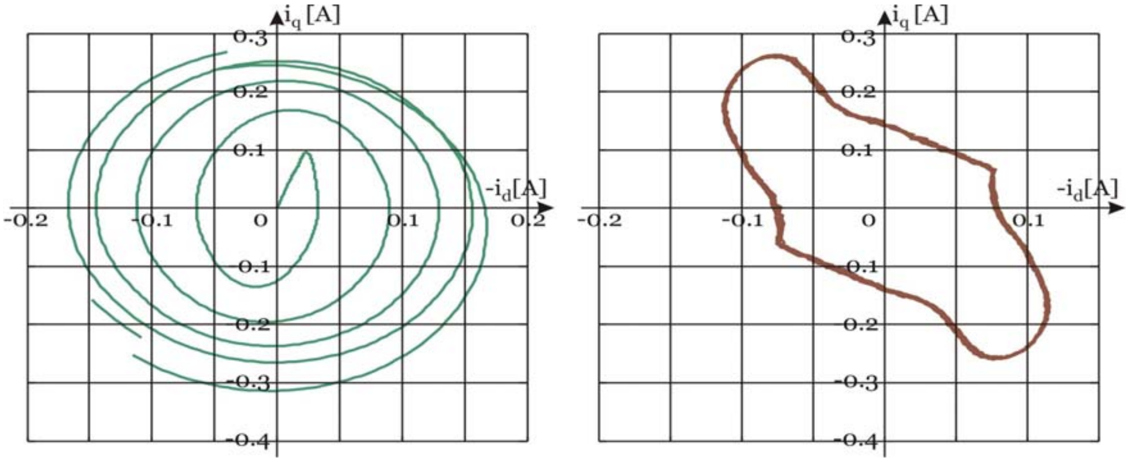

Figure 2: The loci of the stator currents space-vector, estimated values- to the left and measured values – to the right.

$$\mathbf{A} = \begin{bmatrix} -\dfrac{1}{T_1 + T_2} & \omega_1 - \omega \cdot \dfrac{T_2}{T_1 + T_2} \\ -\left(\omega_1 - \omega \cdot \dfrac{T_2}{T_1 + T_2}\right) & -\dfrac{1}{T_1 + T_2} \end{bmatrix} \quad T_1 = \frac{L_1}{R_1}, T_2 = \frac{L_2^{'}}{R_2^{'}} \tag{3}$$

$$\mathbf{B} = \frac{T_1}{T_1 + T_2} \cdot \begin{bmatrix} 1 & 0 \\ 0 & 1 \end{bmatrix} \tag{4}$$

$$\mathbf{C} = \frac{T_1}{T_1 + T_2} \cdot \begin{bmatrix} 1 & \omega \cdot T_2 \\ -\omega \cdot T_2 & 1 \end{bmatrix} \tag{5}$$

$$\mathbf{D} = \frac{T_1}{T_1 + T_2} \cdot \begin{bmatrix} T_2 & 0 \\ 0 & T_2 \end{bmatrix} \tag{6}$$

Input variables $\begin{bmatrix} v_{1d} & v_{1q} \end{bmatrix}^T$

Output variables $\begin{bmatrix} i_{1d} & i_{1q} \end{bmatrix}^T$

State variables $\begin{bmatrix} \Psi_{1d} & \Psi_{1q} \end{bmatrix}^T$

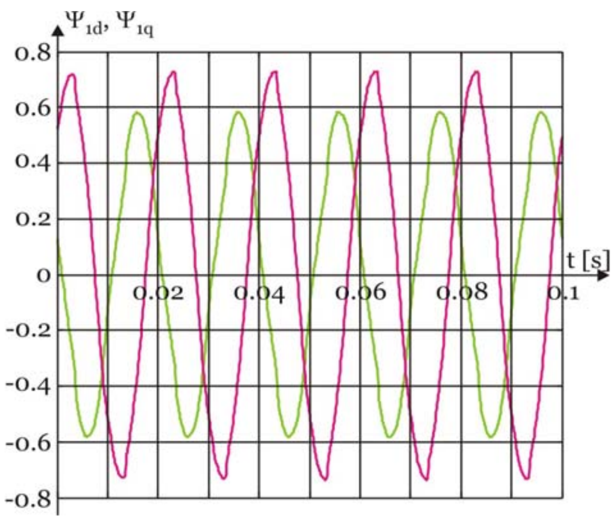

Figure 3: time-dependencies of the estimated flux components.

The Luenberger observer reconstructs the flux-linkage components based on the measurements of the input and output variables. Then the estimations are corrected in closed-loop with a term $K \cdot \left(i_{1d} - \hat{i}_{1d}\right)$ where the gain is determined with a Kalman filter.

3. DISSCUSIONS/RESULTS/ANALYSES

The motor under the investigation was a MSP311 type. The nominal parameters of the motor are given in Table 1.

3.1. The determination of the flux-linkage components with the FEM method

In Figure 1 the spectra of the magnetic field components are presented, [4]. The spectra have been determinate within the MAXWELL SV software environment and a geometrical representation of the cross-section of the machine.

The computations performed with the field calculator give the following values for the self inductances of the stator: $L_{1d} = 0{,}665\,H$ and $L_{1q} = 0{,}358\,H$. A remark issued at the implementation of the method is that the estimate is dependent on the values of the magnetic permeability of the on the magnetization curve. If an experimental determination of the magnetization curve is not available the estimation will be performed carefully and several data sets shell be used to increase the accuracy of the estimate.

Table 1: The Nominal Parameters of the MSP311 Motor

Denomination	Rated supply voltage	Rated frequency	Rated angular speed	Number of pair poles	Capacitor
Units	[V]	[Hz]	[rpm]	[-]	[μF]
Value	220	50	2820/420	1/6	14

3.2. The determination of the magnetic flux with state observers

The measurements used within the observer's implementation are presented in [4]. The implementation of the state observer is associated to the model in notation (2). The loci of the stator currents space-vector, estimated values and measured values are depicted in Figure 2.
From the analysis follows that the estimator cannot describe the non-linearity effects into the model but the information about the magnitude of the variables is conserved. The time-dependencies of the estimated flux components are presented in Figure 3.

4. CONCLUSIONS/FURTHER PROPOSALS

In this paper, the implementation of two different methods – the FEM method and an observer-based method - for the magnetic field components estimation is presented. The model under investigation was a single/two-phase capacitor-run induction machine.
The FEM method is widely used at the design level; the state observer is implemented in the adaptive control. From the analysis above, both methods provide

REFERENCES

[1.] G. GRELLET and G. CLERC, Actionneurs électriques. Principes/Modèles/Commande, Eyrolles, 2000
[2.] A. NICOLAIDE, Bazele Fizice ale Electrotehnicii, Scrisul Românesc, 1983
[3.] GH. MÎNDRU, M.M. RĂDULESCU, Analiza numerică a câmpului electromagnetic, Editura Dacia, 1986
[4.] A. DANILA, I.MARGINEANU, R. CAMPEANU, C. SUCIU, I. BOIAN, The Optimization of the Single/Two Phase Induction Motor Start-Up with Electronically Switched Capacitor, 2008 IEEE International Conference on Automation, Quality and Testing, Robotics. Proceedings – Tome III pp 450-454

INTERNATIONAL SYMPOSIUM on
ADVANCED ENGINEERING & APPLIED MANAGEMENT
– 40th ANNIVERSARY in HIGHER EDUCATION (1970-2010)
4 – 5 November, 2010, Hunedoara, ROMANIA

[1.]Cornelia Victoria ANGHEL

CONNECTING PC VIA WIRELESS NETWORK PERFORMANCE OF EQUIPMENT

[1.] EFTIMIE MUTGU UNIVERSITY OF REŞIŢA, FACULTY OF ENGINEERING,
COMPUTER SCIENCE DEPARTMENT, REŞIŢA, ROMÂNIA

ABSTRACT:
Increasing popularity of wireless networks has led to a rapid decrease in the price of wireless devices along with a marked improvement in their technical performance. A wireless network infrastructure can now be achieved with much lower costs than a traditional cable. In this way, there are prerequisites to achieve cheap and easy Internet access local communities, with all the benefits resulting. Access to information is a source of global network.

KEYWORDS:
computers, Wireless Network, drivers

1. INTRODUCTION

Increasing popularity of wireless networks has led to a rapid decrease in the price of wireless devices along with a marked improvement in their technical performance.

A wireless network infrastructure can now be achieved with much lower costs than a traditional cable. In this way, there are prerequisites to achieve cheap and easy Internet access local communities, with all the benefits resulting.

2. METHODOLOGY

2.1. Connecting the Device

Before installing the Router, please make sure your broadband service provided by your ISP is available. If there is any problem, please contact with your ISP. After that, please install the Router according to the following steps. Don't forget to pull out the power plug and keep your hands dry.

1. 1. Locate an optimum location for the Router. The best place is usually near the center of the area in which your PC will be wirelessly connected. The place had better accord with the Installation Environment Requirements.
2. Adjust the direction of the antenna. Normally, upright is a good direction.
3. Connect the PC(s) and each Switch/Hub in your LAN to the LAN Ports on the router.
4. (If you have the wireless NIC and want to use wireless function, you can skip this step.)
5. Connect the DSL/Cable Modem to the WAN port on the router.

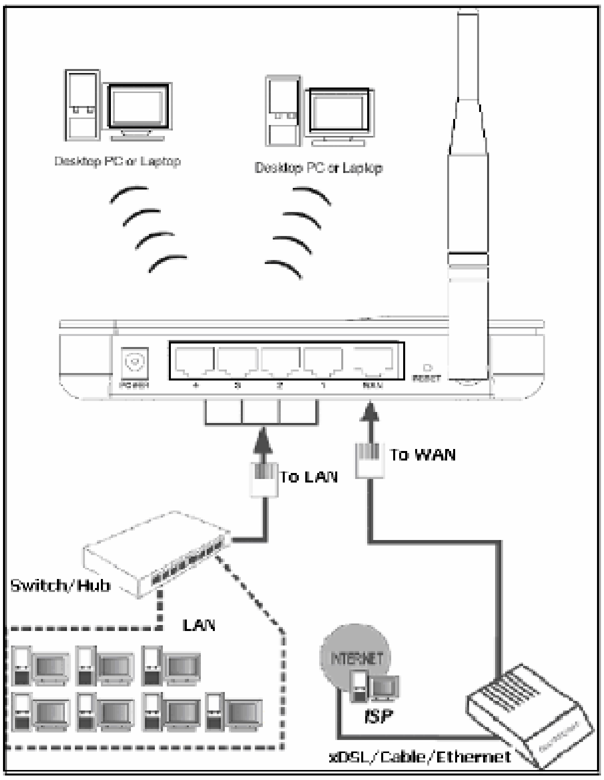

Figure 1. Hardware Installation of the Router

6. Connect the AC power adapter to the AC power socket on the router, and the other end into an electrical outlet. The router will start to work automatically.
7. Power on your PC and Cable/DSL Modem.

2.2. Configure our PC

Our PC needs a network adapter. You may directly connect your adapter to the Router, or you may connect your adapter to a Hub/Switch, and then connect the Hub/Switch to the Router.

Follow the instructions below to configure a computer running Windows XP to be a DHCP client.

1. From the **Start** menu on your desktop, go to **Settings**, and then click on Network Connections.
2. In the **Network Connections** window, right-click on LAN (Local Area Connection), then click Properties.
3. In the **General** tab of **Internet Protocol (TCP/IP) Properties** menu, highlight Internet Protocol (TCP/IP) under "This connection uses the following items:" by clicking on it once. Click on the Properties button.
4. Select "Obtain an IP address automatically" by clicking the radio-button. Click OK .

2.3. Configure the IP address manually

1. 1. Open TCP/IP Properties of the LAN card in our PC, enter the IP address. Now, we can run the Ping command in the command prompt to verify the network connection between your PC and the Router.
2. 2. Open a command prompt, From the Start menu on your desktop, select run tab, type **cmd** in the field, and complete the numbers of *ping* on the screen that appears, and then press Enter.

If the connection between our PC and the Router is correct the LEDs of LAN port which link to on the device and LEDs on our PC's adapter should be lit.

3. PERFORMANT EQUIPMENTS FOR CONNECTING PC VIA WIRELESS NETWORK

3.1. 1W AMPLIFIER 1000MW WIRELESS 6DBI

Art equipment that allows us to receive signals wirelessly at distances up to 3,000 meters and 5,000 meters in urban areas without major obstacles.

Increase signal reception power of over 5 times!

It is compatible with all types of laptop.

BGN 2.4 GHz wireless adapter, antenna 6dBi, MIMO technology, 100Mbps, notebook support

Compatible with IEEE 802.11n draft 3.0 wireless 802.11a/b/g Standards

- 2.4GHz frequency band, MIMO (Multiple Input Multiple Output)
- Complies with Universal Serial Bus Rev. 2.0

Specifications TX

- High speed transfer data rate up to 150 Mbps
- High speed transfer data rate up to 300 RX Mbps
- Supports WPS by S / W
- Supports Wireless Data Encryption with 64/128-bit WEP, WPA, WPA2, TKIP, AES.
- Wide Range coverage
- Compliant with FCC Part 15.247 for U.S., ETS 300 328 for Europe
- Supports drivers for Windows 2000, XP 32/64, Vista 32/64, Linux (2.4.x/2.6.x), Mac (10.4.x/10.5.x) Power PC & PC

3.2. DIRECTIONAL WLAN ANTENN (2.4GHz, 17 dB)


Figure 2. Directional WLAN Antenna

This model has thus having a high resistance grounding surge caused by storms and lightning. The antenna is small and is easily installed on the roof or balcon, not special support required, it can be used in access-point and the client (please make sure you have plugged into the equipment, otherwise it will be necessary cables and adapters). It can operate in both polarization (horizontal or vertical) depending on how it is mounted

Most often, vertical polarization antenna is used in this way it can be changed by rotating the 90° antenna. The radiator can be unscrewed and no position can be changed. If the antenna must operate with a sectorial antenna, it has to be put in horizontal position as in the picture below.

4. RESULTS

The results are detailed in the graphic representation:

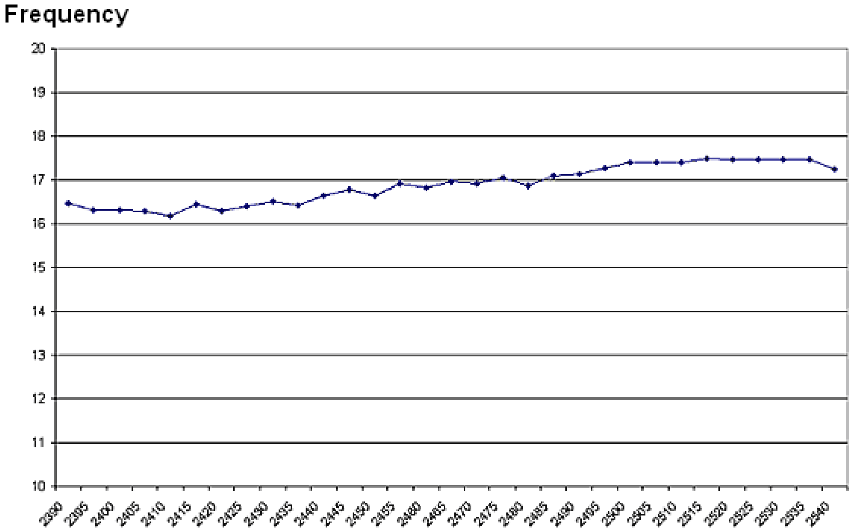

Figure 3. The graphic representation

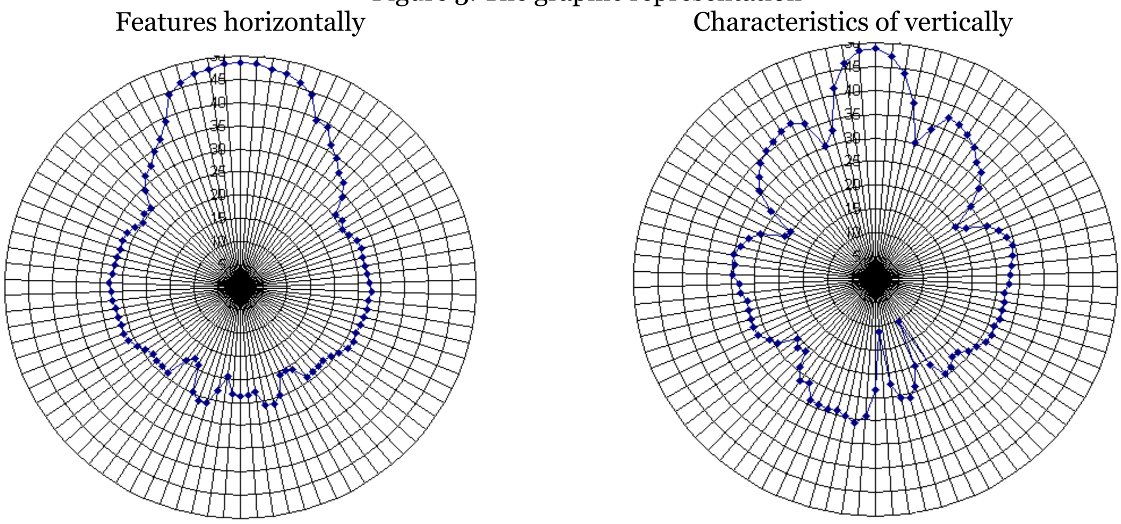

Figure 4. The representation of horizontally and vertically characteristics.

The specifications and characteristics are presented in Table 1.

Table1: Specifications and characteristics

Name	Directional WLAN Anthen
Gain	17dB
Band	2390-2540 MHz
Polarization	V / H
Report of the wave state. (VSWR)	<1.9
Report front / rear	25 dB
Half power beam - H	30 °
Half power beam - E	15 °
Impedance	50 ohms
Connector	N-socket (female)
Size	450 x 390 x 285 mm
Mounting Diameter	35-40mm

5. CONCLUSIONS

Wireless computer networks are intended for applications where cable installation is not possible or where necessary to terminal mobility.

The performance equipments presented in this article allows our PC to receive signals wirelessly at distances up to 3,000 meters and 5,000 meters in urban areas without major obstacles.

REFERENCES

[1.] Anghel, C.V. – „Consideraţii privind conectarea la o reţea Wireless securizată" Al XII-lea Simpozion Internaţional "Tinerii şi Cercetarea Multidisciplinară", 11-12 noiembrie, Timişoara, 2010
[2.] Dixit, R. Prasad (eds.), Wireless IP and Building the Mobile Internet, Artech House, 2003
[3.] M. Mallick, Mobile and Wireless Design Essentials, Ed. John Wiley & Sons, 2003
[4.] Tanenbaum A. - Reţele de calculatoare (ediţia a patra), Ed. Byblos, Tg.Mureş, 2003
[5.] Raab S. et al. - Mobile IP Technology and Applications, Cisco Press, 2005

INTERNATIONAL SYMPOSIUM on ADVANCED ENGINEERING & APPLIED MANAGEMENT
– 40th ANNIVERSARY in HIGHER EDUCATION (1970-2010),

INTERNATIONAL SYMPOSIUM on
ADVANCED ENGINEERING & APPLIED MANAGEMENT
– 40th ANNIVERSARY in HIGHER EDUCATION (1970-2010)
4 – 5 November, 2010, Hunedoara, ROMANIA

[1.]Diana Alina BISTRIAN, [2.]Mihaela OSACI, [3.]Marcel TOPOR

SOLUTIONS TO ACCELERATE MATLAB PROGRAMS WITH GPU COMPUTING

[1-3.] "POLITEHNICA" UNIVERSITY OF TIMISOARA, FACULTY OF ENGINEERING OF HUNEDOARA, DEPARTMENT OF ELECTRICAL ENGINEERING AND INDUSTRIAL INFORMATICS, ROMANIA

ABSTRACT:
The present paper presents recent advances in computational technology using the computational power offered by modern graphic processing units (GPUs). The technology is applied in Matlab scientific computations. Two different software solutions are evaluated and compared in order to reveal the main features and particularities from the point of view of a scientific computation user. The benefits and the drawbacks of this new technology are pointed out.
KEYWORDS:
CUDA technology, GPU computing, accelerating algorithms

1. INTRODUCTION

Over the past few years, graphics processing units (GPUs) have advanced at an astonishing rate and gained significant popularity as powerful tools for high performance computing (HPC). A GPU is a highly parallel computing device designed for the task of graphics rendering. However, the GPU has evolved in recent years to become a more general processor, allowing users to flexibly program certain aspects of the GPU to facilitate sophisticated graphics effects and even scientific applications. In general, the GPU has become a powerful device for the execution of data-parallel, arithmetic (versus memory) intensive applications in which the same operations are carried out on many elements of data in parallel. Example applications include the iterative solution of PDEs, video processing, machine learning, and 3D medical imaging.

The design philosophy of the GPUs has historically been motivated by the fast growing video game industry that exerts tremendous economic pressure for the ability to perform massive numbers of floating point calculations in advanced games. Therefore, the design goal for GPU vendors is to look for ways to maximize the chip area and power budget dedicated to floating point calculations. The general philosophy for GPU design is to optimize for the execution of massive number of threads. The hardware takes advantage of a large number of execution threads to find work to do when some of them are waiting for long-latency memory accesses, minimizing the control logic required for each execution thread. Small cache memories are provided to help control the bandwidth requirements of these applications so that multiple threads that access the same memory data do not need to all go to DRAM. As a result, much more chip area is dedicated to the floating-point calculations.

CUDA stands for **Compute Unified Device Architecture** and is a software architecture and API geared towards the utilization of the GPU as a computing device rather than a graphics rendering device. The CUDA software includes a GPU device driver, a runtime system that serves as an abstraction over the driver, and also runtime libraries that CUDA applications may link to in order to provide GPU-enabled FFT and BLAS support, among others. CUDA also includes a compiler tool chain which provides extensions onto the C/C++ languages for the construction of GPU applications. While programming the GPU with the CUDA tool chain, the GPU is viewed as a coprocessor to the CPU, or host, which orchestrates the executions carried out by the GPU as needed. In order to utilize the GPU to its fullest potential, the CPU must minimize data communication with the GPU, due to limited bus bandwidth, and maximize data parallelism in the tasks given to the GPU to maximize usage of GPU processors. Though the GPU can be viewed as capable of executing a large number of general threads in parallel, GPU programming is still typically accomplished through the specification of kernels which operate across an array of data elements. These kernels are limited in their length and the amount of local memory they use. The potential bottlenecks involved in computing with the GPU include memory allocation, memory transfer, and kernel execution. In the ideal case, each of these tasks is done sparingly to ensure that minimal overhead is accrued over the lifetime of an application.

The CUDA software stack is composed of several layers: a hardware driver, an application programming interface (API) and its runtime, and two higher-level mathematical libraries of common usage, CUFFT (The Fast Fourier Transform implementation) and CUBLAS (Basic Linear Algebra Subprograms implementation).

The Fast Fourier Transform is a divide-and conquer algorithm for efficiently computing discrete Fourier transform of complex or real-valued data sets. CUFFT is the CUDA FFT library that provides a simple interface for computing parallel FFT on an NVIDIA GPU. It allows users to leverage the floating-point power and parallelism of the GPU without having to develop a custom GPU-based FFT implementation.

Implementation of the Basic Linear Algebra Subprograms on top of CUDA driver provides the interface for parallel computation of basic models of matrix and vector objects in GPU memory space, filling objects with data, calling sequence of CUBLAS functions, retrieving data from GPU, creating and destroying objects in GPU space, writing data to and retrieving data from objects.

The hardware has been designed to support lightweight driver and runtime layers, resulting in high performance. When programmed through CUDA, the GPU is viewed as a compute device capable of executing a very high number of threads in parallel. It operates as a coprocessor to the main CPU, or host. In other words, compute intensive portions of applications running on the host are off-loaded onto the device. CUDA has hierarchical and non-unified memory access and both the host and the device maintain their own DRAM, referred to as host memory and device memory, respectively. One can copy data from one DRAM to the other through optimized API calls that utilize the device's high-speed Direct Memory Access (DMA) engines [1].

There are two ways to speed up the solver by CUDA:

- ❖ keeping at least the spirit of the current algorithm, and
- ❖ developing a totally new algorithm considering the new architecture.

We chose for the work presented in this report the first alternative believing that the second one is quite timely.

To keep the current algorithm, we partially-modified the algorithm without changing its underlying paradigm, implementing it in CUDA, and then porting it to Matlab. Although CUDA is a new architecture, there is a large amount of related work in the academic and a few in industrial scales. However, they have mostly not been applied to the field of equation solvers. Reference [2] reports a practice on CG solver.

2. SOLUTIONS FOR USING GPUs IN SCIENTIFIC COMPUTING

Finding parallelism in a program has been a challenge for at least the past twenty years of research in parallelism, and is still one today. But with the arrival of GPU chips capable of executing many instructions in parallel, available to average users, it become even more important to be able to utilize this power so that the end-users of computers can benefit from it and not only elite or research members.

Languages should evolve and low-level languages like C are not well suited for programming complex parallel tasks. It is a necessity to give to programmers new tools to effectively develop parallel program while reducing the need of a full parallelism comprehension and good knowledge of the underlying architecture. Matlab [3] is a high-level language with a powerful matrix-based system. It is often used for easy prototyping in early development stages because it relieves the programmer of many details like memory management and has an impressive library of built-in many matrix functions. Hence, it is a useful tool for many simulation domains like fluid mechanics, biology or mechanical engineering, especially for people whose first domain of competence is not computer science and are programmers by necessity.

There already exist different ways to speed up the computation of Matlab programs using GPUs, including several third-party toolboxes. Some options available, all built on top of the Compute Unified Device Architecture (CUDA) developed and provided by NVIDIA to access its GPUs will be presented in forthcoming sections.

2.1 GPUMAT LIBRARY

GPUmat is a freeware library, in a more advanced state that GPUlib, so memory management on the GPU is automated, even if data movements still need to be explicit. This is done through the addition of a new type of variables, GPUsingle, which makes use of GPU memory transparent for users. Deletion of unused variables is taken care of by a garbage collector so as not to clobber the GPU memory. This is important as data processed by GPUs tend to be very big since computations are based on data-parallelism. The use of this new type allows Matlab functions to be overloaded so that either the GPUmat or the original Matlab function is called depending on the type of the arguments.

The start command for GPUmat library *GPUstart* generate the following output in Matlab command window

>> GPUstart
Copyright gp-you.org. GPUmat is distribuited as Freeware.
By using GPUmat, you accept all the terms and conditions
specified in the license.txt file.
Please send any suggestion or bug report to gp-you@gp-you.org.
Starting GPU
There is 1 device supporting CUDA
CUDA Driver Version: 2.30
CUDA Runtime Version: 2.30
Device 0: "GeForce 9500 GT"
CUDA Capability Major revision number: 1
CUDA Capability Minor revision number: 1
Total amount of global memory: 1073414144 bytes
Number of multiprocessors: 4
Number of cores: 32
- CUDA compute capability 1.1
...done
- Loading module EXAMPLES_CODEOPT
- Loading module EXAMPLES_NUMERICS
-> numerics11.cubin
- Loading module NUMERICS
-> numerics11.cubin

GPUmat enables Matlab code to run on the Graphical Processing Unit. The following is a summary of GPUmat most important features:

- ❖ GPU computational power can be easily accessed from Matlab without any GPU knowledge.
- ❖ Matlab code is directly executed on the GPU. The execution is transparent to the user.
- ❖ GPUmat speeds up Matlab functions by using the GPU multi-processor architecture.
- ❖ Existing Matlab code can be ported and executed on GPUs with few modifications.
- ❖ GPU resources are accessed using Matlab scripting language. The fast code prying capability of the scripting language is combined with the fast code execution on the GPU.
- ❖ GPUmat can be used as a Source Development Kit to create new functions and extend the library functionality.
- ❖ GPU operations can be easily recorded into new functions using the GPUmat compiler.

The following example presents the computational solution of the wave equation using the discrete Fast Fourier Transform. Consider the variable coefficient wave equation

$$\frac{du}{dt} + c(x)\frac{du}{dx} = 0, \quad c(x) = 0.3 + \cos^3(x-1), \tag{1}$$

for $x \in [0, 2\pi], t > 0$, with periodic boundary conditions. As an initial condition we take $u(x,0) = \exp\left(-100(x-1)^2\right)$. This function is not mathematically periodic, but it is so close to zero at the ends of the interval that it can be regarded as periodic in practice.

In the first case the process is based on a CPU computation (Program 1), while in the second case the solving is executed using the GPU unit (Program 2). The *fft* function was realized using GPU instructions with the help of GPUmat library.

Comparative with the GPU results, the CPU results have a better accuracy (Figure 1), while the computation using the GPUmat *fft* function introduced the occurrence of spurious dispersion. In Figure 2 can be noticed that the algorithm loses its stability with oscillations that will grow exponentially and swamp the solution. The code requires another corrections to increase the accuracy.

Program 1.

```
clc;clear all;
tic;
N = 128; h = 2*pi/N; x = h*(1:N); t = 0; dt = h/4;
c = 0.3 + cos(x-1).^3;
v = exp(-100*(x-1).^2); vold = exp(-100*(x-.2*dt-1).^2);
tmax = 8; tplot = .15; clf, drawnow
plotgap = round(tplot/dt); dt = tplot/plotgap;
nplots = round(tmax/tplot);
data = [v; zeros(nplots,N)]; tdata = t;
for i = 1:nplots
for n = 1:plotgap
t = t+dt;
v_hat = fft(v);
w_hat = 1i*[0:N/2-1 0 -N/2+1:-1] .* v_hat;
w = real(ifft(w_hat));
vnew = vold - 2*dt*c.*w; vold = v; v = vnew;
end
data(i+1,:) = v; tdata = [tdata; t];
end
waterfall(x,tdata,data), view(10,70), colormap([0 0 0])
axis([0 2*pi 0 tmax 0 5]), ylabel t, zlabel u, grid off;  toc
```

Program 2.

```
clc;clear all;
tic;
N = 128; h = 2*pi/N; x = h*(1:N); t = 0; dt = h/4;
c = 0.3 + cos(x-1).^3;
v = exp(-100*(x-1).^2); vold = exp(-100*(x-.2*dt-1).^2);
tmax = 8; tplot = .15; clf, drawnow
plotgap = round(tplot/dt); dt = tplot/plotgap;
nplots = round(tmax/tplot);
vGPU=GPUsingle(v);    % transfer variable v to GPU memory
data = [v; zeros(nplots,N)]; tdata = t;
for i = 1:nplots
for n = 1:plotgap
t = t+dt;
v_hatGPU = fft(vGPU); % perform Fast Fourier Transform  on GPU
v_hat =single(v_hatGPU);  % copy v_hat in CPU memory
w_hat = 1i*[0:N/2-1 0 -N/2+1:-1] .* v_hat;
w_hatGPU=GPUsingle(w_hat);   % transfer variable w_hatGPU to GPU memory
wGPU = real(ifft(w_hatGPU)); % perform Inverse Fast Fourier Transform on GPU
w=single(wGPU);    % copy w in CPU memory
vnew = vold - 2*dt*c.*w; vold = v; v = vnew;
end
data(i+1,:) = v; tdata = [tdata; t];
end
waterfall(x,tdata,data), view(10,70), colormap([0 0 0])
axis([0 2*pi 0 tmax 0 5]), ylabel t, zlabel u, grid off
toc
```

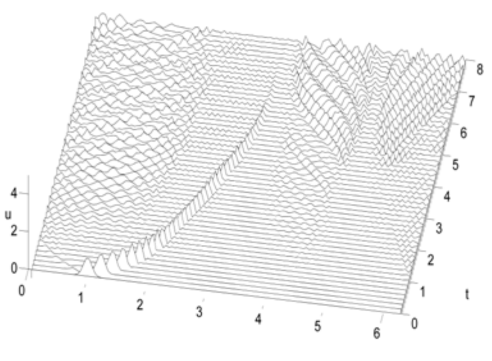

Figure 1. Program 1 output: solution of the wave equation (1) computed on CPU.

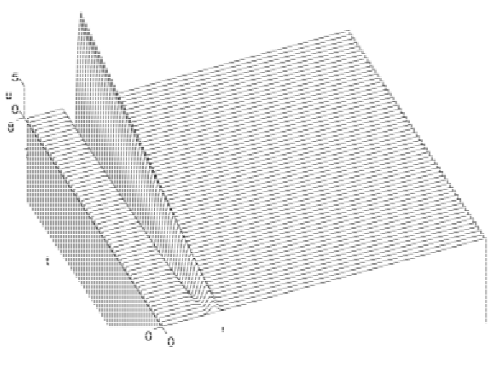

Figure 2. Program 2 output: solution of the wave equation (1) computed using GPUmat- algorithm loses its stability

2.2. JACKET PLATFORM FOR GPU COMPUTING WITH MATLAB

Jacket is a software platform designed for engineers, scientists, and analysts who want maximum application performance, minimum programming difficulty and maximum leverage of available technical computing resources, including laptops, desktops, servers, clusters and the Cloud. Jacket provides a middleware approach to GPU programming, with MATLAB as the fronted point of interaction for the user [4]. MATLAB with millions of users worldwide is the platform of choice for engineers and scientists alike, for rapid algorithm prototyping. MATLAB is an extensible interactive programming environment for numerical analysis built on a vector language called M. The M-language, like other vector languages, provides users with a high-level interface at which operations may be specified over large sets of data at once making the expression of data-parallel algorithms natural. M is also dynamically typed, adheres to pass-by-value semantics, and is integrated into a well developed interpreted environment. With these characteristics, M has proven to be a powerful, user-friendly language. Using Jacket, the M-language and MATLAB transparently adapt to GPU computing. Unlike other GPU solutions, Jacket provides GPU computation and graphics ability from a language which is inherently parallel and interpreted, thereby providing a standard, extensible, and simple method of programming for the GPU in an already proven rapid prototyping environment. Jacket adds few GPU-specific data types to MATLAB with overloaded operators and entire CPU-bound MATLAB programs can be converted into GPU-enabled programs through as little as adding a '*g*' prefix onto memory allocation commands. Otherwise, the user interacts with MATLAB as they normally would either from the command line or when running scripts.

Changing the data type allows the user to tap into the GPUs tremendous computational power. All standard data types are supported, including real and complex versions of singles, doubles, and integars. CUDA-capable GPUs of all types are supported. For instance, NVIDIA's Fermi-based Tesla C2050 contains 448 cores that are now fully accessible with Jacket, but those with lesser budget can also run Jacket on GeForce and Quadro GPUs.

Performance tests were performed on a desktop configuration of dual core CPU and Windows 2010 64 bite operating environment, using Matlab 2010a with Jacket v1.4. The GPU used is CUDA enabled GeForce 9500 GT with CUDA drivers.

Let us considered again the wave equation (1) with the CPU computed solution depicted in Figure 1. Program 3 represents the modified Jacket code for solving the wave equation (1) using the Fast Fourier Transform on Graphic Processing Unit.

Program 3.

```
clc;clear
tic;
N = 128; h = 2*pi/N; xx=1:N; % CPU variables
x = h*xx; t = 0; hCPU=h;  % CPU variables
dt = hCPU/4;
c = 0.2 + cos(x+1).^2 + sin(x+1).^2; % CPU variable
%c = 0.3 + cos(x-1).^3;
v = exp(-100*(x-1).^2); % CPU variable
vold = exp(-100*(x-.2*dt-1).^2); %CPU variable
tmax = 8; tplot = .15; clf, drawnow
plotgap = round(tplot/dt); dt = tplot/plotgap;
nplots = round(tmax/tplot);
data = [v; zeros(nplots,N)];
tdata = t;
nplots=gsingle(nplots);  %transfer variable on GPU
plotgap=gsingle(plotgap);% transfer variable on GPU dt=gsingle(dt);       % transfer
variable on GPU
data=gsingle(data);     % transfer variable on GPU
for i = 1:nplots
for n = 1:plotgap
t = t+dt;
v_hat = fft(v);  % perform FFT on GPU
w_hat = 1i*[0:N/2-1 0 -N/2+1:-1] .* v_hat;
w = real(ifft(w_hat));  % perform IFFT on GPU
vnew = vold - 2*dt*c.*w; vold = v; v = vnew;
end
data(i+1,:) = v; tdata = [tdata; t];
end
x=single(x);tdata=single(tdata);data=single(data);  % transfer variables back to CPU
waterfall(x,tdata,data), view(10,70), colormap([0 0 0])
axis([0 2*pi 0 tmax 0 5]), ylabel t, zlabel u, grid off;  toc
```

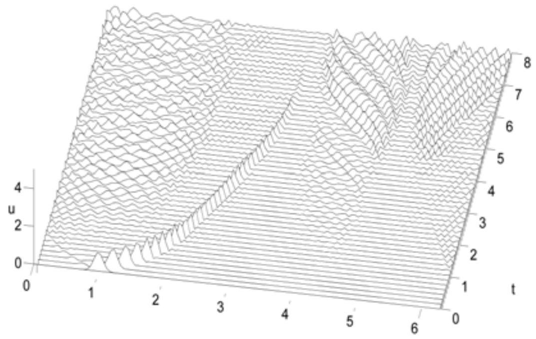

Figure 3 Program 3 output: solution of the wave equation (1) computed on GPU with Jacket v1.4.

Figure 3 shows the output of the Program 3. It can be noticed no difference between the output of the CPU code presented in Figure 1.

3. LIMITATIONS IN EXISTING ACCELERATION SOLUTIONS

Jacket provides an extensive list of Matlab functions with their state of support, ranging from "fully supported," meaning that they should work in any situation authorized by the original Matlab function, to "not supported," which cannot be used with *gsingle* arguments and there is no plan to support them in the immediate future. The number of supported functions is much bigger in Jacket than in GPUmat at the time of this writing. Because of no dynamic matrices with Jacket, hence the assignment

data = [v; zeros(nplots,N)];

is not valid as computed on GPU, it was necessary a two-way directional transfer of variables between the GPU and the CPU for the source Program 3. This increases the elapsed time, despite of the performance improvement obtained by using the GPU processing. In Table 1 a comparison between the CPU computation time of the wave equation (1) and the GPU computation time of the same is presented.

Table 1 Comparison between the computation time of the wave equation, on CPU and GPU.

Elapsed time of computation on CPU	Elapsed time of computation on GPU
0.883485	1.539880

Since our GPU works only with single precision floats, hence gives a less precise calculations, the conclusion is that this technology is not mature enough to be used effortlessly by the average user.

4. CONCLUSION

Some reasons for which Jacket is not suitable for development of our stability investigation algorithms are the facts that Jacket are a rather limited functions for matrix operations (for example diag(M) *diagonal scaling* is not supported), there is no eigenvalue solver supported by Jacket (as *qz factorization for generalized eigenvalue problems* is not currently supported, eigs *largest eigenvalues and eigenvectors of matrix* are unsupported), except some trials, these being insufficient for a generalized eigenvalue problem, at the time being.

That is the reason that most applications will use both CPUs and GPUs, executing the sequential parts on the CPU and numeric intensive parts on the GPUs. This induces a significant overhead of memory transfers between the host CPU and the GPU. In general, the overhead of time spent in sending data to the GPU and bringing it back neutralizes any performance benefit obtained by computing on the GPU.

REFERENCES

[1.] NVIDIA CUDA development team: NVIDIA CUDA Compute Unified Device Architecture Programming Guide, NVIDIA corporation,2007.
[2.] Wiggers, W.A., Bakker, V., Kokkeler, A.B.J., Smit, G.J.M., Implementing the conjugate gradient algorithm on multi-core systems, *IEEE International Symposium on System-on-Chip*, Finland, 2007.
[3.] http://www.mathworks.com
[4.] Jacket v1.4 *Getting Started Guide*, http://www.accelereyes.com/

INTERNATIONAL SYMPOSIUM on
ADVANCED ENGINEERING & APPLIED MANAGEMENT
– 40th ANNIVERSARY in HIGHER EDUCATION (1970-2010)
4 – 5 November, 2010, Hunedoara, ROMANIA

[1]Manuela PĂNOIU, [1]Caius PĂNOIU, [1]Anca IORDAN, [1]Cosmina ILLES

SOFTWARE PACKAGE FOR ANALYSIS THE PERFORMANCES OF BACKPROPAGATION NEURAL NETWORKS TRAINING ALGORITHM

[1-4] UNIVERSITY POLITEHNICA TIMISOARA, FACULTY OF ENGINEERING HUNEDOARA,
ELECTRICAL ENGINEERING AND INDUSTRIAL INFORMATICS DEPARTMENT, ROMANIA

ABSTRACT:
In this paper we present a software package use to analysis the performances of backpropagation neural networks training algorithm. It was analyze the dependency of performances with the learning rate of the algorithm. The software was implemented in Java language. The software was designed with the aim of offering a very easy-to-use user interface. It can be use as an educational tool for teach the basic concepts of backpropagation neural networks.

KEYWORDS:
neural networks, Java, learning algorithm, backpropagation algorithm

1. INTRODUCTION

Artificial neural networks (ANNs) are tools that have proved to be valuable to solve complex problems in many different application fields of science and technology [1, 2]. As a result, it is increasingly usual to find notions of neural networks included in the curricula of many Engineering studies [1].

Neural networks are interdisciplinary and have been used extensively in various fields ranging from electrical engineering to computer science from biology to image processing. Neural networks can solve prediction, estimation, classification, clustering, forecasting, control and decision making problems accurately and quickly [2].

Studying and researching neural networks, results the mathematical nature and underlying complexity. For this reason many students find the neural networks behavior difficult [9]. Moreover, neural networks are dynamic systems, which evolve in time, especially during their design and training phases. For engineering students, the most important is to understand this dynamic nature, and the real utility and operation of neural networks. Classroom-based teaching, books, and lecture notes are not sufficient to transmit this kind of knowledge [1].

Neural Networks have ability to learn from its environment and improve the performance through learning. The procedure used to selflearning process of an NN is called a learning algorithm. Some important application areas of neural networks are: Engineering and industrial applications, Business and financial applications, Medical applications. Some engineering and industrial applications are [2]: control, monitoring and modeling; process engineering; technical diagnosis; nondestructive testing; power systems; robotics; transportation; telecommunications; remote sensing; image processing.

The use of neural networks offers the many useful properties and capabilities [2]: nonlinearity; adaptivity; contextual information; fault tolerance; uniformity of analysis and design; neurobiological analogy.

In this paper is described an educational software useful for a better understanding the basic concepts of backpropagation neural networks and their training algorithm.

2. THE INFORMATICS SYSTEM DESIGN AND IMPLEMENTATION

The application was implemented in Java using NetBeans platform. The graphical user interface for this application is presented in figure 1. Using main menu for the application you could select the main options that are available.

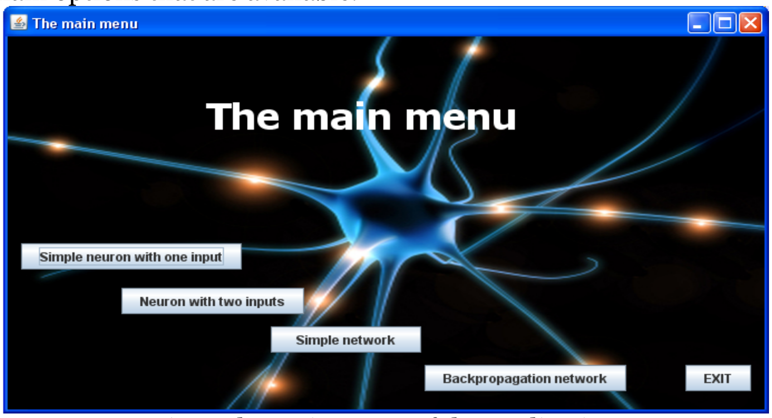

Fig. 1 The main menu of the application

The first and second options present the principle of the simplest artificial neuron operating. The simplest model of artificial neuron is represented by a nonlinear limiting or threshold element which excites if their inputs activation, fig. 2.

In according to threshold-logic units model each of continuous-valued input signals shall represent the electrical activity on the corresponding input line, or alternatively, the momentary frequency of neural impulses delivered by another neuron to this input.

The output frequency y is approximated by a function

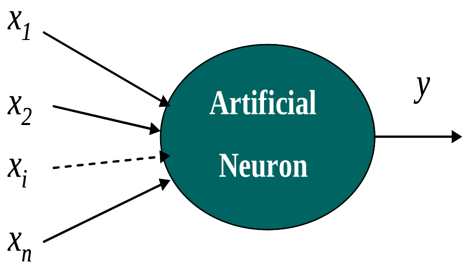

Fig. 2 The simplest model of the artificial neuron

$$y = c \cdot f\left(\sum_i x_i w_i - \theta\right), \tag{1}$$

where f() is the Heaviside function:

$$f(\cdot) = \begin{cases} 1, \text{ for positive argument} \\ 0, \text{ for negative or zero argument} \end{cases} \tag{2}$$

The principle of a single input neuron operating is present in fig. 3a and in fig. 3 b the principle of multiple inputs neuron operating.

In both these windows it can be separately select the input, the threshold, the weight and the activation function.

For implement this software package it was design a Java class, Neuron, was implemented. This Java class was use in all modules of the package software.

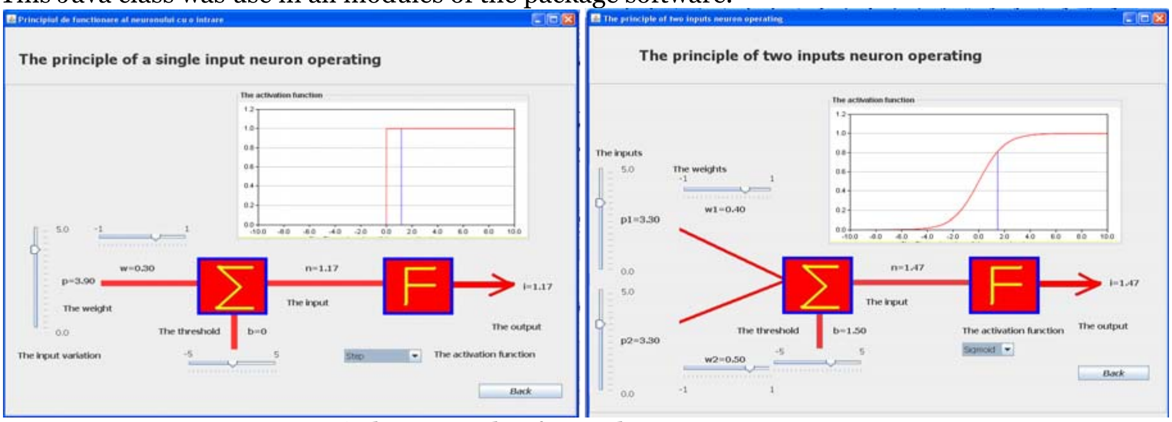

Fig. 3. a)The principle of a single input neuron operating
b) The principle of two inputs neuron operating

The "Simple network" option is design in order to analyze a simple neural network operating mode. Like the other two previous options it can be separately select the input, the threshold, the weight and the activation function for each neuron.

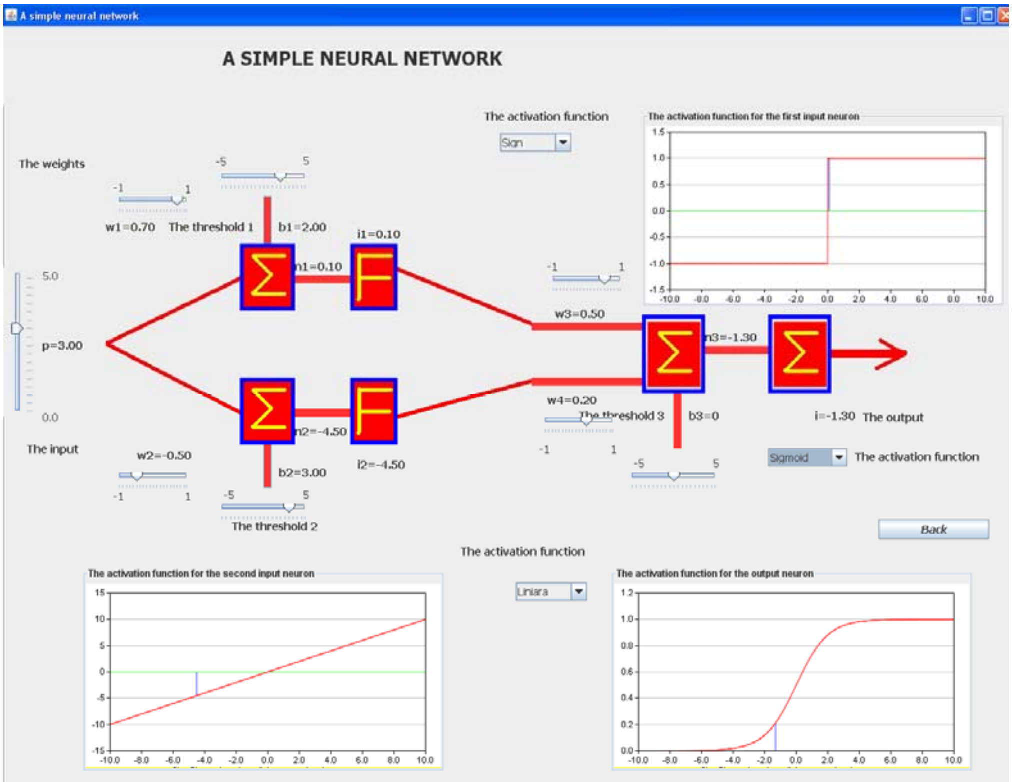

Fig. 4. The principle of a simple neural network operating

The last option of the software package is design in order to study the backpropagation network and the training algorithm for this network.

A BackPropagation network consists of at least three layers of units: an input layer, at least one intermediate hidden layer, and an output layer (see Figure 5) Typically, units are connected in a feed-forward fashion with input units fully connected to units in the hidden layer and hidden units fully connected to units in the output layer. When a BackPropropagation network is cycled, an input pattern is propagated forward to the output units through the intervening input-to-hidden and hidden-to-output weights [3].

With BackPropropagation networks, learning occurs during a training phase in which each input pattern in a training set is applied to the input units and then propagated forward. The pattern of activation arriving at the output layer is then compared with the correct (associated) output pattern to calculate an error signal. The error signal for each such target output pattern is then back propagated from the outputs to the inputs in order to appropriately adjust the weights in each layer of the network. After a BackPropagation network has learned the correct classification for a set of inputs, it can be tested on a second set of inputs to see how well it classifies untrained patterns. Thus, an important consideration in applying BackPropagation learning is how well the network generalizes [3]. Backpropagation, or propagation of error, is a common method of teaching artificial neural networks how to perform a given task [4]. The backpropagation algorithm is:

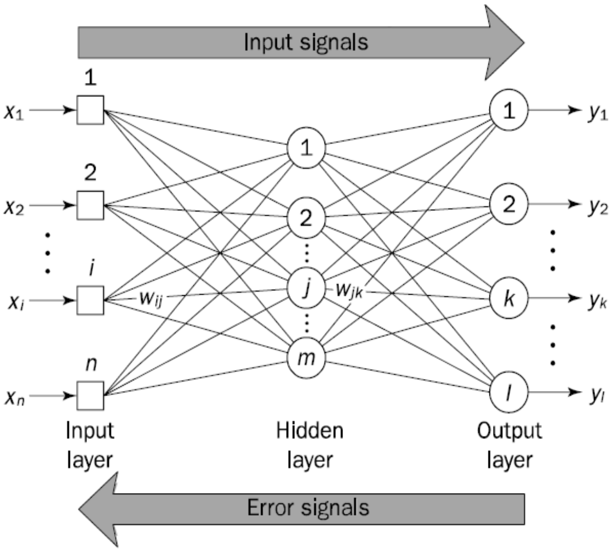

Fig. 5 A three layer backpropagation network

Step 1. Initialisation.

Set all the weights and threshold levels of the network to random numbers uniformly distributed inside a small range[5], typically (-2.4/Fi , 2.4/Fi), where Fi is the total number of inputs of neuron i;

Step 2. Activation

Activate the back-propagation neural network by applying inputs $x_1(p), x_2(p),..., x_n(p)$, and desired outputs $y_{d,1}(p), y_{d,2}(p),..., y_{d,n}(p)$,

(a) Calculate the actual outputs of the neurons in the hidden layer:

$$y_j(p) = \mathrm{sigmoid}\left[\sum_{i=1}^{n} x_i(p) \cdot w_{ij}(p) - \theta_j\right] \tag{3}$$

(b) Calculate the actual outputs of the neurons in the output layer

$$y_k(p) = \mathrm{sigmoid}\left[\sum_{j=1}^{m} x_{jk}(p) \cdot w_{jk}(p) - \theta_k\right] \tag{4}$$

Step 3: Weight training

Update the weights in the back-propagation network propagating backward the errors associated with output neurons.

(a) Calculate the error gradient for the neurons in the output layer

$$\delta_k(p) = y_k(p) \cdot [1 - y_k(p)] \cdot e_k(p) \tag{5}$$

(b) Calculate the weight corrections

$$\Delta w_{jk}(p) = \alpha \cdot y_j(p) \cdot \delta_k(p) \tag{6}$$

Update the weights at the output neurons

$$w_{jk}(p+1) = w_{jk}(p) + \Delta w_{jk}(p) \tag{7}$$

(c) Calculate the error gradient for the neurons in the hidden layer

$$\delta_j(p) = y_j(p) \cdot [1 - y_j(p)] \cdot \sum_{k=1}^{l} \delta_k(p) \cdot w_{jk}(p) \tag{8}$$

Calculate the weight corrections and update the weights at the hidden neurons

Step 4: Iteration

Increase iteration p by one, go back to Step 2 and repeat the process until the selected error criterion is satisfied.

In fig. 6 is show the graphical user interface for training algorithm. As can see, it can be selected some options, the learning rate, the number of training cycles and the logical function for approximation.

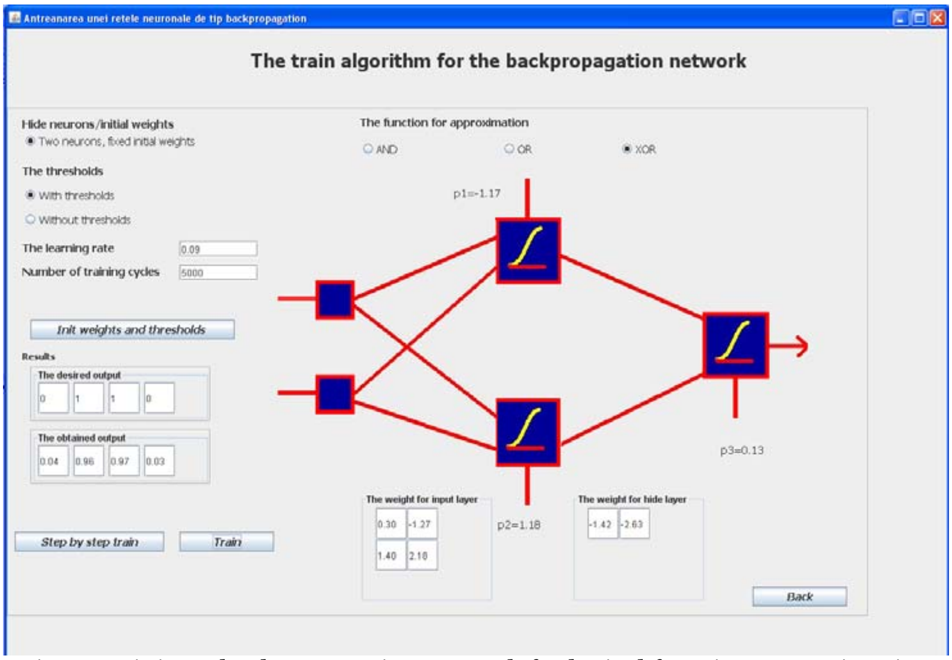

Fig. 6 Training a backpropagation network for logical function approximation

In the figures 7, 8 and 9 are the results of a study that show the dependency of mean square error to the learning rate for 500, 3000 and 5000 training cycles.

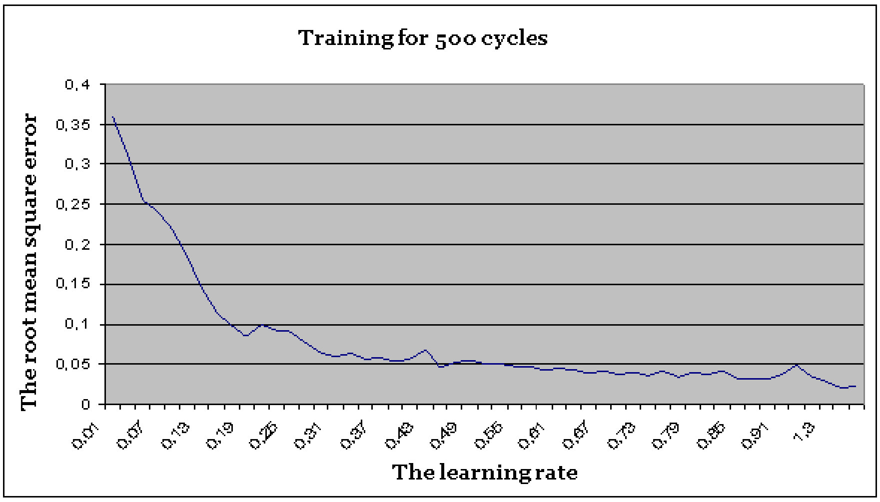

Fig. 7. The dependency of mean square error to the learning rate for 500 cycles

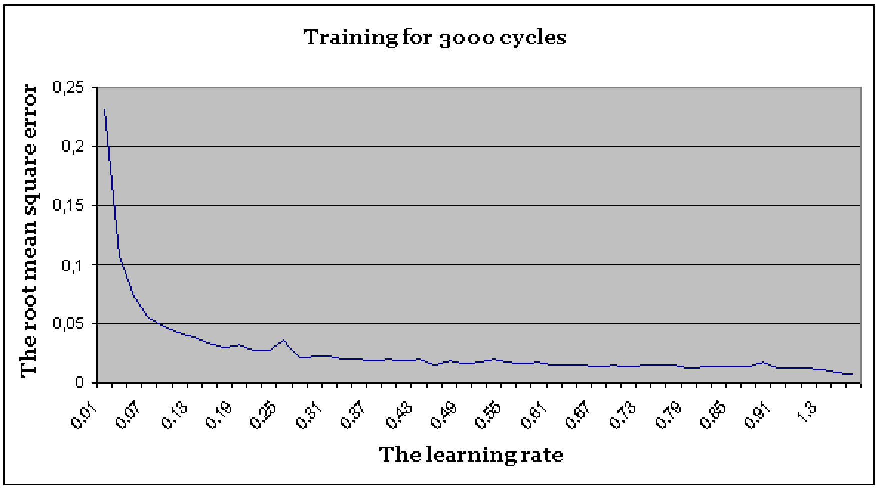

Fig. 8. The dependency of mean square error to the learning rate for 3000 cycles

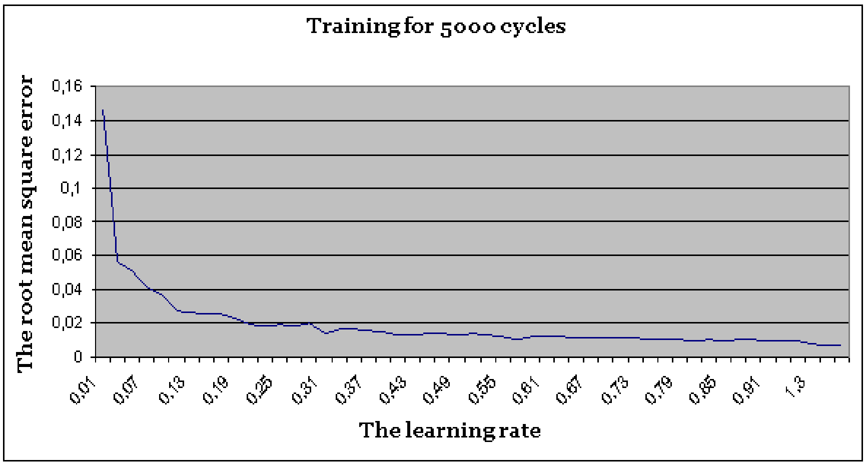

Fig. 9. The dependency of mean square error to the learning rate for 5000 cycles

3. CONCLUSIONS

In this paper an interactive software package was describe. The software can be use as a educational tool for a better understand of neural networks especially of backpropagation neural networks. It was also present some results of running the backpropagation algorithm and the dependency of mean square error to the learning rate of the algorithm. Using object oriented design and Java language allowed us to ease extendibility for the software.

REFERENCES

[1.] Emilio Garcia Rosello , Jose B. Garcia Perez-Schofield, Jacinto Gonzalez Dacosta, Manuel Perez-Cota, Neuro-Lab: A Highly Reusable Software-Based Environment to Teach Artificial Neural Networks, Computer Application in Engineering Education, vol 11, Issue 2, pp 93-102, 2003
[2.] Aybars Ugur, Ahmet Cumhur Kinaci , A Web-Based Tool For Teaching Neural Network Concepts, Computer Application in Engineering Education, Volume 18, Issue 3, pages 449–457, September 2010
[3.] http://www.itee.uq.edu.au/~cogs2010/cmc/chapters/BackProp/
[4.] http://en.wikipedia.org/wiki/Backpropagation
[5.] Michael Negnevitsky - Artificial Intelligence A Guide to Intelligent Systems, editura Addison-Wesley,2005

INTERNATIONAL SYMPOSIUM on
ADVANCED ENGINEERING & APPLIED MANAGEMENT
– 40th ANNIVERSARY in HIGHER EDUCATION (1970-2010)
4 – 5 November, 2010, Hunedoara, ROMANIA

[1.]Diana Alina BISTRIAN, [2.]Mihaela OSACI, [3.]Marcel TOPOR

NUMERICAL INVESTIGATION OF SWIRLING FLOWS STABILITY USING MATLAB DISTRIBUTED COMPUTING SERVER ON A WINDOWS OPERATING SYSTEM ENVIRONMENT

[1-3.] "POLITEHNICA" UNIVERSITY OF TIMISOARA, FACULTY OF ENGINEERING OF HUNEDOARA, DEPARTMENT OF ELECTRICAL ENGINEERING AND INDUSTRIAL INFORMATICS, ROMANIA

ABSTRACT:
This paper presents an evaluation of the parallel processing for meshless algorithm for solving Navier-Stokes problems in fluid dynamics. The fluid dynamics existing solvers take use of finite element methods which are cumbersome and very exhaustive in computational resources. Meshless algorithms uses a different approaches using high level eigenvalue solvers. In order to evaluate the parallel processing performance, a cluster using Matlab development environment was build. Using the Matlab parallel and distributed toolbox it was possible to perform a profiling of the algorithm and to observe the eventual bottlenecks and flaws of the algorithm. Using this approach we obtained a very effective tool for processing the numerical stability investigation of the swirling flow in the Francis hydropower turbine.
KEYWORDS:
Cluster technology, parallel computational algorithms, fluid dynamics spatial stability, swirling flow, meshless method

1. CONSIDERATIONS ABOUT PARALLEL COMPUTING

Parallel programming and the design of efficient parallel programs have been well established in high-performance, scientific computing for many years. The simulation of scientific problems is an important area in natural and engineering sciences of growing importance. More precise simulations or the simulations of larger problems need greater and greater computing power and memory space. In the last decades, high-performance research included new developments in parallel hardware and software technologies [1-4] and a steady progress in parallel high-performance computing can be observed. Popular examples are simulations of weather forecast based on complex mathematical models involving partial differential equations or crash simulations from car industry based on finite element methods [5].

Other examples include drug design and computer graphics applications for film and advertising industry [6]. Depending on the specific application, computer simulation is the main method to obtain the desired result or it is used to replace or enhance physical experiments. A typical example for the first application area is weather forecast where the future development in the atmosphere has to be predicted, which can only be obtained by simulations [7]. In the second application area, computer simulations are used to obtain results that are more precise than results from practical experiments or that can be performed with less financial effort. An example is the use of simulations to determine the air resistance of vehicles [8]. Compared to a classical wind tunnel experiment, a computer simulation can give more precise results because the relative movement of the vehicle in relation to the ground can be included in the simulation. This is not possible in the wind tunnel, since the vehicle cannot be moved. Crash tests of vehicles are an obvious example where computer simulations can be performed with less financial effort.

Computer simulations often require a large computational effort. A low performance of the computer system used can restrict the simulations and the accuracy of the results obtained significantly. In particular, using a high-performance system allows larger simulations which lead to better results. Therefore, parallel computers have often been used to perform computer simulations. Today, cluster systems built up from server nodes are widely available and are now often used for parallel simulations. To use parallel computers or cluster systems, the computations to be performed must be partitioned into several parts which are assigned to the parallel resources for execution. These computation parts should be independent of each other, and the algorithm performed must provide enough independent computations to be suitable for a parallel execution. This is normally the case for scientific simulations. To obtain a parallel program, the algorithm must be formulated in a suitable programming language. Parallel execution is often controlled by specific runtime libraries or compiler directives which are added to a standard programming language like C, Fortran, or Java [9-13].

MATLAB [14] is currently the dominant language of technical computing with approximately one million users worldwide, many of whom can benefit from the increased power offered by widely available multicore processors and multinode computing clusters. MATLAB is also an ideal environment for learning about parallel computing, allowing the user to focus on parallel algorithms instead of the details of the implementation.

Higham & Higham [15] and Moler [16] offer an introduction to MATLAB in their surveys. In [17] Jeremy Kepner introduces the theory, algorithmic notation, and an „under the hood" view of distributed array programming. He discusses metrics for evaluating performance and coding of a parallel program. A selected survey of parallel application analysis techniques are presented in this book, with a particular emphasis on how the examples used in the book relate to many wider application domains. In [18], Rauber and Runger take up the new development in processor architecture by giving a detailed description of important parallel programming techniques that are necessary for developing efficient programs for multicore processors as well as for parallel cluster systems or supercomputers. Both shared and distributed address space architectures are covered.

Parallel programming is an important aspect of high-performance scientific computing but it used to be a niche within the entire field of hardware and software products. However, more recently parallel programming has left this niche and will become the mainstream of software development techniques due to a radical change in hardware technology. Major chip manufacturers have started to produce processors with several power efficient computing units on one chip, which have an independent control and can access the same memory concurrently. Normally, the term core is used for single computing units and the term multicore [19, 20] is used for the entire processor having several cores. Thus, using multicore processors makes each desktop computer a small parallel system. The technological development toward multicore processors was forced by physical reasons, since the clock speed of chips with more and more transistors cannot be increased at the previous rate without overheating. Multicore architectures in the form of single multicore processors, shared memory systems of several multicore processors, or clusters of multicore processors with a hierarchical interconnection network will have a large impact on software development. In 2009, dual-core and quad-core processors are standard for normal desktop computers, and chip manufacturers have already announced the introduction of oct-core processors for 2010. It can be predicted from Moore's law [21] that the number of cores per processor chip will double every 18–24 months. According to a report of Intel, in 2015 a typical processor chip will likely consist of dozens up to hundreds of cores where a part of the cores will be dedicated to specific purposes like network management, encryption and decryption, or graphics [22].

As computational fluid dynamics (CFD) matures so rise the expectations of what it can or should deliver. Practitioners and designers are no longer content with qualitative statements on trends, but judge the utility and value of CFD by its ability to provide quantitatively accurate predictions for property fields and engineering parameters derived therefrom. In the extreme, theoretical fluid dynamicists expect fully-resolved simulations of turbulence to provide fundamental information on turbulence mechanics of greater accuracy and detail than can be derived from the most sophisticated experimental techniques.

In computational fluid dynamics, several software packages solving either the Euler or the Navier-Stokes equations around complex geometries have been developed and are currently used by aircraft or engine manufacturers. The use of unstructured meshes is one of the most efficient ways to solve complex problems, because they allow high flexibility in specifying a geometry. The possibility of using the modern parallel machines even for unstructured mesh based codes implies the necessity of dealing with two problems: the first one lies on the strategies and algorithms which can be used for the partitioning of the grid and the mapping of the subdomains among the processors; the second one is related to the structure of the code, which has to be designed is such a way that the features of the modern parallel machines are fully exploited.

The first efficient implementation of a 2D unstructured flow solver on MIMD parallel computers was presented by Venkatakrishnan et al [23] in 1992: they demonstrated that a good supercomputer performance can be reached and that a careful implementation of the message passing routines is a critical point, even for an explicit code. In 1995, Lanteri [24] developed a parallel version of an industrial code based on a mixed finite element/finite volume method. The parallelization strategy combines mesh partitioning and message passing programming model: basically, the same old serial code is going to be executed within every subdomain. Modifications occurred in the main loop in order to take into account the assembly phases of the subdomain results.

The literature on these topics can be considered exhaustive for two-dimensional applications and parallel machines of the old generation. The same cannot be said for three-dimensional complex flows and for the new machines in terms of optimization of the performances and assessment of algorithms and techniques (i.e. [25-28]).

2. CLUSTER CONFIGURATION

In this paper we have build and tested a small scale cluster based on a Matlab Parallel Processing Toolbox. Using the internal cluster manager from Matlab we were able to evaluate the algorithm behaviour using a distributed process. In this situations we have perform the profiling and we have noticed a speed increase of the algorithm compared to a single computer run. The cluster was conceived using homogenous hardware

Dell Optiplex 755

Intel(R) Core(TM)2 Duo CPU, 2.66GHz 1.97 GHz, 1.95 GB of RAM

MATLAB Distributed Computing Server (MDCS) is a toolbox that lets users solve computationally and data-intensive problems by executing MATLAB and Simulink based applications on a computer cluster.

For numerical investigation of swirling flows stability, a Windows operating system cluster was configured in Computer Aided Mathematics and Numerical Analysis Laboratory of the Engineering Faculty of Hunedoara (Figure 1).

Figure 1. Computer Aided Mathematics and Numerical Analysis Laboratory at the Engineering Faculty of Hunedoara.

The first step to set up the cluster configuration was to install the MDCS on a node called the head node. The license manager was also installed on the head node. After performing this installation, the MDCS was installed on the other cluster nodes, called worker nodes. Figure 2 shows the installations that was performed on our MDCS cluster nodes.

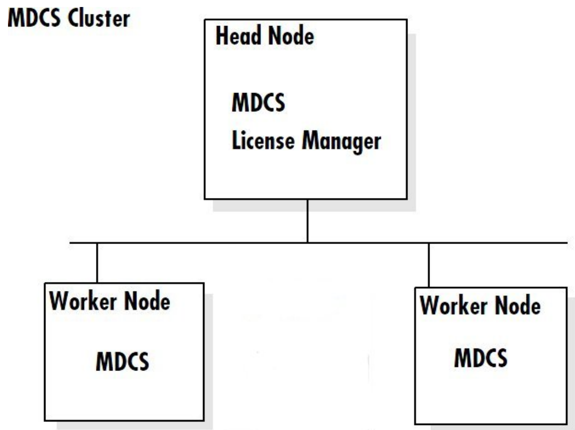

Figure 2. MDCS cluster with local access configuration.

The MDCS service must be running on all machines being used for job managers or workers. This service manages the job manager and worker processes. One of the major tasks of the MDCS service is to recover job manager and worker sessions after a system crash, so that jobs and tasks are not lost as a result of such accidents. To run the MDCS, the license manager must be running on the head node.

We made sure the license manager was running by performing a Status Enquiry. The next step in configuring the cluster was to start the job manager and workers. From the Admin Center, the setup and monitoring utility for the Matlab Distributed Computing Server, we select the list of the hosts in the text box. When Admin Center completed the update, the listing looked like the following Figure 3.

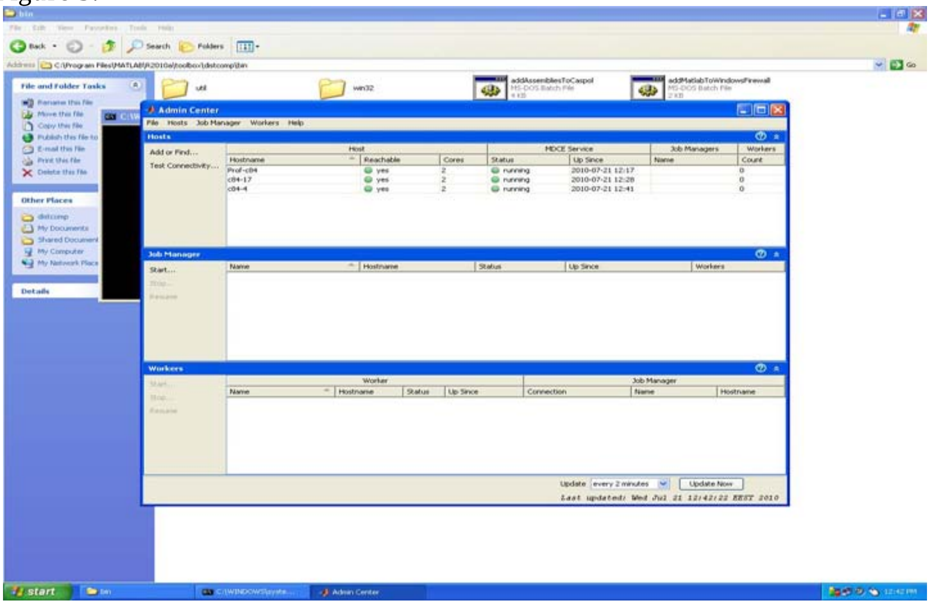

Figure 3. Nodes added in the configuration of the cluster.

At this point, the connectivity between nodes was tested. This assures that the cluster can perform the necessary communications for running MDCS processes. After the cluster configuration was completed, a job manager have been started using the Job Manager module. In the Start Workers dialog box, we specify the number of workers to start on each host, a value that cannot exceed the total number of licenses we have. A number of two workers was set for each host. The Connectivity Testing dialog box shows the results of the last test, reported in Figure 4.

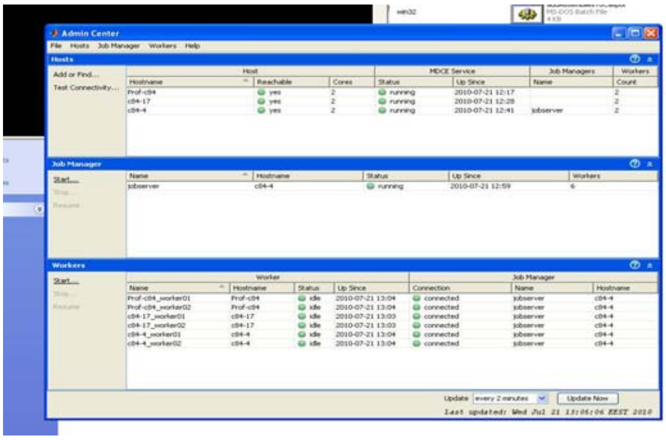

Figure 4. The connectivity test of the configuration of the cluster passed.

3. PARALLEL AND DISTRIBUTED INVESTIGATION OF THE VORTEX ROPE MODEL

The helical vortex breakdown (also known as precessing vortex rope) is a self-induced instability of a swirling flow, encountered in the draft tube cone of hydraulic Francis turbines operated far from the best efficiency. Figure 5 shows the axial and the swirl velocity profiles of the vortex rope model used in our stability analysis.

Let us define the eigenvalue problem governing the hydrodynamic stability in operator formulation

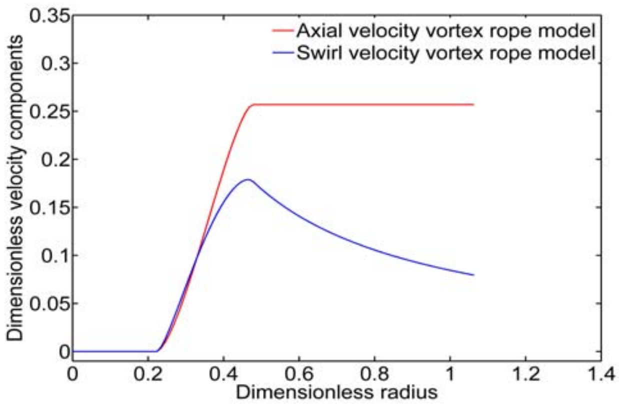

Figure 5 Axial and circumferential velocity profiles.

$$\left(k\,L^{[k]}+\omega L^{[\omega]}+L\right)\mathbf{u}=0,\quad \mathbf{u}=\begin{pmatrix}F & G & H & P\end{pmatrix}^{T} \tag{1}$$

where

$$L^{[k]}=\begin{pmatrix} r & 0 & 0 & 0\\ 0 & U & 0 & 0\\ 0 & 0 & rU & 0\\ U & 0 & 0 & 1\end{pmatrix},\quad L^{[\omega]}=\begin{pmatrix} 0 & 0 & 0 & 0\\ 0 & -1 & 0 & 0\\ 0 & 0 & -r & 0\\ -1 & 0 & 0 & 0\end{pmatrix},\quad L=\begin{pmatrix} 0 & 1+d_r & -m & 0\\ 0 & mW/r & 2W/r & -d_r\\ 0 & W+rdW/dr & mW & m\\ mW/r & dU/dr & 0 & 0\end{pmatrix} \tag{2}$$

The boundary relations are translated into equations that complete the computational model and can be transposed as

$$\sum_{1}^{N}(-1)^{k+1}g_k=\sum_{1}^{N}(-1)^{k+1}h_k=0\,, \tag{3}$$

$$f_2\frac{2}{r_{\max}}+\sum_{\substack{3\\ k\ odd}}^{N}f_k\frac{2(k-1)}{r_{\max}}\left[\sum_{\substack{r=k-1\\ k\ even}}^{2}(-2)\right]+\sum_{\substack{4\\ k\ even}}^{N}f_k\frac{2(k-1)}{r_{\max}}\left[\sum_{\substack{r=k-1\\ k\ odd}}^{2}2+1\right]=0\,, \tag{4}$$

$$p_2\frac{2}{r_{\max}}+\sum_{\substack{3\\ k\ odd}}^{N}p_k\frac{2(k-1)}{r_{\max}}\left[\sum_{\substack{r=k-1\\ k\ even}}^{2}(-2)\right]+\sum_{\substack{4\\ k\ even}}^{N}p_k\frac{2(k-1)}{r_{\max}}\left[\sum_{\substack{r=k-1\\ k\ odd}}^{2}2+1\right]=0\,, \tag{5}$$

$$\frac{2W_{r\max}}{r_{\max}}\sum_{1}^{N}h_k-p_2\frac{2}{r_{\max}}-\sum_{\substack{3\\ k\ odd}}^{N}p_k\frac{2(k-1)}{r_{\max}}\left[\sum_{\substack{r=k-1\\ k\ even}}^{2}2\right]-\sum_{\substack{4\\ k\ even}}^{N}p_k\frac{2(k-1)}{r_{\max}}\left[\sum_{\substack{r=k-1\\ k\ odd}}^{2}2+1\right]=0\,, \tag{6}$$

$$\sum_{1}^{N}g_k=0\,,\ (kU_{r\max}-\omega)\sum_{1}^{N}h_k=0\,,\ k\left(U_{r\max}\sum_{1}^{N}f_k+\sum_{1}^{N}p_k\right)-\omega\sum_{1}^{N}f_k=0\,. \tag{7}$$

The numerical investigation employed both the positive and the negative modes. Let us define by the critical frequency that temporal frequency corresponding to a maximum growth rate for a given mode number. The numerical results are summarized in Table 1.

Table 1 The critical frequency and the maximum growth rates obtained for the investigated modes

Mode m	–3	–2	–1	0	1	2	3
Critical Frequency	0.1	0.3	0.3	0.3	0.3	0.3	0.35
Maximum Growth Rate	14.129	11.947	6.932	0.043	0.544	0.535	0.395

Figure 6 presents the three dimensional map of the growth rate as function of the frequency and mode number and the density map of the growth rate. The negative modes present an amplitude increase depending on the mode number. However, these amplitude growth rates increase linear up to a frequency of 0.25 both for the positive and negative modes.

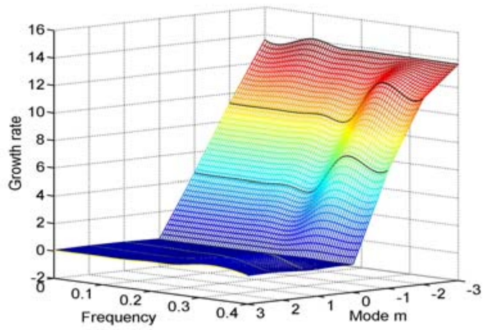

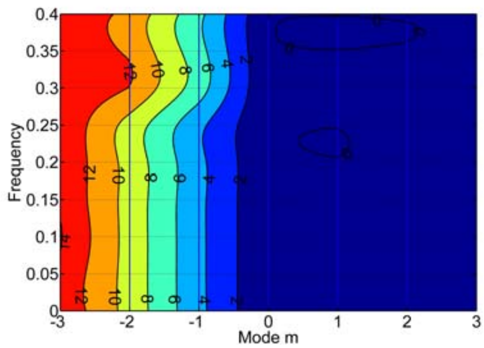

Figure 6. Plot of the growth rate as function of frequency and mode (left) and density map (right).

The convergence behavior of the collocation algorithm for $m=-1$ case is reported in Table 2 on few cluster configurations with six, four and two labs, respectively. It is noticeable that the time increase is relevant when the numerical experiments run on four labs configuration instead of 2 labs configuration. The time increase becomes irrelevant when the number of cluster nodes is increased at six labs, thus the conclusion that the cluster has no need to be extended for numerical improvements of our stability analysis.

Table 2. Elapsed time (in seconds) of the numerical computation for mode $m = -1$, on three cluster configurations.

N	Critical frequency	Elapsed time on 2 labs	Elapsed time on 4 labs	Elapsed time on 6 labs
5	0.25	1.463658	0.196285	0.211601
6	0.1	1.569234	0.225536	0.193199
8	0.1	1.584621	0.210344	0.222434
10	0.25	1.611874	0.328014	0.341408
12	0.3	1.632951	0.345925	0.360558
16	0.3	1.751369	0.431654	0.431196
17	0.3	1.836951	0.460168	0.451093
19	0.3	1.854693	0.519268	0.524420
29	0.3	2.234852	1.005637	1.015383
32	0.3	2.672955	1.479596	1.448778
37	0.3	2.895647	1.682333	1.726657
40	0.3	3.269854	2.064365	2.087408
46	0.3	4.125965	2.942432	2.948638
61	0.3	8.264985	6.453132	6.318485

4. CONCLUSION

The cluster technology represents the state of the art in computational technology. This extends the limit imposed by the single computer analysis, reducing in a large manner the amount of time required for solving complex mathematical models. Using a rather usual hardware (desktop PCs) it is possible to obtain a significant acceleration of the computation process. However, the acceleration depends on the algorithm structure and it is necessary to perform a profiling of the solving process (that means to analyze carefully the behavior of the computational process- the number of steps required, the mathematical operations involved, the size of matrix variables) in order to avoid the eventual bottlenecks in the algorithm.

REFERENCES

[1.] Culler, D.E., Singh, J.P., Gupta, A., Parallel Computer Architecture: A Hardware Software Approach, Morgan Kaufmann, San Francisco, 1999.
[2.] Conway, M.E., A Multiprocessor System Design, In Proceedings of the AFIPS 1963 Fall Joint Computer Conference, volume 24, pages 139–146, Spartan Books, New York, 963.
[3.] Chin, A., Complexity Models for All-Purpose Parallel Computation, In Lectures on Parallel Computation, chapter 14. Cambridge University Press, Cambridge, 1993.
[4.] Bertsekas, D.P., Tsitsiklis, J.N., Parallel and Distributed Computation, Athena Scientific, Nashua, 1997.
[5.] Braess, D., Finite Elements, 3rd edition, Cambridge University Press, Cambridge, 2007.
[6.] Krikelis, A., Parallel Multimedia Computing, Parallel Computational Fluid Dynamics Recent Developments and Advances Using Parallel Computers, Elsevier Science B.V., 1998.
[7.] Gulzow, V., Diehl, T., Foelkel, F., About the Parallelization of Climate Models, Parallel Computing: Fundamentals, Applications and New Directions, Elsevier Science B.V., 1998.
[8.] Reid, J., Supalov, A., Thole, C.A., PARASOL Interface to New Parallel Solvers for Industrial Applications, Parallel Computing: Fundamentals, Applications and New Directions, Elsevier Science B.V., 1998.
[9.] Allen, R., Kennedy, K., Optimizing Compilers for Modern Architectures, Morgan Kaufmann, San Francisco, 2002.
[10.] Bishop, P., Warren, N., JavaSpaces in Practice, Addison Wesley, Reading, 2002.
[11.] Bodin, F., Beckmann, P., Gannon, D.B., Narayana, S., Yang, S., Distributed C++: Basic Ideas for an Object Parallel Language. In Proceedings of the Supercomputing'91 Conference, pages 273–282, 1991.
[12.] Dongarra, J., Performance of various Computers using Standard Linear Equations Software in Fortran Environment. Technical Report CS-89–85, Computer Science Department, University of Tennessee, Knoxville, 1990.
[13.] Kennedy, K., Koelbel, C., Zima, H., The Rise and Fall of High Performance Fortran: An Historical Object Lesson. In HOPL III: Proceedings of the Third ACM SIGPLAN Conference on History of Programming Languages, pages 7–1–7–22, ACM, New York, 2007.

[14.] www.mathworks.com
[15.] Higham, D.J., Higham, N.J., MATLAB Guide, Second Edition, SIAM, Philadelphia, 2005.
[16.] Moler, C., Numerical Computing with MATLAB, SIAM, Philadelphia, 2004.
[17.] Kepner, J., Parallel MATLAB for Multicore and Multinode Computers, SIAM, Philadelphia, ISBN 978-0-898716-73-3, 2009.
[18.] Rauber, T., Runger, G., Parallel Programming for Multicore and Cluster Systems, Springer-Verlag Berlin Heidelberg, ISBN 978-3-642-04817-3, 2010.
[19.] Jaja, J., An Introduction to Parallel Algorithms, Addison-Wesley, New York, 1992.
[20.] Lenoski, D.E., Weber, W., Scalable Shared-Memory Multiprocessing, Morgan Kaufmann, San Francisco, 1995.
[21.] Koch, G., Discovering Multi-core: Extending the Benefits of Moore's Law, Intel White Paper, Technology@Intel Magazine, 2005.
[22.] Kuck, D., Platform 2015 Software-Enabling Innovation in Parallelism for the Next Decade, Intel White Paper, Technology@Intel Magazine, 2005.
[23.] Venkatakrishnan, V., Simon, H.D., Barth, T., A MIMD implementation of a parallel Euler solver for unstructured grids, The J. of Supercomputing 6, pp. 117-137, 1992.
[24.] Lanteri, S., Parallel solutions of Three-Dimensional compressible flows', INRIA, Rapport de recherche n. 2594, June 1995.
[25.] Diurno, W.G., Higher Order Solution of the Compressible Viscous Flows Arising in Aerothermodynamics Using a Finite Element Method, Proc, AIDAA Congress, Roma (Italy), 11-15 September 1995.
[26.] Barth, T.J., Aspects of Unstructured Grids and Finite-Volume Solvers for the Euler and Navier Stokes Equations, VKI - AGARD R 787, 1992.
[27.] Peraire, J., Peiro, J., Morgan, K., Multigrid Solution of the 3-D Compressible Euler Equations on Unstructured Tetrahedral grids, Int. J. Num. Meth. in Engin. 36, 1993.
[28.] Bucchignani, E., Diurno, W.G., Parallel computation of inviscid 3D flows with unstructured domain partitioning: performances on SGI-Power Challenge Supercomputer, Parallel Computing: Fundamentals, Applications and New Directions Elsevier Science B.V., 1998.

INTERNATIONAL SYMPOSIUM on ADVANCED ENGINEERING & APPLIED MANAGEMENT
– 40th ANNIVERSARY in HIGHER EDUCATION (1970-2010).

INTERNATIONAL SYMPOSIUM on ADVANCED ENGINEERING & APPLIED MANAGEMENT
– 40th ANNIVERSARY in HIGHER EDUCATION (1970-2010),

INTERNATIONAL SYMPOSIUM on
ADVANCED ENGINEERING & APPLIED MANAGEMENT
– 40th ANNIVERSARY in HIGHER EDUCATION (1970-2010)
4 – 5 November, 2010, Hunedoara, ROMANIA

[1] Stela RUSU-ANGHEL, [2] Lucian GHERMAN, [3]Sergiu MEZINESCU

USING THE MATLAB-SIMULINK SIMULATION FOR OPERATING ACTIVE FILTERS ORDERED BY DIGITAL SIGNAL PROCESSOR (DSP)

[1-3] UNIVERSITY POLITEHNICA OF TIMISOARA, FACULTY OF ENGINEERING FROM HUNEDOARA, ROMANIA

ABSTRACT:
The paper proposes the use of a DSP family ADMC330 several ways to control an active filter. It is made available as filter simulation in Matlab-Simulink environment, and the results confirm the effectiveness of the filter.
KEYWORDS:
DSP family, simulation, Matlab-Simulink

1. INTRODUCTION

Figure 1.1. is a schematic diagram of a DSP controlled active filter. The Rp resistors are denoted preloading the filter capacitor C, necessary to limit the current drawn from the converter to the mains connection.

Signals from voltage / current transducers are taken through LEM type, and block 'Adaptation Signals' are made in the range of 0.3 - 3.2 V analog converters acceptable entry - digital. To order using a digital converter evaluation board CMDA signal processor 330 - control processor specifically designed for electric cars.

ADMC330 microprocessor family is part of the signal processor (DSP) which operates fixed-point math calculations. It's characteristics is recommended for high performance control of electrical drives. Among these we mention below the most important:

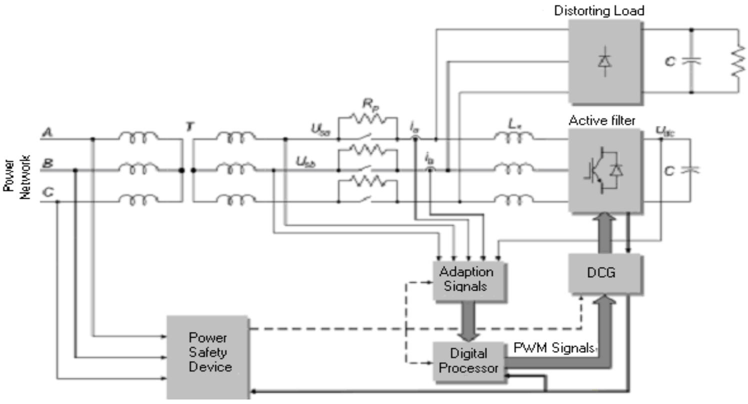

Fig. 1.1. Schematic diagram

- ❖ 20 MHz clock frequency;
- ❖ Seven analog inputs for external signal acquisition;
- ❖ Data acquisition synchronized with the PWM signal;
- ❖ Control signal generator for PWM voltage inverter (Pulse width modulation in - pulse width modulation)
- ❖ Programmer detection dead time and minimum pulse;
- ❖ Minimum inverter frequency 2.5 kHz;
- ❖ Maximum inverter frequency 25 kHz;
- ❖ Generator for the space vector control inverter;
- ❖ Program counter and address two generators;
- ❖ Two 8-bit timers for PWM generation;
- ❖ Eight ports of entry and exit;
- ❖ Implementation of 20 MIPS (million instructions per second);

- Arithmetic logic unit for executing mathematical calculations;
- Mathematical operands displacement unit;
- 50 ns instruction cycle time;
- Type 16-bit timer watchdog to reset the DSP;
- Two synchronous serial ports;
- 2k x 24 bit program memory and data RAM 1k x 16 bits;
- 2k x 24 bit program memory ROM.

The flexibility of the internal structure ADMC330 signal processor, allow for the following operations in a machine cycle (50 ns)

- Generating new program addresses;
- Taking the next instruction stack;
- Achieving two data moves;
- Loading two data pointers with addresses;
- Performing a calculation operation.

The processor can also independently control the peripherals that are fitted, so while it may do the following:

- Generation of three PWM signals for inverter;
- Generation of the two auxiliary PWM signals generators;
- The acquisition of four analog channels;
- Control of eight digital input / output pin;
- Decrementing timer control program (Watchdog).

ADMC330 processor includes internal memory as we have seen, so the 2K monitor ROM program is to interface with a PC UART for serial communication interface, boot loader, mathematical tables to implement the following functions: sine, cosine, tangent and inverse tangent, logarithm and inverse logarithm, square root, inverse function, divide unsigned, transformations from Cartesian to polar marker, functions for interpolation.

2. SOFTWARE SIMULATION SYSTEM USING MATLAB-SIMULINK

Four schemes were carried out using both types of construction, with and without feedback loop, for three-phase voltage sources but nonlinear loads balanced (neutral wireless). The first two schemes will be presented using real-time Fourier analysis of the currents on each phase.

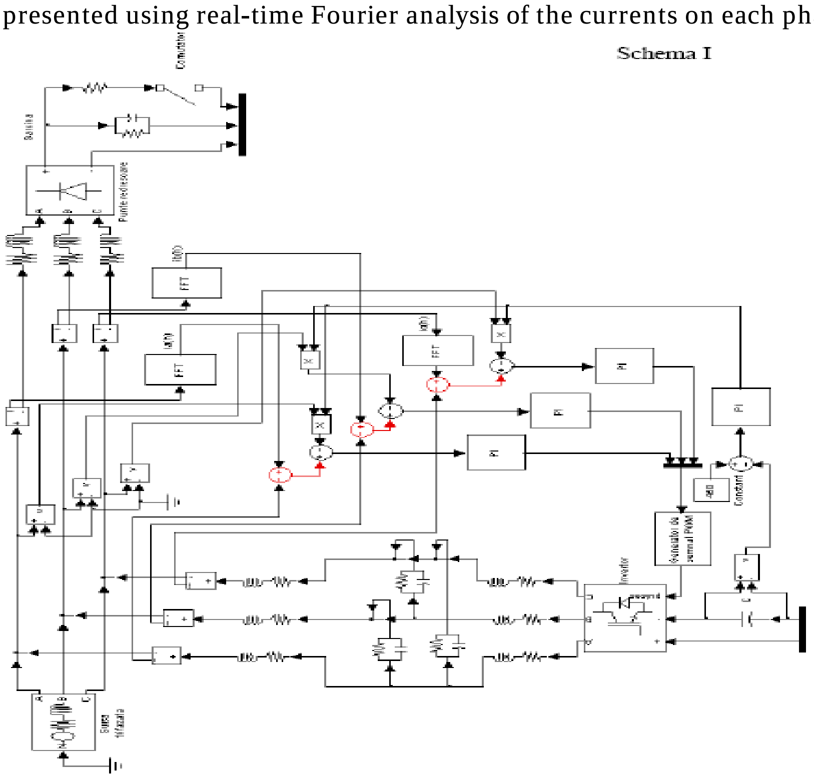

Fig. 2.1. FFT alternative work schedule

Fourier transform is calculated using the fastest FFT algorithm. By Fourier analysis of the currents on each phase has succeeded in its breakdown of its component harmonics. Recomposed signal using only the higher order harmonics (less than first harmonic), it is a signal that will be introduced in the network with the sign reversed. So the grid will run a first harmonic signal. This method is applied to the first scheme.

A second solution is to calculate only the fundamental harmonic is then subtracted from the total current network to produce the higher harmonic current is given by the opposite sign is the reference active filters. Such an approach is adopted in the sliding mode option, which is shown in diagram two.

In the following we present diagrams made for each model calculation and simulation results obtained.

FFT block in the current decomposition of its component harmonics. Computer program called the block "MATLAB Function" allows the extraction of harmonics first. IFFT block recomposed signal using only higher order harmonics, resulting in a signal that will be introduced in the network with the sign reversed.

Below are the results obtained by simulation.

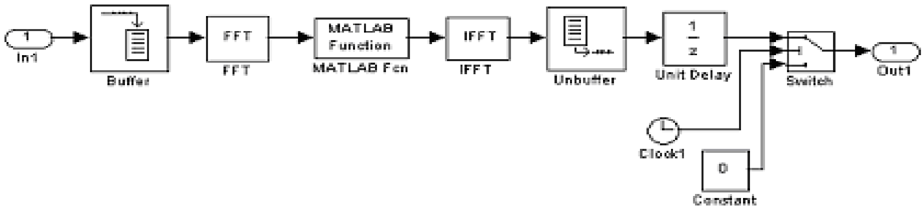

Fig. 2.2. FFT block

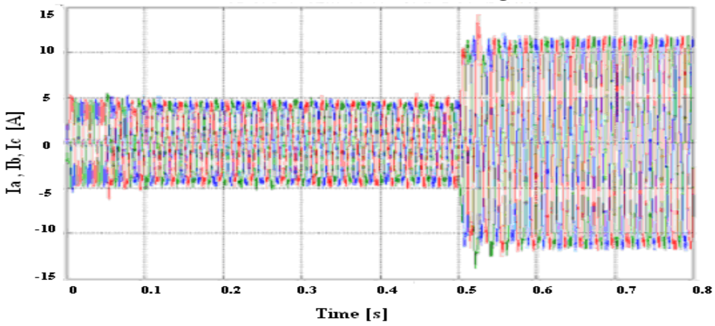

Fig. 2.3. The mains currents

In Fig 2.3 the currents are presented mains throughout the simulation period. In the interval (0 - 0.1) current network is not filtered, at time 0.1 comes into the active filter. 0.5 At the burden is doubled.

In Fig. 2.4 phase currents are given power to the system without active filter. It can be seen as their harmonic due to the presence of higher order harmonics.

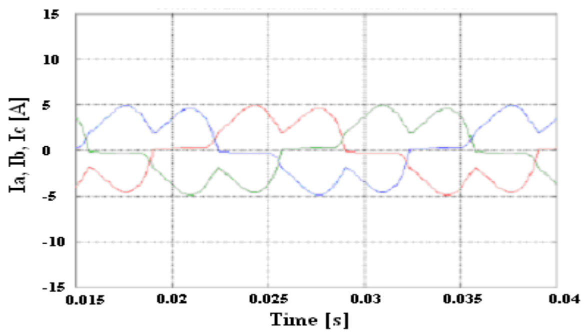

Fig. 2.4. The mains currents without filter

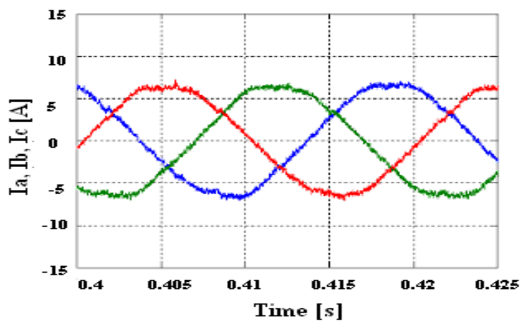

Fig. 2.5. The mains currents active filter

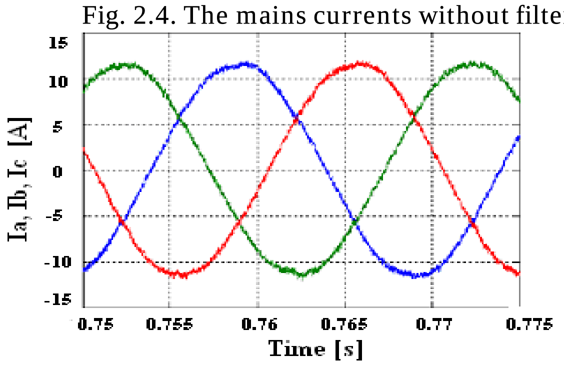

Fig. 2.6. Power supply currents for

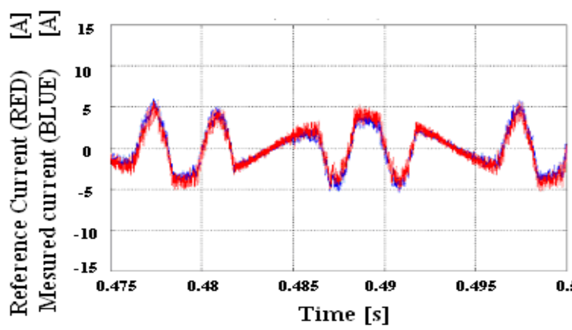

Fig. 2.7. Current compensation
the double burden

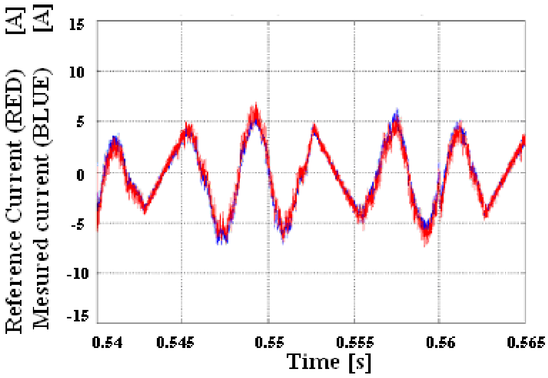

Fig. 2.8. Current produced by the active filter compensation

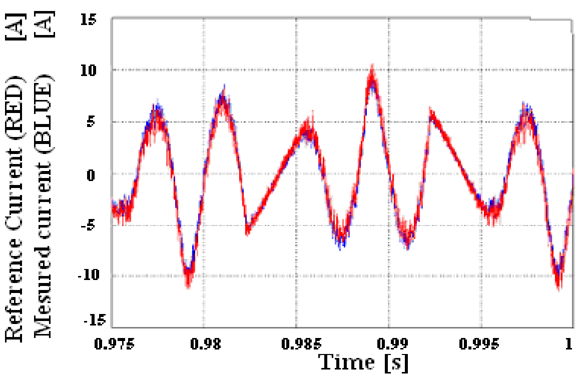

Fig. 2.9.Curent double load compensation

From Fig. 2.5 can be observed that with the arrival of an active filter, three-phase currents are sinusoidal mains.

In Fig. 2.6 we presents three mains currents, the active filter for a dual task.

In Figures 2.7 , 2.8 and 2.9, the reference current (red) are harmonics with opposite sign that must be placed on the network. The blue is injected currents in inverter network.

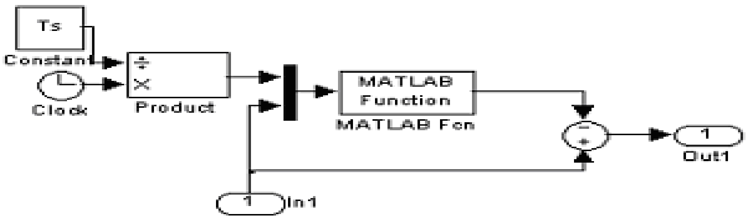

Fig.2.10. Sliding FFT block

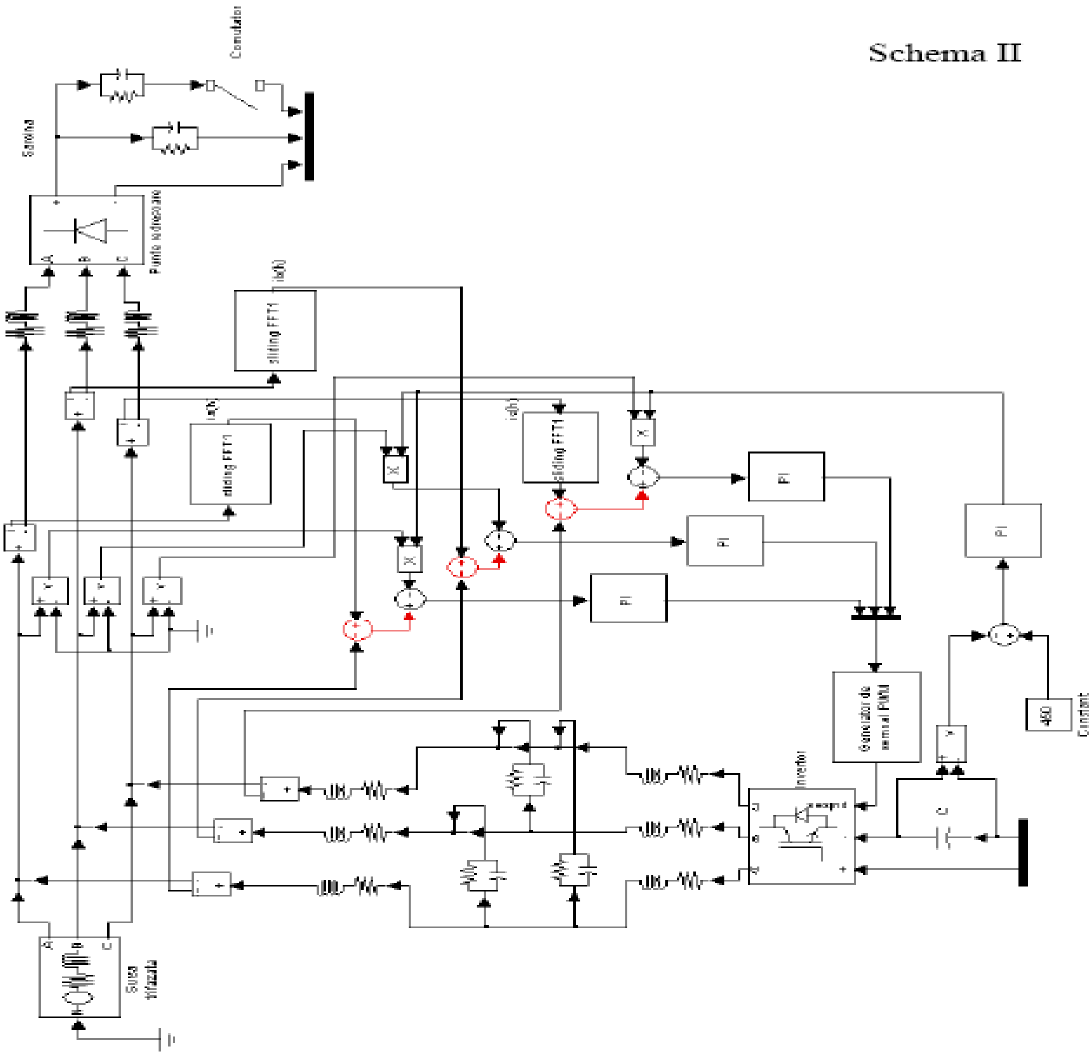

Fig. 2.11. Alternative work schedule with sliding FFT mode

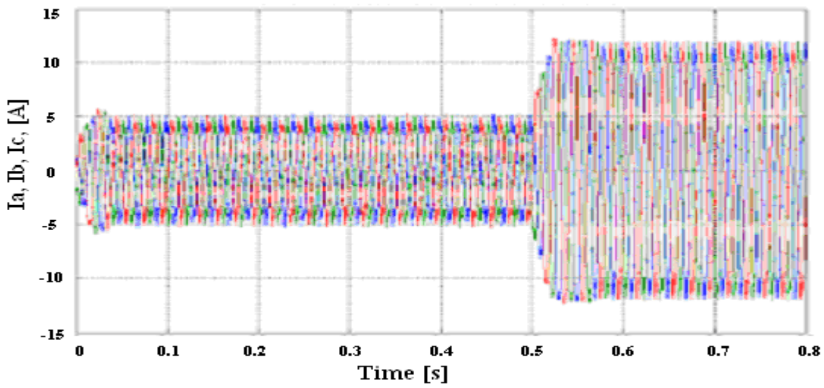

Fig. 2.12. The mains currents throughout the simulation time

Extract the first harmonic sliding FFT block which then decreased the current network consists of harmonics resulting in a higher power.

In the following we present scheme for model calculation carried in variant sliding mode.

In Fig. 2.12. currents are presented mains throughout the simulation period. Results obtained from simulation with the sliding mode method are similar to those obtained in the FFT version. The only notable difference is that there is an increasing burden smooth current growth.

Unfortunately, this method has the disadvantage that it requires real-time applications using DSP with large memory. This leads to the impossibility of using cheap DSP having more than one Kb of RAM. In this case we propose another solution that enables the calculation based on the fundamental harmonic active and reactive power (by averaging the instantaneous value).

In the following experimental results will be presented.

On the basis of this technique is that transfers of active and reactive power defined as the product of the fundamental harmonic voltage and currents is real only on the first harmonic current harmonic currents rest do not give power. Unfortunately, in some applications the source voltage contains higher harmonics. For this reason the calculation of power is no longer used that tension, but tension given by a PLL circuit realized by software and implemented on a DSP which provides as output a sinusoidal signal in phase with the fundamental harmonic amplitude equal to unity. This signal is subtracted from the total current network to produce the higher harmonics given the current reference is changed in sign of active filter.

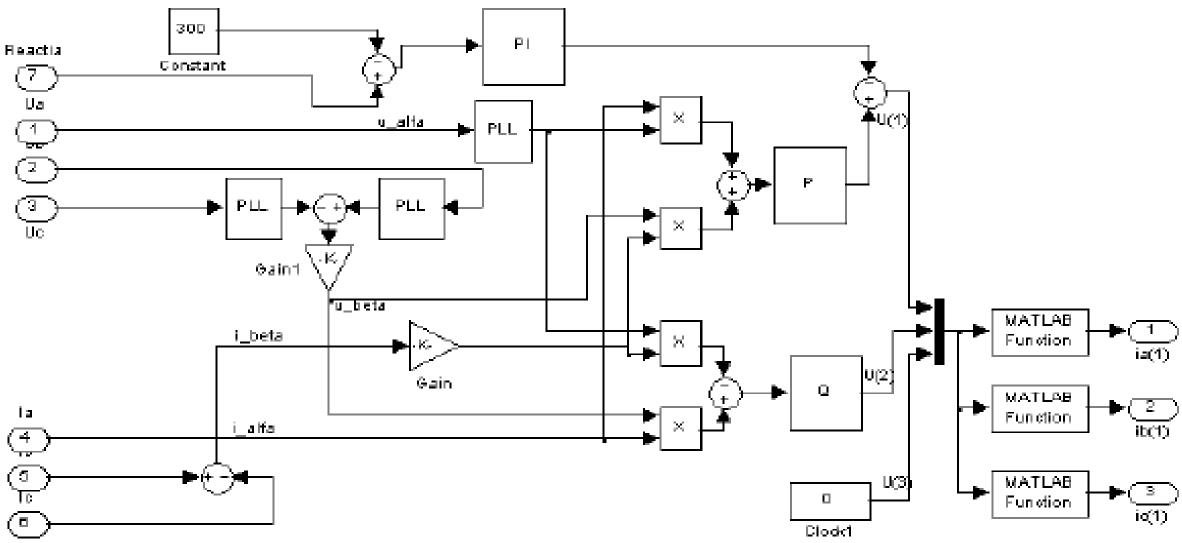

Fig. 2.13. PQ Building

In this block currents and voltages are introduced in three phases. Calculate the first-order harmonic currents. They will then be subtracted from a signal resulting network consists of higher order harmonics to be introduced into the network with the sign reversed.

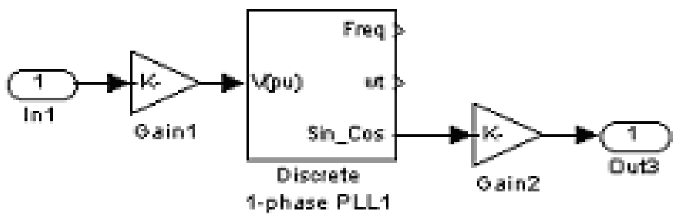

Fig. 2.14. PLL block

In Fig. 2.14. PLL block is presented which provides as output a sinusoidal signal in phase with the fundamental harmonic amplitude equal to unity.

Have been developed for this model two types of construction, with and without feedback loop. In the following we present schemes for the two models made constructive and results obtained from simulation. The former alternative presented feedback loop variant.

Results will be presented in the following experimental. In Fig.2.17 currents are presented mains throughout the simulation period. Note that at time 0.3 with a double load variation occurs due to sudden changes in voltage on the load current, the variation is shown in the figure below. This surge current limiter can be removed from power.

Block P-Q is presented in Fig. 2.13. The difference between the two modes of constructive notice is observed in the manner of placing the measure voltages and currents in relation to the inverter, and how the taxation of reference.

Figures 2.19, 2.20 and 2.21 are shown the three phase currents at different moments in time simulation.

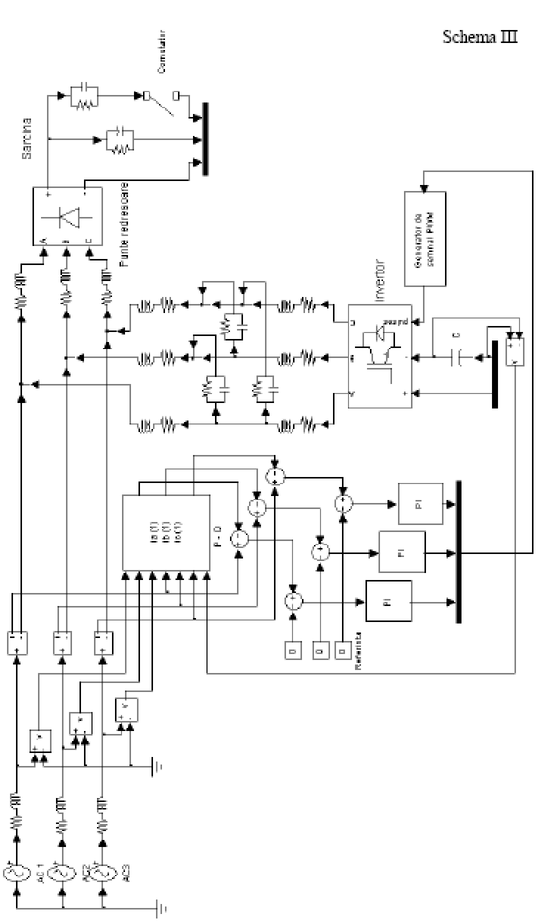

Fig. 2.15. Alternative work schedule PQ-loop response

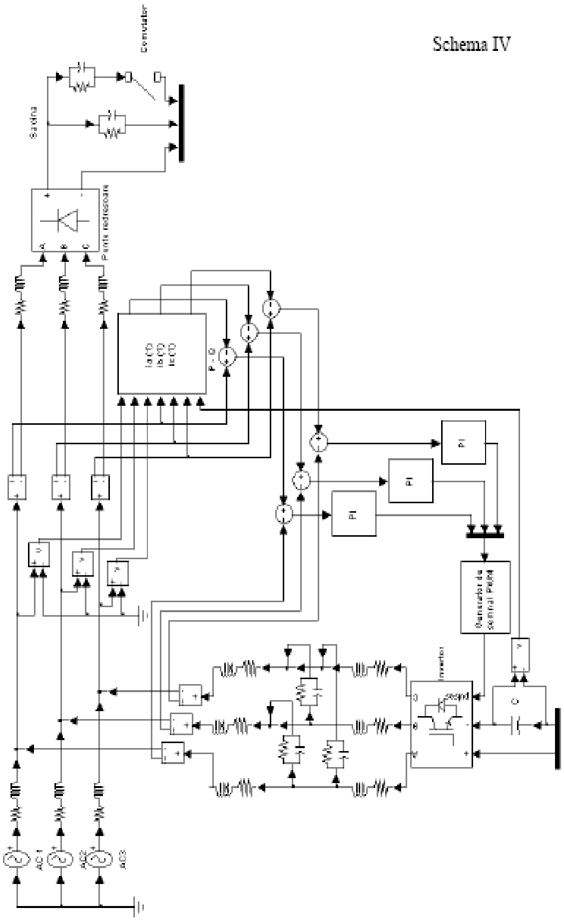

Fig. 2.16. PQ alternative work schedule without feedback loop

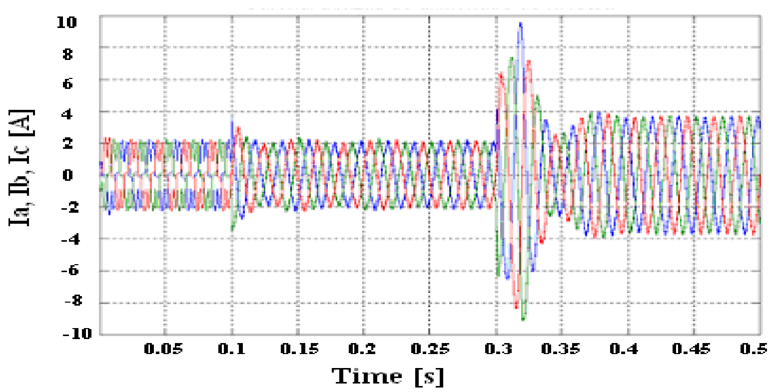

Fig. 2.17. Mains currents throughout the simulation time

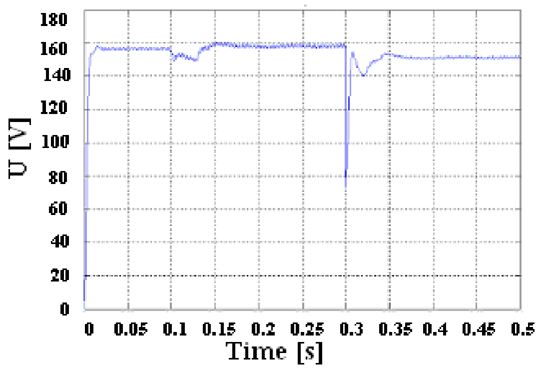

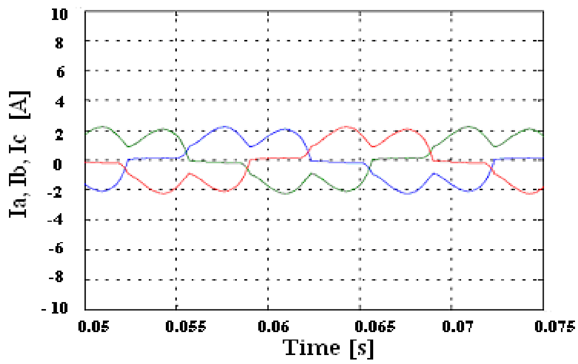

Fig. 2.18. Voltage on the load
the mains supply without active filter

Fig. 2.19 Three-phase currents from

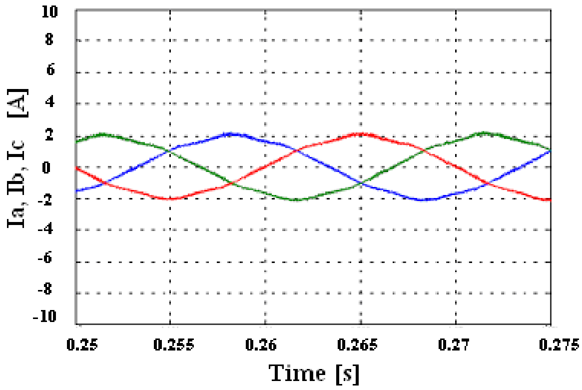

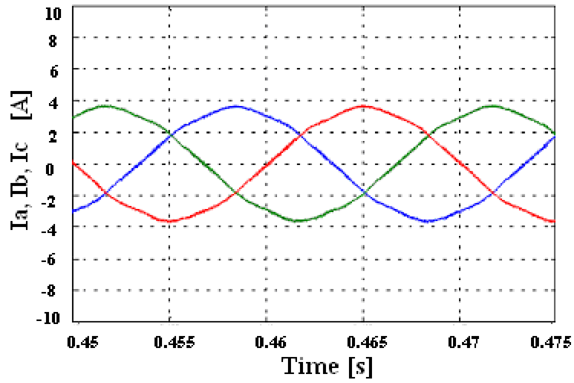

Fig. 2.20. Phase currents from the power
network with active filter

Fig. 2.21 Three-phase currents from the
mains supply for dual task

In the following we present the results obtained from simulation for this type of construction.

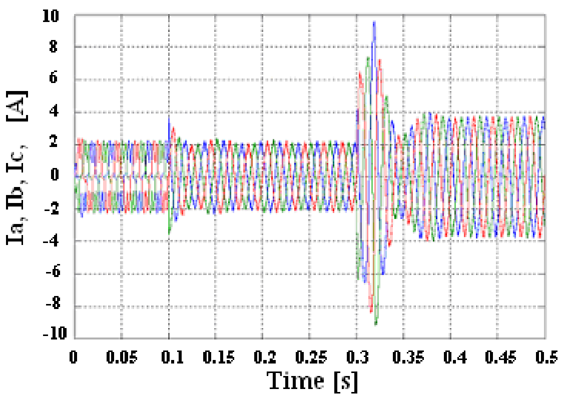

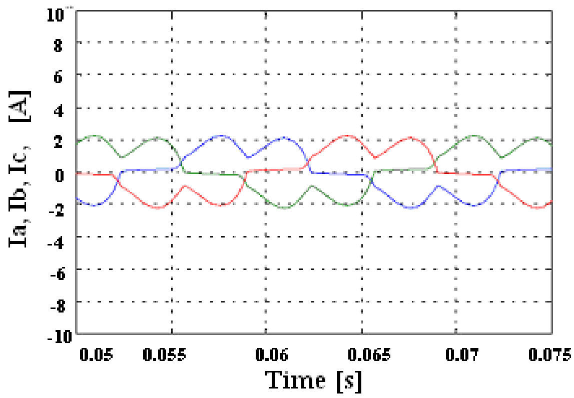

Fig. 2.22 Three-phase currents from the power
supply throughout the simulation time

Fig. 2.23. Phase currents from the power
network without active filter

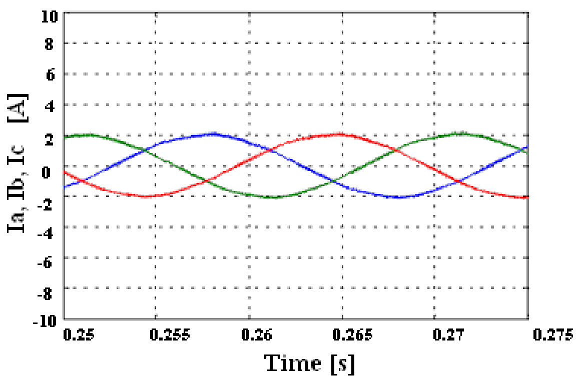

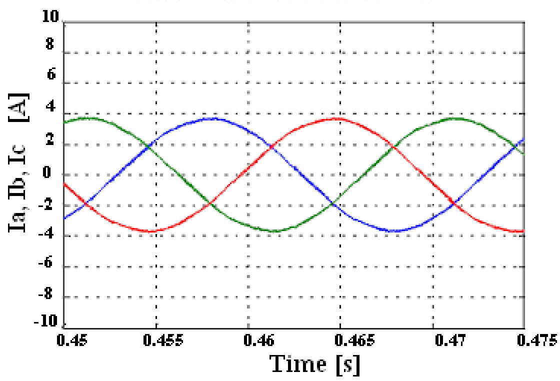

Fig. 2.24 three-phase currents mains
an active filter

Fig. 2.25. Phase currents from the mains
supply for dual task

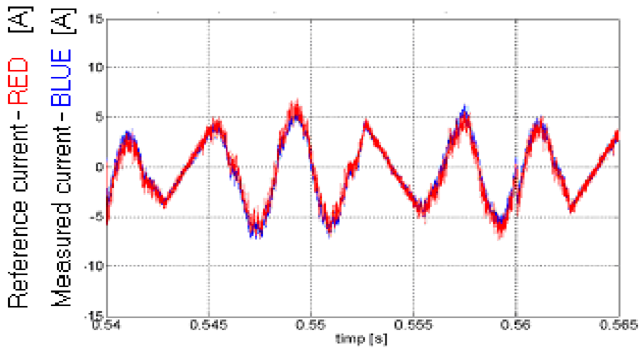

Fig. 2.26. Compensation current produced from the active phase of growth after pregnancy

3. CONCLUSIONS

This paper presents four schemes using both types of construction, with and without feedback loop, for three-phase voltage sources but balanced nonlinear load (no neutral wire). The first two schemes use a calculation method based on real-time Fourier analysis of the currents on each phase. The other two schemes propose another solution that enables the calculation based on the fundamental harmonic active and reactive power (by averaging the instantaneous value). Simulation of these schemes was done in Matlab-Simulink environment. In all cases observed sharp decrease distorting effect caused by pregnancy. Using sliding mode version requires use of a DSP but need large memory.

REFERENCES

[1.] Gelu-Ovidiu Tirian, Stela Rusu-Anghel – Automatizarea Proceselor Continue, Editura Mirton, Timisoara, 2008

[2.] Anghel Stela, Tirian Gelu-Ovidiu – Teoria Sistemelor si Reglaj Automat, Aplicatii in Matlab, Editura Mirton, Timisoara, 2007

[3.] Task Force on Harmonics Modeling and Simulation, IEEE PES Harmonic Working Group: „Characteristics and Modeling of Harmonic Sources – Power Electronic Devices”, IEEE Trans on Power Delivery, Vol 16, No 4, october 2004, pp. 791-800.

INTERNATIONAL SYMPOSIUM on
ADVANCED ENGINEERING & APPLIED MANAGEMENT
– 40th ANNIVERSARY in HIGHER EDUCATION (1970-2010)
4 – 5 November, 2010, Hunedoara, ROMANIA

[1] Stela RUSU-ANGHEL, [2] Lucian GHERMAN, [3]Sergiu MEZINESCU

MANAGEMENT FLOW CONTROL ROTOR INDUCTION MACHINE USING FUZZY REGULATORS

[1-3] UNIVERSITY POLITEHNICA OF TIMISOARA, FACULTY OF ENGINEERING FROM HUNEDOARA, ROMANIA

ABSTRACT:
Commands based on static characteristics of induction motor inevitably produce a number of undesirable effects on the dynamic behavior of the engine. These disadvantages can be partially eliminated by appealing to the orientation control strategy flow. The paper proposes the use of fuzzy controllers for rotor flow and electromagnetic torque, and simulation in Matlab-Simulink them. The results show that using fuzzy controllers compared with conventional methods allow a quick start and a small error rate in both task and goal.
KEYWORDS:
fuzzy controllers, Matlab-Simulink, induction motor

1. INTRODUCTION

Perturbations introduced by the inverter are most stator voltage and stator flow so. Instead, the rotor flow does not vary depending on the stator current with a time constant Tr so great. Vector diagram in Figure 1.1 describes the principle of rotor flow orientation with respect. Also the rotor flow estimation and adjustment can be made with a larger sampling period than the average of Stroke inverter.

So after the rotor flow orientation allows us to combine the requirements in terms of rapidity and computing performance. In addition to orientation relative to the rotor flow, allows decoupling of flow and electromagnetic torque regulation.

Ψ_r rotor flow vectors and stator current is moving at the speed of the mobile coordinate system ω_s synchronism. It is found that the flow vector is in phase with the real component of stator current phasor $i_{s\alpha}$ and therefore is out of phase by 90 degrees from the imaginary component $i_{s\beta}$. Also, the rotor flow is purely real $\left(\underline{\psi}_r = \psi_{r\alpha}, \psi_{r\beta} = 0\right)$ in mobile reference system. $I_{s\alpha}$ real component of current flow while producing so imaginary component $i_{s\beta}$ produce electromagnetic torque. Because of this dynamic coupling of the engine components are independent in terms of operation. Flow and torque can also be ordered individually.

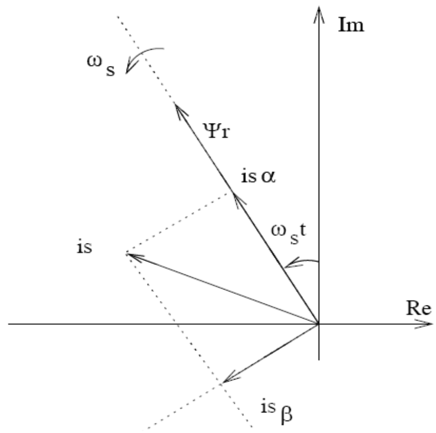

Figure 1.1. Vector diagram in mobile reference system command oriented in relation to the flow rotor

In Figure 1.2 is a circuit schematic diagram of power, control and control of a controlled induction motor rotor relative to the flow. Logic control signals, but (i = 1 ... 6) are determined from the adjustment phase currents. In principle, adjusting the phase currents are made just like the current order - variable stator frequency. Phase current shape is determined by the block (6) by making measurements $i_{s\alpha}$ and $i_{s\beta}$ mobile reference system fixed reference system with stator frequency f_s estimated.

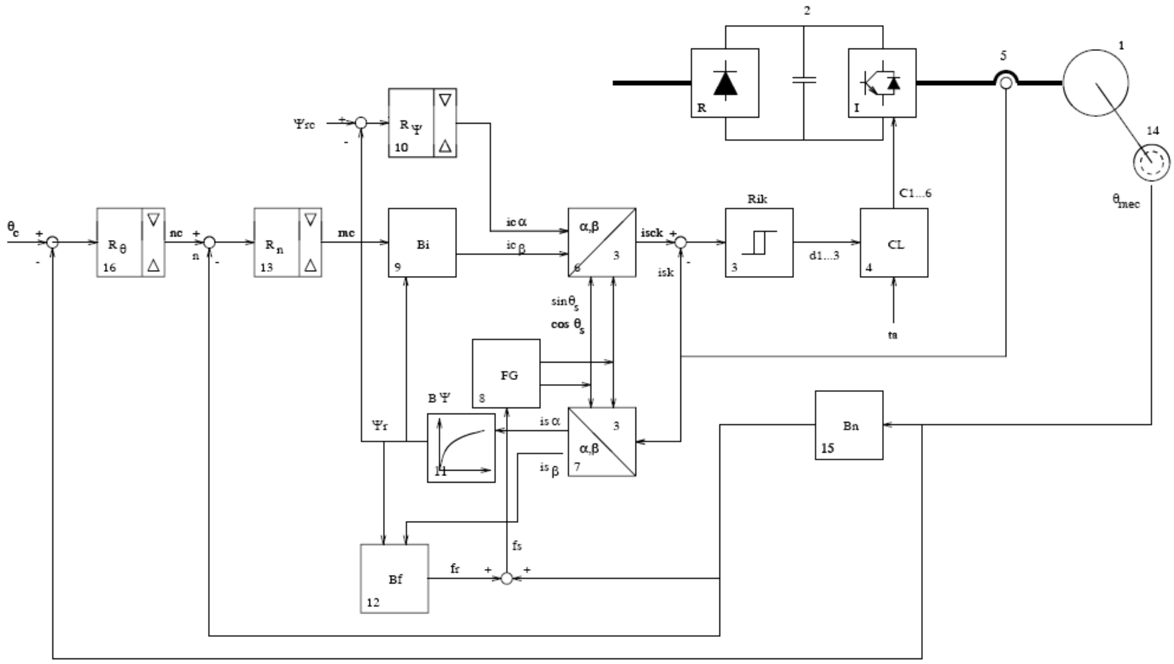

Figure 1.2. The schematic diagram of a control circuit after the rotor flow oriented

Rotor flow adjustment is achieved through a flow regulator which is maintained by negative reaction to the amount imposed. RΨ flow controller output will give us the desired shape of the real component of current $i_{c\alpha}$, while the desired shape for the imaginary component icβ current signal is calculated from the speed controller output obtained from MC and the estimated value of rotor flow Bloc (9). This calculation is derived from the expression of electromagnetic torque as:

$$m_e = \frac{x_h}{x_r} \cdot \psi_r \cdot i_{s\beta} \tag{1.1}$$

Size mc prescribed torque comes from the speed controller, while the constant flow is imposed ($\Psi_{rc} = \Psi_{rn}$) to ensure maximum torque reserve. Rotor flow can also be imposed under the principle of reducing the field to high rotational speeds. By overlaying the speed and position regulator allows adjustment of the induction motor speed and position.
Current regulator can be relised in the rotor coordinate system with the advantage that steady state values of stator current required $i_{c\alpha}$ and $i_{c\beta}$ are constant and independent of the stator frequency f_s.

2. FUZZY CONTROL

As we know, the engine parameters vary depending on the magnetic circuit saturation regime and temperature are also the dispersion due to their manufacturing process.

To control the orientation of the induction motor rotor flow will be used two fuzzy controllers, one for controlling the flow through the rotor stator current $i_{s\alpha}$ real component and a second controller to control the electromagnetic torque, so the rotational speed through the imaginary component $i_{s\beta}$ stator current. Block diagram of rotor flow control the orientation using fuzzy controllers is presented in Figure 2.1.

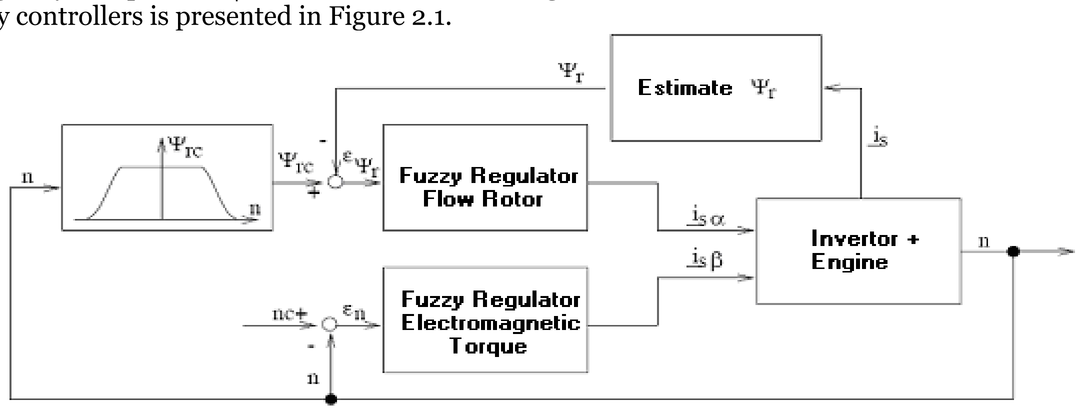

Figure 2.1. Order flow target rotor block diagram, using fuzzy controllers

Numerical simulation was done in Matlab - Simulink using real data of a 133Hz engine. The mathematical model of rotor flow control the orientation is shown in Figure 2.3., And the induction motor model used in this type of order is shown in Figure 2.2.

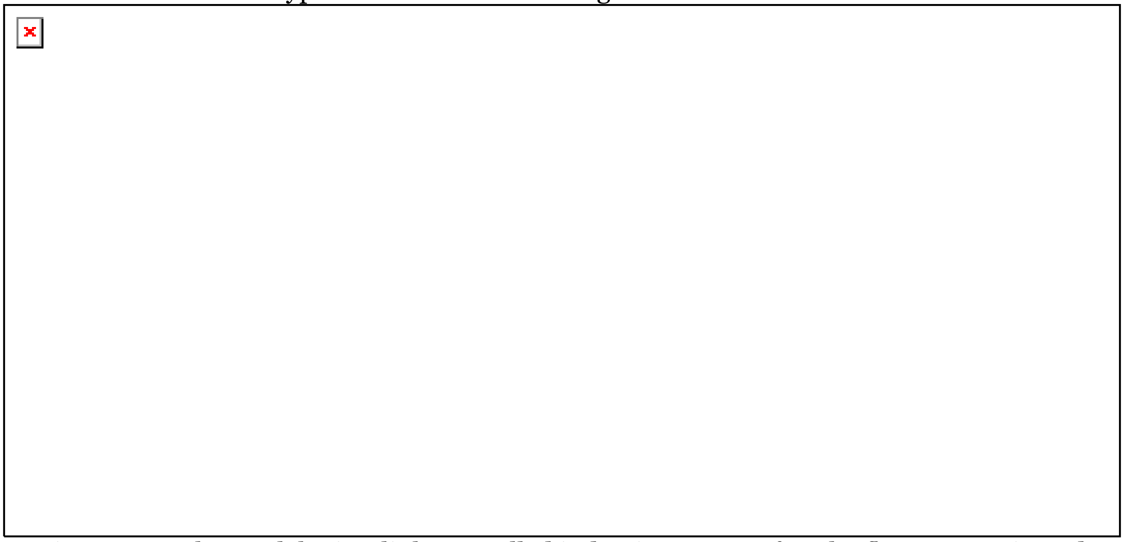

Figure. 2.2. The Matlab Simulink controlled induction motor after the flow rotor oriented

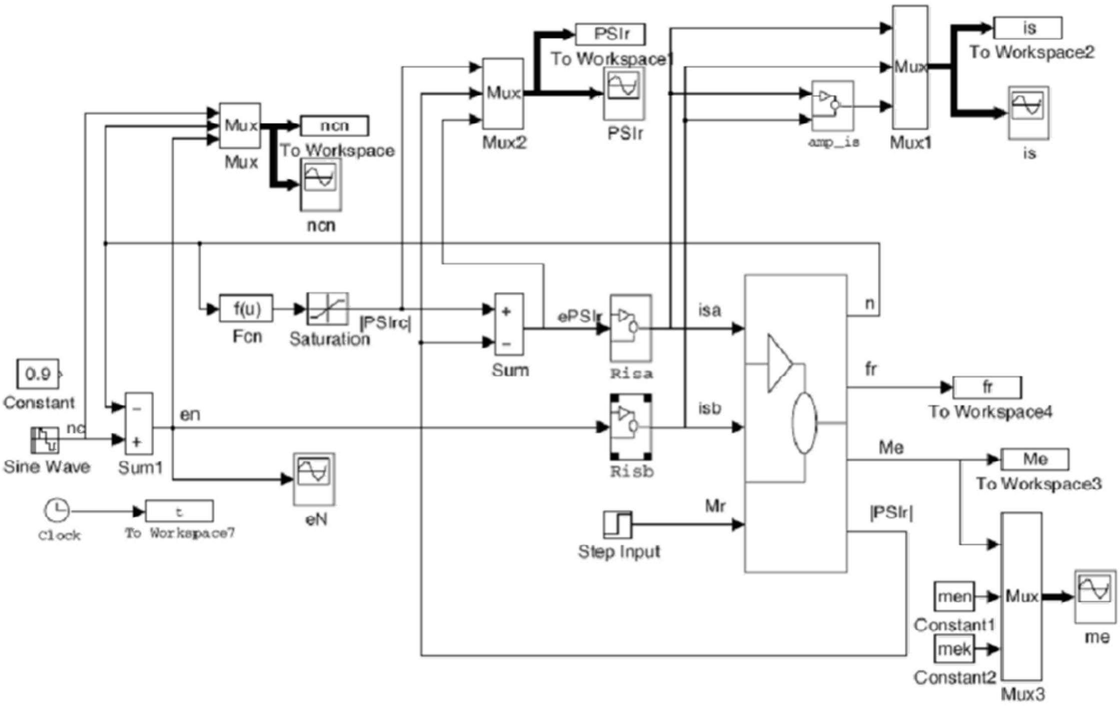

Figure 2.3 .. The Matlab Simulink-controlled induction motor
rotor flow oriented by using fuzzy controllers

Obtained speed at the exit block that models the asynchronous motor (Figure 1.4.) Block is applied to determine the rotor flow imposed, which is then limited to the nominal value of rotor flow. Using the rotor flow modulus value obtained in the block that models the asynchronous motor and the rotor flow value imposed by loss of control error to determine the rotor flow will apply fuzzy controller that will calculate the real component of stator current $i_{s\alpha}$, which would apply to model induction motor.

$I_{s\beta}$ imaginary component of stator current is determined by the second fuzzy controller based on speed error.

3. DESIGNING FUZZY CONTROLLERS

3.1. FUZZY REGULATOR FOR FLOW ROTOR

Ψr rotor flow is controlled by the real component of stator current $i_{s\alpha}$. The block diagram of this controller is shown in Figure 3.1.

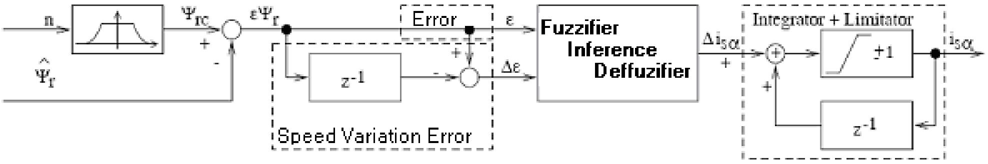

Figure 3.1. Block diagram of fuzzy controller to control flow rotor oriented control after the flow rotor

Ψr rotor flow current value is taken from the induction motor model, but in practice it can be determines the stator currents depending on the stage. Rotor flow Ψrc prescribed value is determined using the rotational speed, not based on static characteristics. The estimated value of rotor flow is calculated.

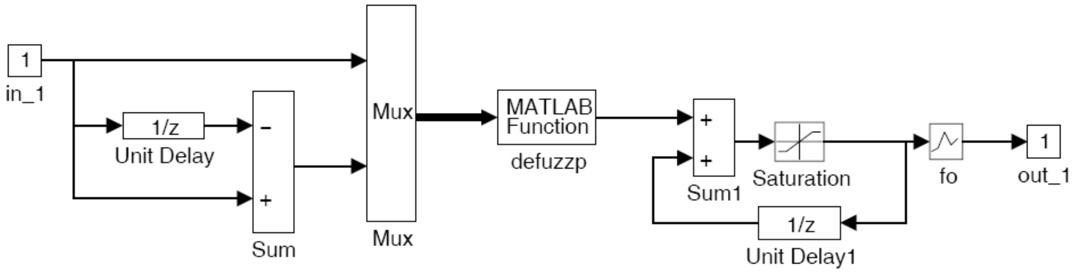

Figure 3.2. Matlab-Simulink model of the fuzzy controller for the rotor flow

Time delay is equal to sampling period TE = 0.001 s. Sampling period was chosen so that a sufficient number of samples to control the rotor flow following engine speed. The sampling period should not be confused with the sampling period to generate the inverter control pulses, the period must be much smaller (~ 500 μs) to have a sufficient number of points to generate the stator current frequency.

Numerical variables εΨr and ΔεΨr fuzzy variables are converted into speech presented fig.3.3 universal and triangular membership functions.

Each universes of discourse is divided into seven fuzzy sets according to a k^n: NL = Negative Large, NM = Negative Medium, NS = Negative Small, ZE = Zero, PS = Positive Small, PM = Positive Medium, PL = Positive Large. The coefficient k is chosen in the range (0.1 - 1.0). Variables εΨr and ΔεΨr inference are processed using the 49 (7 x 7) rules , type If ... then ..., shown in Figure 3.4., using the min / max.

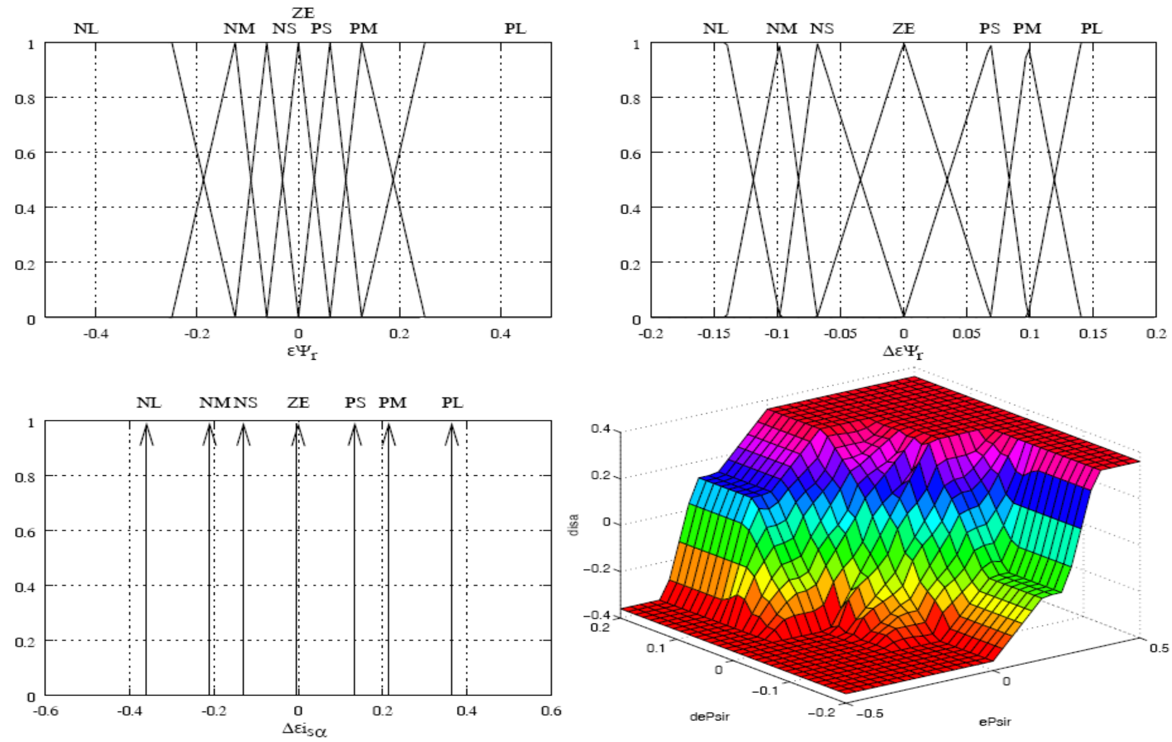

Fig. 3.3. The inputs εΨr and ΔεΨr; the output Δisα and the command surface of fuzzy controller proposed

For defuzzification centroid method was used. Command area of fuzzy controller is presented in Figure 3.3.

$\varepsilon\Psi_r$ \ $\Delta i_{s\alpha}$ / $\Delta\varepsilon\Psi_r$	NL	NM	NS	ZE	PS	PM	PL
NL	NL	NL	NL	NL	NL	NL	NL
NM	NL	NL	NL	NL	NM	NS	PS
NS	NL	NL	NL	NL	NM	NS	PS
ZE	NL	NM	NS	ZE	PS	PM	PL
PS	NS	PS	PM	PL	PL	PL	PL
PM	NS	PS	PM	PL	PL	PL	PL
PL	PL	PL	PL	PL	PL	PL	PL

Figure 3.4. Table of proposed rules of fuzzy controller

3.2. FUZZY REGULATOR FOR ELECTROMAGNETIC TORQUE

Electromagnetic torque and rotational velocity is controlled by imaginary component of stator current $i_{s\beta}$. The proposed controller error as input rotational speed, and speed variation ε_n this error $\Delta_{\varepsilon n}$. Error rate is obtained by the difference between the prescribed speed, n_c, and the actual value of rotor speed n - Matlab Simulink model of this controller is shown in Figure 3.5.

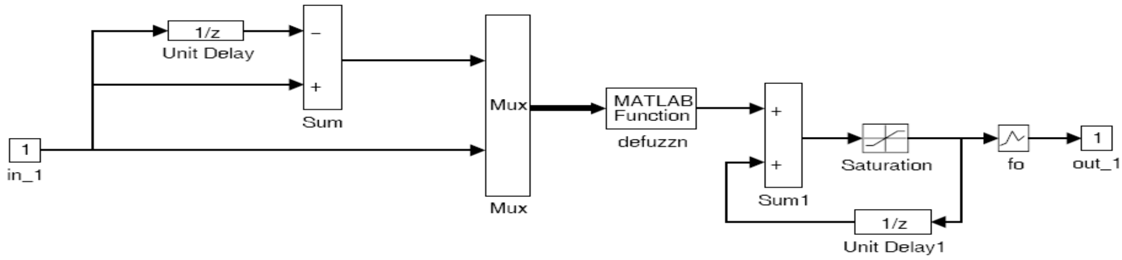

Figure 3.5. Matlab-Simulink model of the electromagnetic torque fuzzy controller

Time delay is equal to sampling period TE = 0.001. Sampling period was chosen so that a sufficient number of samples to control and track engine speed.

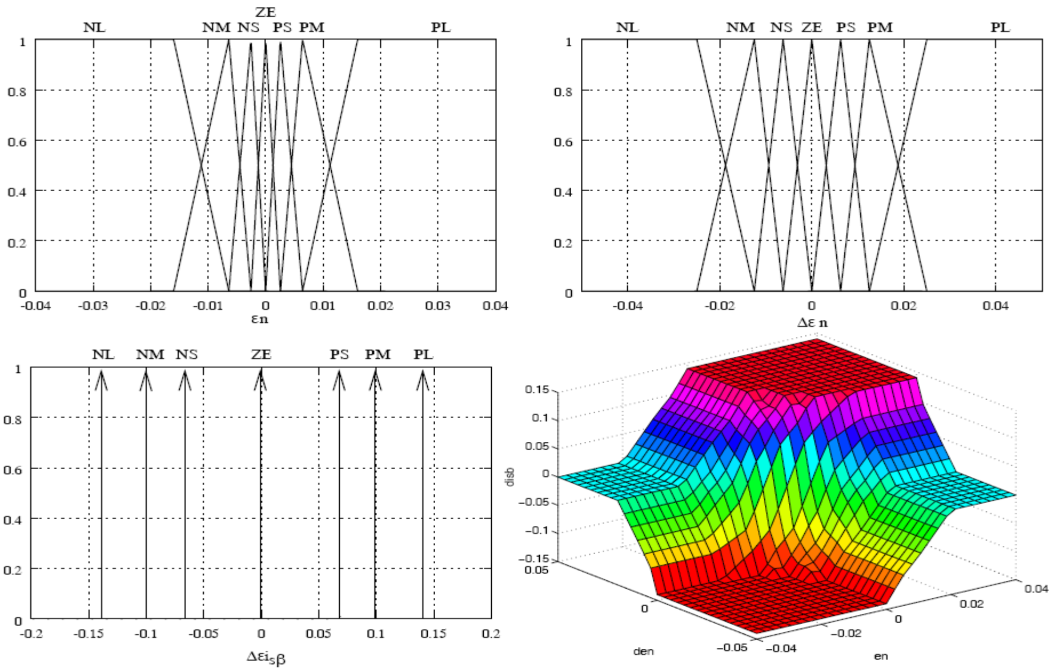

Figure 3.6. The inputs ε_n and $\Delta_{\varepsilon n}$; output $\Delta_{is\beta}$ and control surface fuzzy controller proposed

Numerical variables εΨn and ΔεΨn fuzzy variables are converted into speech presented fig.3.6 universes and triangular membership functions. Each universe of discourse is divided into seven fuzzy sets according to a k^n: NL = Negative Large, NM = Negative Medium, NS = Negative Small, ZE = Zero, PS = Positive Small, PM = Positive Medium, PL = Positive Large. The coefficient k is chosen in the range (0.1 - 1.0).

After optimization of the system were determined universes of speech and sharing factor k of the law in language degrees. ε_n variable universes of discourse is [-0.04 ÷ 0.04], the variable is $\Delta_{\varepsilon n}$

[-0.05 ÷ 0.05], and the output is $\Delta_{is\beta}$ [-0.2 ÷ 0.2]. For entry ε_n factor k = 0.4 for entry $\Delta_{\varepsilon n}$ factor k = 0.5 and k = 0.7 exit $\Delta_{is\beta}$ factor.

$\Delta i_{s\beta}$ (ε_n \ $\Delta\varepsilon_n$)	NL	NM	NS	ZE	PS	PM	PL
NL	NL	NL	NL	NL	NM	NS	ZE
NM	NL	NL	NL	NM	NS	ZE	PS
NS	NL	NL	NM	NS	ZE	PS	PM
ZE	NL	NM	NS	ZE	PS	PM	PL
PS	NM	NS	ZE	PS	PM	PL	PL
PM	NS	ZE	PS	PM	PL	PL	PL
PL	ZE	PS	PM	PL	PL	PL	PL

Figure 3.7. Fuzzy inference table of the controller proposed

Variables ε_n and $\Delta_{\varepsilon n}$ inference are processed using 49 (7 x 7) rules, type If ... then ..., shown in Figure 3.7., using the min / max.

Table rules underlying fuzzy speed regulator is shown in Figure 3.7 has been determined using the following logic: if the component of stator current imagination, $i_{s\beta}$, it will grow and grow me electromagnetic torque generated by the engine. For defuzzification centroid method was used. Fuzzy control surface of the controller is presented in Figure 3.6.

4. RESULTS NUMERICAL SIMULATION

To simulate the operation of induction motor rotor flow controlled by using two independent fuzzy controllers for the rotor flow and electromagnetic torque respectively, was done in Matlab. For numerical integration of differential equations resulting system was used Runge-Kutta algorithm of order 5. For simulation we use a 133 engine Hz/160W.

The mathematical model implemented in Matlab Simulink-Target Order of the rotor flow is shown in Figure 2.1. At the current fed induction motor stator variable in Figure 2.2. And the two fuzzy controllers used to control rotor flow and electromagnetic torque are shown in Figure 3.1. and Fig.3.2

Speed, n, and rotor flow | Ψr | obtained from the induction motor model is applied to the two control loops, the rotor flow and electromagnetic torque. Rotor flow imposed Ψrc is calculated based on the actual rotor speed. Since rotor flow is dependent only real component of stator current, $i_{s\alpha}$, the fuzzy controller will only control the rotor flow $I_{s\alpha}$. Also, because the electromagnetic torque depends only on the imaginary part of the stator current, $i_{s\beta}$, then the controller will only control the electromagnetic torque $i_{s\beta}$.

To study the static behavior and response to the step signal of the current controlled induction motor with rotor flow orientation after two tests were performed. These tests, which are part of the first set of tests, consisting in imposing a constant speed n_c = 0.9 [pu], and the first engine test was considered void start (Mr = 0) at t = 0.5s and applying a torque resistant equal to the nominal torque (Mr = men). For the second test was also considered imposing a constant speed n_c = 0.9 [p.u.], but starting the engine in charge (Mr = m_{men}) and at t = 0.5s resistant torque cancellation. Graph of the main parameters can be simulated in Figure 4.1 follow.

In Fig. 4.1. prescribed speed is presented charts, still, the rotor speed, n, electromagnetic torque, me, speed error, ε_n, the rotor flow modulus, | Ψr | and stator current ($i_{s\alpha}$ real component, imaginary component and module $i_{s\beta}$ | i_s | the first set of tests. From these graphs you can see a great variation in the behavior of the prescribed speed gear so the engine speed error in the gap, and with the engine load.

The transitional arrangement is very short settling speed prescribed in 0.14 and up, without a long-harmonic regime. Study the dynamic regime controlled induction motor operation in the stator current with rotor flow orientation was made after the imposition of a speed, yet, to form sinusoidal amplitude 0.2 [p.u.] and the frequency of 6Hz. Frequency was chosen maximum speed acceleration imposed.

Otherwise that is approximately equal to the maximum acceleration that the engine can have rated load. For the first test of this set of tests, Fig 4.2 we considered to start in goal, (Mr = 0), and applying a torque at t = 0.5s electromagnetic torque is equal to the nominal resistance, and for the second test, Fig 4.3. , To start the task (Mr = men) and at t = 0.5s, strong torque cancellation.

From the study of dynamic graphics system (Figure 4.4.) shows that using fuzzy controllers to get a quick start and a small error rate in both task and goal.

The principle of command guidance after the rotor flow using fuzzy proposed to impose independent stator current components, compared with the methods described above, and leads to obtain very good results both in steady and dynamic conditions.

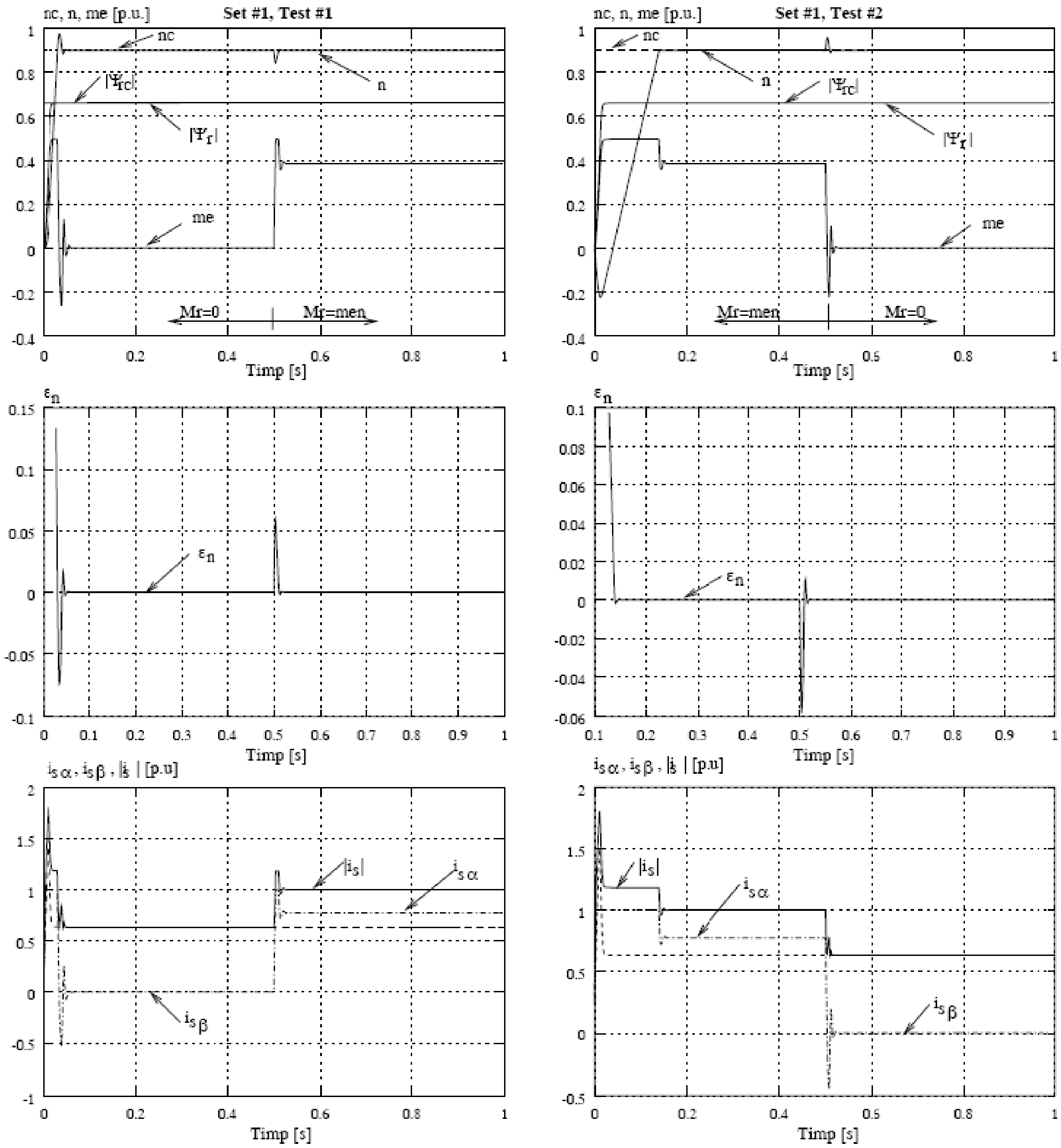

Fig. 4.1 . Speed n electromagnetic torque me, rotor flow module | Ψr |, εn speed error and stator current (real part isα, isβ imaginary component and module is) the first set of tests

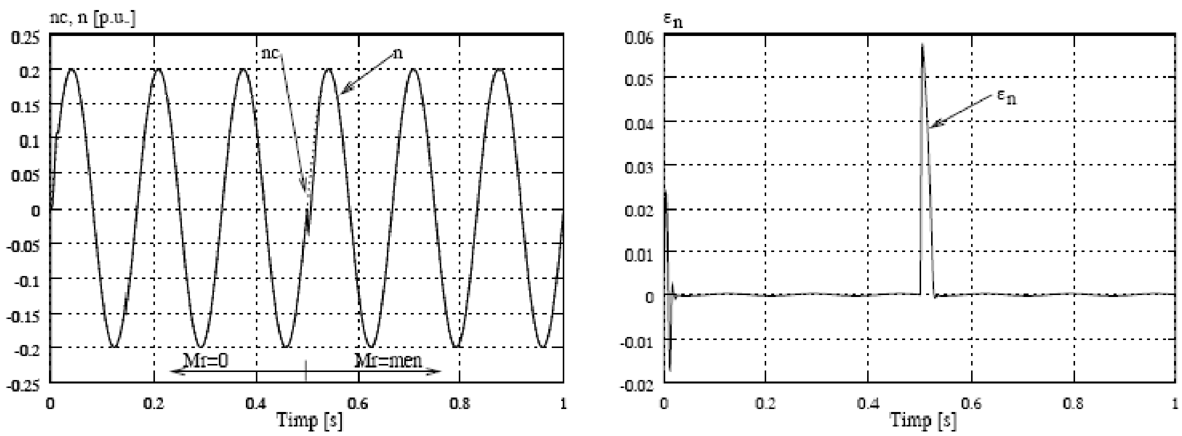

Fig. 4.2. Rotor speed n, rpm still imposed, and the speed error εn 1 test 2 test kit.

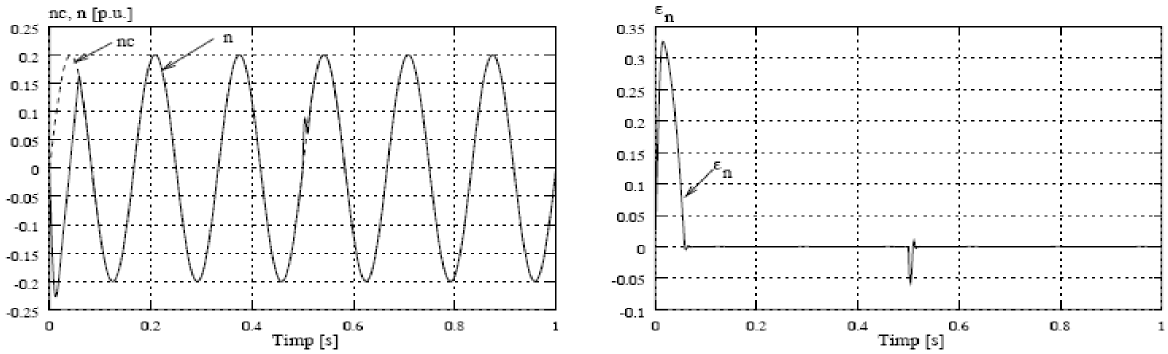

Fig. 4.3. Rotor speed n, rpm still imposed, and the speed error εn Test 2 of 2 set of tests.

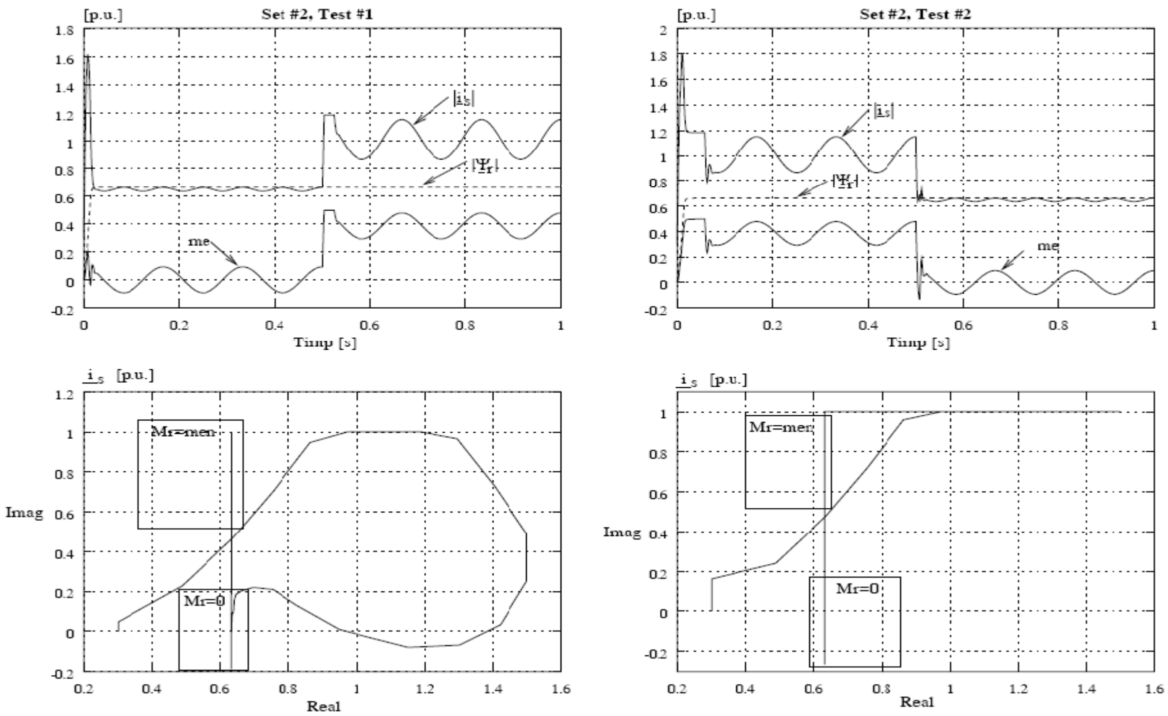

Fig. 4.4. Variation of stator current phasor module, | is |, is the stator current phasor, the rotor flow phasor module, | Ψr | and electromagnetic torque, me 2 test kit.

5. CONCLUSIONS

It can highlight the following conclusions: asynchronous motor is a nonlinear system described by a 7-order differential equations with variable parameters, the inverter, the control algorithm and the limitations imposed on the hysteresis, inter switching times is also a powerful nonlinear, speed control motors, control methods studied impugn regulators with variable coefficients depending on the operating point of engine controllers to drive motors implementation requires knowledge of how real operating parameters, and their evolution, the parameters may vary The magnetic circuit saturation and / or temperature, quality tuning fuzzy actually requires a wider range of motion controllers used in applications for robotics, machine tools, transportation, etc.

REFERENCES

[1.] Gelu-Ovidiu Tirian, Stela Rusu-Anghel – Automatizarea Proceselor Continue, Editura Mirton, Timisoara, 2008

[2.] Anghel Stela, Tirian Gelu-Ovidiu – Teoria Sistemelor si Reglaj Automat, Aplicatii in Matlab, Editura Mirton, Timisoara, 2007

[3.] Peter Vas. Electrical machines and Drives – a Space – Vector Theory Approach, Volume 25 of Monographs in electrica land Electronical Engineering. Oxford science Publications, Waltron Street, Oxford OX2 6DP, 1992.

[4.] Fariba Moghaddam Butzberg. Etude et Comparaison de Differentes Strategies de Reglage et de Commande de Servomoteurs Asynchrones. These no. 1414 pour l'obtention du grande de docteures sciences techniques, Ecole polytechnique federale de Lausanne, Department d'Electricite, 1995.

INTERNATIONAL SYMPOSIUM on
ADVANCED ENGINEERING & APPLIED MANAGEMENT
– 40th ANNIVERSARY in HIGHER EDUCATION (1970-2010)
4 – 5 November, 2010, Hunedoara, ROMANIA

[1]Ion COPACI, [2]Aurelia TĂNĂSOIU

THE REDUCTION OF THE ACCELARATION LEVELS CONVEYED TO THE FREIGHT HAULED ON CARRIAGES FITTED WITH LONG-RUN BUFFERS

[1-2] UNIVERSITATEA "AUREL VLAICU" ARAD, ROMANIA

ABSTRACT:
The current trend towards the increase of speeds in the railway traffic and the ever growing gain weight on the axles has brought about a series of special problems concerning the impact stress which occurs at collision.
In order to isolate the shock that occurs longitudinally, the rail vehicles are fitted with shock dampers:
- ❖ Buffers or main coupling dampers
- ❖ Long-rung buffers fitted on the platform wagons, meant as an additional safety measure for the goods loaded on the storage platform

Long-rung buffers fitted on the platform wagons are reducing the level of the longitudinal accelaration.
KEYWORDS: shock, collision, long-run damper, acceleration, contraction, mobile longeron, storage platform, mobile covering

1. INTRODUCTION

The collision of the rail vehicles takes place under shunting conditions while the carriages are being coupled and during traffic following the start-ups and brakings of the set of cars.

The stress produced at the collision of the rail vehicles generates the transmission of certain forces and accelerations of considerable value that convey acceleration to the goods hauled. This acceleration, in its turn, may jeopardize their integrity and their anchoring, fixing and packing systems.

Fig. 1 shows Rijmmns- 600, a 4-axle platform wagon fitted with a long-run buffer fixed on a 76-350 mm OLEO INTERNATIONAL mobile longeron .

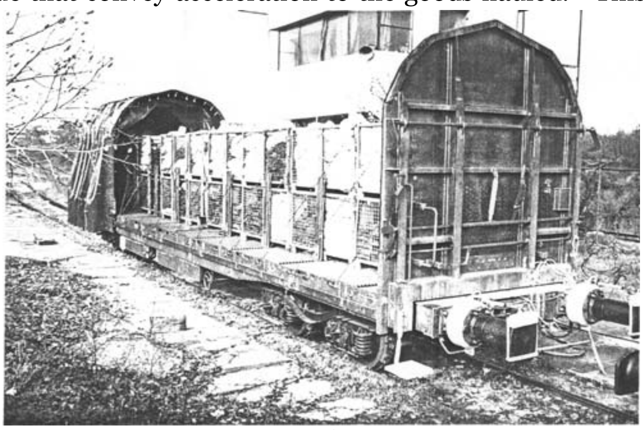

Fig. 1

2. COLLISION TEST

Fig. 2 shows the way in which damper (1) is fixed, in between the mobile longeron and the storage platform, as well as the mounting of force cell (2) that determines the force conveyed through damping.

The collided wagon was loaded with pellets and small products in two different variants:
- ❖ Variant 1: a half-load for a tare weight of 56,960 kg ;
- ❖ Variant 2: a total load for a tare weight of 90,000 kg;

The colliding wagon was a a gondola car loaded with sand at a tare weight of 80 t., fitted with A category buffers in keeping with UIC 526-1. During the tests the following parameters were determined as response functions of the collided car:

- F1; F2 [kN] – the forces conveyed through the buffers of the car;
- D1, D2 [mm] – the contraction of the buffers;
- FL [kN] – the force conveyed by the mobile longeron to the long-run buffer;
- DL [mm] – the contraction of the long-run buffer;
- as [g] – the acceleration imparted to the undercarriage on which the hauled goods are fixed;
- aL [g] – the acceleration of the longeron;

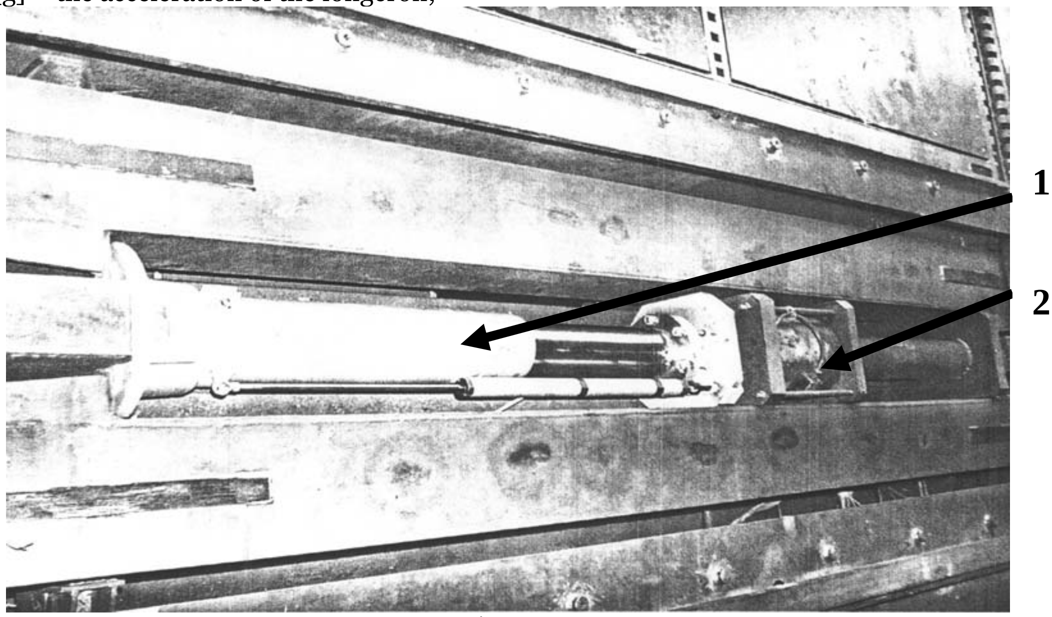

Fig. 2

The colliding car was launched from an incline and it collided into the tested car which was lined up at various collision speeds. The results of the collision tests are shown in Tabel no.1

The analysis of the results for the second collision variant (V= 11.68 km/h), shows that the collision process lasts 0.75 s. By the integration of the curve of the undercarriage acceleration as a function of time, we determined the evolution of the speed correlated with time during the process of collision, as shown in Fig. 3.The evolution in time of the undercarriage acceleration as is illustrated in Fig. 4.

Tabel no. 1

Parametri masurati	Vagon tara 56.960 kg									Vagon tara 90.000 kg				
	Viteza (km/h)													
	7,1	8,12	8,93	8,91	8,95	10,16	10,84	11,61	12	8,29	8,95	10,22	10,87	11,68
F_1 (kN)	118	142	158	158	158	190	208	229	241	152	168	199	211	238
F_2 (kN)	106	129	152	153	151	186	199	224	235	142	158	194	207	232
F_L (kN)	219	282	340	345	347	427	472	534	565	346	390	486	499	570
D_1 (mm)	32	38	40	41	41	48	51	56	59	35	38	46	50	55
D_2 (mm)	27	32	32	35	35	41	46	49	53	27	31	37	44	49
D_L (mm)	289	312	318	318	317	329	336	340	340	337	340	347	350	350
a_s (g)	0,67	0,86	0,92	0,92	0,92	1,44	1,63	1,67	1,74	0,65	0,7	0,95	1,05	1,22
a_p (g)	0,72	0,83	0,93	0,91	0,94	1,43	1,5	1,55	1,62	0,69	0,75	0,85	0,98	1,14
a_L (g)	4,13	4,54	4,69	4,67	4,65	6,17	6,58	6,68	6,92	5,09	5,3	6,13	6,44	6,95

The figure shows speeds at time t=0, the start –up of collision and at time t= 0.75 s, the end of collision. We have to point out also time t1,2 =0.27 s, the moment when the process of turning the kinetic energies of the masses taking part in the collision into stored potential strain energy came to an end and the masses of the vehicles were running at the same speed.

Making up the energetic balance for the collision of the car having a tare weight of 90,000 kg at a speed of V= 11.68 km/h, we concluded the following:

- the strain energy stored by the shock dampers is We = 180.46 kJ , so that the potential strain energy stored in by the resistance structures of the vehicles and the freight becomes W_{v+i} = 43.32 kJ;
- the strain energy dispersed by the shock dampers is W_a = 139.44 kJ and consequently the strain energy dispersed by the resistance structures of the vehicles and the freight becomes W_{v+i} =22,26 kJ.

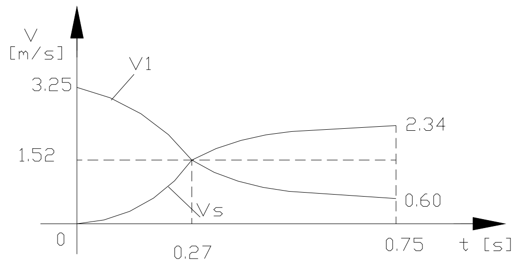

Fig. 3

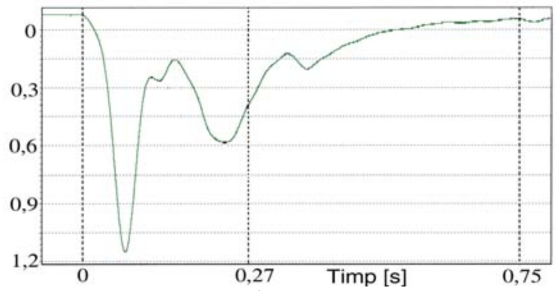

Fig. 4

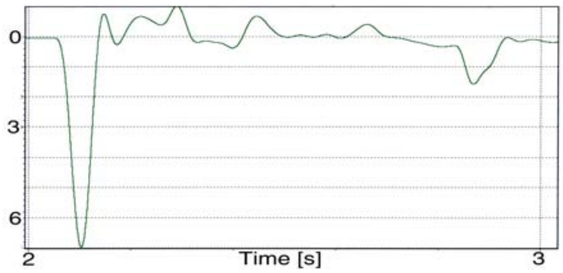

Fig. 5

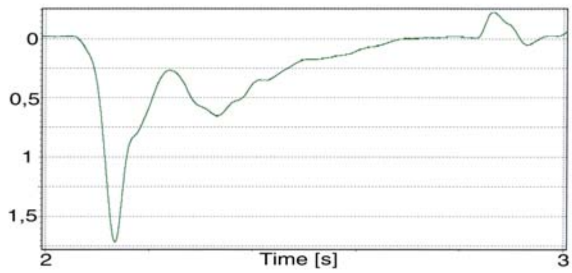

Fig. 6

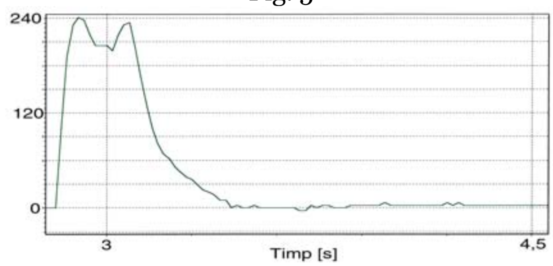

Fig. 7

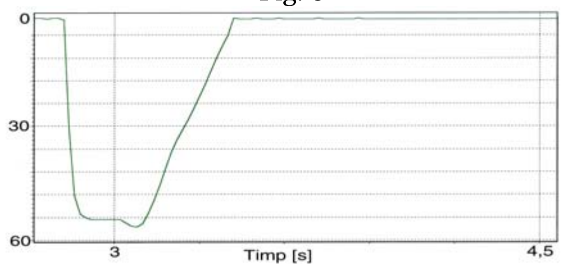

Fig.9

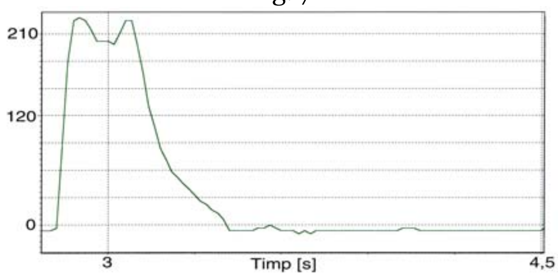

Fig. 8

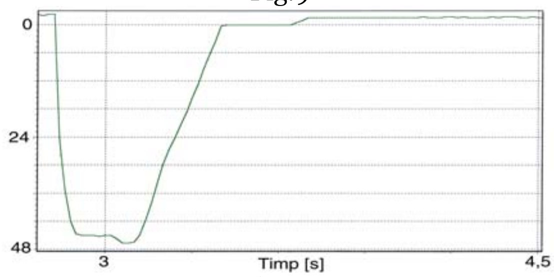

Fig. 10

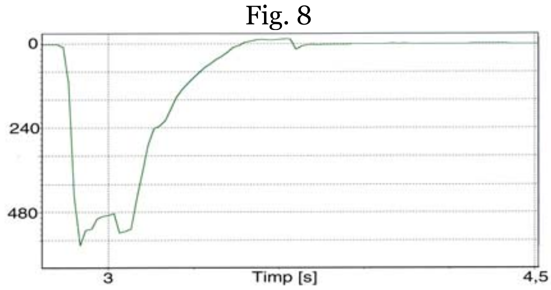

Fig. 11

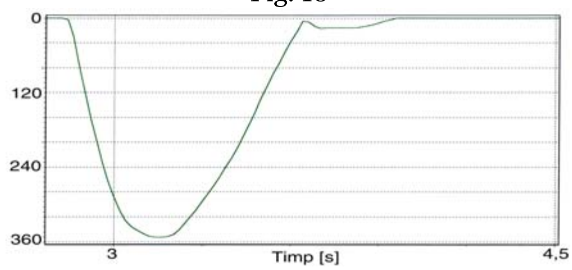

Fig. 12

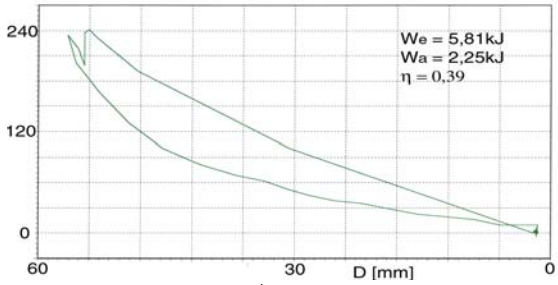

Fig. 13

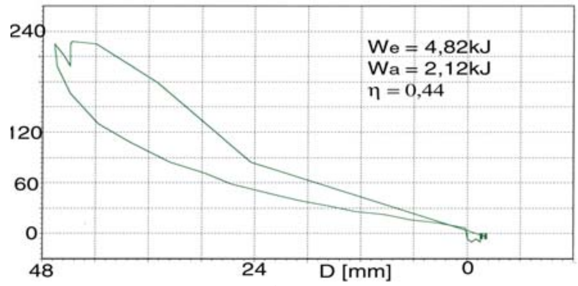

Fig. 14

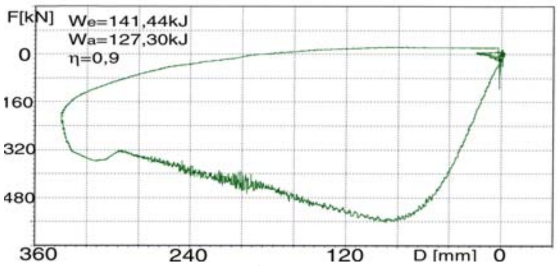

Fig. 15

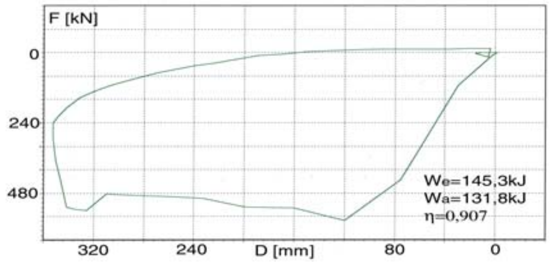

Fig. 16

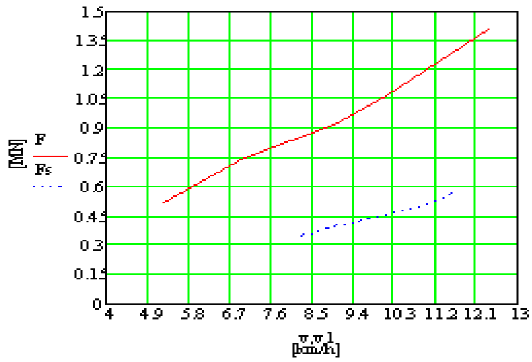

Fig. 17

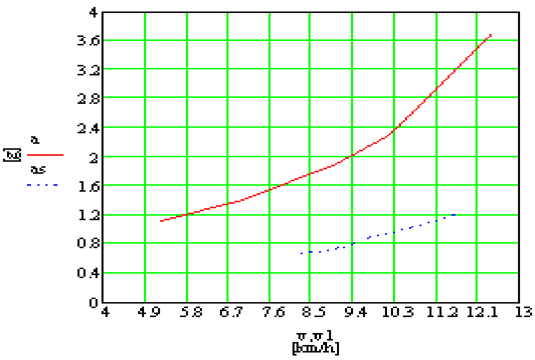

Fig. 18

Fig. 5 and 6 shows the variation of the mobile longeron acceleration and that of the undercarriage in variant 1 of collision at a speed of 12 km/h.

Fig. 7, 8, 9, 10 show F1; F2; D1; D2 correlated with time in variant 2 of collision at a speed of 11.68 km/h. Fig. 11 and 12 show $F_{L,} D_L$ correlated with time in the same variant of collision. Fig. 13, 14 and 16 show the graphs characteristic for buffer 1; buffer 2 and the long-run damper in collision variant 2. Fig. 15 shows the characteristic of the long-run damper in collision variant 1.

Fig.17, 18 illustrate the variation of the forces conveyed and of the acceleration of the car undercarriages in the following situations:

- collision of 80 t→90 t cars fitted with buffers of category C (full line graph);
- collision variant 2 of a 80 t car→ 90 t car fitted with long-run dampers.

3. CONCLUSION

The utilization of long-run dampers leads to a significant reduction of the level of forces conveyed, of the accelerations imparted to the cars and of the potential and dispersed energies which apply to the resistance structures of the cars and freight hauled. Fig. 17 and 18 show that the conveyed forces decrease approx. with 60 %, while the accelerations imparted with approx. 50 % as compared to a collision in which the cars are fitted with buffers of category C – 70kJ, buffers which have the highest capacity of energy storage.

REFERENCES

[1.] UIC 529- Amortizori hidrodinamici de cursă lungă- 1998
[2.] Cyril M. Harris, Charles E. Crede – Shock and Vibration Handbook – McGraw Hill Book Company – New York 1961
[3.] Louis – Marie Cleon, Henri Lagneau – Physique du choc et accidentologie, Revue generale des chemins de fer, November 1993
[4.] Tyrell D., Severson K., Perlman A. – Single Passenger Rail Car Impact Test Volume I: Overview and Selected Results, US Department of Transportation, Federal Railroad Administration, March 2000
[5.] Severson K., Tyrell D.,Perlman A. – Single Passenger Rail Collision Test: Analysis of structural Mesurements, ASME Winter Annual Meeting 2000
[6.] Severson K. – Development of Collision Dynamics Models to Estimate the Result of Full-scale Rail Vehicle Impact Tests, Tufts University Master's Thesis, November 2000

INTERNATIONAL SYMPOSIUM on
ADVANCED ENGINEERING & APPLIED MANAGEMENT
– 40th ANNIVERSARY in HIGHER EDUCATION (1970-2010)
4 – 5 November, 2010, Hunedoara, ROMANIA

[1] Lucian GHERMAN, [2] Stela RUSU-ANGHEL, [3]Sergiu MEZINESCU

USING DSP TO ORDER ACTIVE FILTERS

[1-4] UNIVERSITY POLITEHNICA OF TIMISOARA, FACULTY OF ENGINEERING FROM HUNEDOARA, ROMANIA

ABSTRACT:
This deformed system power supply networks of different consumers is increasingly common. At European level there are rules limiting factors distorting the values strict enough. This goal can be achieved using active harmonic filters. The present paper shows how to control such an active filter using a digital signal processor (DSP) DSP family of 56 F805.
KEYWORDS:
DSP family, digital signal processor, active harmonic filters

1. INTRODUCTION

1.1. P-Q-N METHOD TO ORDER ACTIVE FILTERS.

If sinusoidal supply voltage, active power and reactive mediated network is taken from the first harmonic. Since it is not perfectly sinusoidal voltage using a PLL circuit which generates a fundamental voltage in phase with equal amplitude but of unity.

Active power is calculated using this voltage and reactive power p = 3·U·I·cosφ, where q=3·U·I·sinφ is the phase angle between voltage and current fundamental harmonic.
This technique called "generalized theory of instantaneous reactive power in three phase circuits" or "PQ theory" was developed in [2]. Change the coordinates from A, B, C in α, β, 0 for three-phase voltages and currents:

$$\begin{bmatrix} u_\alpha \\ u_\beta \\ u_0 \end{bmatrix} = \sqrt{\frac{2}{3}} \cdot \begin{bmatrix} 1 & -\frac{1}{2} & -\frac{1}{2} \\ 0 & \sqrt{\frac{3}{2}} & -\sqrt{\frac{3}{2}} \\ \frac{1}{\sqrt{2}} & \frac{1}{\sqrt{2}} & \frac{1}{\sqrt{2}} \end{bmatrix} \cdot \begin{bmatrix} u_a \\ u_b \\ u_c \end{bmatrix} \tag{1.1}$$

and reverse:

$$\begin{bmatrix} i_\alpha \\ i_\beta \\ i_0 \end{bmatrix} = \sqrt{\frac{2}{3}} \cdot \begin{bmatrix} 1 & -\frac{1}{2} & -\frac{1}{2} \\ 0 & \sqrt{\frac{3}{2}} & -\sqrt{\frac{3}{2}} \\ \frac{1}{\sqrt{2}} & \frac{1}{\sqrt{2}} & \frac{1}{\sqrt{2}} \end{bmatrix} \cdot \begin{bmatrix} i_a \\ i_b \\ i_c \end{bmatrix} \tag{1.2}$$

can be obtained:

$p = u_\alpha \cdot i_\alpha + u_\beta \cdot i_\beta$ - Instantaneous active power

$q = u_\beta \cdot i_\alpha - u_\alpha \cdot i_\beta$ - Instantaneous reactive power (1.3)

$n = u_0 \cdot i_0$ - Instantaneous homopolar power

To improve the performance of this method and to simplify calculations, instead of the three instantaneous voltages will use three generators PLL output which will produce three sinusoidal signals of amplitude and phase of a fundamental supply voltage (this assumption is valid only in the absence of even harmonics).

To call these virtual voltage: 1A (1), 1B (1), 1C (a) and corresponding powers:

$$\begin{bmatrix} p_1 \\ q_1 \\ n_1 \end{bmatrix} = \begin{bmatrix} 1_\alpha^{(1)} & 1_\beta^{(1)} & 0 \\ 1_\beta^{(1)} & -1_\alpha^{(1)} & 0 \\ 0 & 0 & 1_0^{(1)} \end{bmatrix} \cdot \begin{bmatrix} i_\alpha \\ i_\beta \\ i_n \end{bmatrix} \tag{1.4}$$

Calculating the average value of this power and knowing that for basic fundamental virtual voltage just currents averaged can give a average value different by zero, we can write:

$$\begin{bmatrix} P \\ Q \\ N \end{bmatrix} = \begin{bmatrix} \frac{1}{T}\int_0^T \left(1_\alpha^{(1)} \cdot i_\alpha^{(1)} + 1_\beta^{(1)} \cdot i_\beta^{(1)}\right)dt \\ \frac{1}{T}\int_0^T \left(-1_\alpha^{(1)} \cdot i_\beta^{(1)} + 1_\beta^{(1)} \cdot i_\alpha^{(1)}\right)dt \\ \frac{1}{T}\int_0^T \left(1_0^{(1)} \cdot i_0^{(1)}\right)dt \end{bmatrix} \tag{1.5}$$

By reversing the relationship (1.5) can be obtained fundamentally load currents iα(1), iβ(1),

$$\begin{bmatrix} i_\alpha^{(1)} \\ i_\beta^{(1)} \end{bmatrix} = \begin{bmatrix} i_\alpha^{(1)} & i_\beta^{(1)} \\ i_\beta^{(1)} & -i_\alpha^{(1)} \end{bmatrix} \cdot \begin{bmatrix} P - N \\ Q \end{bmatrix} \tag{1.6}$$

Respective reference currents of active filter i_{AH}*, i_{BH}*, i_{CH}* if SFFT site.

If we do not have the neutral wire to calculate the instantaneous active power and instantaneous reactive power we use (1.7).

$$\begin{bmatrix} p \\ q \end{bmatrix} = \begin{bmatrix} u_\alpha & u_\beta \\ u_\beta & -u_\alpha \end{bmatrix} \cdot \begin{bmatrix} i_\alpha \\ i_\beta \end{bmatrix} \tag{1.7}$$

This solution enables the calculation based on the fundamental harmonic active and reactive power (through mediation instantaneous value). On the basis of this technique lies that transfer of active and reactive power defined as the product of the fundamental harmonic voltage and currents is real only on the first harmonic current harmonics current remaining power fail.

Unfortunately, in some applications the source voltage contains higher harmonics. For this reason the calculation of power no longer use this tension, but tension time achieved by a PLL circuit implemented on a DSP software and providing an output sinusoidal signal in phase with the fundamental harmonic and amplitude equal to unity. This signal is subtracted from the total current network and thus obtain higher current harmonics which are given by reference to the sign change of active filter.

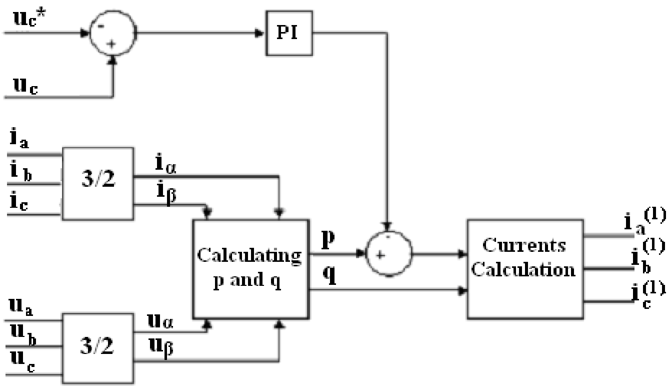

Fig. 1.1. Order active filter with instantaneous power control

1.2. THE FFT AND SFFT METHOD TO ORDER ACTIVE FILTERS.

It is known that a periodic signal can be decomposed into spectral components whose frequency is a multiple of the fundamental frequency. These components are known as harmonic components. A periodic signal can be represented by a Fourier series:

$$V(t) = \frac{1}{2}a_0 + \sum_{k=1}^{n}\left(a_k \cdot \cos k\omega t + b_k \cdot \sin k\omega t\right) \tag{1.8}$$

where ½ . a_0 is the DC component of the signal.

Coefficients a_k and b_k of the series can be defined as:

$$a_0 = \frac{2}{T}\int_t^{t+T} v(t)dt \tag{1.9}$$

$$a_k = \frac{2}{T}\int_t^{t+T} v(t)\cos(k\omega t)dt \qquad (1.10)$$

$$b_k = \frac{2}{T}\int_t^{t+T} v(t)\sin(k\omega t)dt \qquad (1.11)$$

The two coefficients a_k and b_k are the amplitudes of spectral components of order k. There is the possibility of formulating such a Fourier series:

$$V(t) = \frac{1}{2}a_0 + \sum_{k=1}^{n} A_k \cdot \cos(k\omega t - \phi k) \qquad (1.12)$$

where A_k represents the signal amplitude and ϕ_k represents the signal phase.

We define two such values:

$$A_k = \sqrt{a_k^2 + b_k^2} \quad ; \quad \varphi_k = \arctan\frac{b_k}{a_k} \qquad (1.13)$$

Fourier transform is calculated using the fastest FFT algorithm. By Fourier analysis of the currents on each phase has succeeded in its breakdown of its component harmonics. Recompose signal using only the higher order harmonics (less than first harmonic), a clear signal that the network will be introduced with the sign reversed. So that the grid will run a first harmonic signal.

A second solution is to calculate only the fundamental harmonic is then subtracted from the total current network and thus obtain higher current harmonics which are given by reference to the sign change of active filter. This method is used in sliding mode option.

2. ORDER AND DATA ACQUISITION SYSTEM WITH DIGITAL SIGNAL FROM DSP56 F805 FAMILY PROCESSOR

Signal processor is part of the family DSP56800 and belongs to class 16-bit processor, the fixed-point, manufactured by Motorola, is the most complex family. It includes all the necessary peripherals and control procurement system in real time. Calculation speed is very high, tens of millions of instructions per second (MIPS), which allows implementation of sophisticated algorithms.

CPU power signal is enhanced by the existence of a very strong package of software development (SDK - System Development Kit) that allows you to write algorithms in high level languages without a significant increase in computing time. Besides software development environment, the processor comes with a hardware development board, which facilitates much effort to implement the control scheme.

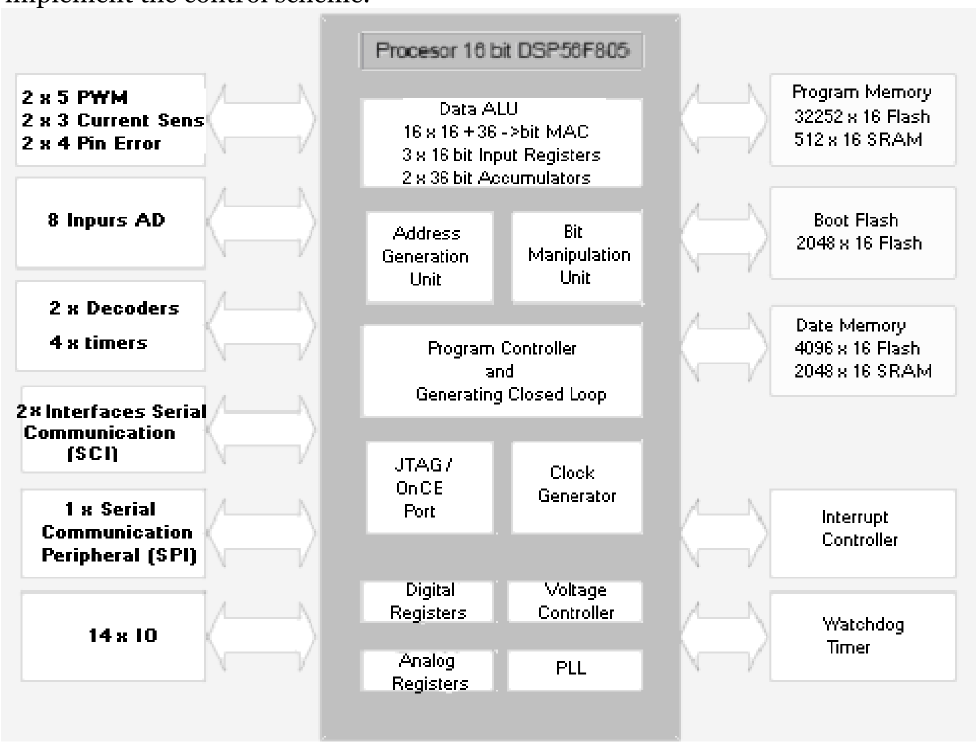

Fig.2.1. The principle scheme DSP56F805

Essential characteristics of the digital signal processor are listed below. Schematic diagram of the component blocks is presented in Fig. 2.1 .

The processor is built on a modified Harvard architecture, with three execution units, able to carry up to six instructions per cycle, or three memory locations to access data or programs, simultaneously. It can execute 40 million instructions per second (MIPS) at a frequency of 80Mhz internal work.

Internal features DSP (core) - site can be grouped as follows:

- 16x16 36-bit - parallel multiplier accumulator (MAC) in a single cycle
- Implementation of hardware DO loops and REP
- Three internal address bus and an external
- Four internal data bus and an external
- Parallel instruction set with unique addressing modes
- Instruction set compatible with that of microcontrollers
- Two 36-bit accumulators, including extension of mark
- 16-bit bidirectional shifter
- Internal memory
- 32,252 words on 16-bit program memory (FLASH)
- 512 words 16-bit program memory (RAM)
- 2k words 16-bit data memory (RAM)
- 4k words 16-bit data memory (FLASH)
- 2k words 16-bit boot memory (FLASH)
- Possible memory expansion Up to 64k program and 64k data
- JTAG interface for debugging programs / OnCETM

Peripherals embedded in DSP56F805 are:

- Second PWM signal generating modules, each with 6 outputs, three inputs of sense of current four error inputs, generating PWM dead time
- Two 12-bit digital analog converters with parallel conversion and 2x4 input multiplexed, the port be synchronized with the PWM module
- Two quadrature decoders, each with four entries
- Two hours dedicated
- Two serial communication interface (SCI)
- Serial peripheral interface (SPI)
- Two dedicated external interruptions
- CAN 2.0 A / B (Controller Area Network)
- 14 output ports of entry for general use; 18 ports multiplexed
- Programmable PLL
- Internal voltage regulators for digital and analog circuits to reduce cost
- Supports standby and stop
- Manufactured in CMOS technology (5V), supports digital TTL inputs
- Single power supply 3.3 V

PWM pulse generation block provides considerable flexibility in configuration. It has the following characteristics:

- Three pairs of complementary pulse generation channels, or six channels independent
- Dead time insertion software
- Current status or via pulse correction software
- Polarity control to arm up or down inverter
- Resolution 15-bit pulse setting
- Programmable protection fault condition

Digital analog converters provide optimum control algorithm necessary. Is it possible to plan how to read their policy. Is the input voltage between 0 and 3.3V. Offset can be set for each channel, and maximum or minimum allowable to digital output. ADC units can work synchronized with the PWM unit. As the PWM generation unit, this unit is assigned its own disruption. Conversion during the 8 channels in the U.S. is 5.5 mode simultaneously.

DSP56F805EVM development board features:

DSP56F805EVM development board is built to facilitate the development of specific applications DSP56F805 signal processor. These include: electric drive applications, remote communications, modems, automatic telephone response, optical cameras. The plate is designed so that the user can easily run and debug programs and data on the host computer. This is done through JTAG interface / OnCETM - which allows software debugging and modification of various internal registers of the processor in real time.

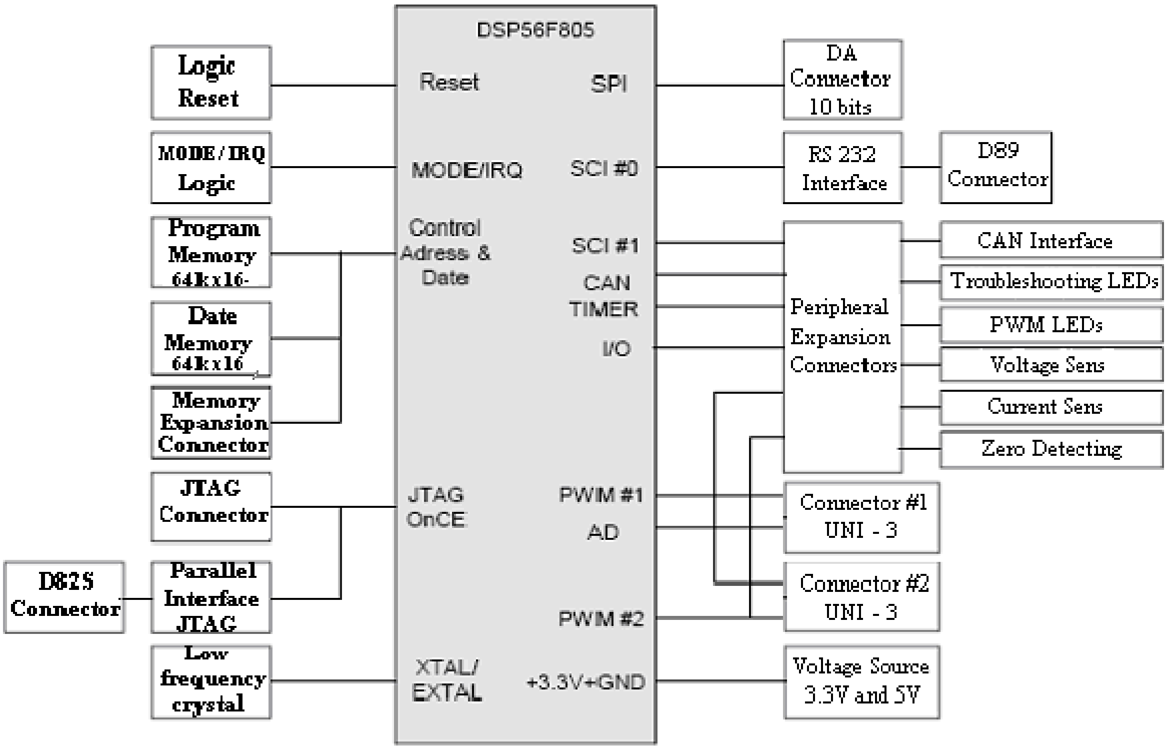

Fig.2.2. Block diagram of DSP56F805EVM

Hardware development can also be very easy, user can connect with existing system in November peripherals, and disconnect peripherals that are not necessary. For this special plugs are designed for specific ports and control and communication applications. Block diagram is shown in Figure 2.2.

The main components of plaque development are described below:

- DSP56F805 signal processor internal working frequency 80Mhz
- Rapid static external memory (FSRAM) with the following configuration
- 64k x 16 program memory 70Mhz
- 64k x16 70Mhz data memory
- Analog digital converter with four channels 10-bit SPI interface
- Frequency oscillator to generate the DSP 8Mhz
- JTAG connector for debugging programs
- SCI interface for connection to a host processor
- 1Mbps CAN interface for fast communication
- UNI interface - 3 for engine control, I / O specific
- Connectors for I / O General purpose
- LED - sites for debugging programs
- LED - sites for PWM outputs
- Disruptions associated external buttons
- Buttons RESET and I / O
- Power source of 3.3V and 5V

Development board is connected via serial and parallel interfaces to the host computer (DB9 DB25 connectors respectively) connector UNI - 3 # 1 inverter and analog acquisition board.

Characteristics of software development:

Motorola offers a wide range of tools for generating and debugging code. Besides these there is a business application developed by Metrowerks particular signal processor produced by Motorola, CodeWarrior. This software includes a C + + compiler, a macro assembler, a librarian, and editor of links, all with an easy to use graphical interface Tools for debugging and system integration including a simulator and a method of assessment.

For ease of software development DSP56F805 processor is a package of routines and specialized functions (Development System Kit). Package software development (SDK) contains predefined control peripheral functions (DSP routines PWM, ADC, etc.), electrical drives functions (Clarke, Park, etc.). C compiler generates machine code in a very efficient way, enabling this rapid development and implementation of control algorithms.

All these applications use for communication with the board JTAG/OnCETM interface development and parallel interfaces, existing host computer.

Manner of application development:

Complexity need to be controlled requires work in phases, with several intermediate stages of development. Simulators existence much easier the implementation effort, assessing system responses to control algorithms. After estimation follows the actual implementation of programs on the processor, while testing them if the values do not depend on the stand have a corresponding dynamic. It can even control the reaction test on samples of data obtained from simulations made in advance, without providing any service bench.

The final phase is starting to stand algorithm implemented, the acquisition of control variables and comparing them with values obtained by simulation.

Phase I - Simulation

Control algorithm is simulated in Simulink - Matlab, so the model should be implemented as close as possible to reality. The results are analyzed, and extrapolated to the real case, eliminating possible simplifying assumptions made in the simulation. If the solution is convenient pass to the next stage.

Phase II - Implementation of the DSP algorithm

Write control program for the DSP. Using both C language and assembly language-specific processor, the compiler is used with CodeWarrior SDK package. Along the way, to create intermediate steps to test the algorithm - partial results of the control is highlighted with embedded debugger (to view specific areas of memory, CPU registers), or towards the end, when appropriate, values are saved in memory card development on the host computer's hard disk using the communication program (TTY.exe). If the results are similar, it’s case to move to the next stage.

Phase III - Implementing the algorithm on bench

The program is developed in the previous phase test bench. At the end of the test are saved and the data acquired control with communication program. These are viewed in Matlab and compared with those obtained by simulation. If the results are similar, the development application is deemed complete.

3. DEDICATED PROGRAMME FOR DSP56F805 PVM TYPE OF ORDER INVERTER ACTIVE FILTERS

```
#include <stdio.h>
#include "805registers.h"
void init_PWM(void);
void init_PORTB(void);
void intr_PWM(void);
int contor=0;
int var=0;
int test=0;
void main(void)
{
init_PWM();
init_PORTB();
// set PWM_reload interrupt vector
asm {
        move #$0076,r0                    // PWMA_reload interrupt vector adress
        move #$e9c8,a                     // JSR
        movem a,p:(ro)+
        move #intr_PWM,a                  // 3 means no address, no there is value
        movem a,p:(ro)+
 };

//  PWM values
*gpr14 = 0 x 7000;                        // set level 7 for PWM_reload
*pwmctl = 0 x 50e0;                       // divide by 8 and 6 in6! ----->25 Hz
            *pwmval0    = 0 x 4000;                   // PWM Channel 0 Value Reg.
            //*pwmval1  = 0 x 0fa0;       // PWM Channel 1 Value Reg.
            *pwmval2    = 0 x 4000;       // PWM Channel 2 Value Reg.
            //*pwmval3  = 0 x 0fa0;       // PWM Channel 3 Value Reg.
            *pwmval4    = 0 x 4000;       // PWM Channel 4 Value Reg.
            //*pwmval5  = 0 x 0fa0;       // PWM Channel 5 Value Reg.
// enable all interrupts
*ipr  = 0 x fe12;
```

```
// Enable maskable (Level 0) interrupts
asm {bfclr #$0002,X:$0e00};
// set LDOK; 0e00 ------>pwmct1
asm {bfset #$0002,X:$0e00};
//set PWM_Enable; 0e00 ------->pwmct1
asm {bfset #$0001,X:$0e00};
while (1)
{           test++;
        // if (test>20) goto stop;                                        };
stop;
asm { bfset #$0001,X:$0e00} ;
while (1)
{           test++;
            // if (test>20) goto stop;                                     };
stop;

asm {bfclr #$0001,X:$0e00} ;          // desable PWM
}
// ISR ---------> PWM_reload
void intr_PWM (void)
{
asm{ bfclr #$0010,X:$0e00 } ;        // Interrupt acknoledge; 0e00 ----->pwmct1
*ipr  =  0 x 0000;                   // disable all external interrupts
// test++;  //timp
var++;
if (var>0)
{           var = 0;
            contor++;
                        if(contor>8) contor=;
                        *pbdr     =          contor;
};
*ipr   =   0 x fe12;                 // enable all interrupts
asm (bfcl #$0200, sr);               // Enable maskable (Level 0) interrupts
}
//initializare PORTB ca port de iesire
void init_PORTB(void)
{           *pbiar              = 0 x 0000;
            *pbien              = 0 x 0000;
            *pbipol  = 0 x 0000;
            *pbiesr             = 0 x 0000;
            *pbper              = 0 x 0000;
            *pbddr              = 0 x ffff;
}
void init_PWM(void)
{           pwmct1              = 0 x 0000;          //PWM Control Reg.
            pwmfct1             = 0 x 0000;          //PWM Control Reg.
            pwmfsa              = 0 x 0000;          //PWM Fault Status & Acknoledge Reg.
            pwmout              = 0 x 8000;          //PWM Output Control Reg.
            pwmcnt              = 0 x 0000;          //PWM Counter Reg.
            pwmcm               = 0 x 7fff;          //PWM Counter Modulo Reg.
            pwmval0                       = 0 x 0000;          //PWM Channel 0 Value Reg.
            pwmval1                       = 0 x 0000;          //PWM Channel 1 Value Reg.
            pwmval2                       = 0 x 0000;          //PWM Channel 2 Value Reg.
            pwmval3                       = 0 x 0000;          //PWM Channel 3 Value Reg.
            pwmval4                       = 0 x 0000;          //PWM Channel 4 Value Reg.
            pwmval5                       = 0 x 0000;          //PWM Channel 5 Value Reg.
            pwmdeadtm           = 0 x 002f;          //PWM Deadtime Reg.
            pwmdismap1          = 0 x 0000;          //PWM Disable Mapping Register 1
            pwmdismap2          = 0 x 0000;          //PWM Disable Mapping Register 2
            pwmcfg              = 0 x 0000;          //PWM Config Register
            pwmccr              = 0 x 0000;          //PWM Channel Control Register.
            pwmport                       = 0 x 0000;          //PWM Port Reg.
}.
```

4. CONCLUSIONS

In this paper we presented the general principles used in order active filters. On the basis of a program designed to drive filters through DSP56F805.

REFERENCES

[1.] Abellan, A. Benavent, J. M. (2001). "A New Combined Control Method for Shunt Active Filters applied to Four-Wire Power Systems", EPE 2001 – Graz

[2.] Afonso, J. Couto, C. Martines, J. (2000) "Active Filter with Control Based on the p-q Theory", IEEE Industrial Electronics Society Newsletter, Vol. 47, No. 3

[3.] Aredes, M. Watanabe, E. H. (1995) "New Control Algorithms for Series and Shunt Three-phase Four-Wire Active Power Filters", IEEE Transaction on Power Delivery, Vol. 10, No. 3

[4.] Fujita, H. Akagi, H. (1998). "The Unified Power Quality Conditioner: The Integration of Series and Shunt-Active Filters", IEEE Transactions on Power Electronics, Vol. 13, No. 2

INTERNATIONAL SYMPOSIUM on ADVANCED ENGINEERING & APPLIED MANAGEMENT
– 40th ANNIVERSARY in HIGHER EDUCATION (1970-2010),

INTERNATIONAL SYMPOSIUM on
ADVANCED ENGINEERING & APPLIED MANAGEMENT
– 40th ANNIVERSARY in HIGHER EDUCATION (1970-2010)
4 – 5 November, 2010, Hunedoara, ROMANIA

[1.]Rastislav PIRNÍK, [2.]Ján HALGAŠ, [3.]Martin ČAPKA

NON-INVASIVE MONITORING OF CALM TRAFFIC

[1-3.] UNIVERSITY OF ŽILINA, FACULTY OF ELECTRICAL ENGINEERING,
DEPARTMENT OF CONTROL AND INFORMATION SYSTEMS, ŽILINA, SLOVAKIA

ABSTRACT:
This paper deals with the use of video detection to identify the occupancy of a parking place from image information. The video detection comes in handy for cases of large and indented car parks. Suitably mounted camera can cover large area and software can locate from its images occupied places. The whole video detection system interprets the situation at car park and information about free parking places could be displayed on navigation panels guiding the drivers to the nearest free places. An added value for the management is the real-time video overview about the situation.
KEYWORDS:
car park occupancy, car park management, video detection, object tracking, calm traffic

1. INTRODUCTION

Today, the frequently discussed problem is how to detect the occupancy of parking places at institutions, park-and-ride areas, shopping centres etc. If there is a way of reliable detection of occupancy of parking place, it could be used for many commercial and security applications as well. Targeting this domain, there was realised a project "Non-invasive monitoring of calm traffic". It solves the problem of recognition of occupancy of parking places at the University of Žilina by using the video detection.

2. ESTIMATION OF CAR PARK OCCUPANCY RATE.

Every kind of car park has its own limited capacity of parking places given by areal possibilities. Already all accessing roads can be considered as a part of the car park system. Depending on many factors, the information about occupied parking places can differ from the real situation. This could lead to misinformation of drivers searching for a parking place. So an early and advisable consideration that the car park is full can prevent the ineffective navigation. The estimation of the maximum rate of occupancy to declare the car park as full depends on type, complexity, area and many other criteria. Generally there are hints helping to estimate the moment to declare the car park as full:
- ❖ To gain information about vehicles routing from/to car park
- ❖ To use zone detection and zone navigation in cases of complex car parks
- ❖ To use time zones during the day with different upper limits to declare the car park as full
- ❖ To leave a gap to take into accounts some critical situations (fire, police, ambulance, guests, etc.)
- ❖ To take into account the capacity and characteristics of car park

3. METHODS FOR OBJECT DETECTION AND TRACING

The content of every image (regardless if standalone or in a video sequence) can be divided into several levels of abstraction hierarchy [4]. The first one consists of pixels, elementary parts of every digital image, containing information about brightness or colours. The next level is aimed at features as edges, corners, curves, areas, etc. The upper level of abstraction combines and interprets this information as objects and their attributes. The top level uses concepts of processing and analyzing of images similar to human perception. These methods couple individual objects and define relations between them. The process of detection of an object in video sequence includes the step of catching its occurrence and locating it as accurate as possible in individual frames for further processing. The principle of tracking the object is generally based on processing the detected changes of its location, size, and shape in consecutive frames. Basic methods used to detect objects:

- Detection of objects based on their features
- Detection based on shape
- Detection based on colour information
- Detection based on pattern matching
- Motion detection

4. CAMERA POSITION

The position of a camera is important to effectively use its images. Therefore this fact has to be taken into account for every car park individually when using a video detection system. There are generally following two rules:

- place the camera to cover most parking places
- place the camera to minimize overlapping of objects (e.g. van vs. sport car)

In our case there were two possible views:

1. To shoot our experimental car park lengthwise, where all parking places were covered. But the problem was the height the camera to be placed (see Figure 1b). The farthermost objects were overlapped. It is important to keep the ratio between the height *h* and length *d* as great as possible to reach higher point of view (Figure 1a)
2. To shoot the experimental car park broad wise, where the ratio was more suitable. Though the angle of view of the camera in this position was limited (Figure 2 - not all parking places were covered) it was sufficient to verify our algorithm to detect the occupancy of a parking place.

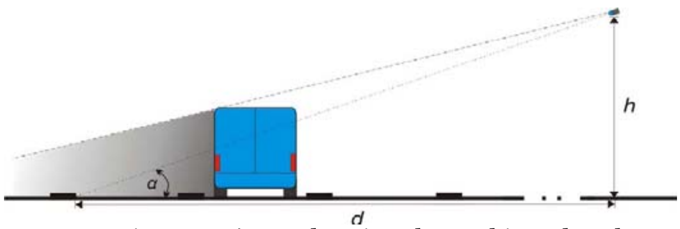

Figure 1. a) Overlapping the parking place by a vehicle, b) general view

5. STRUCTURE AND DESCRIPTION OF THE PROGRAMM

The program implements methods of detection of object based on its motion and colour information. It was written in the C++ language using the “OpenCV” – a library for computer vision. The source code was written according to the specification given in [1]. The structure of the application is explained in following text.

Definition of Region of interest - ROI

There are defined three ROI for each parking place. Two of them are used to gain relevant data (Figure 2: blue, the narrower ROI1, the wider ROI2). The ROI3 is used to visually inform about the occupancy of a parking place (Figure 2: green=free, red=occupied). For every ROI are defined four basic pixel values of its position in the frame: top, left, width and height.

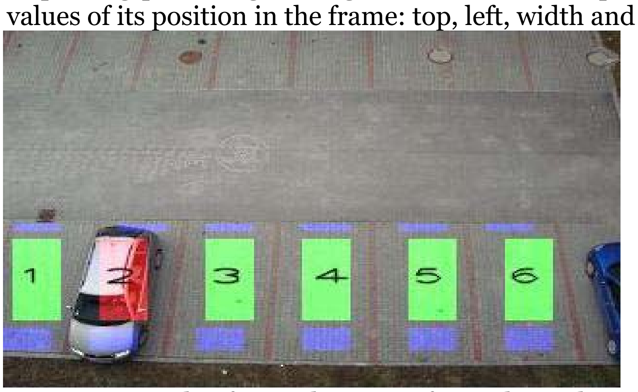

Figure 2. Example of ROI placement for parking places

Detection of moving object

For the proper run of the application it is important to accurately designate the moving objects and to interpret their impact on the parking place. Therefore the following schema illustrates the most important part of the application (Figure 3).

Block of initialization of variables

Definition and initialization of variables used during the application run for storing data

Block of getting image

The reading of image data into variables. There are three alternatives of getting the image data:

- Reading the video from connected camera (integrated webcam, camera connected through supported interfaces)
- Reading the video directly from a local storage in AVI format
- Reading the image directly from a local storage as a simple file

Block of conversion

Because of further processing, here takes the conversion from colour to greyscale place

Block R1

Because there is nothing before to compare with the first image, the application stores it in a variable to compare it with the next one.

Block of computation of changes

Computation of data changes takes place. Figure 4 shows us an example of detected changes in two consecutive frames.

Threshold block

The value of change for each pixel varies in range from 0 to 255. Processing such data structure would be complicated. Therefore a transformation to binary values is needed. It is important to set properly the threshold value [2]. The following example shows the presence of a shadow as an unwanted element when setting the threshold too low. The threshold value has to remove the artefacts and to preserve the best compactness of pixels of the moving object. The threshold value was estimated experimentally (Figure 5).

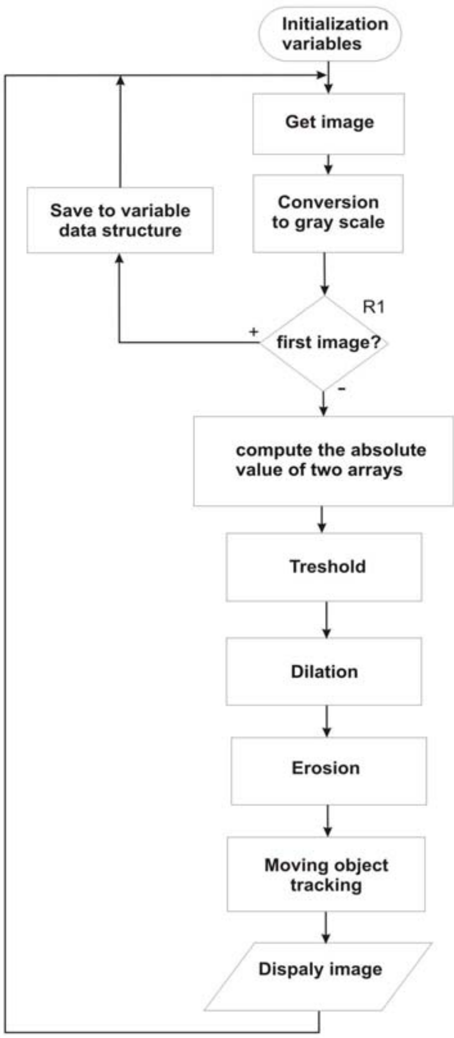

Figure 3. Block diagram of detection of a moving object

Figure 4. Example of comparing two consecutive frames in time of 0,5s

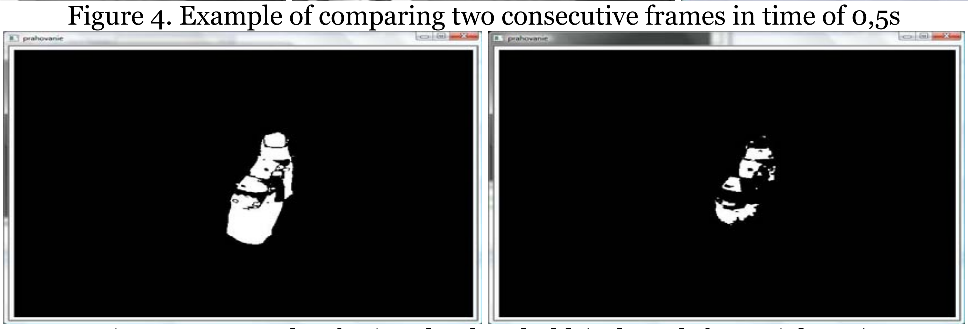

Figure 5. Example of using the threshold (values: left 35, right 80)

Blocks of dilatation and erosion

Even after an ideal threshold, the information about changed pixels will be insufficient to locate the moving object as a whole. To overcome this, several morphological transformations are used [3], [5]. The goal can be reached by their appropriate combination and properly set structural elements. All pixels of a moving object will be then compact. The modified binary image matches the moving object. In this state, there is no problem to find the object (Figure 6).

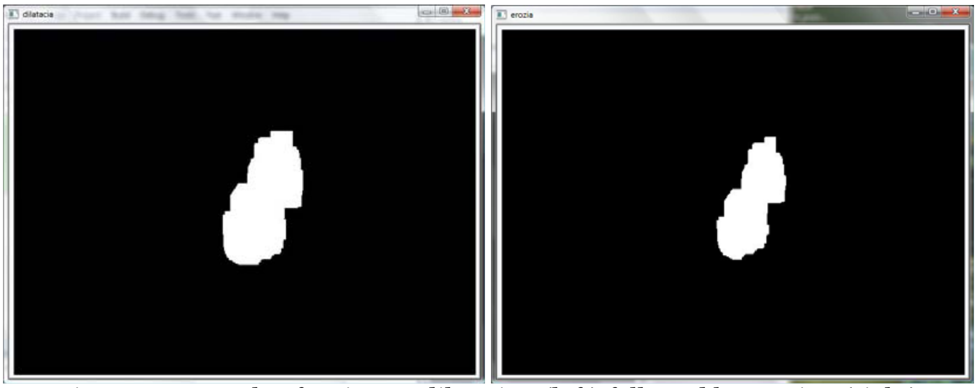

Figure 6. Example of an image dilatation (left) followed by erosion (right)

Block of moving object detection

Using mentioned modifications we can locate moving objects by finding their borders after the erosion step. The application gains data about the binary object and stores them. Based on the saved data as well, we can detect and display the moving object in actual frame to demonstrate this way the process we described.

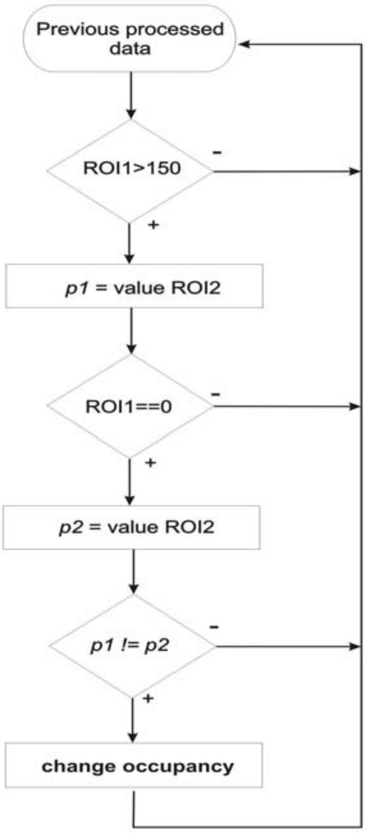

Figure 8. Algorithm of occupancy changes

Figure 7. Example of visual location of an object

The visual location of an object is done by a function drawing a rectangle around it (Figure 7). There are some limitations on accuracy according to the speed limits and refresh rate.

Evaluation of parking place occupancy

If required data for evaluation of occupancy are available (detected motion of an object in ROI1 and colour information from ROI2), the application is driven by the algorithm of evaluating changes of parking place occupancy (Figure 8.).

6. CONCLUSION

There was proposed an algorithm for evaluation of parking place occupancy by joining two methods of object detection. The algorithm is resistant to influence of weather conditions and walking pedestrians on car park. It is based on attributes of objects (speed and size of vehicles) that need to be detected. The functionality of the application was proved at the car park of university (Figure 9, 10). The proper evaluation of parking place occupancy was only influenced by vehicles moving too fast.

Figure 9. Filling of parking places

Figure 10. Freeing of parking places

ACKNOWLEDGEMENT

This paper was supported by the operation program "Research and development" of ASFEU-Agency within the frame of the project "Nové metódy merania fyzikálnych dynamických parametrov a interakcií motorových vozidiel, dopravného prúdu a vozovky". ITMS 26220220089 OPVaV-2009/2.2/03-SORO co financed by European fond of regional development. "We support research activities in Slovakia / The project is co financed by EU".

REFERENCES:

[1.] HALGAŠ, J., *Riadiaci videodetekčný parkovací systém:* diplomová práca. Žilina: Žilinská univerzita v Žiline, 2010. 45s.

[2.] HUDEC, R., Snímanie obrazu, vysokoškolská učebnica, EDIS, August 2008, 150 strán, ISBN 978-80-8070-880-1.

[3.] R. HUDEC, M. BENČO: Systém automatickej identifikácie dopravných priestupkov, Medzinárodná konferencia „Research in Telecommunication Technology 2006", Part II. pp. 133-136, September 11th - 13th 2006, Nové Město na Moravě, Czech Republic, ISBN 80-214-3243-8.

[4.] JURIŠICA, L. - HUBINSKÝ, P. - KNOT,J. *Detekcia a sledovanie objektov.* In *AT&P journal.* [online]. 2005, číslo 6. www.atpjournal.sk/casopisy/atp_05/pdf/atp-2005-06-69.pdf

[5.] P. LUKÁČ, M. BENČO, R. HUDEC, Z. DUBCOVÁ: Color image segmentation for retrieval in large image-databases, TRANSCOM 2009, pp. 113-116, Žilina, Slovakia. ISBN 978-80-554-0039-6.

INTERNATIONAL SYMPOSIUM on ADVANCED ENGINEERING & APPLIED MANAGEMENT
– 40th ANNIVERSARY in HIGHER EDUCATION (1970-2010),

INTERNATIONAL SYMPOSIUM on
ADVANCED ENGINEERING & APPLIED MANAGEMENT
– 40th ANNIVERSARY in HIGHER EDUCATION (1970-2010)
4 – 5 November, 2010, Hunedoara, ROMANIA

1. Martin VESTENICKÝ, 2. Peter VESTENICKÝ, 1. Martin VACULÍK, 2. Mária FRANEKOVÁ

SENSOR NETWORK FOR VEHICLES TRANSPORTING DANGEROUS GOODS

1, 3. UNIVERSITY OF ŽILINA, FACULTY OF ELECTRICAL ENGINEERING,
DEPARTMENT OF TELECOMMUNICATIONS AND MULTIMEDIA, ŽILINA, SLOVAKIA
2, 4 UNIVERSITY OF ŽILINA, FACULTY OF ELECTRICAL ENGINEERING,
DEPARTMENT OF CONTROL AND INFORMATION SYSTEMS, ŽILINA, SLOVAKIA

ABSTRACT:
The described sensor network has been designed to enable real-time monitoring of dangerous goods status during transport. The network is based on well known CAN bus which is widely used in automotive industry. The sensors measure temperature, LPG concentration, vehicle inclination and pressure. Status of the sensor is transferred via OBU into monitoring centre by GSM network.
KEYWORDS:
Sensor, LPG, inclination, temperature, pressure, CAN bus, on-board unit

1. INTRODUCTION

The dangerous good transport by road network is everyday threat for population and environment close roads which are being used for these transports. Despite of respecting of all regulations there always exists possibility of technical failures, crashes and malfunctions. For elimination of these risks an information system for the monitoring of the dangerous good transport has been developed. This system uses standard communication technologies GPS, GSM/GPRS and CAN (Controller Area Network). The whole project of dangerous goods transport monitoring was solved as a part of the project CONNECT [1] which was funded by the European Commission.

The sensor network for vehicles transporting dangerous goods has been designed to monitor selected parameters of the dangerous goods during transport. Conception of the sensor network is open to enable flexible selection of number and types of the sensor units. For connection to the vehicle OBU (On Board Unit) a standard industrial CAN bus has been selected. CAN bus is often being used in automotive industry for its robustness, resistance against the external environment and fault management [7]. Topology of designed sensor network is shown in Fig. 1.

2. CONCEPTION OF THE SENSOR UNITS

Because standard types of analog or digital sensor elements have not direct CAN bus interface the conception of intelligent sensor units has been selected. Every sensor is equipped with its own microcomputer which performs several functions: communication, diagnostic and data processing. During the design steps of sensor network the reliability and autodiagnostic properties have been emphasized [6]. The microcomputer of sensor unit periodically checks the checksums of program memory and configuration memory. Next diagnostic mechanism built in sensor unit is self test of used sensor elements. The simple sensor elements (contacts, temperature sensor etc.) are doubled and the microcomputer compares if both elements give similar data in the predefined tolerance field. All sensor units have the same block diagram which is in Fig. 2. Except for the sensor element the unit contains microcomputer with CAN bus support and driver of CAN physical layer. The sensor unit has linear DC stabilizer for supplying of electronic circuits. The current consumption is from 50 to 80 mA in dependence on the sensor type.

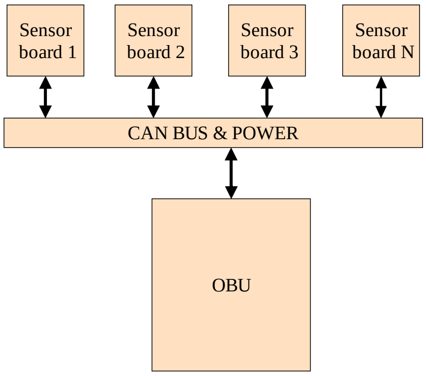

Figure 1. Interconnection of the sensor network

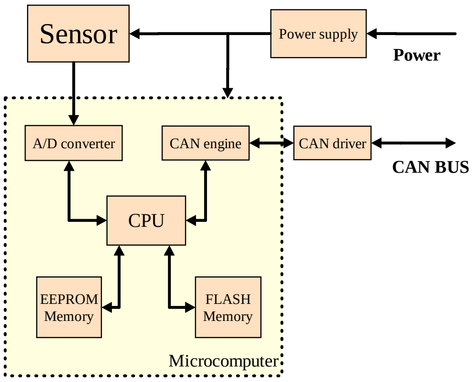

Figure 2. Block diagram of sensor unit

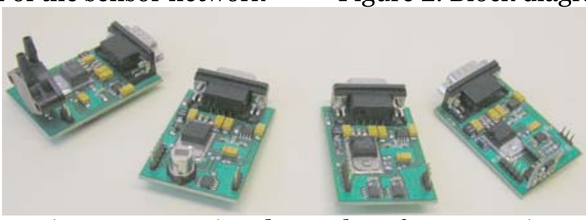

Figure 3. Functional samples of sensor units

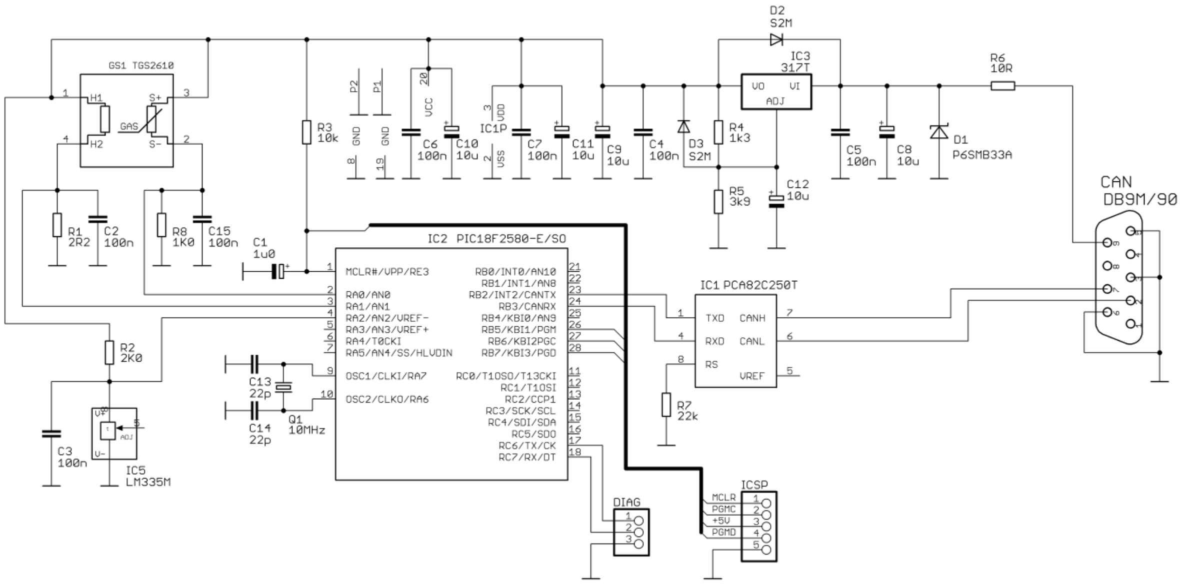

Figure 4. Schematic diagram of LPG sensor unit

For verification of selected conception these functional samples of sensor units have been designed and produced:

- Temperature sensor unit
- Gas detector unit (LPG)
- Unit for measurement of vehicle inclination and detection of overturning
- Unit for measurement of absolute or relative pressure of transported medium.

All four samples of sensor units are shown in Fig. 3, detailed schematic diagram of LPG concentration sensor is shown in Fig. 4 and detail of the vehicle inclination sensor is in Fig. 5.

Physical communication medium of vehicle sensor network is created by STP cable of category 5e which is mostly being used in local area networks. The cable has suitable impedance and wire cross section. One pair is used for data communication and next pair is used for powering of sensor elements. Other two pairs are not used. Connectors used in functional samples and their pinning are compliant with specification [2]. In case of real usage in vehicle environment more suitable cable and connectors will be chosen.

3. FIRMWARE OF THE SENSOR UNITS

Firmware of the sensor unit consists of several key parts which enable to perform all required functions. These functions are defined as follows:

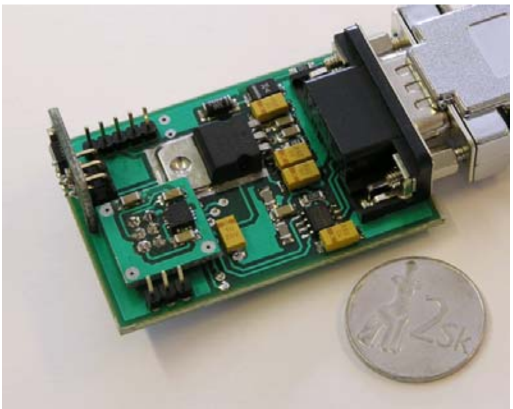

Figure 5. Detail of vehicle inclination sensor unit

- Initialization of sensor unit i. e. definition of input and output ports of microcomputer, initialization of A/D converter, CAN engine, interrupt system and loading of calibration constants.
- Autodiagnostic of the sensor unit consists from test of microcomputer [4] and test of sensor elements. The test of microcomputer is the same for all kinds of sensor units. During this test the checksums of program (FLASH) memory and configuration (EEPROM) memory are computed and compared with predefined values which are stored at the last addresses of program memory and configuration memory. The test of sensor element depends on the type of sensors. Temperature sensors are tested by comparison of values from two identical sensors placed close together. The test result is positive if absolute value of difference of both temperatures is less than predefined constant. Accelerometers and pressure sensors have self test mechanisms integrated and they can be activated by a logical signal from microcomputer. After activation of self test known value is added to sensor output voltage and the test result is positive if this voltage increase is registered by microcomputer. The LPG sensor is tested by monitoring of heating DC current which must be in predefined interval.
- Data processing - the sensor elements provide analog signals which are digitalized by 10 bit A/D converter built in the microcomputer. The sampling rate in all sensor units has been set to 8 kHz. This value is sufficient for processing signal spectrum generated by used sensors. In the next step the sampled signals are digitally filtered by averaging filter with length of 8 samples and decimated by ratio 1:8 because the computational power of used microcomputer is limited. From preprocessed signal the value of observed quantity is calculated in accordance with mathematical formulae given for sensor elements. For example, gas concentration (in ppm) can be calculated from these equations:

$$C = 10^{-\frac{\log\frac{R_{S20}}{R_0 \cdot K}}{\alpha}} \quad (1)$$

$$R_{S20} = \frac{R_S}{T_{C1} \cdot T_{MEAS} + T_{C2}} \quad (2)$$

$$R_S = R_8 \cdot \frac{1024 - RES_{AD}}{RES_{AD}} \quad (3)$$

where α, K, T_{C1}, T_{C2} are specific constants for given type of gas sensor (Table 1), R_0 is sensor resistance at gas concentration 1800 ppm and temperature 20 °C, R_S is sensor resistance before temperature compensation, R_{S20} is sensor resistance after temperature compensation (2), R_8 is 1 kΩ resistor in series with the sensor (see Fig. 4) and RES_{AD} is the result of A/D conversion. The calculations are performed in the space of integer numbers. In the calculation process the compensation and calibration data are taken into account. If the result values exceed the boundary values an alarm message is sent into the OBU.

- The communication with the OBU is on the physical and data link layers performed by the CAN bus controller which is integrated into the microcomputer. The CAN controller after proper configuration performs all needed communication functions without CPU intervention. For communication on the application layer a simple protocol has been designed. The role of the CPU is to read and write data and configuration registers of the CAN controller, evaluation of its status, receiving of commands from the OBU and sending responses or alarms to the OBU.

4. COMMUNICATION PROTOCOL ON THE APPLICATION LAYER

A simple communication protocol has been designed for communication between sensor units and the OBU. Standardized application protocols working on the CAN bus (CANOpen, DeviceNet) have not been used for their complexity. The protocol is based on command – answer principle. Protocol data units are transferred by using standard data frames with 8 octet data field in accordance to CAN 2.0A specification [3]. The PDU structure is given in the Table 2. The CAN message identifier (11 bits) is used to address group of sensor units which measure the same quantity (000H – OBU, 010H – inclination sensors, 020H – pressure sensors, 030H – gas sensors, 040H – temperature sensors). The sensor unit uses CAN filter to select only the messages relevant for its group. The whole sensor network is addressed by message with identifier 000H. Individual sensors can be addressed on the application layer by the 16 bits sensor unit number SENS_NBR.

The command, answer or alarm is identified by the CMD_ID/ANS_ID field (Table 3). Command parameters or measured values are transferred in the fields VAL1_L – VAL0_H. If longer message must be fragmented the field MES_NBR gives number of fragments (4 bits) and fragment order (4 bits). An example of communication shows Fig. 6.

Table 1. The Constants for LPG Sensor FIGARO TGS2610

α	K	T_{C1}	T_{C2}	R_0
0.5413	57.82	-0.02	1.4	1.46 kΩ

Table 2. Structure of The PDU

ID	D0	D1	D2	D3	D4	D5	D6	D7
SENS_ID	CMD_ID/ ANS_ID	MES_NBR	SENS_NBR_L	SENS_NBR_H	VAL_1_L	VAL_1_H	VAL_0_L	VAL_0_H

Table 3. Definition of Commands, Answers and Alarms

CMD_ID/ ANS_ID	TYPE	Description
00H	CMD	Get sensor unique identifier
01H	ANS	Number of sensor unit
02H	CMD	Set number of sensor unit
04H	CMD	Get sensor unit status
05H	ANS	Sensor unit status
06H	CMD	Get actual sensor data
07H	ANS	Actual sensor data
08H	CMD	Set sensor limit value
0AH	CMD	Get sensor limit value
0BH	ANS	Sensor limit value
0DH	ALM	Upper limit exceeded
0FH	ALM	Lower limit exceeded
11H	ALM	Sensor error
12H	CMD	Sensor reset
13H	ANS	OK
15H	ANS	Error

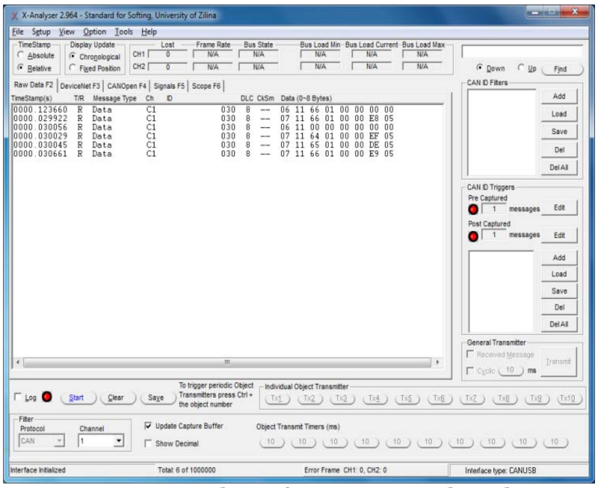

Figure 6. Snapshot of CAN protocol analyzer

Example of communication among the OBU and he sensor units shows the measurement of LPG concentration. Three gas sensors with identification numbers SENS_NBR 0164H, 0165H and 0166H respectively have been used and they have been placed into environment with LPG concentration approximately 1500 ppm. The first two lines in Fig. 6 show communication between the OBU and the sensor with number 0166H which returned value 05E8H (1512 ppm), the third line shows multicast communication from the OBU to the sensors (SENS_NBR=0000H). Last three lines are answers from all three sensor units, respectively.

5. CONCLUSION

The project CONNECT [1] solved in domain 4 (Traveler Information Services) and in its subdomain 4.9 problems of creation “Dangerous goods monitoring and information system.” At present a new project EasyWay [5] continues in solving of similar themes focused on intelligent transport systems.

The described design of the sensor network is an integral part of the subdomain 4.9 system solution. For the test purposes three sets of OBUs and sensor networks have been manufactured. The tests have been performed on the territory of north Slovakia by staff of Transport Research Institute, Inc. and University of Žilina. Results of the tests prove full functionality of manufactured OBU prototypes, sensor networks and real time data transfer into the monitoring centre. Next development will be focused on design of new sensor units, for example “black box” for road traffic accident analysis.

In addition to the technical development of the information system for dangerous good transport monitoring the questions about standardization and legislative are interested, for example the standardization of sensors in vehicles, integration of the various functions into the OBU, the international cooperation on dangerous good monitoring etc.

ACKNOWLEDGMENT

This work was created as a part of solution of international project "Coordination and Stimulation of Innovative ITS Activities in Central and Eastern European Countries – CONNECT", TEN-T Programme EC. Project number: Addition no. 3 to Contract no. 472/VÚD 2002.

This work has been supported by the Grant Agency VEGA of the Slovak REPUBLIC, grant No. 1/0023/08 "Theoretical Apparatus for Risk Analysis and Risk Evaluation of Transport Telematic Systems."

REFERENCES

[1] CONNECT, Co-ordination and Stimulation of Innovative ITS Activities in Central and Eastern European Countries. [online]. URL <http://www.connect-project.org/>

[2] CiA 303-1 DR V1.7: CANopen additional specification – Part 1: Cabling and connector pin assignment

[3] CAN specification, Version 2.0. Robert Bosch Gmbh. 1991. [online] URL <http://www.semiconductors.bosch.de/pdf/can2spec.pdf>

[4] HOTTMAR, V., SCHWARTZ, L., TRSTENSKÝ, D.: End User Box for Interactive Cable Television. IEEE Transactions on Consumer Electronics, May 2007, volume 53, number 2, pp. 412-416, ISSN 0098-3063

[5] EasyWay, [online]. URL <http://www.easyway-its.eu/>

[6] ZOLOTOVÁ, I., LANDRYOVÁ, L.: Knowledge model Integrated in SCADA/HMI System for Failure Process Prediction. WSEAS Transaction on Circuits and Systems, Issue 4, Volume 4, April 2005, pp. 309-318, ISSN 1109-2734

[7] BALOG, R., BÉLAY, I., DORNER, J., DRAHOŠ, P.: Industrial Communications. Slovak Technical University, Bratislava, 2001, ISBN 80-227-1600-6 (in slovak)

INTERNATIONAL SYMPOSIUM on ADVANCED ENGINEERING & APPLIED MANAGEMENT
– 40th ANNIVERSARY in HIGHER EDUCATION (1970-2010),

INTERNATIONAL SYMPOSIUM on ADVANCED ENGINEERING & APPLIED MANAGEMENT
– 40th ANNIVERSARY in HIGHER EDUCATION (1970-2010),

INTERNATIONAL SYMPOSIUM on
ADVANCED ENGINEERING & APPLIED MANAGEMENT
– 40th ANNIVERSARY in HIGHER EDUCATION (1970-2010)
4 – 5 November, 2010, Hunedoara, ROMANIA

[1.]Martin VYSOCKÝ, [2.]Pavol LIPTAI, [3.]Zuzana FARKAŠOVSKÁ

ACOUSTIC QUALITY OF ELECTROMOTOR

[1-3.] TECHNICAL UNIVERSITY IN KOŠICE, FACULTY OF MECHANICAL ENGINEERING, DEPARTMENT OF ENVIRONMENTAL STUDIES AND INFORMATION ENGINEERING, KOŠICE, SLOVAKIA

ABSTRACT:
Article trial above all about acoustic quality of products, then relationship between source and recipient of noise. Concrete oneself dealt one of major sources a noise near appliance and it is a noise of electromotor. Electromotor is able to cause unfavourably on man and there are several criterion that are in this article designated. Modification on given spoil whether position of electromotor is able improve acoustic quality of products.
KEYWORDS:
electromotor, acoustic quality of products, appliance

1. INTRODUCTION

On introduction this contributions is needed to say, what this is in fact acoustic quality of products and why it is important for presentation. Noise us round everywhere about, at home, in the streets, in work, in industries, transport etc. But a noise we can to find on appliance too, whether already is going about fridge, washing machine or mixer and when is more friendly for man, thereby we can to talk about higher acoustic quality of products. It doesn't need to be quite eliminated, even though is this most ideal solution, but be enough, as far as is possible identify and partly lower.

2. ACOUSTIC QUALITY OF PRODUCTS

Designers make choices regarding structure, materials and components in a product. The tools they use should allow them to anticipate the effect of these choices on sound quality. This discussion recounts the role of psychoacoustics in product design and product acceptability and notes the results of that work in metrics for sound quality and consumer/ user perceptions about the product.[1]

Sounds of assistance can be displeased, but also can be luck to. Every engineer should be take note of product by managerial views, because analysis of acoustic signal, humane perception, design and coast-benefit analysis to general profit too are criterion for quality assurance of products. Responsibilities designer, whether manager is propose and try quality of products, remove limitations still during testing products and take to high-class product on market. All these products are before application on market testing and feigned. Important factor for arbitration qualities of products is department psychoacoustics.

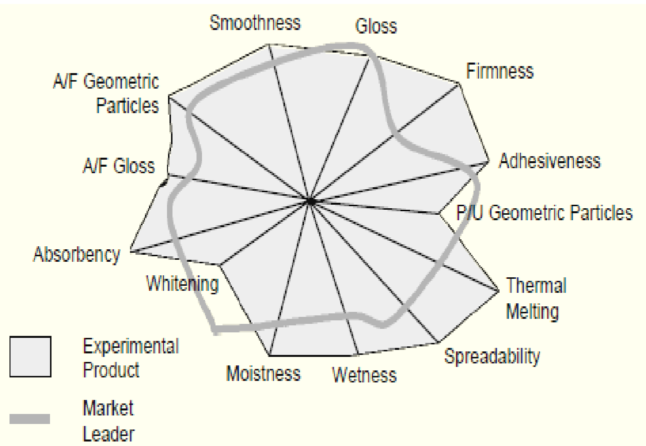

Figure 1. Sensory profiles of two skin care products [2]

Psychoacoustics is science or study that is dealt thereby, how given product perceive single man, and then centre his acoustic receptors on surroundings extraditing sound whether noise. Main aid of psychoacoustics is alternate testing, where people are asked to reception various sound, then are testing and there are additionally producing specific performance chart about sound. Industries use near for training experts a panel or "sensory profiles" (Figure 1.).[2]

3. SOURCES OF NOISE ELECTROMOTOR

Electromotor we can classify as one of major source of transmission sound from appliance and it is needed more closely present of this problem. Electromotor is machine, wherein is electric energy turn on kinetic energy revolving sections of electromotor, rotor. Electromotores utilize physical phenomenon electromagnetics, but there have been motores bottom on by other electromechanical phenomenon e.g . electrostatics, piezoelectric phenomenon and below. Every electromotor is unloaded from duo basic sections - statically boot immobile sections - stator, and mobile sections (usually spinning) rotor. (Figure 2.).

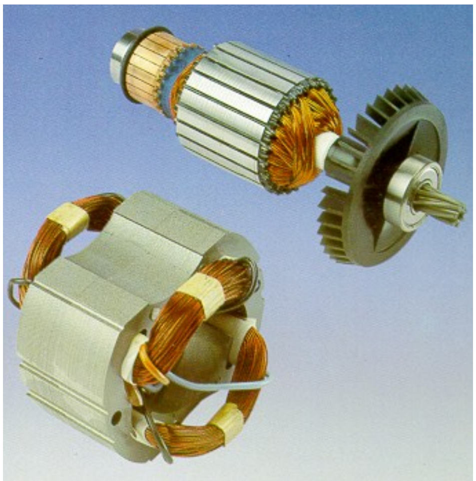

Figure 2. Electromotor of appliance

Between general sources of noise in electromotor belong:

- ❖ Unbalance of electromotor,
- ❖ Bearing of electromotor,
- ❖ Commutators,
- ❖ Aerosound (scoring on rotor).

a) Unbalance of electromotor

Concerning noise electromotor by his unbalance, is this narrowly linear just with vibration of rotor in electromotor, then given noise is doing single vibrations, it is unbalance rotor. We can to say, that unbalance is one from source judder.

Judder are considered as very suitable operating parameter, by that is possible assess AF - audio frequency dynamic construction sequence cases. On creation of vibration in construction sections of electromotor is sharing different sorts of source vibration, mainly recollection unbalance and further mechanical clearance of mounting, resonance of construction, abnormal wear bearing or snap small shovel rotor.

Suitable cap for creation exciting vibration in the working condition machinery is half-round placing rotor and stator of electromotor (Figure 3.). Inaccuracy production rigger ganglion (rotor - bearing - stator) and his consistent working resort influence mutual dynamic eccentricity to excitement vibration. [6].

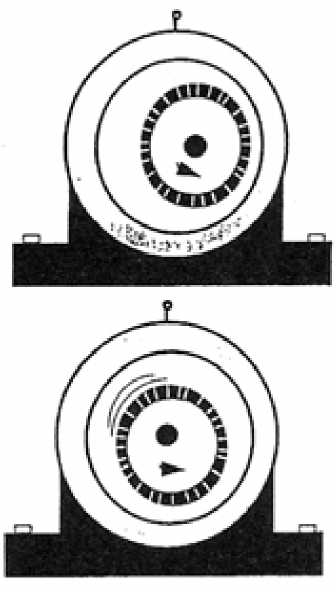

Figure 3. Drive vibrations in electromotor [6]

Figure 4.Bearing of electromotor for appliance Source: http://www.okokchina.com

b) Bearing of electromotor

On part of electromotor in appliance are bearing, that are be instrumental to placing rotor in electromotor (Figure 4.). They are next possible of cause noise of electromotor and thanks for bearing is raising life of electromotor and products or appliance too.

Good and effective diagnostics is able to prevent crash and meaningly to lower repair for costs. Providing electromotor allows timely revelation "inadmissible" technical conditions bearing with exchange bearing in optimally time in several tenth euro without serious after-effects or damage prominent sections of electromotor. If electromotor isn't monitoring, is able to come about disintegration of bearing, in pursuance of st. (under working arrangements) is rotary part aggrieving stator and resort to destruction winding or to deformation mechanical sections and in extremeness case to complete destruction of electromotor. [4]

c) Commutators

Commutators (Figure 5.) create conductive half-ring uncross isolating layer. Every commutator is connected with one end of reel and act motion of rotation included with cateterisation. Brushes invariable one's position, and are conductivity connection with district and source. Commutator and brushes still baffle whereupon is reel turn on drowe energy. This machinery we are talking about electromotor.[5]

Figure 5. Commutator

Good commutantion lead the way assumption of correct functions commutator to dress. Below concept commutantion is understand complex march in reel winding rotor, that are near turning curl grind from influence one's pole below another pole. Near this change is through the medium commutator changing direction flow in reel. Volts every commutating reel, in who is turn direction flow, arrive together toward connecting briefly over brushes and lamella of commutator. [5]

d) Aerodynamic noise of electromotor

Tone noise is editing providing, when flow over blown space too. It's infliction shift of backward whirls, that are stroke on border wall and further are throw back about additional walls. Flow further and form new maelstroms (Figure 6.).

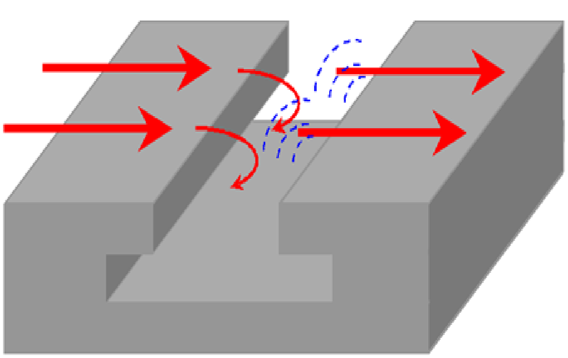

Figure 6. Flowinf of sound in hollow spaces [3]

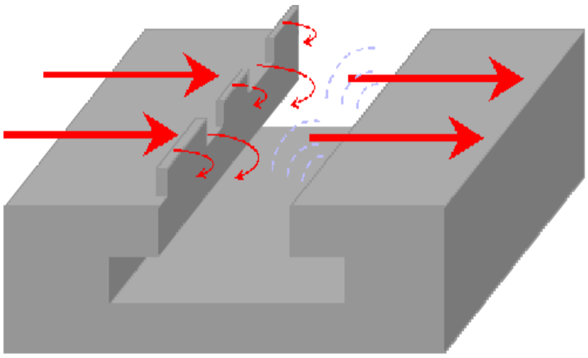

Figure 7. Measure for cut-down aerodynamic noise in hollow spaces [3]

Flowing acoustic coupling can be cut-down additional groove on front edge of sections walls (Figure 7.).

As a result is turbulence with different length weight and thereby creation small constructive sound of windy. In the last analysis is concerned the same thought, in to have be near falling noise around cylindral surface sections electromotor.[3]

4. CONCLUSION

This article apprised reader not only with acoustic quality of products and main sources of noise in electromotor for appliances too, but also abets possibilities of improvements acoustic qualities of products, then possibility noise reduction on electromotor.

Acknowledgement

This paper was supported by projects APVV-0176-071/0453/08 and KEGA 3/7426/09.

REFERENCES

[1.] B. G. Churcher and A. J. King, "The Performance of Noise Meters in Terms of the Primary Standard," Journal of the Institute of Electrical Engineers, (London) Vol 81, pp 59-90, 1937.
[2.] H. Fletcher and J. A. Munson, "Loudness, Its Definition, Measurement, and Calculation," Journal of the Acoustical Society of America, Vol. 5, pp 82-108, 1933.
[3.] Aerodynamic noise electric motor: Available online 10.09.2010 on http://www.diracdelta.co.uk/science/source/a/e/aerodynamic%20noise/source.html
[4.] Bearing of electromotor: Available online 15.09.2010 on http://www.atpjournal.sk/casopisy/atp_09/pdf/atp-2009-06-16.pdf
[5.] Commutators: Available online 08.09.2010 on http://lazo.czechian.net/elektrika/dynamo.htm
[6.] Unbalance of electromotor: Available online 26.09.2010 on http://web.tuke.sk/fvtpo/casopis/pdf07/3-str-75-78.pdf

INTERNATIONAL SYMPOSIUM on ADVANCED ENGINEERING & APPLIED MANAGEMENT
– 40th ANNIVERSARY in HIGHER EDUCATION (1970-2010),

INTERNATIONAL SYMPOSIUM on
ADVANCED ENGINEERING & APPLIED MANAGEMENT
– 40th ANNIVERSARY in HIGHER EDUCATION (1970-2010)
4 – 5 November, 2010, Hunedoara, ROMANIA

[1] Anjan KUMAR KUNDU, [2] Bijoy BANDYOPADHYAY, [3] Sugata SANYAL

A MICROWAVE IMAGING AND ENHANCEMENT TECHNIQUE FROM NOISY SYNTHETIC DATA

[1-2.] INSTITUTE OF RADIOPHYSICS & ELECTRONICS, UNIVERSITY OF CALCUTTA, KOLKATA, INDIA.
[3] TATA INSTITUTE OF FUNDAMENTAL RESEARCH, INDIA

ABSTRACT:
An inverse iterative algorithm for microwave imaging based on moment method solution is presented here. The iterative scheme has been developed on constrained optimization technique and is certain to converge. Different mesh size for the model has been used here to overcome the Inverse Crime. The synthetic data at the receivers is contaminated with different percentage of noise. The ill-posedness of the problem is solved by Levenberg - Marquardt method. The algorithm is applied to synthetic data and the reconstructed image is then further enhanced through the Image enhancement technique.
KEYWORDS: Microwave Tomography, Levenberg-Marquardt Method, Inverse crime, Percentage noise, Image Adjustment

1. INTRODUCTION

For the last few decades, microwave tomography techniques for biomedical applications have been received increasing interest. Intensive studies in this field able to give an efficient solution to quantitative imaging. We had proposed several algorithms [1-2] which though reconstructed the image without any misfit, yet the mesh size remains the same both in the forward and the inverse problem leading to inverse crime. This paper represents an iterative algorithm based on Levenberg-Marquardt regularization technique with necessary considerations to avoid inverse crime. The reconstructed image is then undergone through image enhancement mechanisms to minimize the noise.

2. THE STUDY

During the past 20 years, immense research has been carried out in microwave tomography to quantitatively reconstruct the complex permittivity distribution of the biological media. Standard spectral diffraction tomography [3-7] which has been investigated with application to microwaves, prove to be very fast and capable of producing reconstructions with good quantitative accuracy for small contrast objects.

Yet it is subjected to various limitations, including the artifacts due to the diffraction effects in strongly inhomogeneous media where Born or Rytov approximations are not valid [8-9]. Several approaches based on moment methods [10-12] have, in past, been explored rigorously, but the stability depends on the measurement accuracy due to ill-conditioning of the matrix. Also the convergence depends on the contrast of the objective.

In recent years, multiplicative regularized contrast source inversion method is applied to microwave biomedical applications [13-14]. The inversion method is fully iterative and avoids solving any forward problem in each iterative step.

In our earlier works [15-16], we had suggested quasi-ray optic SIRT-style algorithms for microwave imaging. In those first generation algorithms it was assumed that only those cells situated within the beamwidth of the transmitter radiation pattern, would effectively contribute to the field at the end of a ray. Those linear and nonlinear algorithms did not reconstruct the image quantitatively to the extent which could be considered to be clinically important.

The earlier algorithms proposed by us [1-2] which, though reconstructed the image without any misfit, yet the same mesh size for both in the forward and the inverse problem leading to inverse crime. This paper represents an iterative algorithm with necessary considerations to avoid inverse crime.

3. ANALYSIS, DISCUSSIONS, APPROACHES AND INTERPRETATIONS

3.1. Forward problem

The forward problem has already been discussed in details in our previous work [2]. A cylindrical object of arbitrary cross section is considered here which is characterized by a complex permittivity distribution ε(x,y). An electromagnetic wave radiated from an open-ended waveguide is used here for the illumination. The incident electric field E^{inc} is parallel to the axis of the cylinder.

The expression for the total electric field E is

$$\vec{E} = \vec{E}^{inc} + \vec{E}^{s} \tag{1}$$

where E_s represents the scattered field which is generated by the equivalent electric current radiating in free space.

The total electric field can be calculated with an integral representation

$$\vec{E}(x,y) = \vec{E}^{inc}(x,y) + \int_s J \int_s (x,y)\, G(x,y;x',y')\ d\ x'\ d\ y' \tag{2}$$

where the Green's function can be given by

$$G(x,y;x',y') = -\frac{j}{4} H_0^2\left(k\sqrt{(x\ \ x')^2+(y\ \ y')^2}\right) \tag{3}$$

Here (x, y) and (x', y') are the observation and source points respectively.

The solution of the forward problem are carried out by moment method [17] using pulse-basis function and point matching technique. The synthetic data at the receivers is then contaminated with different percentage of noise as our main objective is to reconstruct the numerical model under noisy conditions.

3.2. Inverse problem

The aim of the inverse problem is to find a stable solution for permittivity distribution ε^* which minimizes the squared error output at the receivers i.e.

$$\|E(\varepsilon) - e\|_2^2 \tag{4}$$

where $e \in C^n$, the n electric fields we measure at receiver points,

$E : C^m \longrightarrow C^n$, a function mapping the complex permittivity distribution with degrees of freedom into a set of n approximate electric field observations, and also $\varepsilon \in Cm$, the complex permittivity distributions with m degrees of freedom.

The Levenberg-Marquardt regularization technique for the minimization of the (4) leads to an iterative solution

$$\varepsilon_{i+1} = \varepsilon_i + \Delta\varepsilon_i \tag{5}$$

where ε_{k+1} is the permittivity distribution at the k+1th iteration.

$\Delta\varepsilon$ can be written as

$$\Delta\varepsilon = (E'(\varepsilon)\dagger E'(\varepsilon) + \lambda\ I)^{-1}\ E'(\varepsilon)^{\dagger}(E(\varepsilon) - e) \tag{6}$$

where E' is the Jacobian matrix, † denotes the conjugate transpose, λ is a monotonically decreasing regularization parameter, I is the identity matrix, $E(\varepsilon)$ is the calculated electric fields at the receivers.

3.3. Numerical Model

To test our algorithm, we have considered the following model as shown in Figure 1.

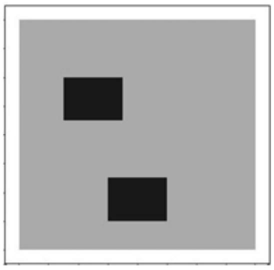

Figure 1. Numerical model

It is a high contrast square biological object 9.6 cm × 9.6 cm consisting of muscle and bone having complex dielectric constants 50-j23 and 8-j1.2 respectively at a frequency of 1 GHz. The object is kept immersed in saline water having complex dielectric constant 76-j40.

The target is illuminated with TE fields radiating from an open ended dielectric filled wave guide having sinusoidal aperture field distribution. The transmitter is moved along four mutually orthogonal directions. For each of the transmitter positions along a particular transmitting plane, the received fields at eighteen locations in the other three orthogonal planes were measured theoretically at a frequency of 1 GHz.

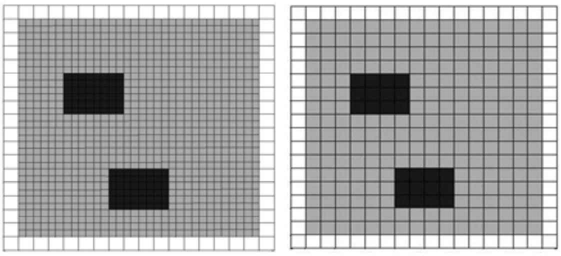

Figure 2. Meshes used to overcome the inverse crime (a) Mesh used in forward problem (b). Mesh used in inverse problem

Different meshes are used to overcome the inverse problem as shown in figure 2. The finer mesh is used in the forward problem (Figure 2(a)) whereas the inverse solver uses the coarse mesh (Figure 2 (b)).

In case of forward problem, the rectangular model is divided into 1024 square cells of dimension 0.3cm X 0.3cm and the saline water region is divided into 32 cells of dimension 0.6cm X 0.6cm. During the inverse problem, the rectangular model together with saline water region is divided into 324 equal square cells 0.6 cm $\times$ 0.6 cm. The measurement set contains 288 independent data.

During the iterative reconstruction, the complex permittivity values of the cells filled up with saline water were assumed to be known, thus rendering the problem of estimating the complex dielectric constants of the remaining 256 cells.

3.4. RESULTS AND DISCUSSIONS

To apply the reconstruction algorithm, it was initially assumed that the biological medium is filled up with muscle only. The received fields at different receiver locations were computed for each transmitter position. The only priori information we have used in our algorithm is that the real part of the complex dielectric constant cannot be negative and the imaginary part cannot be positive. The iteration is stopped when the 2-norm error output is of the order of 10^{-4}.

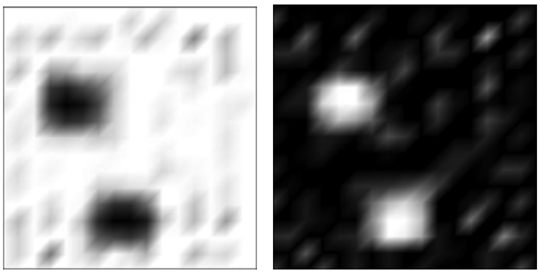

Figure 3. Reconstructed model with 1%noise (a) Real part (b) Imaginary part

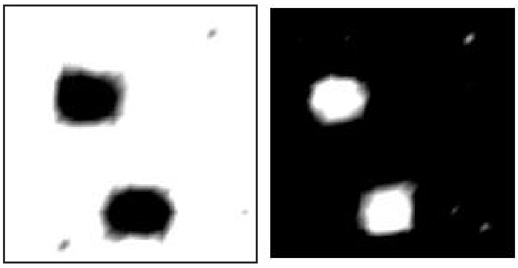

Figure 4. Reconstructed model with 1%noise after using image adjustment technique (a) Real part (b) Imaginary part

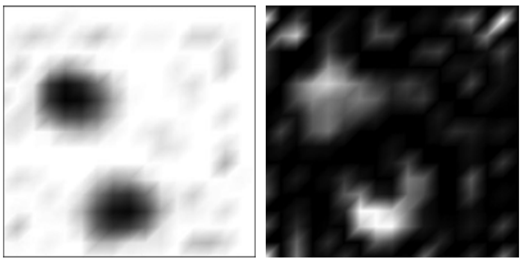

Figure 5. Reconstructed model with 2%noise (a) Real part (b) Imaginary part

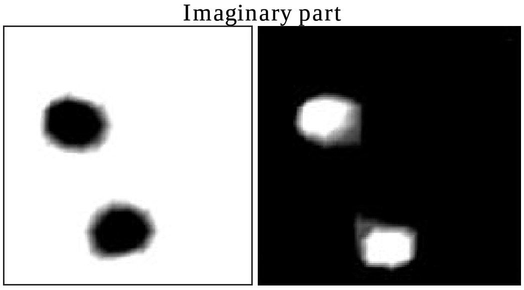

Figure 6. Reconstructed model with 2%noise after using image adjustment technique (a) Real part (b) Imaginary part

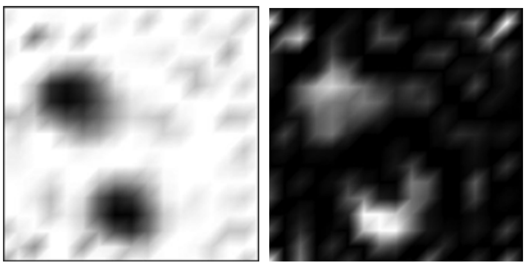

Figure 7. Reconstructed model with 5%noise (a) Real part (b) Imaginary part

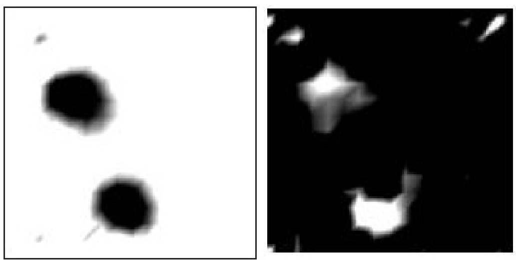

Figure 8. Reconstructed model with 5%noise after using image adjustment technique (a) Real part (b) Imaginary part

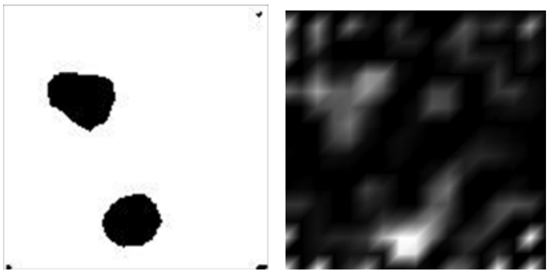

Figure 9. Reconstructed model with 10%noise (a) Real part (b) Imaginary part

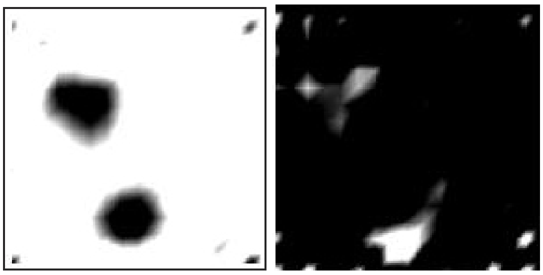

Figure 10. Reconstructed model with 10%noise after using image adjustment technique (a) Real part (b) Imaginary part

The reconstructed models for different percent of noise in the synthetic data are then undergone through image enhancement filter in particular through the histogram equalization technique to have an improved quality of reconstructed model in terms of noise. The figures 3 to 10 display the reconstructed models for different percent of noise and their enhancement in quality after using the Image adjustment technique.

4. CONCLUSIONS

Thus using the different mesh sizes in the forward and reverse problem, the inverse crime has been avoided in this proposed algorithm. Also the clarity of the reconstructed images for different percentage of noise has been improved through Image adjustment technique. This work can be further extended by incorporating different other regularization techniques along with other image enhancement techniques for a comparative study.

REFERENCES

[1.] A.K.Kundu, B.Bandyopadhyay "Reconstruction Algorithm for Microwave Tomography Using Iterative Regularized Gauss-Newton Method", International Conference on Computer and devices for Communication (CODEC 06), Kolkata, India, 2006
[2.] B.Bandyopadhyay, A.Kundu, and A.N.Datta, "An Iterative Algorithm for Microwave Tomography Using Levenberg-Marquardt Regularization Technique", Ind J Pure & Appl Physics, 43, 649 – 653, 2005
[3.] Adams F M & Anderson A P, Inst Elec Eng Proc-H, Microwaves, Opt, Antennas, 129(1982)83.
[4.] Bolomey J C, Izadnegahdar A, Jofre L, Pichot C , Peronnet G & Solaimani M, IEEE Trans Microwave Theory Tech, 30(1982)1998.
[5.] Bolomey J C & Pichot C, Int J Imag Syst Tech, 1(1990) 119.
[6.] Devaney A J, IEEE Trans Biomed Engg, 30(1983)377.
[7.] Rius J M, Ferando M., Jofre L & Broquetas A, Electron Lett, 23(1987)564
[8.] Slaney M., Kak A C & Larsen L E , IEEE Trans Microwave Theory Tech, 32(1984)860.
[9.] Bolomey J C, Pichot C & Gaboriaud G, Radio Sci, 26(1991)541.
[10.] Ney M N, Smith A M & Stuchly S S, IEEE Trans Med Imaging, 3(1984) 155.
[11.] Wang Y M. & Chew W C , Int J Imag Syst Tech, 1(1989)100.
[12.] Caorsi S, Gagnani G L & Pastorino M, IEEE Trans Microwave Theory Tech, 38(1990) 981.
[13.] P.M. van den Berg and A. Abubakar, "Contrast source inversion method: State of Art", Progress in Electromagnetics Research, PIER 34, 189-218, 2001
[14.] Aria Abubakar, Peter M. van den Berg and Jordi J. Mallorqui "Imaging of Biomedical data Using a Multiplicative Regularized Contrast Source Inversion method" IEEE transactions on Microwave theory and Techniques. Vol. 50, No. 7, July 2002
[15.] A.N. Datta, and B. Bandyopadhyay, "An SIRT style reconstruction algorithm for microwave tomography", IEEE Trans. Biomed. Engg., vol 32, pp 719-723, 1985
[16.] A.N. Datta, and B. Bandyopadhyay, "Non-linear extension of moment method solution for microwave tomography", Proc. IEEE. vol. , pp.604 - 605, 1986.
[17.] J.H. Richmond, "Scattering by a dielectric cylinder of arbitrary cross- section shape," IEEE Trans. Antennas and Propagation, vol. 13, No. 3, 334-341, 1965

INTERNATIONAL SYMPOSIUM on
ADVANCED ENGINEERING & APPLIED MANAGEMENT
– 40th ANNIVERSARY in HIGHER EDUCATION (1970-2010)
4 – 5 November, 2010, Hunedoara, ROMANIA

[1] Pavel DRABEK, [2] Martin PITTERMANN

CALCULATION OF INTERHARMONICS OF POWER ELECTRONIC CONVERTERS – USING OF HARMONIC ANALYSIS

[1-2] UNIVERSITY OF WEST BOHEMIA IN PILSEN, FACULTY OF ELECTRICAL ENGINEERING,
DEPT. OF ELECTROMECHANICS AND POWER ELECTRONICS, CZECH REPUBLIC

ABSTRACT:
Paper deals with problems of using Fourier progression for harmonic analysis of unfavourable effects in power grid made by power semiconductor converters. Detailed theoretical analyze has been made and useful mathematical equations for interharmonics calculation were derived. Several simulations and experimental measurements for analytical calculation verification have been realized.
KEYWORDS:
Fourier Series, EMC, Harmonic Analysis, Interharmonics, Power Converters

1. INTRODUCTION

The power quality is primarily influenced by the electric appliances connected to the power grid. If a linear load such as resistive heater is connected to the power grid, the resulting current will be a sine wave and, therefore, only the fundamental frequency will be introduced. However, if the load is non-linear, drawing short pulses of current within each cycle, the current shape will be distorted (non-sinusoidal) and higher frequency current components (e.g. characteristic and non-characteristic harmonics, interharmonics – see Fig.1 and 2) will occur in the frequency spectrum of phase current.

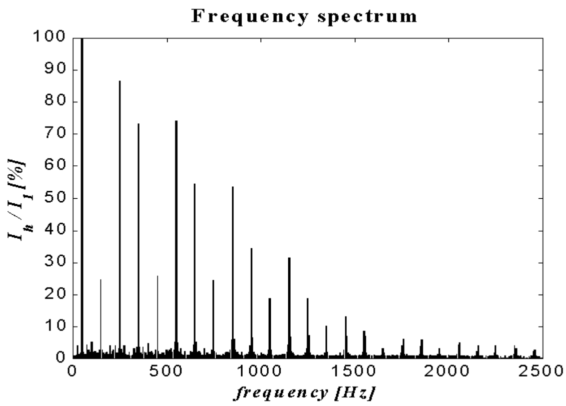

Figure 1. Frequency spectrum of phase current taken by uncontrolled 3phase bridge rectifier (e.g. frequency converter)

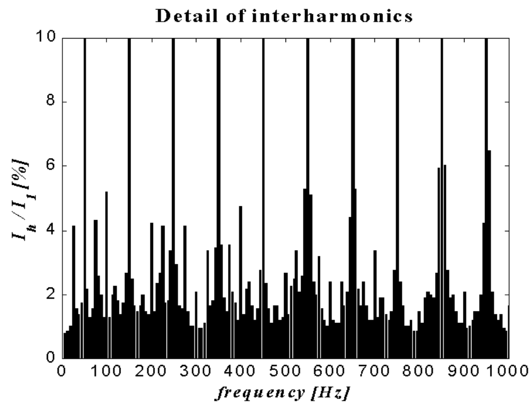

Figure 2. Detail of frequency spectrum of phase current with focus on interharmonic components (defined below)

Thus, the resulting current will be composed of the fundamental and higher frequency components. These frequency components are transferred to the power grid, where they can cause distortion of supply voltage, disturbance of connected equipment (e.g. ripple control devices, compensation units), etc [1,2].

This paper looks mainly at the problem how to calculate these harmonic components. According to standards the low-frequency interference is considered on a frequency range 2.5 kHz and the frequency components can be defined as follows:

Harmonic	f = h * f1 where h is an integer > 0
DC	f = 0 Hz (f = h* f1 where h = 0)
Interharmonic	f * h * f1 where h is an integer > 0
Sub-harmonic	f > 0 Hz and f < f1

Where f1 is the fundamental power system frequency (50 Hz).

2. HARMONIC ANALYSIS

For calculation of the frequency components in the power grid we can use Fourier progression which is defined for periodical functions. We can show its use at the following example of taken phase current of the 3-phase uncontrolled diode rectifier (see Fig.3). The typical waveform of a taken phase current under ideal operating conditions (symmetrical power supply, ideal power semiconductor devices, indefinite short circuit power etc.) is shown in Fig.4. The non-sinusoidal waveform of a phase current creates higher frequency current components. For the harmonic components calculation of phase current it is necessary to simplify the phase current wave as is shown in Fig.4.

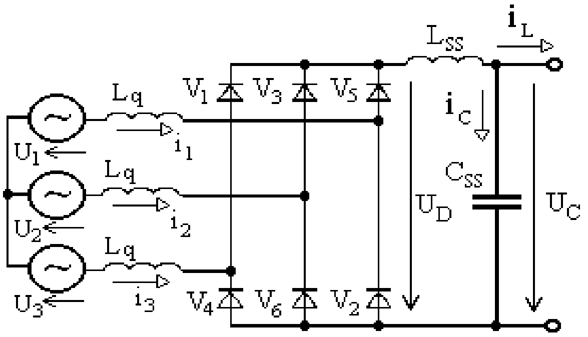

Figure 3. Three-phase bridge rectifier configuration

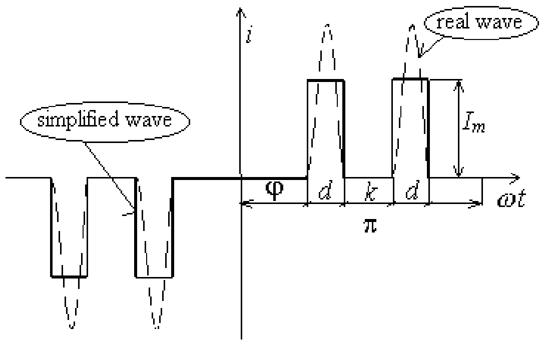

Figure 4. Real and simplified phase current wave

Amplitude Im is constituted so that the area of both currents will be identical for the same parameter d (where d is a diode conduction time). From the figure it is obvious that used simplification is rough in commensurate with the value of parameter d. The error of used simplification decreases with the decreasing of parameter d and for small value d corresponds to reality.

Using the well-known quotation for Fourier analysis [1,3] we can calculate coefficients a_h and b_h:

$$f(t) = \frac{a_0}{2} + \sum_{h=1}^{\infty} \left[a_h \cos(h\omega t) + b_h \sin(h\omega t) \right]. \qquad (1)$$

For Fourier coefficients valid:

$$a_0 = \frac{2}{T}\int_0^T f(t)dt\,, \qquad a_h = \frac{2}{T}\int_0^T f(t)\cos(h\omega t)dt\,, \quad b_h = \frac{2}{T}\int_0^T f(t)\sin(h\omega t)dt, \qquad h = 1,2,\ldots$$

Since the current waveform from Fig.4 is symmetrical odd function, coefficients a_h are zero and we can solve coefficients b_h only:

$$b_h = \frac{2}{\pi}\int_0^{\pi} i_f(\omega t)\sin(h\omega t)d\omega t \qquad (2)$$

After editing we will get:

$$b_h = -\frac{4I_m}{h\pi}\left[\sin\left(\frac{hk}{2}\right) - \sin\left(\frac{hk}{2} + hd\right)\right]\cdot\sin\left(\frac{h\pi}{2}\right)$$

For symmetrical power network is valid d+k=600 and relation (2) we can convert to:

$$b_h = \frac{8I_m}{h\pi}\cdot\sin\frac{hd}{2}\cdot\cos\frac{h\pi}{6}\cdot\sin\frac{h\pi}{2} \qquad (3)$$

The Back expression of current i by Fourier progression is:

$$i_f(\omega t) = \sum_{h=1}^{\infty} \frac{8I_m}{h\pi} \sin\frac{hd}{2}.\sin\frac{h\pi}{2}.\cos\frac{h\pi}{6}.\sin(h\omega t) \tag{4}$$

For higher current harmonics amplitudes is valid:

$$I_h = \frac{1}{h} I_1 \cdot \frac{\sin\frac{hd}{2}}{\sin\frac{d}{2}} \tag{5}$$

where

$$I_1 = \frac{8I_{fm}}{\pi} \cdot \sin\frac{d}{2} \cdot \cos\frac{\pi}{6} = 2{,}205.I_{fm}.\sin\frac{d}{2}$$

When we use the relation (4), we find out that only harmonics of a definite order (5., 7., 11., 13. etc.) will appear on a frequency spectrum. These harmonic orders are called characteristic harmonics and their amplitudes are solved by an equation (5) so-called "1 over h rule". Under real conditions, unbalanced power source - amplitude or phase non-symmetry, the considered problem becomes more complicated and in the frequency spectrum we can find also non-characteristic components. In contrast to characteristic harmonics for calculation amplitudes of non-characteristic harmonics we can not use equation (5) and we have to apply numerical Fourier analysis (DFT or FFT). Power source non-symmetry causes distortion of phase currents and drift of basic harmonic wave of phase current against phase voltage [2,3,4,5].

Excepting characteristic and non-characteristic harmonics discussed in the previous paragraph, we can also find interharmonic components in frequency spectrum of consumed current (see Figure 1). The interharmonics occur as a consequence of dynamic changes of circuit parameters (power supply voltage dips, load variation etc.). The interharmonic current magnitudes are relatively small in comparison with characteristic and non-characteristic harmonic components, but they may impact the proper function of neighbouring appliances (e.g. interference of ripple control and tuned filters). However frequency of the interharmonic is not integer multiple of the fundamental grid frequency 50Hz, therefore we cannot use standard Fourier quotations (1). For an explanation occurrence of the frequency components in the power grid it is necessary to derive new multipurpose quotations which allow calculating interharmonic components.

If function *f(t)* is defined and integrable in the close interval <-*l*, *l*> so valid $f \in L\,(-l,l)$:

$$f(t) = \frac{1}{2}a_0 + \sum_{n=1}^{+\infty}\left(a_n \cos\frac{n\pi\omega t}{l} + b_n \sin\frac{n\pi\omega t}{l}\right) \tag{6}$$

For Fourier coefficients valid:

$$a_n = \frac{1}{l}\int_{-l}^{l} f(t)\cos\frac{n\pi\omega t}{l}\, d\omega t \quad (n = 0, 1, 2, \ldots) \quad ,$$

$$b_n = \frac{1}{l}\int_{-l}^{l} f(t)\sin\frac{n\pi\omega t}{l}\, d\omega t \quad (n = 1, 2, \ldots) \tag{7}$$

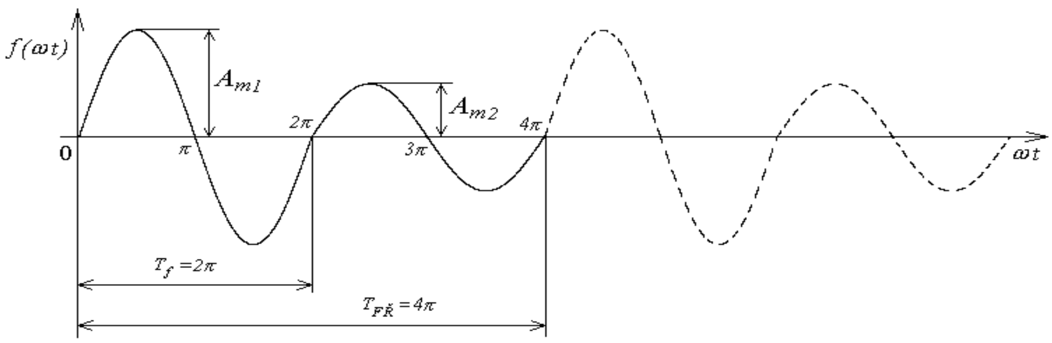

Figure 5. Harmonic waveform of function f(ωt) for interharmonic components analysis

For the function waveform in the Fig. 5 valid following coefficients calculation:

$$a_h = -\frac{(A_{m1} - A_{m2})4}{(h-2)(h+2)\pi}$$

$$\text{for} \quad h \neq 2 \quad \text{and} \quad h = 1, 3, 5, 7, \ldots$$

$$b_2 = \frac{2\pi A_{m1} + 2\pi A_{m2}}{4\pi} = \frac{A_{m1} + A_{m2}}{2} \tag{8}$$

Other coefficients b_h are zero.

Now it is necessary to verify these new equations (6-8) for interharmonics calculating, we make harmonic analysis of periodical function in Fig.5 with period T_f=2π (50Hz). It changes amplitude each period from value A_{m1} to A_{m2} and so on. From the function behaviour it is evident, that Fourier progression of the function have double period T_{FR}=4π (25Hz).

In relation to difference between function period and Fourier progression period we can expect relation between frequency of first harmonic of time function f_1 and frequency of first harmonic of Fourier progression time function f_{FR1}:

$$f_1 = \frac{1}{T_f} = \frac{1}{2\pi}, \quad f_{FR1} = \frac{1}{T_{FR}} = \frac{1}{4\pi} \quad \Rightarrow \quad f_1 = 2 f_{FR1} \tag{9}$$

Therefore we can expect frequency components as multiple of 25 Hz although the function waveform has period 50 Hz as shown in Figures 6-8 (frequency component 50 Hz is 100% and it is second component in the figures).

3. SIMULATION AND EXPERIMENTAL RESULTS

Simulation

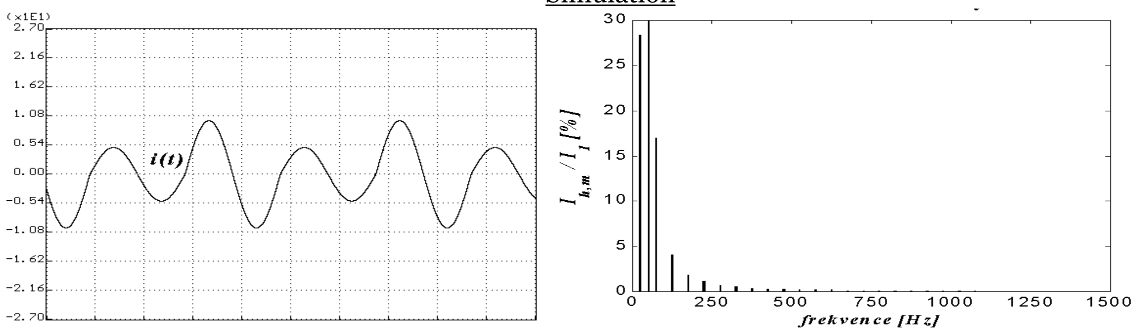

Figure 6. Simulation results of function waveform harmonic analysis

Measurement

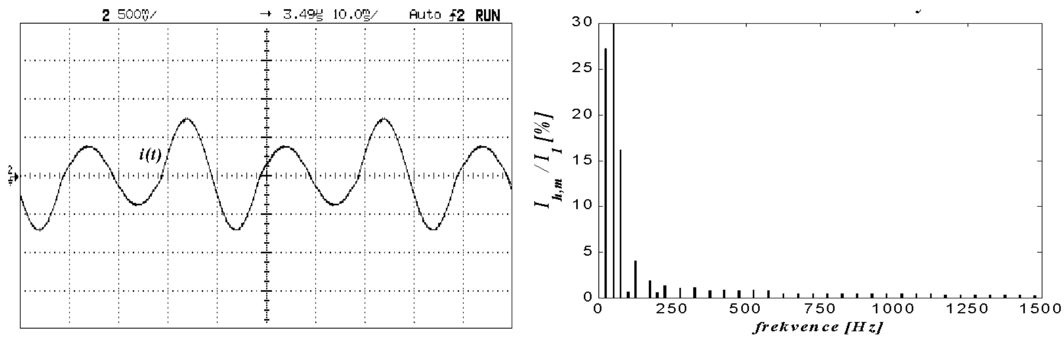

Figure 7. Measurement results of function waveform harmonic analysis

Analytical calculation – equation

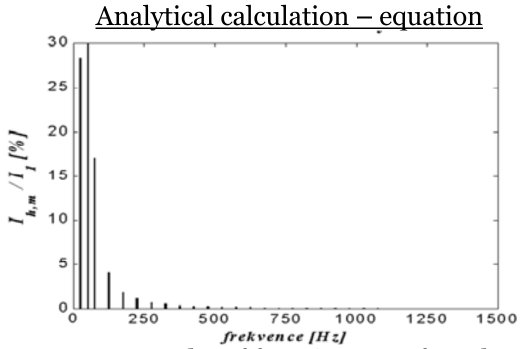

Figure 8. Measurement results of function waveform harmonic analysis

4. CONCLUSION

Detailed theoretical analyze has been made and useful mathematical equations for interharmonics calculation were derived. Several simulations and experimental measurements for analytical calculation verification have been realized. Results from simulation and measuring confirm that frequency of first harmonic of time function f_1 and frequency of first harmonic of Fourier progression time function $f_{FŘ1}$ should not be the same thing.

ACKNOWLEDGMENT

This research work has been made within research project of Czech Science Foundation No. GACR 102/09/1164.

REFERENCES / BIBLIOGRAPHY

[1] Bauta, M., Grötzbach, M., "Noncharacteristic Line Harmonics of AC/DC Converters with High DC Current Ripple," In: 8th IEEE-ICHQP, Athens, Proc. Vol. II, pp. 755-760, 1998.

[2] Drábek, Pavel; Kůs, Václav. EMC Issues of Power Electronic Converters. In IEEE SYMPOSIUM EMC 2009. Austin: IEEE, 2009. s. 296-301. ISBN: 978-1-4244-4267-6.

[3] Drábek, P., Peroutka, Z.: Electromagnetic Compatibility Issues of Variable Speed Drives. In: IEEE SYMPOSIUM on Electromagnetic Compatibility 2002. Minneapolis, Minnesota, USA 2002, pp. 308-313

[4] KŮS, V.; PEROUTKA, Z.; DRÁBEK, P. Non-characteristic harmonics and interharmonics of power electronic converters. In 18th International conference and exhibition on electricity distribution. Turin: IEE, 2005. p. 1-5.

[5] KŮS, V.; DRÁBEK, P.; FOŘT, J.; PITTERMANN, M. Harmonic currents of frequency converters with voltage source inverters. In International 15 symposium Micromachines and servosystems. Warszawa : Wydawnictwo Ksiazkowe Instytutu Elektrotechniki, 2006. s. 45-50. ISBN 83-922095-1-6.

[6] DRÁBEK, P.: Harmonic analysis use for investigation of semiconductors converters EMC. Transcom 2007, Žilina 2007.

[7] Drábek, P.,: EMC issues of controlled rectifiers. In 2007 European Conference on Power Electronics and Applications. Piscataway: IEEE, 2007. s. 4801-4807. ISBN: 978-90-75815-11-5.

INTERNATIONAL SYMPOSIUM on ADVANCED ENGINEERING & APPLIED MANAGEMENT
– 40th ANNIVERSARY in HIGHER EDUCATION (1970-2010),

INTERNATIONAL SYMPOSIUM on ADVANCED ENGINEERING & APPLIED MANAGEMENT
– 40th ANNIVERSARY in HIGHER EDUCATION (1970-2010),

INTERNATIONAL SYMPOSIUM on
ADVANCED ENGINEERING & APPLIED MANAGEMENT
– 40th ANNIVERSARY in HIGHER EDUCATION (1970-2010)
4 – 5 November, 2010, Hunedoara, ROMANIA

[1.] Cornelia Victoria ANGHEL

DATA SECURITY IN WIRELESS NETWORKS

[1.] EFTIMIE MUTGU UNIVERSITY OF REŞIŢA, FACULTY OF ENGINEERING,
COMPUTER SCIENCE DEPARTMENT, REŞIŢA, ROMÂNIA

ABSTRACT:
Wireless networks are relatively less secure than wired network because of easier access of unauthorized persons in coverage areas of access points. There is implicit in the implementation of wireless networks, different barriers that form the so-called basic security of wireless networks, which prevents unintended access of foreigners network in the coverage of an access point.
Security barriers (basic security) protocols have been provided in Wi-Fi networks provide a relatively low level of security of these networks, which has slowed development somewhat.

KEYWORDS:
Wireless Network, data security, Mac Filtering, WEP, WAN

1. INTRODUCTION

Wireless networks are relatively less secure than wired network because of easier access of unauthorized persons in coverage areas of access points. There is implicit in the implementation of wireless networks, different barriers that form the so-called basic security of wireless networks, which prevents unintended access of foreigners network in the coverage of an access point.

Security barriers (basic security) protocols have been provided in Wi-Fi networks provide a relatively low level of security of these networks, which has slowed development somewhat.

In June 2004, was adopted 802.11i standard which improves Wireless network security.

Basic security of wireless networks is ensured by the following features implemented:

- SSID (Service Set Identifiers);
- WEP (Wired Equivalent Privacy);
- Address validation MAC (Media Access Control).

SSID is a code that defines membership of a particular wireless access point. All wireless devices that will communicate on a network must have its own SSID, set the same value as the value of SSID access point to achieve connectivity.

Normally the access point transmits its SSID every few seconds. This mode can be stopped so that an unauthorized person can not automatically find the SSID and the access point. But since the SSID is included in any sequence ul1 wireless beacons, it is easy for a hacker equipped with monitoring equipment to discover and bind the value network.

WEP can be used to improve ongoing problem SSID transmission by encrypting traffic between wireless clients and access point. This is accomplished by an authentication with a key (shared-key authentication). Wireless client access point transmits a challenge that he must return it encrypted. If the access point can decrypt the client's response, the key is valid proof that it possesses and is entitled to join the network. WEP encryption has two options - to 64-bit key or 128-bit.

WEP does not provide much security. Hacker equipped with monitoring equipment can receive and record first challenge away from the access point and then answer the customer's encrypted on the basis of processing can determine the key that can then be used to join the network.

Checking the MAC address. It can enhance network security, if the network administrator is using MAC address filtering, in the access point is configured with the MAC addresses of clients are granted network access.

Unfortunately, even this method does not provide much security.

A hacker can record footage from traffic and, after analysis, can extract a MAC address that can then be used to join the network.

2. METHODOLOGY

Wireless MAC Filtering is the simplest method for limiting access in a Wireless Network.

Only wireless equipment, who has been previously, registered MAC address of the router or Access Point can connect to wireless network.

SSID Hiding (Wireless Broadcast SSID Disabled) is a method for limiting unauthorized access to a wireless network.

Securing the network can be done with WEP or WPA.

- **WEP** (Wired Equivalent Protection) is an encryption method:
  - using 64 bits (10 hexa characters) or 128 bits (26 hexa characters). Hexa characters are: 0-9 and A - F
  - authentification: Open or Shared Key Now the 64-bit WEP encryption can be cracked in minutes, and the 128 bits in a few hours, using public applications.
- **WPA-PSK** (WPA Preshared Key or WPA-Personal) is a much safety method such as WEP.
- **WPA2** is the safest encryption method is an improved version of WPA method.

Also, those encryptions (WPA and WPA2) can be broken if the password contains fewer characters or a word found in the dictionary. To break this encryption makes it impossible to use long passwords, randomly generated.

3. ANALYSES

We use the TL-WR340G/TL-WR340GD 54Mbps Wireless Router. This router provides dedicated solution for Small Office/Home Office (SOHO) networks. With our network all connected, our local wired or wireless network can share Internet access, files and fun for multiple PC's through one ISP account. In addition, this device supports Bridge mode which can make two AP's communicate with each other wirelessly.

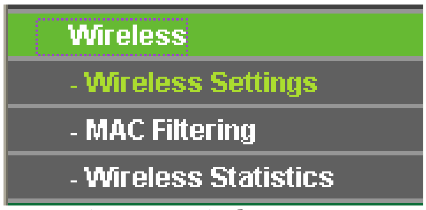

Figure 1. Wireless menu

There are three submenus under the Wireless menu (shown in Figure 1): **Wireless Settings**, **MAC Filtering** and **Wireless Statistics.** Click any of them, and we should be able to configure the corresponding function. The detailed explanations for each submenu are provided below.

SSID - Enter a value of up to 32 characters. The same name (SSID) must be assigned to all wireless devices in our network. The default SSID is TP-LINK, but it is recommended strongly that we change our networks name (SSID) to a different value. This value is case-sensitive. For example, *TP-LINK* is NOT the same as *tp-link*.

Region - Select our region from the pull-down list. This field specifies the region where the wireless function of the router can be used. It may be illegal to use the wireless function of the router in a region other than one of those specified in this field. If the country or region is not listed, we can contact the assistance.

The default region is United States. When we select our local region from the pull-down list, we click the **Save** button**,** then the Note Dialog appears. Then we click OK.

Channel - This field determines which operating frequency will be used. It is not necessary to change the wireless channel unless we notice interference problems with another nearby access point.

Mode - Select the desired wireless mode. The options are:

- **54Mbps (802.11g) -** Both 802.11g and 802.11b wireless stations can connect to the router.
- **11Mbps (802.11b) -** Only 802.11b wireless stations can connect to the router.

Enable Wireless Router Radio - The wireless radio of this Router can be enabled or disabled to allow wireless stations access. If enabled, wireless stations will be able to access the router. Otherwise, wireless stations will not be able to access.

Enable SSID Broadcast - If we select the **Enable SSID Broadcast** checkbox, the Wireless Router SSID will broadcast its name (SSID) on the air.

Enable Bridges – If we select the **Enable Bridges** checkbox, we can input MAC address of other AP's to communicate with them wirelessly in Bridge mode.

MAC of AP (1-6): Input the MAC address of the AP which we want to communicate with. There are six entries can be configured.

The AP's can communicate with each other in Bridge mode unless they know each other's MAC address. For example, if the router whose MAC address is 00-13-56-A8-9E-1A wants to communicate with an AP whose MAC address is 00-13-56-A8-9E-1B in Bridge mode, we should do as following:

Enable Wireless Security – The wireless security function can be enabled or disabled. If disabled, the wireless stations will be able to connect the router without encryption. It is recommended strongly that we choose this option to encrypt our wireless network. The encryption settings are described below.

Security Type - We can select one of the following authentication types:

- ❖ **WEP -** Select WEP authentication type based on 802.11 authentications.
- ❖ **WPA-PSK/WPA2-PSK -** Select WPA/WPA2 authentication type based on pre-shared passphrase.
- ❖ **WPA /WPA2 -** Select WPA/WPA2 authentication type based on Radius Server.

Security Options - We can select one of the following Security options:

When we select **WEP** for authentication type we can select the following authentication options:

- ❖ **Automatic -** Select Shared Key or Open System authentication type automatically based on the wireless station request.
- ❖ **Shared Key -** Select 802.11 Shared Key authentication.
- ❖ **Open System -** Select 802.11 Open System authentication.

When we select **WPA-PSK/WPA2-PSK** for authentication type we can select **Automatic**, **WPA –PSK** or **WPA2-PSK** as authentication options. When we select **WPA/WPA2** as an authentication type we can select **Automatic WPA** or **WPA2** as authentication option.

WEP Key Format - We can select **ASCII** or **Hexadecimal** format. ASCII Code Format stands for any combination of keyboard characters in the specified length. Hexadecimal format stands for any combination of hexadecimal digits (0-9, a-f, A-F) in the specified length.

WEP Key settings - Select which of the four keys will be used and enter the matching WEP key information for our network in the selected key radio button. These values must be identical on all wireless stations in our network.

Key Type - We can select the WEP key length (**64-bit**, or **128-bit,** or **152-bit**) for encryption. "Disabled" means the WEP key entry is invalid.

- ❖ For **64-bit** encryption **-** we can enter 10 hexadecimal digits (any combination of 0-9, a-f, A-F, zero key is not permitted) or 5 ASCII characters.
- ❖ For **128-bit** encryption **-** we can enter 26 hexadecimal digits (any combination of 0-9, a-f, A-F, zero key is not permitted) or 13 ASCII characters.
- ❖ For **152-bit** encryption **-** we can enter 32 hexadecimal digits (any combination of 0-9, a-f, A-F, zero key is not permitted) or 16 ASCII characters.

Encryption - When we select **WPA-PSK/WPA2-PSK** or **WPA/WPA2** for **Security Type** we can select **Automatic**, **TKIP** or **AES** as **Encryptions.**

The Wireless MAC Address Filtering feature allows we to control wireless stations accessing the router, which depend on the station's MAC addresses.

MAC Address - The wireless station's MAC address that we want to access.

Status - The status of this entry either **Enabled** or **Disabled**.

Privilege - Select the privileges for this entry. We may select one of the following **Allow** / **Deny**.

Description - A simple description of the wireless station.

First, we must decide whether the unspecified wireless stations can access the router or not. If we desire that the unspecified wireless stations can access the router, please select the radio button **Allow the stations not specified by any enabled entries in the list to access**, otherwise, select the radio button **Deny the stations not specified by any enabled entries in the list to access**.

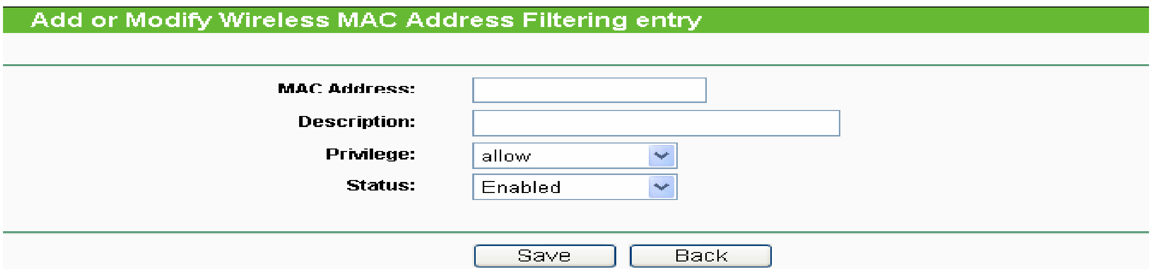

Figure 2. Add or Modify Wireless MAC Address Filtering entry

To Add a Wireless MAC Address filtering entry, click the **Add New...** button. The "**Add or Modify Wireless MAC Address Filtering entry"** page will appear, shown in Figure 2.

4. CONCLUSIONS

The article presents some aspects about the router configuration on a safety wireless network by Mac Address Filtering. An example used use the TL-WR340G/TL-WR340GD 54Mbps Wireless Router, is detailed. This router provides dedicated solution for Small Office or Home Office (SOHO) networks.

REFERENCES

[1.] Anghel, C.V. – *„Consideraţii privind conectarea la o reţea Wireless securizată"* Al XII-lea Simpozion Internaţional "Tinerii şi Cercetarea Multidisciplinară", 11-12 noiembrie, Timişoara, 2010
[2.] Dixit, R. Prasad (eds.), *Wireless IP and Building the Mobile Internet*, Artech House, 2003
[3.] M. Mallick, *Mobile and Wireless Design Essentials*, Ed. John Wiley & Sons, 2003

INTERNATIONAL SYMPOSIUM on
ADVANCED ENGINEERING & APPLIED MANAGEMENT
– 40th ANNIVERSARY in HIGHER EDUCATION (1970-2010)
4 – 5 November, 2010, Hunedoara, ROMANIA

[1.] Corina Maria DINIŞ, [2.] Angela IAGĂR,
[3.] Corina Daniela CUNŢAN, [4.] Gabriel Nicolae POPA

STUDY OF THE VOLTAGE RESONANCE IN ELECTRIC CIRCUITS

[1-4.] UNIVERSITY POLITEHNICA TIMIŞOARA, FACULTY OF ENGINEERING HUNEDOARA, ROMANIA

ABSTRACT:
This work is presenting the study of the voltage resonance in the a.c. R-L-C series circuits, as well as the practical implications of this phenomenon in electrotechnics.
In order to verify the voltage resonance phenomena by simulation, there have been achieved applications using the programsEWB -Multisim 9 and LabVIEW 7.1.
KEYWORDS:
Voltage resonance, R-L-C series circuit, variable frequency, variable inductivity, variable capacity

1. INTRODUCTION

The voltage resonance takes place in the R-L-C series circuit supplied by the alternate voltage $u(t) = U\sqrt{2}\sin\omega t$, when the reactive power absorbed by the circuit at the terminals is null Q=0, e.g. when is obtained a null phase-difference (φ=0) between the voltage applied to the circuit and the absorbed current's intensity. In this case, the inductive reactance X_L becomes equal with the capacitive reactance X_C. This equality is obtained either by modifyong the inductance L or capacity C, or by supplying the circuit with a voltage of variable frequency.

The resonance condition can be obtained:

- ❖ at pulsation's, respectively supply voltage frequency's variation, keeping constant the inductance *L* and capacity *C*: $\omega_r = \frac{1}{\sqrt{LC}}$ respectively $f_r = \frac{1}{2\pi\sqrt{LC}}$, ω_r and f_r being called pulsation, respectively resonance frequency;

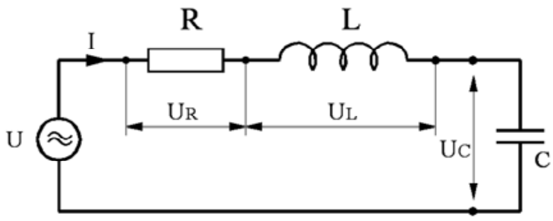

Fig. 1 R-L-C series A.C. circuit

- ❖ at inductance's variation, supplying the circuit from a fix frequency source and keeping constant the capacity *C*: $L_r = \frac{1}{\omega^2 C}$, L_r being called resonance inductance;

at capacity's variation, supplying the circuit from a fix frequency source and keeping constant the inductance *L*: $C_r = \frac{1}{\omega^2 L}$, C_r being called resonance capacity.

2. PROBLEM STUDY

In case of a R-L-C series circuit operating in permanent sinusoidal regime, in resonance conditions, is obtained:

- the complex impedance of the R-L-C series circuit is:

$$\underline{Z} = R + j\cdot(X_L - X_C) \tag{1}$$

- having the module $Z = \sqrt{R^2 + (X_L - X_C)^2}$. (2)

According to the Ohm's Law, the current from circuit is:

$$\underline{I} = \frac{\underline{U}}{\underline{Z}} = \frac{\underline{U}}{R + j(X_L - X_C)} \tag{3}$$

- The current's effective value is determined by the relation:

$$I = \frac{U}{\sqrt{R^2 + (X_L - X_C)^2}} = \frac{U}{\sqrt{R^2 + \left(\omega L - \frac{1}{\omega C}\right)^2}} \tag{4}$$

- The phase-difference between current and voltage is given by the relation:

$$tg\varphi = \frac{X_L - X_C}{R} = \frac{\omega L - \frac{1}{\omega C}}{R} \tag{5}$$

$$\varphi = arctg\left(\frac{U_L - U_C}{U_R}\right) = arctg\left(\frac{X_L - X_C}{R}\right) \tag{6}$$

- At resonance, $\mathbf{X_L = X_C}$, and the current through the circuit is reaching the maximum value:

$$I_{rez} = \frac{U}{R} \tag{7}$$

During the experiment, the R-L-C series circuit could be foud in the following situations: $X_L > X_C$ (inductive character, fig. 2.1); $X_L = X_C$ (voltage resonance, fig. 2.2); $X_L < X_C$ (capacitive character, fig. 2.3).

The phase diagrams of voltages and currents for the three cases are presented in the following figures:

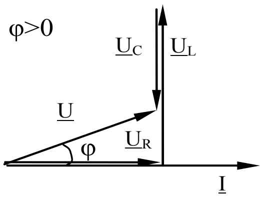

Fig. 2.1

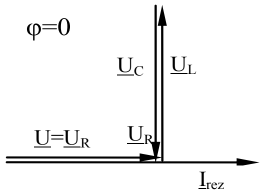

Fig. 2.2

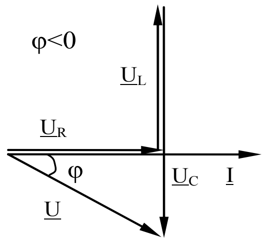

Fig. 2.3

For the circuit in fig.1, the variation of impedance Z, resistance R and reactance X_L and X_C, as well as the phase-difference angle φ between the voltage applied at the circuit's terminals and the current through the circuit are presented in fig. 3.

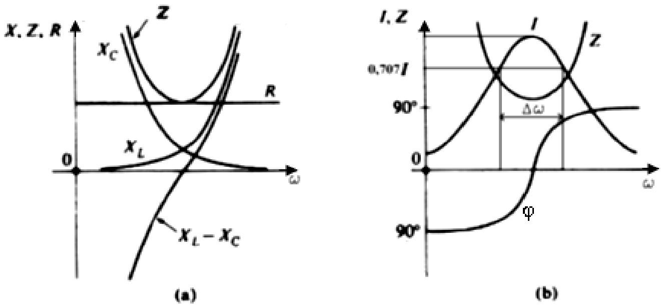

Fig. 3

We notice that at the resonance frequency (pulsation), the circuit's impedance is minimum and equal with R, and the current is maximum: $I_{rez} = I_0 = \frac{U}{R}$. The voltage drops U_L and U_C are equal and in phase opposition, and they can be much higher than the supply voltage, reason for which the resonance in the R-L-C series circuit is also called *voltage resonance*.

3. APPLICATIONS ACHIEVED IN MULTISIM 9 FOR THE VOLTAGE RESONANCE STUDY

For the study of the R-L-C series circuit's operation, there have been achieved the applications from figure 4, 6 and 8. The circuit components are linear and constant or variable (constant resistor, variable coil, variable capacitor). This allows us to analyze the circuit's operation at inductivity, respectively variable capacity.

The applications emphasize the phenomena of voltage resonance achieved by one of the three ways:

- ❖ inductivity variation
- ❖ capacity variation
- ❖ frequency variation

Further, are presented the circuits implemented in simulations with Multisim 9 for verifying the voltage resonance in the R-L-C series single-phased A.C. circuits de c.a. The circuits' resonance moment is emphasized aslo by means of oscilloscope, on which screen being noticed the two voltage and current signals, which are in phase.

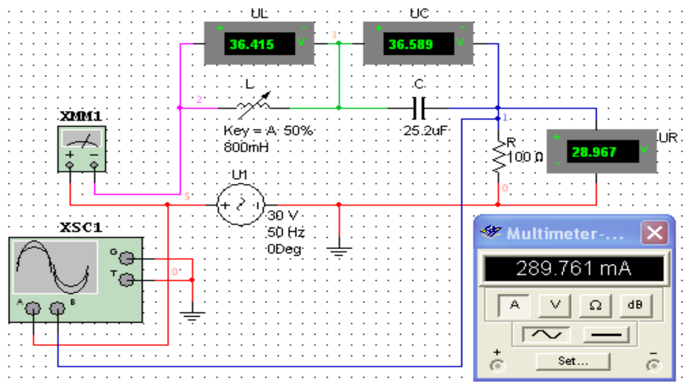

Fig. 4

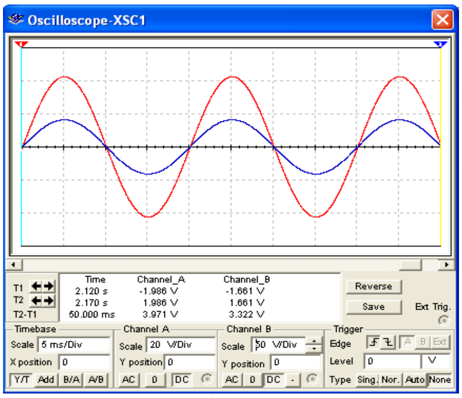

Fig. 5

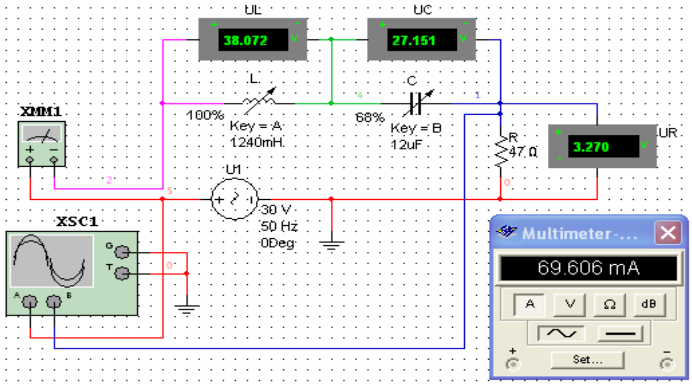

Fig. 6

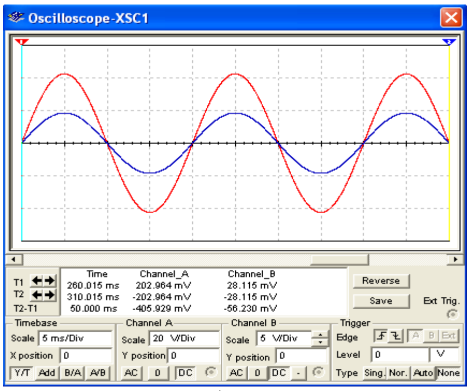

Fig. 7

In fig. 8, the supply source is a signal generator, to which can be modified both the amplitude and the frequency of the circuit's supply voltage, which allows us the analysis of its operation at variable frequency.

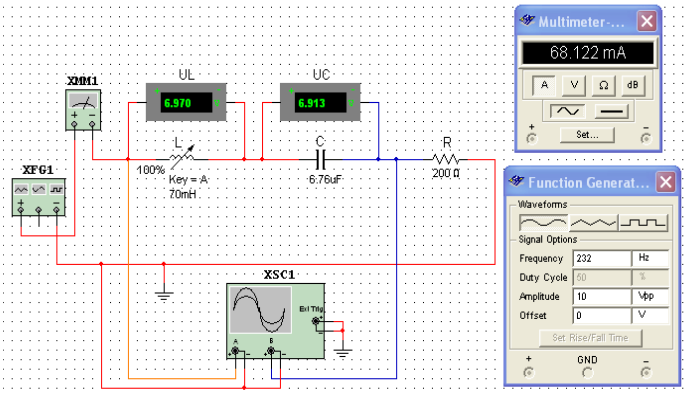

Fig. 8

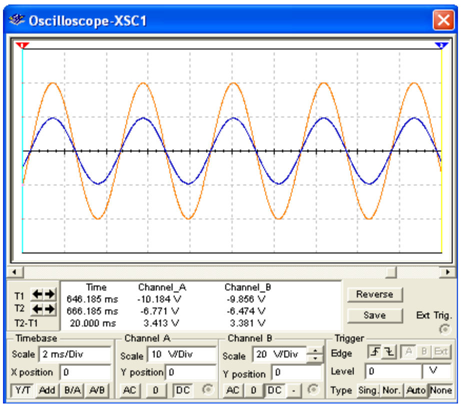

Fig. 9

4. EXPERIMENTAL RESULTS

For the circuits from fig. 4, 6 and 8 were obtained the experimental results presented in tables 1, 2 and 3.

Table 1. RLC series circuit at variable inductivity

L, [mH]	I, [mA]	U_R, [V]	U_L, [V]	U_C, [V]
100 %	184,819	18,482	46,454	23,339
90 %	208,537	20,847	47,160	26,332
80 %	234,931	23,485	47,243	29,665
70 %	261,307	26,130	45,980	33,006
60 %	281,988	28,190	42,534	35,607
50 %	289,761	28,976	36,427	36,6
40 %	281,181	28,118	28,285	35,507
30 %	260,026	25,996	19,622	32,836
20 %	233,537	23,353	11,768	29,499
10 %	207,237	20,723	5,260	26,177

where $L_{max} = 800$ mH (100%)

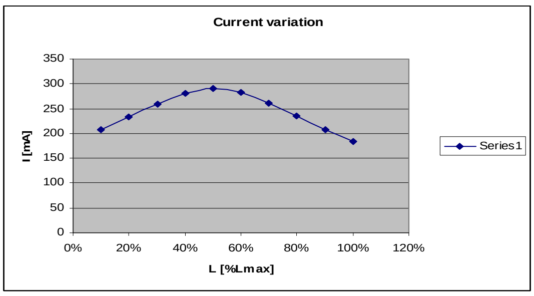

Fig. 10

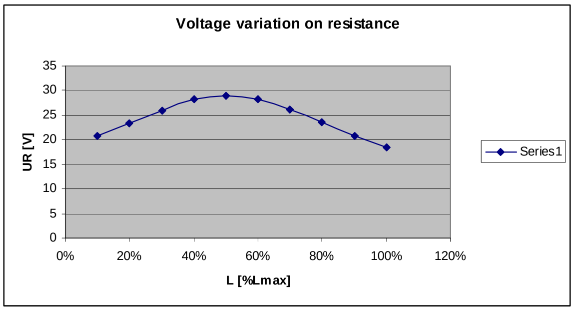

Fig. 11

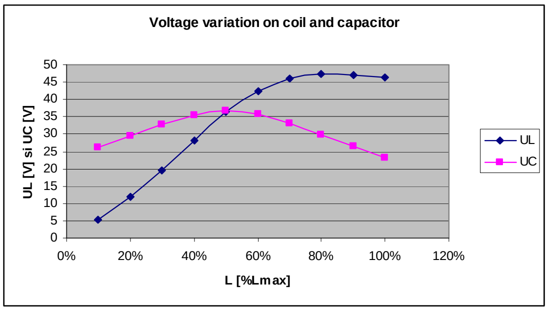

Fig. 12

Table 2. RLC series circuit at variable capacity

C, [μF]	I, [mA]	U_R, [V]	U_L, [V]	U_C, [V]
100 %	66,882	3,143	36,571	17,736
90 %	67,982	3,195	37,183	20,029
80 %	68,985	3,242	37,732	22,873
70 %	69,585	3,269	38,048	26,361
68%	69,606	3,271	38,072	27,142
60 %	69,093	3,247	37,791	30,545
50 %	66,155	3,108	36,175	35,095
40 %	58,762	2,762	32,140	38,956
30 %	45,723	2,149	25,009	40,416
20 %	29,093	1,367	15,912	38,572
10 %	13,022	0,612	7,123	34,541

where $C_{max} = 12$ μF (100%)

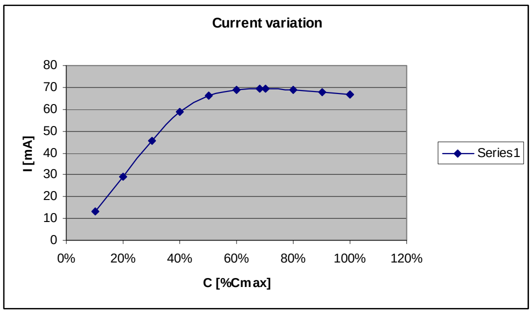

Fig. 13

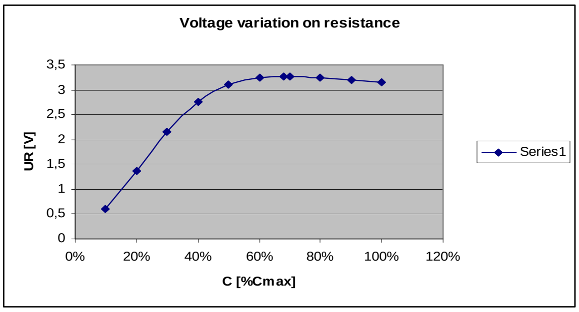

Fig. 14

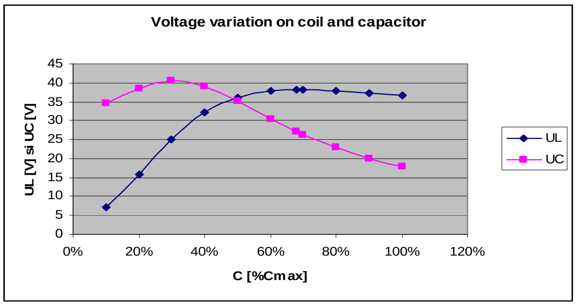

Fig. 15

Table 3. RLC series circuit at variable frequency

f, [Hz]	I, [mA]	U_R, [V]	U_L, [V]	U_C, [V]
150	62,394	12,478	4,144	9,793
170	65,125	13,025	4,894	9,019
190	66,872	13,374	5,611	8,286
210	67,817	13,563	6,285	7,603
230	68,122	13,624	6,911	6,973
232	68,123	13,624	6,971	6,913
240	68,08	13,615	7,205	6,678
260	67,68	13,536	7,757	6,128
280	66,948	13,389	8,26	5,629
300	65,97	13,194	8,719	5,177

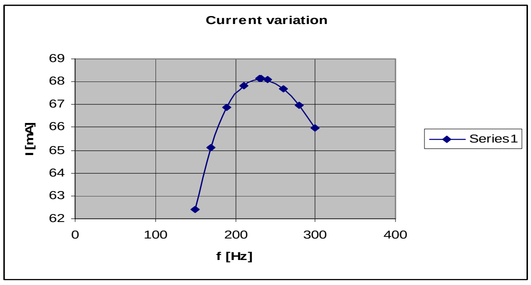

Fig. 16

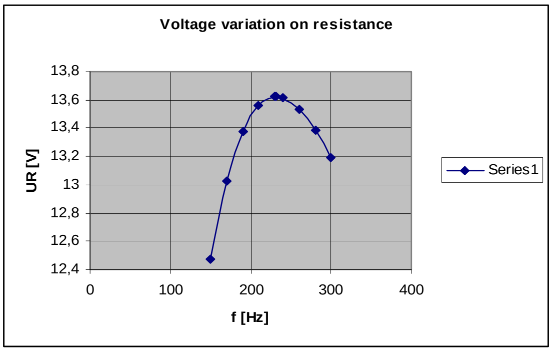

Fig. 17

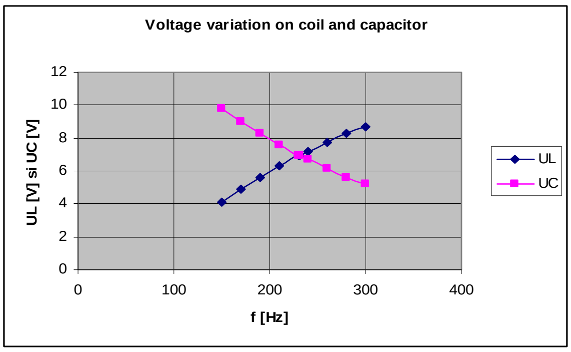

Fig. 18

5. APPLICATION LABVIEW 7.1 FOR THE VOLTAGE RESONANCE's STUDY

For a thoroughly study of the voltage resonance phenomena, it's been achieved the application with the front pannel presented in fig.19 and fig.20.

The front pannel is organized on three zones:

- supply zone (voltage with variable effective value and frequency)
- circuit components zone (variable resistance, inductivity, capacity)
- display and visualizing zone (digital indicators, oscilloscope).

The application allows:

- modification of the supply voltage effective value within [0 ; 220] V
- modification of the supply voltage frequency within [0 ; 10000] Hz
- modification of the circuit components' parameters:
  - resistance – within [0 ; 200] Ω
  - inductivity – within [0 ; 1240] mH
  - capacity – within [0 ; 25,2] μF
- selection of the variable parameter (frequency, inductivity, capacity) depending on which are analyzed certain measures and against which is emphasized the resonance;
- visualizing variation graphics of certain measures depending on the selected variable parameter:
  - effective values of the supply voltage and the voltage on resistance;
  - voltages on inductivity and capacity;
  - impedance
  - current's intensity
  - active power
  - phase-difference between the supply voltage and current;
  - selecting the measures visualized at a certain moment;
  - possibility to use some cursors which, fixed on a certain point of a wave form, should indicate its coordinate;
- displaying of some important values of certain parameters, respectively electric measures:
  - variable parameter's value for which the resonance is obtained
  - impedance at resonance
  - current intensity's effective value at resonance
  - effective values of voltages on resistance, inductivity and capacity at resonance
  - maximums of the effective values of voltages on inductivity and capacity
  - active power at resonance.

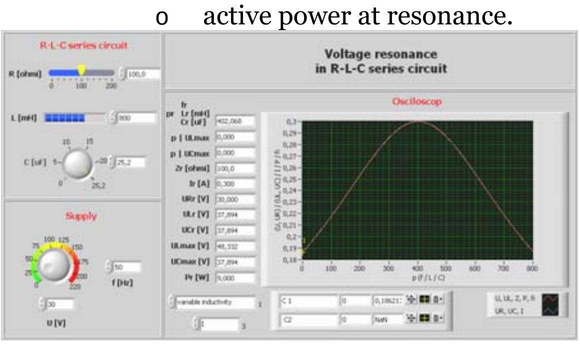

Fig. 19 Study of the voltage resonance in R-L-C series circuit at variation of the coil's inductivity –front panel

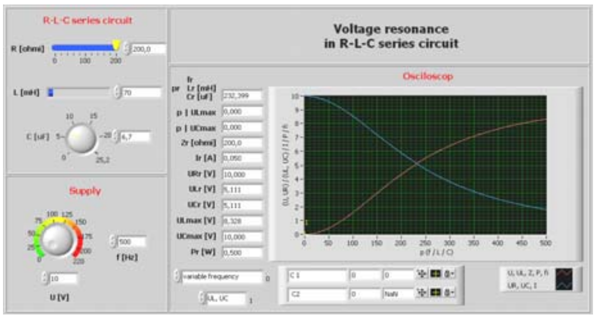

Fig. 20 Study of the voltage resonance in R-L-C series circuit at variation of the frequency – front panel

The application's block diagram is presented in fig.21. The values of the parameters set at a given moment are transformed in step-type, respectively ramp-type signals (in case of the ones against which is made the graphic representation), obtaining this way a set of values for the respective parameters, corresponding to the variation interval of the variable parameter (frequency, inductivity, capacity).

For calculating the pulsation, reactances, impedance, voltage drops, power and phase difference are used „formula"-type blocks.

For selecting the parameter against which is made the circuit's analysis, as well as for selecting the visualized graphics, at a given moment, are used „Case" structures, inside which are made the suitable operations.

For detecting the minimum or maximum values of certain analyzed measures, which correspond the resonance, are used dedicated subprograms from the functions library of the programming environment.

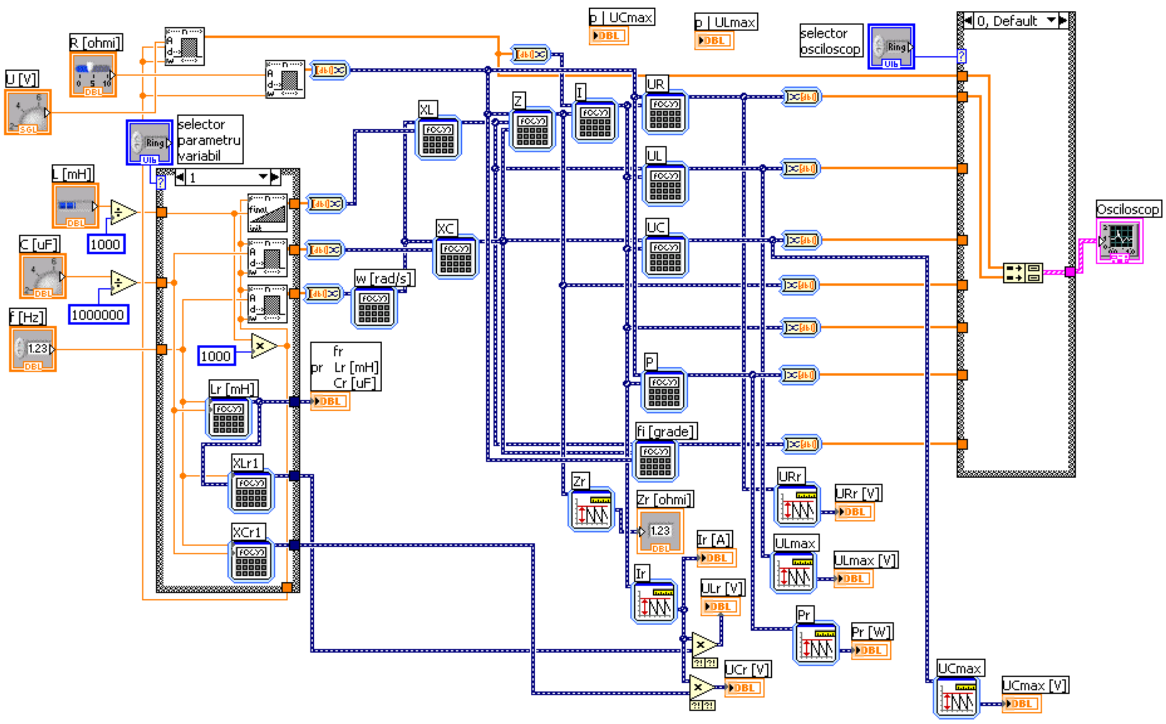

Fig. 21 Study of the voltage resonance in R-L-C series circuit – block diagram

6. CONCLUSIONS

In conclusion, in resonance regime:

- the (real) impedance, equal with the circuit's resistance, has minimum value,
- the power factor is maximum,
- the voltage on resistance has maximum value,
- the current, in phase with the voltage, has maximum value,
- the voltage on coil and capacitor are equal in effective values, and of contrary sign, and can exceed the voltage applied to the circuit, e.g. in the circuit appear *over voltages*. From this reason, the series resonance is also called voltage resonance.

The main advantage provided by the simulation program Electronic Workbench – Multisim 9 consists in high flexibility as regards the modification of the analyzed electric circuits' structure and their operation regimes, fact that allows an analysis and a diagnose of those circuits within a much more reduced time interval, than the case when these would be phisically achieved, allowing in addition a facile storage and in large quantities of the information about the circuit's operation in different implementation versions.

To be noticed the time savings and the possibility of further processing of data, especially of graphic dependencies for different measures, by means of the Electronic Workbench – Multisim 9 program.

Utilization of the simulation program Electronic Workbench – Multisim 9 in the university educational activity, at disciplines with electric and electronic profile, allows the educational process to become more attractive, providing the students a large perspective in their professional training.

LABVIEW was materialized into a versatile development environment, based, mainly, on the advantages of graphic programming, in detriment of the traditional one.

Combining the special features of the LabView environment with the computing power and high flexibility of the current generation computers, can be implemented powerful instruments for the analysis of some systems from various activity fields.

The significant obtained avantages (the created unit is very powerful from the calculations viewpoint, easy to use – due to the friendly graphic interface, easy to configure and a much lower price compared with the classic testing system) indicate the facy that the virtual instrumentation represents an adequate solution for implementatin of some complex testing systems, reliable and, not the least, advantageous from financial viewpoint.

The present and future measuring systems cannot be conceived without virtual instruments, that should replace the actual dedicated measuring devices and instruments.

REFERENCES

[1.] C.M. Diniş, A. Iagăr, C.D. Cunţan, Fundaments of electric and electronic engineering, Experimental themes, Politehnica Publishing House, Timişoara, 2009.
[2.] E. Cazacu, I. Nemoianu, a.o., Special issues about electric circuits theory, Elements of theory and applications, Vol. 1 and Vol. 2, MatrixRom Publishing House, Bucharest, 2005.
[3.] H. Gavrilă, Electrotechnics and electric Equipments, Vol. I, Didactic and Pedagogic Publishing House, RA, Bucharest, 1993.
[4.] A. Saimac, C. Cruceru, Electrotechnics, Didactic and Pedagogic Publishing House, Bucharest, I981.
[5.] * * * – Electronics Workbench/ Multisim 9 – User's guide.
[6.] V. M. Popa, Electrotechnics' Basics, Alma Mater Publishing House, Sibiu, 2002.
[7.] Mariana Milici, Concepts of electric circuits theory – Signals. Laws, theorems and analysis methods, MatrixRom Publishing House, Bucharest, 2005.
[8.] Mariana Milici, Electric circuits – Sinusoidal and particular operation regimes, MatrixRom Publishing House, Bucharest, 2005.
[9.] Cottet Francis, Ciobanu Octavian, Programming bases in LabVIEW, Matrix Rom Publishing House, Bucharest, 1998.
[10.] M. Dobriceanu, Introduction in virtual instrumentation and LabView, Universitaria Publishing House, Craiova, 2005.
[11.] M.V. Drăgoi, Data acquisition-distribution systems, Programming bases in LabVIEW, Transilvania University Publishing House from Braşov, 2001.
[12.] V. Dogaru-Ulieru, ş.a., Aplicatii LabVIEW in measurements, Ed.CONPHYS, Rm. Vâlcea, 2002.
[13.] * * * NI , LabVIEW Basic Introduction, Manual Course.
[14.] Gabriel Gorghiu, Applications of virtual instrumentation in education, Bibliotheca Publishing House, Targoviste, 2007

INTERNATIONAL SYMPOSIUM on ADVANCED ENGINEERING & APPLIED MANAGEMENT
– 40th ANNIVERSARY in HIGHER EDUCATION (1970-2010),

INTERNATIONAL SYMPOSIUM on ADVANCED ENGINEERING & APPLIED MANAGEMENT
– 40th ANNIVERSARY in HIGHER EDUCATION (1970-2010),

INTERNATIONAL SYMPOSIUM on
ADVANCED ENGINEERING & APPLIED MANAGEMENT
– 40th ANNIVERSARY in HIGHER EDUCATION (1970-2010)
4 – 5 November, 2010, Hunedoara, ROMANIA

[1] Gelu Ovidiu TIRIAN, Camelia BRETOTEAN - PINCA[2], Marcel TOPOR[3]

SIMULATION OF NEURAL AND FUZZY SYSTEM TO PREDICT, DETECT AND ELIMINATE CRACKS IN CONTINUOUS CASTING

[1-3.] UNIVERSITY POLITEHNICA OF TIMISOARA, FACULTY OF ENGINEERING FROM HUNEDOARA, ROMANIA

ABSTRACT:
This paper work present Simulink implementation of a neural and a fuzzy system for prediction, detection and rejection of cracks in continuous casting processes. The neural and fuzzy system is made up by a neural network used for fissures detection and a fuzzy controller for predicting and rejecting them, who uses the signal from neural network and a part of data in the process to correct the casting speed and the primary cooling water.
KEYWORDS:
Neural system, fuzzy controller, control, crack

1. INTRODUCTION

Control systems [3] ensure the right working algorithms required by an appropriate system working– both technologically and generally speaking –, and also in case of classical systems based on PID numerical controller. Usually, there are no measures for crack prediction, thus rejects results from the process (in terms of tenth of tones of steel). In such case, working staff changes the working methods of the installation, based on internal instructions. The casting programmer is not appropriate and that has important economical implications [4].

Worldwide, there is research [1], [2], [5], [6], [7] who might lead to already-made crack detection (inside the crystallizing apparatus) and damaged goods. Currently used methods do not entirely eliminate the cracks; they are effective only if some features are being accomplished (crack detection at both exits of the crystallizing apparatus, a pretty slow phenomenon feature as far as the cracking correction is concerned etc.).

In [8], [9], [10], it is proposed a number of original solutions allowing the complete crack rejection from the cast material, outside the crystallizing apparatus. Therefore, it is designed a neural network [8] allowing us to detect any primary crack, by a thorough predictive analysis of the information received from a thermo-couple matrix. Information is used by a system based on fuzzy logics [10], which enables corrections of the casting speed and of the cooling water flow. Since this method does not lead to a complete crack rejection (although specialized literature refers to correcting the casting speed alone, in addition to that we have proposed to change the cooling water flow as well), we have adopted a new predictive principle who diminishes any possible cracking. Thus, the fuzzy system [10] analyzes a number of characteristic measurements and, although the neural network [8] has not yet acknowledged any crack, but it considers they may occur they perform casting speed corrections and cooling water flow occurs. Certainly, the solution we have proposed also implies a more complex fuzzy controller, using two sets of distinct set of rules [10].

2. METHODOLOGY AND DISCUSSION

A. System description

To review the functioning of neural and fuzzy systems, we carry out the simulation in a Matlab-Simulink environment. Scheme implementation is given in fig.1.

Block temperature data generation

In principle, we used recordings of the unfolding process. The best solution is to use two separate sets, one normal and one in case there is a crack. To switch between the two sets of data, we use a switch - control implemented in Simulink - Stateflow. Depending on a given parameter to the entry of this block, it switches between the two sets of data (1 - with crack, 0 – no crack). Block "CT Temperature" operate successively (every 120 s), the data "0" or "1", which basically makes the crack to occur or not. All data are memorized in „look-up data" tables.

Neural data processing block

We are able to identify any fissure if using data received from the 48 thermocouples mounted in 12 rows and 4 columns (on one side of the crystallizing apparatus). For each thermocouple, a dynamic neural network processes 10 consecutive temperature values. Any data received from a dynamic network is then processed by a space network who analyzes the values received from the two adjacent thermocouples. The input size value of such space networks (0 or 1) is introduced into a logical SAU (OR) block [9].

Figure 2 describes the connection amongst two dynamic networks and of a space network for data processing from two adjacent thermocouples.

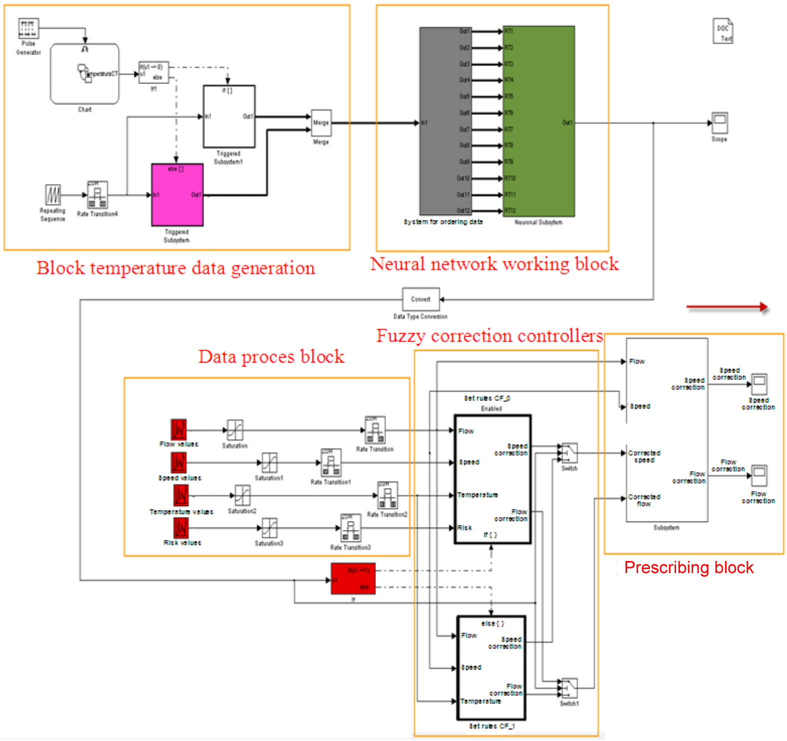

Fig. 1. Implementation in Matlab - Simulink of system

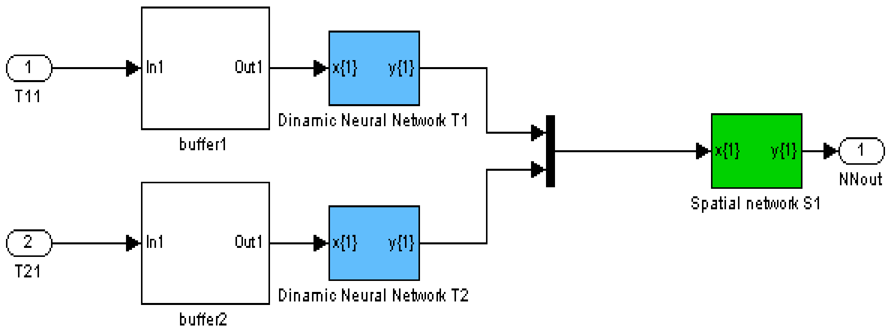

Fig. 2. Connecting two dynamic networks to space network for data processing from two thermocouples

According to the results of the logical SAU operation (we have analyzed output values of the space networks), when leaving the neural block we get a 0-value (there is no primary crack), and a 1-value (there is a primary crack).

Fuzzy Controller (RG-F)

According to the value of the output value of the neural network, RG-F starts two different base sets: a corresponding base in case there are no cracks for „0" (225 rules), and a corresponding base in case there are some primary cracks (75 rules) [7]. The first set has four entries (casting speed, primary cooling water flow, distributor temperature, and technological risk). They are all read from the process (in real situations).

We have used the „Process data block" to simulate it. The „technological risk" parameter is not necessary for the second set of rules, because its value is the highest since we have already detected some cracks. The two outputs of the RG-F (p_v - correction of speed, and p_q - correction of flow), are used for the limitation block [10]. Figure 3 describes the implementation of RG-F "0", and in figure 4. we describe the implementation of RG-F "1" in the environment Matlab-Simulink.

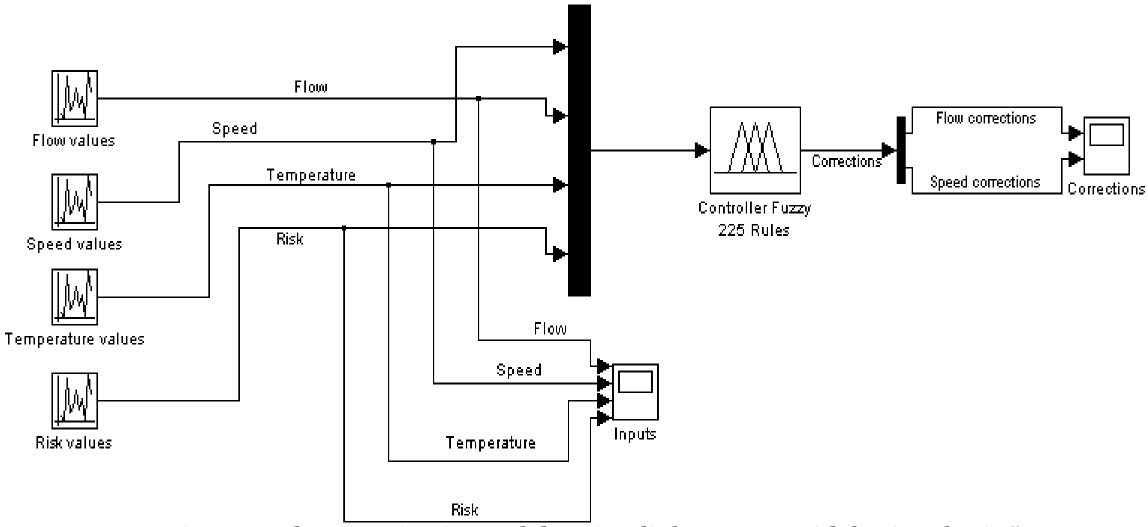

Fig. 3. Implementation in Matlab - Simulink to RG-F with basic rules “0”

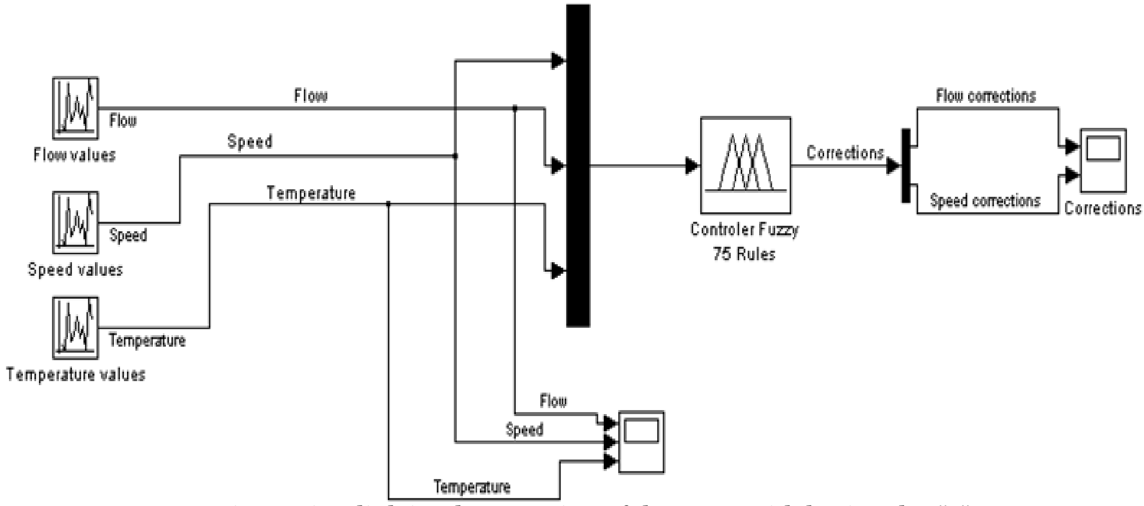

Fig. 4. Simulink implementation of the RG-F with basic rules "1"

Block prescribing

Block prescribing is replacing the values required for speed and flow (v *, q *), from the installation of automation existing in their new corrected values v_c, q_c), resulting in RG-F outputs. For simulation, the values v * and q * were considered equal to those measured sizes of the process (from "Block data processing").

B. Validation of simulated system operation

For validation of simulated system operation, for the entry fissures detection neural network we have applied two different sets of data measured during the current process and stored in tables. One of the sets refers to the situation when there are no cracks and the other one in case there is a crack. Neural network outputs reach 0 and 1 value and they show the network works correctly and it has detected the crack (in case they occur).

For each of the two cases generated at RG-F input, there are several input values (flow, speed, temperature, risk – if the neural network has produced a „0” output – there are no cracks or flow, speed, temperature; - if the neural network has produced an ”1” output value – there are primary cracks). These values are described in figures 5. and 6. : a) – time variation (120 seconds) of RG-F input values; b) – speed correction and new speed values; c) – flow correction and new flow values.

Figure 5. describes the situation during the first 30 simulation seconds, when the cooling water flow is low, the casting speed is low, the temperature inside the crystallizing apparatus is high, and the technological risk is low. Speed correction is very low, hence required casting speed is almost unchanged. During the next simulation 30 seconds, the technological risk increases, the fuzzy controller causes speed correction, and also avoids any crack (casting speed decreases). During the whole time, cooling water flow increases significantly. We can see that the other two simulation rounds are similar.

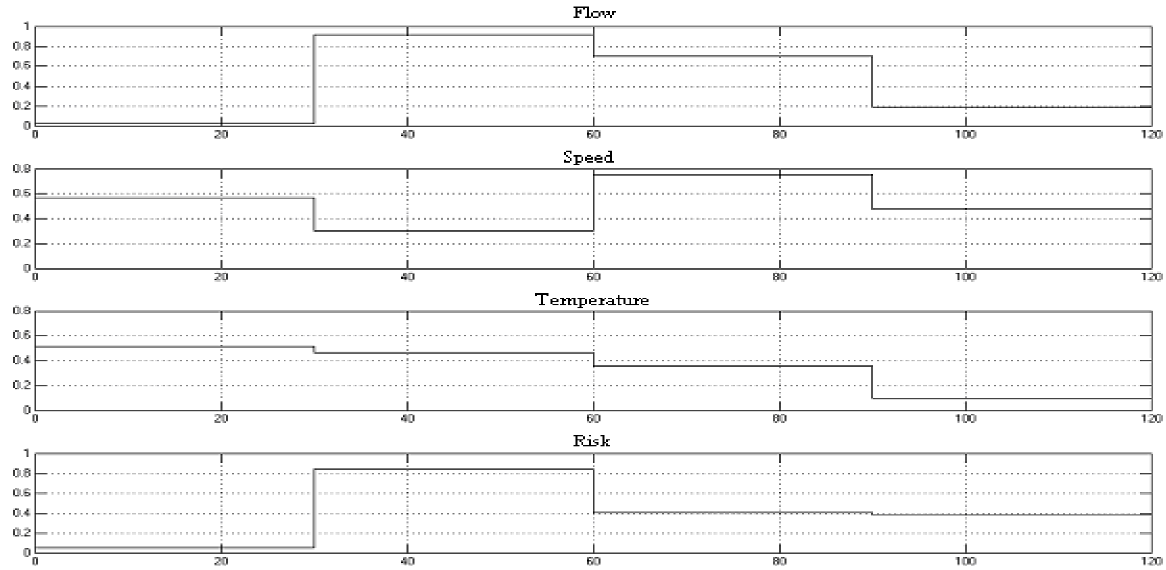

a) RG-F Input Data

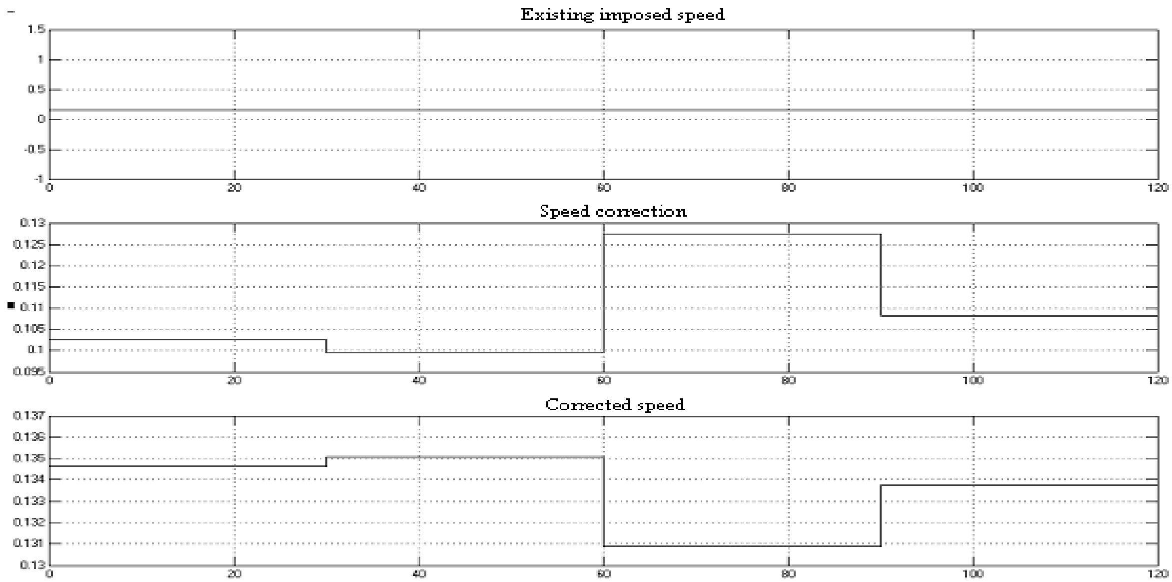

b) Output data – speed

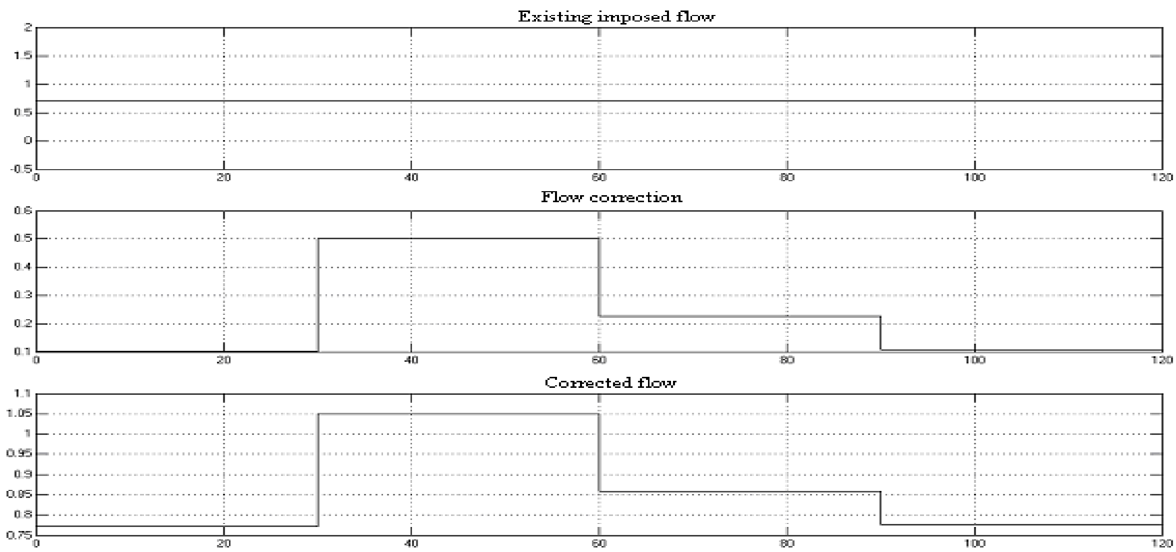

c) Output data - flow

Fig. 5. RG-F Validation (RN=0)

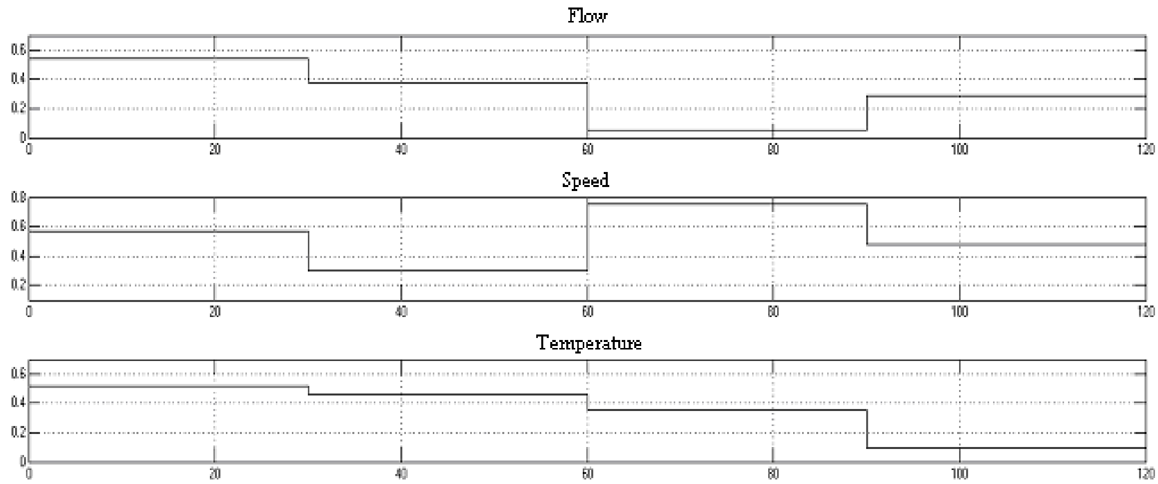

a) RG-F input data

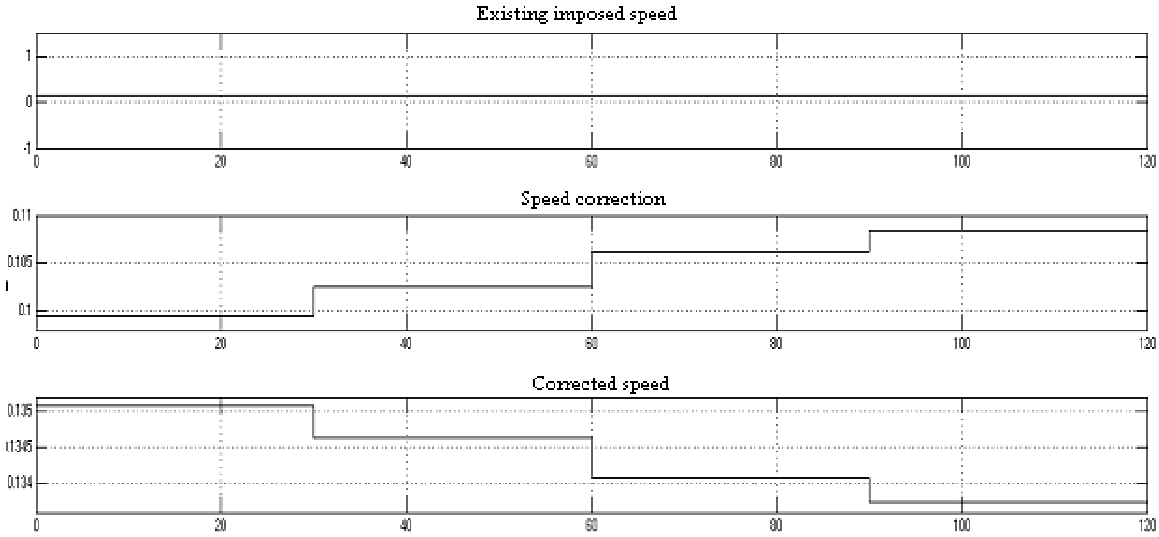

b) Output data – speed

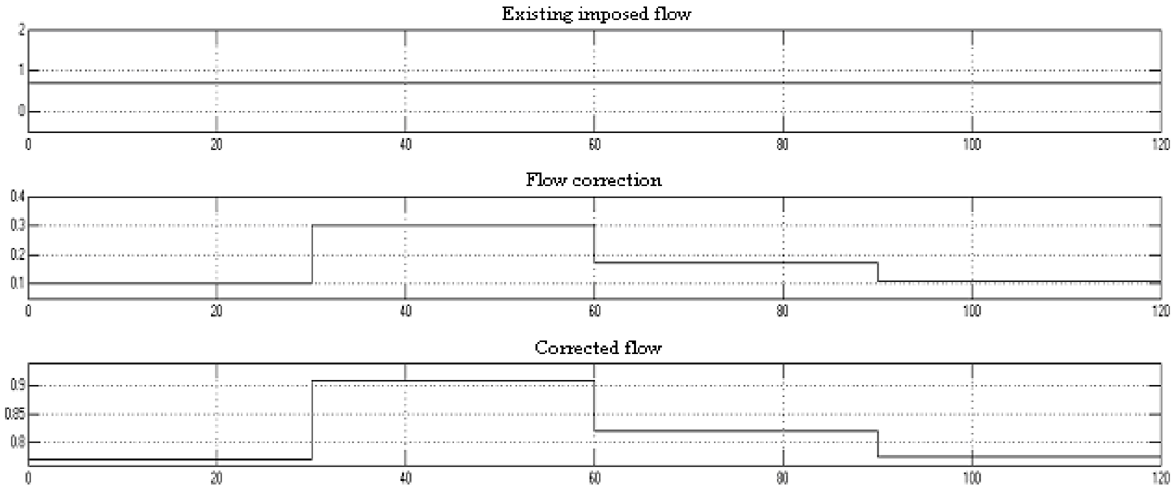

c) Output data - flow

Fig. 6. RG-F validation (RN = 1)

When analyzing all cases described in figures 5. and 6, we draw the following conclusions:

- RG-F analyzes the input values and elaborates speed corrections and water flow correctly, according to two base sets connected to each output of the neural network;

❖ Fore-writing block corrects all required values for speed and flow, according to RG-F outputs.

By simulating in Matlab-Simulink, we have proved that all solutions are correct – predicting, detecting, and rejecting any crack during continuous casting. Such simulation is made for performing a check out on the fuzzy system. During operation, all size values do not change so fast, hence some input values combinations are not that predictable. Once the system is implemented, the rules referring to such situations could be eliminated.

3. CONCLUSIONS

We have performed a Matlab-Simulink simulation of the entire system. Considering this aspect, we have designed the simulation design and designed input sign generators, a neural network, a fuzzy regulator, and the fore-writing block for speed and flow values. When using this method, we have been able to use several input data sets, and the design has correctly generated all output values, acknowledging the whole system.

REFERENCES

[1.] J. Adamy - Device for early detection of run-out in continuous casting, United States Patent, No.5, 904,202, Date of Patent 18 may (1999).

[2.] C. Avila , Y. Tsuji, - Crack width prediction of RC structures by Artificial neural networks, Adaptive and Natural Computing Algorithms, Springer Viena, pg.92-95, 12.dec.(2005).

[3.] S. Bouhouche, et. all - Quality Monitoring Using Principal Component Analysis and Fuzzy Logic. Application in Continuous Casting Process, American Journal of Applied Science (AJAS), 4(9),, ISSN: 1546-9239, 2007, pp.637-644.

[4.] Drainkov, et. all. - An Introduction to Fuzzy Control, Springer-Verlag, Berlin, 1993.

[5.] L. Herbert Gilles, J. Shipman - Method and apparatus for controlling heat removal by varying casting speed, United States Patent, No.4,235,276, Date of Patent 25 nov. (1980).

[6.] T. Nakamura, K. Kazuho - Breakout prediction system in a continuous casting process, United States Patent, No.5, 548,520, Date of Patent 20 august (1996).

[7.] F.P. Pleschiutschnugg, - Method and apparatus for the early recognition of ruptures in continuous casting of steel with an oscillating mold, United States Patent, No.US 6,179,041 B1, Date of Patent 30 jan.(2001).

[8.] G.O.Tirian, - Neural system for detecting cracks in the wire of the continuous casting, 12th International Research/Expert Conference–Trends in the Development of Machinery and Associated Technology, pp. 649-652 Istanbul, Turkey, August 2008.

[9.] G.O. Tirian, S. Anghel, M.Pănoiu, C.Pinca-Bretotean - Control of the continuous casting process using neural networks, Proceedings of the 13th WSEAS International. Conference on Computers, Rodos Island, Greece, July 23-25, ISSN:1790-5109, ISBN:978-960-474-099-4, 2009, pp.199-204.

[10.] G.O.Tirian, O. Prostean, S. Rusu-Anghel, Pinca B. C, D.Cristea - Fuzzy system for implementing the cracks control during the continuous casting, Annals of DAAAM &Proceedings of the 20th International DAAAM Symposium, Volume 20,No.1, ISSN 1726-9679, ISBN 978-3-901509-70-4, pp.1661-1662, 25-28th November 2009, Vienna, Austria.

INTERNATIONAL SYMPOSIUM on ADVANCED ENGINEERING & APPLIED MANAGEMENT
– 40th ANNIVERSARY in HIGHER EDUCATION (1970-2010),

INTERNATIONAL SYMPOSIUM on
ADVANCED ENGINEERING & APPLIED MANAGEMENT
– 40th ANNIVERSARY in HIGHER EDUCATION (1970-2010)
4 – 5 November, 2010, Hunedoara, ROMANIA

[1]Mihaela OSACI, [2] Ioana Sonia DRAGAN, [3]Iulia TRIPA

STUDIES ABOUT MAGNETIC HYPERTHERMIA WITH SUPERPARAMAGNETIC NANOPARTICLES

[1.]POLITEHNICA UNIVERSITY OF TIMISOARA, HUNEDOARA ENGINEERING FACULTY, ROMANIA
[2.]SCHOOL GROUP TELECOMMUNICATIONS AND PUBLIC WORKS HUNEDOARA, ROMANIA
[3.]HIGH SCHOOL TEACHERS "SABIN DRAGOI" DEVA, ROMANIA

ABSTRACT:
The hyperthermias, as an alternative choice for the cancer therapy, are more and more interesting for many researches. When applying the hyperthermia, the cancerous cells are destroyed by increasing their temperature. The idea of using superparamagnetic nanoparticles in hyperthermia is up-to-date, because it offers the possibility of direct inoculation in the target places of the human body, where they remain locally by applying a magnetic field. If the magnetic field is radio-frequency alternating, the magnetic losses that lead to temperature increase are caused by the Neel relaxation processes. The matrix where they are dispersed and the physical properties of the nanoparticles have a crucial importance in the magnetic hyperthermia applications. In this article, we undertake to realise a analytic study about specific absorption rate behavior that characterise the heating in hyperthermia.
KEYWORDS:
magnetic hyperthermia, superparamagnetic nanoparticles, specific absorption rate

1. INTRODUCTION

Electromagnetic (EM) radiation is a fundamental tool in cancer therapy [1], extensively used for both diagnostics and therapy. Physical interactions between EM waves and living matter can be very different depending on the portion of the electromagnetic spectrum considered. A variety of clinical tools have been established in physical medicine based on direct emission and detection of EM waves such as x-ray radiography, computer tomography scanning (CT scan) and gamma-ray radiotherapy from radioactive isotopes. Many other techniques rely on indirect uses of EM radiation such as positron-emission tomography (PET), magnetic resonance imaging (MRI), and microwave hyperthermia (MWH). In fig. 1 [1] it present a frequency ranges for some of the most used diagnostic/therapy equipments (MFH = Magnetic Fluid Hyperthermia, MRI = Magnetic Resonance Imaging). B. The respective main physical mechanisms at each frequency range. Also shown in (C) is the common nomenclature for the electromagnetic waves at each region: RF = radiofrequency; MW = microwaves; IR = infrared; Vis = visible; UV = ultraviolet and X-Ray.

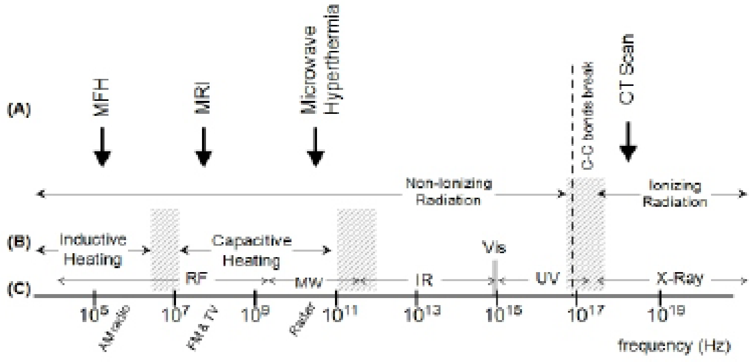

Fig 1.

2. METHODOLOGY

The hyperthermia in oncology consists of increasing the temperature of the cancerous tumours in order to destroy them [3,4,5], and can be used concurrently with other therapeutic techniques, as chemotherapy or radiotherapy. Lately, the magnetic hyperthermia attracted more and more interest [2, 6, 7, 8, 9, 10 ...], being one of the basic subjects debated at the International Conference of Magnetism that took place, during 26th-31st July 2009, in Karlsruhe, Germany. As a ground rule, the magnetic germs or particles are inoculated directly in the tumour zone. Under the action of the alternative magnetic field, the magnetic particles can generate heat via four different mechanisms [9, 10, 11]:

1) generation of the Foucault currents in conductor materials;
2) losses through hysteresis;
3) losses through Neel magnetic relaxation in superparamagnetic nanoparticle systems;
4) losses through Brown magnetic relaxation Brown in the nanoparticle systems found in slimy suspensions.

The mechanism of producing Foucault currents in conductor materials in a time-variable magnetic field is governed by the electromagnetic induction law. Through this mechanism, a significant heating effect is obtained if the material is under an alternative magnetic field. An example of hyperthermia that uses this method is the inoculation of acicular copper particles in the tumour zone, followed by their excitation in a radiofrequency magnetic field. The significant losses through hysteresis are characteristic to the ferromagnetic materials. But, the usage of this mechanism in hyperthermia is problematical [11] due to the temperature control in a quite limited domain (41-48 °C). A solution can be the usage of certain materials that have their Curie points around the heating temperature (41-48 °C), but it's very difficult to find such materials due to their chemistry [11]. A less traumatic solution consists of using an "intelligent" polymer-base ferrogel.

In case of mono-domain particles, where there are no domain walls, when the particles are immersed into a solid matrix or when dispersed particle systems are in high frequency magnetic fields, the inversion of the particle magnetization is realised through the rotation of the particle, and these rotation processes cause losses due to the Neel relaxation processes. In case the magnetic particles are in a liquid matrix, if the frequency of the excitation magnetic field is not too high, the particles tend to rotate until they reach a minimum energy position. These rotation processes lead to losses due to the Brown relaxation.

The measure that characterize the efficiency of the transformation of these losses, via those four mechanisms described above, it is known in the literature as the *specific absorption rate* (SAR), and it is defined as the absorbed power per the mass unit of the tumour material, at a given strength of the excitation magnetic field.

The SAR amplitude is given by

$$\mathrm{SAR}= A.f, \tag{1}$$

where A is the specific area of the hysteresis loop (i.e. specific losses) at the frequency and magnetic field at which the experiment is conducted.

Recent experimental researches [12] showed that, at a given amplitude of the excitation field, at the same frequency, the specific absorption rate is higher in case of using superparamagnetic nanoparticles in radiofrequency fields. These observations, and the fact that the magnetic nanoparticles can be more easily inoculated in the tumour, explain the interest for using them in the magnetic hyperthermia.

To calculate A and interpret hyperthermia experiments, two models -valid in different regimes- can be used. First, when the applied magnetic field is small compared to the saturation field of the NPs, the linear response theory can be used. In this case [12],[13],[14], the hysteresis loop is an ellipse of area [12]:

$$A=\frac{\pi\mu_0 H_{\max}^2}{\rho}\cdot\chi''(f), \tag{2}$$

$$\chi''=\frac{\mu_0 M_s^2 V}{3k_B T}\cdot\left(\frac{f\tau_N}{1+(f\tau_N)^2}\right) \tag{3}$$

Ms is the saturation magnetization, ρ the density of the material (for magnetite 8300 kg/m³).

$$\tau_N=\tau_0\exp\left(\frac{KV}{k_B T}\right) \tag{4}$$

is the Néel relaxation time, and τ0 the interwell relaxation time. The linear theory is suitable to interpret hyperthermia experiments on superparamagnetic NPs, since the rather weak magnetic field used (generally up to 30 mT) is far from the saturation field of the NPs.

If we consider Brown relatation time:

$$\tau_B = \frac{3\eta V_H}{k_B T}, \tag{5}$$

where η is the liquid matrix dinamic viscosity coefficient, V_H is hydrodynamic magnetic nanoparticles volume, in eq. 1 and 2 τ_N becomes total relataxion time $\tau = \tau_N + \tau_B$.

3. DISCUSSION

The most studied superparamagnetic nanoparticles for hyperthermia are those of magnetite, due to their very low toxicity. To be possible to be used in hyperthermia, the magnetic nanoparticles are coated with a carbon layer, to make them biocompatible, and immersed in dextran [15] or polymers (for example, polyvinyl alcohol [16]), to make them biodegradable. For a better penetration of the nanoparticles in the cancerous cells, they are coated with a bioactive compound, as antibodies or proteins [15].

Jennifer L. Phillips, in the paper "A Topical Review of Magnetic Fluid Hyperthermia", available online on the Internet network, describes the possibility of using magnetic fluids in hyperthermia. The superparamagnetic nanoparticles are dispersed in water or hydrocarbon with neutral ph and physiological salinity. The resulted ferrofluid is directly injected in the tumour and a radiofrequency magnetic field is applied.

If the problem of the magnetic nanoparticle inoculation in the tumour zone is rather solved, there are no complex studies to clearly present the relation between the physical properties of the nanoparticle systems and their thermal efficiency in the hyperthermia therapy, or the modality to control the thermal efficiency by controlling the physical proprieties in a way that implies low costs and small technological efforts.

The heating capacity of a magnetic material or electromagnetic device is quantified through the specific absorption power rate (SAR), defined as the amount of energy converted into heat per time and mass. In terms of the usual experiments and parameters for magnetic colloids, the loss power per gram of Fe3O4 is obtained from the heating curves within the initial T temperature rising interval through the definition [1] where c_s is the sample heat capacity, defined as a mass-weighted mean value for a given concentration of magnetic material, calculated as

$$SAR = c_s \frac{\Delta T}{\Delta t} \cdot \frac{1}{m_{mag}} \tag{6}$$

$$c_s = \frac{m_{mag} c_{mag} + m_l c_l}{m_{mag} + m_l} \tag{7}$$

with c_{mag}, m_{mag} and c_l, m_l being the specific heat capacities and masses of magnetic material and liquid carrier, respectively.

The study we performed on spherical magnetite nanoparticles with specific heat capacities c_{mag} = 0.67 J/gK, mass m_{mag} = 1g and diameter 9 nm in water with mass 5 mg and specific heat capacity c_l = 4.18 J/gK and dinamic viscosity coefficient $\eta=0.633 \cdot 10^{-3}$ Ns/m². The physical properties of the magnetite nanoparticles is: saturation magnetization $M_s = 4.7 \cdot 10^5$ A/m and effective anisotropy constant K=1900 J/m³. Initially we consider the system temperature 37.5 degrees Celsius. We believe that the maximum intensity alternating magnetic field applied is between 100 mT 1mT's frequency range between 10kHz and 100 kHz.In first phase we study how depend SAR of frequency and maxim magnetic intensity of magnetic field applied.Rezult is present in fig.2,3.

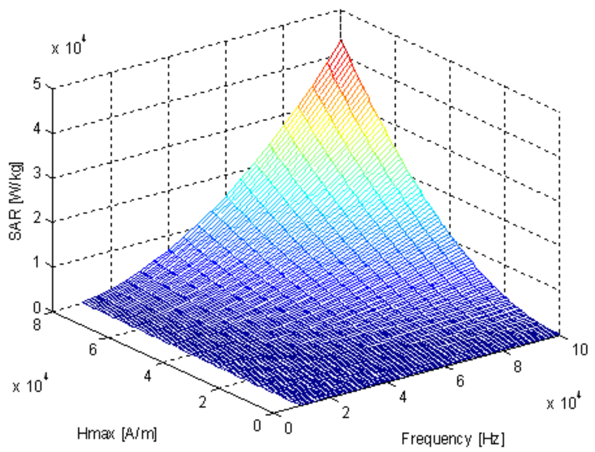

Fig.2

From Fig. 2.3 Note that SAR increases with increasing frequency and amplitude of applied magnetic field.

In Figure 3 is seen as keeping the value constant amplitude magnetic field intensity, it can get a SAR increase if applied field frequency increases.

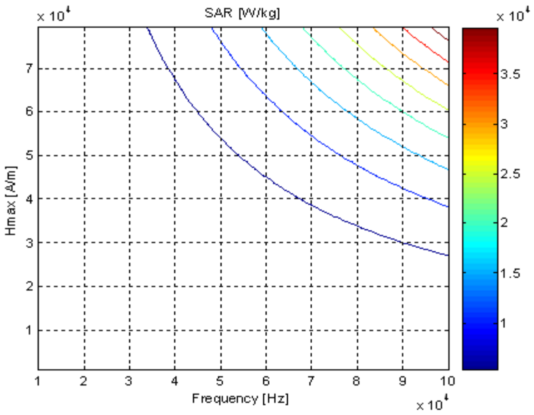

Fig. 3

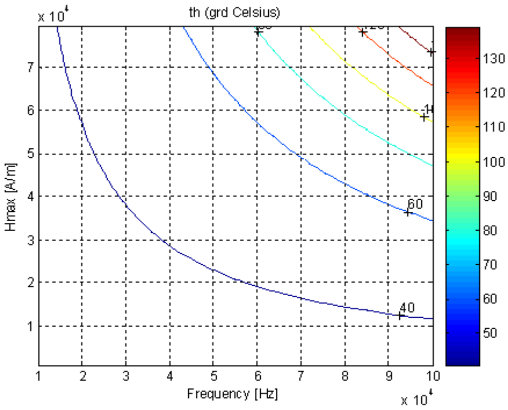

Fig. 5

Then we study how depend the temperature growth of of frequency and maxim magnetic intensity of magnetic field applied. Result is present in fig.4,5.

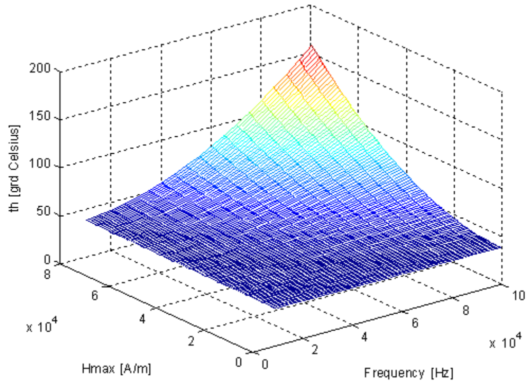

Fig. 4

From Fig. 4.5 Note that the tumor tissue temperature increases with increasing frequency and amplitude of applied magnetic field.

In Figure 5 is observed as a nursery for the temperature ment units when working in weak magnetic fields should work at high frequencies.

4. CONCLUSIONS

In this article, we realise a analytical study that implies the analysis how certain physical properties that maxim intensity of magnetic field applied and frequency of magnetic field, influence the temperature in the tumour zone and, in the same time, to obtain a theoretical tool for controlling the temperature in the magnetic hyperthermia by controlling this physical properties.

REFERENCES

[1.] http://esm.neel.cnrs.fr/2007-cluj/abs/Ibarra2-abs.pdf
[2.] Y.Akin, I.M. Obaidat, B. Issa, Y. Haik, Cryst. Res. Technol., 44, no.4, 388-390
[3.] P. Wust, B. Hildebrandt, G. Sreenivasa, B. Rau, J. Gellermann, H. Riess, R. Felix, and P. M. Schlag, Lancet Oncol. 3, 487 (2002).
[4.] C. C. Vernon, J. W. Hand, S. B. Field, D. Machin, J. B. Whaley, J. van der Zee, W. L. J. van Putten, G. C. van Rhoon, J. D. P. van Dijk, D. G. Gonzalez, F. F. Liu, P. Goodman, and M. Sherar, Int. J. Rad. Oncol. Biol. Phys. 35, 73 (1996).
[5.] J. J. W. Lagendijk, Phys. Med. Biol. 45, R61 (2000).
[6.] M. Kawashita, Y. Iwahashi, T. Kokubo, T. Yao, S. Hamada, and T. Shinjo, J. Ceram. Soc. Jpn. 112, 373 (2004).
[7.] S. Deger, K. Taymoorian, D. Boehmer, T. Schink, J. Roigas, A. H. Wille, V. Budach, K. D. Wernecke, and S. A. Loening, Europ. Urol. 45, 574 (2004).
[8.] S. Mornet, S. Vasseur, F. Grasset, and E. Duguet, J. Mat. Chem. 14, 2161 (2004).
[9.] Q. A Pankhurst, J. Connolly, S. K. Jones and J. Dobson, J. Phys. D 36, R167 (2003).
[10.] R. Hergt, W. Andra, "Magnetic Hyperthermia and Thermoablation" in "Magnetism in Medicine", Eds. W. Andra and H. Nowak, Second Edition (Wiley-VCH Verlag 2006).
[11.] Proc. First Intl. Bioengg. Conf., F.K. Fuss, S.L. Chia, S.S. Venkatraman, S.M. Krishnan and B. Schmidt (eds.), Singapore, p.69 (2004).
[12.] M. Zeisberger et al., J. Magn. Magn. Mater. **311**, 22 (2007)
[13.] R. Hergt et al., J. Magn. Magn. Mater. **270**, 345 (2004)
[14.] X. Wang, H. Gu and Z. Yang, J. Magn. Magn. Mater. **293**, 334 (2005)
[15.] Gruttner C., Rudershausen S. and Teller J. (2001) "Improved properties of magnetic particles by combination of different polymer materials as particle matrix", J. Magn. Magn. Mat. Vol. 225 (1-2), pp. 1-7
[16.] Pardoe H., Chua-anusorn W., St Pierre T.G. and Dobson J. (2001) "Structural and magnetic properties of nanoscale iron oxide particles synthesized in the presence of dextran or polyvinyl alcohol", J. Magn. Magn. Mat. Vol. 225 (1-2), pp. 41-46

INTERNATIONAL SYMPOSIUM on
ADVANCED ENGINEERING & APPLIED MANAGEMENT
– 40th ANNIVERSARY in HIGHER EDUCATION (1970-2010)
4 – 5 November, 2010, Hunedoara, ROMANIA

[1.] Zsolt Csaba JOHANYÁK, [2.] Kálmán Milán BOLLA

DEVELOPMENT OF A TOOLBOX SUPPORTING FUZZY CALCULATIONS

[1,2]KALMÁR SÁNDOR INSTITUTE OF INFORMATION TECHNOLOGIES,
KECSKEMÉT COLLEGE, KECSKEMÉT, HUNGARY

ABSTRACT:
Alpha-cut based calculations are widely used in fuzzy arithmetic and fuzzy rule interpolation based reasoning. One of the key issues of the successful development of these applications is the availability of a toolbox that makes possible the quick and efficient calculation of the α-cuts' endpoints. In this paper, after reviewing some basic theoretical concepts, we present the methods of the α-cut calculation in case of the most used membership function types. The presented methods were also implemented in C# in form of a dynamic link library, which is easy useable in every .NET or traditional Windows or Linux targeting software applications.

KEYWORDS:
α-cut calculation, fuzzy set, toolbox

1. INTRODUCTION

Fuzzy sets can be seen as an extension of the traditional set concept. In case of a crisp (traditional) set (A) every x element of a universe of discourse X can be evaluated only two-way, either as part of the set ($x \in A$) or as not belonging to the set ($x \notin A$). Contrary to this all-or-nothing approach the fuzzy concept [11] makes possible a more colorful interpretation of boundaries. It allows the expression of the membership's measure not only by 0 and 1 but also by any value of the unit interval.

The fuzzy approach has been successfully applied in several areas of the science and the everyday life. Thus has been emerged the fuzzy arithmetic (e.g. [2],[3]) and one can find many practical applications in the field of control (e.g. [9],[4]) or fuzzy modeling of processes and systems (e.g. [6]). A huge amount of these applications does the computations α-cut wise based on Zadeh's extension principle [3]. One of the key issues of the successful practical application is the availability of a toolbox that supports the auxiliary calculations, i.e. the quick and efficient determination of the α-cuts.

In this paper, after reviewing some important theoretical concepts, we present the α-cuts' calculation methods for the most often used membership function types. The methods being presented were also implemented in C# in form of a dynamic link library, which is easy useable in every .NET or traditional Windows or Linux targeting software applications.

2. FUZZY SETS AND RELATED CONCEPTS

In this section we review briefly some concepts and definitions that are strongly related to the α-cut calculation and its applications.

Universe of discourse. Notation: X or U.

The universe of discourse is a crisp (traditional) set, also called domain, from which the members of a fuzzy set are taken. For example the set of the real numbers ($\Re$) can be an universe of discourse.

Fuzzy set. Notation: capital roman letter, e.g. *A*.

The fuzzy set can be seen as an extension of the traditional set concept. While in case of the crisp sets each member of the universe of discourse can be tagged squarely as member of the set or outsider, in case of fuzzy sets one can assign a membership level as well.

Membership function. Notation: μ_A.

The function $\mu_A : X \to [0,1]$ expresses in which measure the members of the universe *X* belong to the fuzzy set *A*.

Normal fuzzy set.

The fuzzy set *A* is considered normal if $\exists x \in X$, for which $\mu_A(x)=1$.

α-cut. Notation: $[A]_\alpha$.

The α-cut of a fuzzy set (*A*) is a crisp set that is defined by

$$[A]_\alpha = \{x \in X \mid \mu_A(x) \geq \alpha; \alpha \in (0,1]\} = [\underline{a}_\alpha, \overline{a}_\alpha], \tag{1}$$

where $\underline{a}_\alpha = \inf\{\ [A]_\alpha\ \}$ and $\overline{a}_\alpha = \sup\{\ [A]_\alpha\ \}$ are the lower respective upper endpoints of the α-cut.

Convex fuzzy set.

A fuzzy set (*A*) is convex when all of its α-cuts are convex sets

$$\mu_A(\lambda x_1 + (1-\lambda)x_2) \geq \min[\mu_A(x_1), \mu_A(x_2)]\ \forall\ x_1, x_2 \in \Re^2,\ \lambda \in [0,1]. \tag{2}$$

Support. Notation: supp(*A*) or $[A]_{0+}$.

The support of a fuzzy set is defined by

$$\text{supp}(A) = \{x \in X \mid \mu_A(x) > 0\}. \tag{3}$$

Core. Notation: core(*A*).

The core of a fuzzy set is crisp set that contains those elements of *X* for which the membership function takes its maximum value

$$\text{core}(A) = \{x \in X \mid \mu_A(x) = \max(\mu_A(x))\}. \tag{4}$$

Compact fuzzy set.

A fuzzy set (*A*) is compact when its support is bounded, i.e. $\exists\ x_1, x_2 \in X$, $\text{supp}(A) \subset [x_1, x_2]$.

Fuzzy number.

A fuzzy set *A* ($\mu_A : \Re \to [0,1]$) is a fuzzy number when fulfills the following requirements [2].

- The set is convex and normal.
- The membership function is at least piece-wise continuous.
- The set is compact on $\Re$.

Reference point. Notation: $RP(A)$

The reference point of a fuzzy set (*A*) is that element of *X*, which is in one or more aspects characteristic to the position of *A*. The reference point is used by several fuzzy methods (e.g. fuzzy rule interpolation based inference techniques) for the characterization of a set's position. Although there are several options for its selection, usually the center point of the set's core is applied for this task [1].

Left/Right flank.

The point $\{RP(A), \mu_A(RP(A))\}$ divides the membership function (set shape) into two parts called left and right flanks of the set.

3. ALPHA-CUT COMPUTATION

Several fuzzy methods use the set's left and right flanks separately for the calculations; furthermore in several cases one needs different α-cuts in case of the two flanks. In order to satisfy this need our toolbox calculates and handles separately the lower and upper endpoints of the cuts. The calculation methods were developed for the most frequently applied convex membership function types, which are the singleton, the triangle, the trapezoidal, the piece-wise linear, the bell-shaped (Gauss), and the LR type.

3.1. SINGLETON TYPE MEMBERSHIP FUNCTION

The α-cut computation is the simplest in case of the singleton type fuzzy sets (see figure 1.a), because one needs to know only the value of the parameter *a*. Here the membership function is described by

$$\mu_{Singleton}(x;a) = \begin{cases} 0 & x \neq a \\ 1 & x = a. \end{cases} \tag{5}$$

All cut endpoints are identical with the value *a*.

3.2. TRIANGLE SHAPED, TRAPEZOIDAL AND CONVEX PIECE-WISE LINEAR TYPE MEMBERSHIP FUNCTIONS

In case of triangle shaped, trapezoidal and convex piece-wise linear type membership functions the α-cut computations are similar, thus we discuss these cases together. First of all let us give a brief description of the formulas used for their calculation. We can describe the triangle shaped membership function (see Fig. 1.b) by

$$\mu_{triangle}(x;a,b,c)=\max\left(\min\left(\frac{x-a}{b-a},\frac{c-x}{c-b}\right),0\right), \tag{6}$$

where the parameters a, b, and c define the break-points of the shape. Similarly the trapezoidal type membership function (see Fig. 1.c) is defined by

$$\mu_{trapezoid}(x;a,b,c,d)=\max\left(\min\left(\frac{x-a}{b-a},1,\frac{d-x}{d-c}\right),0\right), \tag{7}$$

where the parameters a, b, c , and d define the break-points of the shape. The i^{th} line segment of a convex piece-wise linear membership function (Figure 1.d) is given by

$$\mu_{pwl}(x;p_i,p_{i+1})=\mu_{p_i}+\left(x-x_{p_i}\right)\cdot\frac{\mu_{p_{i+1}}-\mu_{p_i}}{x_{p_{i+1}}-x_{p_i}},\ x\in\left[x_{p_i},x_{p_{i+1}}\right]. \tag{8}$$

where $p_i=\{x_i,\mu_i\}$ and $p_{i+1}=\{x_{i+1},\mu_{i+1}\}$ are the bounding points of the line segment.

In case of the membership function types (6)-(8) the computation of the α-cuts is based on similar triangles. A third point is assigned to the two endpoints of the line segment (Fig. 2) in order to form a rectangular triangle. p_i and p_{i+1} are adjacent points where the x and μ values (co-ordinates) are known. The sides of the triangle can be calculated by their help.

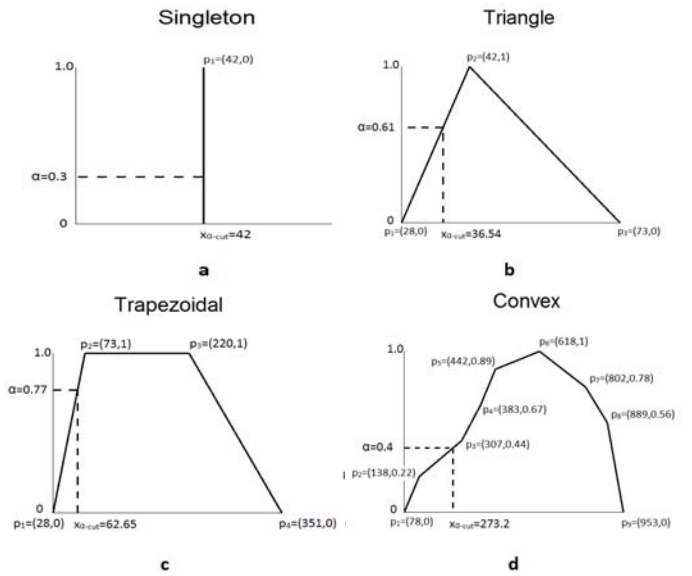

Figure 1 Singleton (a), triangle shaped (b), trapezoidal (c), convex piece-wise linear (d) membership functions and the lower endpoints of their α-cuts

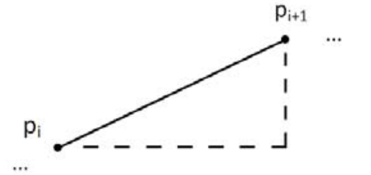

Figure 2. The *i*th linear segment of the set shape

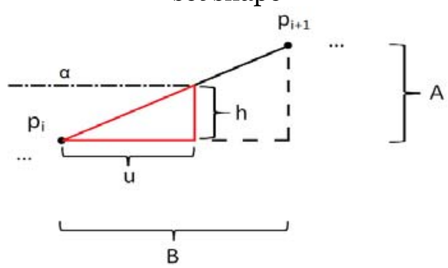

Figure 3. Similar triangles

The determination of a left endpoint of an α-cut is shown in Fig. 3 (the computation of the right endpoint is similar). The figure also shows that the α-cut creates a new triangle. The two existent triangles are similar ones. Their most important feature is that the corresponding sides are in the same ratio. The α-cut computation becomes straightforward owing to this feature.

Fig. 3 shows that the two known sides of the first triangle are A and B. The corresponding sides of the triangle created by the α-cut are h and u, where the size of h is known. Our task is to determine u. In case of the α-cut's left endpoint the x co-ordinate of p_i plus the size of u give the endpoint we are looking for (in case of the α-cut's right endpoint u is subtracted from the abscissa of the p_{i+1} point). For the computation of u the following equations are used.

$$\frac{A}{h}=\frac{B}{u}. \tag{9}$$

$$u=\frac{B\cdot h}{A}. \tag{10}$$

3.3. SMOOTH MEMBERSHIP FUNCTIONS

In case of smooth membership functions (e.g. Gaussian, LR, etc) the α-cut computations are similar, thus we discuss these cases also together. An example of a Gaussian type membership function is shown in Fig. 4. It is calculated by the formula:

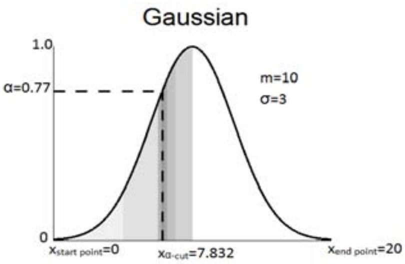

Figure 4 Gauss type membership function and the lower endpoint of its α-cut

$$\mu_{Gauss}(x;\sigma,m)=e^{-\frac{(x-m)^2}{2\sigma^2}}, \quad x\in[x_{start},x_{end}] \tag{11}$$

where σ is the variance and m is the expected value, and x_{start}, x_{end} are the lower repective upper bounds of the partition.

One calculates the LR function by

$$\mu_{LR}(x;\alpha,\beta,c)=\begin{cases}\sqrt{\max\left(0,1-\left(\frac{c-x}{\alpha}\right)^2\right)} & x<c\\ e^{-\left|\frac{x-c}{\beta}\right|^3} & x\geq c\end{cases},$$

$$x\in[x_{start},x_{end}]. \tag{12}$$

Here we use the bisection method for the calculation of the endpoints of the cuts. After bisecting an interval, one calculates the membership value for the resulted abscissa value (x) using the equation (11) or (12). One continues the search in that half interval which contains the demanded α-value. Fig. 4 illustrate the steps of the algorithm. After each bisection one chooses the darker half interval containing the α value. The stopping condition of this method is the execution of 100 iterations, which usually provides a sufficiently good approximation.

4. CONCLUSIONS

The presented calculation methods were implemented in C# in form of a dynamic link library (DLL). The lower and upper endpoints of the α-cuts can be calculated by calling the *AlphaCut* method. It takes as parameters the membership function type (we defined an enumeration type for this purpose), the actual parameters of the shape, two array containing the α-levels for which the lower and upper cut-endpoints have to be calculated, as well as two references for the two arrays in which the results will be returned.

We applied the toolbox successfully in course of the development of the software support for a fuzzy arithmetic based student evaluation method (FUSBE) [5], as well as in course of the implementation of an α-cut based fuzzy rule interpolation method called LESFRI [7].

Further research plans include the consideration of other possible quicker algorithms for the calculation of the α-cuts in case of smooth membership function types.

REFERENCES

[1] Baranyi, P., Kóczy, L. T. and Gedeon, T. D.: A Generalized Concept for Fuzzy Rule Interpolation, in IEEE Transaction on Fuzzy Systems, Vol. 12, No. 6, 2004. pp 820-837.
[2] Fodor, J., and Bede, B.: Arithmetics with fuzzy numbers: a comparative overview, in Proceedings of the 4th Slovakian-Hungarian Joint Symposium on Applied Machine Intelligence (SAMI 2006), Herlany, Slovakia, 2006, pp. 54-68.
[3] Hanss, M.: Applied Fuzzy Arithmetic. An Introduction with Engineering Applications, Springer, Berlin, 2005.
[4] Hladek, D., Vascak, J., Sincak, P.: Multi–Robot Control System For Pursuit–Evasion Problem; Journal of Electrical Engineering, Vol. 60, No. 3, 2009, pp. 143–14.
[5] Johanyák, Z.C.: Fuzzy set theory based student evaluation, Procededings of IJCCI 2009 - International Joint Conference on Computational Intelligence, 5-7 October, Funchal-Madeira, Portugal, pp. 53-58.
[6] Johanyák, Z.C., Ádámné, M.A.: Fuzzy Modeling of the Relation between Components of Thermoplastic Composites and their Mechanical Properties, Proc. of the 5th Int. Symp. on Appl. Comp. Int. and Informatics, 2009, Timisoara, Romania, pp. 481-486.
[7] Johanyák, Z. C., Kovács, S.: Fuzzy Rule Interpolation by the Least Squares Method, 7th Int. Symp. of Hung. Res. on Comp. Int. (HUCI 2006), 2006 Budapest, pp. 495-506.
[8] Klir, G. J. and Folger, T. A.: Fuzzy Sets , Uncertainty, and Information, Prentice-Hall International Inc., Binghamton, 1988.
[9] Precup, R.E. Doboli, S., Preitl, S.: Stability analysis and development of a class of fuzzy systems. Engineering Appl. of Art. Int., vol. 13, no. 3, June 2000., pp. 237-247.
[10] Škrjanc, I., Blažič, S., Oblak, S., Richalet, J.: An approach to predictive control of multivariable time-delayed plant: Stability and design issues, ISA Transactions, vol. 43, no. 4, Oct. 2004, pp. 585-595.
[11] Zadeh, L. A.: Fuzzy Sets, in Information and Control, Vol. 8, 1965, pp. 338-353.

INTERNATIONAL SYMPOSIUM on
ADVANCED ENGINEERING & APPLIED MANAGEMENT
– 40th ANNIVERSARY in HIGHER EDUCATION (1970-2010)
4 – 5 November, 2010, Hunedoara, ROMANIA

[1.]Mária FRANEKOVÁ, [2.]Karol RÁSTOČNÝ, [3.]Aleš JANOTA, [4.]Peter CHRTIANSKY

SAFETY ANALYSIS OF CRYPTOGRAPHY MECHANISMS USED IN GSM FOR RAILWAY

[1,2,3.] UNIVERSITY OF ŽILINA, FACULTY OF ELECTRICAL ENGINEERING, DEPARTMENT OF CONTROL AND INFORMATION SYSTEMS, ŽILINA, SLOVAKIA
[4.] TEMPEST, A. S., GBC IV, GALVANIHO 17/B, 821 04 BRATISLAVA, SLOVAKIA

ABSTRACT:
The paper deals with problems related to safety analysis of cryptography mechanisms that are applied in the GSM-R system. Within introduction the authors briefly describe necessary background and position of the GSM-R and Euroradio in the European Train Control System. To ensure required safety level, in the context of OSI Reference Model an additional safety layer must be implemented consisting of two sub-layers: Euroradio Safety Layer and Safety Application Interface. The authors address only the former when paying attention to safety analysis of cryptographic mechanisms applied. To demonstrate and verify some of theoretical findings, an experimental part has been involved to show results of the particular attack to the DES algorithm, in this case an attack based on the birthday paradox realised via UML.

KEYWORDS:
safety-related communication, Euroradio, GSM-R, cryptoanalysis, block cipher, CBC-MAC, 3-DES

1. INTRODUCTION

Any railway infrastructure operator operating in the Central Europe area should endeavour to modernize trans-European corridor lines as fast as possible, with the highest investment priority. Requirement for corridors modernization results from a need to provide the best quality of railway infrastructure respecting both technological and legislative bases according to the latest technologies and European standards.

To fulfil really this requirement means to implement the European Train Control System (ETCS) as a part of the European Rail Traffic Management System (ERTMS) [1] that has been developed since early 90-ties of the 20th century. The main objective of the ERTMS programme is to design a standardized European rail system, common for all EU countries, which will make possible movement of trains equipped with the ETCS wherever within the European railway network. Based on the track-side ERTMS/ETCS equipment the ETCS may be built on one of three basic application levels L1, L2 and L3 [2]. For the ETCS level L2 and higher the technical solution also must inevitably comprise the Global System for Mobile Communications – Railway (GSM-R) which provides radio information transmission between a stationary and mobile part of the ETCS system.

The GSM-R network, as a technological base for open communication system in the railway transport was chosen and specified within the EIRENE and MORANE projects solved under the auspices of the International Union of Railways (UIC). The project EIRENE led to specification of system and functional requirements representing a fundamental interoperability frame for mobile radio communication at lines of the European conventional railway system according to TSI CCS (Technical Specifications for Interoperability Control-Command and Signalling). The final documents [3] and [4] define a set of requirements to the railway radio communication system. The GSM-R system specification results from a technological platform of digital public cell radiophone GSM system extended for specific requirements of railways and properties required from the professional radio system dedicated to railway operation. From the topology point of view, the GSM-R system is a line system, unlike the public GSM system with an area topology. The GSM-R cells are typically overlapped, sometimes up to a half cell; due to ability to serve a mobile station MS reliably at any place. Assumed velocities within the GSM-R network are up to 350 km/h and frequency bands reserved for data transmission are „uplink“ (876 – 880 MHz) and „downlink“ (921 – 925 MHz).

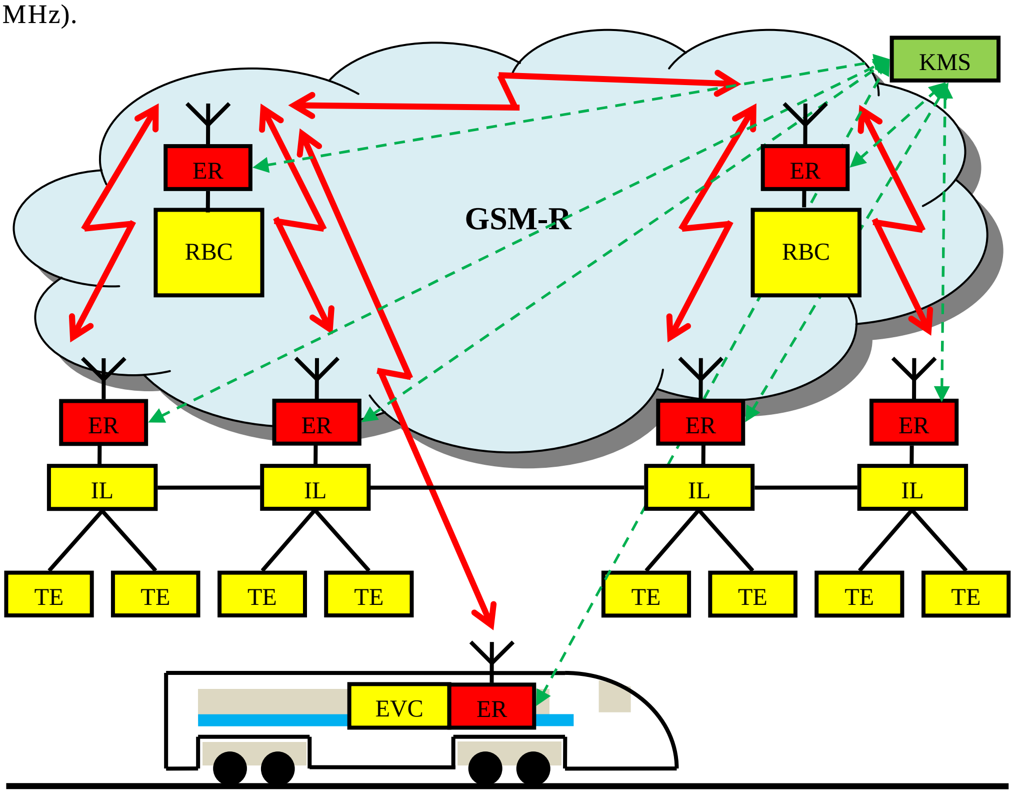

Figure 1. Localisation of GSM-R and ER systems in ETCS architecture

Figure 1 shows usage of the GSM-R system within the ETCS L2. Information needed for railway traffic control (train position, vacancy of track sections, etc.) obtained from Trackside Elements (TE) is concentrated to classical railway interlocking and signalling systems (IL) and from there transmitted via Euroradio (ER) system and the GSM–R communication network. On the base of that information the Radio-Block Centre (RBC) transmits move permissions to individual trains together with other information, again using Euroradio (ER) and the GSM-R communication network. A train sends backward information on its position and other train data to RBC. All functions related to supervision and controls of train velocity are performed by the central European Vital Computer (EVC) located on board the locomotive. Euroradio needs a key management system (KMS) due to management of keys used in cryptographic algorithms.

2. SAFETY OF GSM-R NETWORK

Since the GSM-R transmission system is classified to open transmission systems (classes 6 and 7 according to [5]) it is necessary to assess risk of unauthorised access and consider all threads listed in the standard [5]. According to [5] messages transmitted by ETCS system correspond to the message model of A1 type utilizing the secure cryptographic code with a secret key. Communication between system components is based on layer principle and meets standardised demands for safety-related communication. Additional safety-related layer, added to standard layers of the Open System Interconnection Reference Model (RM OSI) is formed by two sub-layers:

- Euroradio Safety Layer (Euroradio SL) [6];
- Safety Application Interface (SAI) [7].

Within the RM OSI they are integrated above transport layer, having an adaptation layer between them. Figure 2 shows a reference structure of the message for functional specification of interface between trackside subsystems A and B. Euroradio Safety Layer is responsible for secure data transmission which implies protection against threats such as corruption, masking or inserting a message, establishment and release of secure communication link together with error handling. Among secure procedures of the layer there are procedures ensuring message authentication and integrity during transmission. They are realized with the help of the cryptographic technique MAC

(Message Authentication Code) which is a function of the message M and the shared key Kc, when applying operation of ciphering C. The formal notation of MAC calculation is:

$$MAC = C_{K_c}(M). \tag{1}$$

MAC is calculated both at the side of transmitter which adds it to the message being sent, and the side of receiver which verifies coincidence of received and self-calculated authentication codes.

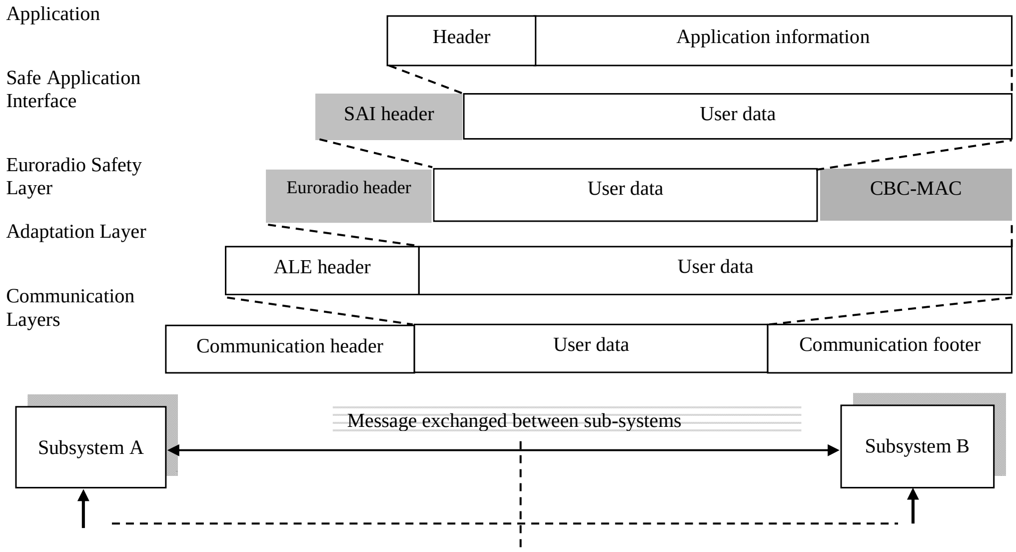

Figure 2. Reference structure of the message

If the codes are equivalent it may be assumed the message has not been corrupted (message integrity), and the message has been sent by the original sender because no one else shares the secret key. To increase safety of procedure for MAC calculation in Euroradion Safety Layer the chained mode of Cipher Block Chaining MAC (CBC-MAC) is used together with the algorithm Triple-DES in EDE mode (Encryption – Decryption - Encryption), also known as a Triple Data Encryption Algorithm (TDEA) defined in ANSI X9.52 [8]. Another safety procedure of the Euroradio SL is procedure for peer entity authentication, which also uses the algorithms CBC-MAC and Triple-DES. In addition to mutual authentication of communicating partner entities the procedure also outputs the session key K_S. The paper only contains a detailed analysis of the Euroradio SL.

3. SAFETY ANALYSIS OF CRYPTOGRAPHY MECHANISMS IN EURORADIO SL

Fundamental requirement of the cryptosystem applied in Euroradio is that implemented cryptographic mechanisms must be able to resist cryptoanalytic attacks during the whole life-cycle of the system. To make assessment of safety and effectiveness of applied cryptographic algorithm those cryptoanalysis methods may be used that are based on complexity theory. Computationally complexity of the algorithm can be determined on the base of asymptotic complexity describing how behaviour of the algorithm changes in dependence on the size of n input data. Operation complexity is usually notated O (called Landau notation or Bachmann-Landau notation) and is a function of input data $O(f(n))$ [9]. It is a limit description of the function curve, so called asymptotic upper limit of the magnitude MG of the function $f(n)$ expressed by other (usually simpler) function $g(n)$. Computation complexity is usually determined by three parameters: space S, time T, and data D.

Algorithm optimisation is then related to minimisation of one out of these three parameters. Algorithms applied in computer science most often have one of the following complexities (m is a real number, $m > 1$):

- Linear complexity: $O(n)$
- Logarithmic – linear complexity: $O(n.log\ n)$
- Polynomial complexity: $O(n^m)$
- Exponential complexity: $O(m^n)$
- Combinatorial complexity: $O(n!)$

The fastest algorithms are considered algorithms with linear, logarithmic-linear or polynomial complexities, algorithms with exponential or combinatorial complexities are realizable in real-time only for low number of inputs n.

Safety analysis of cryptographic algorithms used to secure GSM-R communication via Euroradio system must be concentrated on safety assessment of the CBC-MAC algorithm based on Triple-DES, which is applied within the Euroradio SL.

As inputs to safety procedure of CBC-MAC calculation based on Triple-DEC the following entities can be seen: the session key K_S with sub-keys K_1, K_2, K_3, message M and cryptographic key K_C shared by transmitter with the source address S_A and receiver with destination address D_A. Addresses S_A and D_A represent entities of the ETCS (e.g. RBC and EVC).

Safety procedure of CBC-MAC calculation in the Euroradio SL can be described in the following way:

1. A flag is set to the value log. 0 in the case of communication initiator (transmitter) or the value log. 1 in the case of respondent (receiver).
2. Destination address D_A is added to beginning of the message: D_A_M (the symbol „_“ represents concatenation).
3. A length of the chain D_A_M (denoted as d, in the form of two octets added ahead the chain: $d\_D_A\_M$.
4. If a length of the chain $d\_D_A\_M$ in bits is not a multiple of 64 (block size), at the end of the message padding p is added: $d\_D_A\_M\_p$.
5. The authentication code MAC is calculated from the chain $d\_D_A\_M\_p$ and the shared key K_C using the chained mode CBC-MAC based on symmetric Triple-DES cipher which can be written in the following way: MAC(M) = CBC-MAC(K_C, $d\_D_A\_M\_p$).

Let the session key consists of three parts of the same length (64 bits) $K_C = (K_1, K_2, K_3)$ with the total length 192 bits, including parity bits (every eighth bit). Let data chain (message) consists of bit blocks $X_1, X_2, X_3, \ldots, X_q$. Every block has a size of 64 bits. Encryption function E is a ciphering operation of the DES algorithm in the basic mode, which performs ciphering of data chain with use of the key K_i for i = 1, 2, 3, and decryption E^{-1} is decryption operation of the DES algorithm. Then individual parts of the key are applied when creating the authentication code MAC in the CBC operation mode for data chain parts X_i using the formula (2). Result of the iteration procedure is H_q = CBC-MAC(M).

$$\begin{aligned} H_0 &= 0, \\ H_i &= E(K_1, H_{i-1} \oplus X_i); i = 1,2,\ldots,q-1, \\ H_q &= E(K_3, E^{-1}(K_2, E(K_1, H_{q-1} \oplus X_q))). \end{aligned} \tag{2}$$

From the cryptoanalytic view, calculation of the authentication code in the chained CBC-MAC mode of the cryptographic Euroradio protocol implies several essential facts:

- 192 bit key K_S is used sliced to 3 equally long parts K_1, K_2, K_3, while every eighth bit of the key is the parity bit.
- Function $E(K,P)$ represents encryption of input P by the block cipher DES with a key K. Function $E^{-1}(K,C)$ is decryption of the C by the cipher DES with a key K. Thus input to procedure is divided to 64 bit blocks $X_1, X_2, \ldots, X_q$.
- Message M is extended using a prefix „$d \mid D_A$“, where d is a length of the chain „$D_A \mid M$“ in octets, and p is padding of the last block X_q to the size 64 bits.
- Hash function CBC-MAC is initialised by zero initialisation vector (IV), formula (2).
- The first q-1 steps of the procedure represent a simple DES cipher in a chained CBC mode.
- The last step q is a cipher Triple-DES in so called EDE mode (Encryption - Decryption - Encryption) only.

It is apparent that using the Triple-DES or DES algorithms in a chained mode (multiple operation mode) increases safety of the DES algorithm but what also should be considered is the fact that in the formula (2) the simple DES is used in q-1 steps.

Quite a lot of cryptoanalytic works have been published, describing theoretical attacks to the DES, faster than brute force attack with computing complexity O (2^{56}). There are known several attacks to all 16 rounds of the DES cipher (thereare also attacks to the reduced version of the cipher having less than 16 rounds of calculation). There are known attacks based on differential cryptoanalysis [10] and linear cryptoanalysis [11]. It seems that so called Davies attack [12] is very efficient, based on assumption of knowledge of a certain number of pairs of input and output data that can be used for determining so called empirical distribution of certain characteristics. In this way several bits of the key may be found, the rest of them can be detected using a brute force attack. For 2^{52} known pairs of input and output data it is possible to determine 24 bits of the key with probability of success about 53%.

Usage of the TDEA or DES algorithms in a chained mode (multiple operation mode) increases safety of the DES algorithm. However, as shown in [13], theoretical power of the algorithm is only O(2^{84}) at 228 known encrypted data, or O(2^{112}) at the use of meet-in-the-middle attack which is under present conditions, permanently growing computing capabilities and in certain applications sufficient only for several coming years. The National Institute of Standard Technology (NIST) confirmed the Triple-DES as a cipher applicable concurrently with the AES for sensitive government data till 2030 year [14]). Meet-in-the-middle attack is a standard technique for cryptoanalysis of the TDEA algorithm, in principle it is similar to a birthday paradox.

In an experimental part of the paper there is realization of an attack based on the birthday paradox which reduces the power of the key by the square root of the key size. This attack can also be extended to the DES applied in a multiple operation mode with an initialisation vector. Then for m multiple mode of the cipher the computing complexity $O(2^{m.k/2})$ is assumed at $2^{k/2}$ known encrypted data, if used in combination with the meet-in-the-middle attack.

Supposed that a head (prefix) of the message (input data) A with a larger number of bits than a key is known, every message has it the same (on each occasion encrypted with a different key), it is possible to obtain one of the keys through this attack (actual for a certain modification of the algorithm) as early as for $2^{k/2}$ messages, where k is size of the encryption key. Let l is a number of casually chosen keys K, which will be used to encrypt a head of the message A and result will be inserted to the table as a pair [$E(K, A)$, K], while encryption result $E(K, A)$ will be an index of the table and K its value. Let's choose a number of obtained encrypted messages n, which will be used to extract encrypted head C. On each occasion when a message is received we can have a look into a table whether C is obtained or not. If yes the value for this row of table is the used encryption key. Another possibility is using two tables and analysing an encrypted message without pre-calculation of casually encrypted heads. Probability of finding one of n used keys is expressed by the formula (3).

$$P_S = 1-\left(1-l.2^{-k}\right)^n = 1-\left(1-\frac{1}{2^k/l}\right) \geq 1-e^{-l.n/2^k} \tag{3}$$

If $l.n \geq 2^k$, probability of finding the key P_S is high (e.g. $l = 2^{k/2}$, $n = 2^{k/2}$). So under given circumstances (known prefix of the message, pre-calculation with casually chosen keys, searching in the table with a constant time) theoretical power of the DES algorithm is only $O(2^{28})$ at 2^{28} known encrypted data. This attack may also be extended to the DES applied in a multiple operation mode with the initialisation vector. Then for the m multiple mode of cipher there is assumed computing complexity $O(2^{m.k/2})$ at $2^{k/2}$ known encrypted data, if used in combination with meet-in-the-middle attacks.

4. EXPERIMENTAL VERIFICATION

Within the experimental verification a simple software application has been developed making possible to verify success of a birthday attack to the DES cipher with effective size of the key 56 bits. For this purpose the Unified Modeling Language UML 2.0 has been used supported by the Enterprise Architect 6.0 tool. A chosen development tool for Java has been Oracle JDeveloper 10.1.3.3. The application has been primarily designed as a console-based with opportunity for later GUI implementation. Logging is solved through the *log4j* frame. Running scripts with pre-set parameters have been written in the shell script. Class diagram of the model is shown in Figure 3. Package of cryptographic attacks pch.crypto.attack contains the following trends necessary for the attack realization:

- **ACryptoAttack** – abstract class creating an implementation frame for particular tasks, requires implementation of the method doAttack() from the descendent class returning instance of the class AttackInfo. Further there are methods implemented for writing to so called log (listing directed to file or to console, depending on configuration *log4j*) and to the standard system console.
- **BirthdayAttack** – implementing class of the birthday attck. Besides the overload method doAttack(*) performing one realization of attack set according to the class attributes, it also contains the overload method doAttacks(*) perfoming a chosen number of attacks and returning instance of the class AttackStats. This class is also the target class for running application from the console, so it contains the method main(String[]).
- **HalfSecureRandom** – descendant of the standard class of the language java.security.SecureRandom, covers the method nextBytes(byte[]) to return a mirror symmetrical field of pseudorandom generated bytes.
- **Routines –** a class of accessory statistic methods.

The package of processing (statistic) data from attacks pch.crypto.stat contains classes for saving mentioned data (beans) and their processing:

- **AttackInfo** – a class with attributes containing data about the course and result of the attack.
- **AttackStats** – a class with attributes containing statistic data obtained from several attacks.

- **AttackStatCollector** – a class containing a container for collectivisation of instances AttackInfo and a method calculateStats() for processing of obtained data and creating the instance AttackStats.

The birthday attack according to variant with the use of two indexed tables without pre-calculation would need 2.2^{28} records (memory places) and the same number of encryptions for successful finding of the first key with high probability provided that within the application simulation of obtaining messages with different keys is also considered. Obviously time needed for writing and lookup in tables must also be calculated. Such large tables (either as objects in the operation memory or database) are practically unrealizable on the current hardware (the laptop HP Compaq nx7300 with two-core processor Intel Centrino Duo with clock frequency 2 GHz and operation memory 2 GB, frequency 997 MHz has been available), especially if feasibility is considered from statistic point of view, that is repeated running of the application with the same input parameters. Therefore it was necessary to reduce complexity of the task and thus decreasing effective size of the key. The simplest solution is to decrease effective size of the key to half so that cryptographic keys are generated in mirror symmetry (in bytes – to avoid problem with parity bites), so if n is a length of the key, the byte b_i is identical with the byte b_{n-i-1} for $i = 0, ..., n-1$. Then the size of necessary tables (and thus also computing complexity) should be on average $2^{14} = 16384$ records for the successful attack.

Experimental results are summarized in Table 1. Expected probability of success P_S has been calculated according to the formula (3), $k = 28$, $l = n = k / 2$. Probability of successful experiment P_S^* is determined by the empirical formula as a proportion of successful and whole realisations of the experiment.

Table 1. Results of verification of the birthday attack to the modified cipher DES

Characteristics	Maximum number of attempts of the 2nd realisation			
	2^{12}	2^{13}	2^{14}	2^{15}
Number of realizations	1000	1000	1000	1000
Number of successful realizations	68	226	639	984
Number of unsuccessful realizations	932	774	361	16
Effective size of the key k [bit]	28	28	28	28
Probability of success P_S^*	0,068	0,226	0,639	0,984
Expected P_S	0,061	0,221	0,632	0,982
Average number of attempts	3949,888	7228,148	10811,649	11353,897
Average time of attack realization [s]	0,077	0,147	0,234	0,282

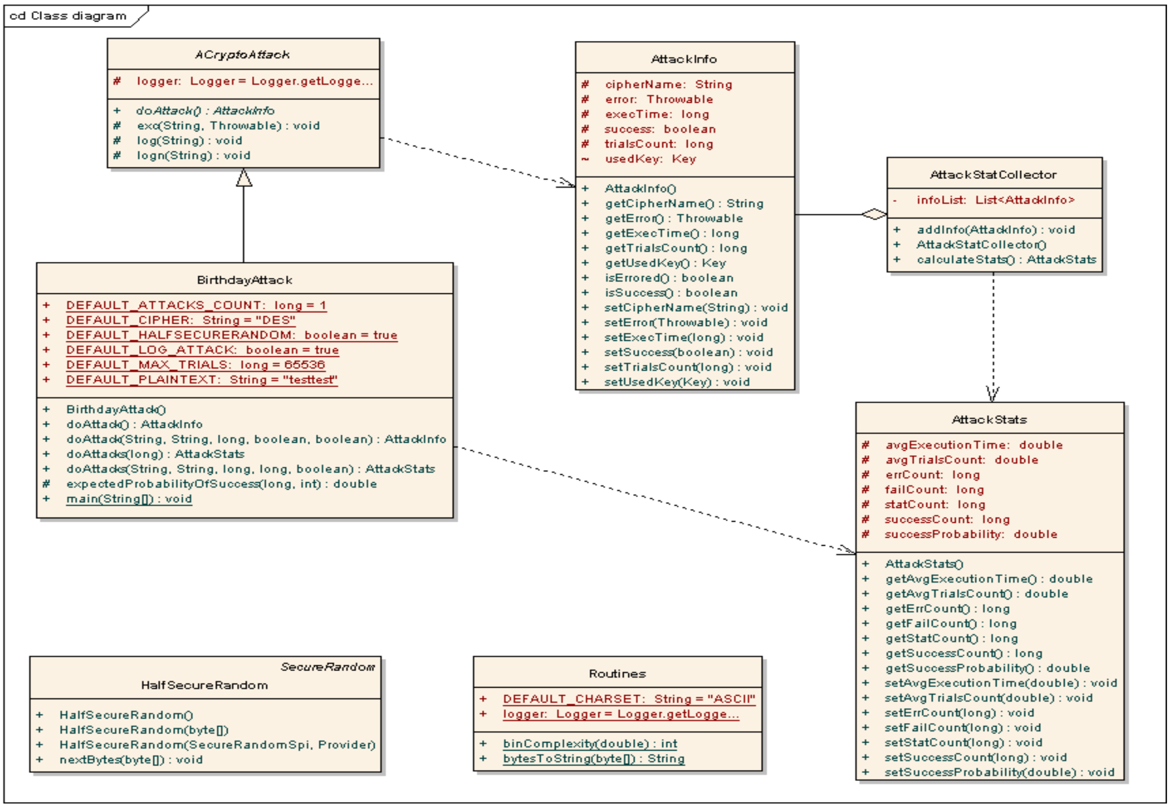

Figure 3. Class diagram of the application BirthdayAttack

On the base of experimental results we can state that theoretical assumes of the birthday attack have been successfully verified for the block cipher with intentionally decreased cryptographic power. On the other side it is necessary to emphasize that possibility of practical realization of such a type of attack in real cryptosystem is extremely low. However, the birthday paradox has been successfully used and applied in different types of theoretical considerations and as we can seen it is also applicable for construction of cryptoanalytic attack.

5. CONCLUSIONS

Safety of the Euroradio SL communication, particularly algorithms CBC-MAC and associated power of encryption of the authentication key, may be theoretically lower than expected.

Operation modes have been projected to reduce propagation of bit errors, they better overlay certain characteristics of input data and protect against attacks with chosen input data (chosen plaintext). Obviously higher safety of operation modes against cryptoanalytic attacks has been assumed. However, theoretical safety is the same in comparison with simple encryption (usage of the key with the same length). Potential shortcomings of the safety procedure MAC may lead to disclosure of the session key. Then it should be mentioned that cryptographic power of the first q-1 steps of the chained CBC-MAC applied in the Euroradio SL is not higher than it is in the case of a simple DES algorithm usage.

Mentioned shortcomings may be improved in several ways. For example the DES cipher or 3-DES could be substituted with the AES cipher which features higher safety limits, higher flexibility of use and higher software efficiency. What's more modifications of safety mechanisms would be minimal. Size of the block would increase to 128 bits and one 192 bit key would be used. Another alternative of how to increase safety of the authentication procedure MAC based on the Triple-DES is to use a proper triple cascade code, for example CBC|CBC|CBC^{-1} [15].

Acknowledgements
This paper was supported by the scientific grant agency VEGA, grant No. VEGA-1/0023/08 "Theoretical apparatus for risk analysis and risk evaluation of transport telematic systems".

REFERENCES

[1.] http://www.ertms.com
[2.] ZAHRADNÍK, J., RÁSTOČNÝ, K.: Safety of Railway Interlocking Systems. (in Slovak), EDIS Zilina, 2006, ISBN 80-8070-546-1.
[3.] UIC EIRENE SRS: System requirements specification. 2006, PSA167D006-15.
[4.] UIC EIRENE FRS: Functional requirements specification. 2006, PSA167D005-7.
[5.] EN 501 59-2: Railway applications: Communication, signalling, and processing systems. Part 2: Safety-related communication in open transmission systems, 2001.
[6.] Subset-037: Euroradio FIS. 2005, v 2.3.0
[7.] FIS SAI: Safe Application Service. 2002, v 8.0, SI/TRK/UP/2.
[8.] ANSI X9.52: Triple Data Encryption Algorithm Modes of Operation.
[9.] http://www.cs.cas.cz/portal/AlgoMath/MathematicalAnalysis/Inequalities/BachmannLandauNotation.htm
[10.] BIHAM, E., SHAMIR, A.: Differential Cryptanalysis of the Data Encryption Standard. Springer-Verlag, 1993, ISBN 3-540-97930-1.
[11.] MATSUI, M.: Linear Cryptanalysis Method for DES Cipher. Advances in Cryptology – EUROCRYPT'93, In: Lecture Notes in Computer Science, Vol. 765, Springer-Verlag, 1993, p. 386-397, ISBN 3-540-57600-2.
[12.] BIHAM, E., BIRYUKOV, A.: An Improvement of Davies' Attack on DES. Advances in Cryptology – EUROCRYPT'94, In: Lecture Notes in Computer Science, Vol. 950, Springer, 1995, p. 461-467, ISBN 3-540-60176-7.
[13.] BIHAM, E.: How to Forge DES-Encrypted Messages in 228 Steps. In: Technical Report, Department of Computer Science, Technion, Haifa, Israel, 1996, CS 884.
[14.] NIST SP 800-67: Recommendation for the Triple Data Encryption Algorithm (TDEA) Blok Cipher. 2004, v 1.0.0.
[15.] BIHAM, E.: Cryptanalysis of Multiple Modes of Operation. In: Technical Report, Department of Computer Science, Technion, Haifa, Israel, 1994, CS 0833.

INTERNATIONAL SYMPOSIUM on ADVANCED ENGINEERING & APPLIED MANAGEMENT
– 40th ANNIVERSARY in HIGHER EDUCATION (1970-2010),

INTERNATIONAL SYMPOSIUM on
ADVANCED ENGINEERING & APPLIED MANAGEMENT
– 40th ANNIVERSARY in HIGHER EDUCATION (1970-2010)
4 – 5 November, 2010, Hunedoara, ROMANIA

[1.]Tibor MORAVČÍK, [2.]Emília BUBENÍKOVÁ, [3.]Ľudmila MUZIKÁŘOVÁ

DETECTION OF DETERMINED EYE FEATURES IN DIGITAL IMAGE

[1-3.]UNIVERSITY OF ŽILINA, FACULTY OF ELECTRICAL ENGINEERING,
DEPARTMENT OF CONTROL AND INFORMATION SYSTEMS, ŽILINA, SLOVAKIA

ABSTRACT:
This paper deals with problem of digital image processing, mainly with localisation of determined interest objects. As application area the eye localisation in a frame of video-sequence has been chosen with continuing in iris and pupil detection. The article contains a theoretical part, with preview of frequently used methods and reasoning of concrete methods selection. The next part presents the actual experiment realised via computing environment MATLAB. In paper conclusion the acquired results are summarised and commented.
KEYWORDS:
Digital image processing, localisation of interest objects, features of human eye, iris, pupil, circular Hough transform, threshold, MATLAB, Image Processing toolbox

1. INTRODUCTION

The localization of interest objects presents the important task of image analysis. At first, for eye image analysis it is necessary to detect the exact eye position, then its main parts and its parameters, e.g. the pupil, the iris, the eyelids, the border of the eyes. This information is used in different applications: monitoring of eye movement, iris extraction for biometrical identification purpose etc. According to the winking frequency it is possible to ascertain driver vigilance, too. In all listed cases several advisable methods of image processing are applied, which afford an opportunity to detect and to locate the interest areas in static image or video-sequence frame. For detection the typical features of eye and of its parts are used, which afford an opportunity to differentiate the particular objects. The resolution of input image is an important factor, which limits the choice of adequate methods. The resolution of eye image for its analysis has a fundamental influence on its precision. Some methods can not be used due to low image resolution because of insufficient details. Generally, image analysis deals with compromise between processing reliability and required processing time. The lower resolution is often used for acceleration of detection process, for working in real time with frames of video-sequence. In these cases the eye area is acquired from the face image cut-out. In the frames of face in resolution 640x480 cut-out of the eye can represent too small part of the frame.

2. LOCALISATION OF HUMAN EYE AND DETECTION OF ITS PARTS

2.1. Features of human eye

The most significant feature in the eye is the iris with a large variety of colours. The iris is the annular part between the pupil and the sclera. Iris and pupil can be taken approximately as non-concentric circles. Apart from these features, the eye has two additional features – the upper and lower eyelid. The ring of the iris might not be completely visible even if the eye is in its normal state, because its top and bottom part are often covered by eyelids and eyelashes. Pupil size varies depending on the light conditions and it is darker than the rest of the eye, even in brown or dark eyes. Sclera is the white visible portion of the eyeball. At a glance with unaided eye, it is the brightest part in the eye region, which directly surrounds the iris. The radius of iris can be defined by the anthropometric measures approximately as 1/6 of the length of the eye. The next constraint for iris detection is that the directions of the edge gradient and the normal to the annulus should not differ more than π/6. The iris is always darker than the sclera no matter what colour it is. In this way the edge of the iris is relatively easy to detect as the set of points that are disposed on a circle. In Fig. 1 are shown all main features in the human eye.

2.2. Methods for localization of eyes

Eyes can be generally localized from face image in two ways. Either is first detected face or eyes are detected from whole image, with using active infrared (IR) based approaches or image-based passive approaches. Eye detection based on active remote IR illumination is a simple effective approach which relies on an active IR light source to produce the dark or bright pupil effects. This method is not widely used, because in many real applications the face images are not IR illuminated. This paper only focuses on the image-based passive methods, which do not affect the input image. In our application we are detecting position of eyes in two steps, the first is locating face to extract eye regions and the second is eye detection from eye window. The face detection problem has been faced up with different approaches: neural network, principal components, independent components, skin colour based methods etc.

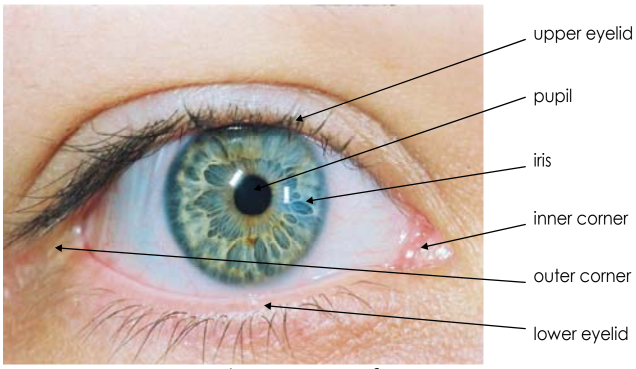

Figure 1. Eye features

We used the method Viola – Jones [1] where face is detected in image with using of AdaBoost classifiers. The image-based passive methods can be classified into three categories. First, template based method, secondly is feature based method and the third is the appearance based method [2]. In the template based method, a generic eye model, based on the eye shape, is designed first. Template matching is then used to search the image for the eyes. While this method can detect eyes accurately, it is normally time-consuming. The appearance based method detects eyes based on their photometric appearance. For this method is needed a large amount of data, representing the eyes of different subjects in different conditions for training classifiers (e. g. neural network or the support vector machine). Feature based methods use for detecting the characteristics of eyes such as contrast difference between iris, pupil and sclera and their edges. This method has a problem with low contrast images. In [3] circular Hough transform is used to detect the iris border where both centre and radius are estimated simultaneously. In some approaches, the iris radius is supposed to be known or limited to a set of expected values.

2.3. Detecting of eye features

The main objective of our work is to detect features such as iris and pupil boundary in eye region. Many distinct approaches have been proposed in this area. [4] Integrodifferential operator is introduced in [5] to find both the iris inner and outer borders. This operator is sensible to the specular spot reflection of non diffused artificial light. Wildes [6] uses for iris segmentation binary edge map followed by circular Hough transform. Liam et al. [7] have proposed a simple threshold method with function maximisation to obtain iris inner and outer borders. Another approach [16] is finding approximate pupil centre as minimum value of the summation of intensity along each row and each column. Then it is applying Canny edge detection and Hough transformation for detection of exact pupil centre. Also morphologic operators, Laplacian or Gaussian operator for edge detection with median filter can be applied to obtain iris borders [2].

In order to locate eye corners, one general approach is utilization of deformable templates [2] which requires a good initialization for correct work, and another common approach is projection functions [9]. Lastly, the proposed methods for eyelids can be classified under two groups: using deformable contour models or curve fitting [2].

In our work we focus on detecting iris and pupil as features of eye. From all approaches mentioned above, we chose circular Hough transform for detecting circles of iris. Hough transform is a very precise technique which can be used to isolate features of a particular shape within an image.

3. APPLICATION OF SELECTED METHODS

In our application we acquire the eye areas proportionally from face dimension. Moreover, these larger areas contain the eye image background too. This background is necessary to be eliminated, than we can work only with the area, which responds to the eye. For distinguishing the objects from background and for the precise eye localisation we used combination of the image segmentation methods, thresholding and edge-based methods. Before using these methods, pre-processing is applied to image for improving the details and adjust the contrast differences. We use histogram equalization, Gamma correction to improve its contrast and brightness and median filter to eliminate the noise [10].

Thresholding is the transformation of an input image f to an output binary image g as follows:

$$g(i,j) = 1 \quad for \quad f(i,j) \geq T, \qquad (1)$$
$$= 0 \quad for \quad f(i,j) < T,$$

where T is the threshold. Since the eye borders are markedly darker, applying adequate threshold allows dividing the background [11]. An example of thresholding method on eye region image is shown in Fig. 2. The result is a binary image with the brightest part of image, which is sclera.

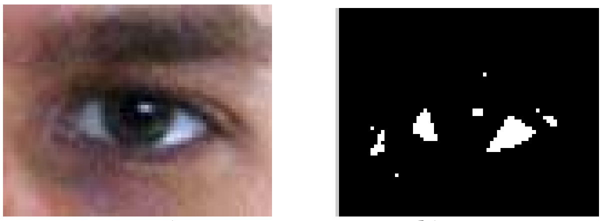

a) b)

Figure 2: a) Original image, b) segmented image

The threshold is added with horizontal and vertical projection [9]. We used variance projection function (VPF) rather than integral (IPF) because variance projection better reflects the difference in image. It is defined with

$$\sigma_H^2(y) = \frac{1}{w} \sum_{i=1...w} [I(x_i, y) - H(y)]^2, \qquad (2)$$

where $H(y)$ is the mean value for the line y, calculated as:

$$H(y) = \frac{1}{w} \sum_{i=1...w} I(x_i, y), \qquad (3)$$

where y is the number of the line, w is the width of the image. With horizontal projection we can determine height of the eye opening. The vertical projection is realised likewise (2), but we don't observe the changes in the rows but in columns.

Thresholds in both normalized projections Fig. 3 a), c) are evaluated based on mean and standard deviation of each function. Green lines represent limitation from horizontal projection while the red ones the limitation from vertical projection. Result from region cropping is on Fig. 3 b). Disadvantage of this method is that the presence of any other significant objects such as glasses or some mark on skin in the eye region affects projection function.

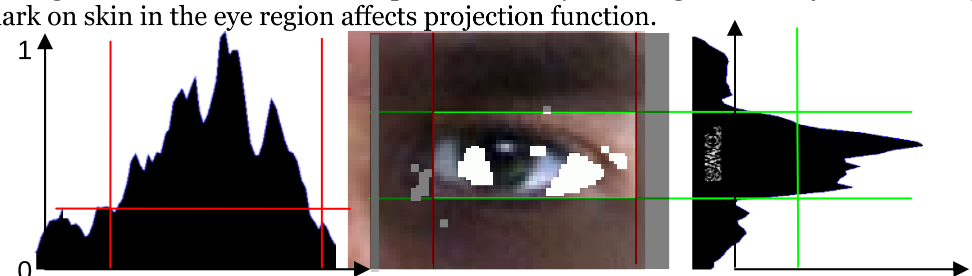

a) b) c)

Figure 3: a) vertical projection, b) result from variance projection function, c) horizontal projection

For the purpose of eye and background segmentation, the Skin-Tone Segmentation method is often used. The skin-tone has specific colour-ranges that distinguish between the colours of the inner parts for eye. Human skin colours can be mapped into one of quadric plane on Cb-Cr chrominance space. But it is necessary to have a colour image in such case.

3.1. Circular Hough transform for iris detection

Having selected the more accurately the region of the eye, the next step is iris detection. For this purpose we used circular Hough transform (CHT), since the iris is nearly circular. The pupil of the eye is plotted as the circle centre and the circular shape of the iris is located and drawn as the circle parameter with its specific radius from the circle centre. As a first, Hough transform is applied to whole eye region, to detect iris. When both centre and radius of iris is detected, then the pupil circle inside iris is localized.

This technique detects imperfect instances of objects within a certain class of shapes by a voting procedure. This voting procedure is carried out in a parameter space, from which object candidates are obtained as local maxima in an accumulator space [3].

The result of Hough transform is an accumulation array in which the higher values represent areas with the occurrence of circles in image with specific radius.

In many cases an edge detector can be used as a pre-processing stage, to obtain image points or image pixels that are on the desired curve in the image space.

Our algorithm is based on the gradient field of the input gray-scale image. A thresholding on the gradient magnitude is performed before the voting process of the Circular Hough transform to remove the 'uniform intensity' image background from the voting process. Thus pixels with gradient magnitudes smaller than gradient threshold are not considered in the computation.

It is not possible to know the exact diameter of the iris, since people can have different iris dimensions and also the system has to manage variable distances between people and the camera. For this reason a range [minimum_radius, maximum_radius] is set to tackle different iris radius. These values are estimated from ratio of iris size to eye width (1/6) mentioned in 2.1. But larger range of radius results in more computational time and memory consumption.

The main advantage of the Hough transform technique is its tolerance to the gaps in feature boundary descriptions and that it is relatively unaffected by image noise.

The circular Hough transform is almost identical to the Hough transform for lines, but it uses the parametric form for a circle:

$$x = x_0 + r\cos\Theta, \qquad (4)$$
$$y = y_0 + r\sin\Theta,$$

where x_0 , y_0 is the coordinate of the circle centre, r is the radius of the circle. When the θ varies from 0 to 360°, a complete circle of radius r is generated.

Gradient of image

To build the accumulation array it is necessary to compute the gradient (5) and the gradient magnitude (6) of the selected eye region (Fig. 4). It is the first derivative of 2D image. The gradient follows the changes in gray level in direction x and y [12]. Gradient ∇I[m, n] of image in direction x and y is defined as:

$$\nabla I = \frac{\partial I}{\partial x}\vec{i}_x + \frac{\partial I}{\partial y}\vec{i}_y = (h_x \otimes I)\vec{i}_x + (h_y \otimes I)\vec{i}_y, \qquad (5)$$

where $\vec{i}_x$ and $\vec{i}_y$ are unit vectors in the horizontal and vertical direction, h_x horizontal derivative and h_y vertical derivative.

Gradient magnitude:

$$|\nabla I| = \sqrt{(h_x \otimes I)^2 + (h_y \otimes I)^2}, \qquad (6)$$

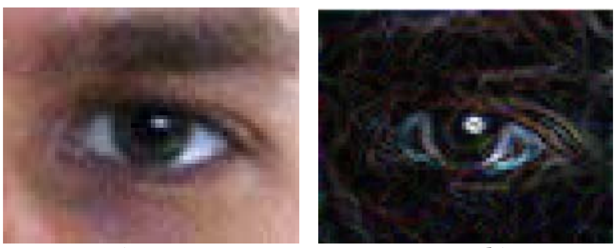

a) b)

Figure 4: a) Original image,
b) gradient magnitude of image

For pixels whose gradient magnitudes are larger than the given threshold, the linear indices, as well as the subscripts are created. The accumulation array of the image consists of the gradient magnitude of the image and its linear indices as

A=accumarray(subs, val);

Accumarray is created by an A array, accumulating elements of the vector val (gradient magnitude) using the subscript in *subs* (linear indices). Each row of the m-by-n matrix subs defines an N-dimensional subscript into the output A. Each element of *val* has a corresponding row in subs. Finally the locating of local maxima in the accumulation array is executed (Fig. 5).

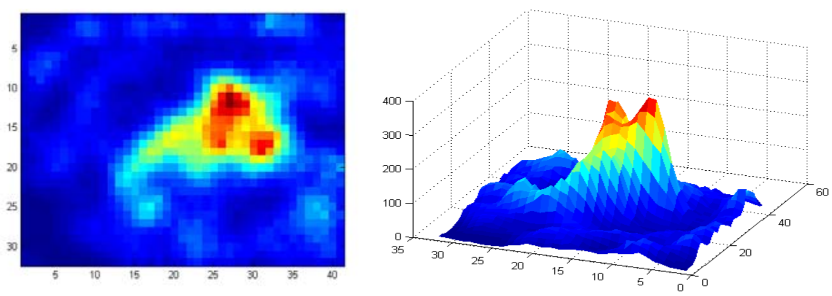

a) b)

Figure 5. Example of accumulator array: a) 2D representation, b) 3D representation

3.2. Experimental results

All methods and algorithms have been implemented in programming environment Matlab, using function from Signal and Image processing toolbox. Input images have been taken from video sequence with resolution 640x480 pixels captured with common web camera.

The set of tested images has contained approximately one hundred video frames from few different people. After face detection, the eye region was cropped for next analysis. One eye region had resolution about 80x80 pixels with some surroundings and the segmented real eye size is only about 50x25 pixels. For its correct function, the CHT Algorithm requires an input image sized 32x32 pixels as a minimum, thus it is necessary to adjust the segmented eye region to this dimension.

Experiments were carried out to test the accuracy of CHT algorithm in iris, using many variations of parameters and input images. For pupil detection, the algorithm is searching for the circle with the smallest average intensity inside localized iris.

Pupil detection requires elimination of reflections on eye; this is done with fill in the brightest parts inside localized iris boundary. In Fig. 6 are presented the examples of testing set of left eye images in many variations of eye gaze and states of eye opening.

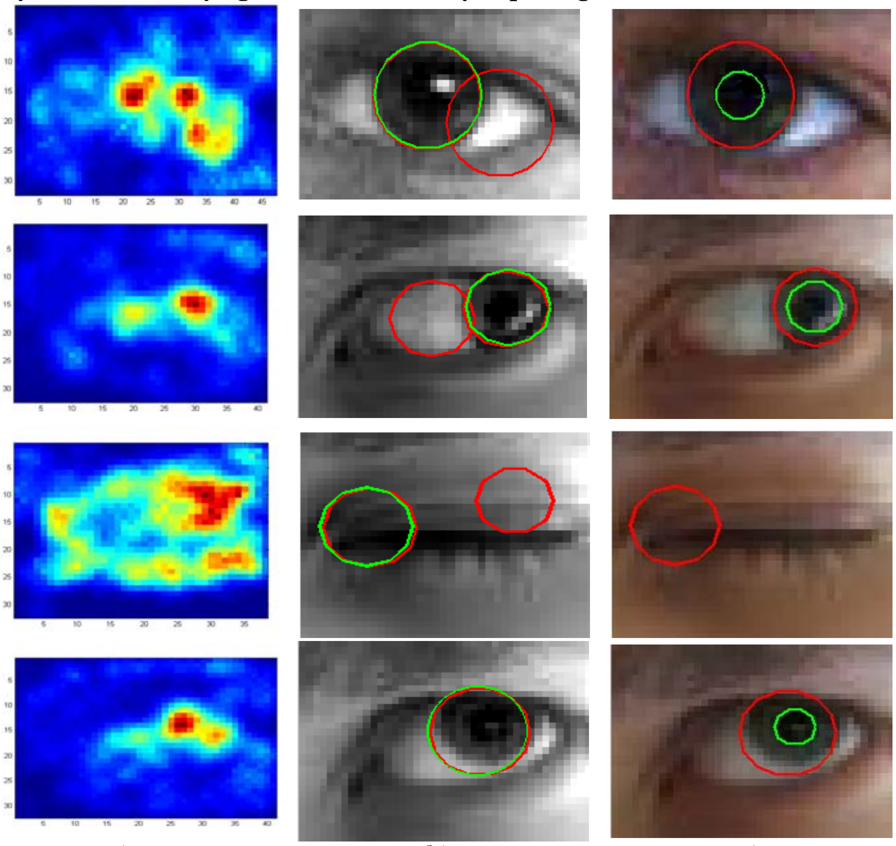

a) b) c)

Figure 6: a) CHT accumulation array,
b) CHT candidates to iris, c) result of iris and pupil detection

4. CONCLUSION

The circular Hough transform (CHT) is very reliable and for a small browsing area it is a fast method for iris detection. This conclusion is valid for our concrete experiment, where the circular object with small resolution has been used. If the iris position changes in the direction towards the eye corner, its precision is slightly worse, due to the loss of circle configuration of the iris, compared with centre position. In this case it is necessary to expand the range of an expected radius. For evaluation and selection from more candidate circles, except local maximum criteria of accumulated area, the darkness criterion of candidate area has been added. This combination helps to eliminate the error detection in some cases. The detection failed only if the opening of eye was not sufficient. For closed eye the dark area in eye corner was detected as iris area. In this case it is necessary to use other methods to evaluate the iris colour.

ACKNOWLEDGEMENT
This work has been supported by the Grant Agency VEGA of the Slovak Republic, grant No. 1/0023/08 "Theoretical apparatus for risk analysis and risk evaluation of transport telematic systems".

REFERENCES

[1.] VIOLA, P. – JONES, M.: Robust Real-Time Face Detection, International Journal of Computer Vision 57(2), 2004, ISSN 0920-5691.
[2.] ŠONKA M. – HLAVÁČ V. - BOYLE R.: Image Processing, Analysis and Machine Vision. Thomson, Toronto, 2008, ISBN 978-0-495-24428-7.
[3.] BALLARD, D. H.: Generalizing the Hough transform to detect arbitrary shapes, Rochester, USA, 1980, ISBN 0-934613-33-8.
[4.] SOMNATH, D. - DEBASIS, S.: An Efficient Approach for Pupil Detection in Iris Images, 15th International Conference on Advanced Computing and Communications, 2007, ISBN 0-7695-3059-1.
[5.] DAUGMAN, J. G.: High confidence visual recognition of persons by a test of statistical independence, IEEE Trans. Pattern Analysis and Machine Intelligence, 1993, 15, (11), pp. 1148–1161, ISSN 0162-8828.
[6.] WILDES, R. P.: Iris Recognition: An Emerging Biometric Technology. Proceeding of the IEEE, 85(9):1348–1363, Sep 1997, ISSN 0018-9219.
[7.] LIAM, L. - CHEKIMA, A. - FAN, L. - DARGHAM, J.: Iris recognition using self-organizing neural network. IEEE, 2002 Student Conf. On Research and Developing Systems, Malaysia, 2002, pp. 169–172, ISBN 0-7803-7565-3.
[8.] MA, L. - TAN, T. - WANG, Y., - ZHANG, D.: Efficient Iris Recognition by Characterizing Key Local Variations. IEEE Trans. on Image Processing, 13(6):739–750, 2004, ISSN 1057-7149.
[9.] FENG, G.C. - YUEN, P.C.: Variance projection function and its application to eye detection for human face recognition, International Journal of Computer Vision. 19 (1998) 899–906, ISSN 0167-8655.
[10.] LUKÁČ, P. – BENČO, M. – HUDEC, R. – DUBCOVÁ, Z.: Color image segmentation for retrieval in large image databases, Conference Transcom 2009, 22-24, Žilina, June 2009, ISBN 978-80-554-0039-6.
[11.] MORAVČÍK, T.: Image Segmentation in Programming Environment MATLAB. OWD 2009, Poland, ISBN 83-922242-5-6.
[12.] WAN MOHD KHAIROSFAIZAL, W. M.– NOR'AINI, A. J.: Eyes Detection in Facial Images using Circular Hough Transform, International Colloquium on Signal Processing & Its Applications, Kuala Lumpur, 2009, ISBN 978-1-4244-4151-8.

INTERNATIONAL SYMPOSIUM on ADVANCED ENGINEERING & APPLIED MANAGEMENT
– 40th ANNIVERSARY in HIGHER EDUCATION (1970-2010),

INTERNATIONAL SYMPOSIUM on
ADVANCED ENGINEERING & APPLIED MANAGEMENT
– 40th ANNIVERSARY in HIGHER EDUCATION (1970-2010)
4 – 5 November, 2010, Hunedoara, ROMANIA

[1]Pavel DRABEK

APPLICATION OF THE SIC COMPONENTS IN POWER ELECTRONICS

[1]UNIVERSITY OF WEST BOHEMIA IN PILSEN, FACULTY OF ELECTRICAL ENGINEERING,
DEPT. OF ELECTROMECHANICS AND POWER ELECTRONICS, CZECH REPUBLIC

ABSTRACT:
This paper presents research motivated by industrial demand for using power semiconductor devices based on SiC (Silicon Carbide). The paper deals with possibility of SiC devices application in traction vehicles. The main attention has been given to the topology of 3-phase voltage-source inverter with free- wheeling SiC schottky diode and 1-phase traction converter with middle frequency converter for auxiliary drives. The theoretical conclusions and simulation results are compared with experimental measurements on laboratory model with rated power of 2kVA
KEYWORDS: Silicon Carbide, Traction application, Power semiconductor device, Hybrid power integration, Electric vehicle

1. INTRODUCTION

Power semiconductor devices based on the SiC substrate is coming more and more popular with increasing development of the power electronics. Due to the advantageous qualities discovered at the SiC this material becomes very interesting object for research and development and subsequent using in the all sorts of applications where bigger and bigger exigencies on efficiency, magnitudes, weight and impact on surroundings are set.

2. SiC PROPERTIES

Crystals of SiC have analogical crystalline structure as diamond and therefore they belong among the hardest known materials, in the Moh's scale of the hardness they reach levels 9-10. Primarily SiC finds use as material called "Carborundum" and it used to exploit for grinding and polishing. Later it was used in the fire-resistant fireclay brickworks and heating shells for industry furnaces or in the composite materials.

With development of the electrotechnics the semiconductor features of SiC were detected and it started to add to the semiconductor substrate of blue shining LED diodes, later in the high shining diodes and in the last few years it has also started to assert in the field of the power electronics.

3. COMPARISON OF THE SIC WITH OTHER MATERIALS

SiC has several unique properties, which make SiC very interesting object for research and development, mainly in the area of high voltage applications. Fig.1 shows these features in comparison with commonly used semiconductor materials (Gallium Arsenide and Silicon).

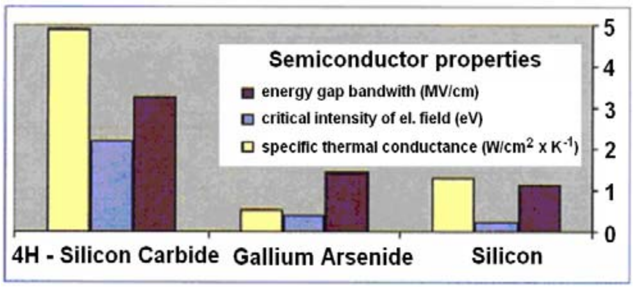

Figure 1. Comparison of individual semiconductor features[3]

4. PRACTICAL USING OF THE SIC

Meantime SiC diodes are the most used devices based on the Silicon Carbide. They are used in many applications. Blocking (freewheeling) diodes in the PFC applications has been the first example of using and it is still frequently used. Rectifying and freewheeling diodes in the switching sources and freewheeling diodes in voltage inverters or active switching rectifiers are the next using of SiC. Further we will discuss possibility of other devices based on the SiC:

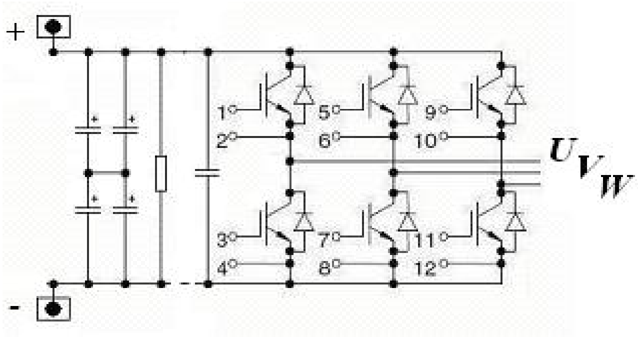

Figure 2. Topology of VSI

At the first we will compare two version of classical 3-phase VSI (see Fig. 2).

The first version of VSI is mounted by classical silicon IGBTs as shown in Fig.3 in left part. The “hybrid” combination of silicon IGBTs and SiC Schottky freewheeling diodes present the second version of VSI (Fig. 3 in right part).

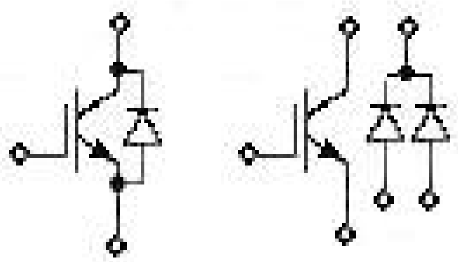

Figure 3. Detailed scheme of used semiconductor devices for VSI

The main advantage of SiC presents following figures 4 and 5 and it is coming-out from Schottky diode properties. The current waveform of silicon diode in the first version of VSI is shown in Fig. 4 and you can clearly see the classical recovering current area.

Against this fact the SiC Schottky diode has very positive waveform of recovering current area (Fig. 5) which is diametrically lower than at Si diode. This is advantage of Schottky structure and SiC material are able produce high voltage Schottky diodes and that is reason of such wave. The double SiC diode module from CREE is used.

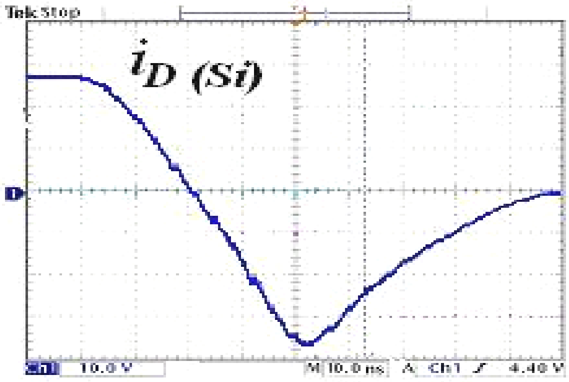

Figure 4. Current waveform of the ultrafast soft recovery epitaxial silicon diode

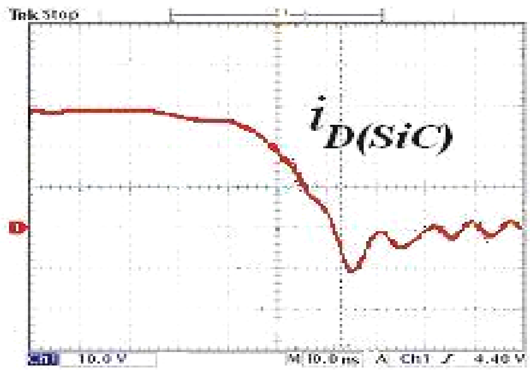

Figure 5. Current waveform of the SiC Schottky diode (produced by CREE as shown in Fig..9)

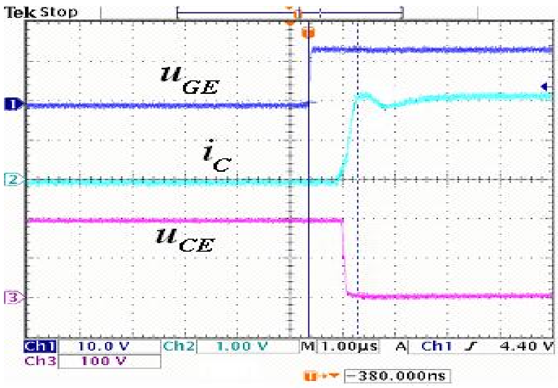

Figure 6. Start up of the hybrid VSI version

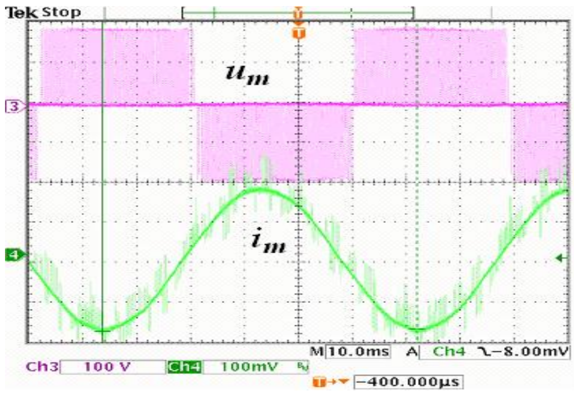

Figure 7. Principal scheme of device J-FET (cascade)

Experimental example of star up of the hybrid VSI version presents Fig. 6. It is evident that using of SiC freewheeling diode has positive influence on current overshoot of collector current of IGBT tranzistor. The testing has been provided under lower supply voltage 200V according to the used devices of 600V range (available free samples).

Typical output waveforms of VSI (line to line voltage UM and phase current IM) are shown in Fig. 7.

Fig. 8 – Fig. 11 present photos of experimental ptotypes of VSI with classical Si IGBTs and hybrid version with Si IGHTS and SiC Schottky diodes.

The hybrid version enables use 5-time higher switching frequency under the same conditions as standard topology with silicon IGBT transistors. It is done by expressively lower losses of SiC schottky diodes (Fig.5). For comparison of the appropriate running condition and losses we have used measuring of circuits values and steady-state temperature of the heat sink.

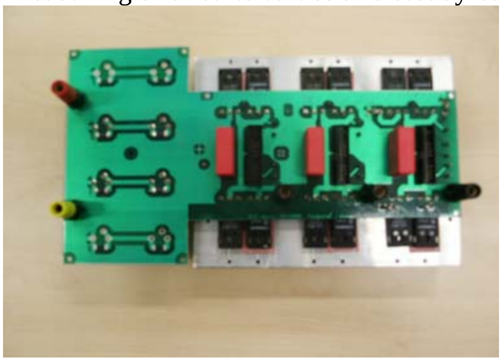

Figure 8. Prototype of hybrid VSI

Figure 9. Detail of hybrid VSI devices

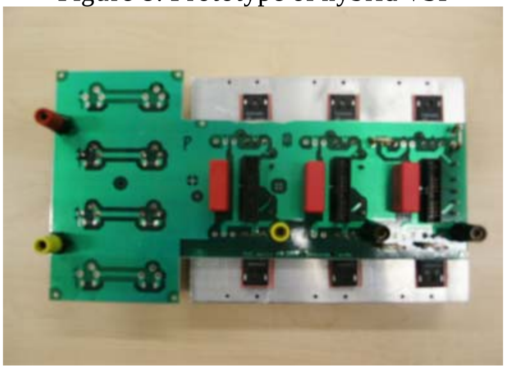

Figure 10. Prototype of VSI with classical IGBTs

Figure 11. Detail of VSI with classical device

The single phase traction converter for auxiliary drives is the second presented application of SiC (Fig. 12). The auxiliary drive converter presents galvanic insulation VSI for auxiliary drives. The input part is directly connected to the DC bus line of main traction converter, it means 1500 V or 3000 V according to the traction vehicle topology. Due to the voltage level the number of serial connections of input 1f VSI has to be placed. Input 1f VSIs fed the middle-frequency transformer (MFT) and the standard diode bride rectifier with SiC is connected on the MFT output. The key is in the using of high switching frequency up to 100 kHz to decrease of weight of auxiliary drive transformer. Output diode rectifier supply DC bus line where several of VSI + auxiliary drives are connected.

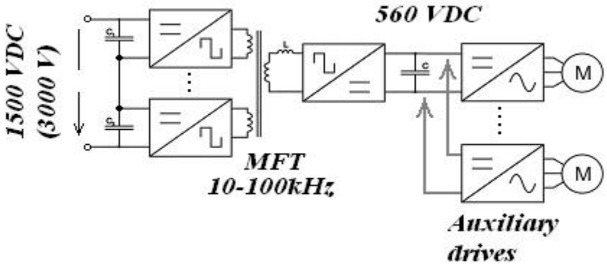

Figure 12. Principal scheme of auxiliary drives traction converter

Fig. 13 presents experimental results of stead state waveforms of MFT voltage and current (output values of input VSI as well). It is evident from the picture that the switching frequency is only 10kHz. This is fact of VSI design with IGBTs and control circuit based on the DSP TEXAS 2812, both aspects limited available switching frequency with reasonable rated power (DSP: A-D converters limited monitoring of analog values, IGBTs limited ratio between switching frequency and reasonable rated power).

The next step is in a new design of the input single phase VSI based on power MOSFETs (to increase switching frequency with reasonable rated power) and mainly using of superior control system based on on analog circuits (analog operational amplifiers) to achieve 100kHz switching frequency.

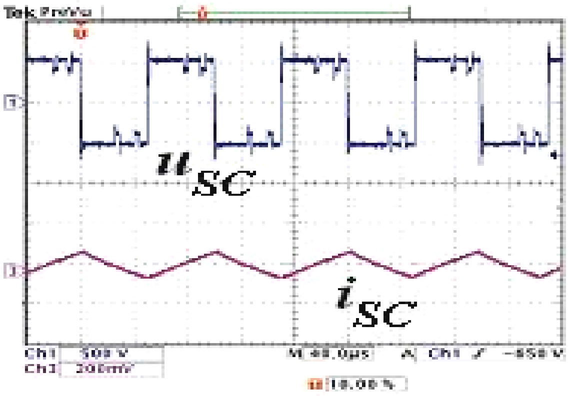

Figure 13. Steady state of voltage and current of MFT, rated power 2kVA

5. CONCLUSION

This paper presents research motivated by industrial demand for using power semiconductor devices based on SiC. The main attention has been given to the topology of 3-phase voltage-source inverter with free-wheeling SiC schottky diode and comparing with topology with classical Si IGBTs. The 5-times increasing of switching frequency with the same loses is the main advantage of this hybrid structure. The second mentioned structure is 1-phase traction converter with middle frequency converter for auxiliary drives. Using SiC diodes in the secondary bridge rectifier brings opportunity to use high switching frequency approximately 50-100kHz. Proposed converter runs at 10kHz according to used devices and control system based on DSP Texas 2812 (problem with conversion speed of standard A-D converters).

ACKNOWLEDGMENT
This research work has been made within research project of Czech Science Foundation No. GACR 102/09/1164.

REFERENCES / BIBLIOGRAPHY

[1] Dahlquist, F. - Frank, W. and Deboy, G. SiC diodes improve boost converter. vyd. Infineon technologies, 2004, 3s, SiC Diodes Improve Boost Converters (PEE 4-04).pdf
[2] Richmond, J. – Hodge, S. and Palmour. J, Silicon karbide power application and roadmap. Publ. Cree inc, 2004, 4s, SiC Power Appl. and Devices Roadmap (PEE 7-04).pdf
[3] Friedrichs, P. – Rupp, R. Silicon Carbide Power Devices - Current Developments and Potential Applications. EPE 2005. ISBN : 90-75815-08-5.
[4] Hruška, M. Application of Silicon Carbide in the power electronics. Publ. in UWB in Pilsen, 2006, 21s.
[5] Kapels, H et. al. A revolutionaly step towards energy saving power Electronic systems. vyd. Infineon technologies AG, 2001, 5s, SIC- PFC Inf. - SiC Schottky Diode - Revolutionary Step to Energy Saving.pdf
[6] Technical documentation, CoolMOS Power transistor – SPW35N60C3. publ. Infineon technologies, 2005, 11s, SPW35N60C3_Rev.2.4.pdf
[7] Technical documentation, SiC diode – SDT12S60. publ. Infineon technologies, 2002, 8s, 1-SDT12S60.pdf

INTERNATIONAL SYMPOSIUM on
ADVANCED ENGINEERING & APPLIED MANAGEMENT
– 40th ANNIVERSARY in HIGHER EDUCATION (1970-2010)
4 – 5 November, 2010, Hunedoara, ROMANIA

[1]Ioan BACIU, [2]Corina Daniela CUNŢAN, [3]Sorin DEACONU, [4]Angela IAGĂR

THE STUDY OF QUALITY INDICATORS OF ELECTRICAL ENERGY IN ELECTRICAL RAILWAY TRANSPORT

[1-4] UNIVERSITY POLITEHNICA TIMIŞOARA, FACULTY OF ENGINEERING OF HUNEDOARA,
ELECTRICAL ENGINEERING AND INDUSTRIAL INFORMATICS DEPARTMENT, ROMANIA

ABSTRACT:
In this work is presenting the study of the electric current's parameters and characteristics, obtained by means of an electric power's quality analyzer. The measurements were made into an AC railway electric traction substation of 27 kV, during more hours, being registered momentary and average values. The data acquired with the electric power's quality analyzer were registered into a computing system, for their further analysis. In order to achieve the adaption between the analyzer's input measures and the traction line's values, the measurements were made in the secondaries of the voltage and current transformers existent in the traction substation.
KEYWORDS: electric power's quality, active power, reactive power, apparent power, harmonic distortion factor, power factor, electric power's quality analyzer

1. INTRODUCTION

The three-phased systems were conceived and achieved to operate in symmetric balanced regimes. In these regimes, all the component elements: generators, transformers, lines and consumers present identical circuit parameters on each phase, and the currents' and voltages' systems in any section are symmetric. If one of the grid's or consumer's elements gets out-of-balance, the regime becomes non-symmetric and the current and voltage systems are losing their symmetry.

The most unfavorable consequence of the voltage unbalance is the circulation of some additional current component (negative and zero) that lead to additional losses, parasite couples at AC electric motors, wear increase, etc.

A prime cause of the unbalances comes from the grid elements: i.e. the non-symmetric space disposition of the aerial electric lines' conductors is translated by impedance differences for the grid's phases, being in this way a source for unbalances. A transposition of the aerial lines' conductors allows, however, the reduction of this unbalance up to the level it becomes negligible. The main cause for non-symmetries is the consumers' supply, great part of them being unbalanced, single-phased and connected between two phases of the grid, or between a phase and null.

The most important unbalances are produced by the high-power industrial single-phased consumers, connected to the medium or high voltage electric grids, e.g: transformation stations for supplying the railway electric traction, welding installations, single-phased electric furnaces, etc.

The non-symmetries provoked by these loads are accompanied most of the times also by other forms of perturbations: harmonics, voltage shocks, voltage holes, etc.

The effects of the current unbalances, indicated by the appearance of the negative and zero sequence components, lead to the increase of longitudinal losses of power and active energy in electric grids. [1]

2. WORK'S PRESENTATION

Conditions for quantities analysis of the harmonic components in the structure of a signal are [58],[71]:

a) Harmonic level – is the ratio, expressed as a percentage of the effective amount of harmonics considered (Fk) and the effective value of the fundamental F1

$$\gamma_K = \frac{F_k}{F_1} \cdot 100\,[\%] \tag{1}$$

b) The deforming residue – represent wave that is obtained from the given wave when is eliminated fundamental harmonic

$$F_d = \sqrt{F^2 - F_1^2} \tag{2}$$

c) Global distortion coefficient (non-sinusoidal shape) – is defined as the ratio, expressed as a percentage of the effective value of deforming residue and the one of fundamental.

$$d = \frac{F_d}{\sqrt{F^2 - F_0^2}} = \frac{\sqrt{\sum_{k=2}^{\infty} F_k^2}}{\sqrt{\sum_{k=1}^{\infty} F_k^2}} \cong \frac{\sqrt{\sum_{k=2}^{\infty} F_k^2}}{F_1} \cdot 100\,[\%] \tag{3}$$

a) Total harmonic distortion, is defined similarly to global distortion coefficient except that the overall distortion is taken into account the first 50 harmonics

$$THD = \sqrt{\sum_{k=2}^{50} \left(\frac{F_k}{F_1}\right)^2} \cdot 100\,[\%] \tag{4}$$

b) Partially weighted harmonic distortion introduced to ensure that when increased rank, descending harmonic and relationship is defined by

$$THD_P = \sqrt{\sum_{k=2}^{50} k \cdot \left(\frac{F_k}{F_1}\right)^2} \cdot 100\,[\%] \tag{5}$$

c) The deformation coefficient of non-sinusoidal periodic wave, ΔF has the expression

$$\Delta F = \frac{|a-b|}{c} \cdot 100\ [\%] \tag{6}$$

where:

- *a* represent y-coordinate of the curve representative for the given periodic wave;
- *b* represent y-coordinate of the curve representative for the fundamental harmonic of the given wave, corresponding to the same x-coordinate as for “a”;
- *c* represent curve amplitude representative for the fundamental harmonic. Determinations of the current harmonics, as well as the THD factor, are made with a three-phased energy analyzer which allows the computing of these parameters according to the following relations.

RMS values for voltage and current:

$$V_{rms}(i) = \sqrt{\frac{1}{N} \cdot \sum_{n=0}^{N} V(i,n)^2} \tag{7}$$

where: N represent the number of samples for the acquisition time;
V_{rms} single RMS voltage $i+1$ phase; $Vavg[i] = Vrms[i]$

$$U_{rms}(i) = \sqrt{\frac{1}{N} \cdot \sum_{n=0}^{N} U(i,n)^2} \tag{8}$$

where: U_{rms} compound RMS voltage $i+1$ phase $Uavg(i) = Urms(i)$

$$Arms(i) = \sqrt{\frac{1}{N} \cdot \sum_{n=0}^{N} A(i,n)^2} \tag{9}$$

where: $Arms(i)$ - Effective current phase $i+1$; $Aavg(i) = Arms(i)$

Computing of harmonic:

By FFT (16 bits) 1024 samples on 4 cycles without windowing (CEI 1000 – 4-7). From real and imaginary parts, each bin computed on each phase V_{harm}, U_{harm} and A_{harm} in proportion to the fundamental value and the angles V_{ph}, U_{ph}, and A_{ph} between each bin and the fundamental.

This computing is done by the following principle:

Module in %: $\mathrm{mod}_k = \frac{c_k}{c_1} \times 100$

angle in degree: ${}_k = \arctan\left(\frac{a_k}{b_1}\right)$

$$\text{With}\quad \begin{cases} c_k = \left|b_k + ja_k\right| = \sqrt{a_k^2 + b_k^2} \\ b_k = \dfrac{1}{512}\displaystyle\sum_{s=0}^{1024} F_s \times \sin\left(\frac{k\pi}{512}s + {}_k\right) \\ a_k = \dfrac{1}{512}\displaystyle\sum_{s=0}^{1024} F_s \times \cos\left(\frac{k\pi}{512}s + {}_k\right) \\ c_o = \dfrac{1}{1024}\displaystyle\sum_{s=0}^{1024} F_s \end{cases} \tag{10}$$

c_k is the amplitude of frequency $f_k = \frac{k}{4} f_1$, F_S is sampled signal, c_o is the DC component, k is the ordinal number (spectral bin).

Computing of the distortion factor (DF):

There are computed two global values that give the relative quantity of harmonics: total harmonic distortion (THD) against the fundamental and the distortion factor (DF) and DF against the effective value (RMS).[2]

$$V_{thd}(i) = \frac{\sqrt{\frac{1}{2}\sum_{n=2}^{50} V_{harm}(i,n)^2}}{V_{harm}(i)} \quad U_{thd}(i) = \frac{\sqrt{\frac{1}{2}\sum_{n=2}^{50} U_{harm}(i,n)^2}}{U_{harm}(i)}$$

$$A_{thd}(i) = \frac{\sqrt{\frac{1}{2}\sum_{n=2}^{50} A_{harm}(i,n)^2}}{A_{harm}(i)} \tag{11}$$

$$V_{df}(i) = \frac{\sqrt{\frac{1}{2}\sum_{n=2}^{50} Vharm(i,n)^2}}{Vrms(i)};\; U_{df}(i) = \frac{\sqrt{\frac{1}{2}\sum_{n=2}^{50} Uharm(i,n)^2}}{Urms(i)} \quad Adf(i) = \frac{\sqrt{\frac{1}{2}\sum_{n=2}^{50} Aharm(i,n)^2}}{Arms(i)} \tag{12}$$

Multiplying the voltage's harmonics factor with the current's harmonics factor, results the power's harmonics factor. Differentiating the voltage's harmonic phase angle with the current's harmonic phase angle, results the power's phase angle.

- different ratios

$PF(i) = \frac{W(i)}{VA(i)}$ power factor, phase $i+1$

Cosinus angle between the voltage's fundamental and the phase current $i+1$

$$\cos[\ (i)] = \frac{\sum_{n=0}^{N-1} VF(i,n)\cdot AF(i,n)}{\sqrt{\sum_{n=0}^{N-1} VF(i,n)^2}\cdot\sqrt{\sum_{n=0}^{N-1} AF(i,n)^2}} \tag{13}$$

Total power factor of various types of energy

$$PF3 = \frac{PF(0) + PF(1) + PF(2)}{3} \tag{14}$$

Active energy consumed $i+1$ phase;

$$Wh(0,i) = \sum_{T\,\mathrm{int}} \frac{W(i)}{3600} \tag{15}$$

Reactive inductive energy consumed $i+1$ phase;

$$VARhL(0,i) = \sum_{T\,\mathrm{int}} \frac{VAR(i)}{3600} \ \text{ for } \ VAR(i) \geq 0 \tag{16}$$

Reactive capacitive energy consumed $i+1$ phase.

$$VARhC(0,i) = \sum_{T\,\mathrm{int}} \frac{VAR(i)}{3600} \ \text{ for } \ VAR(i) \leq 0 \tag{17}$$

The measurements were made in the traction station CFR Deva, by means of the electric power quality's analyzer CA 8334B. During the data acquisition it was caught a passing from one supply transformer to another power factor or distortion factor. Further is presented the variation form of the line voltage and current at a given moment (Fig. 1). One can notice a reduced modification in the voltage form, and a pronounced one in the current's variation form.

Variation of the power factor's measures PF (Fig. 2), of the voltage's harmonic distortion factor V_{thd} (Fig. 3) and of the current's harmonic distortion factor I_{thd} (Fig. 4) is presented during the entire acquisition period, where from can be determined the fluctuation of the determined measures, fluctuation that leads to distortions in the general power supply grid [3].

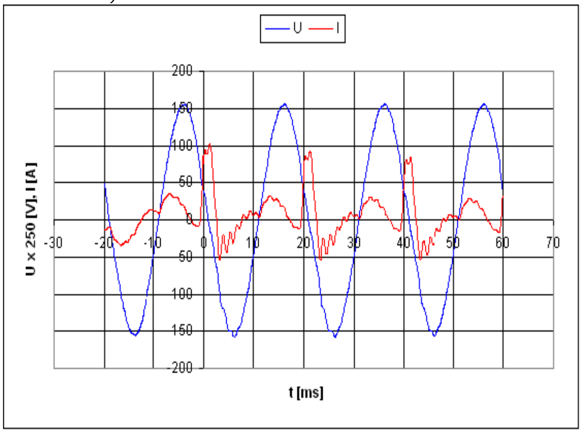

Figure 1 Variation form U,I

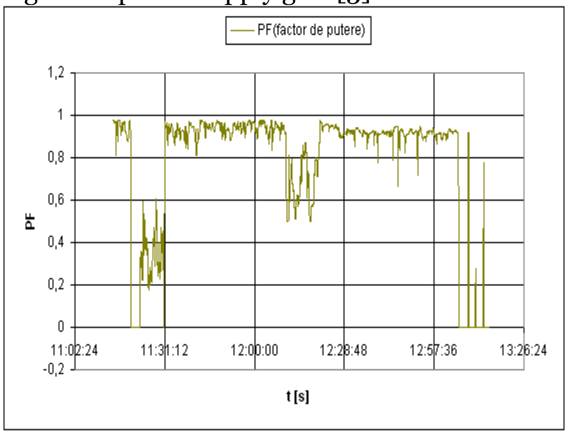

Figure 2 Power factor

Depending on these obtained values, can be designed diverse compensation systems of the perturbations introduced in the grid [4][5].

Within the AC electric traction of 50Hz with DC motors and implicitly with converters [6], was obtained a harmonic distortion factor of the voltage (Fig. 5), relatively reduced, of 4,5% in conditions of a normal traffic, and the values of the voltage harmonics are also reduced.

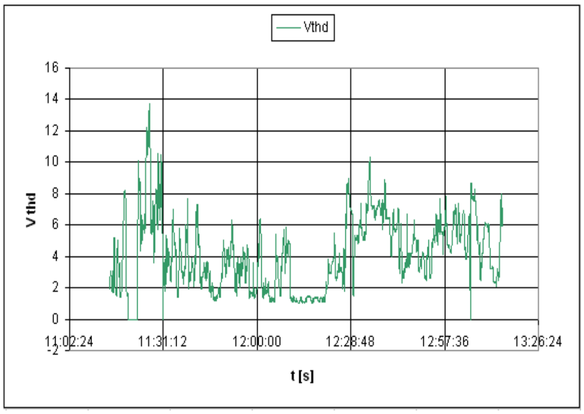

Figure 3 Voltage's harmonic distorsion factor

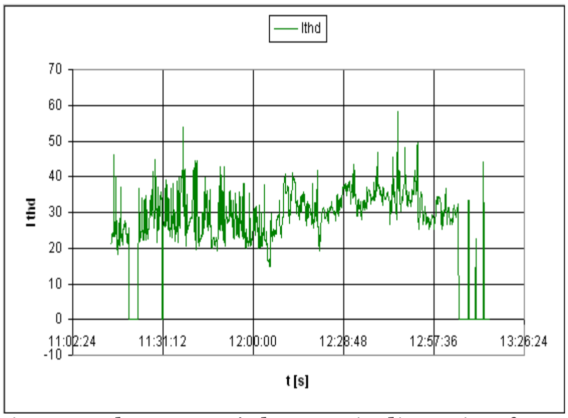

Figure 4 The current's harmonic distorsion factor

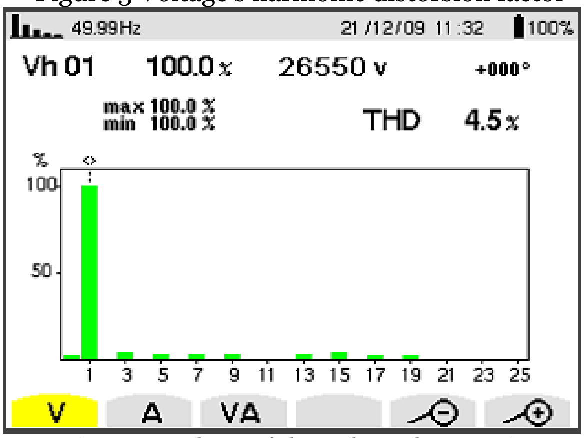

Figure 5 Values of the voltage harmonics

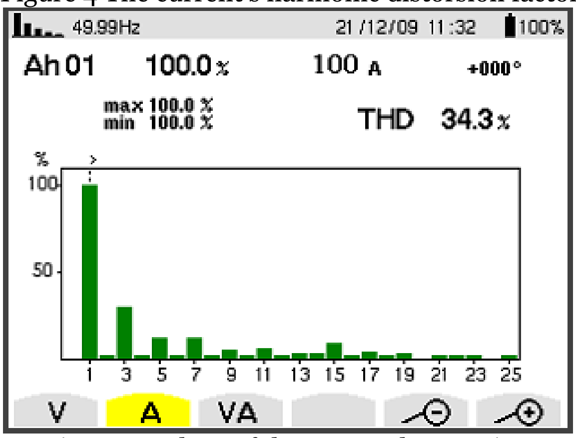

Figure 6 Values of the current harmonics

For the current harmonics (Fig. 6) things are changed, we have high THD of 34,3% and harmonics' individual values also high, up to 25% from the fundamental harmonic, that should be eliminated.

For eliminating the current harmonics, can be introduced passive filters of LC type [4][5], that should eliminate the low-rank harmonics, and for the superior rank ones it can be used the solution of the active power filter, which cannot be connected on the locomotive but only in the traction station. Dimensioning of the passive filters (for the harmonics 3,5,7 can be made on the minimum reactive power criteria, thus being possible to reduce the reactive power consumption [1].

The LC-type filters use coils with variable inductivity by modifying the iron core's penetration depth inside the copper winding. By modifying the inductance, it is modified the LC circuit's tuning frequency, influencing the current absorbed from the power supply system, both as value and shape. For the computing of L and C elements, it was chosen the minimum reactive power criteria.

For each current harmonic that is possible to be introduced is used such a resonant circuit. The elements of each filter are dimensioned in such way that for the resonance frequency that coincides with the respective current harmonic frequency result impedance very small.

$$Z_k = k\omega_1 L - \frac{1}{k \cdot \omega_1 \cdot C} \tag{18}$$

where: Z_k is the equivalent impedance of the resonant circuit for the harmonic of k order (the equivalent resistance of the coil of capacitors and electric connection elements were neglected).
ω_1 = fundamental current pulsation.
Pulsation:

$$\omega_k = k\omega_1 = \frac{k}{\sqrt{LC}} \tag{19}$$

is quite the resonance pulsation of LC circuit.

Usually, the absorbing filters are installed for the harmonics with the highest amplitudes, which correspond in general to the low order of harmonic.

Designing of filters' inductivity and capacity is made by applying of some algorithms that could be differentiated first depending on the filters' role from the viewpoint of reactive power compensation on the fundamental. All the resonant circuits will have capacitive character on the fundamental's frequency, so they will produce, no matter what, a capacitive transversal compensation of the network.

Even though this is a rare solution, it could be taken into account in boundary situations when the deformant regime in current is very pronounced. Even the reactive power compensation is not a primary objective, the filter will generate in the grid reactive power on fundamental. Therefore, the filter's dimensioning criteria, more specifically of the capacity from its componency, is to minimize the installed capacitive reactive power (which, beside a minimum cost of the battery, leads to a minimum influence on the active power circulation in the grid):

$$Q_c = Q_{c\min} \tag{20}$$

This reactive power will have two components corresponding to the two above mentioned currents, the current corresponding to the fundamental and the current corresponding to harmonic k on which the resonance is taking place:

$$Q_c = Q_{c1} + Q_{ck} = U_c^2 \cdot \omega_1 \cdot C + \frac{I_k^2}{k \cdot \omega_1 \cdot C} \tag{21}$$

where: Q_{c1} - reactive power supplied by the filter's capacitor on fundamental;
Q_{ck} - reactive power supplied by the filter's capacitor on k harmonic;
U_c - voltage at the capacitor's terminals;
I_k - harmonic current that follows to be filtered.

Making the partial derivate depending on the capacity of the installed capacitive reactive power equation and canceling it, we obtain the equation of the filter's capacity:

$$C = \sqrt{\frac{1}{k}} \frac{I_k(k^2 - 1)}{U_1 \cdot \omega_1 \cdot k^2} \tag{22}$$

The L filter's coil inductivity is determined from the resonance condition of the filter's LC:

$$L = \frac{1}{\omega_k^2 C} = \frac{1}{k^2 \cdot \omega_1^2 \cdot C} \tag{23}$$

By introducing of such resonant filters on the odd harmonic frequencies, we can study the influence on each filter in part, as well as the effect of many filters connected in parallel. Beside the amplitude value, is aimed also the phase-difference introduced by each harmonic against the fundamental.

Will be analyzed the current harmonics for three different loading situations of the generator, respectively three values for the slide potentiometer, at three different supply voltages [1][7][8].

3. CONCLUSIONS

From the analysis of the obtained graphics, can be seen the need to reduce the existent perturbations in the grid. Introduction of the passive filters beside the active filter only reduces the harmonics' values, without having a major influence upon the reactive power and especially upon the non-symmetry of the supply system. The passive filters can be connected either on the locomotive, or in substation, their dimensioning being specific to each case in part. The non-symmetries introduced in the grid by the single-phased supply of the railway electric traction system can be reduced only in the traction substation; therefore we must act on more plans simultaneously to obtain satisfactory results regarding the reduction of the perturbations induced in the supply grid.

For a better study is needed to examine the variation form of voltage and current on the train in case of normal traction. Depending on the results obtained can find appropriate ways to compensate harmonic regime.

REFERENCES

[1.] Adrian Buta, Adrian Pană, Symmetrization of the Electric Distribution Grids' Load, „University Horizons", Timişoara, 2000.
[2.] C.A. 8334B, Three Phase Power Quality Analyser, Chauvin Arnaux, France, 2007.
[3.] Steimel A., Electric Traction Motive-Power and Enrgy Supply. Basics and Practical Experience, Oldenbourg Industrie Gmbh, 2008.
[4.] Pănoiu, M., Pănoiu, C., Osaci, M., Muscalagiu, I., Simulation result about harmonics filtering using measurement of some electrical items in electrical installation on UHP EAF, WSEAS Transactions on Circuits and Systems 7 (1), pp. 22-31, ian 2008;
[5.] Angela Iagar, Gabriel Nicolae Popa, Ioan Şora, Analysis of electromagnetic pollution produced by line frequency coreless induction furnaces, Wseas Transactions on Systems, January2009,volume 8, Issue 1, ISSN 1109-2777;
[6.] Corneliu Botan, Vasile Horga, Florin Ostafi, Marcel Ratoi, Minimum Energy and Minimum Time Control of Electrical Drive Systems, WSEAS Transactions on Power Systems, Issue 4, Volume 3, April 2008, ISSN: 1790-5060.
[7.] Pănoiu M, Pănoiu C, Osaci M,Muscalagiu I. Simulation result about harmonics filtering for improving the functioning regime of the UHP EAF, Proceedings of the 7th Wseas International Conference on Signal Processing, Computational Geometry and Artificial Vision (iscgav'-07), aug 24-26, 2007 Vouliagmeni, GREECE, Pages: 71-76;
[8.] Alan k. Wallace, Rene Spee, The Effects of Motor Parameters on the Performance of Brushless d.c. Drives, IEEE Transactions on Power Electronics, vol.5, no.1, January 1990;

INTERNATIONAL SYMPOSIUM on
ADVANCED ENGINEERING & APPLIED MANAGEMENT
– 40th ANNIVERSARY in HIGHER EDUCATION (1970-2010)
4 – 5 November, 2010, Hunedoara, ROMANIA

[1.]Iosif POPA, [2.]Gabriel Nicolae POPA, [3.]Sorin Ioan DEACONU

THE SIZING OF THE BRANCH THREE-PHASE LOW VOLTAGE POWER LINES THROUGH SUPERPOSITION METHOD

[1-3.]DEPARTMENT OF ELECTROTECHNICAL ENGINEERING AND INDUSTRIAL INFORMATICS, FACULTY OF ENGINEERING HUNEDOARA, POLITECHNICA UNIVERSITY TIMIŞOARA, ROMANIA

ABSTRACT:
Traditionally, the main and branch three-phase distribution lines are dimensioned by the minimum conductor-material volume method or that of the moments method.
The paper introduces a new method of designing the power distribution lines. Its advantage consists in the fact that it is simple and easy to apply. It is based on the superposition method used in solving the three-phase electric circuits.
KEYWORDS:
sizing, three-phase distribution lines, superposition method

1. INTRODUCTION

Usually, the branch three-phase low voltage distribution power lines can be size by the admissible maximum voltage drop method, the minimum conductor material volume method and the moments' method [1,2,3,4]. These methods can be use easy, when is not necessary the admissible maximum current correction by a specify cross-section, depending on duty type of the consumer. If is necessary to use this correction, the sizing of the branch three-phase power lines is made simple, through superposition method propose in this paper. This method consists in compute of simple power lines cross-section that composes the complex branch power lines through the admissible maximum voltage drop method. For the common cross-section lines, these are compute like sum of the determinate cross-section for every line partly.

The paper gives an example of sizing the branch three-phase low voltage power lines through superposition method.

2. METHODOLOGY. THE SIZING OF THE BRANCH THREE-PHASE POWER LINES THROUGH SUPERPOSITION METHOD

It is consider the general case for a simple branch power line (fig.1) that supplies n three-phase inductions motors. Each motor works in intermittent periodical duty with the different relative duty cycles, DA_i (i = 1,2,...,n). These motors have the powers P_{ci}[W] (i = 1,2,...,n).
First time, is calculate the currents I_{ci} [A] for every n motors:

$$I_{ci} = \frac{P_{ci}}{\sqrt{3}\cdot U_{ln}\cdot \eta_{ci}\cdot \cos\varphi_{ci}}\ [A] \quad (1)$$

In this relation U_{ln} [V] is the line rated voltage, η_{ci} [-] is the efficiency, and $\cos\varphi_{ci}$ [-] is the power factor for every motors.

The branch line is decomposing in n simple branch lines (fig.2), every line will be calculated with the admissible maximum voltage drop method. The lengths L_i of the simple lines, in that case, become:

$$L_i = l_o + l_i,\ i = 1,2,\ldots,n \quad (2)$$

Will be size the simple lines from fig.2 that compose the branch line from fig.1. For this reason it is approximate compute the reactive voltage drop for every line:

$$\Delta U_{lri} = \sqrt{3} \cdot X_i \cdot I_{ci} \sqrt{1-\cos^2 \varphi_{ci}} \ [V], i=1,2,...,n \tag{3}$$

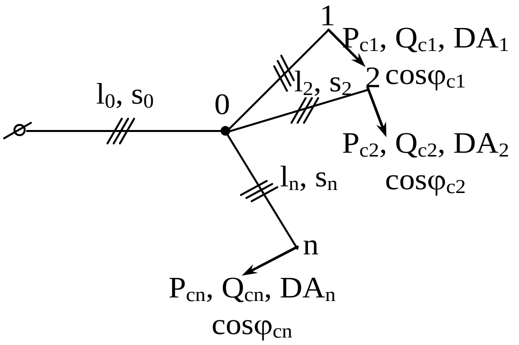

Figure.1 The branch three-phase power lines that feeds with electric energy n consumers

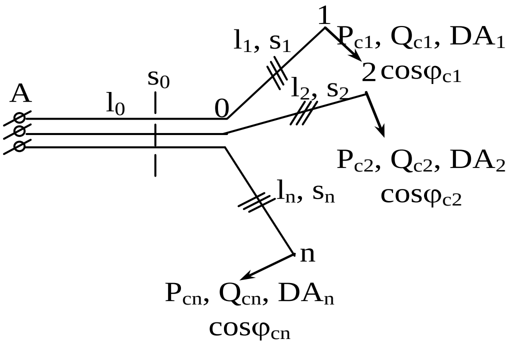

Figure.2 Decomposition of the branch three-phase power lines from figure 1 in n simple power lines

The reactances X_i [Ω] for every simple line are compute with:

$$X_i = 2\pi \cdot f \cdot L_{01} \cdot (l_0 + l_i) \tag{4}$$

In this relation L_{01} [H/m] is the specific line inductance, for underground cable, in the first phase it is calculated with [1]:

$$L_{01} = (2.6...3.2) \cdot 10^{-7} \ [H/m], \text{ for underground cable with } U_{ln} \leq 15 \text{ kV}$$
$$L_{01} = (3.2...3.9) \cdot 10^{-7} \ [H/m], \text{ for underground cable with } U_{ln} > 15 \text{ kV} \tag{5}$$

For overhead line the specify reactance is estimate with: $X_{01} = 0.4 \cdot 10^{-3}$ [Ω/m].
In this case:

$$X_i = X_{01} \cdot (l_0 + l_i) [\Omega] \ i = 1,2,...,n \tag{6}$$

The total active voltage drop for n simple lines, it is calculate with:

$$\Delta U_{l\max} = \frac{\Delta U_l[\%]}{100} \cdot U_{ln} \ [V] \tag{7}$$

For motors $\Delta U_l[\%] = 5$.
Now it computes the active voltage drops for n simple lines:

$$\Delta U_{lai} = \Delta U_{l\max} - \Delta U_{lri} \ [V] \ i = 1...n \tag{8}$$

Using the admissible maximum voltage criterion, the simple three-phase cross-sections are calculated with:

$$s_i = \frac{\sqrt{3} \cdot \rho \cdot I_{ci} \cdot \cos\varphi_{ci}}{\Delta U_{lai}} \cdot (l_0 + l_i) \tag{9}$$

Afterwards, it is choose for lines normalized cross-sections s_{ni}, by an immediate superior value ($s_{ni} \geq s_i$).

The choose cross-sections are further performed to warm check of the conductors. For this, the admissible maximum current I_{max} [A] from the tables [3,5], depending on real temperature θ_{02}[°C] and on duty cycle of the motor:

$$I'_{max} = c_\theta \cdot c_l \cdot I_{max} \tag{10}$$

The temperature correction coefficient c_θ of admissible maximum current is calculated with [4]:

$$c_\theta = \sqrt{\frac{\theta_{max} - \theta_{02}}{\theta_{max} - \theta_{01}}} \tag{11}$$

Here, θ_{max} [°C] is the admissible maximum temperature of conductor insulation, and θ_{01}[°C] is temperature for the maximum value of current I_{max}.

The correction coefficient c_l of maximum current depending on duty cycle and it is calculated with [3]:

$$c_l = \frac{0.875}{\sqrt{DA}}; \ c_l = 0.875 \cdot \sqrt{\frac{t_c}{t_f}} \tag{12}$$

The relative duty cycle DA it is compute with:

$$DA = \frac{t_f}{t_f + t_p}; \ DA = \frac{t_f}{t_c} \tag{13}$$

where t_f[s] is a work time of motor, t_p[s] is pause time of motor and t_c[s] is cycle time:

$$t_c = t_f + t_p \tag{14}$$

The motors feed with electric energy through branch line work in intermittent periodical duty if the maximum time cycle is by 10 minutes and the work time of motor is by 4 minutes. For copper conductors with cross-sections under 10 [mm²] and for aluminium conductors with cross-section under 16 [mm²], c_l=1 both in intermittent periodical duty and in permanent duty.

The line cross-sections will not warm, if are valid the relations:

$$I_{ci} \le I_{max\,i},\quad i = 1,2,\dots,n \tag{15}$$

After will find the normalized cross-sections s_{ni}, i = 1,2,…,n of simple three-phase line, it can be calculating the main cross-section line:

$$s_o = s_{n1}+s_{n2}+\dots+s_{nn};\quad s_0 = \sum_{i=1}^{n} s_{ni} \tag{16}$$

After that, are calculate the voltage drop when the motors are start for the line from fig.1. It is consider that one motors start and the other work at rated values. These voltage drops are calculated with:

$$\Delta U_{p1} = \sqrt{3}\Big[R_{010}\cdot l_0\cdot\Big(k_{p1}\cdot I_{c1}\cdot\cos\varphi_{c1}+\sum_{i=2}^{n} I_{ci}\cdot\cos\varphi_{ci}\Big)+ \\ +R_{011}\cdot l_1\cdot k_{p1}\cdot I_{c1}\cdot\cos\varphi_{c1}+X_{010}\cdot l_0\cdot\Big(k_{p1}\cdot I_{c1}\cdot\sin\varphi_{c1}+ \\ +\sum_{i=2}^{n} I_{ci}\cdot\sin\varphi_{ci}\Big)+X_{011}\cdot l_1\cdot k_{p1}\cdot I_{c1}\cdot\sin\varphi_{c1}\Big] \tag{17}$$

$$\Delta U_{p2} = \sqrt{3}\Big[R_{010}\cdot l_0\cdot\Big(I_{c1}\cdot\cos\varphi_{c1}+k_{p2}\cdot I_{c2}\cdot\cos\varphi_{c}+ \\ +\sum_{i=3}^{n} I_{ci}\cdot\cos\varphi_{ci}\Big)+R_{012}\cdot l_2\cdot k_{p2}\cdot I_{c2}\cdot\cos\varphi_{c2}+ \\ +X_{010}\cdot l_0\cdot\Big(I_{c1}\cdot\sin\varphi_{c1}+k_{p2}\cdot I_{c2}\cdot\sin\varphi_{c2}+\sum_{i=3}^{n} I_{ci}\cdot\sin\varphi_{ci}\Big)+ \\ +X_{012}\cdot l_2\cdot k_{p2}\cdot I_{c2}\cdot\sin\varphi_{c2}\Big] \tag{18}$$

…

$$\Delta U_{pn} = \sqrt{3}\Big[R_{010}\cdot l_0\cdot\Big(k_{pn}\cdot I_{cn}\cdot\cos\varphi_{cn}+\sum_{i=1}^{n-1} I_{ci}\cdot\cos\varphi_{ci}\Big)+ \\ +R_{01n}\cdot l_n\cdot k_{pn}\cdot I_{cn}\cdot\cos\varphi_{cn}+X_{010}\cdot l_0\cdot\Big(k_{pn}\cdot I_{cn}\cdot\sin\varphi_{cn}+ \\ +\sum_{i=1}^{n-1} I_{ci}\cdot\sin\varphi_{ci}\Big)+X_{01n}\cdot l_n\cdot k_{pn}\cdot I_{cn}\cdot\sin\varphi_{cn}\Big] \tag{19}$$

The cross-sections have been chosen, when are true the relations:

$$\Delta U_{pi} \le \Delta U_{p\,max} = \frac{12}{100} U_{ln}\quad (i=1,2,\dots,n) \tag{20}$$

In relations (17), (18), (19), R_{010}, R_{011}, …, R_{01n}, X_{010}, X_{011}, …, X_{01n} are the specific resistances and reactances for main line and for the lines with cross-sections s_{no}, s_{n1}, s_{n2}, …, s_{nn}. Can be determining with accuracy the voltage drops on branch simple line when the motor works at rated values:

$$\Delta U_{l1} = \sqrt{3}\cdot\Big(R_{010}\cdot l_0\cdot\sum_{i=1}^{n} I_{ci}\cdot\cos\varphi_{ci}+R_{011}\cdot l_1\cdot I_{c1}\cdot\cos\varphi_{c1}+ + X_{010}\cdot l_0\cdot\sum_{i=1}^{n} I_{ci}\cdot\sin\varphi_{ci}+X_{011}\cdot l_1\cdot I_{c1}\cdot\sin\varphi_{c1}\Big) \tag{21}$$

$$\Delta U_{l2} = \sqrt{3}\cdot\Big(R_{010}\cdot l_0\cdot\sum_{i=1}^{n} I_{ci}\cdot\cos\varphi_{ci}+R_{012}\cdot l_2\cdot I_{c2}\cdot\cos\varphi_{c2}+ \\ +X_{010}\cdot l_0\cdot\sum_{i=1}^{n} I_{ci}\cdot\sin\varphi_{ci}+X_{012}\cdot l_2\cdot I_{c2}\cdot\sin\varphi_{c2}\Big) \tag{22}$$

…

$$\Delta U_{ln} = \sqrt{3}\cdot\Big(R_{010}\cdot l_0\cdot\sum_{i=1}^{n} I_{ci}\cdot\cos\varphi_{ci}+R_{01n}\cdot l_n\cdot I_{cn}\cdot\cos\varphi_{cn}+ + X_{010}\cdot l_0\cdot\sum_{i=1}^{n} I_{ci}\cdot\sin\varphi_{ci}+X_{01n}\cdot l_n\cdot I_{cn}\cdot\sin\varphi_{cn}\Big) \tag{23}$$

In these relations:

$$\sin\varphi_{ci} = \sqrt{1-\cos^2\varphi_{ci}},\quad i = 1,2,\dots,n \tag{24}$$

These voltage drops are calculate on the following ways $l_o - l_1$ (21), $l_o - l_2$ (22) and $l_o - l_n$ (23). The calculate voltage drops with relations (21), (22), (23) must be under admissible maximum voltage from (7).

3. DISCUSSION. EXAMPLE OF SIZING THE BRANCH THREE-PHASE POWER LINES WITH SUPERPOSITION METHOD

It is supposed the size of the branch three-phase power line (presented in fig.1) made from appearance cable with plastic insulator that has copper conductors (ρ=0.017 $\Omega \cdot mm^2/m$), through feed three motors (three-phase inductions motors M_1, M_2, and M_3), that work in intermittent periodical duty (t_{f1} = 200s, t_{c1} = 420s, t_{f2} = 180s, t_{c2} = 460s, t_{f3} = 230s, t_{c3} = 560s), which characteristics are present in table 1. In the same table gives the relative duty cycle for these three motors determine with relation (13).

Table 1: The motors characteristics feed through main line and relative duty cycle

Motor symbols	P_{ci} [kW]	η_{ci} [%]	$\cos\varphi_{ci}$	U_{ln} [V]	$k_{pi}=\frac{I_{pi}}{I_{ci}}$	DA_i (13)
M_1	37	90	0.855	380	7	0.476
M_2	15	88	0.845	380	7	0.391
M_3	18.5	89	0.845	380	7	0.411

The medium temperature that are place the line is θ_{02} = =+16 °C (θ_{max} = 70 °C). The line parts have the following lengths l_o = 30 m, l_1 = 60 m, l_2 = 50 m, and l_3 = 70 m. The admissible maximum currents for different cross-sections on warm criterion are presented in table 2.

Table 2: The admissible maximum currents for different cross-sections, for copper appearance cable, with plastic isolation at θ_{01} = +25 °C temperature

s[mm²]	2.5	4	6	10	16	25	35	50	70	95	120	150
I_{max}[A]	25	34	44	60	80	105	130	160	200	245	285	325

For the line sizing are use data from table 3. The compute results of main line through superposition method are present in tables 4.a, b, c and d.

Table 3: The specify values resistors and reactances for copper armoured cable, up to 1kV

s[mm²]	2.5	4	6	10	16	25	35
R_{01i}[Ω/km]	7.54	4.71	3.14	1.88	1.17	0.75	0.53
X_{01i}[Ω/km]	0.098	0.095	0.090	0.073	0.068	0.066	0.064

s[mm²]	50	70	95	120	150	185	240
R_{01i}[Ω/km]	0.37	0.26	0.198	0.157	0.125	0.101	0.078
X_{01i}[Ω/km]	0.063	0.06	0.060	0.059	0.058	0.056	0.054

Table 4.a

Com-pute values	I_{ci} [A] (1)	l_o+l_i [m] (2)	ΔU_{lri} [V] (3)	X_L [Ω] (4)	L_{01} [H/m] (5)	ΔU_{lmax} [V] (7)	ΔU_{lai} [V] (8)	s_i [mm²] (9)	s_{ni} [mm²]	s_o [mm²]
1	73.05	90	0.48	0.0074	$2.61 \cdot 10^{-7}$	19	18.52	8.94	10	20
2	30.65	80	0.19	0.0066			18.81	3.24	4	
3	37.37	100	0.28	0.0082			18.72	4.97	6	

Table 4.b

	c_θ [-] (11)	c_l [-] (12)	I_{maxi} [A] (Table 2)	I'_{maxi} [A] (10)	s_{ni} chose [mm²]
0	1.095	1.325	105	152.34	25
1		1.268	60	83.34	10
2		1.400	34	37.25	4
3		1.365	44	48.2	6

Tabel 4.c

Computer values	ΔU_{pmax} [V] (20)	ΔU_{pi} [V] (17),(18), (19)	$\sin\varphi_{ci}$ [-] (24)	R_{01i} [Ω/km] table 3	X_{01i} [Ω/km] table 3	R_{010} [Ω/km] table 3	X_{010} [Ω/km] table 3
1	45.6	110.48	0.519	1.88	0.073	0.75	0.066
2		96.44	0.535	4.71	0.095		
3		98.41	0.535	3.14	0.09		

Table 4.d

Computer values	s_{n1} [mm²]	s_{n2} [mm²]	s_{n3} [mm²]	s_{no} [mm²]	R_{01i} [Ω/km] table 3	X_{01i} [Ω/km] table 3	ΔU_{pi} [V] (17)...(19)	ΔU_l [V] (21)...(23)
	Increase until the inequality (20) is true							
0	35	10	16	50	0.37	0.063	-	-
1					0.53	0.064	36.4	6.24
2					1.88	0.073	40.2	6.87
3					1.17	0.068	39.1	7.19

To compute the line voltage drop when the motors starting, the equations system (17), (18), (19), was simplify for the branch line that feeds with electric energy three motors.

From table 4.a for cross-sections: s_{no} = 25 mm², s_{n1} = 10 mm², s_{n2} = 4 mm², and s_{n3} = 6 mm², the voltage drops when motors M_2 and M_3 are starting, overtakes the admissible maximum values. These cross-sections increase step by step until the inequality (20) is true.

The final values of branch line cross-sections are present in table 4.d. For these cross-sections, with relations (21),(22),(23) (that was simplify for branch power line with three lines), was compute the total voltage drops when the motors work at rated values. These are smaller than admissible maximum voltage drop ΔU_{lmax} = 19 V.

4. CONCLUSIONS

The superposition method use to sizing the branch three-phase power lines is to decomposition the lines in a number of simple lines that are equal with the consumer number that are feed with electric energy. This method it is simple and easy to apply and it is useful to sizing lines that are supply motors that work in intermittent periodical duty. The superposition method is an economical sizing for electric power lines. This method may be applied, also, to sizing complex three-phase power lines with different configuration: the branches, the mains, the complexes, the lines that are supply from two or many feed point, and so on.

REFERENCES

[1.] D. Comşa and other, Proiectarea instalaţiilor electrice industriale, Editura Didactică şi Pedagogică, Bucureşti, 1976.
[2.] N. Gheorghin, Aparate şi reţele electrice, Editura Didactică şi Pedagogică, Bucureşti, 1971.
[3.] T. Ionescu, O. Pop, Ingineria sistemelor de distribuţie a energiei electrice, Editura Tehnică, Bucureşti, 1998.
[4.] M. Păsculescu and other, Instalaţii electrice miniere, Editura Tehnică, Bucureşti, 1988.
[5.] I. Popa, G.N.Popa, Instalaţii electrice, vol.I, Editura Mirton, Timişoara, 2000.
[6.] G.N.Popa, I. Popa, Instalaţii electrice, Editura Mirton, Timişoara, 2005.

INTERNATIONAL SYMPOSIUM on ADVANCED ENGINEERING & APPLIED MANAGEMENT
– 40th ANNIVERSARY in HIGHER EDUCATION (1970-2010),

INTERNATIONAL SYMPOSIUM on ADVANCED ENGINEERING & APPLIED MANAGEMENT
– 40th ANNIVERSARY in HIGHER EDUCATION (1970-2010),

INTERNATIONAL SYMPOSIUM on
ADVANCED ENGINEERING & APPLIED MANAGEMENT
– 40th ANNIVERSARY in HIGHER EDUCATION (1970-2010)
4 – 5 November, 2010, Hunedoara, ROMANIA

[1.]Radovan HOLUBEK, [2.]Matuš VLÁŠEK

PLC PROGRAMMING IN LABORATORY OF PRODUCTION SYSTEM PROGRAM CONTROL

[1-2] SLOVAK UNIVERSITY OF TECHNOLOGY, FACULTY OF MATERIALS SCIENCE AND TECHNOLOGY,
INSTITUTE OF PRODUCTION SYSTEMS AND APPLIED MECHANICS, TRNAVA, SLOVAKIA

ABSTRACT:
Currently, the emphasis on improving the effectiveness of automation in industry. One of the base parts for automation is control devices such as different PLC systems and programming environments. This programming environment for PLC system use in laboratory of production system program control. Base for the control of real output per axis manipulator, a schemes is possible in the virtual software followed by simulated and tuning errors. Thus the scheme is then verified recorded in PLC control and prepared to manage the various movements of the manipulator.
KEYWORDS:
PLC systems, manipulator, automation, sensor, virtual laboratory

1. INTRODUCTION

Within the solution of KEGA grant task, which is being solved at the Institute of Production systems and Applied Mechanics STU Bratislava in years 2009-2011, there is an opportunity to develop the abilities and skills that employers usually expect from the graduates of technical universities. The main goal of this project is to create a virtual laboratory of manufacturing devices programming control and build a suitable system of teaching that will support the creation and consolidation of professional key competences. The result presents both virtual programming PLC with a feedback simulation and checking the graduates´ skills that would support their preparing for practice and whole-life education. The demands on graduates´ skills and their job market preparedness are deeply analyzed.

2. PRINCIPLE OF PROGRAMMABLE LOGIC CONTROLLER OPERATION

Operation of PLC – the program stored in memory periodically evaluates input signals and set the output.

Using PLC – PLC is used in machine tools, material handling, automated assembly, and in many other industrial applications.

2.1 Preparation of PLC and its structure, types of input and output units

The basic structure of the PLC:

2.1.1 Compact (Fixed Hardware Style)

This copy is cheap and is used more for simpler applications. Configuration variability is low with it. Usually have a limited number of digital inputs, digital outputs or analog input or output. Some compact PLCs also have the option to extend the variability of configurations using additional modules.

2.1.2 Modular (Modular Hardware Style)

It is suitable for demanding applications. This allows much more variable configuration. The basis of the frame (rack, chassis), which in its left is the resource. The rear frame is driven internal bus on which the connector module. Frame length varies according to the number of slots for insertion module (unit). As the first module from the right source plugins CPU (processor) and then followed by further input / output modules (I / O modules).

2.2 Function parts PLC:

CPU - central processing unit

- control all operations in the PLC,
- performs programmed sequence of instructions stored in memory,
- CPU can be implemented as a separate module that can add input and output circuits (ie, other modules).

Memory - into PLC memory is stored

- technology program management process,
- titles and operating system PLC.

Input and output circuits

- connecting PLC to sensors and actuators, where the galvanic separation of signals,
- A / C and C / A conversion of continuous variables (current, voltage, resistance),
- each input and output PLC has a (unique) address through which they can access it (write to it or read it).

Programming the device

- configuration and PLC programming [1].

Programmable logic controller PLC is a digital computer consisting of a programmable memory for internal instructions saving. It performs different specific functions such as logical, sequential, timing and start-stop functions by means of digital or analogue input and output modules. More simplified, PLC can be characterized as an industrial digital computer designed especially for controlling in the field of industry [2].

Type of PLC depends on the complexity of controlled technology. Choice of PLC type depends on the application in service. Small PLC is sufficient for plants with simple technological cycle. For automated production and assembly halls it is suitable to use big PLC mainly because of the possibility to extend it by input or output modules and communication interface integration.

Nano PLC and Micro PLC are used as substitutions for switching relay. They control devices like parking automata, manipulators, and machine tools. Their size is very similar to a relay. Small PLC, sometimes called SLC (small logic control), is suitable for plants where PLC performs independently. PLC usually contains an integrated pushbuttons package and an internal LCD display.

2.3 Fundamental structure of PLC systems

Fundamental structure of PLC systems is identical for any PLC (fig.1). Differences are mainly in other options of its expansion. PLC structure is composed of the following parts:

- power supply,
- control processor,
- inputs and outputs (binary, analogue),
- program memory, memory for variables,
- connector interface for program loading,
- other peripherals (floating battery, memory card, RTC, communication conductor bar).

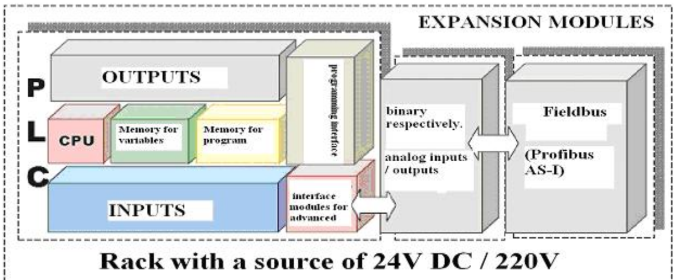

Fig. 1 Structural diagram of PLC

PLC Programming Alpha used in the laboratory of manufacturing devices programming control, is performed by assembling functional blocks of logic with the help of members [3].

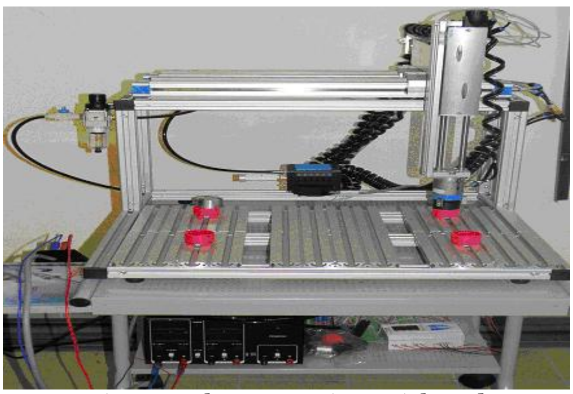

Fig. 2 Real construction „Pick and Place"manipulator controlled by PLC

3. PROGRAMMING METHOD

Controlling and programming of these devices is a very important field of study. For particular manipulator (Fig.2), we used PLC Alpha Controller for cycle automation.

3.1 The workplace of one purpose manipulator "Pick & Place"

The one purpose manipulator consists from pneumatics actuators and components and the main frame is realized out of aluminum profiles [4].

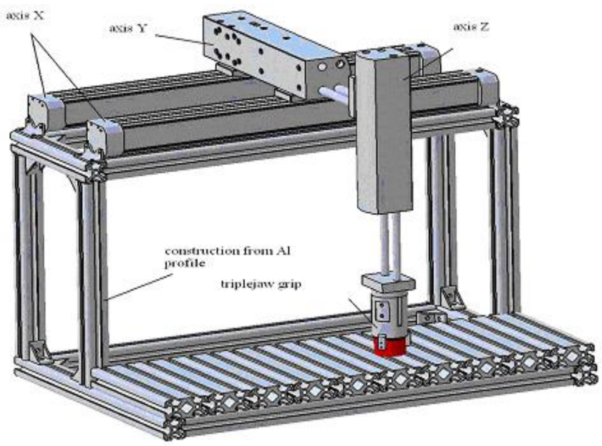

Fig. 3 Three-axis pneumatic „Pick and Place“ workstation design

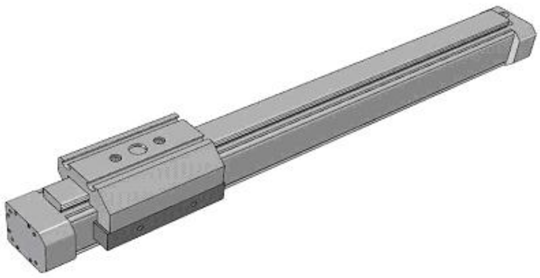

Fig. 4 The X - axis drive (direct pneumatic driver DGPL-25-350-PPV-A-GF-B)

3.1.1 The X - axis drive

The X-axis drive is marked as DGPL-25-350-PPV-A-GF-B. It is linear pneumatic actuator with plain bearing. .

- ❖ DGPL – linear actuator,
- ❖ 25 – piston diameter [mm],
- ❖ 350 – stroke [mm],
- ❖ PPV – adjustable pneumatic absorbing of end positions,
- ❖ A – magnetic proximity switch possibility,
- ❖ GF – bead fixation,
- ❖ B – actuator generation B

Supplementary data:

- ❖ Synchronization principle by shape connection,
- ❖ Position detection,
- ❖ Work pressure (2 – 8 bar),
- ❖ Double acting motion,
- ❖ Work medium – filtered, oiled or no-oiled compressed air.

3.1.2 The Y - axis drive

The Y-axis drive is marked as HMPL-20-200-AI-VP-2A3. This actuator is one of type category of pneumatic actuated linear axes for assembly and manipulation equipment and devices. It is possible directly to combine between actuators and loads into axis systems and thereafter to complete into manipulators units “Pick & Place”. The category HMPL is included into modular technique for assembly and manipulation HMT. It is supplemented this category by it in its construction size and utility mass to down direction. The horizontal axis with vertical axis HMPL creates system “Pick & Place”. It is optimized to stiffness, dynamics and function.

The main characteristics of this actuator are:

- ❖ HMPL – pneumatic linear axis,
- ❖ 20 – piston diameter [mm],
- ❖ 200 – stroke [mm],
- ❖ AI – absorbing of position,
- ❖ VP – armature plate desk,
- ❖ 2A3 –proximity switch position.

Supplementary data:

- ❖ Assembly position,
- ❖ Ball bearing,
- ❖ Work pressure – (4 - 8 bar),
- ❖ Double acting motion.

Fig. 5: The Y- axis driver (linear pneumatic driver HMPL-20-200-AI-VP-2A3)

3.1.3 The Z - axis drive

The z-axis drive is marked as HMPL-16-160-AI-VP-2A3.

- ❖ HMPL – pneumatic lienar axis,
- ❖ 16 - piston diameter [mm],
- ❖ 160 – stroke [mm]
- ❖ AI – absorbing of position,

The actuator axis Z is one of type category as actuator axis Y. the different is only in piston diameter and stroke.

This PLC (Fig. 6) is able to process binary or analogue electric signals.

Programming can be realized either with using the buttons on the front panel or by PC (software Alpha-PCS-WIN-E). By reason of user accessibility, we use the programming language FBD (functional block diagram) for programming. Then we load the following into PLC Alpha by the real output implementation from the created program in given software. Pick and Place manipulator performs single moves on the ground of sensors which are installed on it [5].

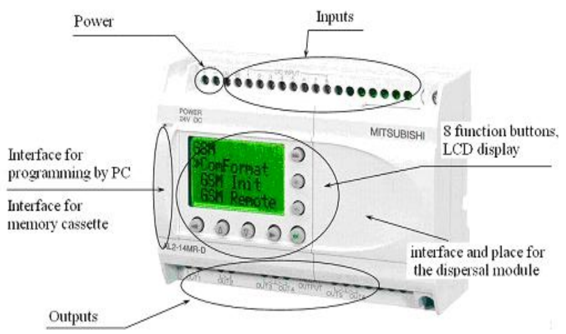

Fig. 6 Programming machine Mishubishi Alpha

It is possible to program in two ways: direct programming or flexible programming. When we use direct programming, it is possible to programmed simplified commands with the help of pushbuttons. All performed changes will be shown on the display. Direct programming is mainly used for controlling and maintenance, eventually a small program change. Flexible programming is performed by interconnection of the functional blocks so they complete the automation task. It is possible to use up-to 200 functional blocks in one program and the individual functions can repeat arbitrarily often.

Functional blocks are available for:

- ❖ simple and complex logical connections,
- ❖ attributes (parameters) setting,
- ❖ timers,
- ❖ visual display of notifications,
- ❖ analogue processing parameter settings (offset / gain).

Functional blocks – a program is created by joining of main components. They enable us to process the information gained from inputs, or other source, and on their ground (according to dependency of a given stored program) switch the corresponding outputs. It is possible to use 22 different functional blocks when compiling a program. These blocks are pre-programmed for performing of specific tasks and they can have different parameters (Fig. 7). Parameters can be changed where necessary [6].

FBD layout – place for positioning programming features (inputs, outputs, functional blocks, memory cells, or keys) during the programming process.

Binary value – variable type (input, output, and memory cell) can have only two states - 0 (Off) or 1 (On).

Analogue quantity – variable type has numeric value.

Program variables of different types can be edited or read by an open protocol. PC communication, utility panels communication or other PA is possible with the help of communication cable RS-232C. Created programs can be password protected. This type of security answers the purpose of programmer's copyright protection because so protected program cannot be copied any more.

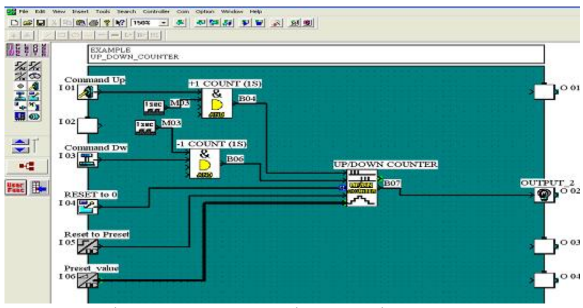

Fig. 7 Programming environment with functional blocks

4. CONCLUSION

At present it is very important to know the flexibility to enter into the controlling process at every moment of the automatic cycle manipulation, or technology operations. Therefore, we in our laboratory program of controlling manufacturing systems to teach students to interact. Whether it is the creation of a virtual program by PLC, but also a change in real time the parameters of input and output units.

Acknowledgement

This paper was created thanks to the national grant KEGA 3/7131/09 – Laboratory of production system program control

REFERENCES

[1] ŽIDEK, K., MAXIM, V., Kurz programovateľných automatov - PLC. J. *INTERNETOVÝ ČASOPIS*, 2009, Vol. 1, č. 1, Bratislava: , 2009, www.oktagon.sk

[2] VARGA G., DUDAS, I.: Intelligent Manufacturing System for Production of Helicoid Surfaces, Gep, Vol.: LI. No.: 09, 2000, pp.: 44-46

[3] DRSTVENŠEK, I., PAHOLE, I., KOVAČIČ, M., BALIČ, J. Intelligent interface in a flexible production environment. J. mater. process. technol.. [Print ed.], 15. maj 2005, vol. 164-165,pp.1309-1316. http://dx.doi.org/10.1016/j.jmatprotec.2005.02.074

[4] HORVÁTH, ŠTEFAN - RUŽAROVSKÝ, ROMAN - VELÍŠEK, KAROL: Flexible assembly system generation by CAD and PPS systems. In: Machine Design. - ISSN 1821-1259. - 2010 (2010), s. 269-272

[5] DANIŠOVÁ, N., VELÍŠEK, K., KOŠŤÁL, P.,: Automated tool changing system in the intelligent manufacturing and assembly cell. In: ISCCC 2009: Proceedings of the 2009 International Symposium on Computing, Communication and Control, October 9-11, 2009, Singapore. - Singapore : International Association of Computer Science and Information Technology Press, 2009. - ISBN 978-9-8108-3815-7. - S. 1-8

[6] JAVOROVÁ, A., HRUŠKOVÁ, E., MATÚŠOVÁ, M.: Automated design of assembly system with computer aided system help. In: MMA 2009. Flexible Technologies: Proceedings. 10th international scientific conference. - Novi Sad, 9.-10.10. 2009. – Novi Sad: Faculty of Technical Sciences, 2009. - ISBN 978-86-7892-223-7. - S. 206-209

INTERNATIONAL SYMPOSIUM on ADVANCED ENGINEERING & APPLIED MANAGEMENT
– 40th ANNIVERSARY in HIGHER EDUCATION (1970-2010),

INTERNATIONAL SYMPOSIUM on
ADVANCED ENGINEERING & APPLIED MANAGEMENT
– 40th ANNIVERSARY in HIGHER EDUCATION (1970-2010)
4 – 5 November, 2010, Hunedoara, ROMANIA

[1.]Tihomir LATINOVIC, [2.]Sorin DEACONU, [3.]Milosav DJURDJEVIC, [4.]Mirko DOBRNJAC

THE BASICS OF DESIGNING CONTROLLERS FOR INDUSTRIAL ROBOTS (EG. ROBOTS ABB IRB 2000)

[1,3,4.] FACULTY OF MECHANICAL ENGINEERING, UNIVERSITY IN BANJA LUKA, BOSNIA & HERZEGOVINA
[2.]UNIVERSITY POLITECHNICA TIMISOARA, FACULTY OF ENGINEERING HUNEDOARA, ROMANIA

ABSTRACT:
The paper explains the basic aspects of designing controllers for an industrial robot control. Industrial robots are basically mechanical devices which, to a certain degree, replicate human motions. They are used whenever there is a need to reduce the danger to a human, provide more strength or accuracy than a human, or when continuous operation is required.
Most industrial robots are stationary, but some move throughout the workplace delivering materials and supplies. While we have the technical ability to produce human robots, industrial robots are actually quite simple devices.
Motions that we take for granted—picking up a something from the table, for instance—are considerably more difficult for a robot. Its mains characteristics of operation, degrees of freedom, etc.
They are solved and the calculations developed to obtain the kinematics and dynamics. The accomplished test to each servomotors and the research about its operation.
Basicaly all industrial robot have a similarly control, because have a similarly actions.
KEYWORDS:
industrial robot control, designing controllers, basic aspects

1. INTRODUCTION

Robotics is a new field of modern technology that crosses traditional engineering boundaries. Understanding the robots and their applications requires knowledge of many areas of engineering, informatics, mechanic and mathematics. We need to know the dynamics, kinematics to control of the robot manipulator. Is the basic to the understanding of the robot operation?

An official definition of such a robot comes the Robot Institute of America (RIA): A robot is a reprogrammable, multifunctional manipulator designed to move material, parts, tools, or specialized devices through variable programmed motions for the performance of a variety of tasks.

In the Laboratory of Intelligent Systems in Faculty of Mechanical Engineering in Banja Luka we have a robot IRB 2000. This robot was starting for this study of design controller.

IRB 2000 is a six-axis robot with a large work volume and is primarily intended for arc welding and glueing/sealing.

The IRB 2000 is also suitable for applications such as assembly, water jet cutting, laser cutting, material handling and stud welding. The handling capacity is 10 kg and the very quick movements of the wrist axis are other important features for the intended applications. The S3 control system makes use of established features like soft keys, joystick and the robot language ARLA for simple and fast programming. The IRb 2000 is in its basic form equipped with an absolute measuring servo system. Another important factor is the interface capacity. The S3 controller has the ability to perform a communication in several different ways. These are digital or analogue I/Os and the serial computer link.

2. THE STUDY

A robot is the main component of a flexible production system (FPS). Other components of this system are machine tools, transport machines, control devices, and different auxiliary elements. A flexible production system is an automatically operating production system that can be easily reprogrammed and adapted to manufacture different products.

Robot centered modules of FPS, called robot modules or robot systems are intended for specified technological operations like welding, surface coating, packaging, etc. The robot module includes one or more robots (with manipulators and control devices), pallets for details or products, auxiliary positioning, transport devices, etc.

Therefore, robot control means control of a complete robot module and a certain part of the production process. The control system has the whole electronic of the system and allows the external communications with peripheral equipment.

Fig. 1 shows main hardware and software components of the IRB2000 robot from ABB.

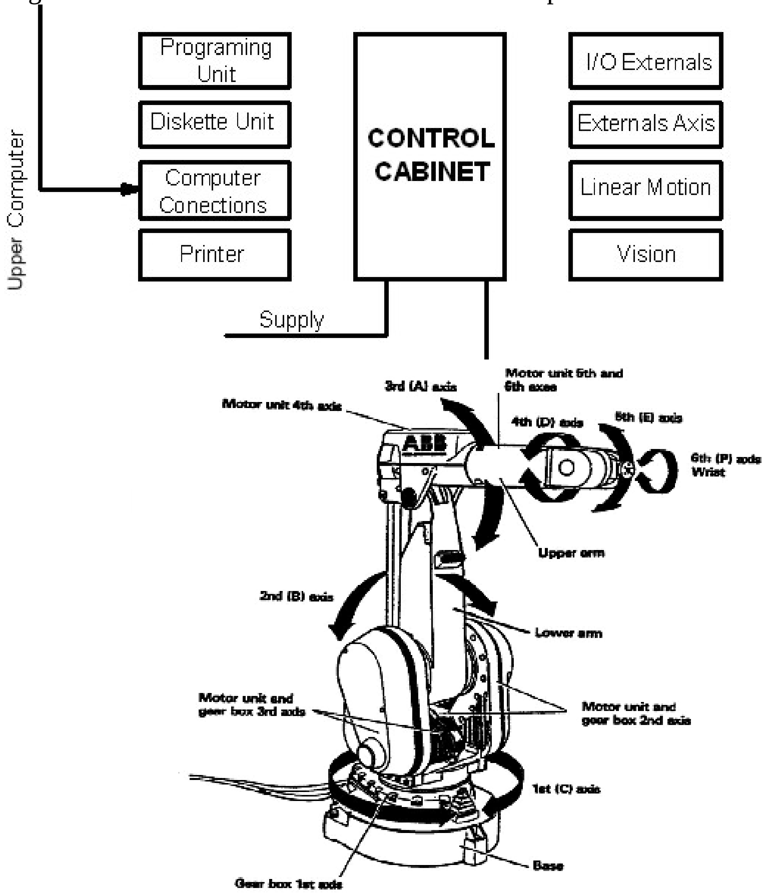

Fig. 1 main ABB IRB 2000 hardware and software components

The mechanical robot is provided with servomotors controlled, in each axes, the servo system have:

- ❖ Speedometer for the speed control.
- ❖ Resolver for the position control.
- ❖ Resolver for the absolute measurement system

The robot is equipped with brakes in each axes, is automatically brake in the emergency stops, power supply fails, or when the motors are disconnected of power supply.

The robot is equipped with brakes in each axes, is automatically brake in the emergency stops, power supply fails, or when the motors are disconnected of power supply. This brakes setting in stand by mode or totally disconnected. While the robot is running and still static the brakes activate automatically after three seconds (automatic operation) or after five seconds. The brakes can turn off manually one by one through of switches in the side of the robot.

3. ANALISES, DISCUSIONS, APPROACHES and INTERPRETĂTIONS

Industrial robots are all-purpose mechanical arms with a number of axes. Regarding movement cycle, route and angle its movements are programmable without mechanical intervention and where required also sensor guided. The mechanical arms are equipped with grippers, other tools and they achieve handling tasks and assembly works.

The path between the positions of robot can be executed in three different coordinate systems: rectangular coordinates, robot coordinates and modified rectangular coordinates.

Each one of the coordinate systems will produce a different path and are used according to the needs of speed, precision and direction. All can be activated through instructions in a robot program.

All the positions of the robot are expressed through the coordinates system that which describe the positions of the robot in the space. This system is setting to the base of the robot with plane X - Y in floor and the axis Z noting upward and concentric to the first rotation shaft.

Space coordinates

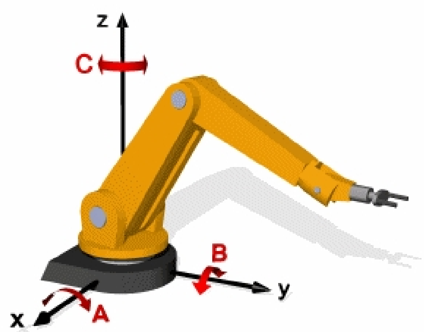

Joint coordinates

The point of origin of the space coordinate system usually is located at the first axis of universal robots. In linear robots the point of origin is located at the intersection point of the three linear axes.

The angle and length description of the particular robot axes describe the orientation of the TCP explicitly. A polar insertion of the coordinates is best.

Gripper coordinates

Gripper coordinates describe the orientation and position of the effector in space.

Workpiece coordinates

The zero point of the coordinate systems is located at the Tool-Center-Point (TCP) of the effector.

If a workpiece has to be processed in different positions, one can site a workpiece coordinate system into one corner of the workpiece.

IRB 2000 manipulates charges in a wide work area, with great rapidity and precision. This robot is particularly adapted for arc welding, application of adhesives and manipulation of materials, because its speed, wide work area and the inherent flexibility of the design of their 6 shafts. The admissible maximum load is of 10 Kg and depends on the distance to the center on the wrist.

The set of points in the space that they can be reached by the extreme of the wrist of the robot constitute its workspace. Remain limited by the maximum angle or linear displacement that permits the joints and the length of the arms.

The movements and degrees of freedom of the robot IRB 2000 are described in table below:

Table 1: Scopes of the robot's axis IRB 2000

Motion	Workspace	Max. Speed
Axis 1: Rotation	+180° -180°	115°/sec
Axis 2: Arm	+100° -100°	115°/sec
Axis 3: Arm	+60° -60°	115°/sec
Axis 4: Wrist	+200° -200°	280°/sec
Axis 5: Lurching	+120° -120°	300°/sec
Axis 6: Draft	+200° -200°	300°/sec

The robot connections for tools and grippers have been designed as a modular system to achieve the best flexibility when accessories are selected. Component can be selected in various ways without limiting the robot working area. Compressed air as well as electrical signals are supplied to the tools via well integrated cablings. Tool exchange can be performed automatically. The exchanger provides a tool fixing plate free from play which allows supply of compressed air and electrical signals fro the tools. Main components in the system are:

- ❖ Connection unit
- ❖ Swivel with cabling carrier
- ❖ Tool exchanger
- ❖ Slip ring
- ❖ Tool attachment
- ❖ Dual grippers

The modular design enables the unit to be offered in many variants.

Computer board contains four microprocessors.

- ❖ Main computer – for overall control
- ❖ Servo computer – for control of servo functions and robot movements
- ❖ Axis computer – for individual control of robot axes
- ❖ I/O computer – for control of communication with operators unit, peripheral equipment, host computer and floppy or cd disk

Safety board contains circuits for the personal safety functions

- ❖ Emergency stop
- ❖ Work hold
- ❖ Safety hold

Digital I/O boards have digital process communication up to 128 inputs and 128 outputs

Analogue I/O board has analogue process communication up to 4 inputs and 4 outputs

Combined I/O board has digital and analogue communication up to 16 digital inputs and 16 outputs + 2 analogue outputs

Control Board for external axes also we have communication via RS 232 interface with computer.

4. CONCLUSIONS

The control panel must to provide full communication with robot system. The emergency stop button and button for resetting the emergency stop function are salient buttons for reasons of safety. The control panel is designed for a demanding industrial environment.

The control panel must includes functions for:

- ❖ Selection of operation modes for the robot system, STANDBY (electronics powered, motor de-energized) and RUN (the entire robot system powered)
- ❖ Synchronization of the robot system
- ❖ Loading of programs from floppy disk or CD
- ❖ Start and stop of programmed operation
- ❖ Emergency stop and re-setting of emergency stop function
- ❖ Locking by key of the programming unit
- ❖ Separate LEDs or LCD for indicating emergency stop and fault status
- ❖ Remote control with joystick

The robot system can be controlled by sensors mounted on the robot or on the object. The robot system can store signal data from sensors , and used then for program. The robot system can receive digital, analog and asyncronics signal with RS232 or other interfaces from the outside computer.

Programming method are point to point method by:

- ❖ Interactive dialogue
- ❖ Manual running with joystick
- ❖ Off-line via terminal
- ❖ Connected with computer

REFERENCES

[1.] Konukseven, E. L. & Abidi, A. (2004). Developmen of man machine interface software for an industrial robot. Proc. of 2004 IEEE Symposium on Virtual Environment, Human-Computer Interfaces and Measurement Systems, (VECIMS), pp. 49-53.

[2.] Pires, Norberto: Industrial Robot Programming, Building Applications for the Factories of the Future. New York; Springer, 2006., 282 str.

[3.] Litzenberger, Gudrun: World Robotics 2007 survey. Frankfurt; IFR Statistcal Department, 2007., URL: http://www.worldrobotics.org/downloads/20071023_Pressinfo_charts.pdf. (05.04.2008.).

[4.] Lundqvist, Rasmus; Söreling, Tobias: New Interface for Rapid Feedback Control on ABB-Robots. Linköping; Linköping University, 2005., URL: http://urn.kb.se/resolve?urn=urn:nbn:se:liu:diva-2762. (20.03.2008.).

[5.] Mihali, Raul C., Sobh, Tarek M., "The Formula One Tire Changing Robot (F1-T.C.R.)", accepted for publication in the Journal of Intelligent and Robotic Systems, April 1999

[6.] Mark W. Spong, M. Vidysagar, "Robot dynamics and control"

[7.] Dr.-ing. Gabriel Hernández López "El origen de la robótica industrial y su desarrollo" in InTech México Automatización pp. 16-22 Octubre-Diciembre 2008

[8.] Reference Manual, ABB Robotics Products, 1993.

[9.] Craig, J.J., "Introduction to Robotics, Mechanics and Control", 2^ Edition, Addison-Wesley, 1989.

[10.] Sciavicco, L., and Siciliano, B., "Modeling and Control of Robot Manipulators"-2"'* Edition, McGraw-Hill, 1996

INTERNATIONAL SYMPOSIUM on
ADVANCED ENGINEERING & APPLIED MANAGEMENT
– 40th ANNIVERSARY in HIGHER EDUCATION (1970-2010)
4 – 5 November, 2010, Hunedoara, ROMANIA

[1.]István MATIJEVICS

REAL AND REMOTE LABORATORIES IN EDUCATION

[1.]INSTITUTE OF INFORMATICS, UNIVERSITY OF SZEGED, HUNGARY

ABSTRACT:
One of the most important areas in the education of students is the laboratory realization of various technical subjects. The institutions are faced the burden of large numbers of students and the high costs of laboratory equipment and staff. In many cases, on top of the afore-mentioned problems comes the lack of space. The most appropriate solution is to develop a laboratory in a given place, this could in an industrial environment, as well, and then in real time establish access via the internet and with user interface and visualization enable two-way data exchange. This way only practice has to be organized, parameter setting, real time running can be achieved any given day or time, and from any location. The already established laboratories are capable of operating as distance laboratories if expanded with internet. At the Institute of Informatics of the University of Szeged the establishment of a distant laboratory has been started. This article shows the development of the server and user interface, and presents its use with a step motor. Since the web server is equipped with standard serial connection, it is suitable for connecting other laboratory instruments, as well, thus for the development of any further practices the internet part does not need to be designed again.
KEYWORDS: Remote control, distant laboratory, education of students

1. INTRODUCTION

It is important that students have experience with microcontrollers. These requirements give for a university with the challenge of establishing in the sufficient laboratory establishment. Other important factors are also the large number of students in the education process, the sometimes limited laboratory space and the financial possibility of the universities.

In an effective way we can use existing Embedded System Laboratory (LAN with PC-s) together with other techniques from the web (Internet) and microcontroller trainer boards. Solutions over the internet open the possibilities for the distance learning. Open source distance learning software gives for the lecturers and students the chance for the distance administration, literature access, rapid and constantly updating the materials, renovation and use of tests. Main standing-point in laboratory-making are the following points: low level investment, using extant pieces of equipment together with the improvement of educational effectiveness. Including trainer boards and the internet in the laboratories does not change the old functions of the Laboratory. This paper presents a project to enhance the embedded system education of students. Some courses provide preliminary knowledge for students who selected microcontroller/microprocessor based classes.

In some obligatory and eligible courses students involve the design and development of microcontroller based technologies, for example in Robotics, Autonomous systems and Mechatronics. These courses include both lecture and laboratory components. In some cases in other courses students do interdisciplinary projects, or diploma works, also using microcontroller applications. Interfacing techniques of embedded systems require some physical and also electrical knowledge from students in microcontroller – external equipment connections. Students must know some electrical lows of electrical engineering: common grounds, voltage/current limitations, noise shielding, timing (delaying) problems. Other courses deal with physical/electrical questions, but the experience is, that a course on microcontrollers needs to remind students of these basics.

Also, we do not forget the mechanical interfacing aspects, this field is always imperfect in educational process of students.

2. DISTANCE EDUCATION

Remote operation and control of the Embedded System Laboratory opens great potentials in distance learning. Educational institutes independent from geographical limitations (distributed laboratories) will integrate material and knowledge potentials into a virtual but very realistic form, a complete unit, in the common educational space. The interactive video link connects two or more laboratories, so the instructor from one laboratory guides all students in the common educational space. Students from far-away workstations can operate through the internet with various remote laboratory equipments 24 hours on 7 days a week. Integrated web-learning environments seem to become more and more accepted. Our College's remote course is basically the traditional one with the big difference that it is remotely accessible over the internet.

3. GENERAL DESCRIPTION OF THE SYSTEM

The general scheme of the application architecture is shown in Figure 1. In this system the software and hardware elements are split into two main blocks: local area (client side) where the user works, and remote area where the whole real system with control elements are located (Laboratory).

The elements of systems are:

- Local area: PC computer with Internet connection and HTTP 4.0 client application,
- Remote area: Internet connection, Web-server, Experimental board, real hardware (stepper motor) and image capture system.

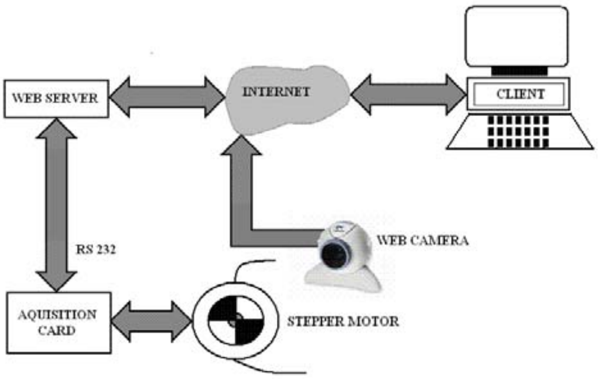

Fig.1. Schematic representation of the Distance Laboratory

The control software communication is RS 232 serial communication. End-user (client) can have access to the process and run step-motor application in real time using TCP/IP. The user can change different parameters: number of steps, direction (left or right) and RUN/STOP status.

4. WEB-BASED STEPPER MOTOR ACQUISI-TION AND CONTROL SYSTEM

The world-wide-web gives method for information transmission. The web enables the control of stepper motor systems from anywhere in the world. The Real system is shown in Figure 2, Lantronix web-server board, self-made experimental printed circuit and stepper motor.

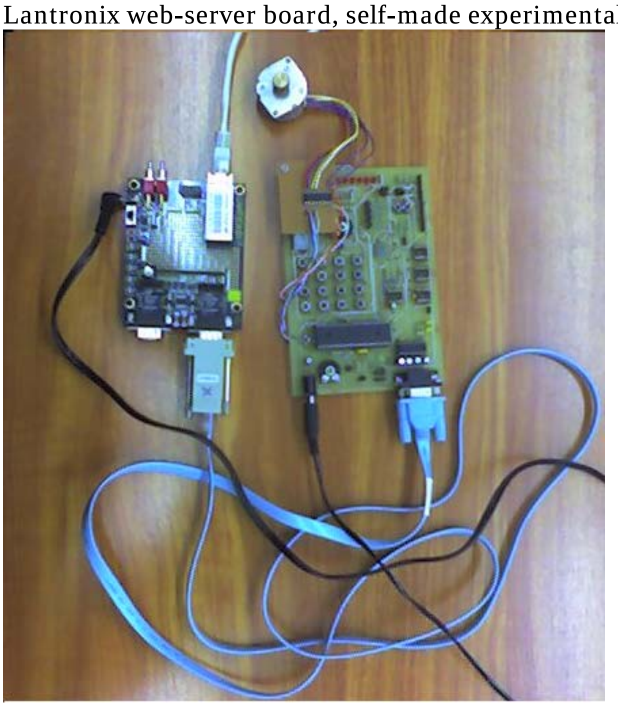
Fig.2. Real system

The first step in the starting the process is to turning-on of the web-camera. After the typing of IP address from web-camera into the browsers address-line the D-Link server sends trough the internet to the client a window with ***login*** and ***password*** requirements (Figure 3).

Fig.3. Login into the camera

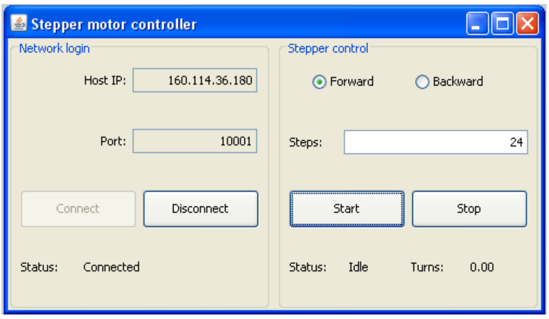

Fig.4. Control panel window on the client side

Fig.5. Real laboratory system in browser using camera picture

The web-server for the camera (D-Link) is integrated onto a circuit board that uses HTML.

The second step is starting the example software, written in Java environment. The Client side network login and stepper control window is shown in Figure 4. Lantronix web-server board needs IP address (160.114.36.180) and Port number (10001) and press the "Connect" button. The connection status is displayed on the bottom part of the window. In the right part of window, in this example there are two buttons for rotational direction (left or right), one stepper motor step is 15 degrees, so full rotation is 24 steps. All our activities are displayed in browser window (Figure 5).

5. COMPARATION OF TWO TECHNICS

In the next table there are some advantages and disadvantages of real and remote laboratories:

Table 1. – comparation of two types of laboratories (rel and remote)

Properties	Real laboratory	Remote laboratory
Contact with system in real work	High-efficiency, full real connection	Indirect relationship, partly real work (programming, parameters)
Delay	There is no immediate response	Internet and internal network-dependent
Financial investment	Great, all exercises should be constructed separately	Smaller, limited to a specific laboratory practices should be established
Other equipment	No	Servers, software and webcams
Student Access	Only under the supervision of a pre-specified times, at night, Sundays and holidays no	7 days in week, 24 hours in day
Supervision	One or more persons	No
Maintenance	Yes	yes
Contribution to the cooperation between the institutions	Limited, it still must be organized	Constant, to be jointly developed curricula should be standardized in the laboratories

6. CONCLUSION

This paper describes the first steps in building combined microcontroller/robotics distance laboratory for several courses in the teaching process of students via the Internet. Teaching microcontrollers for robotics and industry applications is feasible for compulsory courses as well as voluntary courses. This piece of laboratory equipment is also appropriate for other microcontroller applications. Applications of internet tools allow building very operative remote controlled laboratories for the teaching of mobile robots and industry control architecture.

REFERENCES

[1.] Cheever E., Molter L.A., Maxwell BA, (2003) A Remote Wireless Sensing and Control Laboratory". Proceedings of the 2003 American Society for Engineering Education Annual Conference & Exposition Copyright 2003, American Society for Engineering Education

[2.] Puerto R., Jiménez L.M., Fernandéz Ó.R.C., Neco R., (2002) Remote Control Laboratory using MATLAB and SIMULINK: Application to a DC Motor Model, Dpto. Ingenieria de Sistemas Industriales, Universidad Miguel Hernandez, Elche (Alicante), 03202 Spain

[3.] Ogot M., Elliot G., Glumac N., (2002) Hands-On Laboratory Experience via Remote Control: Jet Thrust Laboratory", Proceedings of the 2002 American Society for Engineering Education Annual Conference & Exposition Copyright 2002, American Society for Engineering Education

[4.] Saad M., Saliah-Hassane H., Hassan H., El-Guetiout Z., Cheriet M., (2001) A Synchronous Remote Accessing Control Laboratory on the Internet. International Conference on Engineering Education, August 6-10, 2001 Oslo, Norway, p.p. 8D1-30-33

[5.] Ciubotariu C., Hancock G. (2004) Work in Progress – Virtual Laboratory with a Remote Control Instrumentation Component. 34th ASEE/IEEE Frontiers in Education Conference, October 20-23, Savannah, GA, p.p. T3C 18-19

[6.] Mester Gy. (2006) Distance Learning in Robotics. Proceedings of the Third International Conference on Informatics, Educational Technology and New Media in Education, pp. 249-245, Sombor, Serbia.

[7.] Kucsera P. (2007) Modular Industrial Mobile Robot Systems, Mobile Robot Docking. Proceedings of the XXV. Science in Practice, pp. 1-5, Schweinfurt, Germany.

[8.] B¨ahring H., Keller J., Schiffmann W.. (2004) A combined virtual and remotely accessible microprocessor laboratory. In Proc. 11th Workshop on Computer Architecture Education (WCAE 2004), pages 136–141, June.

[9.] Mester Gy., Pletl Sz.: Rugalmas robotok hibrid irányítása, Gép, IV. Évfolyam, 2004/6, 1-2 oldal, 2004.

[10.] www.lantronix.com

[11.] www.chipcad.com

INTERNATIONAL SYMPOSIUM on
ADVANCED ENGINEERING & APPLIED MANAGEMENT
– 40th ANNIVERSARY in HIGHER EDUCATION (1970-2010)
4 – 5 November, 2010, Hunedoara, ROMANIA

[1.] Gabriel Nicolae POPA, [2.] Sorin Ioan DEACONU, [3.] Iosif POPA, [4.] Corina Maria DINIŞ

NEW TRENDS IN DETECTION OF BACK-CORONA DISCHARGES IN PLATE-TYPE ELECTROSTATIC PRECIPITATORTS

[1.-4] DEPARTMENT OF ELECTROTECHNICAL ENGINEERING AND INDUSTRIAL INFORMATICS, FACULTY OF ENGINEERING HUNEDOARA, POLITECHNICA UNIVERSITY TIMIŞOARA, ROMANIA

ABSTRACT:
Current voltage characteristics are the main tool to control the operation of the ESP fields and to detect the back Corona.
The collecting efficiency of an ESP depends on the large number of parameters. An important parameter is the current emitted from the discharge electrodes and collecting plates. Generally, the higher secondary current the better are collecting performances. Some parameters, like back Corona discharges, high resistivity fly ash reduce the collecting performances of the ESP.
The paper presents some new methods detection of back-Corona discharges in plate-type electrostatic precipitators.
KEYWORDS:
electrostatic precipitators, negative Corona, back Corona discharge

1. INTRODUCTION

An important un-dust device is plate-type electrostatic precipitator (ESP). It is used in power plant, cement, steel and glass industries. In classical design, a d.c. high voltage (up to 100 kV) is used to generate the Corona effect through discharge wires. The electrons bombard the dust particles from the gas, and after a period of time the particles have negative charges, that are moved toward collecting plates, where the particles are collected [1].

In an ESP a negative applied voltage between a discharge wires (connected at negative polarity) and a collecting plates (connected at positive polarity) produce a negative Corona at discharge wires (fig.1).

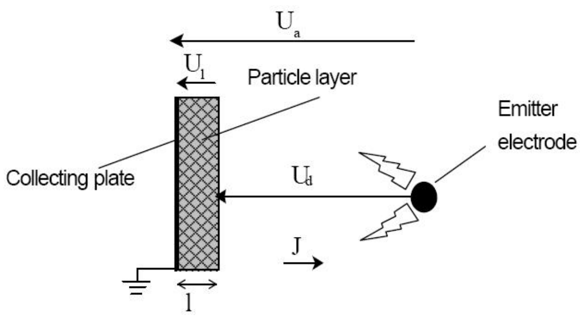

Fig.1. Principle of negative Corona discharge

The collecting high resistance dusts with ESP it is a not well resolved problem. The back-Corona phenomenon is specific for high resistance dust and consists in a series of micro-discharges between the particles from dust layer on the collecting plates. The current-voltage characteristics changes and decrease the efficiency of the ESP.

The back-corona is a non-linear phenomenon [2,3].

A method to determine the occurrence of back-Corona, in a section of ESP, is the measured the current-voltage (i-u) curve. It is important the slope of i-u curve: if the slope is infinite or negative, a back-Corona occurs in a section. The practical experience shows that the mean current depending on minimum value of the precipitator voltage is the better indication of back-Corona [4].

The new voltage control unit include back-Corona detector device. The old back-Corona detector device has the principle of slope of i-u curve. The main disadvantage of this method is that the power must be reduced to detect the back-Corona.

Another method is based on the minimum value of the precipitator voltage, before and after a spark. If the minimum voltage after spark has higher value than the value before the spark, the back-Corona is detected. It is a better method than the first one. If it is not a spark, a blocking period is induced, when the thyristors are not fired. The current is measured before and after this blocking period of time.

2. METHODOLOGY

The back Corona effect occur when the particle of the dust has a very high resistivity, especially when is burning low quality coal in power plants, sinter plants, and cement plants. When the particulates have high resistivity, a voltage drop can develop on the layer on the collecting plates. If this voltage drop is high can occurs breakdown between discharge wires and the surface of the layer. A hole of dust results in the layer, on the collecting plates. The electric field increased near this hole (fig.2).

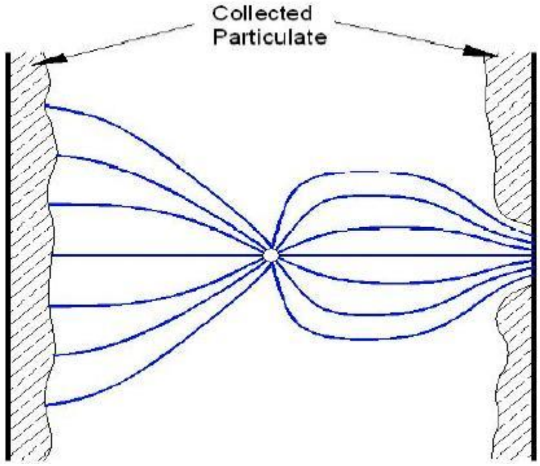

Fig.2. The back Corona between the electrodes

A strong positive field (instead negative field) occurs in the hole, which generates positive ions which neutralize the charged of the particles in the gas. The dust particles may have positive charged and they migrate towards discharge wires. The operation of the electrodes is upside down. This phenomenon (back Corona) is self perpetuating. Many holes occur on the dust layer on the collecting plates, dust particles will be attaching on the discharge wires. A voltage drop will be on the dust layer. Electrically, a high current occurs on the low voltage operation, and specify to back Corona, the rise current-voltage characteristic is different then fall current-voltage characteristic (fig.3) [5,6].

A positive back-Corona discharge occurs when the Corona discharge and layer resistivity are high (10^{10}-10^{11} Ω·cm). The positive ions from the dust layer drift towards the discharge wires and charged the dust particles with positive charges. The discharge wires become the collecting wires, but the total surface it is not large enough and the particles remain un-collected. The collecting efficiency of ESP drastically decreases.

Usually, the value of electric field in a dust layer is 10-20 kV/cm, and the value of electric field of air is 26 kV/cm.

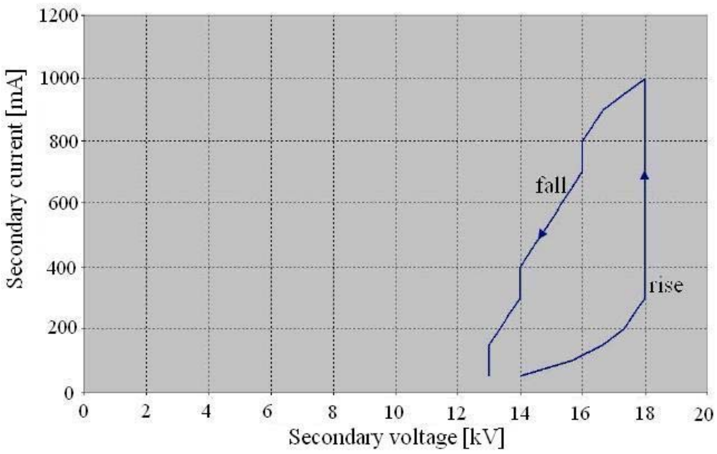

Fig.3. Secondary current as function of secondary voltage in case of back Corona discharges

The back Corona density J_b may be computed with:

$$J_b = k_b \cdot I^{0.4} \cdot (E_l - E_t)^2 \quad (1)$$

Where k_b is the power of the particle layer thickness, E_l is the average electric field in the layer, and E_t is the average electric threshold.
The average electric field in the layer depends on resistivity of the dust ρ, and current density J:

$$E_l = \rho \cdot J \quad (2)$$

In time, various methods have been proposed to detect the back Corona. The ratio between the peak and the mean value of the secondary voltage depends on the back Corona. Other electrical parameters that depend on back Corona are: power supply impedance, supply frequency, precipitator load characteristics.

A method is to inhibit the thyristors pulses for a period of time, and than applied pulses for a period of time t_1. The controller monitors the effect of the decay voltage. In this period of time is analyzing the decay characteristics of the voltage. Back Corona is detected when is available the equation:

$$U_{ref} - U_{offset} > U_{decay} \tag{3}$$

where U_{ref} is a reference voltage in the non back Corona condition, U_{offset} is the offset voltage to determine the sensitivity of the detection and it is a controller parameter, and U_{decay} is a decay voltage that is measure Corona onset voltage. The secondary voltage is recorded after the time t_1.

3. DISCUSSION

At operation of the ESP it is necessary to avoid the negative effects of the back Corona discharges.

In fig.4 are present the computed current-voltage characteristics for different dust resistivities. The dust thickness is 0.1 cm. The characteristics were made in a model ESP into laboratory [3].

For high resistance dust (over $1 \cdot 10^{11}$ $\Omega \cdot$cm) the slope of i-u curve is infinite that indicates the back Corona discharges.

The dust resistivity strongly influences the current-voltage characteristics. The thickness of the dust modify the current-voltage characteristics. In fig.5 the dust resistivity is $6 \cdot 10^{10}$ $\Omega \cdot$cm.

The thicknesses of dust layer increase the current from source. For high value of the voltage, the i-u curve is spreads. The computed and experimental characteristics are likewise.

In fig.6 is present a comparison of collecting efficiency, experimentally by different authors, depending on dust resistivity. Starting at a resistivity about $5 \cdot 10^{10}$ $\Omega \cdot$cm the efficiency drastically decreasing [4,7].

In the following figures are present current-voltage characteristics from the industrial ESP connected at a 600 MW coal burning boiler. The ESP has 5 fields, the first one and the last one are equipped with traditional d.c. power supply, while the other 3 fields have d.c. switching power supplies (with low voltage ripple ±1%) [8].

The static current voltage characteristics (fig.7 and 8) have been measure with slowly speed increasing voltage.

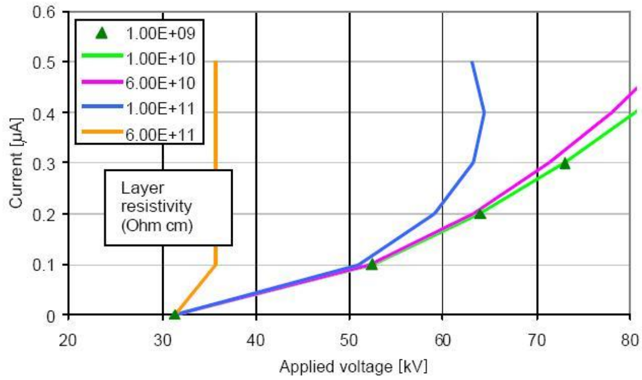

Fig.4. The current-voltage characteristics as function of dust resistivity

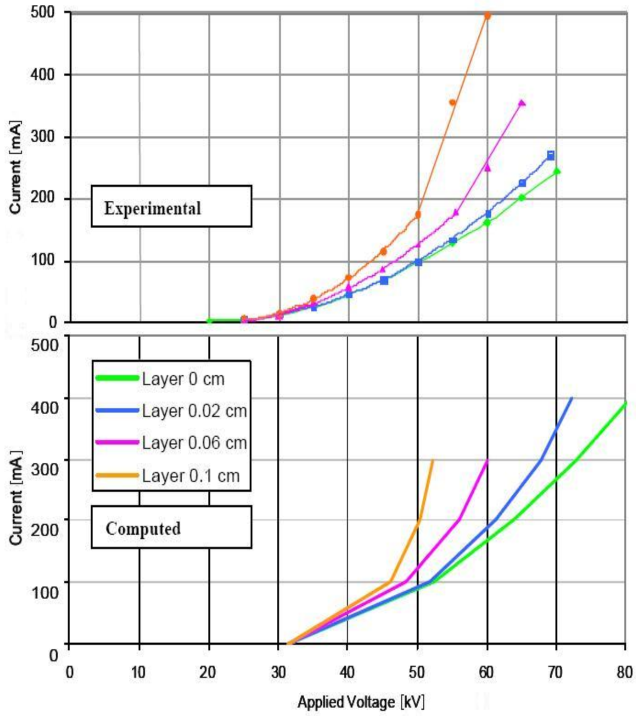

Fig.5. Computed and experimental current-voltage characteristics depending on dust particles thickness

The characteristics from fig.7 was made for a fly ash resistivity $7 \cdot 10^{10}$ $\Omega \cdot$cm. Under approx. 28 kV, the characteristics are the same, and above this value, the current is higher for the characteristics with dust layer.

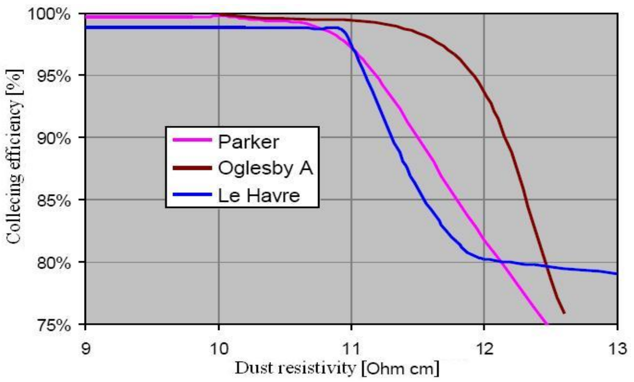

Fig.6. Collecting efficiency depending on dust resistivity

In fig.8 are present three current-voltage characteristics made from different fly ash resistivity: a. high value ($2 \cdot 10^{11}$ $\Omega \cdot$cm), b. medium value ($7 \cdot 10^{10}$ $\Omega \cdot$cm) and c. low value ($3 \cdot 10^{9}$ $\Omega \cdot$cm).

The presence of the back Corona can be made with dynamic (the voltage rise and fall rapidly) current voltage characteristics. The rise and the fall characteristics (the shape of „8”) identify the back Corona discharges.

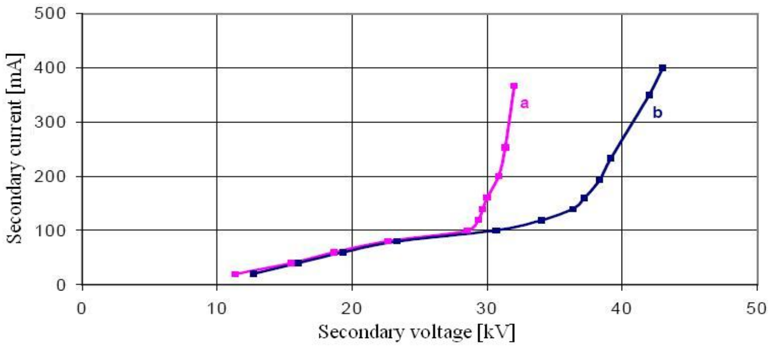

Fig.7. Current voltage characteristics: a. with dust layers; b. without dust layers on the collecting plates

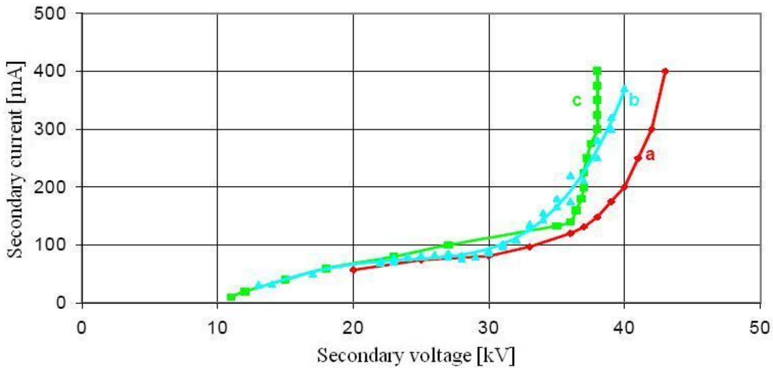

Fig.8. Current voltage characteristics:
a. high, b. medium, c. low resistivity fly ash

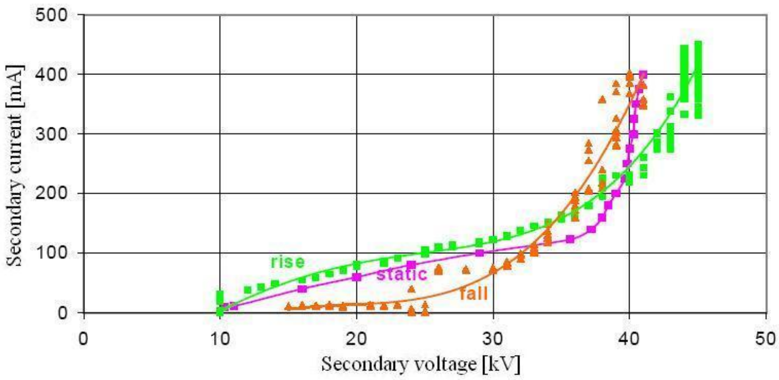

Fig.9. Dynamic current voltage characteristics: at fast rise voltage and at fast fall voltage

In fig.9, is present the dynamic current voltage characteristic for a high resistivity of the dust. For comparison, on the same graph is the static current voltage characteristic.

4. CONCLUSIONS

For an ESP that collects high resistivity dust the presence of back Corona discharges is inevitable problem. The negative resistance area from a current voltage characteristics (if the characteristics depending on minimum voltage) is a result of back Corona discharges. With modern control techniques and with adapted algorithm the back Corona may be detected.

The back-Corona phenomenon is diminish if is burn coal with better characteristics. Another solution to diminish back Corona discharges is to modify the dust resistivity by condition the flue gas (with sulphur and ammonia). Using another control technique, intermittent energisation or pulse energisation will be decreasing the back Corona discharges.

REFERENCES

[1.] K. Huang – *Spark and its Effect on Electrostatic Precipitators*, the Xth International Conference on Electrostatic Precipitation (ICESP), Cairns, Queensland, Australia, july, 2006, no. 5B1, 12 pp.

[2.] W. Wang, R. Li, F. Cao, A. Fang, S. Chen, A. Pei – *The Newest Research Results for Collection of High Specific Resistance Dusts with Electrostatics Precipitators*, the Xth International Conference on Electrostatic Precipitation (ICESP), Cairns, Queensland, Australia, july, 2006, no. 3B2, 11 pp.

[3.] G. Bacchiega, I. Gallimberti, V. Arrondel, N. Caraman, M. Hamlil – *Back Corona Model for Prediction of ESP Efficiency and Voltage-Current Characteristics*, the Xth International Conference on Electrostatic Precipitation (ICESP), Cairns, Queensland, Australia, july, 2006, no. 3B3, 11 pp.

[4.] K.R.Parker and other – *Applied Electrostatic Precipitation*, Chapman and Hall, Londra, U.K., 1997.

[5.] J.M.Leach, S.J. Duddy – *The Development of an Algorithm for the Dynamic Adjusment of the Pulse Repetition Frequency for Minimising Back Corona in Electrostatic Precipitators*, the IXth International Conference on Electrostatic Precipitation (ICESP), Mpumalanga, South Africa, may 17-21, 2004, 9 pp.

[6.] W. Weixue, F. Aimin, C. Feng – *The Newest Technical Results Capable of Remarkably Increasing ESP Efficiency*, the IXth International Conference on Electrostatic Precipitation (ICESP), Mpumalanga, South Africa, may 17-21, 2004, 10 pp.

[7.] S. Oglesby, G. Nichols – *Electrostatic Precipitation*, Dekker, New York, U.S.A., 1978.

[8.] G. Bacchiega, I. Gallimberti – *Static and Dynamic Back-Corona Characteristics*, the IXth International Conference on Electrostatic Precipitation (ICESP), Mpumalanga, South Africa, may 17-21, 2004, 11 pp.

INTERNATIONAL SYMPOSIUM on ADVANCED ENGINEERING & APPLIED MANAGEMENT
– 40th ANNIVERSARY in HIGHER EDUCATION (1970-2010),

INTERNATIONAL SYMPOSIUM on ADVANCED ENGINEERING & APPLIED MANAGEMENT
– 40th ANNIVERSARY in HIGHER EDUCATION (1970-2010),

INTERNATIONAL SYMPOSIUM on
ADVANCED ENGINEERING & APPLIED MANAGEMENT
– 40th ANNIVERSARY in HIGHER EDUCATION (1970-2010)
4 – 5 November, 2010, Hunedoara, ROMANIA

[1.]Constantin OPREA, [2.]Cristian BARZ

CONTRIBUTION TO AUTOMATE REGULATION AFTER THE SPEED OF ACTIONS WITH ASYNCHRONIZED SYNCHRONOUS MOTOR

[1-2] UNIVERSITY OF NORTH, FACULTY OF ENGINEERING BAIA MARE, ROMANIA

ABSTRACT:
The actions with asynchronous synchronous motor must assure every overload, which should not depend on the electric parameters of motor, in conditions in which the power of supply sources and mechanical robust allow this thing. At the same time the system of regulation must also assure the possibility of command the reactive power in such way as to maintain at an economical level impose. In this paper, we consider a synchronous motor with a symmetrical wind in stator, supplied from the network and a three-phase symmetrical wind of excitation, alimentated from a static converter with thyristor. The structural scheme of the motor and automate regulator for reactive moment and power; structures which have at basis the Park relations, following as on base of these structures to realize the system model.
KEYWORDS:
asynchronous synchronous motor, automate regulator, structural scheme

1. INTRODUCTION

The utilization of electric motors by direct current in actions, assure the system a high precision and rapidity for regulation of rotation speed at a pre-establish level, but it presents and a series of disadvantages as well. Because of this cause, it has tried the passing to actions with motors of alternative current without collector synchronous and asynchronous synchronous [1, 4].

In particular, the motors synchronous asynchronous (MSA) must not be less accurate than the ones of continuous current with regard to the quality of regulation, must assure any overload necessary to action without depending on the electric parameters of motor. One of the very important conditions imposed to this type of action consists of the fact that, the system of regulation must assure the possibility of command of the reactive power in such a way to maintain it at an economical level imposed.

2. THE FUNCTIONAL SCHEME OF SYSTEM REGULATION

By MSA we understand a synchronous motor with a symmetrical wind in the stator, alimentated from a network of alternative current and a wind bi- or tri- phased symmetrical of excitation alimentated from a static converter of frequency with thyristor (for example with direct link).

This system can be processed in the limits of a close system of automate regulation of the reactive moment and power of the motor, as in figure 1, where: 1 – MSA; 2 – transducers of rotor current; 3 – static

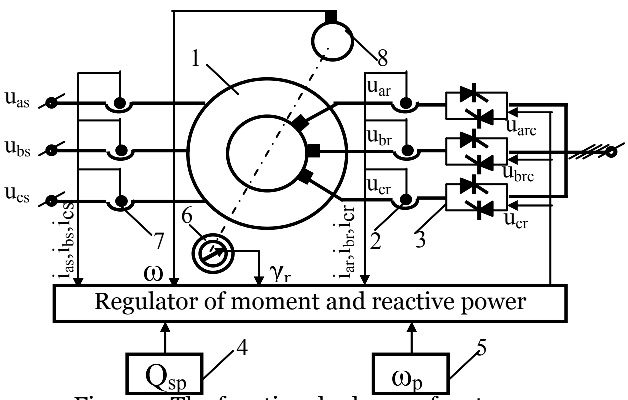

Figure 1. The functional scheme of system

reversible converter with thyristor; 4 – command sensor of reactive power; 5 – command sensor of rotation speed; 6 – angle transducer; 7 – transducers of stator current; 8 – tahogenerator.

Upon the regulator of reactive moment and power, activate the command signals after speed ω_p and after reactive power Q_{sp}, as well as the signals of stator currents, rotor currents, the angular position of rotors ν_r and ω. Under the action of this signals, the regulator will process the command signals u_{arm}, u_{brm}, u_{crm} which activate at the entrance of the supply sources of rotor phases. The regulator of the reactive moment and power is synthesized in such a way that the system assures in stationary regime the maintaining of ω and Q at the given level, indifferent of the load at motor tree.

The system synthesis and analysis simplifying assumptions: at MSA with symmetrical three phases winds in stator and rotor are not be taken in consideration the iron losses and the change of saturation rank at this; the stator network supply is considered as infinite; the rotor supply sources are presumed to be electric generators without inertia, with electromotor tensions proportional with the entrance signal, that is: $U_{ar} = U_{arm}$, $U_{br} = U_{brm}$, $U_{cr} = U_{crm}$.

3. THE STRUCTURAL SCHEME OF MSA

Take into account the simplifying assumptions taking in to consideration a system of coordinates round synchronous after axes α, β [2, 3, 5], the functional ecuations of system can be written under the forms:

$$\begin{aligned}
\frac{d\Psi_{\alpha s}}{dt} &= u_{as} + \omega_s \cdot \Psi_{\beta s} - r_s \cdot i_{\alpha s};\\
\frac{d\Psi_{\beta s}}{dt} &= u_{\beta s} - \omega_s \cdot \Psi_{\alpha s} - r_s \cdot i_{\beta s};\\
\frac{d\Psi_{\alpha r}}{dt} &= u_{\alpha r} + (\omega_s - \omega) \cdot \Psi_{\beta r} - r_r \cdot i_{\alpha r} \qquad (1)\\
\frac{d\Psi_{\beta r}}{dt} &= u_{\beta r} - (\omega_s - \omega) \cdot \Psi_{\alpha r} - r_r \cdot i_{\beta r}\\
\frac{d\omega}{dt} &= \frac{1}{J}(M_e - M_r)
\end{aligned}$$

where:

$$\begin{aligned}
&\Psi_{\alpha s} = x_s \cdot i_{\alpha s} + x_m \cdot i_{\alpha r};\ \Psi_{\alpha r} = x_m \cdot i_{\alpha s} + x_r \cdot i_{\alpha r};\\
&u_{\alpha s} = U_{sm} = 1;\ u_{\beta s} = 0;\ u_{\alpha r} = u_{\alpha rc};\ u_{\beta r} = u_{\beta rc};\\
&\Psi_{\beta s} = x_s \cdot i_{\beta s} + x_m \cdot i_{\beta r};\ \Psi_{\beta r} = x_m \cdot i_{\beta s} + x_r \cdot i_{\beta r}
\end{aligned} \qquad (2)$$

The reactive power of stator circuits will be:

$$Q = u_{\beta s} \cdot i_{\alpha s} - u_{\alpha s} \cdot i_{\beta s} = -U_{sm} \cdot i_{\beta s} \qquad (3)$$

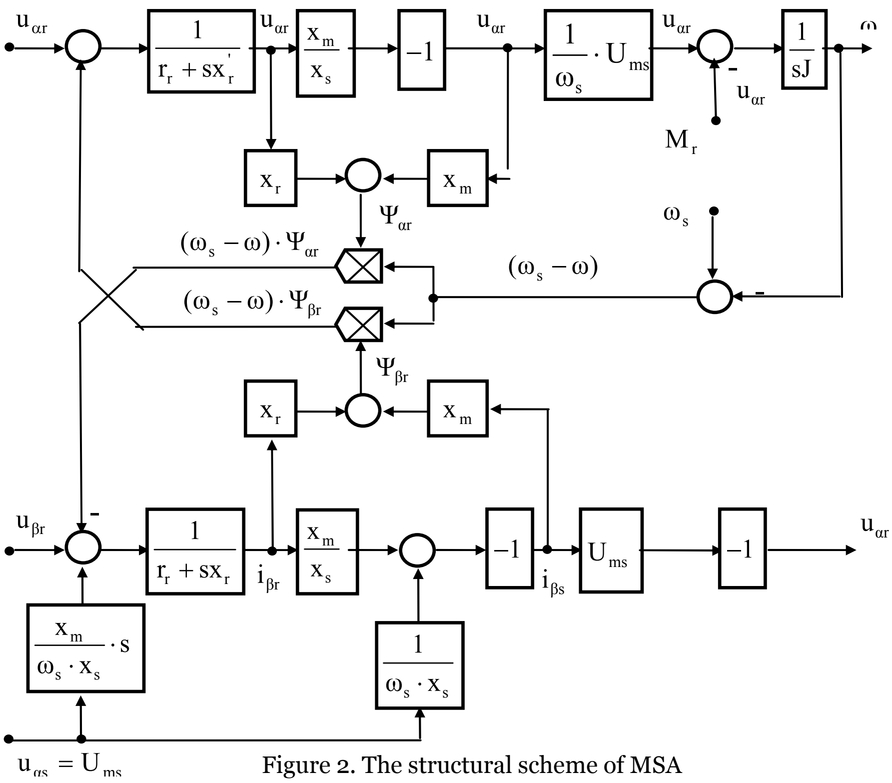

Figure 2. The structural scheme of MSA

With the specifications that in (1) all sizes are expressed in relative units.
The variables on axes α, β are connected through:

$$\begin{aligned} i_{\alpha s} &= \tfrac{2}{3}[i_{as}\cdot\cos\omega_s t + i_{bs}\cdot\cos(\omega_s t - \tfrac{2\pi}{3}) + i_{cs}\cdot\cos(\omega_s t + \tfrac{2\pi}{3})] \\ i_{\beta s} &= \tfrac{2}{3}[i_{as}\cdot\sin\omega_s t + i_{bs}\cdot\sin(\omega_s t - \tfrac{2\pi}{3}) + i_{cs}\cdot\sin(\omega_s t + \tfrac{2\pi}{3})] \\ i_{\alpha r} &= \tfrac{2}{3}[i_{ar}\cdot\cos\nu_r + i_{br}\cdot\cos(\nu_r - \tfrac{2\pi}{3}) + i_{cr}\cdot\cos(\nu_r + \tfrac{2\pi}{3})] \\ i_{\beta r} &= \tfrac{2}{3}[i_{ar}\cdot\sin\nu_r + i_{br}\cdot\sin(\nu_r - \tfrac{2\pi}{3}) + i_{cr}\cdot\sin(\nu_r + \tfrac{2\pi}{3})] \end{aligned} \tag{4}$$

where ν_r is the electric angle between the rotor axes and the coordinate system which turns synchronously.

The reverse pass towards the command tensions of rotor phases is made through the relations:

$$\begin{aligned} u_{ar} &= u_{\alpha rc}\cdot\cos\nu_r - u_{\beta rc}\cdot\sin\nu_r \\ u_{br} &= u_{\alpha rc}\cdot\cos(\nu_r - \tfrac{2\pi}{3}) - u_{\beta rc}\cdot\sin(\nu_r - \tfrac{2\pi}{3}) \\ u_{cr} &= u_{\alpha rc}\cdot\cos(\nu_r + \tfrac{2\pi}{3}) - u_{\beta rc}\cdot\sin(\nu_r + \tfrac{2\pi}{3}) \end{aligned} \tag{5}$$

The system (1) gives the possibility of constructing the scheme of structure MSA, represented in figure 2, observing that the structure contains some non-linear elements as well as a cross reaction created by the presence of the electromotor force of rotation in the stator and rotor circuit, as well as of the magnetic links of these circuits.

The structural scheme can be simplified considerably if the secondary links (by ord. II) are eliminated in particular admitting the elimination of active resistor R_s and a transistor process in statoric circuit. Under these conditions from (1) the fluxes can be determinate:

$$\Psi_{\beta s} = -\tfrac{1}{\omega_s}\cdot u_{\alpha s} = -\tfrac{1}{\omega_s}\cdot U_{sm} = -1;\quad \Psi_{\alpha s} = 0 \tag{6}$$

the electromagnetic moment becoming:

$$M_e = -\Psi_{\beta s}\cdot i_{\alpha s} = \tfrac{1}{\omega_s}\cdot U_{sm}\cdot i_{\alpha s} \tag{7}$$

4. THE STRUCTURAL SCHEME OF THE REGULATOR

As it was mention, the actions with MSA must present the characteristics at similar performance of action case with motors of direct current, carrying out at the same time the part of synchronous compensators as well. From this point of view, we must totally take into account the dynamic proprieties of the regulate object, it is indicated that the regulator be construct not in phase coordinates, but in synchronous coordinates α, β, taking into account (4) and (5).

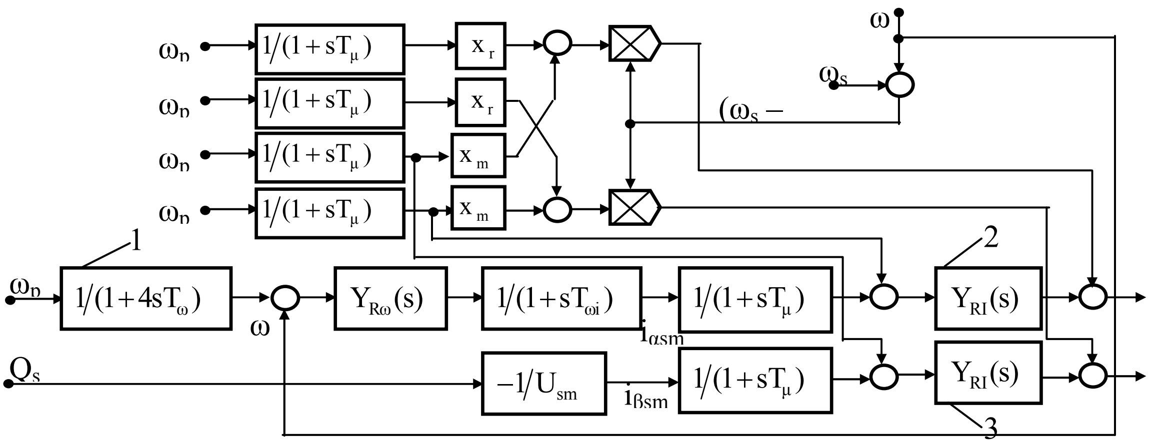

Figure 3. The structural scheme of regulator

From the structural scheme (figure 2), we can observe that, if in the regulator of reactive moment and power, the compensation condition of electromotive force of rotation at rotor is carried ut (ω_s -) and (ω_s -). Then appears the possibility of separate regulation of active current $i_{\alpha s}$ (electromotive moment and ω) and reactive current $i_{\beta s}$ (power Q_s), with the help of voltage $U_{\alpha r}$, $U_{\beta r}$. Thus, on the channel $U_{\alpha r} - \omega$, the structure analyzed is analogous with the motor structure of direct current compensated and the regulation is subordinated to the method with series correction. So, the regulator exit of speed represent the regulator entrance of current, and the motor moment is proportional with the regulator exit of speed.

On the channel $U_{\beta r} - Q_s$, for the regulation it is enough to work only the current regulator.

Taking into account those presented based on figure 2, was obtained the structural scheme of the regulator of reactive moment and power of the MSA from figure 3, at the basis of the regulator synthesis being the general methods of synthesis subordinated to the regulation with series correction.

Through the supply of rotor winds from the static converter of frequency with thyristor, with direct link, the speed is regulated in the approximate limits $(1\pm0.3)\cdot\omega_s$. Beside, the speed regulator, in the structural scheme there appear another two regulators: 2 – regulator of active current and 3 – regulator of reactive current, at the regulator entrance 2 appears the command from the regulator exit of speed, again at the regulator entrance–3 it is applied the command of reactive power Q_{sm}.

The transfer functions of regulator are established starting from the optimum transfer functions of the regulation systems in close circuit [2, 6]. So, the transfer function of the current regulator can be give by:

$$Y_{RC}(s) = (r_{rech} + x_r^{'})/2 \cdot s \cdot T_\mu \tag{8}$$

where T_μ – represent the time constant of measurement filters and its chosen according to the necessary action speed of the regulation circuits of current.

In some cases [4] for increasing the fiability of frequency converters it is indicated that the entries of the regulator non-inertial reverse supplementary connection be introduced after the faze currents, through this the aspect of the transfer function is not modified, only an increase of the equivalent resistance being necessary to be introduced init. The transfer function of the speed regulator can be written under the following aspect, taking into consideration a regulation law PI:

$$Y_{R\omega}(s) = J \cdot (1 + 4 \cdot s \cdot T_\omega)/8 \cdot s \cdot T_\omega^2 \tag{9}$$

where T_ω – time constant which characterizes the regulation loop of speed and in general $T_\omega \geq 2T_\mu$.

In the regulation, loop of speed a supplementary tuning filter can be introduced as well, whose time constant to be $T_{\omega i} = T_\omega - 2T_\mu$.

5. CONCLUSIONS

The establishing of structural scheme allows the model of electric actions with MSA, this model being made taking into account the machine-static converter assemble. The compensation of the electromotor tension of the rotor and the selection of the activating speeds of the regulation loop constitutes a special problem because it can lead to the worsening of the transitory processes and the apparition of oscillations. In the structural scheme, the compensation of the internal reverse reaction is presented after the rotation electromotor tension through the multiplication elements 4 and 5.

Since the results of the modelation on a red case are not finalized, then results will be presented in the future, taking into account [7] as well.

REFERENCES

[1.] Boldea I., Parametrii maşinilor electrice, Ed. Academiei Române, Bucureşti,1991.
[2.] Botvinnik M., M., Asinhronizirovannaia sinhronnaia maşina, Gosenergoizdat, Moskva, 1960.
[3.] Câmpeanu A., Introducere în dinamica maşinilor electrice de curent alternativ, Ed. Academiei Române, Bucureşti, 1998.
[4.] 4. Ferraz, C.A.M.D., de Souza, C.R., Reluctance synchronous motor asynchronous operation, Electrical and Computer Engineering, 2002. IEEE CCECE 2002. Canadian Conference ,
[5.] pg: 195 – 200, vol.1.
[6.] Gayadhar Panda, Sidhartha Panda and Cemal Ardil , Automatic Generation Control of Interconnected Power System with Generation Rate Constraints by Hybrid Neuro Fuzzy Approach, World Academy of Science Engineering and Technology 52, pg. 543-548, 2009.
[7.] Lebedev E., D., Neimark B., E., Upravlenie ventilnîmi elektropribodami postoiannovo toka, Moskva, 1970.
[8.] Oprea C., Barz Cr., The contributions at modeling sincron machine trough utilization of Labview language, Buletinul Institutului Politehnic din Iaşi, Tom. XLVIII(LII), pg. 117-121, 2002.
[9.] Soran I.F., Kisch D.O., Sîrbu G.M., Modelarea sistemelor de conversie a energiei, Editura ICPE, Bucureşti, 1998.

INTERNATIONAL SYMPOSIUM on
ADVANCED ENGINEERING & APPLIED MANAGEMENT
– 40th ANNIVERSARY in HIGHER EDUCATION (1970-2010)
4 – 5 November, 2010, Hunedoara, ROMANIA

1. Cristian BARZ, 2. Constantin OPREA

STUDY OF ELECTROMAGNETIC FIELD IN CLAW-POLES ALTERNATOR

1-2 UNIVERSITY OF NORTH, FACULTY OF ENGINEERING BAIA MARE, ROMANIA

ABSTRACT:
The paper presents the tridimensional analysis of electromagnetic field of an claw poles alternator, in whose construction has been used non-magnetic material, such aluminum, that form the rings in the rotor's structure. This structure aims to establish lower levels of saturation in the claw-pole of Lundell alternator. Reducing the level of saturation in the rotor, lead to reduction of the losses in hysteresis, the power will be exchangeable in the output of the machine, while achieving its growth the performances.
KEYWORDS:
3D analysis, claw-pole alternator, simulation, finite element method

1. INTRODUCTION

Due to the gradual replacement of hydraulic and mechanical organs of the auto vehicles with electrical devices, power demand in automobiles has greatly increased, where electricity plays a decisive role, the conventional vehicle generator (Lundell alternator) tends rapidly to the maximum that can charge.

The Lundell alternator is the most common power generation device used in cars. It is a wound-field three-phase synchronous generator containing an internal three-phase diode rectifier and voltage regulator. The rotor consists of a pair of stamped pole pieces (claw poles), secured around a cylindrical field winding. The field winding is driven from the voltage regulator via slip rings and carbon brushes. The output voltage of the alternator is maintained at about 14V DC, as this is the nominal charging voltage of a 12V lead-acid battery. The voltage is regulated at 14V by an internal controller that continuously samples the battery voltage and adjusts the field current accordingly.

Electromagnetic behavior of the alternator with claw-poles and its interaction with the bridge rectifier, the load and the vehicle power system is generally considered as a spatial-temporal feature. Thermal model was validated by comparing calculation of temperature distribution with the measured values. [1]

Some studies are based on the idea of increasing the power out and efficiency of the alternator, while maintaining the alternator operating point in the optimum zone. Theoretical expectations are compared with experimental results using a car alternator; the output power increases to 200% and significant improvement of efficiency are demonstrated at high speeds. [2]

Utilization of computational analysis allows for the substitution of expensive prototype construction at early design stages. Authentic simulations of the real machine behaviour require advanced component modelling.

Methods using numerical simulations based on finite elements are often used because permit a better precision performance of the devices. Using these methods can overcome all the surveys and the assumptions made to establish an analytical model often long and hard to build.

Analytical models allow preliminary design studies, so the numerical simulations as an opportunity to validate and refine solutions based on analytical methods.

Henneberger S.A, Damerdash S.A., Viorel S.A. investigated the electromagnetic and thermal phenomena of Lundell alternator using the finite element method.

Perreault's studies have investigated ways to extract more power from existing claw-pole alternators by using a rectifier switching system. Have also been proposed alternators driven by inverter, these can provide energy to a capacitive power factor and being able to extract about twice as much power from alternative to the low speeds.

Proposed solutions include also other types of electric machines: asynchronous machines, variable reluctance machines, synchronous machines with permanent magnet for surface and permanent magnet for interior: Boldea, Naidu, Liang, J.M. Miller s.a. The proposed alternators systems are expensive because the power electronics and the complex control. [3]

Schulte describes two approaches for calculating the mutual inductance between rotor and stator of the synchronous alternator with claw-poles about the claw shape. If the prototypes are available, mutual inductance can be calculated from the voltage measured at no load. Description of the mutual inductance obtained can be used to implement the circuit based on numerical simulations. [4]

2. NUMERICAL ANALYSIS OF THE ELECTROMAGNETIC FIELD - THE CONCEPT

The numerical analysis 3D by finite element method for the electromagnetic field produced by electric drives, is currently, in terms of reliability of results obtained, one of the most powerful means for analyzing the electromagnetic field, for determining the parameters of these complex structures, indifferent of the field shape or the existence or absence of some symmetry.

2.1.Formulation for the finite elements method

The software used in this paper is MagNet, 6.24.1 version, a product of Infolytica. Without many details, it will be still specified that for this software the general 3D formulation is based on the T-Ω method in which the magnetic field is represented as the sum of two parts: the gradient of a scalar potential and, in conductors, an additional vector field represented with vector-edge elements.

In a conducting medium, the equation to be solved is one in $\overline{H}$ of the following form:

$$\nabla \times [\nabla \times \overline{H}] + \overline{\overline{\sigma}}\,\overline{\overline{\mu}} \frac{\partial \overline{H}}{\partial t} + \overline{\overline{\varepsilon}}\,\overline{\overline{\mu}} \frac{\partial^2 \overline{H}}{\partial t^2} = 0 \tag{1}$$

where $\overline{\overline{\mu}}$ is magnetic permeability tensor, $\overline{\overline{\sigma}}$ is electric conductivity tensor, $\overline{\overline{\varepsilon}}$ is electric permittivity tensor and $\overline{H}$ is magnetic field strength.

In a non-conducting medium, $\overline{H}$ can be written as:

$$\overline{H} = -\nabla \psi + \overline{H}_s \tag{2}$$

where $\overline{H}_s$ is any source field that satisfies $\nabla \times \overline{H}_S = \overline{J}_S$, where $\overline{J}_s$ is the current density in an eventual stranded coil, and ψ -scalar potential. [6]

2.2. The Newton-Raphson method

Finite elements method is a numerical method based on the application of variation principles to solve equations with partial derivatives. In technique, was first developed to solve the problems of resistance material, its application to calculate electric and magnetic fields are relatively recent.

Finite element method is suitable for work with non-linear components such as electromagnets with materials ferromagnetic who manifest anisotropic phenomenal that and saturation.

Relationships formed between magnetic flux (B) and magnetic field (H) are generally nonlinear, over some materials present hysteresis, in "state" BH for a particular point in space and time depends on the previous magnetic values.

To extend the procedure for finite elements to include non-linear properties of materials are required a mathematical model to describe the properties of the material.

The software of field analysis used is based on the calculation method Newton Raphson who converges quickly, providing sufficient initial values. So, if $u^{(0)}$ is a matrix of values of the initial solution, u(1) can be write:

$$u^{(1)} = u^{(0)} + \delta u^{(0)} \tag{3}$$

where: δu(0) – matrix of errors values.

$$(K(u) - Q) = F(u) = 0 \tag{4}$$

where Q is independent by u, the factor F define in equation (4) can be extended from multidimensional Taylor series.

The simple iteration scheme (9) Newton Raphson, as illustrated in Figure 1. b), it may not converge if the initial assumptions are not close enough solution. For this reason, is usual in practice, to get the initials startup by completing several steps of iteration before applying Newton Raphson method

In Newton Raphson is essential that curves made it to be smooth, this allowing to be made a better estimation of derivatives. [5].

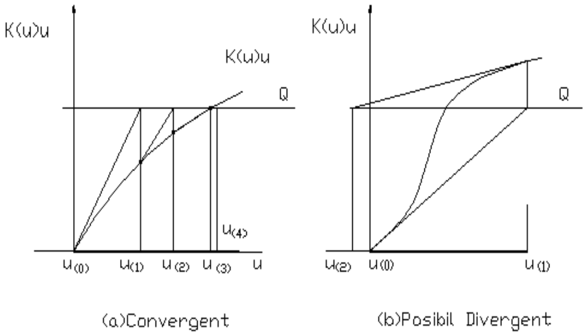

Fig. 1. Simple iteration scheme Newton-Raphson

The treatment of nonlinearities with the Newton-Raphson method and application of finite element method to solve the problems of field, for every iteration, is currently the most used method of analysis of the magnetic field of rotating electrical machines.

3. THE REALIZATION OF NUMERICAL MODEL OF THE ALTERNATOR WITH CLAW-POLES

Complex construction of the alternator with claw poles, the existence of magnetic fields both radial and axial, the lack of symmetry plane-parallel magnetic field study require the car to be achieved through three-dimensional finite element numerical modeling.

It highlights sub domains characterized by different magnetic properties: magnetic core of the rotor (polar components as claws), axis machine made from the magnetic material, coil excitation, the stator magnetic core provided with notches in which are placed winding induced.

Starting from the model of alternator with claw-poles in the experimental study, and checking in the same time the geometric dimensions of its design, was performed three-dimensional model of the alternator to following the behavior of this. There are various studies related to various forms of cut or teeth geometry [3], we tried to make some options for changing them, to follow in the subsequent analysis of the influences on the electromagnetic field of alternative.

The program allows saving the models (Fig. 2) and retrieving of this for further modifications to the building with new data, which are made by environmental Magnet 6.11

```
CALL saveDocument("D:\doctorat\MODELE ALTERNATOR\scripturi\stator.mnte", infoMinimalModel)
Call getDocument().getView().addRotation(0, 45, 0)
Call getDocument().getView().addRotation(0, 0, 10)
Call getDocument().getView().addRotation(10, 0, 0)
Call getDocument().getView().rotateToAxis(infoPositiveZAxis)
Call getDocument().getView().rotateToAxis(infoPositiveXAxis)
CALL closeDocument()
msgbox("")
'deschidere fisier
CALL openDocument ("D:\doctorat\MODELE ALTERNATOR\scripturi\stator.mnte")
'setarea unitatilor in milimetrii
Call getDocument().beginUndoGroup("Set Default Units", true)
Call getDocument().setDefaultLengthUnit("Millimeters")
Call getDocument().endUndoGroup()
'introducere dimensiuni
dim Rrext,Rrint,Hrdinte,Lrdinte,npoli,Rgheara,Lrbaza,Lgdinte,dist,Rrbaza,Lrotor,gizol
```

Fig. 2. The saving model

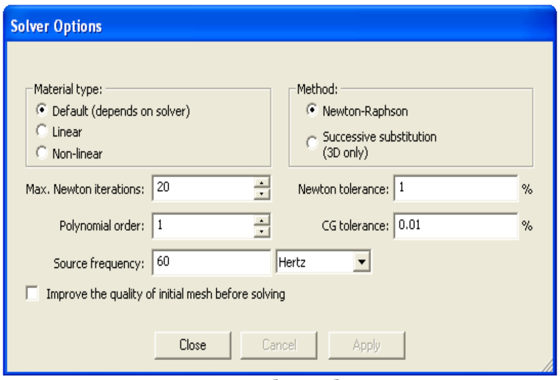

Fig. 3. The solver options

Accessing computing environment for the analysis magnet field define boundary conditions, the currents that cross both the involution stator and the rotor.

Magnet computing environment allows the choice of several ways of calculating the field, find the most used Newton Raphson method, and also choose the orders of the polynomial calculation. (Fig. 3)

Realizing some analysis of the shape and size of the volume of air surrounding the model alternator (Fig.4), brings us attention over some influence of that, on energy stored in the model.

By interpreting the results obtained in the analysis field (Fig. 5), can automatically change the input data to obtain a new constructive model to be analyzed.

It won a precious time with automatic model building constructively us needs another soft drawing a constructive model.

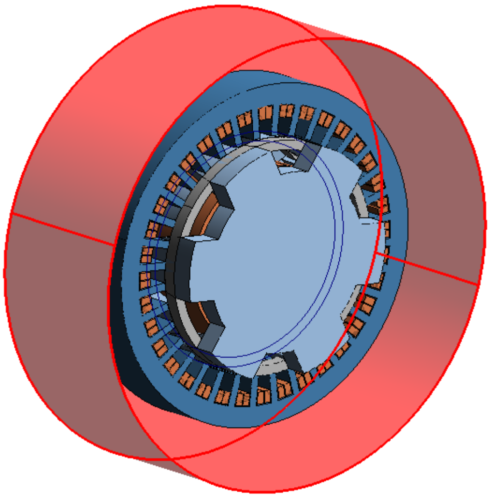

Fig. 4. The volume of air surrounding the alternator model

The uniform level of magnetic saturation in the whole magnetic circuit is usually required, but it is seen that the magnetic flux density in the claw-poles roots is significantly higher in comparison with other magnetic circuit components and areas.

The representation of the magnetic induction along the claw-poles as so on the axis claws, but also on its edges for different excitation currents is made in Fig. 6.

The construction and optimal sizes of the claw poles are required by their role to converting the axial flow produced by the excitation winding in radial flow in air gape.

Begin from the experimental data, in the tridimensional analysis of the alternator with claw poles, we can make comparisons with different configurations of the numerical model of the alternator.

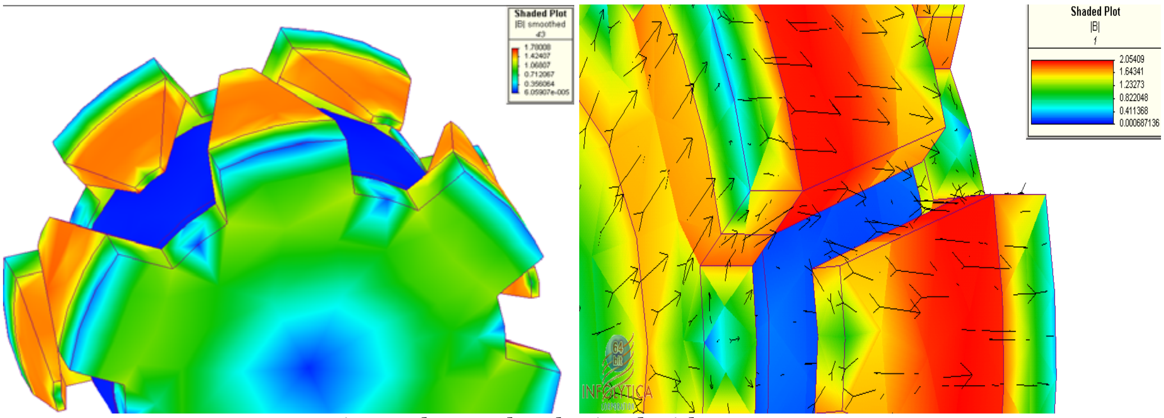

Fig. 5. The results obtained with Magnet 6.11

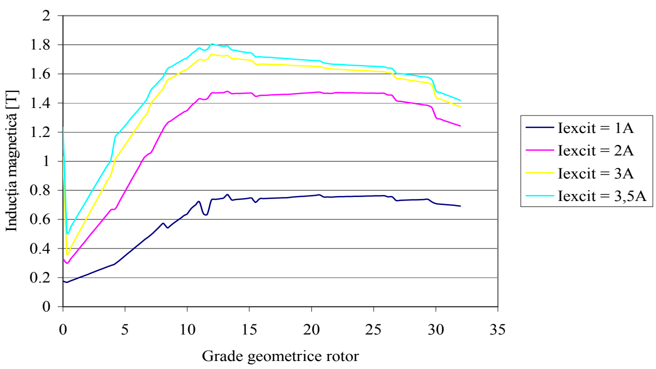

Fig. 6. The representation of the magnetic induction along the claw-poles.

Thus, we can observe how the inductance of the claw poles depends by the geometry and the nature of material from the rotor is achieved.

The uniform level of magnetic saturation in the whole magnetic circuit is usually required, but it is seen that the magnetic flux density in the claw-poles roots is significantly higher in comparison with other magnetic circuit areas and components. Improvement of claw-pole design is therefore advisable. On the other side, increasing the cross-section area of the claw-pole root causes reduction of exciting winding space.

The numerical analysis carried out covering two constructive variants of the rotor unit.

The first variant considered involves a distribution of aluminum between the rotor claws, replacing the air gape with aluminum (Fig. 7. a.). The second consists in a ring shape build on the crown of the rotor to reduce the saturation level, but only space between the claws (Fig. 9. b.).

In Fig. 8. have represented the magnetic induction over along the claw pole for the cases: simple alternator, resulting from design and build the model studied, for the case when the air gap between the claws is replaced with aluminum, and, the case when the aluminum is used as the ring shape on the crown of the rotor, but only in free space of the claw.

It can be notice, an increase in saturation along the axis of claw pole in the first case, with the aluminum between the claws beside to the case of standard alternator.

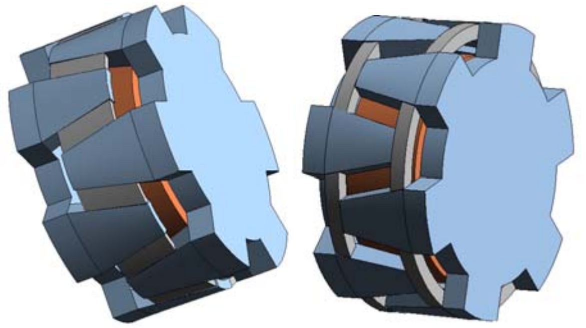

a) b)

Fig. 7. The repartition of aluminum in the rotor structure of the alternator

In the second case study, however, is important the decrease of saturation by 15%, when the aluminum is in the shape of rings on the crown of the rotor. There is a sharp reduction in magnetic saturation in the aluminum zone, but the decreased saturation is present and to the claw pole tip (up to 5%), there is initial a lower saturation.

The results obtained from experimental measurements, from the aluminum version of the crown ring rotor, show us that reducing the saturation, are going to decrease the output power of the alternator with claw-poles.

Changing the magnetic circuit of the alternator is based on the perspective to optimization the results to be included in designing a prototype of the alternator with claw-poles.

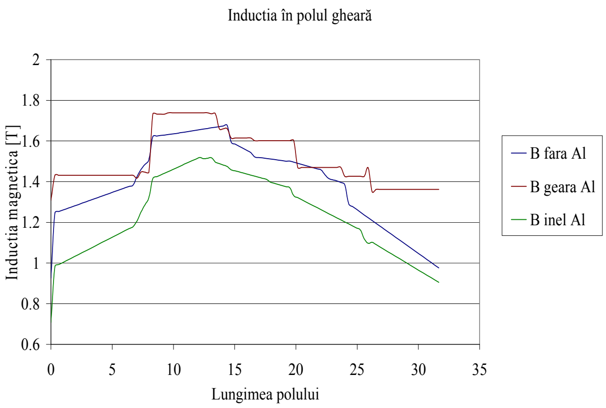

Fig. 8. The magnetic induction over along the claw-pole axis

4. CONCLUSIONS

The programs which realized field analysis based on the finite element method, come in help of the designer from the checks who can be make in usually time and with high precise, thus removing any errors made during in the design of electric machines, providing reached the designer intended purpose. These programs of analysis and verification ensure the safety of a proper design of the electric cars.

Numerical investigations carried out aimed at optimizing the machine design by reducing the magnetic saturation of the poles' alternator which is due to the interaction of aluminum segments enter into the construction of the rotor.

- ❖ The present paper deals with specific issues concerning modeling and numerical analysis of an alternator with claw-poles, with certain portions of nonmagnetic material (Al), using the finite element method.
- ❖ The introduction of the nonmagnetic materials in the rotor assemble as the rings shape on the rotor crowns, try to establish some lowest levels of the saturation in different parts of magnetic circuit (teeth, yokes) and to increase the useful power of the alternator.

REFERENCES

[1.] Sai Chun Tang, Member, IEEE, Thomas A. Keim, and David J. Perreault, Member, IEEE, „*Thermal Modeling of Lundell Alternators*", IEEE TRANSACTIONS ON ENERGY CONVERSION, VOL. 20, NO. 1, MARCH 2005, pag 25

[2.] Ceuca, E.; Joldes, R.; Olteanu, E „Simulation of automotive alternator - solution for increasing electrical power". Automation, Quality and Testing, Robotics, 2006 IEEE International Conference on Volume 1, Issue , 25-28 May 2006 Page(s):292 – 297

[3.] V. Comnac, M. Cernat, A. Mailat, J. Vittek, R. Rabinovici, „New 42 V Automotive Supply System Based on Conventional 14 V Alternator", in Proccedings OPTIM 2008, Brasov, Romania, 22-24 May 2008, vol. II, pp. 271-276

[4.] St. Schulte, K. Hameyer „Computation of the Mutual Inductance between Rotor and Stator of Synchronous Claw-Pole Alternators regarding Claw Chamfers", Institute of Electrical Machines, RWTH Aachen University, Schinkelstr. 4 52056 Aachen Germany, 2005

[5.] Barz C., Oprea C., Chiver O., ,,Modelig of Lundell alternator", 6-th Japanese-Mediteranean Workshop on Applied Electromagnetic Engineering for Magnetic, Superconducting and Nano Materials, Bucuresti, 2009.
[6.] O. Chiver, E. Micu si C. Barz, „Stator winding leakage inductances determination using finite elements method", OPTIM 2008, Proceeding of the 11 th International Conference on Optimization of Electrical and Electronic Equipment, 22-23 May 2008, Braşov, IEEE XPLORE INSPEC, pag. 69-74

INTERNATIONAL SYMPOSIUM on
ADVANCED ENGINEERING & APPLIED MANAGEMENT
– 40th ANNIVERSARY in HIGHER EDUCATION (1970-2010)
4 – 5 November, 2010, Hunedoara, ROMANIA

[1.]Sorin Ioan DEACONU[1)], [2.]Lucian Nicolae TUTELEA,
[3.]Gabriel Nicolae POPA, [4.]Tihomir LATINOVIC

ARTIFICIAL LOADING FOR ROTATING ELECTRIC MACHINES

[1,3.] DEPARTMENT OF ELECTRICAL ENGINEERING AND INDUSTRIAL INFORMATICS,
FACULTY OF ENGINEERING HUNEDOARA, UNIVERSITY "POLITEHNICA" TIMISOARA, ROMANIA
[2.] DEPARTMENT OF ELECTRICAL ENGINEERING, ELECTROTECHNICAL FACULTY,
UNIVERSITY "POLITEHNICA" TIMISOARA, ROMANIA
[4.] DEPARTMENT OF ROBOTICS, UNIVERSITY OF BANJA LUKA, BOSNIA & HERTEGOVINA

ABSTRACT:
The paper presents many methods to produce synthetic loading of rotating electric machines (induction, synchronous and DC) without load to the shaft using power converter. The required equipment is simple. Setting-up time is considerably reduced because it is not required to connect an external load to the machine's shaft. The range of r.m.s. current control is large beginning from no-load current to overload at rated speed and temperature, that the total losses in the machine can be identified by taking the average of the measured power over one cycle of synthetic loading of the machine.
KEYWORDS:
Ytterberg's method, DC machine, induction machine, synchronous machine, synthetic loading

1. INTRODUCTION

The machine temperature at full load represents an essential parameter of rotating electric machine. The conventional method is to produce the shaft's load using another electric machine. The cost of test equipment and setting-up procedure for mechanical coupling make the conventional method prohibitively expensive, especially for large machine or for high speed machine. Thermal test of vertical mounted machines is quite impossible due difficulties to fit the vertical load [1].

Hence, currently there is no cost-effective method of assessing the state of a machine on-site and whether or not it would be economically and environmentally beneficial to replace it. However, the regulations are not retrospective and so many poor performing machines will remain in service for many years to come. A method of evaluating the efficiency of machines currently in service to ascertain whether or not it should be replaced needs to be developed [2], [3], [4].

The dual frequency method was proposed in 1921 by Ytterberg [5] in order to produce synthetic loading of induction machine.

Now, using power converters several methods have been developed. Dynamic thermal loading [6], [7], [8], constant speed method [9], sweep frequency method [10] and also the dual frequency method [10], [11], [12], [13], [14], can be implemented using power converters.

2. THEORETICAL STUDY

The essence of the dual frequency method is to produce a supply voltage containing two distinct frequencies. This way, two magnetic fields are produced, rotating at different speeds. The shaft speed can not change quickly, so the machine is oscillating between motoring and regenerating. This way, the r.m.s. motor current is increased compared to the no-load current [1].

In Ytterberg's method the loading machine is supplied from two series three-phased symmetrical systems having different frequencies. One of the sources has a fixed frequency f_1

(frequency of the network's power supply) and is called "base source" and the other one has a variable frequency f_2, usually less than f_1, and it is called "auxiliary source". The emf's supply by the two sources can be written as:

$$u_1 = \sqrt{2} \cdot U_1 \cdot \sin \omega_1 t \,, \tag{1}$$

$$u_2 = \sqrt{2} \cdot U_2 \cdot \sin \omega_2 t \,. \tag{2}$$

Consequently, the resulting wave has amplitude modulated by a frequency equal to the difference between f_1 and f_2. In the rotating rotor winding is induced a voltage with the frequency equal to the difference between the frequencies f_1 and f_2. The interaction between rotoric current and the rotating magnetic field in the core creates an electromagnetic torque which in a semi-period acts as an accelerating torque, while in the next semi-period acts as a generating torque, reducing the rotating speed of the rotor. In other words, in the first semi-period the machine absorbs active power from the source, while in the next semi-period it releases active power to the source. The resulting voltage has the following expression [15], [16]:

$$u(t) = \sqrt{2} \cdot U_1 \cdot \sin \omega_1 t + \sqrt{2} \cdot U_2 \cdot \sin \omega_2 t \,, \tag{3}$$

$$u(t) = \sqrt{2} \cdot (U_1 - U_2) \cdot \sin \omega_1 t + \sqrt{2} \cdot U_2 \cdot (\sin \omega_1 t + \sin \omega_2 t) \,. \tag{4}$$

In figure 1 is presented the current in the machine's windings

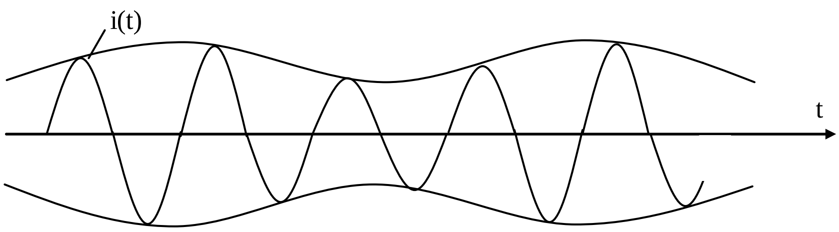

Fig. 1 The current i(t) for synthetic charge loading

Further, we introduce the following notation:

$$\alpha = \omega_1 - \omega_2 \,, \tag{5}$$

$$\beta = \frac{\omega_1 + \omega_2}{\omega_1 - \omega_2} \,, \tag{6}$$

$$\beta \cdot \alpha = \omega_1 + \omega_2 \,. \tag{7}$$

By combining equations (5) and (6) results:

$$(\beta + 1) \cdot \alpha = 2\omega_1 \,. \tag{8}$$

Thus equation (4) becomes:

$$u(t) = \sqrt{2} \cdot \left[(U_1 - U_2) + U_2 \cdot \cos \frac{\alpha t}{2} \right] \cdot \sin \frac{\alpha \beta}{2} \cdot t \,. \tag{9}$$

We can observe that this voltage varies periodically with the frequency ω_1 and is modulated with the frequency $\frac{\alpha}{2}$.

In dynamic thermal loading, the rotor's inertia moment will produce the electromechanical load during the acceleration and brake cycle. The induction machine will be repeatedly motor and generator. The average value of electromagnetic torque is close to zero, but not zero, in order to compensate the ventilation and mechanical losses. This method can be implemented as torque control or speed control.

In torque control implementation the reference will be a rectangle wave with a small positive offset. The amplitude of reference torque controls the stator and rotor load current. The offset value of reference torque controls the average value of speed. The average reference speed will be the rated speed in order to keep the same cooling conditions and mechanical loss as in conventional loading [1].

The internal air-gap voltage of an unloaded induction machine is very close in magnitude and phase angle to the applied armature voltage and no load current is small. As the machine becomes loaded, the load angle increases and a larger armature current is produced. The principle of equivalent loading is to increase the internal load angle without connecting any mechanical load onto the shaft. The inertia of the rotor acts as an energy storing device [17].

The constant speed method keeps the flux speed constant and changes only its amplitude. This method works in much the same way as a transformer in which the primary and secondary windings are magnetically coupled by varying flux magnitude. A small oscillating torque will be produced due to interaction of rotor current and the resultant rotating flux. The rotor speed will be close to rated speed ensuring equivalent cooling conditions. In order to produce the flux magnitude oscillating around rated flux value a higher then rated voltage is necessary in DC link circuit [1].

The other method to produce artificial loading is the sweep frequency method [1], [9]. In this method the supply voltage of induction machine is the result of standard frequency modulation. This voltage, as in the two frequency method, produces a flux wave which varies both in magnitude and angular velocity.

For synchronous machines, there are two loading methods in artificial load: by sub-excitation or over-excitation, and active loading by passing repeatedly from the motor regime in generator regime.

The reactive loading presents the advantage that it only intervenes upon excitation, so it will be adjusted small powers. The synchronous machine can be reactively loaded by sub-excitation or over-excitation, according to the excitation currents I_{min} and I_{msx}. These currents being different by the rated value, the condition to have the same losses distribution is not respected. The average heating of the excitation winding can be achieved if the machine passes periodically form a loading regime to the other.

Thus, during t_{sub} the current through excitation will have the value I_{min} and during $T\text{-}t_{sub}$ will have the value I_{max}. The period T will be chosen in such way that the duration of the transitory processes to be negligible against the duration of the stabilized process and sufficiently small compared with the thermal time constants of the machine.

The active loading is achieved by accelerating the machine in motor regime, than braking in generator regime. During loading, the machine's speed is oscillating around the rated speed. Loading is achieved by controlling the internal angle θ by means of a voltage inverter and a control system. The position of d-axis can be known either using a position transducer, or is estimated knowing the machine's parameters and the variation dynamics of currents and voltages.

The reactive loading can also be done by means of a voltage inverter that modifies the stator voltage (it increases it in the sub-excited regime and decreases it in over-excited regime in such way that the operation point at rated current to be within the stability field, respectively the excitation current to not reach to high values).

The synthetic on-load charging of the DC machines is achieved by producing an oscillating couple that has the average value approximately equal to zero and amplitude close to the rated value. This condition is met if the average couple developed in the machine equals the couple of mechanical losses produced when the machine operates at rated speed. For the DC machines with separate excitation, in derivation or with permanent magnets, the artificial load can be obtained by supplying from a 4-quadrant chopper or by connecting the machine between two branches of a three-phased inverter. Occurrence of some small errors in estimating the mechanical losses depending on speed is producing high deviations of the average speed. Is imposed the utilization of a speed regulator, and for speed's control can be used a speed transducer or a speed estimator.

At the DC machines with serial excitation is needed an additional voltage source, of reduced value and high currents, which during the test to supply separately the excitation and to have the possibility of voltage adjustment. Utilization of a single chopper for testing of some machines with much different voltages is possible by adapting the variator's supply voltage to the rated voltage of the tested machine, or only by adjusting the variator's output voltage. By using of a three-phased inverter, with the 3rd branch can be achieved the source in commutation for supplying the serial excitation winding.

3. DIAGRAMS FOR EXPERIMENTAL TESTS

A. Synthetic loading for induction machine. The first block diagram of the dual frequency method is presented in fig. 2. Autotransformer (AT) plays the role of the base source supplying the voltage with the constant frequency f_1 = 50Hz. Static frequency converter (SFC) supplies a voltage with variable amplitude and frequency f_2, and plays the role of an auxiliary source which gives the power of the machine that can be loaded. Adapting block controls the level of the signals provided by the transducers to the input of the data acquisition system, which acquires analog signals and convert them to digital. The computing system compares the data received from the transducer to the default set of the loading machine and controls the change of the voltage sources' parameters until one obtains the default value of the artificial charge. The shunts play the role of current transducers.

In fig. 3 is presented another system for synthetic loading [17]. The driver motor D_o is on the same shaft with generators G_1 and G_2. Generator G_1 of system (1) is rated at the maximum power rating P_{max} of the test rig (highest motor rating to be tested), and feeds the motor M_1 under test. The test motor could be either a wound rotor machine or a squirrel cage machine. Both the generator G_2

and the recovery machine M_2 of the system (2) are rated at P_{max}. If the field modulation of each generator is in opposition of phase, the power generated by each system is also in opposition of phase and, therefore, when one system absorbs power, the other generates it and vice-versa. By adjusting the magnitude of the excitation swing of generator G_2, one can adjust the power exchange with system (2) to exactly match the power swing of system (1). When this equilibrium is reached, the driver motor D_0 needs to provide only the losses in all five machines. Driver D_0 is preferably a synchronous motor, but can be a DC motor or an induction motor with low slip. In the latter case, the motor would have to be slightly over rated in order to perform the test at close to synchronous speed. It's been shown that the optimal performance to reach full rated load is achieved with a 10 Hz modulation depth (55 to 65 Hz).

Fig. 4 presents the diagram of artificial loading using a single supply source. The static frequency converter (SFC) is supplied from the power system and is controlled by a computing system. The frequency converter supplies the induction machine with the free shaft. Before the start, in the computing system are introduced the prescribed values. Depending on the rated speed n_N, is chosen the maximum speed n_{max} and minimum speed n_{min} values. The values of voltage and current are controlled by the computer with the adapting block and transducers. The power delivered towards the SFC in the generating period is consumed by the broke resistance in the DC link of SFC. The speed can be adjusted until the rated value is obtained.

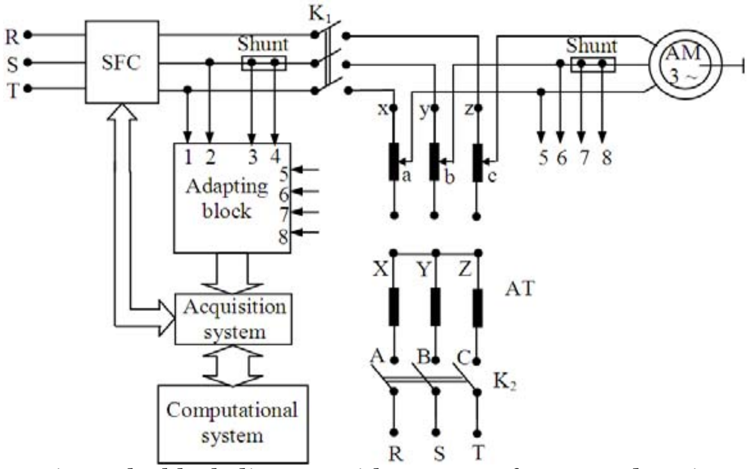

Fig. 2 The block diagram with autotransformer and static frequency converter

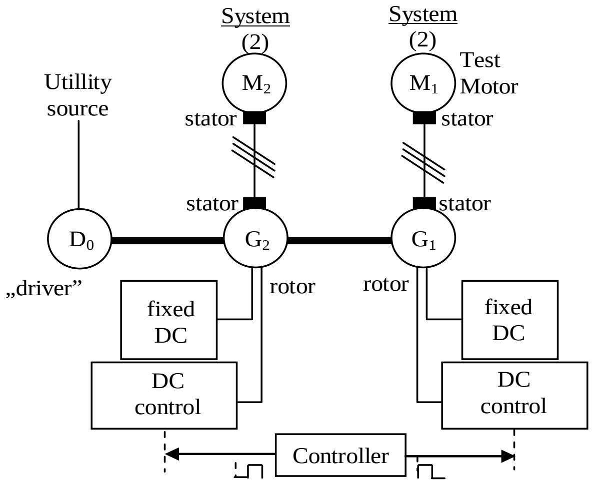

Fig.3 Diagram for large induction machines with no feedback into the power system

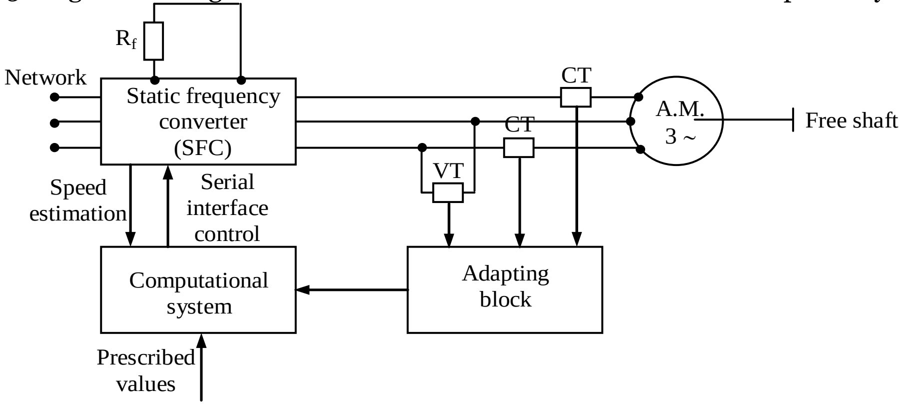

Fig. 4 Artificial loading of induction machine using a single supply source

B. Synthetic loading for synchronous machines

The diagram presented in fig. 5 allows the utilization of the synthetic charge of the synchronous machines (SM) both by using the reactive loading method and the active loading method. The AC/DC converter allows the excitation's supply both in sub-excited regime and in over-excited regime, and the static frequency converter (SFC) allows the modification of the voltage and stator frequency. The rotor position is obtained by means of a position transducer.

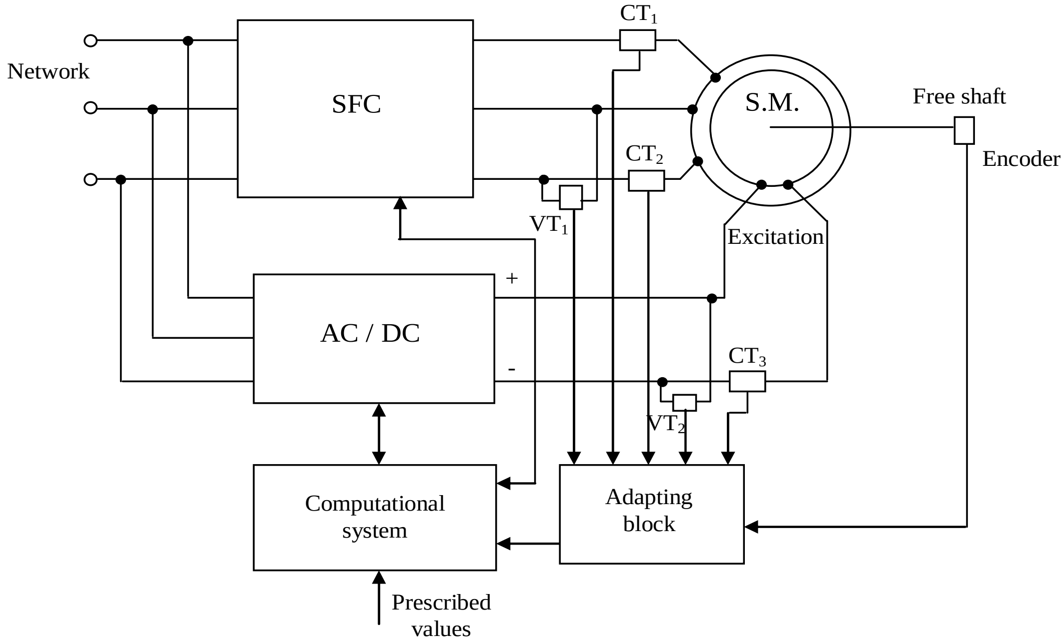

Fig.5 Reactive and active artificial loading for synchronous machines

C. Synthetic loading for DC machines

A synthetic on-load charging diagram of the DC machine using a 4-quadrant chopper is presented in fig. 6.

For a DC machine perfectly compensated, the induced voltage is directly proportional with speed. The proportionality factor between voltage and current is the flux produced by excitation which can be read from a table depending on the measured current.

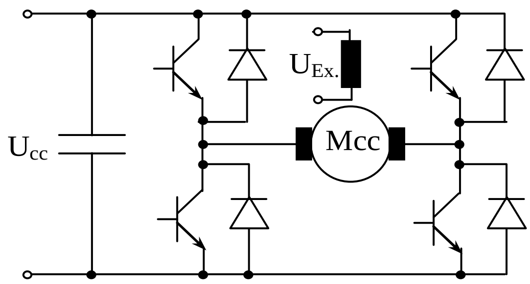

Fig.6 Artificial loading with DC machine by using 4Q chopper

4. EXPERIMENTAL RESULTS

The test machine was an induction motor with the following rated values: shaft power P_N = 2,2 kW, voltage U_N = 380 V, speed n_N = 1420 rpm, current I_N = 4,7 A, stator winding resistance R_1 = 2,75 Ω, rotor winding R_2 = 2,1 Ω at 20°C and R_1 = 3,7 Ω, R_2 = 2,85 Ω at 90°C. The temperature of the stator winding was measured using electrical sounders.

In table I we present the variation of the loading current, average speed, voltage and efficiency as a function of the source's frequency.

Table I

Frequency [Hz]	Average speed [rpm]	Voltage U[V]	Loading current I[A]	Efficiency [%]
45	1445	377,6	4,75	84,9
46	1450	378,2	4,73	85,2
47	1447	378,6	4,77	85,4
48	1453	379,1	4,8	85,6
49	1441	379,5	4,66	85,9
50	1420	380	4,68	86,2
51	1418	379,9	4,72	86,15
52	1425	380,2	4,71	86,0
53	1433	380,1	4,73	85,9
54	1435	380,3	4,74	85,7
55	1438	380	4,725	85,1

The final over-temperature on artificial loading was higher than for shaft loading and sinus supply by about 5°C (10 %) for windings and about 6°C (12 %) for core. The voltage supply from inverter source contains high harmonics which are increasing the core losses and copper losses.

The main problem indentified during the experimental port was the need for a closed-loop control to maintain the constant ratings on the test motor and the matching power exchanged with the recovery system.

Further this, the variation of efficiency with auxiliary frequency is only small, namely 1% as shown in Table I. The friction and winding losses will only be marginally higher since the average speed during synthetic loading is near to the rated speed.

5. CONCLUSION

The artificial on-load testing of the rotating electric machines is a modern solution for the simple verification, low-cost, of parameters and characteristics. In the specialty literature is insisted more on testing the induction machines, but of great interest becomes the testing of the synchronous machines and DC machines, including the ones where the inductor field is produced with permanent magnets.

Synthetic loading, the two frequency method, dynamic thermal loading and the constant speed methods of evaluating the efficiency of electric machines has been confirmed, using computer modeling and simulation techniques, as accurate, and able to indentify the total losses in the machine under test. Experimental results agree with the modeled synthetic loading and measured steady-state efficiencies.

REFERENCES

[1.] I. Boldea, L. Tutelea and Klumpner C., "Artificial loading of induction machines: a review", Workshop on Electrical Machine's Parameters, Technical University of Cluj-Napoca, 26th of May, 2001, pp. 9-14.
[2.] D.J. McKinnon and C. Grantham, "Experimental Confirmation of On-Site Efficiency Evaluation of Three-Phase Induction Motors using Synthetic Loading Techniques", Australasian Universities Power Engineering Conference AUPEC 2004, 26-29 September 2004, Brisbane, Australia, pp. 78-83.
[3.] D. McKinnon, D. Seyoum and C. Grantham, "Novel dynamic model for a three-phase induction motor with iron loss and variable rotor parameter considerations", Journal of Electrical & Electronics Engineering, Australia, Vol. 22, No. 3, The Engineers Australia College of Electrical Engineers, 2003, pp. 219 - 225.
[4.] D.J. McKinnon, D. Seyoum and C. Grantham, "Investigation of parameter characteristics for induction machine analysis and control", Conf. Proc. Of the Second International Conference on Power Electronics, Machines and Drives, (PEMD 2004), Universityof Edinburgh, UK, 31 Mar. – 2 Apr. 2004, pp. 320-325.
[5.] A. Ytterberg, "Ny method for fullbelasstning av electrisca maschiner utan drivmotor eler avlastningsmaskin", s.k. skakprov, Teknisktidskrift, 1921, S42-44.
[6.] P. Templin, M. Alacula, M. Gertmar, "Dynamic Thermal Loading of an inverter fed Induction Machine", IEEE /KTH Stocckhlom Power Tech. Conference, 1995, pp. 241-244.
[7.] P. Lesage, M. Alacula, L. Gertmar, "The dynamic thermal loading of an induction machine", Record ENE'97 vol.2 pp. 520-525.
[8.] C. Klumpner, I. Boldea, F. Blaabjerg, "Artificial loading of the induction motors using a matrix converter", Proceedings of PEMD London 2000, pp. 40-45.
[9.] C. Grantham and M. Sheng, "The synthetic loading of three-phase induction motors using microprocessor controlled power electronics", Record IEEE Catalogue No. 95TH8025/1995, pp. 471-476.
[10.] D.J. McKinnon and C. Grantham, "Modeling of synthetic loading for efficiency evaluation of three-phase induction motors", Proc. AUPEC 2003, Christchurch, New Zeeland, 28 Sept. – 1 Oct. 2003.
[11.] C. Grantham, "Full load testing of three phase induction motors without the use of a dynamometer" ICEMA, 14-16 September 1993 Adelaide Australia, pp. 147-152.
[12.] S. Garvey, I. Kolak and M.T. Wright, "Aspect of mixed frequency testing for induction machines", Record of ICEM-1994, D14, Paris, France.
[13.] I. Boldea, L. Tutelea and N. Muntean, "A new approach to inverter-fed mixed frequency testing of induction machines", Proc. Electromotion'97, Cluj-Napoca, Romania, pp. 82-87.
[14.] L. Tutelea, I. Boldea, E. Ritchie, P. Sandholdt and F. Blaabjerg, "Thermal testing for inverter-fed induction machines using mixed frequency method", Proceedings of ICEM'98 Istanbul, vol.1, pp.248-253.
[15.] M. Biriescu, "Testing elements of electric machines", Politechnica Publishing House, Timisoara, Romania, 1994 (in Romanian).
[16.] S.I. Deaconu, G.N. Popa and L. Gherman, "Diagram for artificial charge loading of asynchronous machine and the study of the influence of the frequency change on the charge loading", Buletin of Politechnic Institute of Iasi, Tom XLVIII, Fasc. 5, 2002, pp. 127-130.
[17.] J. Soltani, B. Szabados, and Gerry Hoolboom, "A New Synthetic Loading for Large Induction Machines With No Feedback Into the Power System" IEEE Transactions on Energy Conversion, Vol. 17, No. 3, September, 2002, pp. 1-7.

INTERNATIONAL SYMPOSIUM on
ADVANCED ENGINEERING & APPLIED MANAGEMENT
– 40th ANNIVERSARY in HIGHER EDUCATION (1970-2010)
4 – 5 November, 2010, Hunedoara, ROMANIA

[1.] Gyula MESTER

CONTRIBUTION TO THE SIMULATION OF BIPED ROBOT USING 19-DOF

[1.] UNIVERSITY OF SZEGED, DEPARTMENT OF INFORMATICS, ROBOTICS LABORATORY, SZEGED, HUNGARY

ABSTRACT:
This paper presents contribution to the simulation of biped robot Kondo robot KHR-1HV using 19-DOF. Studies in the area of humanoid robotics have recently made a remarkable progress. The modeling of the Kondo KHR-1HV humanoid robot motion is analyzed. A kinematic scheme of a 19-DOF biped locomotion system is used in simulation. The simulation results in the Matlab /Simulink and Robotics Toolbox for Matlab/Simulink environment show the validity of the proposed method.
KEYWORDS: Modeling, dynamic model, Lagrangian dynamics simulation, biped locomotion, humanoid robot motion, Kondo robot KHR-1HV, 19-DOF, rigid segments, joints, bipedal walking, locomotion mechanism

1. INTRODUCTION

In recent years, there has been a growing interest in modeling, simulation and control of the humanoid robot motion. Currently many researches in robotics are dealing with different problems of humanoid robot motion. This paper deals with the simulation of biped robot Kondo robot KHR-1HV using 19-DOF.

The modeling of the Kondo humanoid robot motion is analyzed. The problem of bipedal motion is a very complex task. Studies in the area of humanoid robotics have recently made a remarkable progress.

The considered humanoid locomotion in this paper has 19-DOF. The simulation results in the Matlab/Simulink and Robotics Toolbox for Matlab/Simulink environment show the validity of the proposed method. The paper is organized as follows:

The paper is organized as follows:

- Section 1: Introduction.
- In Section 2 modeling of the Kondo robot motion is proposed.
- In Section 3 the simulation results of the Kondo humanoid robot motion are illustrated.
- Conclusions are given in Section 4.

2. MODELING OF THE KONDO ROBOT MOTION

The Kondo KHR-1HV humanoid robot's body consists of a number of rigid segments interconnected with joints. During the bipedal walking, some kinematic chains in their interaction with the unknown environment transform from open to closed type of kinematic chain.

The dynamic model of the locomotion mechanism of the robot in a vector form is:

$$\mathbf{H}(\mathbf{q})\ddot{\mathbf{q}} + \mathbf{h}(\mathbf{q},\dot{\mathbf{q}}) = \boldsymbol{\tau} + \mathbf{J}^T(\mathbf{q})\mathbf{F} \tag{1}$$

where:

H(q) – is the inertia matrix of the mechanism,
h – is the vector of centrifugal, Coriolis and gravitational moments,
J(q) – is the Jacobian matrix of the system,
q – is the vector of the internal coordinates,
F – is the vector of external forces and moments,
τ – is the vector of the driving torques at the robot joints.

Biped locomotion of humanoid robots is a very complex process to modeling. The bipedal walking of the robot consists of several phases that are periodically repeated: single-support phases and double-support phases.

The dynamics of the locomotion mechanism can be expressed by the Lagrangian dynamics. Computed Torque Control method is applied for control of the humanoid robot motion. The widely-known method to generate a stable trajectory for a biped robot is based on the Zero-Moment-Point (ZMP) equation. The concept of Zero-Moment-Point was first introduced by Miomir Vukobratovic and has an essential role both in scientific research and practical applications of bipedal motion of humanoid robots. The Zero-Moment-Point is the center of pressure at the feet on the ground, and the moment applied by the ground about the ZMP is zero.

The considered humanoid locomotion mechanism used in simulation in this paper has 19-DOF. The scheme of a 19-DOF biped locomotion system, masses and dimensions of the biped Kondo KHR-1HV humanoid robot is presented in Fig. 1.

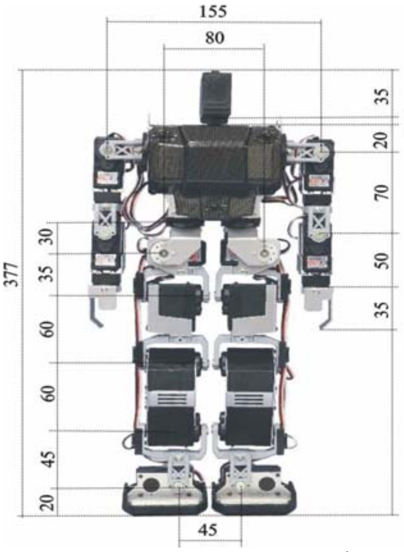

Part	Body measures length [m]	mass [kg]
head	0.035	0.052
torso	0.11	0.678
single leg	0.22	0.264
single arm	0.155	0.126
whole body	0.377	1.51

Link	mass [kg]	Moments of inertia [kg m^2] sagital axis (Ix)	lateral axis (Iy)	vertical axis (Iz)
head	0.052	0.0704X10^(-4)	0.1224X10^(-4)	0.0867X10^(-4)
torso	0.678	0.0007	0.0005	0.0011
upper arm	0.062	0.1244X10^(-4)	0.1764X10^(-4)	0.0867X10^(-4)
forearm	0.06	0.0704X10^(-4)	0.1224X10^(-4)	0.0867X10^(-4)
hand	0.004	0.1225X10^(-5)	0.1225X10^(-5)	0.0100X10^(-5)
thigh	0.07	0.4164X10^(-4)	0.3807X10^(-4)	0.0704X10^(-4)
shank	0.116	0.5178X10^(-4)	0.4983X10^(-4)	0.2448X10^(-4)
foot	0.078	0.1395X10^(-4)	0.3473X10^(-4)	0.3142X10^(-4)

Fig.1. The Kondo KHR-1HV humanoid robot

3. SIMULATION RESULTS OF THE KONDO HUMANOID ROBOT MOTION

Simulation experiments are commonly used for the initial system analysis and control design while the experimental scalable tested system has to be used in the final phase of system evaluation and control verification. The obtained results and control architecture can be afterwards adapted to the different application of mobile robots. Based on this, the important task in system development is accurate and valuable modeling of the observed system.

Simulation of the humanoid robot motion was performed using Matlab/Simulink and Robotics toolbox for Matlab/Simulink. In the simulation the biped robot walks on a flat horizontal plane. The simulation time is 3 s. The results of the simulation of Kondo robot motion are shown in Fig. 2-6.

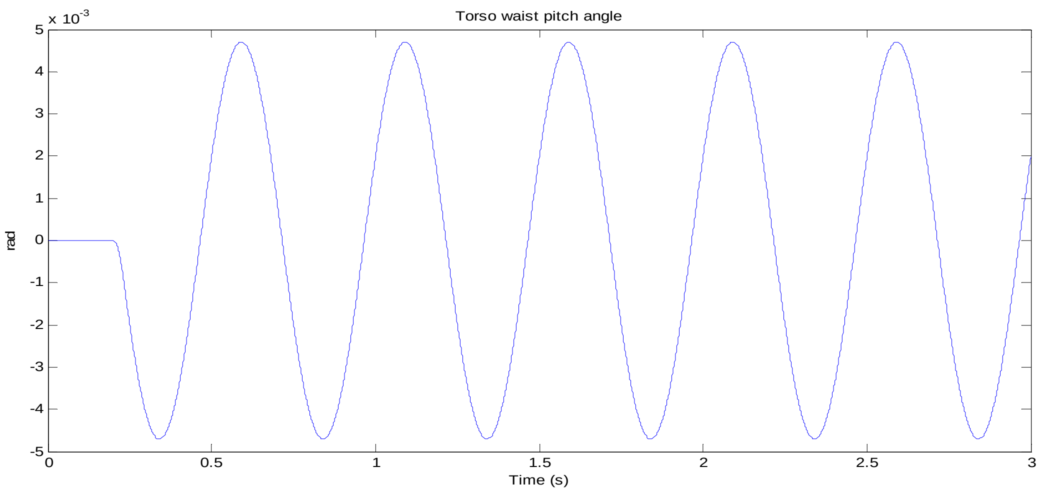

Fig.2. Torso waist pitch angle

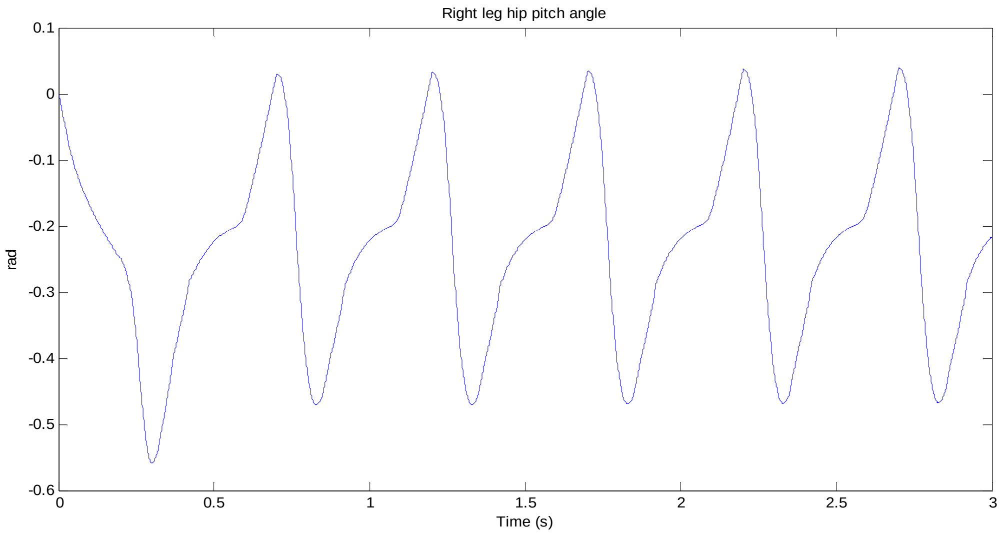

Fig.3. Right leg hip pitch angle

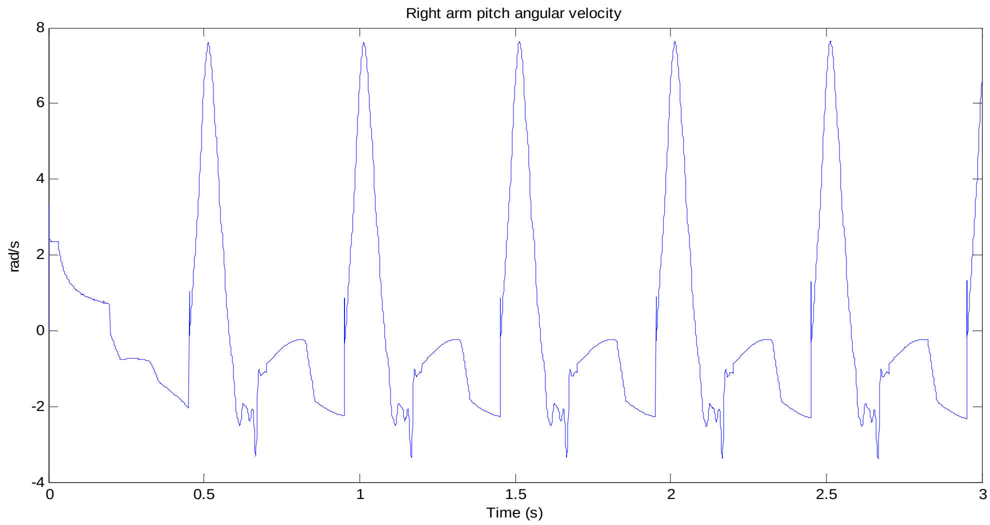

Fig.4. Right arm pitch angular velocity

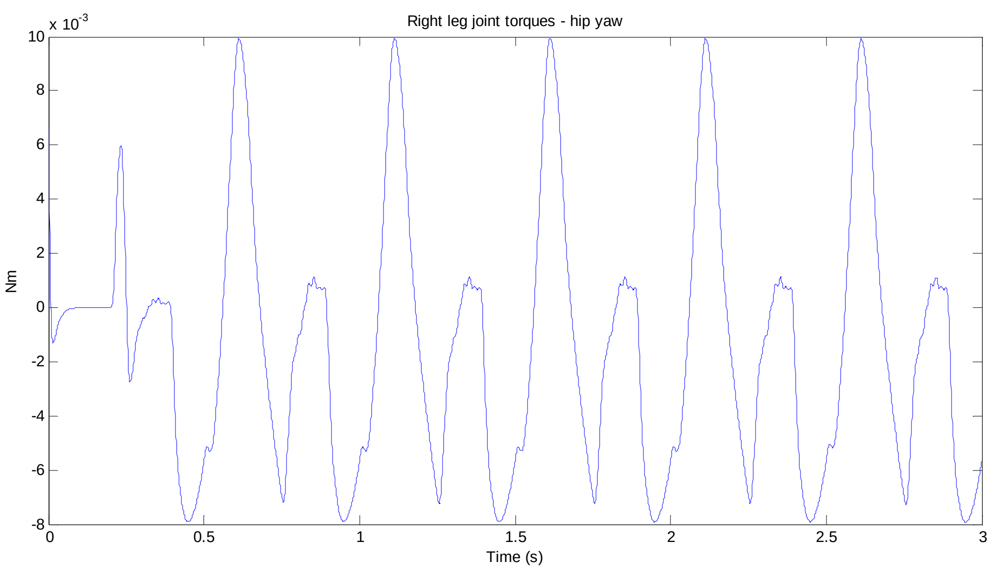

Fig.5. Right leg joint torques – hip yaw

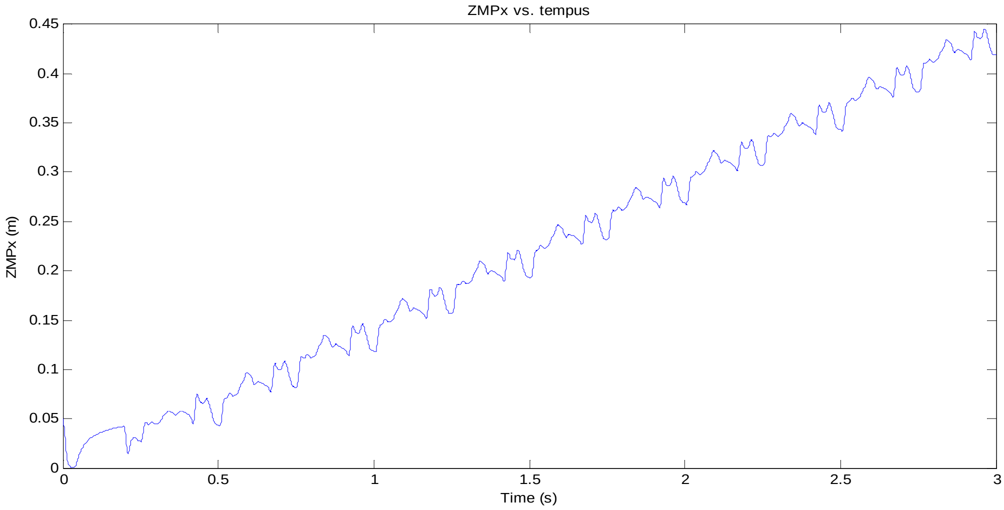

Fig.6. ZMP x trajectory

4. CONCLUSION

This paper will deal with the modeling and simulation of the autonomous motion of KONDO KHR-1HV humanoid robots. A scheme of a 19-DOF biped locomotion mechanism of the anthropomorphic structure is used. The simulation results in the Matlab/Simulink and Robotics Toolbox for Matlab/Simulink environment show the validity of the proposed method.

REFERENCES

[1.] Vukobratović M. et al., Biped Locomotion-Dynamics, Stability, Control and Application, Springer Verlag, Berlin, Germany, 1990.

[2.] S. Kajita, K. Tani, Experimental study of biped dynamic walking in the linear inverted pendulum mode. Proceedings of the IEEE International Conference on Robotics and Automation, pp. 2885-289,1Nagoya, Japan, 1995.

[3.] J. H. Park, K. D. Kim (1998) Biped robot walking using gravity-compensated inverted pendulum mode and computed torque control. Proceedings of the IEEE International Conference on Robotics and Automation, Leuven, Belgium, 1998.

[4.] T. Furuta et al., Design and construction of a series of compact humanoid robots and development of biped walk control strategies. Robotics and Autonomous Systems, pp. 81-100, 2001.

[5.] A.Rodić, D.Katić, M.Vukobratović," The Connectionist Compensator for Advanced Integrated Road Vehicle Controller", International Journal Engineering & Automation Problems, vol..2, no.1, pp.27-39, 2001.

[6.] A.Rodić, D.Katić, M.Vukobratović,"The Connectionist Compensator for Advanced Integrated Vehicle", Proceedings of the IEEE International Conference on Control Applications, Mexico City, Mexico, September 2001.

[7.] A.Rodić, D.Katić, M.Vukobratović, "The Neural Compensator for Advanced Vehicle Controller", Proceedings of the 6. Workshop Application of Neural Networks in Electrotehnics - NEUREL'02, Belgrade, Yugoslavia, September 2002.

[8.] D.Katić, A.Rodić, "Neural Control Techniques For Humanoid Robots", Proceedings of the 47. ETRAN Conference, Herceg-Novi , Serbia & Montenegro , June 2003, vol. 4, pp..386-389.

[9.] A.Rodić, M. Vukobratović, M. Filipović, D. Katić, " Modellling and Simulation of Locomotion Mechnanisms of Antropomorphic Structure Using Contemporary software tools", ", Proceedings of the 47. ETRAN Conference, Herceg-Novi, Serbia & Montenegro, June 2003, Vol.4, pp.347-350.

[10.] A.Rodić, D.Katić, M.Vukobratović," The Advanced Vehicle Control Algorithm Using Neural Networks", Proceedings of the European Control Conference ECC 2003., Cambridge,UK, September 2003.

[11.] J. H. Park, Fuzzy-Logic Zero-Moment-Point Trajectory Generation for Reduced Trunk Motions of Biped Robots. Fuzzy Sets and Systems 134, pp. 189-203, 2003.

[12.] Vukobratović M., Rodić A.: Contribution to the Integrated Control of Artifical Human Gait. Proceedings of the SISY 2004, Symposium on Intelligent Systems, Subotica, Serbia, pp. 59-70, 2004.

[13.] Vukobratović M, Potkonjak V, Rodić A (2004) Contribution to the Dynamic Study of Humanoid Robots Interacting with Dynamic Environment. Robotica. Vol. 22, pp. 439-447

[14.] M.Filipović, A.Rodić, D.Katić, " An Analysis of Movement of Elastic Robotic System under the influence of environment dynamics", Proceedings of 29. HIPNEF 2004, Vranjačka Banja, Serbia & Montenegro, May 2004.pp.385-390.

[15.] M.Filipović, D.Katić, A.Rodić, " An Analysis of Movement of the Flexible Robotic System in Horizontal Plane", Proceedings of the 7th DQM-2002 Dependability and Quality Management, Belgrade, Serbia & Montenegro, June 2004.
[16.] M. Vukobratovic, V. Potkonjak, A. Rodic, "Contribution to the Dynamic Study of Humanoid Robots Interacting with Dynamic Environment", Robotica, CAMBRIDGE university press, United Kingdom, Vol. 22, pp. 439-447, 2004
[17.] A. Rodić, D. Katić, "Intelligent Control of Road Vehicles by Implementation of Artificial neural Networks", Technics-Mechanic Engineering, No. 5/04, pp. 1-12, in Serbian, 2004
[18.] M. Filipović, A. Rodić, D. Katić, "Motion Analysis of Elastic Robotic Systems Under Influence of Dynamic Environment", Proceedings of 29th szmposium HIPNEF 2004, pp.385-390, Vrnjačka Banja, Serbia, May, 2004
[19.] M. Filipović, D. Katić, A. Rodić, " Motion Analysis of Elastic Robotic Systems in Horizontal plane", Proceedings of the 7th DQM-2004 Dependability and Quality Management, Belgrade, Serbia & Montenegro, June, 2004
[20.] M. Vukobratović, A. Rodić, "Contribution to the Integrated Control of Artificial Human Gait", Proceedings of 2nd Serbian-Hungarian Joint Symposium on Intelligent Systems, SISY 2004, pp. 59-70, Subotica, Serbia & Montenegro, 2004
[21.] Metta G, Sandini G, et. all (2005) The RobotCub Project – an open framework for research in embodied cognition. Proc. of the 2005 IEEE-RAS Int. Conf. On Humanoid Robots
[22.] K. Addi, D. Goeleven, A. Rodic, "Nonsmooth Mathematical Modelling and Numerical Simulation of a Spatial Vehicle Dynamics", *Zeitschrift für Angewandte Mathematik und Mechanik (ZAMM)*, Wiley-VCH Verlag GmbH & Co. KGaA - Weinheim, DOI 10.1002/zamm.200410235, pp. 1-25 (2005)
[23.] A. Rodić, D. Katić, M. Filipović, "Control of Dynamic Balance and Trunk Posture of Humanoid Robots in Service Tasks", in Proceedings of 49th Conference on ETRAN, Vol. IV, pp. 347-350, Serbia & Montenegro, Budva, 2005
[24.] Rodić A, Vukobratović M (2006) Control of Dynamic Balance of Biped Locomotion Mechanisms in Service Tasks Requiring Appropriate Trunk Postures. Engineering & Automation Problems. ISSN 0234-6206, Vol. 5, No. 1, pp. 4-22.
[25.] D. Katić, A. Rodić, "Control Algorithm for Humanoid Robots Walking Based on Learning Structures", in Proceedings of 49th Conference on ETRAN, Vol. IV, pp. 355-358, Serbia & Montenegro, Budva, 2005
[26.] A. Rodić, M. Vukobratović, "Intelligent Integrated Control of Vehicle Stability Characteristics", in Proceedings of EAEC2005 European Automotive Congress, Serbia & Montenegro, Belgrade, June, 2005
[27.] A. Rodić, E. Schnieder, "Hybrid Model-Based – Knowledge-Based Control of Driver-Vehicle System Performances", in Proceedings of EAEC2005 European Automotive Congress, Serbia & Montenegro, Belgrade, 2005
[28.] A. Rodić, "User Oriented Software Toolbox for Advance Modeling, Control Synthesis and Simulation of Automotive Systems", in Proceedings of EAEC2005 European Automotive Congress, Serbia & Montenegro, Belgrade, June, 2005
[29.] A. Rodić, K. Addi, G. Dalleau, "Contribution to the Mathematical Modeling of Multi-point, Non-smooth Impact/Contact Dynamics of Human Gait", in Programe resume of the 6th International Conference AIMS 2006 "Dynamic Systems, Differential equations and Applications", pp. 101-102, University Poitiers, Poitiers, France, 2006
[30.] K. Addi, G. Dalleau, A. Rodic, "Linear Complementarity Problem Formulation Used for Modeling of Impact/Contact Dynamics of Byped Locomotion Mechanisms", in Proceedings of ETRAN 2006, Belgrade, Serbia, 2006
[31.] A. Rodic, M. Vukobratovic "Multi-feedback Dynamic Control of Byped Robots", in Proceedings of ETRAN 2006, Belgrade, Serbia, June, 2006
[32.] Katić D, Rodić A, Vukobratović M (2007) Reinforcement Learning Control Algorithm for Humanoid Robot Walking. International Journal of Information & Systems Sciences. Vol.4, No.2, pp.256-267
[33.] Vukobratović M, Rodić A (2007) Contribution to the Integrated Control of Biped Locomotion Mechanisms. International Journal of Humanoid Robotics. World Scientific Publishing Company. New Jersey, London, Singapore. Vol. 4, No. 1, pp. 49-95
[34.] Gyula Mester: „ Bipedal Walking in Robots", Proceedings of the IV. Európai kihivások nemzetközi konferencia, pp. 703-707, Szeged, Hungary, 2007.
[35.] A. Rodić, "Towards Sustainable Transport and Active Traffic Safety – Synthesis of Hazard Prevention Control System based on Modeling of Cognitive Driver Behavior", UNESCO Program – Education for All by 2015, 11th Education and Training Workshop, Belgrade, Serbia, 22th – 28th October, 2007
[36.] Gyula Mester, „Lépegető humanoid robotok mozgástervezése", MTA, VMTT konferencia, pp.267-273, Novi Sad, Serbia, 2007.
[37.] Gyula Mester, „Dynamic Modeling for a Walking Robot", Proceedings of the SIP 2008, 26th International Conference SCIENCE IN PRACTICE, pp.87-89, ISBN 978-953-6032-52-4, Osijek, Croatia, 2008.
[38.] Mester Gyula, „Kétlábon járó robot modellezése", Informatika a felsőoktatásban 2008, Konferencia kiadvány, pp. 1-8, ISBN 978-963-473-129-0, Debrecen, 2008.
[39.] Gyula Mester, „Simulation of Humanoid Robot Motion", Proceedings of The KANDÓ CONFERENCE, pp. 1-8, ISBN 978-963-7154-74-4, Budapest, 2008.

[40.] Rodić A, Vukobratović M, Addi K, Dalleau G (2008) Contribution to the Modeling of Non-smooth, Multi-point Contact Dynamics of Biped Locomotion – Theory and Experiments., Robotica. CAMBRIDGE Univ. Press. Vol. 26, Issue, 02, pp. 157-175

[41.] Katić D, Rodić A, Vukobratović M (2008) Hybrid Dynamic Control Algorithm For Humanoid Robots Based On Reinforcement Learning. Springer Journal of Intelligent and Robotic Systems. No.1, pp.3-30

[42.] D. Katić, A. Rodić, "Intelligent Autonomous Locomotion of Humanoid Robots through Perception, Learning and Spatial Reasoning", in Proceedings of the ETRAN 2008, Subotica, Serbia, June, 2008

[43.] A. Rodić, V. Potkonjak, "Towards Advanced Personal Robot Platform – Concept of Intelligent Service Robot of High Performances", in Proceedings of the ETRAN 2008, Subotica, Serbia, June, 2008

[44.] A. Rodić, D. Katić, "Trajectory Prediction and Path Planning of Autonomous Biped Robots – Learning Locomotion and Fuzzy Reasoning", in Proceedings of the 9th Symposium on Netwotk Applications in Electrical Engineering, Electrotechnic Faculty, Belgrade, Serbia, September, 25-27, 2008

[45.] D.Katić, A.Rodić, "Dynamic Control Algorithm for Biped Walking Based on Policy Gradient Fuzzy Reinforcement Learning", in Prioceedings of the 17th IFAC World Congress, Seoul, Republic of Corea, July 2008.

[46.] D. Katić, A. Rodić, "Intelligent Autonomous Locomotion of Humanoid Robots through Perception, Learning and Spatial Reasoning", in Proceedings of the ETRAN 2008, Subotica, Serbia, June, 2008

[47.] D.Katic, A.Rodic, M.Vukobratovic," Reinforcement Learning Control Algorithm for Humanoid Robot Walking ", International Journal of Information & Systems Sciences, Vol.4, No.2, pp.256-267, 2008.

[48.] A. Rodić, D. Katić, "Trajectory Prediction and Path Planning of Autonomous Biped Robots – Learning Locomotion and Fuzzy Reasoning", in Proceedings of the 9th Symposium on Netwotk Applications in Electrical Engineering, Electrotechnic Faculty, Belgrade, Serbia, September, 193-197, 2008

[49.] D.Katic, A.Rodic, M.Vukobratovic, "Hybrid Dynamic Control Algorithm For Humanoid Robots Based On Reinforcement Learning" ,Journal of Intelligent and Robotic Systems, vol.51,No.1,pp.3-30, January 2008,

[50.] Siciliano, Khatib editors, Springer Handbook of Robotics, Springer-Verlag Berlin Heidelberg, 2008.

[51.] Gyula Mester, Aleksandar Rodic, "Autonomous Locomotion of Humanoid Robots in Presence of Mobile and Immobile Obstacles", Studies in Computational Intelligence, Towards Intelligent Engineering and Information Technology, pp. 279-293, ISBN 978-1-642-03736-8, Library of Congress: 2009933683, DOI 10.1007/978-3-642-03737-5-_20, Springer, 2009.

[52.] Aleksandar Rodić, Dusko Katić, Gyula Mester, "Ambient Intelligent Robot-Sensor Networks for Environmental Surveillance and Remote Sensing", Proceedings of the IEEE SISY 2009, pp. 39-44, IEEE Catalog Number: CFP0984C-CDR, ISBN: 978-1-4244-5349-8 Library of Congress: 2009909575, DOI 10.1109/SISY.2009.5291141, Subotica, Serbia, 2009.

[53.] Web-page (2009) http://world.honda.com/ASIMO/

[54.] Web-page (2009) http://jp.fujitsu.com/group/labs/downloads/en/business/activities/actties-4/fujitsu-labs-robotics-005-en.pdf

[55.] Web-page (2009) http://www.sony.net/SonyInfo/News/Press_Archive/200312/03-060E/

[56.] Rodic A (2009) Humanoid Robot Simulation Platform – HRSP. Matlab/Simulink Software Toolbox for Modeling, Simulation & Control of Biped Robots. Robotics Lab. Mihajlo Pupin Institute. http://www.institutepupin.com/ RnDProfile/ ROBOTIKA/comprod.htm.

INTERNATIONAL SYMPOSIUM on
ADVANCED ENGINEERING & APPLIED MANAGEMENT
– 40th ANNIVERSARY in HIGHER EDUCATION (1970-2010)
4 – 5 November, 2010, Hunedoara, ROMANIA

[1.]Angela IAGĂR, [2.]Gabriel Nicolae POPA, [3.]Corina Maria DINIŞ

STUDY UPON THE THERMAL FIELD FROM A RESISTANCE OVEN

[1-3]POLITECHNICA UNIVERSITY TIMIŞOARA, FACULTY OF ENGINEERING HUNEDOARA, ROMANIA

ABSTRACT:
This work presents a study of the thermal field from an indirect resistance oven. Temperature acquisition was achieved with a Conrad Electronic data acquisition board and 8 integrated temperature sensors LM35DH. The utilized software, Ser10bit, allowed the data saving both as list of values and multi-graphics, for being further processed.
It's been analyzed the influence upon the thermal regime of the oven by its operation steps and heating period.
KEYWORDS:
indirect resistance oven, data acquisition system, thermal field

1. INTRODUCTION

The most used temperature sensors are currently the thermo-resistances, thermistors, thermocouples and integrated sensors.

For the temperature sensors, very important are the following features: sensitivity, reproductibility, low response time, linearity on an increasing range, rapid and easy mounting and inter-changeability [1-4].

In order to chose correctly the temperature sensor, should be analyzed: the temperature range in which it should operate, response time, sensitivity, precision for establishing the temperature, maximum temperature to which the sensors will be submitted, utilization time, if the determination is made with or without contact and, not the last, the costs, which are directly proportional with the sensor's precision and with its mounting mode [4, 7, 9].

The integrated temperature sensors (or IC - Integrated Circuit sensors) are precision ones, and easy to calibrate, being much used in digital applications for temperature measuring and control, because they produce an output signal proportional with temperature [1, 2].

The temperature sensors with semi-conductors have a high level of the output signal, but they cover a relatively limited temperature range [1, 2].

2. TEMPERATURE ACQUISITION SYSTEM FROM THE RESISTANCE OVEN

The temperature sensors used within experiments where of LM35DH type, in TO-46 capsule.

LM35DH is a very precise integrated sensor, of which output voltage varies linearly with the temperature measured in Celsius degrees, within -60°C and +180°C; the sensor's sensitivity is 10 mV/°C. Is supplied by a continuous voltage within 4…30 V, the current absorbed being below 60 μA.

The temperature sensors from the LM35 series don't need external calibration or adjustment to ensure a typical precision of ±1/4°C at the chamber's temperature and ±3/4°C within the temperature range −55…+150°C. The same sensors have low output impedance (0,1 W for a load current of 1 mA), linear output, accurate calibration, and the interface to the reading or control circuits is achieved easily.

The output voltage expression is:

$$V_T = V_{T0} \cdot \frac{T}{T_0}, \tag{1}$$

where V_{To} is the output voltage at temperature T_o.

For measuring the temperature inside the resistance oven it was used a Conrad Electronic data acquisition board (fig. 1).

The module's supply can be achieved directly from PC (switch 82 Int) or externally from a 9 V d.c. source (switch 82 Ext by the supply between GND - ground and external UB +9 V).

Communication with the PC is made by serial interface, by duplex communication. Transmission is achieved on 16 bits out of which 12 are used for measuring, and 4 bits are used for the selected channel's address and the measurement type (unipolar or differential).

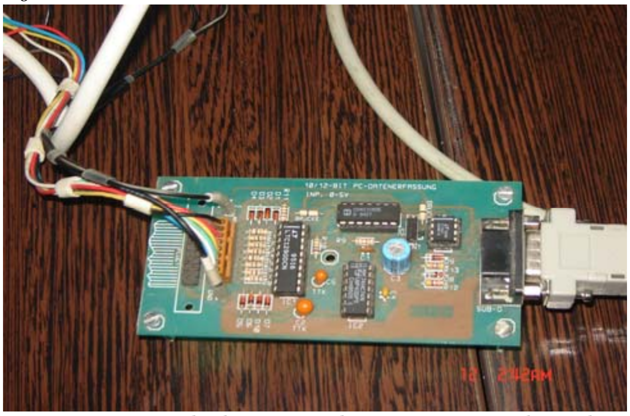

Fig. 1. Conrad Electronic data acquisition board

An analogue signal is unipolar at module's input, when the applied signal (within 0-5 V) is with the positive potential to a channel, and the negative potential is connected to ground. In this way can be measured 8 analogue signals.

An analogue signal is differential at module's input, when the signal is applied between two inputs (without using ground); in this way is measured the difference between the two signals. Thus, can be measured 4 analogue signals. The current absorbed by the module is 8mA to an impedance ≤1 kΩ.

The module's basic integrated circuit is LTC 1290 (CI l, 12-bit converter A/D, precision 0,02%), which, in principle, has two base blocks: a multiplexer with 8 analogue channels (CH0, CH1, ..., CH7) and a 12-bit analogue-digital converter (CAN). Each of these two modules has a register, which establishes for the multiplexer what channel to read, and for CAN allows the serial data transfer towards the PC. The transfer is achieved based on the successive approximation principle.

For operation, this circuit needs a supply source of proper precision and stability. In this purpose is used the integrated circuit LT 1021-5 (CI 4, with 0,05% accuracy) which is a precision stabilizer of 5 V.

Between the measurement part (the integrated circuit LTC 1290) and PC is ensured the separation of signals by means of the trigger-Schmitt inverter circuits (6 pcs.). These inverters are in the circuit 40106 (CI 3). The first inverter circuit (1-2) produces the tact of 300 Hz for the CAN's control, while the serial tact (shift clock) for introducing the command word and reading the measurement comes from PC.

Is used also a bi-stabile (of D-type) of CMOS type, high speed, from the circuit 74C74 (CI 2). This integrated circuit has two D-type bi-stabiles, out of which is used only one.

Within experiments, the acquisition board was connected to the serial interface RS 232 (with 9 poles) and by COM1 to a PC. The software used by PC was Ser10bit (achieved in Basic). Communication was achieved on the hexa-decimal addresses which are activated by the Basic INP and OUT controls.

The Ser10bit Program has a main menu with the following submenus:

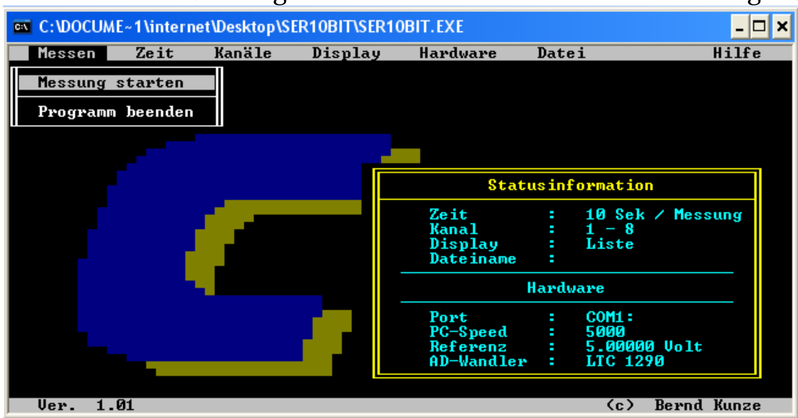

Submenu Measurements (Messen):
- Measurements achievement (Messung starten);
- Exit program (Program beenden).

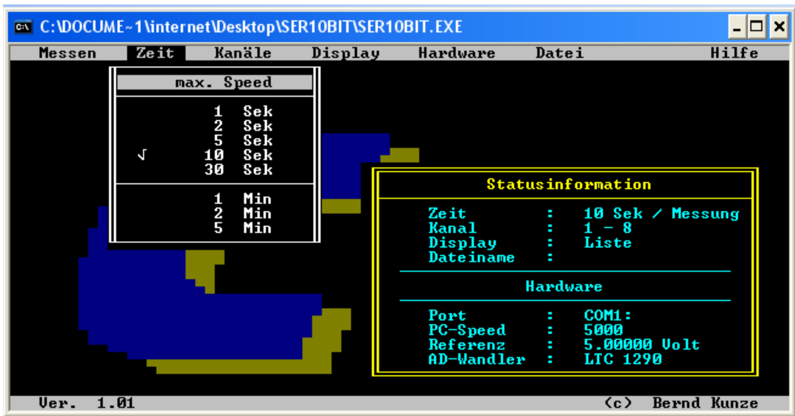

Submenu Sampling Speed (Zeit):

- maximum speed (max Speed);
- l s, 2 s, 5 s, 10 s, 30 s;
- l min, 2 min, 5 min.

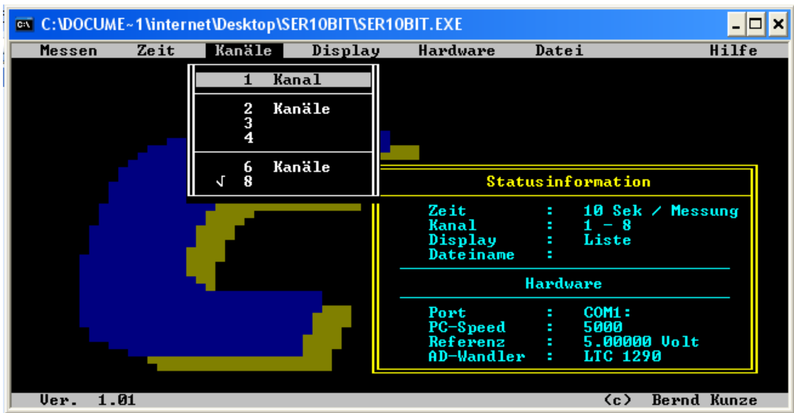

Submenu Number of Channels (Kanale):

-1, 2, 3, 4, 6, 8.

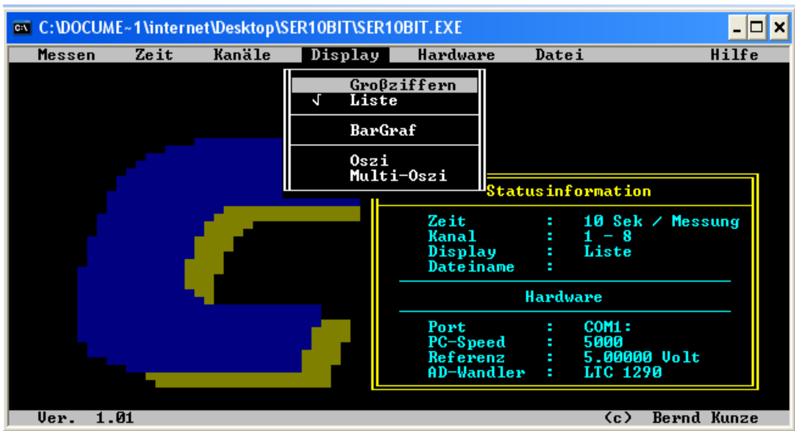

Submenu Display Mode (Display):

- Multimeter (Groβziffern);
- Values List (Liste);
- Voltmeter Bar (Bargraf);
- Graphic (Oszi);
- More graphics (Multioszi).

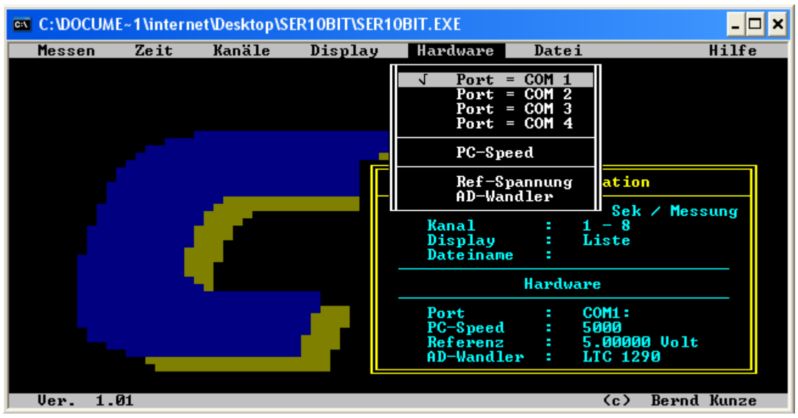

Submenu Hardware:

- COM 1, COM 2, COM 3, COM 4;
- PC speed (PC speed):0, 10, 20, 50, 100, 200, 500, 1000, 2000, 5000;
- reference voltage (Ref-Spannung) 5 V;
- CAN-type (AD-Wandler):
  LTC 1090 (conversion on 10 bit);
  LTC 1290 (conversion on 12 bit).

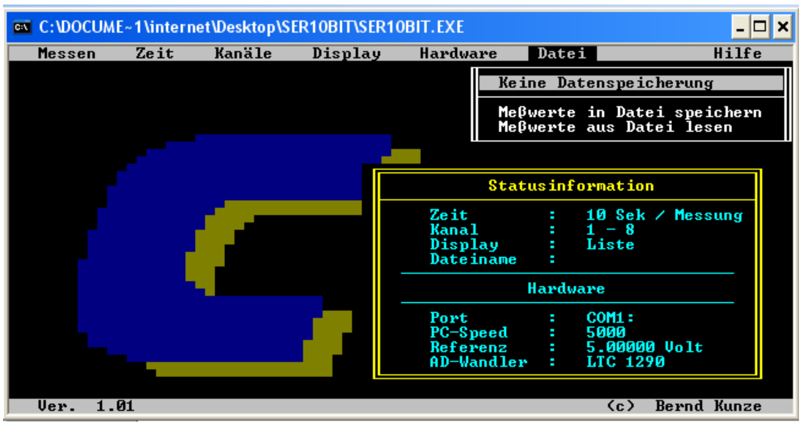

Submenu Data (Datei):
- No data (Keine Datenspeicherung);
- Creating a file for saving data (Meβwerte in Datei speichern);
- Opening a file already created (Meβwerte aus Datei lessen).

To the previously described submenus is added also the submenu **Help (Hilfe).** Passing from one submenu to another is achieved only with the arrows from the keyboard. The files' extension is of *.mwt type.

3. EXPERIMENTS

Within the experiments was used a resistance oven, model KWS1015J-FB, with rated power of 1000 W and capacity of 15 l (fig. 2).

The oven is provided with 4 stainless heating elements that ensure 3 operation steps: all heating elements (or up-down), two heating elements in the upper part, or two heating elements in the lower part.

The oven's walls are made by two metallic layers (steel) separated by an air layer. The temperature from the oven can be adjusted within 90 - 230°C, and the operation time can be adjusted within 0 – 60 minutes. The oven is supplied from the single-phased voltage grid (220 V, 50 Hz).

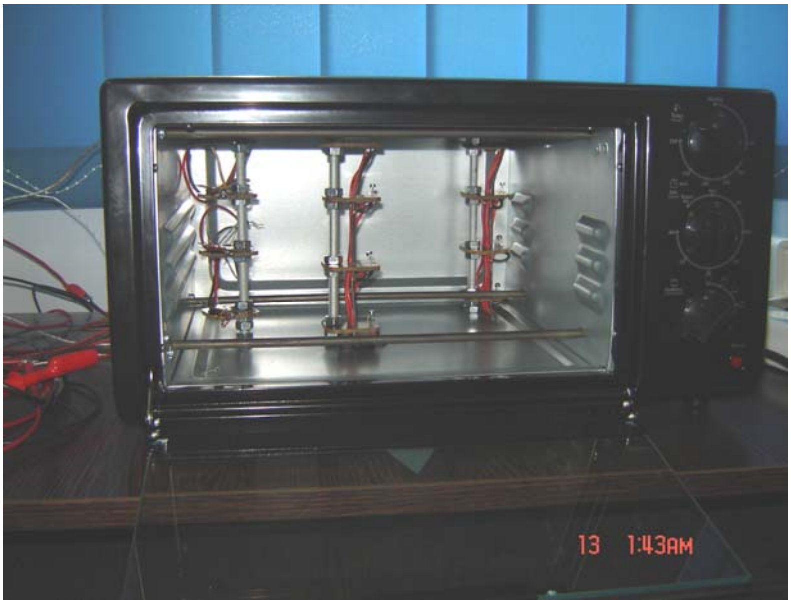

Fig. 2 Placing of the 8 sensors LM35DH inside the resistance oven

In fig. 2 is presented the location of the sensors LM35DH inside the resistance oven. For supplying the temperature sensors it was used a stabilized voltage source (0 – 20 V). Position of the temperature sensors LM35DH (measured against the oven's bottom) is shown in table 1.

Within the experiments, the data acquisition was achieved on 8 channels, with a sampling period of 10 seconds.

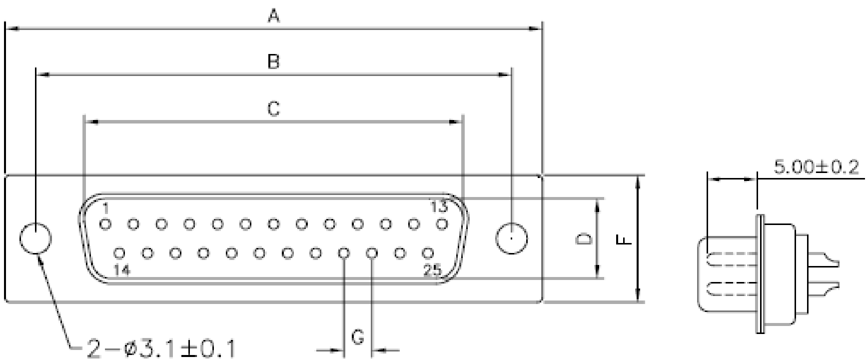

Fig. 3 Connector DB25.

Table 1 – Position of temperature sensors LM35DH

Temperature Sensor	LM35DH Sensor's position
Sensor no. 1	Right (h1=15,5 cm)
Sensor no. 2	Right (h2=11,5 cm)
Sensor no. 3	Right (h3=6,5 cm)
Sensor no. 4	Right (h4=1,5 cm)
Sensor no. 5	Right (h5=16 cm)
Sensor no. 6	Right (h6=12 cm)
Sensor no. 7	Right (h7=7 cm)
Sensor no. 8	Right (h8=2 cm)

Table 2 – Sensors location at connector DB25 and configuration of its pins

DB25 connector's pin	Pins' configuration
1, 2, 14	+5 V
12, 13, 25	GND
7	Sensor no. 8
8	Sensor no. 7
9	Sensor no. 6
10	Sensor no. 5
16	Sensor no. 1
17	Sensor no. 2
18	Sensor no. 3
19	Sensor no. 4

Table 3 – Pins' configuration on the strip from the data acquisition board

Strip's pin from the acquisition board	Acquisition board's channel	Temperature sensor
1	CH8	Sensor no. 1
2	CH7	Sensor no. 2
3	CH6	Sensor no. 3
4	CH5	Sensor no. 4
5	CH4	Sensor no. 5
6	CH3	Sensor no. 6
7	CH2	Sensor no. 7
8	CH1	Sensor no. 8
9	GND	

There have been analyzed the following cases:

a. oven supplied on step II (2 resistances up): initial temperature $\theta_i = 27°C$, adjusted temperature $\theta_r = 110°C$, heating period $t_i = 60$ *minutes*;

b. oven supplied on step I (2 resistances down): initial temperature $\theta_i = 27°C$, adjusted temperature $\theta_r = 110°C$, heating period $t_i = 60$ *minutes*;

c. oven supplied on step III (4 resistances up-down): initial temperature $\theta_i = 27°C$, adjusted temperature $\theta_r = 110°C$, heating period $t_i = 30$ *minutes*, cooling period $t_r = 54$ *minutes*.

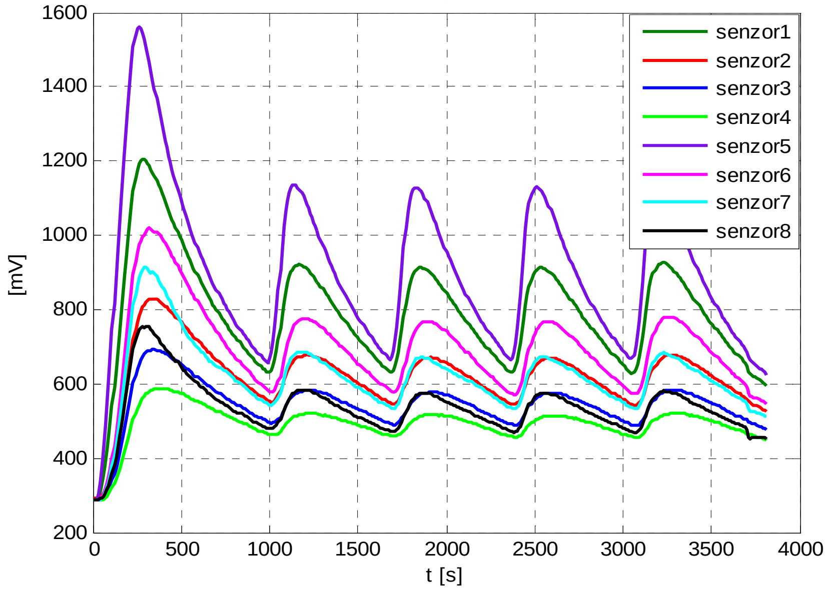

Fig. 4 Output voltages on sensors LM35DH in case a.
Oven supplied on step II (2 resistances up), $\theta_r = 110°C$, $\theta_i = 27°C$, $t_i = 60$ *min*.

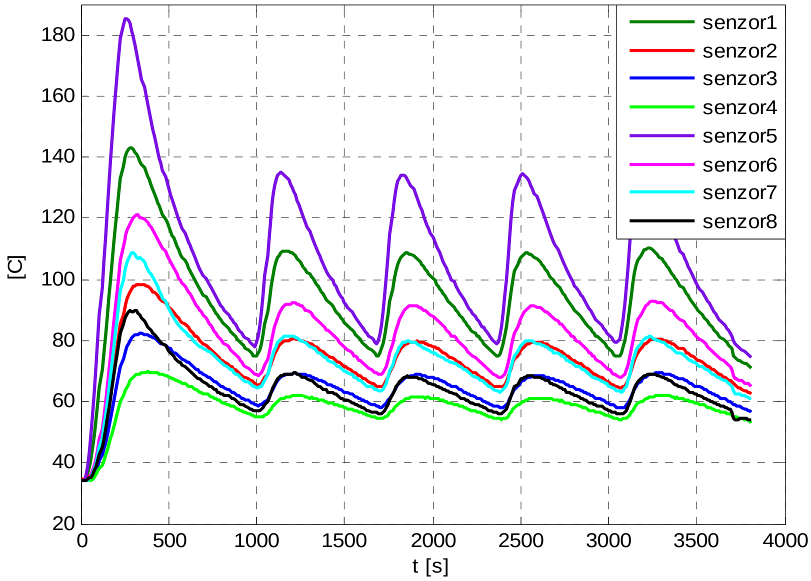

Fig. 5 Temperatures indicated by sensors LM35DH in case a. Oven supplied on step II (2 resistances up), $\theta_r = 110\,^\circ C$, $\theta_i = 27\,^\circ C$, $t_i = 60$ *min.*

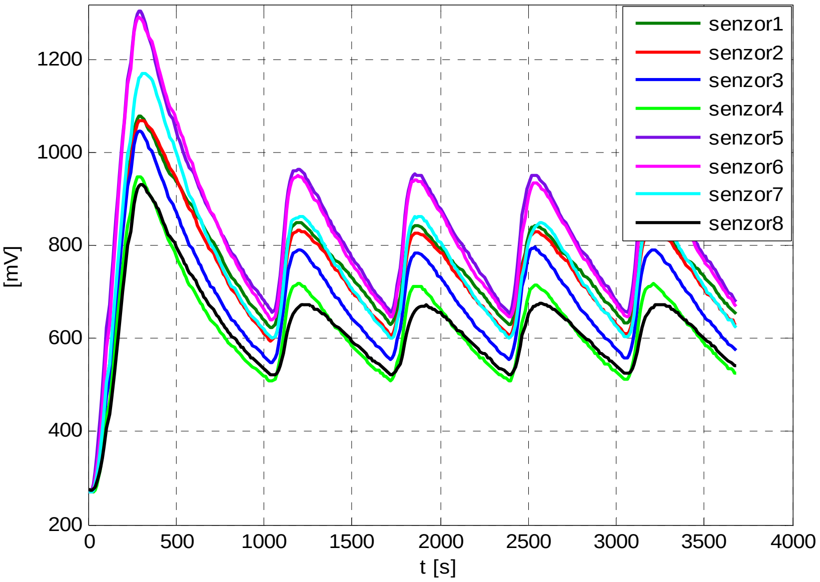

Fig. 6 Output voltages on sensors LM35DH in case b. Oven supplied on step I (2 resistances down), $\theta_r = 110\,^\circ C$, $\theta_i = 27\,^\circ C$, $t_i = 60$ *min.*

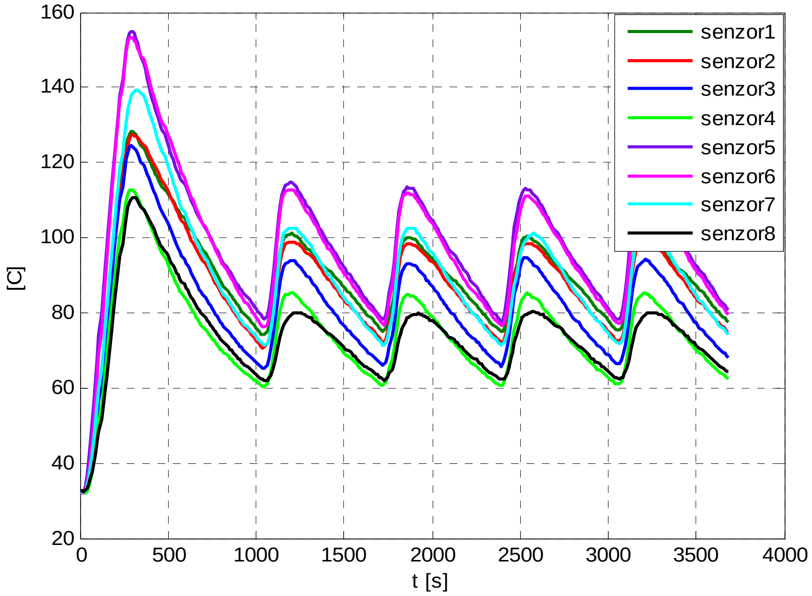

Fig. 7 Temperatures indicated by sensors LM35DH in case b. Oven supplied on step I (2 resistances down), $\theta_r = 110\,^\circ C$, $\theta_i = 27\,^\circ C$, $t_i = 60$ *min.*

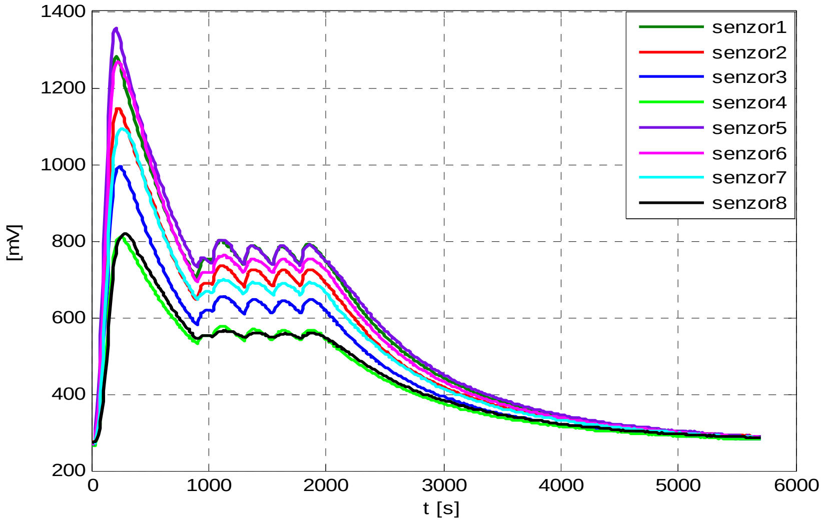

Fig. 8 Output voltages on sensors LM35DH in case c.
Oven supplied on step III (4 resistances up-down), θ_r =*110 ℃*, θ_i =*27℃*, t_i =*30 min*, t_r =*54 min*.

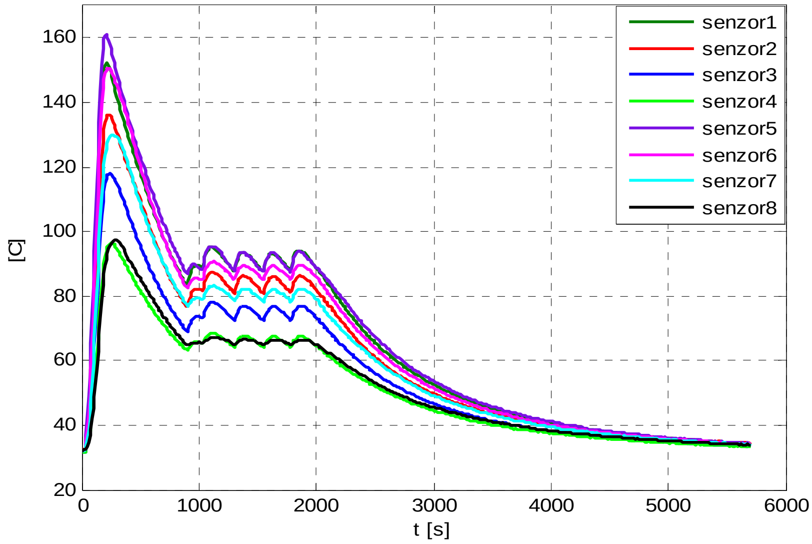

Fig. 9 Temperatures indicated by sensors LM35DH in case c.
Oven supplied on step III (4 resistances up-down), θ_r =*110 ℃*, θ_i =*27℃*, t_i =*30 min*, t_r =*54 min*.

4. CONCLUSIONS

In the first analyzed case is registered the greatest non-homogeneity of the temperature inside the oven, because the heat was transmitted from the resistances placed in the upper part of the oven.

The maximum temperature difference (120°C) between the upper part (sensor 5) and the lower one (sensor 4) of the oven's enclosure was recorded at t=210 s. At this moment the temperature inside the oven has reached the maximum value (185°C), and then were disconnected the oven's resistances (by the bimetallic element), up to t=1000 s; further, the heating's intermittent periodical regime had a cycle duration (connecting-disconnecting) t_c=700 s.

Within t=1000 s...3500 s the up-down temperature difference inside the oven was 70°C, and in final, 25°C.

The temperature from the oven's enclosure had the maximum value in the area of sensor 5, placed in centre at maximum height (h5=16 cm). The temperature from the up-right corner (indicated by sensor 1, placed at height h1=15,5 cm) is lower than the one from centre (up) by approximately 15°C. Sensor 6, placed in centre at height h6=12 cm indicates a higher temperature by approximately 12°C against sensor 2, placed on right side at a height of 11,5 cm.

Sensor 2 and sensor 7 (placed in centre, h7=7 cm) have indicated approximately the same temperature (the values max/min were 80°C/65°C). Sensor 3 (placed on right side, h3=6,5 cm) and sensor 8 (placed in centre, h8=2 cm) have indicated approximately the same temperature (values max/min: 70°C/58°C). The minimum temperature's value from the oven's enclosure was registered in the right-down corner (the temperature indicated by sensor 4 was within 55°C...65°C).

In the second case, the heat was transmitted from the resistances placed in the lower part of the oven, which determined a non-homogeneity of the oven temperature more reduced compared with the previous situation.

The maximum temperature difference between the upper part (sensor 5) and the lower one (sensor 4) of the oven's enclosure was of 45°C; within t=1020 s...3500 s the up-down temperature difference inside the oven was 35°C, and at the end of the recording period, it was 15°C.

After the first 1020 s the transient state disappears. The steady-state of the oven was intermittent periodic duty-type (with a cycle duration of t_c=700 s) in this case.

Sensors 5 and 6 (placed in centre at h5=16 cm and h6=12 cm) have indicated the same temperature (the values max/min being 115°C/78°C). Sensors 1, 2 (placed on right side at h1=15,5 cm and h2=11,5 cm) and sensor 7 (placed in centre, h7=7 cm) have indicated the same temperature (the values max/min being 105°C/70°C).

Within t=1020 s...3500 s the max/min temperature values indicated by the other sensors were the following: sensor 3 - 95°C/65°C, sensor 4 - 85°C/60°C, sensor 8 - 80°C/63°C.

In the last case were supplied all the 4 resistors of the oven (up-down). This has determined a non-homogeneity of the temperature inside the oven much more reduced compared with the previous cases.

The maximum temperature difference (65°C) was registered at t=210 s; within t=1000 s...3000 s the up-down temperature difference inside the oven was 30°C, and at the end of the recording period, the temperature inside the oven was homogeneous.

In the first 210 seconds from the heating's beginning, the temperature inside the oven reached the maximum value (161°C), and then were disconnected the oven's resistances (by the bimetallic element), up to the moment in time t=1020 s; further, the heating intermittent periodic regime had a cycle duration (connecting-disconnecting) t_c=250 s.

After the first 1020 s the max/min temperatures indicated by sensors were: sensors 1 and 5 - 95°C/90°C, sensor 6 - 90°C/85°C, sensor 2 - 85°C/81°C, sensor 7 - 83°C/79°C, sensor 3 - 78°C/73°C, sensors 4 and 8 - 68°C/65°C. At supplying of all the oven's resistances (up-down) the variations max/min indicated by each sensor were much more reduced than the previous cases.

Is found that, to obtain a thermal field as uniform possible, is necessary to be supplied all the heating elements of the oven (up-down).

The thermal regime of the resistance oven is very much influenced by its operation steps (resistances up-down, or only resistances up, respectively down), but also by the heating duration (due to the bimetallic elements that adjust the temperature from the oven).

REFERENCES/BIBLIOGRAPHY

[1.] Şt. Laurenţiu, Temperature transducers (III). Semiconductor transducers, Conex Club Magazine, pp. 18-21 (October 2004).
[2.] Şt. Laurenţiu, Temperature transducers (I). Semiconductor transducers, Conex Club Magazine, pp. 12-16 (July-August 2004).
[3.] A. Heler, Şt. Hărăguş, Transducers and measuring the non-electric measures, Politehnica University from Timişoara, 1997.
[4.] V. Dolga, Sensors and transducers, Eurobit Publishing House, Timisoara, 1999.
[5.] A. Ignea, Electric measurement of non-electric measures, Western Publishing House, Timişoara, 1996.
[6.] N. M. Bârlea, Semiconductors, dielectrics and applications, Blue Publishing House, Cluj-Napoca, 2002.
[7.] Monica-Anca Chita, Sensors and transducers, MatrixROM Publishing House, Bucharest, 2003.
[8.] M. Saracin, Cristina Saracin, Electric and electronic measurements, MatrixROM Publishing House, Bucharest, 2003.
[9.] M. Saracin, Cristina Saracin, Transducers. Interfaces. Data acquisition, MatrixROM Publishing House, Bucharest, 2010.
[10.] D. Comşa, Industrial electrothermal installations, vol. I şi II, Technical Publishing House, Bucharest, 1986.
[11.] I. Şora, N. Golovanov et all, Electrothermal conversion and electrotechnologies vol 1 (in Romanian), Technical Publishing House, (Bucharest, Romania), 1997.
[12.] 12. Marilena Ungureanu, M. Chindriş, I. Lungu, Utilisations of electric power, E.D.P. R.A. Bucharest, 1999.
[13.] A. C. Metaxas, Foundations in Electroheat, A unified approach, John Wille&Sons Ltd, Baffins Lane, Chichester, West Sussex England, 1996.

INTERNATIONAL SYMPOSIUM on
ADVANCED ENGINEERING & APPLIED MANAGEMENT
– 40th ANNIVERSARY in HIGHER EDUCATION (1970-2010)
4 – 5 November, 2010, Hunedoara, ROMANIA

[1]Ionel MUSCALAGIU, [2]Manuela PĂNOIU, [3]Diana Maria MUSCALAGIU, [4]Anca IORDAN

THE IMPLEMENTATION OF THE MULTI-ROBOT EXPLORATION PROBLEM IN DisCSP-NetLogo

[1-4] UNIVERSITY „POLITEHNICA" OF TIMISOARA, FACULTY OF ENGINEERING OF HUNEDOARA, ROMANIA

ABSTRACT:
The implementation and evaluation of asynchronous search techniques can be done in any programming language allowing a distributed programming. Nevertheless, for the study of such techniques and for their evaluation, it is easier and more efficient to implement the techniques under certain distributed environments, such as NetLogo and are open-source. Recently, for evaluation of this algorithm it is used a multi-robot exploration problem. This problem is a natural application of Distributed Constraint Reasoning in which each robot is represented by an agent/variable; the different values for agents are the future directions they may move. The aim of this article is to introduce an model of study and evaluation for the asynchronous search techniques in NetLogo using a multi-robot exploration problem, model model calling DisCSP-NetLogo.
KEYWORDS: Artificial intelligence, distributed programming, constraints, agents

1. INTRODUCTION

The constraint programming is a model of the software technologies, used to describe and solve large classes of problems as, for instance, searching problems, combinatorial problems, planning problems, etc. A large variety of problems in the A.I field and other domains specific to computer sciences could be regarded as a special case of constraint programming. Lately, the A.I community showed a greater interest towards the distributed problems that are solvable through modeling by constraints and agents. The idea of sharing various parts of the problem between agents that act independently and that collaborate between them using messages, in the prospective of gaining the solution, proved itself useful, as it conducted to obtaining a new modeling type called Distributed Constraint Satisfaction Problem(DisCSP) [1][7],[8].

Many algorithms to solve Distributed Constraint Satisfaction Problems (DisCSP) have been introduced in the literature There exist complete asynchronous searching techniques for solving the DCSP, such as the ABT (Asynchronous Backtracking) and DisDB (Distributed Dynamic Backtracking) [1],[7],[8]. There is also the AWCS (Asynchronous Weak-Commitment Search) [7],[8] algorithm which records all the nogood values. The ABT algorithm has also been generalized by presenting a unifying framework, called ABT kernel [1]. From this kernel two major techniques ABT and DisDB can be obtained.

The evaluation of the asynchronous search techniques depends on at least two factors: the types of problems used at the evaluation and the units of measurement used. Each problem can be used with a certain efficiency of a certain technique, depending on the problem's difficulty. For the CSP modeling there were used some types of classic problems: the n queens problem, the graph coloring problems, uniform random binary or the SAT problem. These problems were taken over for the analysis of the DisCSP techniques in the distributed formulation in which the variables where taken over by agents. For these problems there are a few parameters that define them. The most important are the dimension of the problem and the density of the constraints graph associated to the DisCSP problem. There should be mentioned that the problem of the coloring of a graph and the randomly generated binary are the most suitable for the evaluation, because they allow different densities for the constraints graph and they have many direct applications in real practice.

Recently, for evaluation of this algorithm it is used a multi-robot exploration problem[2][3][4]. This problem is a natural application of Distributed Constraint Reasoning (DCR) in which each robot is represented by an agent/variable; the different values for agents are the future directions they may move. We will observe that using both classical and real world problem is interesting to obtain a better and more precise comparison.

The implementation of asynchronous search techniques based on distributed constraints can be done in any programming language allowing a distributed programming, such as Java, C, C++ or other. Nevertheless, for the study of such techniques, for their analysis and evaluation, it is easier and more efficient to implement the techniques under certain distributed environment, which offer various facilities, such as NetLogo [12], [9],[10],[11].

NetLogo, is a programmable modelling environment, which canl be used for simulating certain natural and social phenomena. It offers a collection of complex modelling systems, developed in time. The models could give instructions to hundreds or thousands of independent agents which could all operate in parallel. NetLogo is the next generation in a series of modeling languages with agents that began with StarLogo [12]. It is an environment written entirely in Java, therefore it can be installed and activated on most of the important platforms (Windows, Unix) .

The aim of this article is to introduce an model of study and evaluation for the asynchronous search techniques in NetLogo using a multi-robot exploration problem in [2][3], by extending the model in [5][6], model calling DisCSP-NetLogo. This model can be used in the study of agents behavior in several situations, like the priority order of the agents, the synchronous and asynchronous case, leading, therefore, to identifying possible enhancements of the performances of asynchronous search techniques. We extend the model in [5][6] with support for the problem a multi-robot exploration problem.

2 DisCSP FOR MULTI-ROBOT COORDINATION

2.1 Distributed Constraint Satisfaction Problems (DisCSP)

This paragraph presents some notions known from the IT literature related to the DCSP modeling[1][7][8].

Constraint satisfaction is a classical and powerfull tool in artificial intelligence whose traditional applications concern planning, scheduling, placement, logistics and so on.

Definition 1.-CSP model. The model based on constraints CSP-Constraint Satisfaction Problem, existing for centralized architectures, consists in:

- n variables $X_1, X_2 ..., X_n$, whose values are taken from finite, discrete domains D_1, D_2, …., D_n, respectively.
- a set of constraints on their values-*C*.

Solving a CSP requires to find for each variable x_i a value in Di which is consistent with set of constraint *C* (i.e. which does not violate any constraint of C).

The concept of distributed CSP has been introduced to formalize and solve naturally distributed decision problems which generally deal with a set of data, shared out among many sites and whose centralization is often impossible.

Definition 2.-The DisCSP model. A problem of satisfying the distributed constraints (DisCSP) is a CSP, in which the variables and constraints are distributed among autonomous agents that communicate by transmitting, messages.

Formally, a DisCSP (X, D, C, A) is an extension of the triplet (X, D, C) where A is a finite set of agents $\{A_1, A_2, ..., A_p\}$ in which each A_k ($1 \le k \le p$) owns a subset of X: X_{A_k} with $\cap_{A_k \in} X_{A_k} = \emptyset$ and a subset of C: CA_k . From the point of view of agent A_k , variables of set XA_k are called "owned variables" whereas the set $X \setminus XA_k$ refers to the "foreign variables".

Most of algorithms to solve disCSP are distributed and asynchronous. To execute such algorithms, an agent has to be able to send messages to any other agents of its accointance set. As the algorithms are asynchronous, delays can occur when messages are exchanged through the communication network. For more details about DisCSP algorithms, readers can consult [1][7][8].

2.2 Modelling the multi-robot exploration problem as a DisCSP

Multi-robot systems (MRS) consist in a set of autonomous mobile robots which collaborate to perform a mission. This collaboration is allowed by communication abilities which usually rely on radio communication technologies. Among the applications of multi-robot system, the exploration of an unknown environment under communication constraint is a difficult problem [2][3][4]. In such an application, it is consider robots with communication abilities and sensing abilities (like laser, sonar, camera).

To perform the exploration, the robots move toward the frontier between open space and unexplored area. In addition, robots have to collaborate to spread out on the ground (requirement to speed up the exploration and use less energy) and to keep in touch with each other (requirement to be able to exchange partial maps during the resolution and maintain a communication link with a control center). In [2][3][4] these two last requirements can be integrated into a coordination scheme as constraints of a DisCSP.

To express the multi-robot exploration as a distributed constraint satisfaction problem [2], [3] will be to discretize the space of actions of robots. The movement of a mobile robot is usually the result of a combination of lateral and longitudinal accelerations. To simplify in [2],[3] it consider 8 possible directions corresponding to the cardinal points of a compass: go to the north, go to the north-east, go to the east, go to the south-east, etc .

Each robot is considered as an agent and owns a variable to instantiate. This variable represents its next heading (in other words, the next direction to explore). The domain of each variable is composed with the 8 cardinal directions: {N,NE,E, SE, S, SW,W,NW}. The assignment of each variable has to satisfy two constraints:

- according to a direction, the future position of a robot does not have to break the connectivity of the network,
- according to a direction, the future position of a robot does not have to create overlapping with the sensor range of its neighbors.
- its future location allows to discover new unexplored areas.

Constraints can be summarized as follows in [2][3]. Thus, the requirement 1. can be expressed as a constraint defined by an inferiority test between two values: the distance between the future positions of the two robots and the communication range (Figure 1). The requirement 3. can be expressed as a specific ordering between the 8 cardinal positions such that the first cardinal position allows to have the lowest distance between the robot and the frontier, the second cardinal position allows to have the second lowest distance, etc. To enforce the efficiency of the exploration by reducing overlaps (requirement 2), we can also impose that the distance between the future positions of any two robots of A have to be superior to the sum of their sensor ranges[2][3].

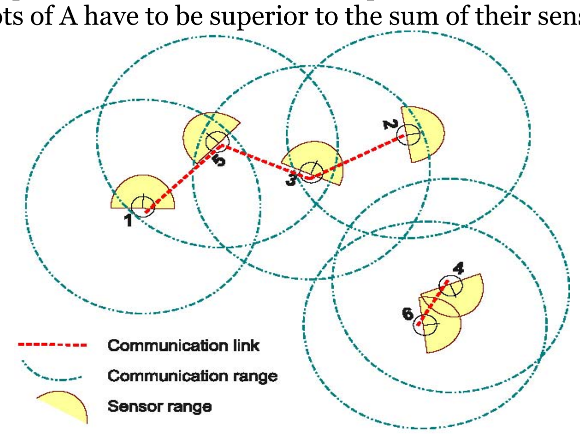

Figure 1: Connectivity constraint between two robots

This previous statement can be expressed as the following disCSP [2],[3]:

- $A = \{A_1, A_2, ..., A_p\}$ denotes a fleet of p robots exploring an unknown environment and sharing a common map of already explored areas.
- $X = \{x_1, x_2, ..., x_p\}$ is composed of variables storing the next heading of each robot of A.
- $D = \{dom(x_1), \ldots, dom(x_p)\}$ with $dom(x_i)$ $(1 \le i \le p)$ is the set of all 8 cardinal directions that a robot A_i can choose to plan its next movement. The domain is ordered by the following relation:

$$v_1 \le v_2 \equiv dist(fp(A_i,v_1), frontier) < dist(fp(A_i,v_2), frontier) \text{ with } (v_1, v_2) \in dom(x_i).$$

- $C = C1 \cup C2$ where:

$$C1 = \{\forall A_i \in A, \exists A_j \in AR_{A_i}, \text{dist}(fp(A_i,x_i), fp(A_j, x_j)) < cr\}$$

$$C2 = \{\forall A_i \in A, \forall A_j \in A \setminus A_i, 2\ sr < \text{dist}(fp(A_i,x_i), fp(A_j, x_j))\}$$

with:

- sr the sensor range of a robot;
- dist(p1 ,p2)the euclidian distance between the position p1 and the position p2 ;
- $fp(A_i,x_i)$the future position of Ai considering its future direction x_i and its current vector speed;
- cr the communication range of a robot.

To explore an unknown environment, the robots of set A have to periodically solve this DisCSP in order to be able to choose a heading compatible with the requirements previously introduced.

3. MODELING AND IMPLEMENTING OF THE MULTI-ROBOT EXPLORATION PROBLEM IN DisCSP-NetLogo

In this section we present a solution of modeling and implementation for the existing agents' process of execution in the case of the asynchronous search techniques for the multi-robot exploration problem in DisCSP-NetLogo. This solution, calling DisCSP-NetLogo will be extended with support for the evaluation of the performances of asynchronous search techniques using a multi-robot exploration problem in [2][3].

This modeling can also be used for evaluation of the asynchronous search techniques, such as those from the AWCS family [7][8], ABT family [1], DisDB [1]. Implementation examples for these techniques can be found on the site in [11].

The modeling of the agents' execution process will be structured on two levels, corresponding to the two stages of implementation.

The definition of the way in which asynchronous techniques will be programmed so that the agents will run concurrently and asynchronously will be the internal level of the model. The second level refers to the way of representing the NetLogo application. This is the exterior level. The first aspect will be treated and represented using turtle type objects. The second aspect refers to the way of interacting with the user, the user interface. Regarding that aspect, NetLogo offers patch type objects and various graphical controls.

3.1.Agents' simulation and initialization

First of all, the agents are represented by the breed type objects (those are of the turtles type). In there fig. 1 is presented the way the agents are defined together with the global data structures proprietary to the agents.

breeds *[agents-robots]*
globals *[variables that simulate the memory shared by all the agents]*
agent-robots-own *[message-queue current-view nogoods messages-received_ok messages-received_nogood total_distance the-neighbors nr_constraintc nr_cycles AgentC_Cost]*
;message-queue contains the received messages.
;current-view is a list indexed on the agent's number, of the form [v_0 v_1 v_2...], v_i = -1 if we don't know the value o that agent or v_i=1,8 (the cardinal directions: {N,NE,E, SE, S, SW,W,NW}).
; nogoods is the list of inconsistent positions [0 1 1 0 ...] where 0 is a good position, and 1 is inconsistent.
; total_distance the total traveled distance by the robots
; nr_cycles -the number of cycles
; nr_constraintc - the number of constraints checked
; AgentC_Cost – a number of non-concurrent constraint checks
; messages-received_ok and messages-received_nogood are variables that count the
; number of ok and nogood messages received by an agent.

Figure 2. Agents' definition in the case of the multi-robot exploration problem

For the evaluation of the multi robot exloration problem in this paper we using the three clasical metrics and the total traveled distance by the robots, from [4]:

- ***the number of messages transmitted during the search***: messages-received_ok, messages-received_nogood, messages-received_removed, etc.
- ***the number of cycles***. A cycle consists in the necessary activities that all the agents need in order to read the incoming messages, to execute their local calculations and send messages to the corresponding agents. This metrics allows evaluating the calculation of the global effort evaluation for a certain technique
- ***the number of constraints checked***. The time complexity can be also evaluated by using the total number of constraints verified by each agent. There is a measurement of the global time consumed by the agents involved. It allows the evaluation of the local effort of each agent. The number of constraints verified by each agent can be monitored using the variables proprietary to each robots called **nr_constraintc**.
- ***a number of non-concurrent constraint checks.*** This can be done by introducing a variable proprietary to each agent, called AgentC-Cost. This will hold the number of the constraints concurrent for the agent. This value is sent to the agents to which it is connected through the messages. Each agent, when receiving a message that contains a value SenderC-Cost, will update its own monitor AgentC-Cost with the new value.
- ***the total traveled distance by the robots***. This metric is specific to this application [4]. It makes it possible to evaluate if an algorithm is effective for mobile and located agents in an unknown environment. Indeed, it is not because an algorithm obtains a low number of cycles or a low number of messages which it is more adapted to obtain a coherent displacement of the robots.

3.2. Representation and manipulation of the messages

Any asynchronous search technique is based on the use by the agents of some messages for communicating various information needed for obtaining the solution. The manipulation of the messages supposes first of all message representation. This thing can be achieved in Netlogo by using some indexed lists. The way of representation of the main messages encountered at the asynchronous search techniques is presented as follows:

- (**list** "ok" agent-robot value agent_costs) – messages of the *ok* type*;value*= cardinal directions.
- (**list** "nogood" agent-robot current-view agent_costs) - messages of the *nogood* type;
- (**list** "addl" agent-robot $_1$ agent-robot $_2$ agent_costs)
- (**list** "removel" agent-robot $_1$ agent-robot $_2$ agent_costs)

3.3. Definition and representation of the environment

As concerning the interface part, it can be used for the graphical representation of the DCSP problem's objects (robots, obstacle etc) of the patch type. It is recommended to create an initialization procedure for the display surface where the agents' values will be displayed. For the case of the multi-robot exploration the representation of robots, links and obstacle is modeled asa a grid with a number de cells. Each cell can be empty, occupied by a robot or an obstacle, explored or unknown.

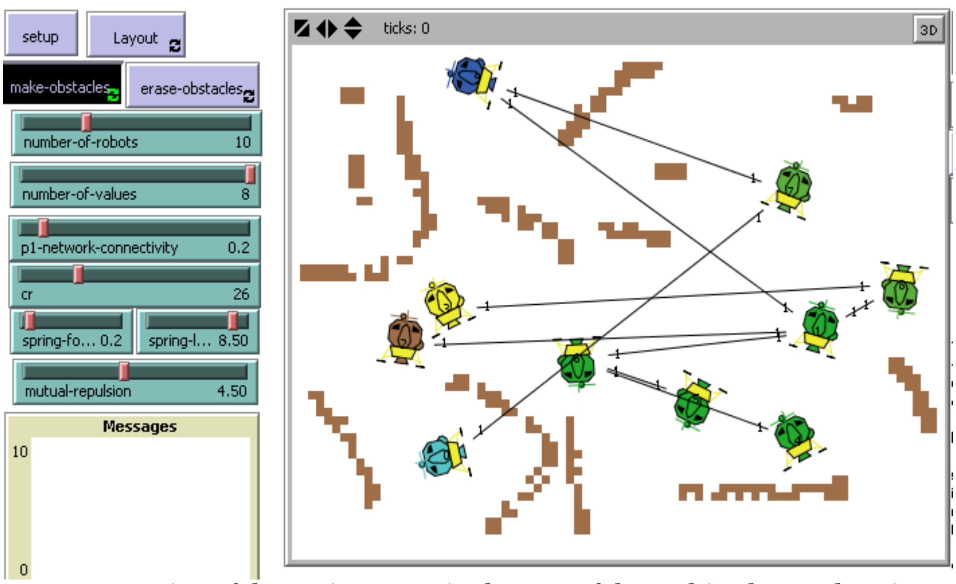

Figure 3. Representation of the environment in the case of the multi-robot exploration problem

To model the surface of the application are used objects of the *patches* type. Depending on the significance of those agents, they are represented on the Netlogo surface. In figure 3 are presented one way in NetLogo for representing the agents of the *robots* type. For this implementation we have considered environments with different levels of complexity depending on: number of obstacles, the size of the obstacles, the density of the obstacles, the minimum distance between two close obstacles.

3.4. Application initialization. "The main program" for the application

The initialization of the application supposes the building of agents and of the working surface for them. Usually, there are initialized the working context of the agent, the message queues, the variables that count the effort carried out by the agent. In figure 4 there are presented the two routines of the application initialization.

The working surface of the application should contain NetLogo objects through whom the parameters of each problem could be controlled: the number of agents, the density of the constraints graph, the number of colors. These objects allow the definition and monitoring of each problem parameters.

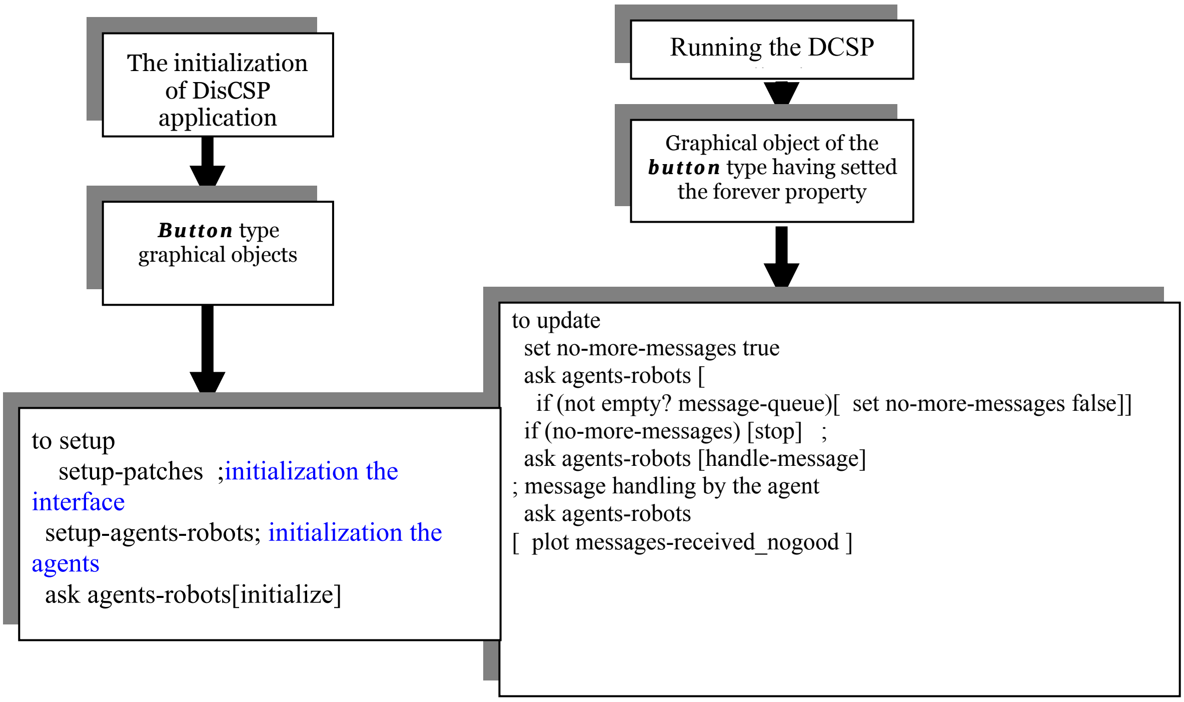

Fig. 4. Initialization and running of the DisCSP application

For the application running there is proposed the introduction of a graphical object of the button type and setting the forever property. That way, the attached code, in the form of a NetLogo procedure (that is applied on each agent) will run continuously, until emptying the message queues and reaching the stop command.

Another important observation is tied to attaching the graphical button to the *observer* [5[6]. The use of this solution allows obtaining a solution of implementation with synchronization of the agents' execution. In that case, the *observer* will be the one that will initiate the stoping of the DisCSP application execution. In this case the *update* procedure is attached and handled by the *observer*. These elements lead to the multi-agent system with synchronization of the agents execution. If it's desired to obtain a system with asynchronous operation, will be used the second method of detection, which supposes another *update* routine. That new *update* routine will be attached to a graphical object of the *buton* type which is attached and handled by the turtle type agents[5][6].

In figure 5. there is captured an implementation of the AWCS for the multi-robot-exploration problem technique that uses the model presented. In figure 5 the update procedure is attached and handled by the observer. These elements lead to the multi-agent system with synchronization of the agents' execution.

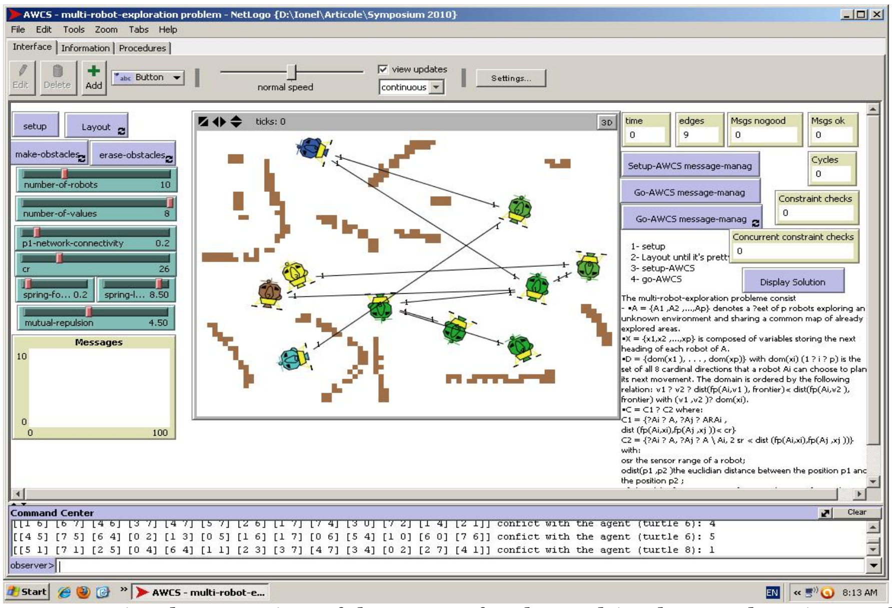

Fig 5. NetLogo implementation of the AWCS for the multi-robot-exploration problem

4. CONCLUSIONS

In this article was analysed the NetLogo environment with the purpose of building a general model of implementation and evaluation for the asynchronous techniques such as they could use the NetLogo environment as a basic simulator in the study of asynchronous search techniques.

In this paper is to introduce an model of study and evaluation for the asynchronous search techniques in NetLogo using a multi-robot exploration problem, by extending the old model, model calling DisCSP-NetLogo. This model can be used in the study of agents behavior in several situations, like the priority order of the agents, the synchronous and asynchronous case, leading, therefore, to identifying possible enhancements of the performances of asynchronous search techniques. We extend the old model in [5][6] with support for the problem a multi-robot exploration problem.

As a general conclusion, we think that the model we achieved can be used for the study and analysis of the asynchronous techniques, the model allowing their complete evaluation. Students can use the models on the site [11] to study, to understand the functioning of the asynchronous search techniques and, perhaps, to extend them.

REFERENCES

[1.] C. Bessiere, I. Brito, A. Maestre,P. Meseguer, Asynchronous Backtracking without Adding Links: A New Member in the ABT Family. Artificial Intelligence, 161:7-24, 2005.

[2.] A. Doniec, N. Bouraqadi, M. Defoort, V-T. Le, and S. Stinckwich. Distributed constraint reasoning applied to multi-robot exploration. In *21st International Conference on Tools with Artificial Intelligence (ICTAI)*, New Jersey, USA, 2009.

[3.] A. Doniec, N. Bouraqadi, M. Defoort, V-T Le, and S. Stinckwich. Multi-robot exploration under communication constraint: a disCSP approach. In 5th National Conference on "Control Architecture of Robots", May 18-19, 2010 - Douai, FRANCE.

[4.] Pierre Monier, A. Doniec, S. Piechowiak and R. Mandiau. Metrics for the evaluation of DisCSP: some experiments on multi-robot exploration. In 2010 IEEE/WIC/ACM International Conference on Web Intelligence and Intelligent Agent Technology, Canana, August, 2010.

[5.] I. Muscalagiu, H. Jiang, H.E. Popa. "Implementation and evaluation model for the asynchronous techniques: from a synchronously distributed system to a asynchronous distributed system", in *Proceedings of the 8th International Symposium on Symbolic and Numeric Algorithms for Scientific Computing (SYNASC 2006)*, Timisoara, Romania, *IEEE Computer Society Press*, 2006, pp. (209-216).

[6.] Muscalagiu, I., Iordan , A., Muscalagiu, D., Panoiu, M.Implementation and evaluation model with synchronization for the asynchronous search techniques. Proceedings of the 13th WSEAS International Conference on Computers, Rhodos Island, Greece, July 23-25, pg. 211-216, 2009.

[7.] Yokoo M., E.H. Durfee, T. Ishida, K. Kuwabara (1998): *The distributed constraint satisfaction problem: formalization and algorithms* . IEEE Transactions on Knowledge and Data Engineering 10 (5).
[8.] Yokoo Makoto (2001): *Distributed Constraint Satisfaction- Foundation of Cooperation in Multi-agent Systems*. Springer.
[9.] MAS Netlogo Models-a. http://jmvidal.cse.sc.edu/netlogomas/
[10.] MAS Netlogo Models-b. http://ccl.northwestern.edu/netlogo/models/ community
[11.] MAS Netlogo Models-c. http://discsp-netlogo.fih.upt.ro/
[12.] Wilensky, U. *NetLogo itself:* NetLogo. http://ccl.northwestern.edu/ netlogo/. Center for Connected Learning and Computer-Based Modeling, Northwestern University, IL, 1999

INTERNATIONAL SYMPOSIUM on ADVANCED ENGINEERING & APPLIED MANAGEMENT
– 40th ANNIVERSARY in HIGHER EDUCATION (1970-2010),

INTERNATIONAL SYMPOSIUM on
ADVANCED ENGINEERING & APPLIED MANAGEMENT
– 40th ANNIVERSARY in HIGHER EDUCATION (1970-2010)
4 – 5 November, 2010, Hunedoara, ROMANIA

[1.]Adela BERDIE, [2.]Mihaela OSACI, [3] Robert RAICH, Daniela CRISTEA

THE COMPONENTISATION EFFICIENCY IN REALIZING A WD ABAP PROJECT

[1-3.]POLITEHNICA UNIVERSITY OF TIMISOARA, ENGINEERING FACULTY OF HUNEDOARA, ROMANIA
[4.] CELLENT AG, STUTTGART, GERMANY

ABSTRACT:
In this paper, we realised a study regarding the efficiency of using the componentisation technique with faceless component, in developing a Web Dynpro ABAP project. The componentisation is possible due to the architecture of the Model View Controller, the base of the Web Dynpro ABAP framework. According to the faceless componentisation technique, a Web Dynpro ABAP project is made of different components, the basic three components being: the *model* that contains the data model, the *view* component in charge with the visual part, and the *controller* component that links them and contains the testing web application. The realised case study was ordered by a company that offered the required support in selecting and recruiting the work force. The Web Dynpro ABAP application is realised with SAP NetWeaver Application Server ABAP 7.0 - trial version.
KEYWORDS:
integrated system, web programming, web dynpro ABAP application

1. WEB DYNPRO ABAP – CONCEPT AND ARCHITECTURE

The current standard for realising web applications in the ABAP environment is represented by the SAP NetWeaver concept, named *Web Dynpro*. This one is a framework integrated into the ABAP Workbench (SE80 transaction) that contains the required execution environment and the graphical development environment with special Web Dynpro tools.

The Web Dynpro architecture is based on the Web Dynpro component. The **Web Dynpro component** is the programmable and reusable entity which represents the „heart" of a Web Dynpro application [3]. It can be considered as a unilateral representation of its parts and can be executed only through a Web Dynpro application. The parts included into a Web Dynpro component are: *component Interface, component controller, component usage, window* and *view* (Fig.1) [4].

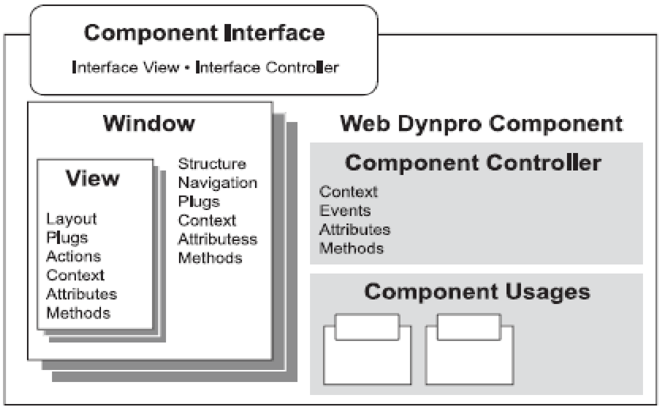

Fig.1 Parts of a Web Dynpro component [5]

The c*omponent interface* enables the component to interact with other components, being made of a visual part (interface view) and a programmable part (interface controller). The c*omponent controller* is in charge with the data transfer and the links among the parts of the component. By defining a component reuse, then in a component can be used other components. The *View* is the part where a visual interface is defined to the user. To be able to be visualised, it must be integrated in a window. The *Window* is the container of views among which the navigation is realised; it has an interface view uniquely associated and connected to the test application Web Dynpro.

This framework is realised according to the Model View Controller (MVC) paradigm. The MVC is an architectural model that divides the implementation of an application in three components: the *model* component, the *view* component and the *controller* component. The *model* component is in charge with data processing and returning the result to the controller; the *view* component is in charge only with the interface displayed to the user, and the *controller* component is in charge with the evaluation of the requests, sending data and instructions to the *model* component, and sending data to the *view* component. In principle, this *controller* component is in charge with the interaction between the *view* component and the *model* component (Fig. 2).

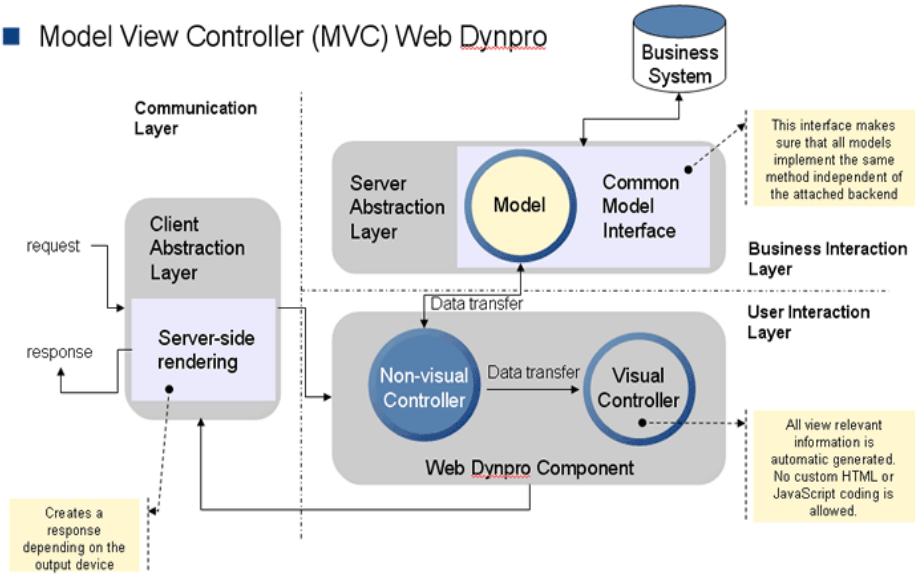

Fig.2 The architecture of the Web Dynpro framework [2]

With the Web Dynpro framework, we can develop user interfaces by using two techniques: declarative (when the interface structure is known before the execution) and dynamic (when the interface structure is partly known during the execution).

The client implementation can be defined for the web browser (Server-Side Rendering) and XML. The implementation of the metadata and the generation of HTML pages with integrated JavaScript functionalities are required for the web browser, and the implementation of XML is currently used for eCATT scenarios (extended Computer Aided Test Tool) and for client integration (*SP Smart Board)* [1].

Some of the advantages, offered by Web Dynpo in developing web applications, are [1], [3], [4]: possibility to use graphical tools, large offer of technologies, e.g. HTTP, HTML, CSS, XML and client-side scripts that are the base of each Web application, strictly separation between the data presentation and processing, possibility of using and reusing the components, easy modification of the application due to the tools it disposes of, possibility to access the data from the application context that remain intact even if the page is changing, automatic transportation of the data through data binding, automatic verification of the inputs, access to the user interface, totally integration in the ABAP development environment.

2. THE CONCEPT OF *COMPONENTISATION WITH FACELESS COMPONENT*

The componentisation is the concept used to structure a large project in Web Dynpro components. The componentisation technique is based on three such components: the *View* component, in charge with the data presentation to the user, the *Model* component, in charge with the logical part of data programming, and the Controller component, in charge with the link between the other two components – *Model* and *View*, the base of the project testing application.

The *View component* will integrate all the components included in the graphical part of the project, defining a usage for each one.

The *Model component* is a Web Dynpro component without graphical elements, i.e. without *window* and *view* (faceless). This component is used to realise the logical part and to structure the data used in the entire project. We can use a faceless component [4] for a componentised application if more than one component of the project uses the same data, and if we want to extend the project.

According to the programming paradigm *Model View Controller* of Web Dynpro ABAP, it is possible to detach the data model (the logical part of the project) from the visual part. This step requires a quite big programming effort, but ensures a high transparency and quality to the project. Through this process, the componentisation methods used in the project, which need to be visible throughout the project, are moved in the *Model* component controller, as interface methods.

The great win of the componentisation based on the design pattern *Model View Controller* is that the individual components of a project are interdependent, can be easily changed and extended, can be reused, the entire project being able to be extended and easily managed and, the last but not the least, we have to mention the possibility to use in common the data models.

3. THE COMPONENTISATION TECHNIQUE IN REALISING A WEB DYNPRO PROJECT

This technique has been implemented based on a case study realised for a company that wanted to put at the visitors' disposal information regarding the activity field, the services and the products of the company, and to offer the available working places to those people who wanted to join the company. The Web Dynpro ABAP application was realised on the *SAP NetWeaver AS ABAP 7.0* trial and consisted of Web Dynpro components.

The steps in realising a complex project, based on the faceless technology, are: realising the database, implementing and preparing the components to be linked in the componentisation structure, preparing the componentisation structure by realising the three components: view, model and controller, linking the components in the structure and detaching the model from the visual part.For realising the database, we need to create and link the tables in the DDIC data dictionary, by using the SE11 transaction (Fig. 3).

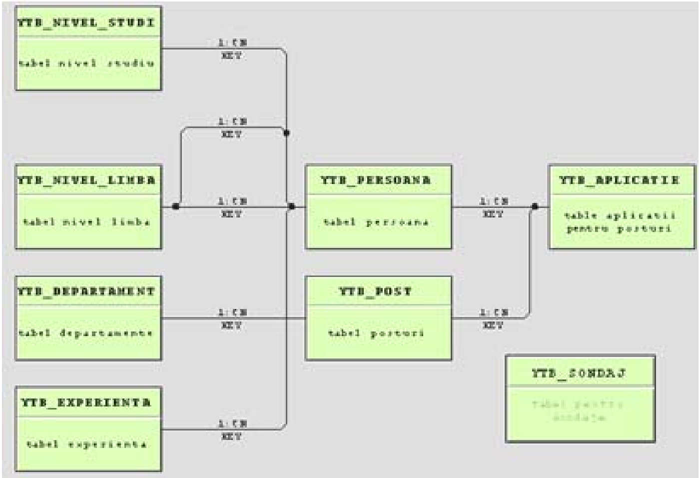

Fig. 3 Database table links

The diagram of componentisation with faceless component, used for this project, is presented in Fig. 4.

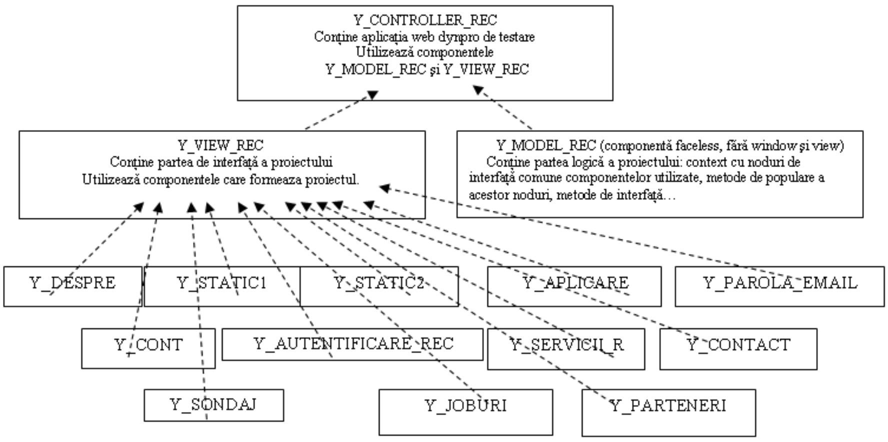

Fig.4 Diagram of componentisation with faceless component

The realisation of the project starts from the main *view* component that defines its components as usage, and realises the entire interface with the user. The data migration is made through direct external mapping. The *Model* or *faceless* component includes the logical part of the project: the common nodes of the components that compose the visual part, the methods of populating these nodes, the interface methods and other methods adequate for the *view* components [6].

Because the navigation from one page to another is the basic element of any web application, the windows of the components embedded into the main *View* component will define outputs (outbound plugs) and inputs (inbound plugs) used to realise the navigation diagram . At the *view* level, the outputs will be linked with the inputs defined in the *window*. The link between the window inputs and outputs is logically realised, by using the interface event handler methods that correspond to the defined inputs.

The *Controller* component links the components *Model* and *View*, defining them as usage, to ensure the data traffic.

Regarding the separation of the data model from the visual part, in the *Model* component, besides the methods used to populate the interface nodes that correspond to the reused components, there are brought all the methods along with their afferent codes from the component controller of the used components which, even without navigation sequences, want to be visible in other components. The reused components will keep the name of the respective methods, but these methods will trigger only interface events. The controller component that links the components *View* and *Model* includes the event handler methods able to call these methods.

4. CONCLUSIONS

Web Dynpo is one of the top technologies used to realise high quality web applications, and the componentisation is the technique used to build web projects on the nowadays SAP platform. The faceless componentisation, as a technique based on the design of the *Model View Controller* pattern, enables the independence of the components along with their interchange and reuse and, in the same time, the easily extension of the project. Although this requires a greater programming effort, it offers a maximum win.

Comparing with other frameworks (e.g. Prado), where the physical creation of the file that runs the application and the interface file are required, the Web Dynpro applications need only the realisation of a component whose window will be attached to the user. The application structure is realised without writing a single line of code, and the interface with the user is a view built with view design elements and programmed according to the requirements.

In conclusion, the Web Dynpro framework is not a tool for creating presentation pages with much animation and sophisticated graphical elements, but for implementing and realising latest generation business applications.

REFERENCES

[1.] Ulli Hoffmann, *Web Dynpro for ABAP*, Publishing House SAP Galileo Press, Bonn, Germania, 2007.
[2.] SAP Developer Network (http://sdn.sap.com).
[3.] SAP Portal - Help (http://help.sap.com).
[4.] Web Dynpro for ABAP (WDA, WD4A, WDF4A), Release NW2004s SP8 (SAP AG Online Help 2006), available in electronic format (pdf) on Internet network.
[5.] Ulli Hoffman, *Get started developing Web – native custom SAP application with Web Dynpro ABAP*, SAP Professional Jurnal, 2007.
[6.] Web Dynpro ABAP Programming Guidelines (SAP AG 2006), available in electronic format (pdf) on Internet network.

INTERNATIONAL SYMPOSIUM on ADVANCED ENGINEERING & APPLIED MANAGEMENT
– 40th ANNIVERSARY in HIGHER EDUCATION (1970-2010),